R73-11

161

AN ANALYTICAL AND EXPERIMENTAL STUDY OF TRANSIENT COOLING POND BEHAVIOR

by

Patrick J. Ryan

and

Donald R.F. Harleman

M.I.T. RALPH M. PARSONS LABORATORY
FOR WATER RESOURCES AND HYDRODYNAMICS

Report No. 161

Prepared under the support of
The Hydrologic Engineering Center
Corps of Engineers, U.S. Army
Contract No. DACW05-71-C-0113
and
National Science Foundation
Engineering Energetics Program
Grant No. GK-32472
and
Duke Power Company
Charlotte, North Carolina

January 1973

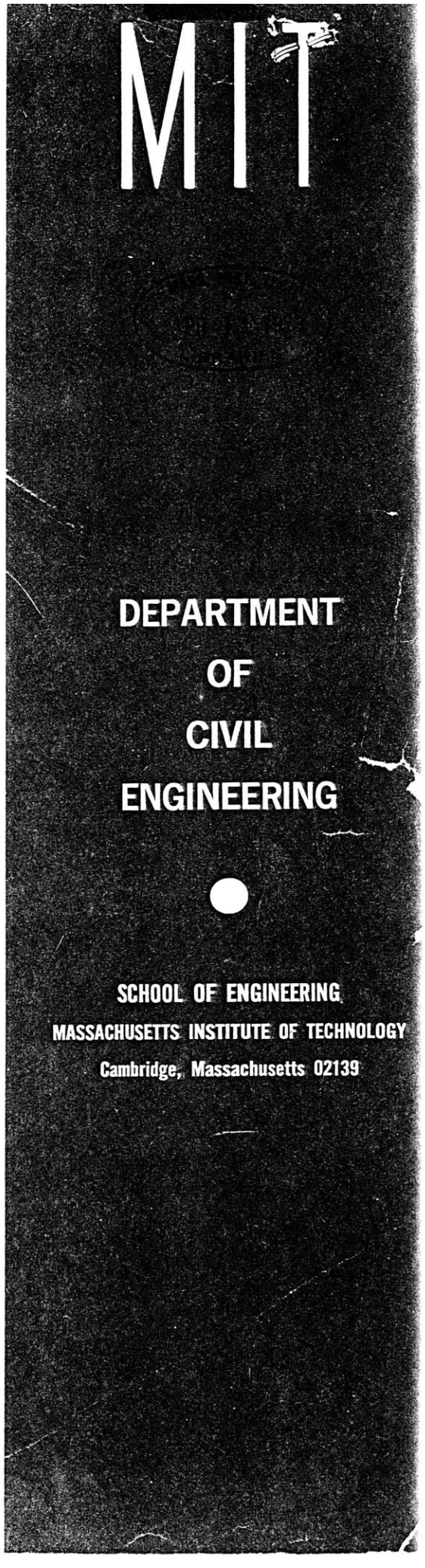

R73-11

DSR 73304
DSR 80004
DSR 80317

RALPH M. PARSONS LABORATORY

FOR WATER RESOURCES AND HYDRODYNAMICS

Department of Civil Engineering

Massachusetts Institute of Technology

AN ANALYTICAL AND EXPERIMENTAL STUDY OF TRANSIENT COOLING POND BEHAVIOR

by

Patrick J. Ryan

and

Donald R. F. Harleman

Report No. 161

Prepared under the support of
The Hydrologic Engineering Center
Corps of Engineers, U.S. Army
Contract No. DACW05-71-C-0113
and
National Science Foundation
Engineering Energetics Program
Grant No. GK-32472
and
Duke Power Company
Charlotte, North Carolina

January 1973

ABSTRACT

Cooling ponds offer many advantages as a means of closed cycle heat dissipation. These are simplicity, low maintenance and power requirements, aesthetic and possible recreational values, and high thermal inertia. A cooling pond is also subject to minimal environmental problems, since fogging tends to be localized, blowdown water can be stored for long periods, and make-up water requirements are intermittent and often lower than for other closed systems. In spite of the above advantages it is presently estimated that less than one-third of the closed cycle power stations built in the next 30 years, will utilize cooling ponds. One reason for this is lack of land, but another reason is the lack of confidence in the ability of existing models to predict cooling pond performance under transient heat loads and meteorological conditions. The use of simple steady state models and various commonly used assumptions as to surface heat loss and circulation patterns can lead to differences of at least 100% in the predicted required land area. Physical models have severe limitations, and this uncertainty in design often results in the rejection of the cooling pond alternative, which may be a mistake from economic, aesthetic and environmental considerations.

An analytical and experimental investigation of cooling ponds is conducted. The guiding principle of this investigation is that a cooling pond can be designed on a rational basis only if the desired pond behavior is first clearly defined and the important mechanisms of heat transfer both within the pond itself, and at the water surface, are isolated and quantified. An efficient pond has been defined in terms of maximum surface heat transfer and maximum response time; this leads to the requirement that a pond be capable of sustaining a vertical temperature stratification, that entrance mixing be a minimum, and that a skimmer wall intake be used.

The various components of heat transfer at a water surface are discussed, and existing empirical formulae are reviewed. Existing formulae for predicting evaporative flux from an artificially heated water surface are found to be unsatisfactory. Field data indicates that commonly used formulae may predict evaporative losses that are too low by as much as 50% for a heavily loaded water surface. A new formulae is proposed which explicitly accounts for mass transfer due to free convection. This can be very significant at low wind speeds. The proposed formula for evaporative flux performs well both in the laboratory and the field.

The effect of entrance mixing and density currents on both the steady state and transient behavior of a cooling pond is examined in the laboratory, and where possible laboratory results are supported by field observations. It is concluded that the reduction of entrance mixing is a very significant factor in improving the pond performance. In a stratified pond density currents can be of paramount importance in

distributing the heat to backwater areas, thus making the pond performance essentially independent of shape.

Steady state analytical models and a numerical transient model for the prediction of cooling pond performance are developed. The steady state models demonstrate the effect of entrance mixing and different circulation patterns. The major components of the transient model are a relatively thin surface region with horizontal temperature gradients overlying a deeper subsurface region with vertical temperature gradients. The entrance mixing is determined using the Stolzenbach-Harleman surface jet model, and the M.I.T. reservoir model is used to simulate the subsurface behavior. Output is given in terms of transient surface temperature distribution (area under isotherms), transient vertical temperature distribution, and transient intake temperatures. The transient model has been tested in the laboratory, and against five years of field data on two ponds with completely different characteristics, with very satisfactory results.

The input data required by the transient model are that which are available before the pond is built, i.e. the model is predictive. The transient mathematical model is relatively simple and inexpensive, with an execution time of less than 1 minute per simulated year on an IBM 370/155. Thus the model can be used as a design tool, or as a component of a management model which compares different heat disposal alternatives.

Design considerations, such as design of outlet and intake, the use of internal diking, and the use of physical models are briefly discussed, and a design approach is recommended.

ACKNOWLEDGEMENTS

This research was supported by the following:

The Hydrologic Engineering Center, Corps of Engineers, Department of the Army, under Contract No. DACW05-71-C-0113 (DSR 73304). The project officer was Mr. Leo R. Beard, Director, Hydrologic Engineering Center, and his successor, Mr. William Eichert.

The Engineering Energetics Program of the National Science Foundation, Grant No. GK32472 (DSR 80004). The project officer was Dr. Royal E. Rostenbach.

The Duke Power Company of Charlotte, North Carolina. The project officer was Mr. Charles A. Dewey, Jr., Principal Environmental Engineer, Duke Power Company (DSR 80317).

The cooperation of the above project officers is gratefully acknowledged.

The research work was conducted under the technical supervision of Dr. Donald R. F. Harleman, Professor of Civil Engineering. Valuable suggestions were made by Mr. Eric Adams and Mr. Gerhard Jirka, Research Assistants in the Ralph M. Parsons Laboratory, and by Dr. Keith D. Stolzenbach, Research Engineer, Tennessee Valley Authority. Experimental work and data reduction was aided by Mr. Edward McCaffrey, Mr. Roy Milley, Mr. Steven Miller and Mr. Michael Ryan. Typing was done by Mss. Pat Swan, Susan Johnson, Kathleen Emperor, Justine Lynge and Stephanie Demeris. All computer work was done at the M.I.T. Information Processing Center.

The excellent field data supplied by the State Electricity Commission of Victoria, Australia, and the Duke Power Company, North Carolina, played a large role in the success of this project. Thanks are due to Mr. Ralph Urie of the S.E.C. and Messrs. Brent Sigmon and James Hendricks of Duke Power Company.

The material contained in this report was submitted by Mr. Ryan in partial fulfillment of the requirements for the degree of Doctor of Philosophy at M.I.T.

TABLE OF CONTENTS

I. Introduction

1.1 Cooling Ponds - Raison d'Etre

Power generating capacity in the U.S.A. is expected to continue to double each decade, with thermal power plants providing the bulk of this extra capacity. Nuclear power plants are expected to show a large growth rate, increasing from 2.4% of the total capacity in 1971 to approximately 30% in 1990 (Electrical World 1972). Present levels of efficiency are about 40% for coal and oil plants, and about 33% for nuclear plants, and thus all thermal plants release large quantities of heat to the environment. These levels of efficiency are determined both by the existing levels of metal technology and the economics of power plant design, particularly the capital cost of items such as turbines and condensers. Water is the only economic cooling fluid for steam condensers in large power plants and at present the costs of its supply and of the heat disposal system do not greatly influence the choice of economic efficiency. Significant technological improvements in the efficiency of conventional steam cycles, or the development of more efficient thermal power generating methods are not foreseen in the near future (22).

Nuclear plants, with their lower efficiency, and no stack losses, produce a water heat load 60-70% higher than a fossil fuel plant. A typical 2000 MW nuclear plant produces waste heat at the condenser at the rate of 13×10^9 BTU/hr. Economic design of the power plant dictates high flow rates and relatively small temperature rises across the condenser. Typical numbers for the 2000 MW plant above are 3000 cfs and 20°F. The result is that the power industry

accounts for approximately ninety percent of industrial water use in the U.S.A., or about 45% of total water use (136).

Heat disposal may be accomplished by closed cycle systems such as cooling ponds or cooling towers, or once-through systems using water from an adjacent river, lake or ocean. Hauser (1969) estimates that by the end of the 1970's the inland sites for once-through cooling, which satisfy the thermal pollution legislation, will have been exhausted. Inland power stations, which will make up about 70% of the new base load, will therefore utilize some form of closed cycle cooling i.e. either a cooling pond ,spray canal, cooling tower, or some combination of these.

The cooling tower has been proposed as the ultimate solution to the thermal pollution problem, but there is ample evidence that the choice is by no means straightforward. The less costly and more efficient "wet" tower dissipates heat directly to the atmosphere by evaporative heat transfer, and thus while thermal water pollution is eliminated, thermal air pollution, in the form of large quantities of fog under conditions of high humidity, can be a serious problem. Chemical pollution, through disposal of the concentrated salt residue, resulting from evaporative processes, is also a potential source of difficulty. Serious objections may be raised, on aesthetic grounds, to the appearance of hyperbolic towers more than 400 feet high. Spray canals avoid many of the above objections, but as yet there is very little data on their performance with large power stations, and furthermore their power requirements are very high. Cooling ponds also have their

disadvantages, the major one being the large amount of land required. Even efficient ponds in regions of relatively low humidity require ~ 0.75 acres per MW_e, and many existing ponds require 1-2 acres/MW_e. If, however, land is available at a reasonable price, then the cooling pond offers such advantages as simplicity, low maintenance, recreational value, ability to operate for extended periods without makeup water, low power requirements and most importantly, high thermal inertia. This last point is most significant, and means that for a properly designed pond the temperature of the intake water will not reflect short term changes in meteorological conditions or plant loadings. Elimination of diurnal fluctuations may be particularly important since high power demand, and minimum heat loss (high intake temperatures, low efficiency) both tend to occur in the early evening period. Also, Brown (1970) points out, if once through cooling is not available, the cooling pond is the most aesthetically pleasing solution. The fogging effect of a pond is minimal, a figure of 200 meters downwind being given by Berman (1961) as the limit of the affected area. This figure may increase substantially with the increased size and heat loading of modern ponds, but because of the large surface area over which heat transfer to the atmosphere takes place, cooling ponds are expected to have less environmental effect than other closed cycle methods.

The problem of supply of make-up water and disposal of blowdown is now becoming significant for all closed cycle systems. The present trend in nuclear plants is towards large central power stations of the order of 5000 MW_e. The make-up water requirement for a station of this type is approximately 200 cfs, with a blowdown of approximately

100 cfs. In general, the water loss from a closed cycle cooling pond varies from 1-3 percent of the pumping rate. This loss is caused by natural and forced evaporation, seepage, blowdown losses, etc. The forced evaporative loss accounts for between 40 and 80% of the waste heat, depending primarily on the wind and water temperature. The higher figure is more typical. The remaining waste heat, usually of the order of 30%, is dissipated primarily by conduction, and also by long wave radiation from the surface. A cooling pond may have a higher or lower consumptive water loss than a tower depending on the supply of make-up water. If a year-round supply of make-up water is available, then the natural evaporation from a cooling pond generally favors the cooling tower, although this loss will be partly offset by rainfall. However, in arid regions like the Southwest the make-up water often has to be stored for part of the year, and then the water losses from the storage reservoir, plus the cooling tower losses, may exceed the cooling pond losses, due to the radiative heat loss from the pond surface. This lower demand on make-up water has been the deciding factor in favor of cooling ponds in some recent installations. The ability to operate for extended periods without blowdown may be important in meeting downstream water quality requirements.

In spite of the above advantages, it is estimated (62) that less than 33% of closed cycle power stations, built in the next 30 years, will utilize cooling ponds. One reason for this is simply lack of land. Another reason, however, is that cooling pond behavior is rather difficult to predict. There is some substance to this belief,

as use of different heat loss formulae, or use of different assumptions as to circulation patterns, can mean differences of at least 100% in the required pond area. This uncertainty leads to the use of poorly based rules of thumb such as 2 acres/MW_e or 4 acres/MW_e. The rejection of the cooling pond alternative, based on one of the above rules could be a mistake from economic, aesthetic and environmental considerations.

1.2 Economic Considerations

Cooling ponds and towers are both costly, being of the order of $5-12/kw of capacity, but as shown by Christianson et.al. (1969), in terms of extra cost to the consumer, the use of cooling ponds leads to an increase of 0.4 to 0.9%, and the use of towers from 0.6 to 3%. Although these figures are disputed by the electric power industry, it seems unlikely that the use of closed cooling systems will prove a serious obstacle to the growth of electrical generation capacity.

Comparisons of costs of different methods of closed cycle cooling tend to be rather unsatisfactory as the design and economics of a power plant with a cooling pond is very much site dependent. However, Hogan, et.al. (1970) have looked at the economics of a hypothetical 2000 MW plant with either a cooling pond or cooling tower. The meteorological conditions assumed are those near Philadelphia. The economic study is based on the capital cost and the operating expenditures for that equipment which differs depending on the cooling system, namely condensers, cooling water pumps, cooling towers/ponds. The loss in capacity due to condenser back pressure is included, but the cost of the make-up water is neglected. Some results are given in Figures 1-1, since these may be of interest. The conclusion of lower overall cost

for cooling ponds than for other closed cycle systems is supported by (21), (37).

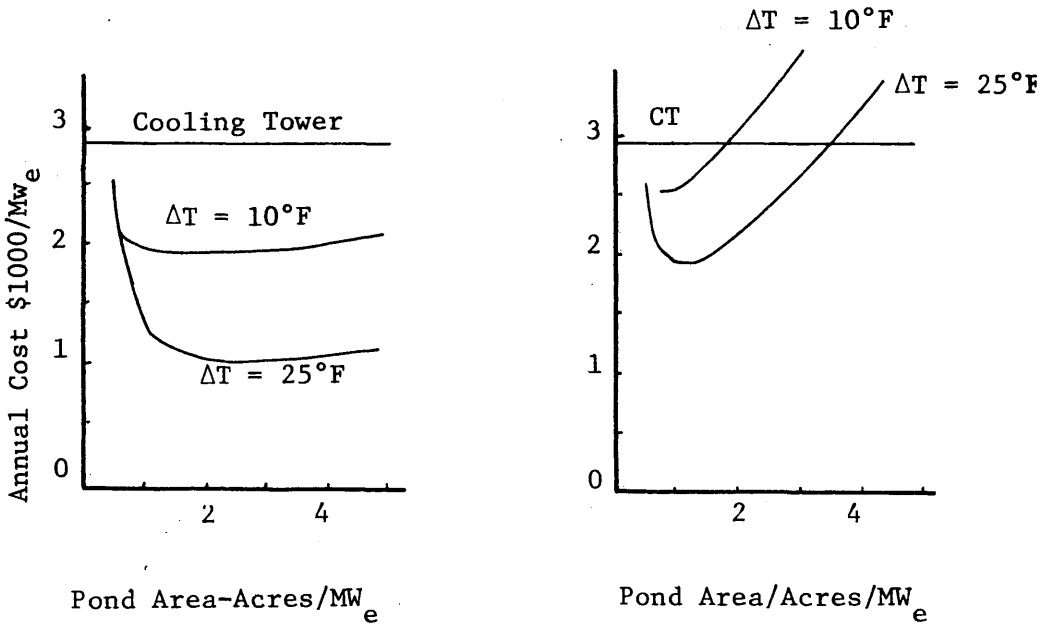

SEE ERRATA Figure 1-1 Annual Cooling Pond Costs (53)

1.3 Classification of Ponds

There is no really satisfactory way to classify cooling ponds. Possible categories are on-stream and off-stream ponds, or deep and shallow ponds, or stratified and non-stratified ponds, or, plug flow and fully mixed ponds, or, artificial and natural ponds, or finally, lightly and heavily loaded ponds. These terms will be used throughout the text, and a brief description of each category will be given.

1.3.1 Definition of Terms

a) An on-stream pond may be created by damming a small river, as shown in Figure 1-2. It may be built as a multi-purpose reservoir e.g. for water supply, hydro power or flood control, as well as heat dissipation. It may even exist as a natural lake. It will usually have an average depth of 20 ft. or greater, be stratified, and often, although not necessarily, be lightly loaded ($< 1/4$ MW_e/acre). Thermal pollution legislation may apply in the pond, as well as to the downstream discharge.

b) An example of an off-stream pond is shown in Figure 1-3. This type of pond is usually created by extensive diking. Make-up water requirements are obtained by pumping from adjacent surface or subsurface supplies. The pond is often shallow (mean depth < 15 ft.), and heavily loaded (up to 1.5 MW_e/acre). The pond may be stratified near the outlet due to the heated discharge floating on the colder bottom layers. Diurnal stratification may also be observed, but seasonal stratification usually will not be present. Thermal pollution legislation will probably apply only at the boundary of the pond.

c) There are three types of stratification, seasonal, diurnal, and artificial (i.e. caused by a heated discharge). A stratified pond is defined as one

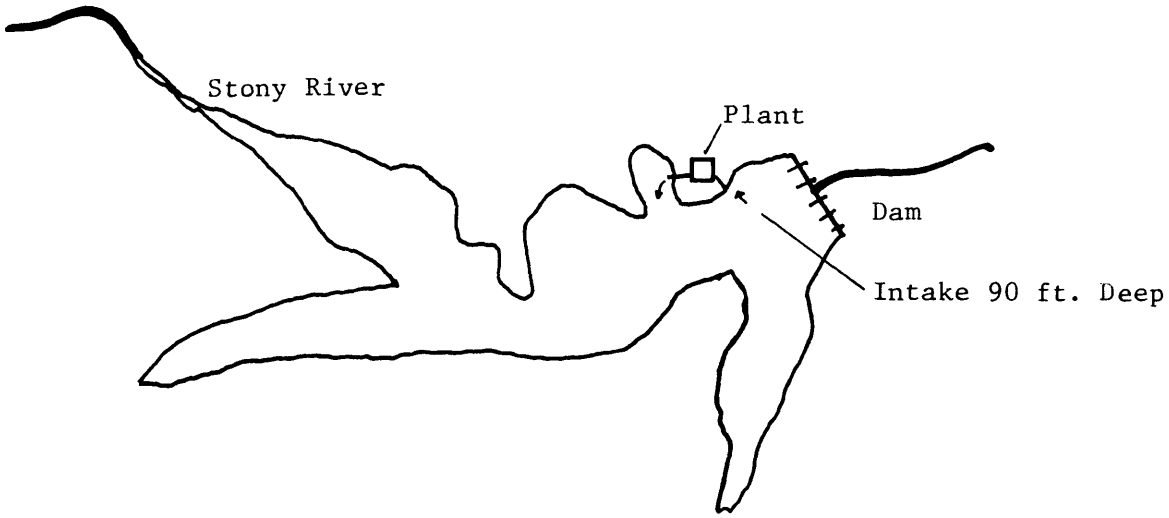

Figure 1-2 On Stream Pond - Mt. Storm

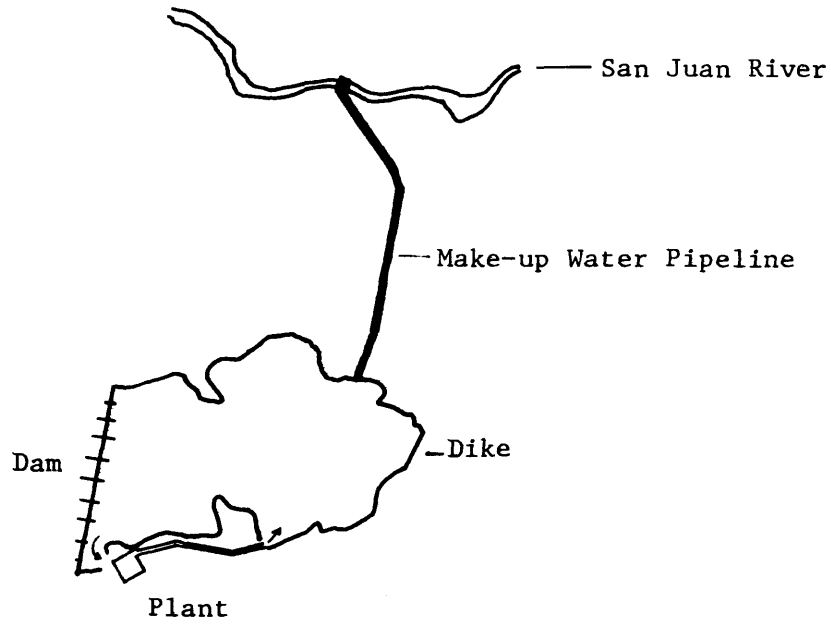

Figure 1-3 Off-Stream Pond - Four Corners

which is artificially stratified over a significant percentage of its surface area. Seasonal and diurnal stratification are incidental, although in many cases the three types of stratification reinforce one another.

d) A plug flow pond is one in which the heated discharge does not mix with the receiving water. Such a pond may or may not be stratified. See Figure 1-4. In practice there will always be some mixing.

e) The fully mixed pond involves high entrance mixing. Simple models exist for these extreme cases. The amount of mixing is determined primarily by the design of the outlet structure. The effect of the mixing is influenced by the shape of the pond.

f) An artificial pond is defined as one built exclusively for heat dissipation, whereas a natural pond already exists as a lake, or a multi-purpose reservoir.

Note that the terms outlet and intake are used from the vantage point of the power plant, not the pond. Thus the outlet is the point at which the heated discharge enters the pond, while at the intake the flow leaves the pond and enters the condenser. Heat loadings in MW_e/acre refer to the waste heat rejected by the generation, by a nuclear plant, (33% efficiency, 5% in-plant losses) of one megawatt for each acre of surface area. A loading of 1 MW_e/acre is equivalent to 3600 BTU/ft^2/day.

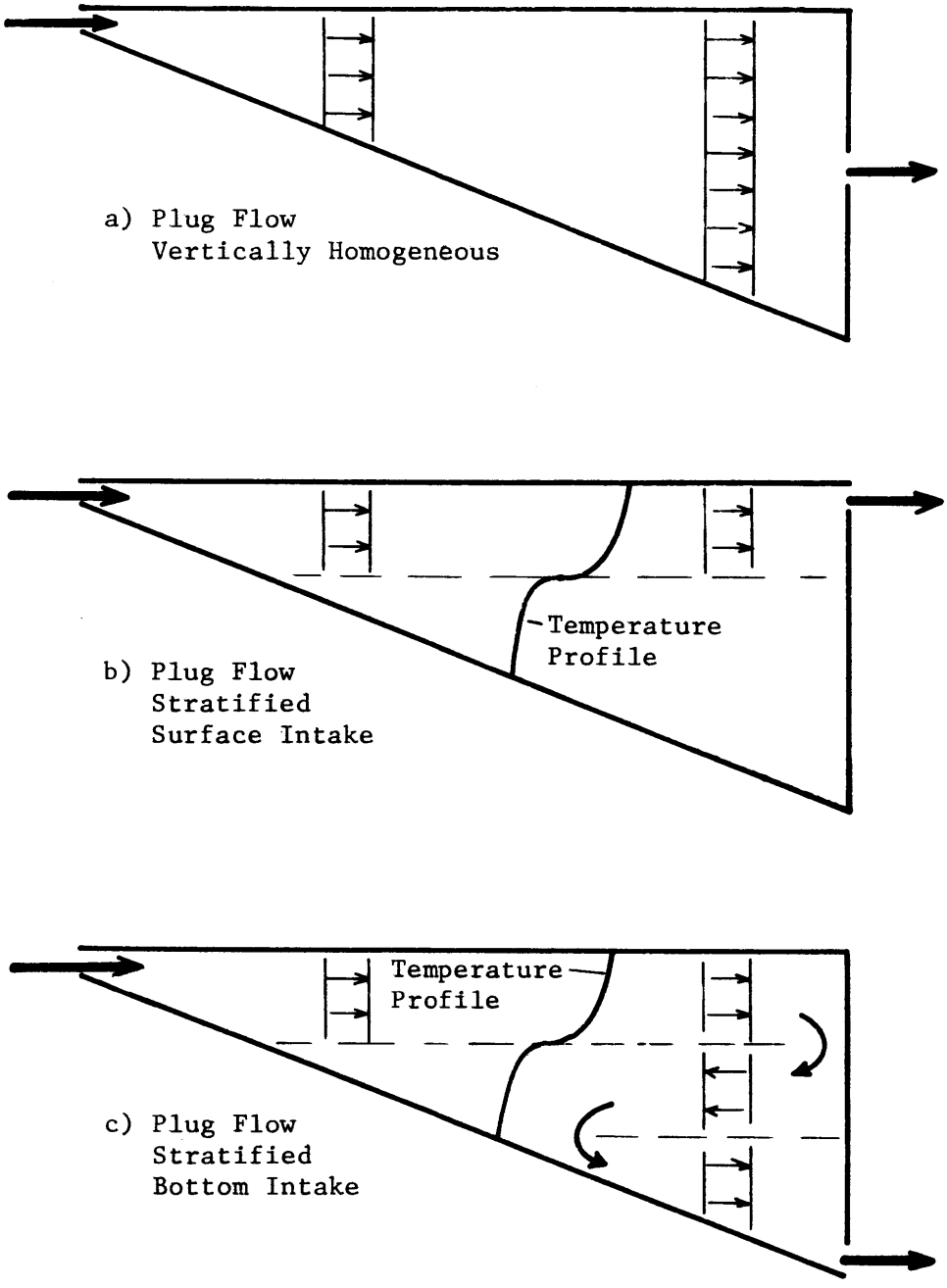

Figure 1-4 Plug Flow Ponds

1.4 Physical Characteristics of Cooling Ponds

1.4.1 Heat and Mass Fluxes

The heat and mass fluxes into a typical closed cooling pond are shown in Figure 1-5.

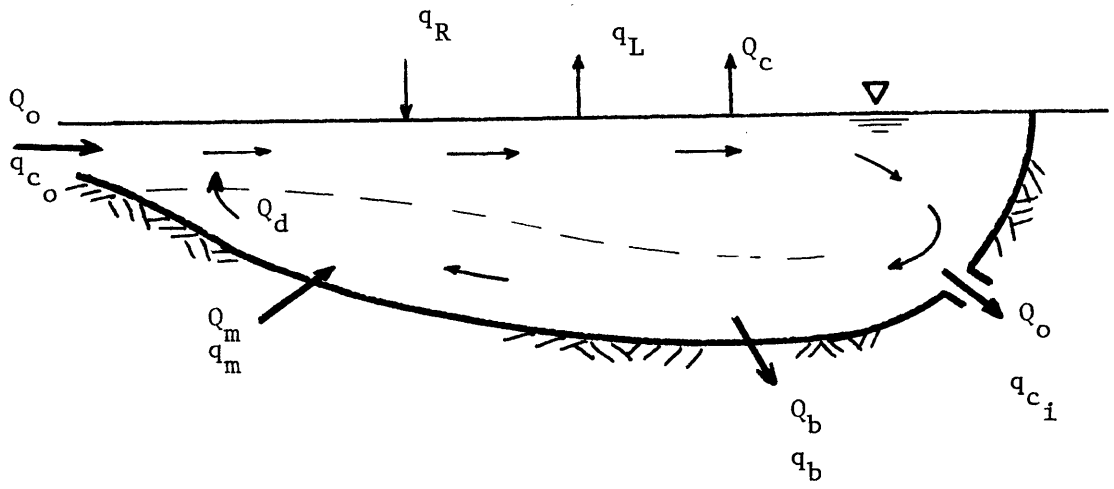

Figure 1-5 Heat and Mass Fluxes in a Typical Pond

The heat balance is given by

$$q_s = q_R + q_{c_o} + q_m - q_L - q_{c_i} - q_b \qquad (1.1)$$

where (units - energy/time)

q_s = rate of change of heat stored in pond

q_R = net heat influx by radiation

q_L = heat flux out of surface

q_{c_o} = heat flux in by advection through outlet

q_{c_i} = heat flux out by advection through intake

q_m = heat flux in by advection (make-up water)

q_b = heat flux out by advection (blowdown)

The mass balance gives

$$\frac{d\forall}{dt} = Q_o + Q_m - Q_o - Q_e - Q_b \qquad (1.2)$$

where

$\forall$ = volume of pond

Q_o = circulating water flow rate (volume/time)

Q_m = make-up water flow rate

Q_e = evaporative rate

Q_b = blowdown flow rate

The heat rejection rate by the power plant, H_p, is given by

$$H_p = q_{c_o} - q_{c_i} \qquad (1.3)$$

1.4.2 Entrance Mixing

As the heated discharge enters the pond, it entrains some of the receiving water at a volume flow rate Q_d. The entrance mixing, r_m is defined as the ratio

$$r_m = Q_d/Q_o$$

and the initial dilution D_s is defined as

$$D_s = \frac{Q_d + Q_o}{Q_o} = 1 + r_m$$

It will be shown (Chapters 3, 4) that the efficiency of the pond,

defined as the average heat loss rate for a fixed circulating water flow rate, Q_o, and outlet temperature, T_o, decreases significantly as T_m (or D_s) increases. For example, for an intake temperature within 10°F of the natural water surface temperature, and a temperature rise across the condenser of 20°F, a pond with no entrance mixing requires only about 60% of the area of a pond with high entrance mixing. SEE ERRATA

1.4.3 Effective Area

The concept of "effective area" is an old one in cooling pond design. The "effective area" is usually defined as the area of a plug flow pond having the same efficiency. The ratio of effective to actual area, k_u, may be obtained from the shape of the pond,or by isothermal model tests (Berman 1961), by intuition (AEC Report 1972), or by calculation using some assumed psuedo dispersion coefficient (Edinger 1971). Often, the effective area concept is used as a fitting coefficient, to help explain inaccuracies due primarily to not accounting for entrance mixing or lack of knowledge of surface heat transfer. It rarely seems to have any physical significance, and plays an analogous role to the "turbulent diffusion" coefficients used in many early reservoir models, i.e. a convenient fitting parameter to explain the performance of existing ponds.

1.5 Ideal Cooling Pond

The prime objective of a cooling pond is to reject as much heat as possible to the atmosphere. The heat rejection rate, q_L, is a strong function of the water surface temperature, and can be written as

$$q_L = K_1 A (T_s - T_E)^n$$

where

K_1 = function of wind speed

T_s = bulk water surface temperature

A = surface area

T_E = equilibrium temperature (see Ch. 2)

n = $f(T_s) \simeq 1.2 - 1.5$

Thus surface temperatures should be as hot as possible, and mixing of the heated discharge with cooler water is to be avoided.

A desirable aspect of cooling ponds is their ability to minimize temperature fluctuations in the intake water. This is best accomplished by storing as large a volume as possible of cooled water, and selectively withdrawing this water at the intake. A large volume of cooled water requires that the hot surface layer be kept relatively thin. Selective withdrawal requires a skimmer wall type intake. Thus the ideal pond is a deep, stratified pond with a skimmer wall type intake. This type of pond may be represented schematically as shown in Figure 1-6.

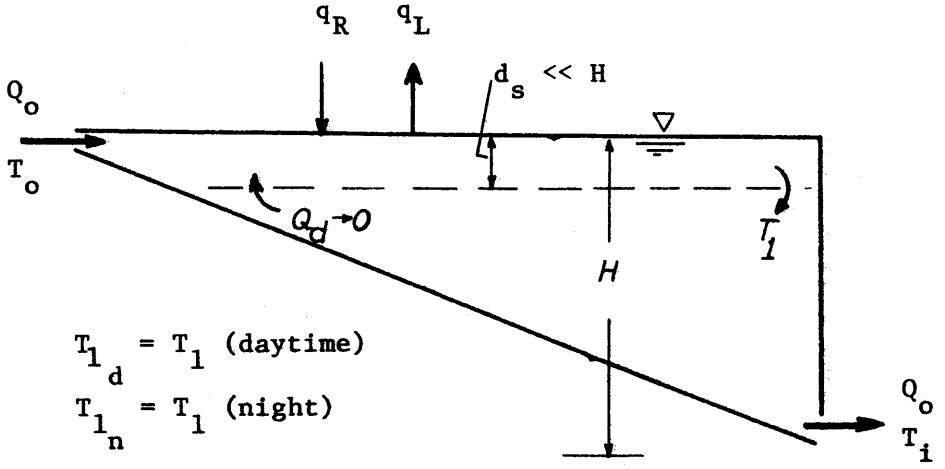

Figure 1-6 Ideal Cooling Pond

The behavior over a diurnal cycle, of an ideal pond will be considered briefly. During the daylight hours q_R increases, and q_L may decrease, leading to a $T_{l_d} > T_i$. This cooled water forms a layer just beneath the hot surface layer. At night, q_R decreases and q_L may increase, leading to $T_{l_n} < T_i$. Water at temperature T_{l_n} overlies T_{l_d}, but since $T_{l_n} < T_{l_d}$ convective mixing occurs at the cooler end of the pond, resulting in an intake temperature T_i (where $T_{l_n} < T_i < T_{l_d}$) that is largely independent of diurnal, or short term load fluctuations.

1.6 Objectives of the Study

Cooling pond design techniques are weak in two areas, prediction of surface heat transfer rates and circulation patterns. Since many existing ponds have a relatively low heat loading (< 0.5 MW_e/acre), poor design has not yet led to serious problems, and in fact the neglect of entrance mixing effects and use of conservative heat loss formulae have tended to compensate for each other. However, for large new nuclear plants the economic incentive to design a high load, efficient pond is quite large, and the penalties for poor design are correspondingly severe. Also, rejection of the cooling pond alternative due to incorrect design methods may lead to a solution which is less attractive from an economic, aesthetic and environmental standpoint. Unfortunately, physical modelling is of rather limited value in predicting pond behavior, except in special cases. Problems arise due to the virtual impossibility of satisfying similarity requirements for entrance mixing, stratified flow and surface heat loss, along with the usual Froude and Reynolds criteria. Thus the need exists to both define what constitutes an efficient cooling

pond, and to develop realistic predictive techniques for such a pond. The ideal cooling pond is shown to be both relatively deep, artificially stratified, and to use an effective skimmer type intake. This study will be limited to this type of pond. The objectives of this study are therefore:

a) To determine the characteristics of an efficient cooling pond.

b) To examine the role in such a pond of factors such as entrance mixing, density currents, pond shape, internal diking and design and location of intake and outlet.

c) To critically examine the various heat loss formulae, and test them against the best available field data.

d) To develop a relatively simple, predictive, transient mathematical model for a stratified pond which will include the effects of all the significant parameters. The model should have the ability to simulate multiple inflows and outflows so that it is also applicable to a multi-purpose reservoir used as a cooling pond.

Laboratory experiments will be conducted on an idealized cooling pond in order to both learn more about cooling pond behavior, and to provide some verification for the mathematical model developed in the study. In the final phase the mathematical model will be applied to two prototype ponds, an artificial and a natural type, for comparison of predicted and observed behavior. Emphasis will be placed on the development of a predictive mathematical model.

The uses and limitations of physical hydro-thermal models as design aids will be examined qualitatively.

1.7 Summary of Study

The guiding principle of this investigation is that a cooling pond cannot be designed on a rational basis until the desired pond behavior is first clearly defined, until the important mechanisms of heat transfer both within the pond itself and at the water surface have been isolated, and until these mechanisms have been quantified.

An efficient pond has been defined in terms of maximum heat transfer, and maximum response time. This type of pond, a relatively deep, stratified pond, with an effective skimmer type intake, has been examined in the laboratory, and where possible the laboratory results have been supported by field observations.

A relatively simple mathematical model has been developed which includes the significant characteristics of an efficient pond. This model has been verified against the laboratory pond and against two widely different types of field ponds. Predictions can be made of transient intake temperatures, surface temperature distribution, and vertical temperature profiles, for given geometric, plant operation, and meteorological conditions. The model may be used either to predict the performance of an artificial pond, or to determine whether the changes induced by waste heat input into a natural lake or reservoir are within thermal standards.

Finally, the problem of using physical models and the limitations of this study are discussed, and some suggestions for future research are made.

II. Surface Heat Transfer

2.1 Introduction

The most important single factor in predicting cooling pond performance is an accurate knowledge of the heat fluxes through the water surface. These fluxes consist of the radiation penetrating the water surface from above, radiation out of the water surface, evaporation, and conduction transfer. These are indicated schematically in Figure 2-1.

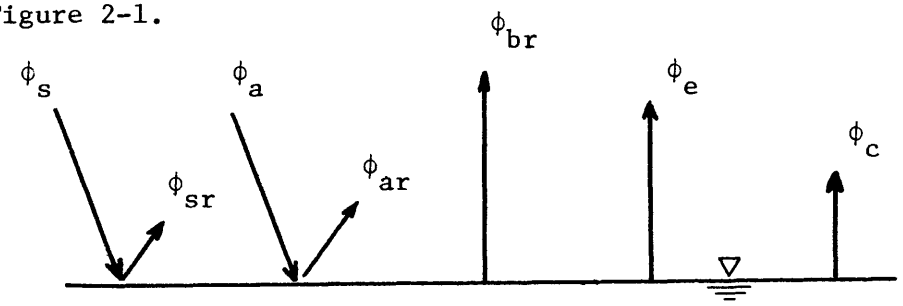

Figure 2-1 Heat Transfer Mechanisms at the Water Surface

in which (units - energy/area - time).

ϕ_s = incident solar radiation (short wave)

ϕ_{sr} = reflected solar radiation

ϕ_{sn} = net incident solar radiation = $\phi_s - \phi_{sr}$

ϕ_a = incident atmospheric radiation (long wave)

ϕ_{ar} = reflected atmospheric radiation

ϕ_{an} = net incident atmospheric radiation = $\phi_a - \phi_{ar}$

ϕ_{br} = long wave radiation from the water surface

ϕ_e = evaporative heat flux

ϕ_c = conduction (sensible) heat flux

Two surface heat fluxes which will not be considered are the fluxes due to the heat contained in the evaporated water, and in direct rainfall, since these are small in comparison with the other fluxes, and also tend to counteract each other.

Empirical methods for estimating the above components of heat transfer for a natural water surface are well established. However, for an artificially heated water surface, such as a cooling pond, the evaporation and conduction components are not well known. A new evaporation formula for an artificially heated water surface, applicable to both the laboratory and the field, will be developed in this chapter. All the other components will be briefly discussed. British units will be used throughout, with the exception of the units for pressure (mm. Hg.) and measurement height (meters). These mixed units are in common use in the electric power industry. The units of ft., days, British Thermal Units (BTU), degrees Fahrenheit (°F), and miles per hour (mph) for windspeed, will be used both in the laboratory and field studies.

2.2 Net Solar Radiation ϕ_{sn}

2.2.1 Incident Solar Radiation ϕ_s

The short wave radiation incident to the outside of the earth's atmosphere comes primarily from the sun. As this radiation passes through the earth's atmosphere it is absorbed by gases of the air, water vapor, clouds, and dust. As a result of these complex processes, the short wave radiation arrives at the earth's surface partly as direct radiation and partly as diffuse radiation. This short wave

radiation can be evaluated by two approaches:

a) direct measurement by suitable instrumentation;

b) indirect evaluation in terms of easily measureable quantities.

Anderson (1954) concluded from the Lake Hefner study that where accuracy greater than approximately 15% was required, direct measurement was essential. A typical instrument for measuring solar radiation is the Eppley pyrheliometer, which has a calibration error of approximately 2%.

When direct measurements of the solar radiation are not available, empirical formulae may be used to estimate the value. Details of these formulae are given in Wunderlich (1972). If daily average values are sufficient, as is usually the case, empirical curves by Hamon et.al. (1954) are very useful. These curves are based on data from 20 weather stations throughout the U.S., and give the daily average insolation as a function of latitude, day of year and percent of possible hours of sunshine. The authors claim that the use of percent of possible sunshine gives more reliable results than the use of cloud cover measurements. However, a reasonable approach would be to obtain the clear sky radiation and modify it as follows:

$$\phi_s = \phi_{sc} (1 - 0.65C^2) \qquad (2.1)$$

where

ϕ_{sc} = clear sky solar radiation obtained using the 100% possible sunshine curve

C = fraction of sky covered by clouds

Alternatively, Equation (2.1) can be used to calculate cloud cover from average daily solar radiation data. This process has been used in calculating evaporative heat losses for the Hazelwood pond (see Sec. 2.4.2.6), and a similar process was used by Brady et.al. (1969).

2.2.2 Reflected Solar Radiation ϕ_{sr}

The reflected radiation may be expressed as a fraction of the incident radiation by Anderson's empirical formula. However due to the lack of accuracy in estimating solar radiation, moderate errors in the reflected radiation (5-10% of the incident radiation) will not be significant. The following table, taken from the Lake Hefner study, (137), should be adequate, and these values are used in this study.

Month	Jan	Feb	Mar	Apr	May	June	July	Aug	Sept	Oct	Nov	Dec
ϕ_{sr}/ϕ_s(%)	9	7	7	6	6	6	6	6	7	7	9	10

Table 2-1

The net incident solar radiation, ϕ_{sn}, is therefore given as

$$\phi_{sn} = \phi_s - \phi_{sr} \simeq 0.94\ \phi_{sc}\ (1 - 0.65C^2) \qquad (2.2)$$

2.3 Longwave Radiation

2.3.1 Net Atmospheric Radiation ϕ_{an}

The thermal radiation from the earth's atmosphere is a very important component in the heat budget. In many cases it is second in

magnitude only to the longwave radiation from the water surface itself. Typical values are 2000-3000 BTU/ft^2/day, about 50% larger than the average solar radiation. Atmospheric radiation is primarily due to the water vapor, carbon dioxide and ozone components of the atmosphere. An approximate emittance spectrum for these three gases is shown in Fig. 2-2. Due to the sharp breaks between the various bands, an analytic description is not feasible, and empirical relations are used. The basic equation for the incident atmospheric radiation, ϕ_a, is given as

$$\phi_a = \varepsilon \sigma T_a^4 \qquad (2,3)$$

where

ε = average emittance of the atmosphere

σ = Stefan Boltzmann constant

T_a = air temperature (°R , °K) (absolute)

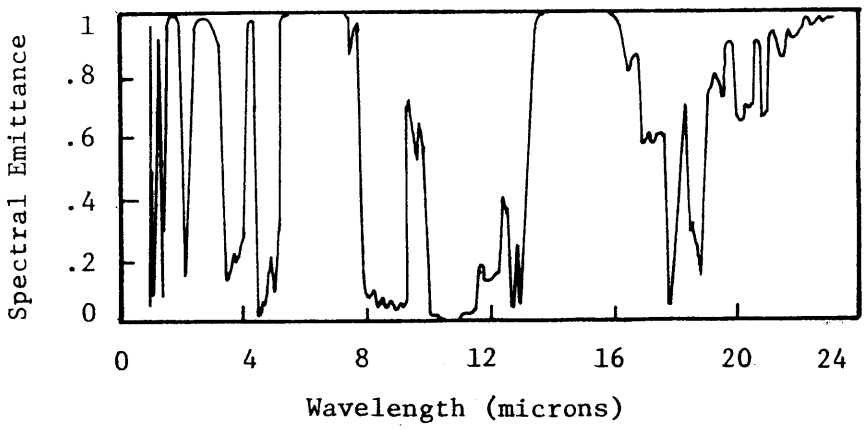

Figure 2-2 Emission Spectrum of Atmosphere at 32°F
Gates (1965)

From Fig. 2-2 it is seen that the emittance is actually a

marked function of wavelength. The average emittance ε is the ratio between the total atmospheric radiation and total blackbody radiation at the same temperature. The emittance varies from about 0.7 for low temperatures and clear skies, to almost unity for higher temperatures and heavy low overcast conditions. However, to assume $\varepsilon = 1$ is usually a serious error, and often involves an overestimation of the atmospheric radiation by ~ 600 BTU/ft^2/day. See Figure 2-3.

Most formulae for atmospheric radiation have been first developed for a clear sky and later modified for the effect of clouds. Some important clear sky formulae will now be considered.

2.3.1.1 Clear Sky Formulae

Two of the earliest and most widely used formulae are those of Brunt (1932) and Angstrom (1918). These assume that ε is a function only of the vapor pressure. Brunt's equation for atmospheric radiation from a clear sky, ϕ_{ac}, is

$$\phi_{ac} = \sigma T_a^4 (a + b\sqrt{e_a}) \qquad (2.4)$$

and Angstrom's

$$\phi_{ac} = \sigma T_a^4 (c - d \exp(- \gamma e_a)) \qquad (2.5)$$

where a, b, c, d, γ are empirical constants.

e_a = vapor pressure (measured at same height as air temperature)

Although good regressions are obtained for most localities, the five

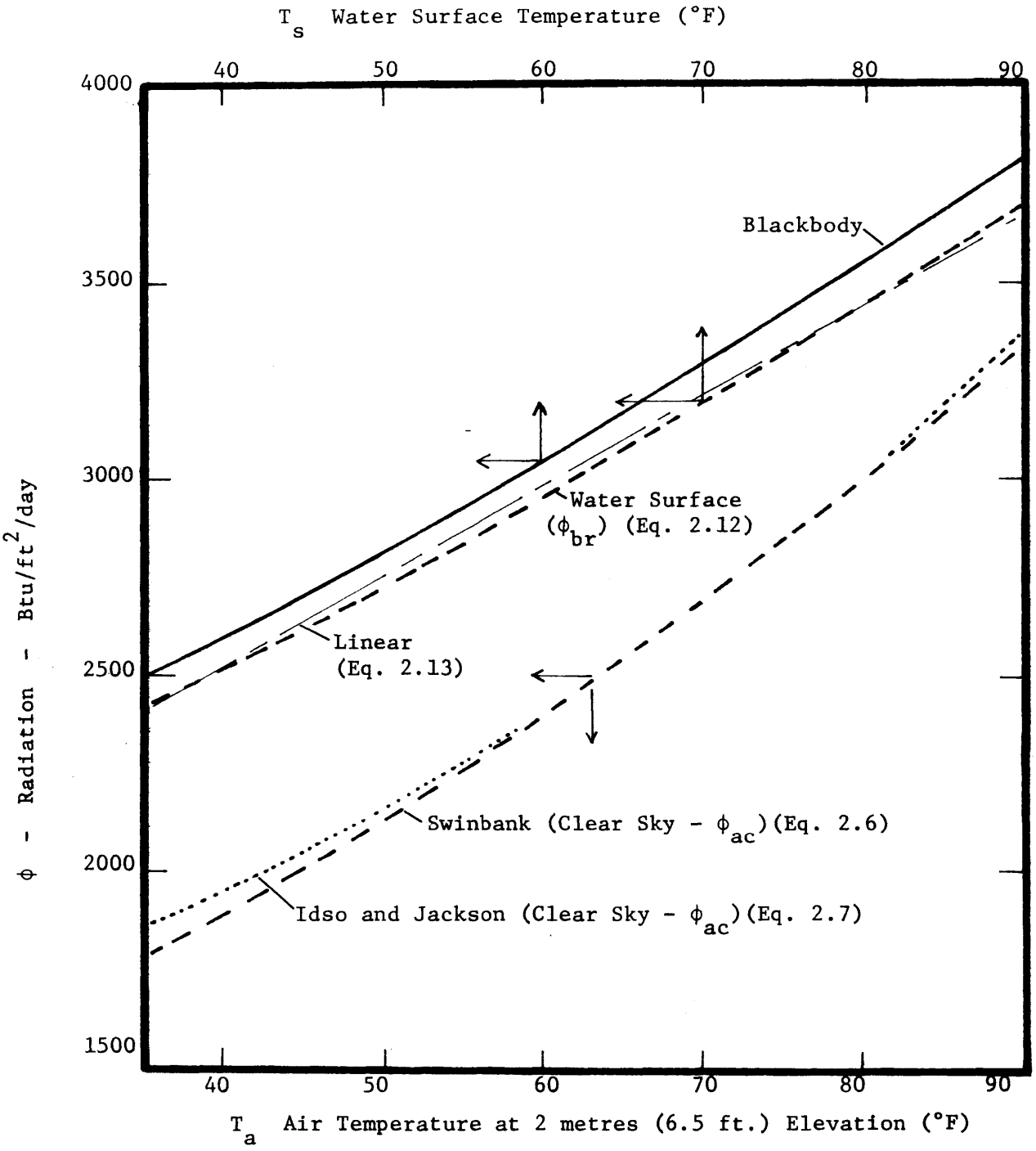

Figure 2-3 Longwave Radiation for Blackbody, Water Surface and Clear Sky

empirical constants tend to be somewhat variable. The above approach provides for no temperature dependence of ε, except through that inherent in e_a. Swinbank noted that this is only true for an atmosphere of constant grayness, which is far from the real case (see Fig. 2-2).

Swinbank (1963) and Idso and Jackson (1969) have proposed formulae in which ε is a function of T_a only. The theoretical justification for this has been provided by Gates (1965). He states that the monochromatic emission of radiation varies with a higher power of T_a than 4 for wavelengths shorter than the modal. Thus, the strong water vapor band at 6.3μ, below the nominal mode of 10μ for 300°K (80°F) blackbody radiation, causes the whole spectrum to radiate at an average power of T_a greater than 4. Idso and Jackson show that a T_a^6 dependence gives best results at low temperatures, as well as providing a good fit at high temperatures. Both formulae have been tested with good results against data from widely separated localities, including Alaska, Australia, Arizona, Tennessee, and the Indian Ocean.

Morgan, Pruitt and Laurence (1971) made a comparative study of the various atmospheric radiation formulae, taking the formulae against clear sky data taken at Davis, California. Best results were obtained using a Brunt-type formula, with coefficients fitted to the Davis data. The standard error was 75 BTU/ft^2/day. The standard error using the Swinbank formula was 96 BTU/ft^2/day. Wunderlich (1972) tested several formulae against data in Tennessee, and found that Swinbank's formula gave the most consistent results. Wunderlich recommends the Swinbank formula, noting that reasonable results are obtained without using

adjustable coefficients. Swinbank's formula has been used throughout this study since air temperatures were almost above 40°F. Below 40°F Idso and Jackson's formula is recommended.

Swinbank's formula is

$$\phi_{ac} = 1.2\ 10^{-13}\ (T_a + 460)^6 \qquad (2.6)$$

and Idso and Jackson's is

$$\phi_{ac} = 4.15\ 10^{-8}\ (T_a + 460)^4\ [1 - .261 \exp\ (-2.4\ 10^{-4}(T_a-32)^2)] \qquad (2.7)$$

where

T_a = air temperature at 2 meters (6.5 ft) in °F

ϕ_{ac} has units BTU/ft^2/day.

Figure 2-3 shows that above 50°F the above two formulae are almost identical.

2.3.1.2 Effect of Clouds

Clouds behave as near-black bodies and hence their effect is to increase the atmospheric radiation. Usually the effect of clouds is included by an adjustment formulae such as the one suggested by Bolz (Geiger 1965). The incident atmospheric radiation, ϕ_a, is given by

$$\phi_a = \phi_{ac}\ (1 + k\ C^2) \qquad (2.8)$$

where

ϕ_{ac} = atmospheric radiation for a clear sky

k = constant

C = cloudiness ratio

Values of k range from 0.04 for cirrus to 0.25 for nimbostratus or fog. Wunderlich (1972) suggests an average value of 0.17, and this value has been used in this study.

2.3.1.3 Reflection

A figure of three percent is usually accepted as reflectance of a water surface to longwave radiation. This figure is probably a little high (Buettner and Kern (1965)), but in view of the inaccuracies in estimating the atmospheric radiation itself, the error involved is of no significance. Thus the net atmospheric radiation is

$$\phi_{an} = 0.97 \ \phi_a . \qquad (2.9)$$

2.3.1.4 Conclusion

Anderson (1954) claims that formulae of the type of Brunt and Angstrom are limited to an accuracy of $\pm$ 10%. Swinbank claims a standard error of $\pm$ 3%. Morgan et.al. (1971) found a standard error of $\pm$ 4-5% for Swinbank's formula. It is concluded that Swinbank's formula (Eq. 2.6) provides a simple, reliable method of determining the atmospheric radiation within a probable error of $\pm$ 5%. The complete formula for net atmospheric radiation is (BTU/ft^2/day)

$$\phi_{an} = 1.16 \ 10^{-13} \ (460 + T_a)^6 \ (1 + 0.17 \ C^2) \qquad (2.10)$$

A useful linear approximation for average cloudy conditions (C = 0.5) is

$$\phi_{an} = 800 + 28 \ T_a \qquad (2.11)$$

2.3.2 Longwave Radiation from a Water Surface, ϕ_{br}

The longwave radiation from a water surface is usually the largest single item in the energy budget. It can be obtained fairly accurately since the emmissivity of a water surface is known within relatively precise limits. However, due to the formation of a thin (.003 ft)cool surface skin on many water surfaces, the actual surface temperature is usually known only to $\pm$ .5°F, at best. Anderson notes that the emmissivity of a water surface is independent of temperature and salt or colloidal concentrations, and gives a value of 0.97 $\pm$.005. Other investigators have found higher values, but the differences are not significant in view of inaccuracies in the water surface temperature T_s. Thus we have ϕ_{br} in units of BTU/ft^2/day,

$$\phi_{br} = 0.97\,\sigma(T_s + 460)^4 \qquad (2.12)$$

$$= 4.10^{-8}\,(T_s + 460)^4$$

where T_s = water surface temperature (°F)

Fig. 2.3 shows both the blackbody and water surface radiation curves.

A simple linearized form for back radiation from a water surface, within $\pm$ 30 BTU/ft^2/day of Equation 2-12 from 35 - 90°F is

$$\phi_{br} = 1600 + 23\,T_s. \qquad (2.13)$$

2.4 Evaporative Heat Flux, ϕ_e

Evaporation from a water surface occurs as a result of both

forced (wind driven) convection and free (buoyancy driven) convection. Above a natural water surface (i.e. no waste heat input) forced convection dominates. Above a heated water surface both forced and free convection may be important. The evaporation from a water surface is usually written (mass/area/time) as

$$E = \rho F(W_z) (e_s - e_z) \qquad (2.14)$$

where

E = mass flux (mass/area - time)

ρ = density of water

W_z = windspeed at height z

$F(W_z)$ = windspeed function for mass flux including both free and forced convection effects (length/time-pressure)

e_s = saturated vapor pressure at temperature of the water surface

e_z = vapor pressure at height z.

A large number of evaporation formulae exist for a natural water surface. It will be seen that the discrepancies between these formulae are not as large as is often suggested. Evaporation from an artificially heated water surface is often calculated using a formula developed for a natural water surface. It will be shown that this is quite inadequate, and a formula will be developed which explicitly considers the effect of free convection, and which gives consistently good results both in the laboratory and the field.

It is convenient to discuss evaporation in heat units

(BTU/ft^2/day). The latent heat of vaporization is usually given as follows for T_s in °F

$$L_v = 1087 - .54\ T_s \quad \text{(BTU/lb)} \tag{2.15}$$

For this chapter, however, L_v will be assumed constant (1060 BTU/lb.). Writing Equation (2.14) in heat units, the evaporative flux, ϕ_e, is given by

$$\phi_e = f(W_z)\ (e_s - e_z) \tag{2.16}$$

where

$f(W_z)$ = windspeed function for heat flux (energy/area-time-pressure)

2.4.1 Natural Water Surface

Evaporation from a free water surface has been the subject of a considerable amount of study since the beginning of this century. The results have been less than satisfactory, with a large number of formulae giving a wide variety of results. Initially there was considerable emphasis on developing formulae on a reasonably sound theoretical basis, using the analogy between momentum and mass transfer. With two exceptions (Sutton (1949) and Sverdrup (1937)) these formulae performed poorly during the Lake Hefner study, and it was found that a simple empirical formula of the form

$$f(W_z) = a + b\ W_z \tag{2.17}$$

where

a,b = constants

give slightly better results.

A serious obstacle to comparing different evaporation formulae is the fact that most of them are derived using differing measurement heights for W_z and e_z, from 0.02- 13 m. (.07-43 ft) above the water surface. In some cases no heights are given. Different lengths of observation times also complicate matters and confusion arises from the fact that some formulae are developed from evaporation pan measurements, and others directly from reservoir studies. For the same W_z, e_s, e_z, evaporation from a 3 ft. diameter pan is about 30 percent greater than reservoir evaporation. This discrepancy is apparently due to the effect of the pan rim on the wind structure and disappears when the pan diameter is 12 ft. or greater. Reducing all formulae to the same measurement levels (2 m. (6.5 ft) for both wind speed and vapor pressure), and taking into account the difference between reservoir and pan evaporation, the scatter between the commonly used formulae is considerably reduced, particularly in the range of windspeed 5-15 mph. See Figure 2-4. The formula with the best data base is the Lake Hefner formula given by Marciano and Harbeck (1954). This formula has also performed satisfactorily at Lake Mead(138), and at Lake Eucumbene in Australia (141). An almost identical formula, based on Russian lakes and reservoirs is given by Budyko et. al. (1955).

Writing the Lake Hefner formula in heat units we have (for windspeed in mph, e_s, e_z in mm. Hg)

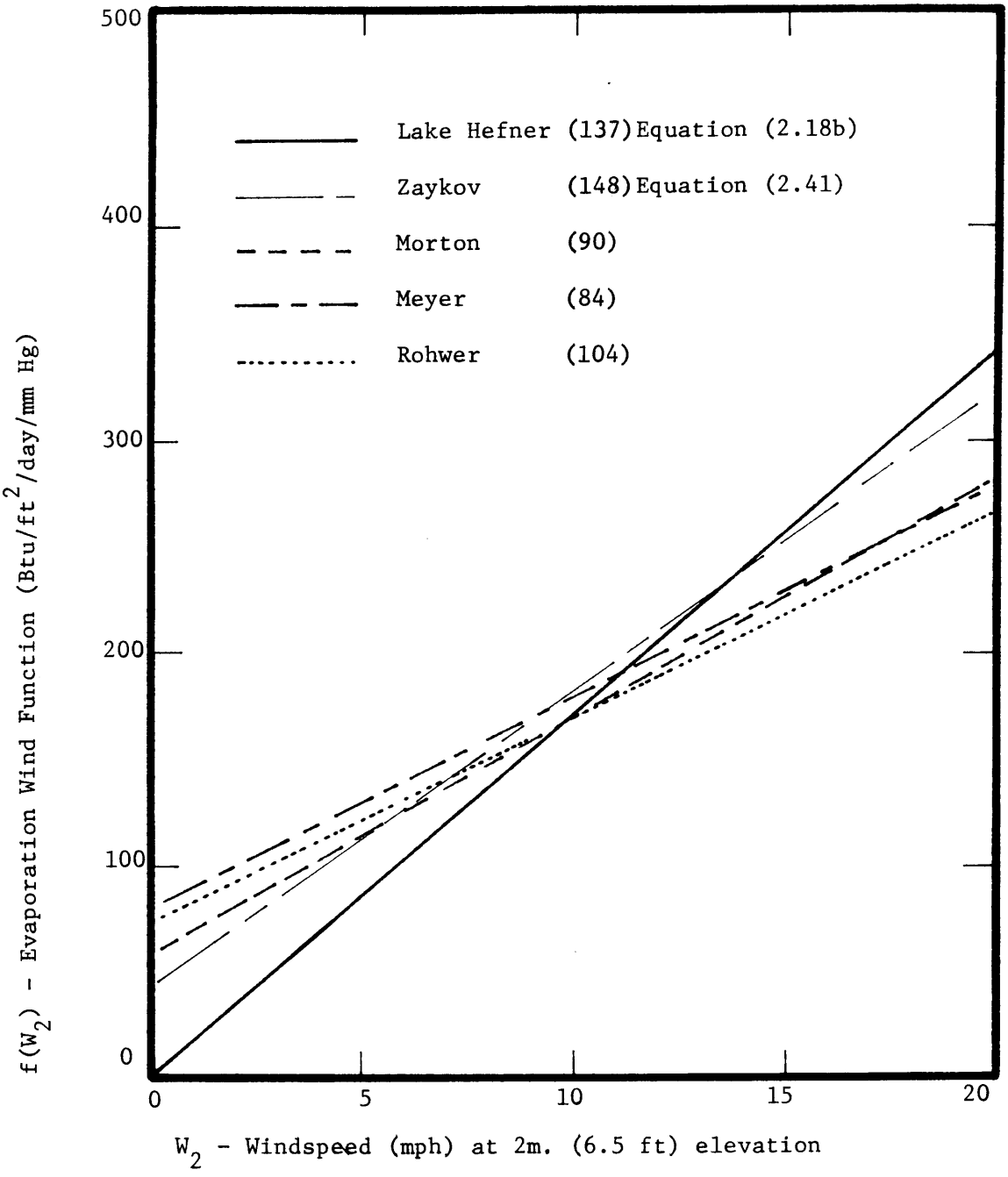

Figure 2-4 Windspeed Functions For a Natural Water Surface

$$\phi_e = 17W_2(e_s - e_2) \qquad (2.18a)$$

or

$$f(W_2) = 17W_2 \qquad (2.18b)$$

The other formulae are based on pan measurements and then modified to apply to reservoirs. The non-zero value of the constant a in Equation (2.17) is probably due to the fact that small local air movements, with velocities less than the anemometer sensitivity, are sufficient to remove excess vapor from above a pan surface. This may not be the case for a large body of water. The air motion may be the result of very light winds or temperature differences between the pan and the surrounding locality.

Table 2-2 shows the basis for commonly used evaporation formulae.

It should be noted that the Lake Hefner formula only performed well at Lake Mead when 2 meter (6.5 ft) wind speeds and vapor pressures were used. The use of 8 meter (26 ft) wind speeds and vapor pressures gave a similar yearly evaporation, but somewhat inconsistent monthly results. For 8 meter values, the stability of the air blanket above the lake appeared to affect the coefficients. Since merely changing measurement height at the same location introduces problems, the validity of using wind speeds and vapor pressures from a different location (e.g. as in the design of a cooling pond) is open to serious questioning.

Table 2-2

EVAPORATION FORMULAE FOR LAKES AND RESERVOIRS

Name	Formula in Original Form	Units	Observation Levels	Time Increments	Water Body	Formula at sea-level, Meas.Ht.Spec.units BTU/ft^2/day mph, mm Hq	Remarks
Lake Hefner	$E=6.25.10^{-4} W_8(e_s-e_8)$	cm/3 hr. knots mb	8m-wind 8m-e_a	3 hrs Day	Lake Hefner Okla. 2587 acres	$12.4W_8(e_s-e_8)$ $17.2W_2(e_s-e_2)$	Good agreement with Lake Mead (138), Lake Eucumbene, Russian Lakes
Kohler	$E=.00304 W_4(e_s-e_2)$	in./day miles/day in. Hg.	4m-wind 2m-e_a	Day	Lake Hefner Okla. 2587 acres	$15.9W_4(e_s-e_2)$ $17.5W_2(e_s-e_2)$	Essentially the same as the Lake Hefner Formula.
Zaykov	$E=[.15+.10\&W_2] (e_s-e_2)$	mm/day m/s mb	2m-wind 2m-e_a		Ponds and Small Reservoirs	$(43+14W_2)(e_s-e_2)$	Based on Russian experience. Recommended by Shulyakovskiy
Meyer	$E=10(1+.1W_8) (e_s-e_8)$	in/month mph in. Hg.	25ft-wind 25ft-e_a	Monthly	Small Lakes and Reservoirs	$(73+7.3W_3)(e_s-e_8)$ $(80+10W_2)(e_s-e_2)$	e_a is obtained daily from mean morning and evening measurements of T_a, R_H. Increase constants by 10% if av. of max. and min. used.
Morton	$E=(300+50W)(e_s-e_a)/p$	in/month mph	8m-wind 2m-e_a	Monthly	Class A pan	$(73.5+12.2W_8)(e_s-e_2)$ $(73.5+14.7W_2)(e_s-e_2)$	Data from meteorological Stations. Measurement Heights assumed.
Rohwer	$E=.771[1.465-.0186B] [.44+.118W] [e_s-e_a]$ where B=atmos.press	in/day mph in. Hg.	0.5-1ft-wind 1 inch-e_a	Daily	Pans 85 ft.diam. tank 1300 acre reservoir	$(67+10W_2)(e_s-e_2)$	Extensive pan measurements using several types of pans. Correlated with tank and reservoir data.

2.4.2 Artificially Heated Water Surface

Above an artificially heated water surface free convection may be the dominant process (e.g. in the laboratory) or both forced and free convection may be important (e.g. in the field). The constant a in the formula $f(W_z) = a + b\ W_z$ may now become very significant. In this section a will first be determined by looking at heat and mass transfer for the case when only free convection applies ($W_z = 0$). Later the problem of combined free and forced convection will be considered.

2.4.2.1 Free Convection

Mass transfer by convection is usually treated by analogy with heat transfer. This analogy involves the assumption that the eddy diffusivities of heat (K_h) and mass (K_m) are identical. There has been considerable controversy about the validity of this assumption for the unstable conditions which characterize free convection. Pasquill (1949) reports that (K_h/K_m) may reach 2 under unstable conditions. Anderson (1954) reports that work by Sutton (1948) and Priestley and Swinbank (1947) supports Pasquill's conclusions. However, more recent work by Rider (1954), Pruitt and Aston (1963), Crawford (1965) and Dyer (1967) all support the theory that K_h/K_m is approximately unity throughout the neutral and unstable range. The situation has been summed up by Monin and Yaglom (1971) who note that all existing data on humidity profiles are in agreement with the above assumption, although at present no rigorous proof exists. They say, therefore, that there is no reason to reject the assumption, but that further verification is necessary.

2.4.2.2 Flat Plate Analogy

A considerable amount of work has been done on free convective heat transfer above a flat plate. From dimensional analysis it can be shown that the heat transfer coefficient (characterized by the Nusselt No.) is a function only of the Grashof (Gr) and Prandtl (Pr) Nos.. For a warm, flat plate, side length L, temperature difference with its surroundings $\Delta\theta$, Fishenden and Saunders give the following empirical expressions:

Laminar Range $10^5 < (Gr.Pr) < 10^8$

$$Nu = 0.54\ (Gr.Pr)^{1/4} \qquad (2.19a)$$

Turbulent Range $(Gr.Pr) > 5 \times 10^8$

$$Nu = 0.14\ (Gr.Pr)^{1/3} \qquad (2.19b)$$

where

$$Nu = \frac{\text{Actual Heat Transfer Rate}}{\text{Heat Transfer Rate into Still Air}} = \frac{H_c L}{k(\Delta\theta)}$$

$$Gr = \frac{\text{Buoyancy Force}}{\text{Viscous Force}} = \frac{\beta' g \Delta\theta L^3}{\nu^2}$$

$$Pr = \frac{\text{Kinematic Viscosity}}{\text{Molecular Diffusivity}} = \frac{\nu}{\alpha}$$

H_c = heat transfer rate

L = characteristic dimension of plate

$\Delta\theta$ = temperature difference between the plate surface, T_s, and the background air, T_a

β' = expansion coefficient for gas

ERRATA

g = acceleration due to gravity

ν = kinematic viscosity of gas

α = molecular thermal diffusivity of gas

In air, at standard pressure and temperature, Equations (2.19a) and (2.19b) can be written in terms of a heat transfer coefficient, h_c.

Laminar Range

$$h_c = \frac{H_c}{\Delta\theta} = 6.5 \left(\frac{\Delta\theta}{L}\right)^{1/4} \quad (BTU/ft^2/day/°F) \qquad (2.20)$$

Turbulent Range

$$h_c = \frac{H_c}{\Delta\theta} = 6.0 \ (\Delta\theta)^{1/3} \quad (BTU/ft^2/day/°F) \qquad (2.21)$$

for

ρ_a = density of air = .076 lb_m/ft^3

c_p = specific heat of air at constant pressure
= .24 $BTU/lb_m/°F$

Also, the Grashof-Prandtl No. is approximately given by (units of ft., °F)

$$Gr.Pr = 2 \times 10^6 \ (L^3 \Delta\theta) \qquad (2.22)$$

Assuming a characteristic $\Delta\theta$ of 10°F, a length scale greater than 2 ft. is needed to ensure turbulent free convection ($Gr.Pr > 10^8$-10^9). Thus in the field it is obvious that free convection is turbulent. However, in the laboratory some investigators, notably Hickox (1946) have operated in the laminar range.

2.4.2.3 Mass and Heat Transfer by Free Convection

Mass flux of water vapor can be written as

$$E = K_m \frac{\partial \rho_v}{\partial z} \simeq K_m \frac{\Delta \rho_v}{\Delta z} \tag{2.23}$$

where

E = mass flux ($ML^{-2}T^{-1}$)

ρ_v = vapor density

Δz = characteristic vertical ordinate

Using the assumption K_h/K_m equal to unity, and the standard gas formulae

$$\rho_v = .622 \frac{e}{RT} \tag{2.24}$$

$$p = \rho_a RT \tag{2.25}$$

where

e = vapor pressure

R = gas constant for dry air

T = absolute temperature of air

p = total air pressure

and noting that

$$H_c = h_c \Delta\theta = \frac{K_h}{\rho_a c_p} \frac{\Delta\theta}{\Delta z} \quad \text{SEE ERRATA} \tag{2.26}$$

we obtain

$$E = \frac{h_c}{\rho_a c_p} \Delta \rho_v$$

$$= \frac{.622}{c_p p} h_c \Delta e \tag{2.27}$$

For turbulent convection, we can substitute Equation (2.21) in Equation (2.27) to obtain

$$\phi_e = .622 \frac{L_v}{c_p p} 6.0(\Delta\theta)^{1/3} (e_s - e_z) \qquad (2.28)$$

For standard conditions we obtain

$$\phi_e = 22.4 (\Delta\theta)^{1/3} (e_s - e_z) \qquad (2.29)$$

In moving from Equation (2.23) to Equation (2.29) it has been assumed that the vertical distance Δz is the same for Δe as for $\Delta\theta$. In a laboratory where the air temperature and vapor pressure reach background values a short distance (<1 ft) from the heated surface, and thus Δe and $\Delta\theta$ are essentially independent of Δz, this assumption is valid. For the field case, the constant may be a function of the measurement height.

Since water vapor is lighter than air, evaporation actually increases the buoyancy forces. This effect is included by substituting a virtual temperature difference ($\Delta\theta_v$) for $\Delta\theta$. $\Delta\theta$ and $\Delta\theta_v$ are now defined as follows:

$$\Delta\theta = T_s - T_a \quad (°F) \qquad (2.30a)$$

where

T_s = bulk water surface temperature (°F)

T_a = dry bulb air temperature at a height of 2 meters (6.5 ft) above the water surface

$$\Delta\theta_v = T_{s_v} - T_{a_v} \qquad (2.30b)$$

where

T_{s_v} = virtual temperature of a thin vapor layer in contact with the water surface

T_{a_v} = virtual air temperature

The virtual temperature of moist air is defined as the temperature of dry air with the same density, and T_{s_v} and T_{a_v} are given by

$$T_{s_v} = (T_s + 460)/(1 - .378\ e_s/p) \quad (°R) \tag{2.31a}$$

$$T_{a_v} = (T_a + 460)/(1 - .378\ e_a/p) \quad (°R) \tag{2.31b}$$

where

e_s = saturated vapor pressure at temperature T_s

e_a = water vapor pressure in the atmosphere at 2 meters (6.5 ft) above the water surface

p = atmospheric pressure

Thus, for the case of a heated water surface in still air we have

$$\phi_e = 22.4\ (\Delta\theta_v)^{1/3}\ (e_s - e_a) \tag{2.32}$$

or

$$f(W_z) = a = 22.4\ (\Delta\theta_v)^{1/3} \tag{2.33}$$

The basic idea of using the analogy between heat and mass transfer to compute evaporation into still air was presented by Hickox (1946). Wunderlich (1972) and Shulyakovsky (1969) both use the flat plate data

to obtain the numerical coefficients. Equation 2.32 will be tested for the turbulent range of free convection in both the laboratory and the field.

2.4.2.4 Laboratory Evaporation ($W_z = 0$)

Estimation of evaporation in the laboratory is necessary in evaluating the performance of thermal models. In this study the performance of the laboratory pond is of the utmost importance, and an accurate determination of surface heat loss is essential. Experimental work on laboratory evaporation has been done by Rohwer (1931), Hickox (1946), and Markofsky (1968). A short description of existing experimental work follows:

a) Rohwer (1931) did careful measurements of evaporative losses from a laboratory tank, 3 ft. square and found the mass transfer rate to be proportional to $(\Delta\theta)^{2/3}$. However, the high exponent is probably due to the fact that the air temperature was measured only one inch from the water surface.

b) Hickox (1946) used a tank only 1 ft. in diameter and found the exponent to be 0.25. His experiments were in the laminar free convection range, and thus the experiments are in agreement with the predictions from flat plate theory (see Equation 2.19a)

c) Markofsky (1968) carried out two series of experiments in a 40 ft. long lucite flume. In the first series heating took place using a warm water inflow. Evapora-

tion was determined by the energy balance approach. In the second series the water was heated from above by quartz-iodine lamps, and evaporation determined by direct measurement. The wind function $f(W_z) = \underline{a}$ was determined for each case.

For the warm water inflow $\underline{a}$ = 157 BTU/ft^2/day/mm Hg

For surface heating $\underline{a}$ = 63 BTU/ft^2/day/mm Hg

d) For this study a series of heat loss experiments were carried out, using a 3.5 ft. square insulated tank, and a 40 ft. x 22 ft. x 1.25 ft. laboratory basin. Details of the experiments are given in Chapter 7. For the small tank the Gr.Pr. No. usually exceeded 5 x 10^8, and for the large basin Gr.Pr. > 10^{10}, so turbulent free convection was always present. Evaporation losses were obtained using an energy budget approach. Sensible heat losses were obtained using the Bowen ratio approach (see Sec. 2.5). Note, however, that the basic assumption in the Bowen ratio approach is that K_h/K_m is unity, and therefore, use of the Bowen ratio does not involve any extra assumptions.

The results for the small insulated tank are shown in Figures 2-5 to 2-7. Figure 2-5 shows that using the actual temperature difference between the air and the water surface ($\Delta\theta = T_s - T_a$) instead of

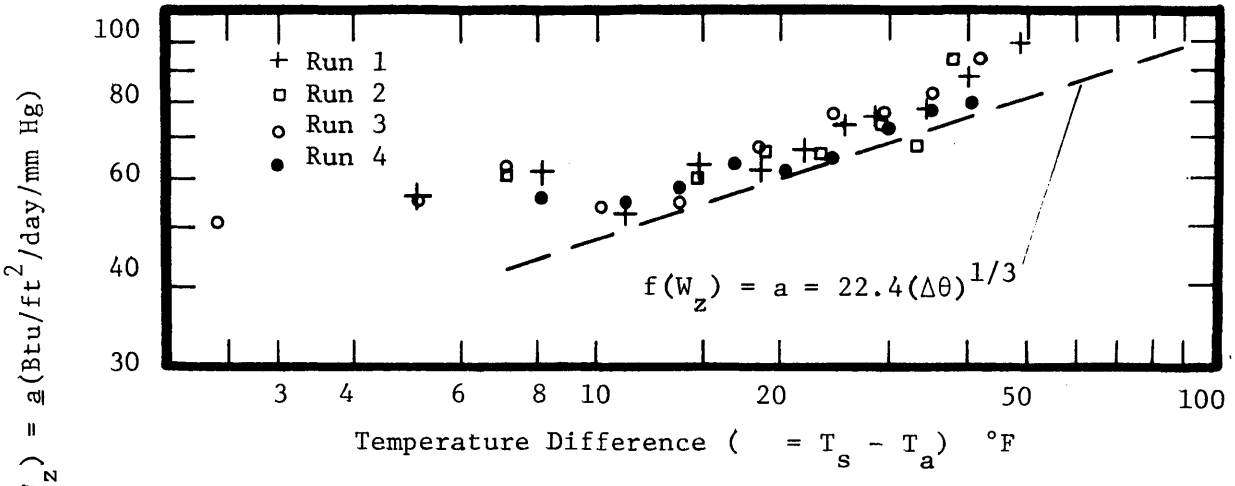

Figure 2-5 Windspeed Function $f(W_z)$ vs Temperature Difference ($\Delta\theta$) for 3.5' x 3.5' Tank

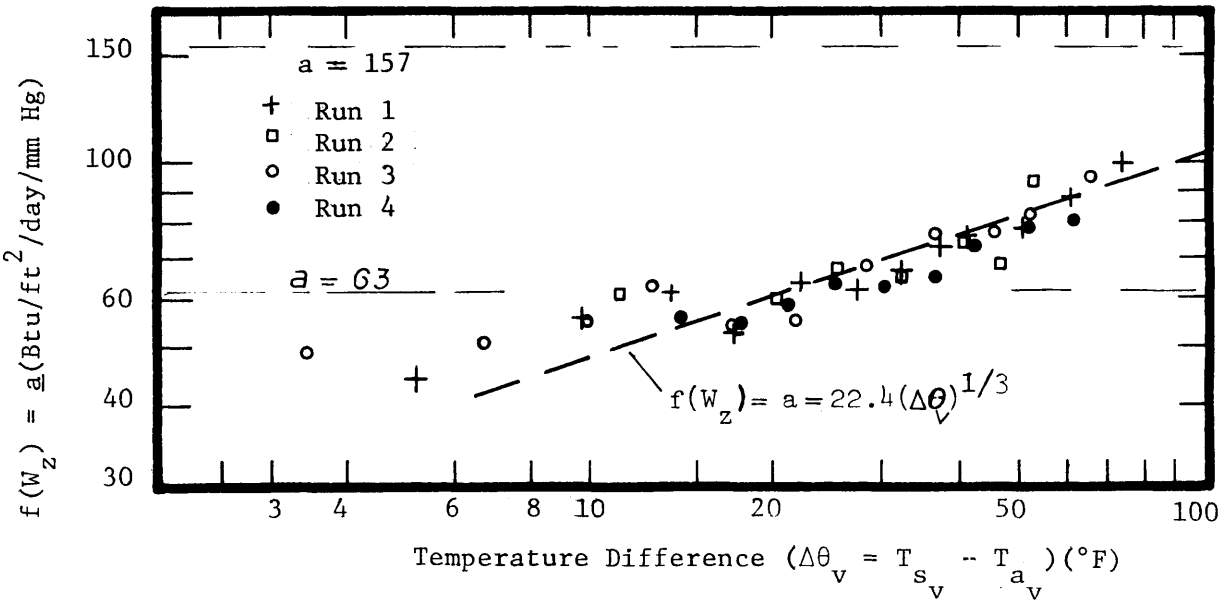

Figure 2-6 Windspeed Function $f(W_z)$ vs Virtual Temperature Difference ($\Delta\theta_v$) for 3.5' x 3.5' Tank

the virtual temperature difference, ($\Delta\theta_v = T_{s_v} - T_{a_v}$), leads to an underestimation of the evaporation. Figure 2-6 shows that Markofsky's experimental constant for the surface heating case (63 BTU/ft^2/day/mm Hg) is quite realistic for $\Delta\theta_v$ in the range 10-30°F. However, his constant for the warm water inflow case appears to be far too high. Figure 2-6 also demonstrates that for $\Delta\theta_v > 15°F$ (Gr.Pr. $> 10^9$), the evaporation coefficient is not a constant, but increases as $(\Delta\theta_v)^{1/3}$. The empirical constant, 22.4, obtained from flat plate theory, appears to be quite satisfactory. Figure 2-7 compares predicted and measured net heat flux, ϕ_n, using Equation 2.32 to predict the evaporative component (see Equation 2.52). The agreement is excellent over the whole range due to the fact that when Equation 2.32 is not valid, the evaporation is a less significant part of the total heat loss.

Figures 2-8 and 2-9 show similar results for the 40' x 20' basin. Here it is also apparent that the evaporation coefficient increases with increasing $\Delta\theta_v$, although the exponent of the line of best fit is closer to 2/3, than 1/3 as predicted. Nevertheless, Figure 2-9 shows that Equation 2.32 leads to quite reasonable predictions of total heat loss.

The relatively large scatter in the results for the basin is partly due to heat transfer and heat storage in the concrete floor. This effect was minimized by allowing the floor to reach equilibrium (a period of 24 to 48 hours) before starting the experiment. The heat loss through the floor was monitored throughout the run and corrections made where necessary, but errors of $\pm$ 5 BTU/ft^2/hr were probably still present.

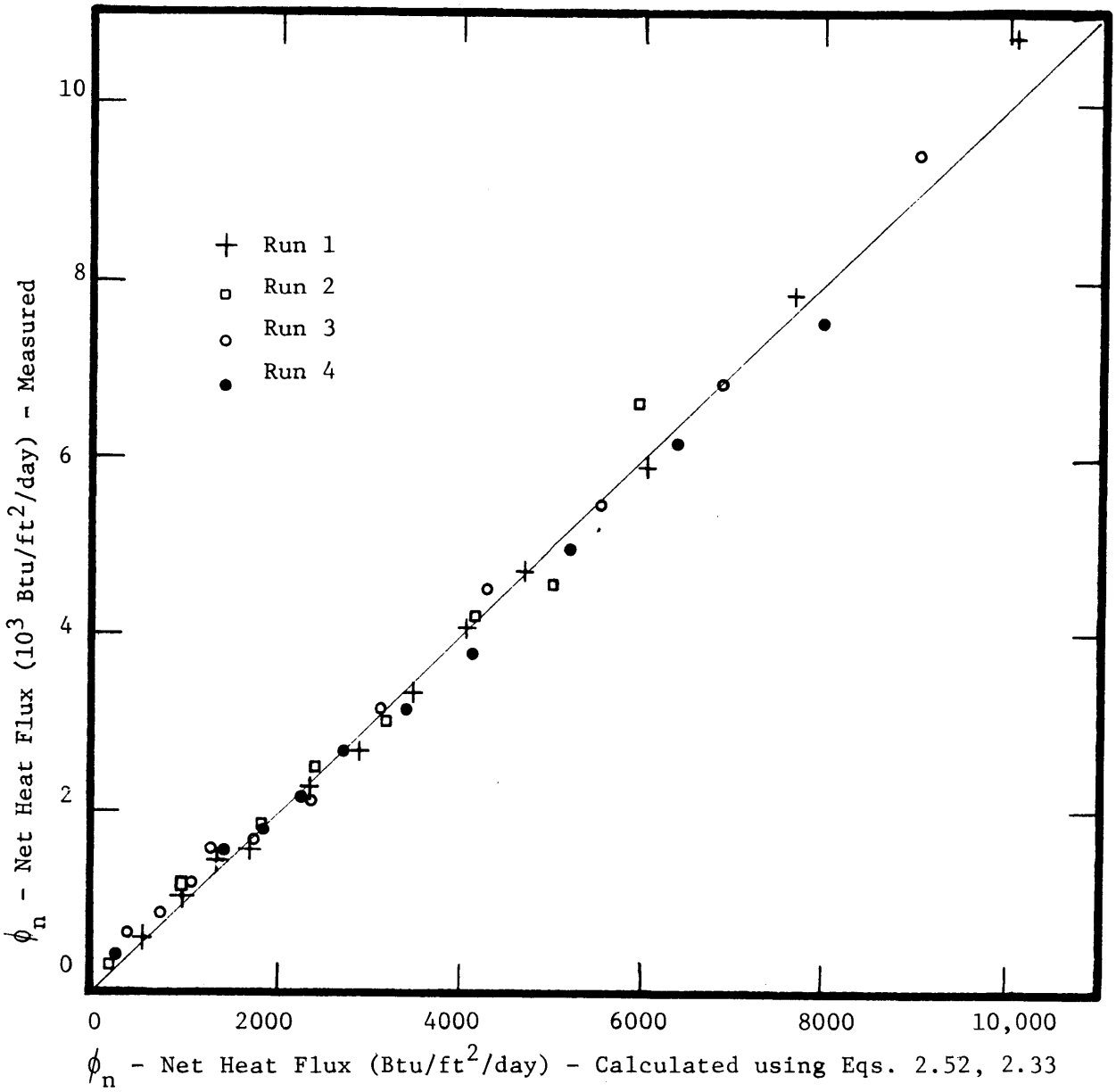

Figure 2-7 Net Heat Flux in 3.5' x 3.5' Tank

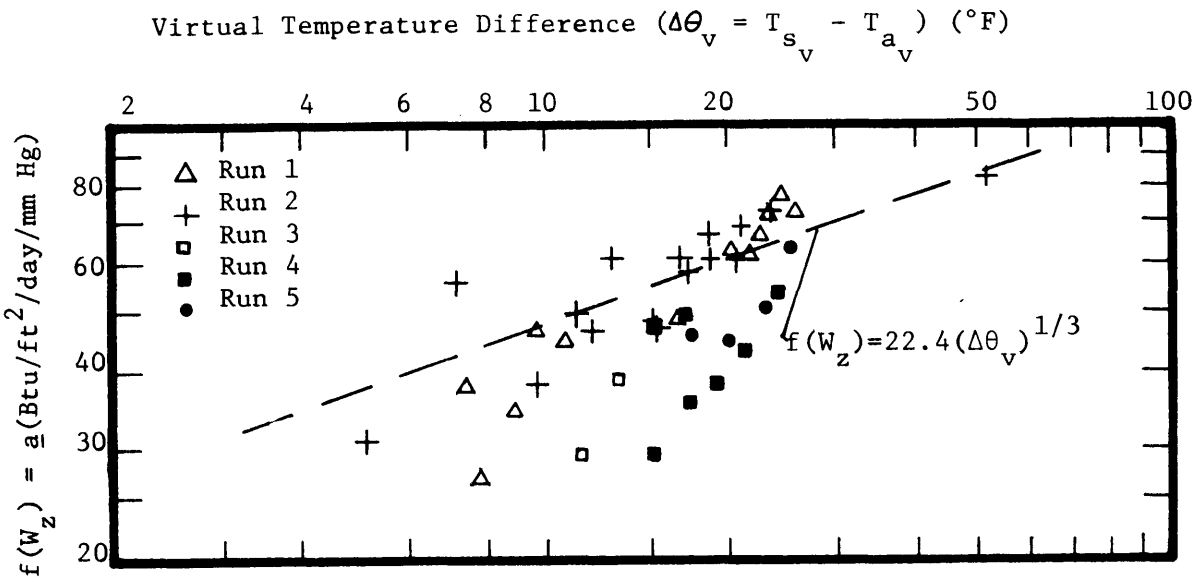

Figure 2-8 Windspeed Function for 20' x 40' Basin

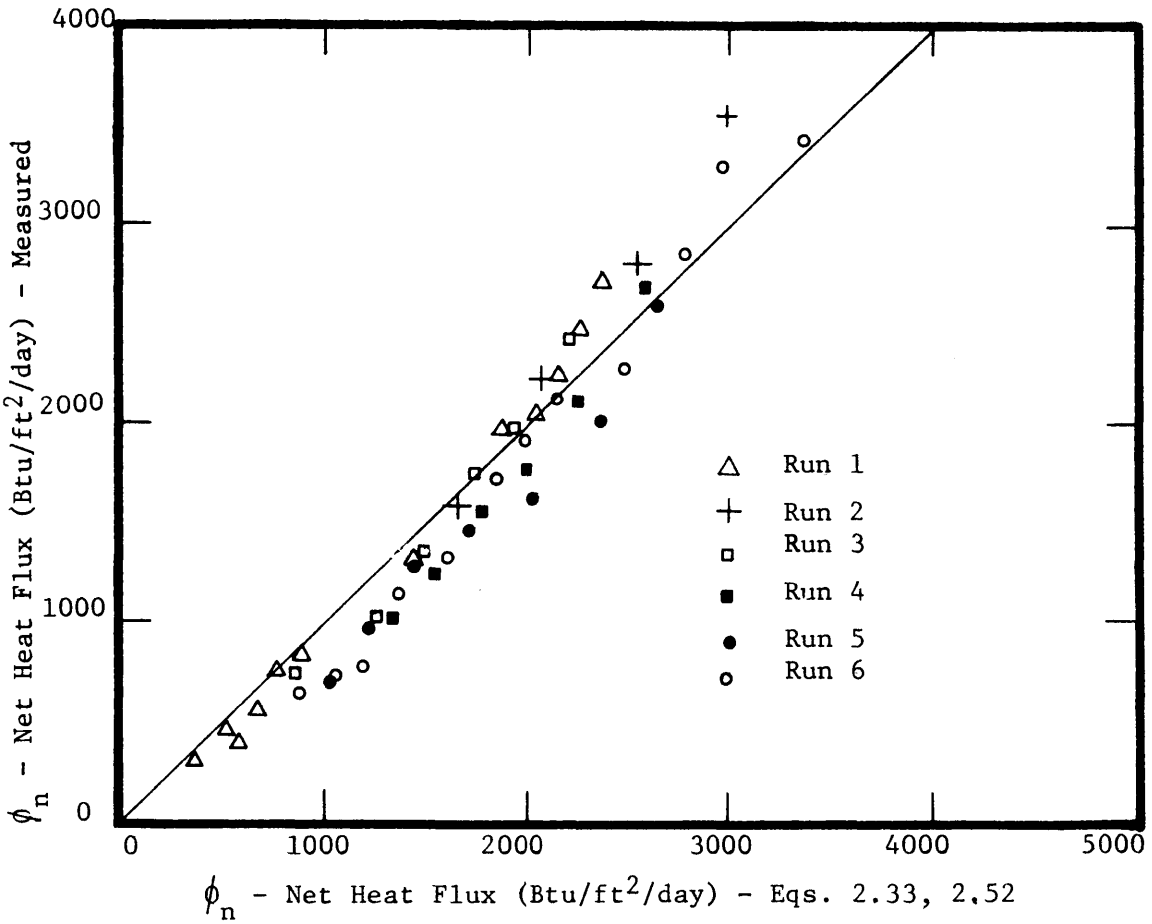

Figure 2-9 Net Heat Flux in 20' x 40' Basin

In conclusion it appears that Equation 2.32 is valid for evaporation from a heated water surface in the laboratory (with $W_z = 0$) as long as the Gr.Pr. No. $>10^9$. The difference in behavior of the small tank and the large basin at $\Delta\theta_v < 15$ ($\Delta\theta < 10$) is very striking, and leads to the tentative conclusion that small tanks may not be very suitable for measuring heat transfer at temperatures near equilibrium, and thus the practice of using small insulated tanks, equipped with heating coils, to determine K for thermal models, could give misleading results.

2.4.2.5 Combined Forced and Free Convection

Evaporation from a prototype cooling pond involves both forced and free convection. The first problem is to determine whether free convection is significant in the presence of forced convection. Unfortunately, there is no flat plate experimental data, similar to that obtained by Fishenden and Saunders (1950) for the case of free convection only. Theoretical solutions are limited to the laminar range ($Re_x < 10^6$). In this range it has been shown that effects of buoyancy on forced convective heat transfer are less than 5-10% if

$$\left|Gr_x\right| < .08(Re_x)^{2.5} \qquad (2.34)$$

where the length scale, x, in both dimensionless numbers is the distance from the upstream edge of the plate (88,114). This result is of no interest in the field, but does explain why Rohwer (1931) and Yen and Landvatter (1970) found evaporation in the presence of forced convection to be independent of buoyancy effects, since nearly all their experimental results satisfy the inequality in Equation 2.34. Thus at

this stage one cannot say a priori that free convection is or is not significant in the presence of forced convection. The only solution, therefore, is to look at a wide range of field data on artificially heated water surfaces, and to determine if a formula which explicitly accounts for free convection performs better than those formulae which ignore free convection, or assume it to be independent of the buoyancy forces which depend on $\Delta\theta_v$.

It was found that none of the existing formulae gave consistent results, and several new formulations were tested against field data. The basis for the proposed formulae is the assumption that the wind function could be represented by Equation 2.17 which gives

$$f(W_z) = a + b\ W_z \qquad (2.17)$$

The constant a is now replaced by the explicit free convective term $22.4(\Delta\theta_v)^{1/3}$. It is assumed that b remains a constant, similar to the value for a natural water surface. From Table 2-2 it is seen that for a windspeed measurement height of 2m. (6.5 ft) the value of b ranges from 10-17 BTU/ft^2-day-mm Hg-mph. Three values of b in Eq. 2.17 were tested, with b = 10, 14 and 17 BTU/ft^2-day-mm Hg-mph. The best results were obtained with b equal to 14, and the resulting formula is called the "proposed formula. For b equal to 17 the resulting formula essentially consists of the Lake Hefner formula with the addition of the free convective term, and is called the Modified Lake Hefner formula. This formula tended to predict too high an evaporative rate. For b equal to 10, the resulting formula predicted about the same evaporation as

the Rohwer or Meyer natural surface formulae, and hence is not of particular interest. The significant new formulae are as follows:

Proposed Formula

$$f(W_2) = 22.4\ (\Delta\theta_v)^{1/3} + 14\ W_2 \qquad (2.35)$$

Modified Lake Hefner Formula

$$f(W_2) = 22.4\ (\Delta\theta_v)^{1/3} + 17\ W_2 \qquad (2.36)$$

A brief historical background to the existing formulae for evaporation from a heated surface will now be given, the data against which all formulae are tested will be described, and the performance of the various formulae will be discussed.

2.4.2.6 Field Performance of Heated Water Surface Formulae

Evaporation from an artificially heated water surface has received relatively little attention in comparison with that from a natural water surface. Work on cooling ponds has been done by Throne (1951), Harbeck (1959) and Brady (1969). None of these explicitly considered the problem of free convection. Formulae including free convection effects have been proposed by Rimsha and Donchencko (1957), Shulyakovskiy (1969) and other Russian workers (13,14). A brief survey of significant work follows.

Throne (1951) used Rohwer's formula to analyze 25 years of data from a small (120-210 acres), but heavily loaded cooling pond (the maximum loading was equivalent to 1 MW_e (nuclear)/acre). Perhaps unwittingly

Throne used a windspeed elevation of 5 ft. instead of the 0.5-1 ft. elevation used by Rohwer. The effect was to increase evaporation by 10-30%. The modified Rohwer formula was used by Throne with considerable success enabling him to predict the mean monthly intake temperatures within ±3°F for over 88% of the 208 months of record. Throne's formula, modified for sea-level altitude, and for 2m. (6.5 ft) windspeed elevation is

$$f(W_2) = 67 + 17\ W_2 \qquad (2.37)$$

Note that Rohwer's windspeed coefficient of 10 BTU/ft^2/day/mm Hg/mph has been increased by 70% (see Table 202). SEE ERRATA The above formula appears to work well for heavily loaded surfaces, and gave excellent results when used by Garrison and Elder (1965) to predict temperature decay downstream from a power station on the Susquehanna River ($\Delta\theta$ from 15 - 25°F).

Harbeck (1959) carried out an energy budget study of Lake Colorado City. Unfortunately, the waste heat loading on the lake was very low (<0.1 MW_e/acre) and thus the data is not of great interest for cooling pond behavior. Harbeck's formula, is

$$f(W_2) = 25\ W_2 \qquad (2.38)$$

The form of Equation 2.38, with zero evaporation loss at zero windspeed, is not in accord with most recent data.

Brady (1969) analyzed three cooling ponds using an energy budget appraoch, and proposed a formula which stressed the importance of evaporative losses at low windspeeds. The data base for the formula

is fairly good. Four hourly records of meteorological and plant operating parameters were taken for an average of one year for each of three cooling ponds in the Texas-Louisiana area. The ponds had surface areas of 605, 650 and 2500 acres and heat loads of 0.4, 0.2 and 0.3 MW_e (nuclear)/acre, i.e. relatively low loading. A minimum of five (5) surface temperatures were taken in any one pond. Due to difficulties in determining changes in heat stored within the pond for short periods, it was found necessary to use periods of one week rather than four hours as originally intended. Two shortcomings are apparent in the analysis of the data. The calculated atmospheric radiation, ϕ_{an}, was 100-200 $BTU/ft^2/day$ higher than that obtained by the formulae recommended in Section 2.3 (Eq. 2.10). The wind speed measurements were obtained at three different heights, 5 ft., 18 ft., and 22 ft. The 5 ft. windspeed was obtained by a rather tenuous correlation with a 39 ft. windspeed at a location 2 miles from the pond. No attempt was made to reduce all these windspeeds to a common height (e.g. 6.5 ft. or 2 meters). Brady's formula is

$$f(W_z) = 70 + .7\ W_z^2 \qquad (2.39a)$$

where the measurement height z is unspecified. This formula is now used fairly extensively, although its performance with other cooling pond data leads to the conclusion that the predicted heat loss by evaporation is somewhat low. Assuming that Brady's formula uses the 8 meter windspeed, we have for 2 meters (6.5 ft)

$$f(W_2) = (70 + W_2^2) \qquad (2.39b)$$

Rimsha and Donchencko (1957) carried out a study of heat loss from ice free reaches in wintertime, and developed an equation which specifically includes a free convection term. The equation is

$$f(W_2) = 61 + 1.47\ (\Delta\theta) + 13.3\ W_2 \qquad (2.40)$$

This equation gave good results in a study of heat dissipation in rivers in wintertime by Weeks, et.al. (1971).

Shulyakovskiy (1969) developed his formula by assuming that mass transfer due to free convection is independent of the mass transfer due to forced convection. The formula of Zaykov (1949) was used to predict the forced convection component. This formula was developed for small natural lakes and ponds, and is shown in Figure 2-4. Zaykov's formula is

$$f(W_2) = 43 + 14\ W_2 \qquad (2.41)$$

The free convection component was obtained by using the flat plate analogy and is given by Equation 2.33. An attempt was made to include the effect of the cool surface skin on evaporation, and skin temperatures (see ref.(109)) rather than bulk surface temperatures were used. Shulyakovskiy's formula, modified to include bulk surface temperatures, rather than the impractical skin surface temperatures, is

$$f(W_2) = 22.4\ (\Delta\theta_v)^{1/3} + 43 + 14\ W_2 \qquad (2.42)$$

This formula gave good results on a 16 ft. diameter evaporation pan, but was not tested for high values of $\Delta\theta_v$. Note that the formula

is the same as the proposed formula (Equation 2.35), with the addition of the constant a (43 BTU/ft^2-day-mm Hg) from Zaykov's formula. Since this term probably represents free convective transfer during periods when $\Delta\theta_v$ is positive, it is felt that it is redundant when free convection is explicitly included. This hypothesis is supported by the fact that Shulyakovskiy's formula gave consistently high results.

All the above formulae were tested against the following data.

a) The data from the three cooling ponds on which Brady based his formula and design charts. Evaporation losses were obtained from Table 6.1 in reference (12), by multiplying Brady's tabulated wind speed function by the calculated vapor pressure difference. Values of ϕ_e are averaged over consecutive periods ranging from 2-5 weeks. Where possible 5-week periods were used. The mean temperature difference between the water surface and the air ($\Delta\theta$) was approximately 10°F, and $\Delta\theta_v$ ranged from 10-20°F with a mean of 14°F.

b) Data from the Hazelwood cooling pond, Australia (D3). The pond has an area of 1250 acres, and was operated during the period under consideration at increasing loadings up to 0.8 MW_e (nuclear)/acre. An interesting feature of the pond is a 70 acre hot pond area, which is followed by a narrow cooling pond outlet channel (see Figure 8.2). The pond is stratified but the cold bottom waters rarely penetrate the outlet channel

as far as the hot pond, which therefore provides a separate source of data, with a mean water-air temperature difference ($\Delta\theta$) of 29°F ($\Delta\theta_v$ from 25-40°F). Temperatures were taken at both the surface and bottom at the end of the hot pond. When bottom temperatures in the outlet channel were more than 2°F less than surface temperatures, indicating possible cold water intrusion, the data was discarded. A 2°F mean difference is explainable on the basis of diurnal stratification. The mean $\Delta\theta$ and $\Delta\theta_v$ for the main cooling pond were 12 and 15°F respectively. The data from Hazelwood are the best presently available. Surface temperatures were recorded continuously at seven (7) locations. Windspeed was measured on site at 2 shore locations. Three hourly wet and dry bulb temperatures were taken. Pan evaporation, solar radiation, and natural surface temperatures in an adjacent isolated pond were also recorded. The data used here are mean monthly data for 1967, 1968 and 1969. Evaporative heat flux ϕ_e was calculated using an energy budget apporach, with Swinbank's equation 2.10 to determine atmospheric radiation. Cloud cover was estimated from solar radiation using Hamon's (1954) chart and Equation 2-1. Changes in heat stored in the pond were included in the energy budget calculation.

The performance of the various evaporative heat flux formulae against Brady's data is shown in Figures 2-10 to 2-13. Figure 2-10

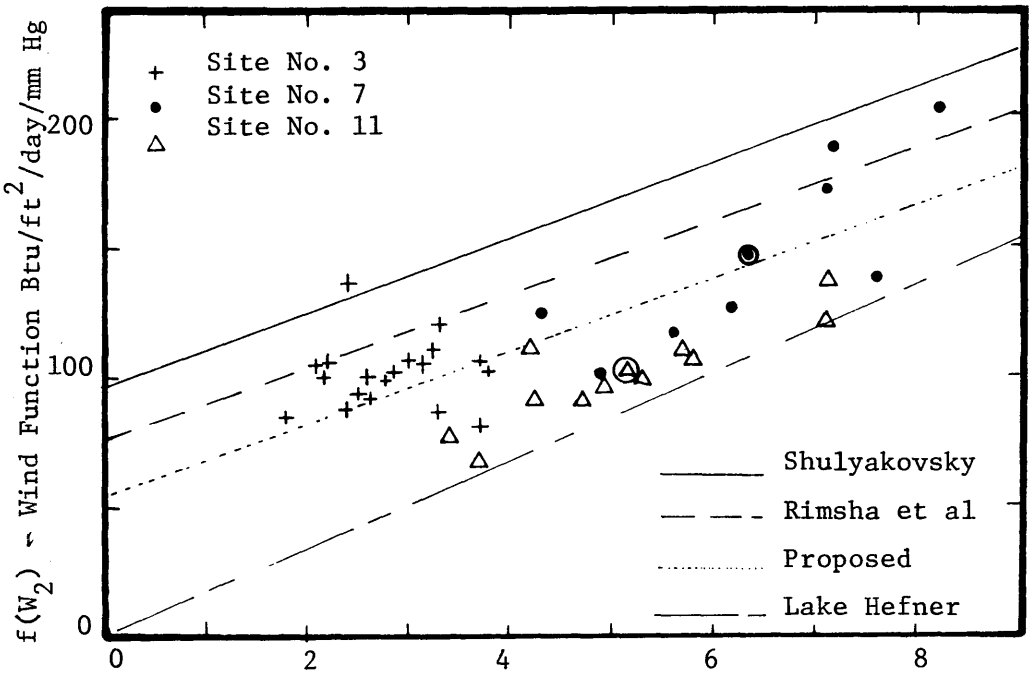

a) W_2 Windspeed at 2 meters (6.5 ft) elevation (mph)

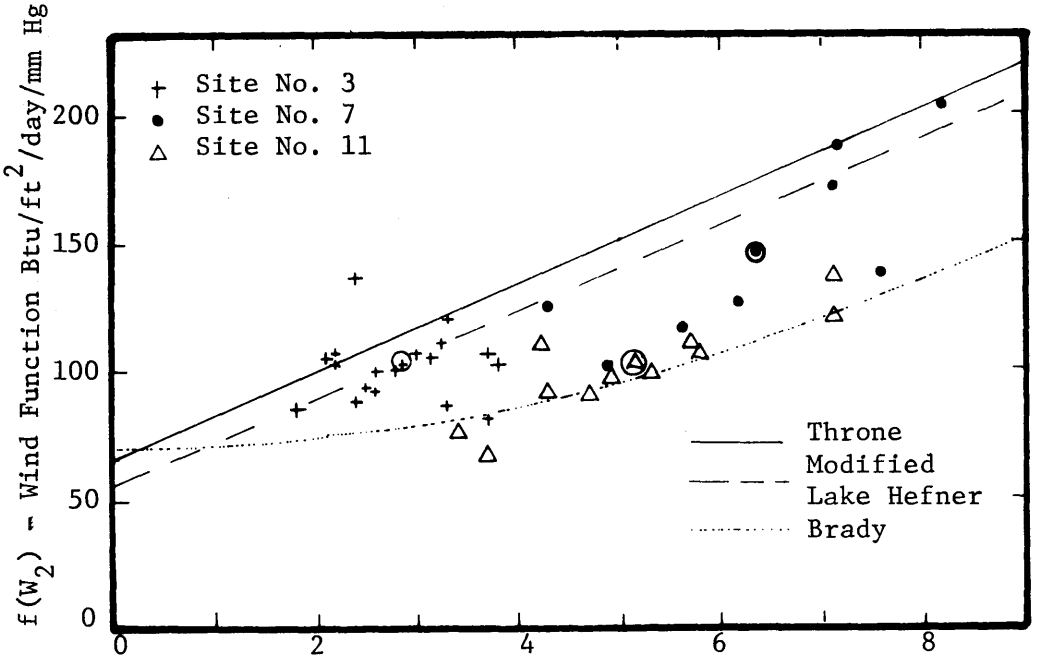

b) W_2 Windspeed at 2 meters (6.5 ft) elevation in (mph)

Figure 2-10 Alternative Wind Functions vs. Data from (Brady (12)

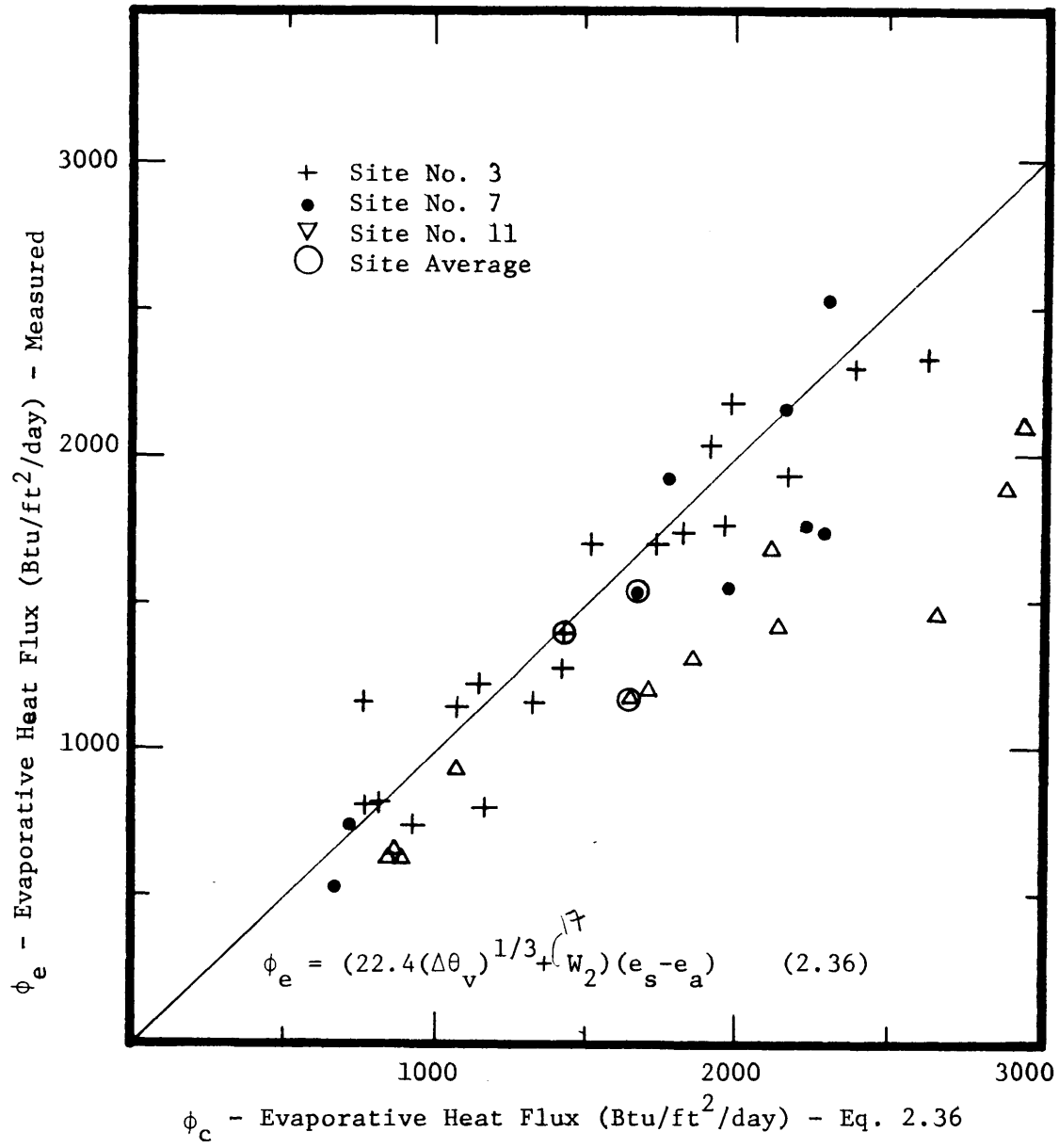

Figure 2-11 Comparison of Modified Lake Hefner Formula with Brady's Data

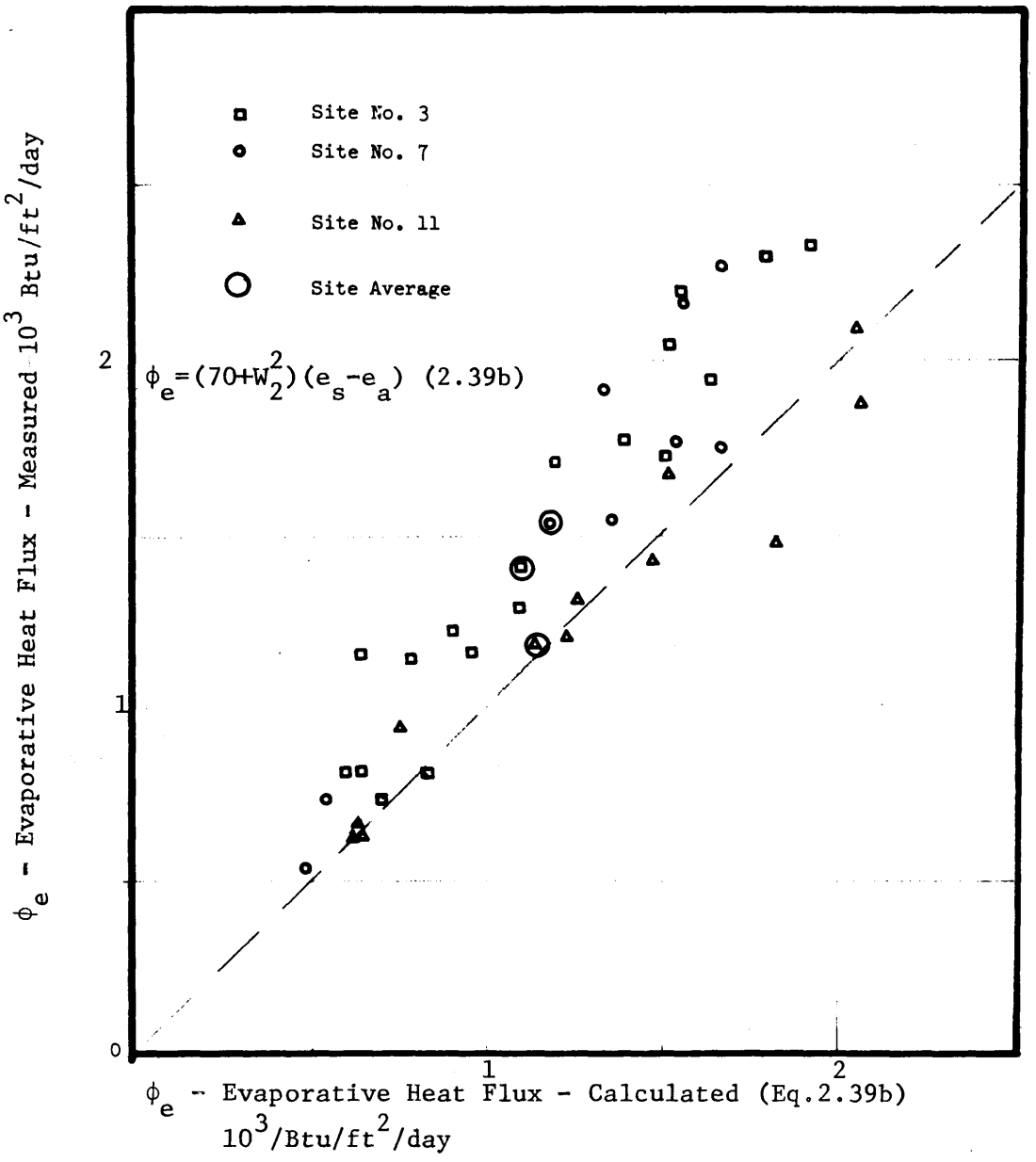

Figure 2-12 Comparison of Brady's Formula and his Data (Monthly Average)

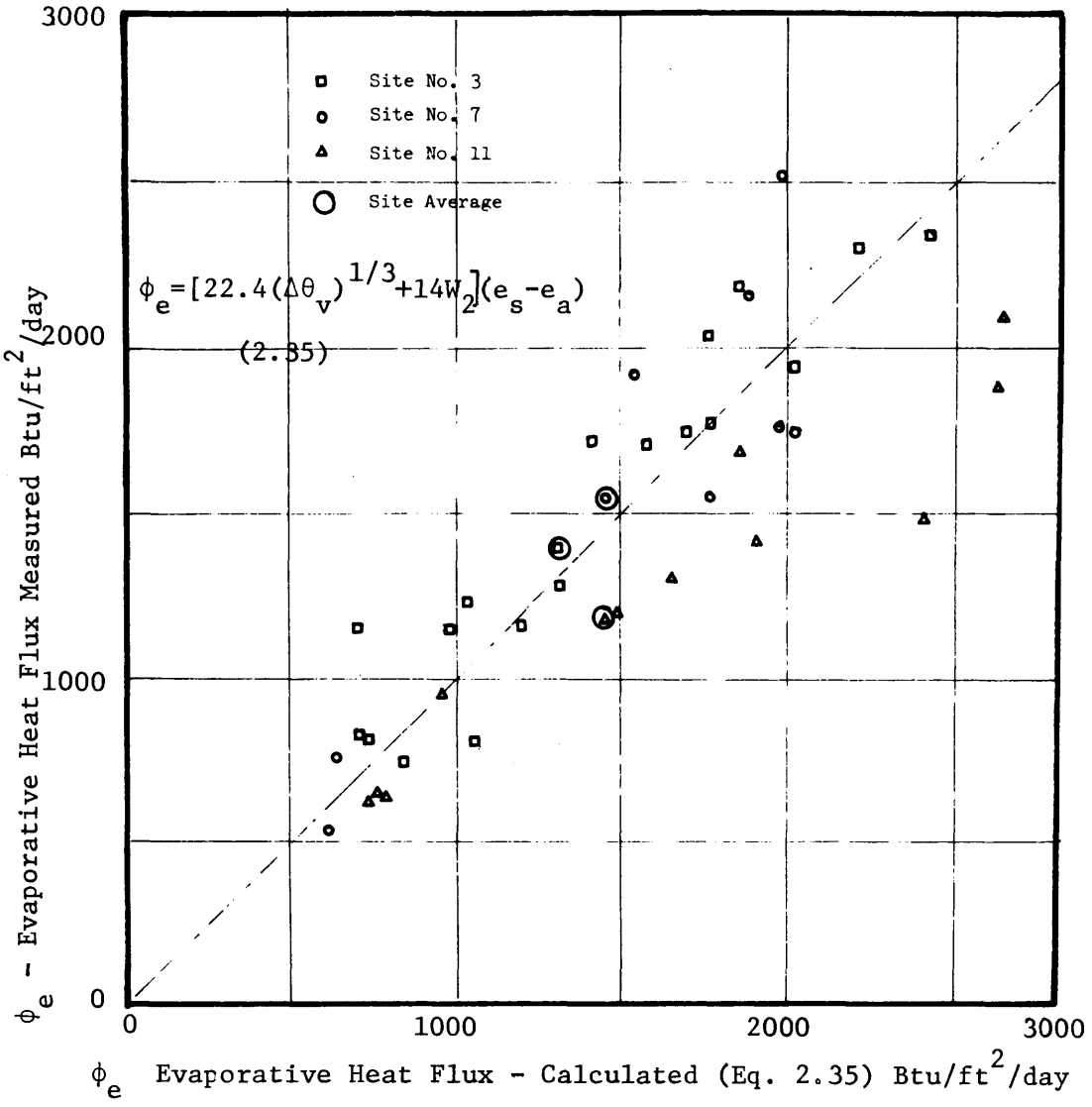

Figure 2-13 Comparison of Proposed Formula with Brady's Data (Monthly Average)

shows that the formulae of Shulyakovskiy, Rimsha and Donchencko, and Throne are too high and the Lake Hefner formula too low by a considerable margin. The modified Lake Hefner formulae is somewhat high, while Brady's formula and the proposed formula perform quite well. Mean values of $\Delta\theta$ and $\Delta\theta_v$ as specified previously were used to obtain the curves in Figure 10. The three formulae with the best performance are shown in equivalence form in Figures 2-11 to 2-13. The modified Lake Hefner formula is still too high, (Figure 2-11), while Brady's formula is somewhat low (Figure 2-12). The best performance, even using Brady's data, is given by the proposed formula (Figure 2-13).

The performance of the various formulae against the Hazelwood data is shown in Figures 2-14 to 2-17. Figure 2-14 compares the predicted vs. measured wind functions for the total pond. Again, it is seen that the formulae of Shulyakovskiy and Throne are far too high, while the Lake Hefner formula and that of Brady are too low by a similar margin. The best fit is given by the proposed formula, while the Rimsha and Donchencko and the modified Lake Hefner formula are somewhat high. The formula with the best performance (the proposed formula), and the closest formulae on the high and low side (the modified Lake Hefner and the Brady formulae) are shown in equivalance form in Figures 2-15 to 2-17. The data from the Hazelwood hot pond showed so much scatter that comparison of performance of wind functions was rather unrewarding. However, this data is included on the equivalence plots. The modified Lake Hefner formula is about 10-20% high for the total pond data, but is somewhat better for the hot pond. The Brady formula is about 25% low for the total pond, and 50% low for the hot pond. The proposed formula gives

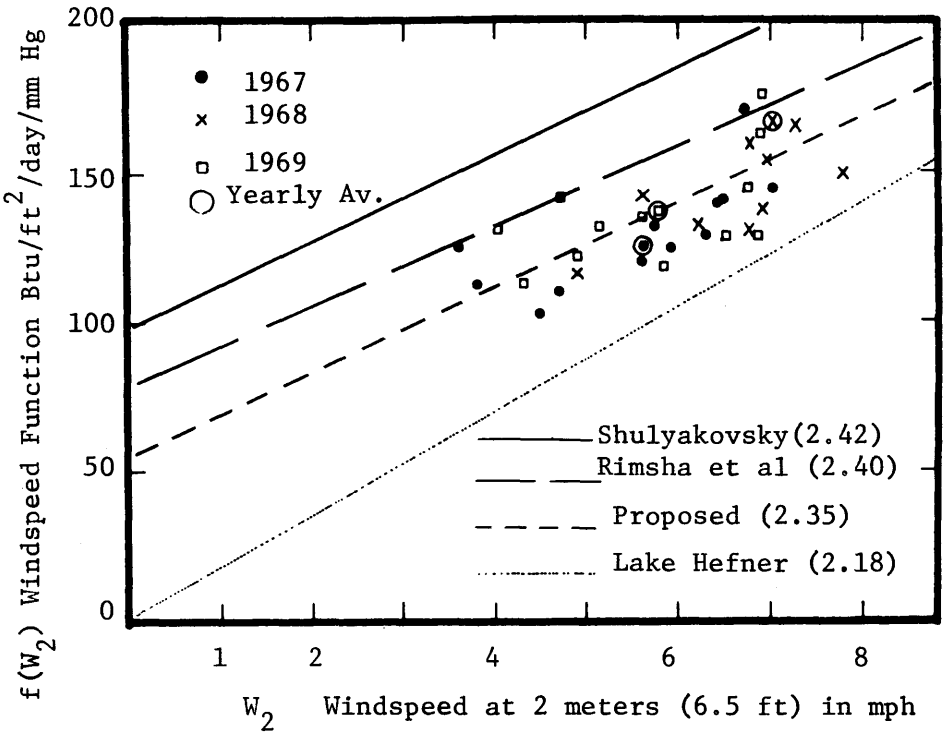

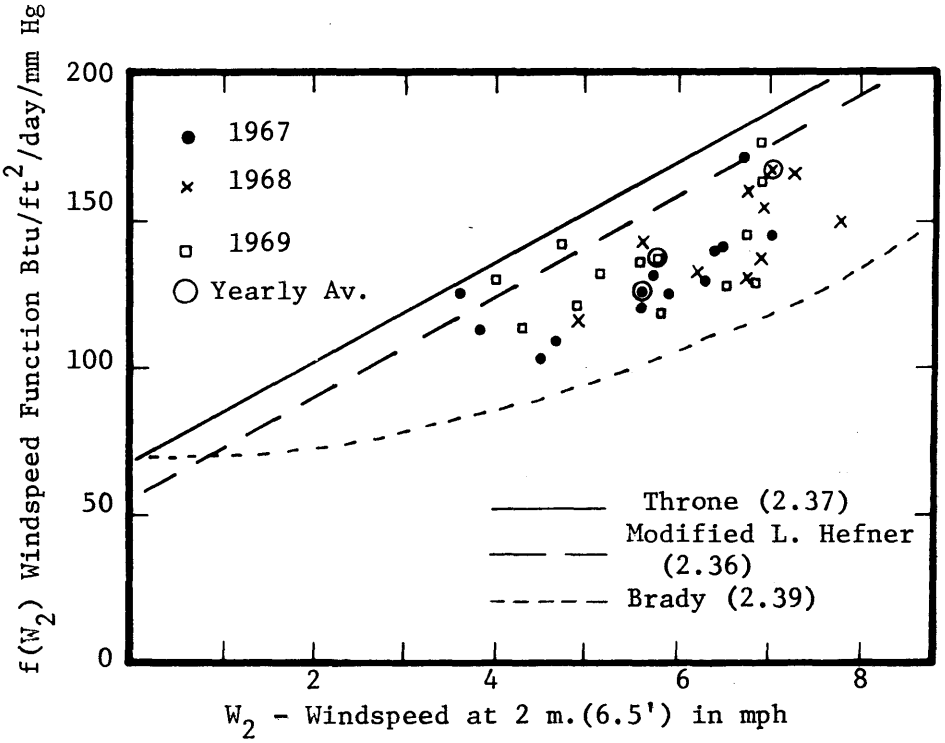

Figure 2-14 Wind Function vs. Windspeed - Hazelwood Total Pond

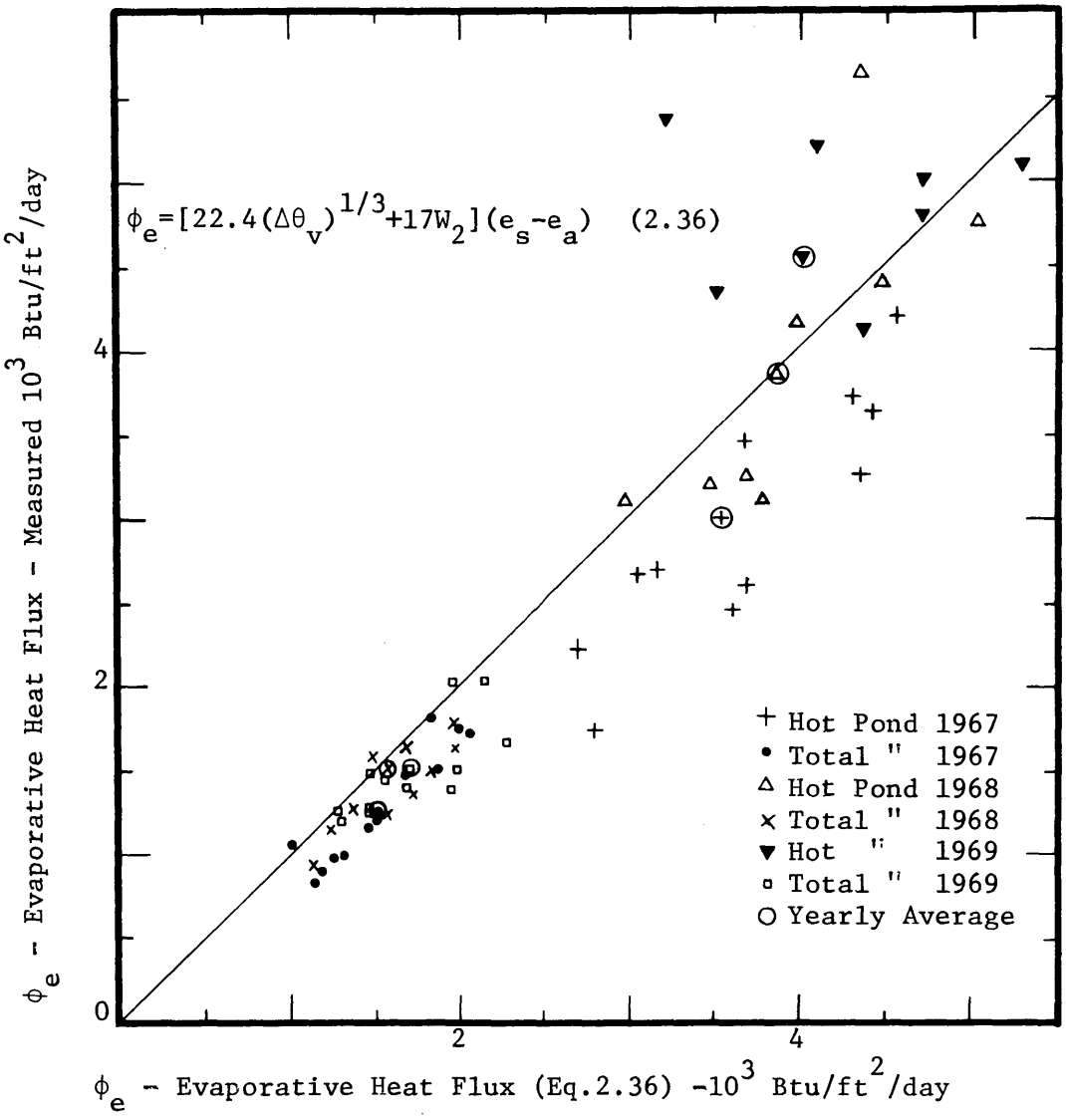

Figure 2-15 Comparison of Modified Lake Hefner Formula with Hazelwood Data

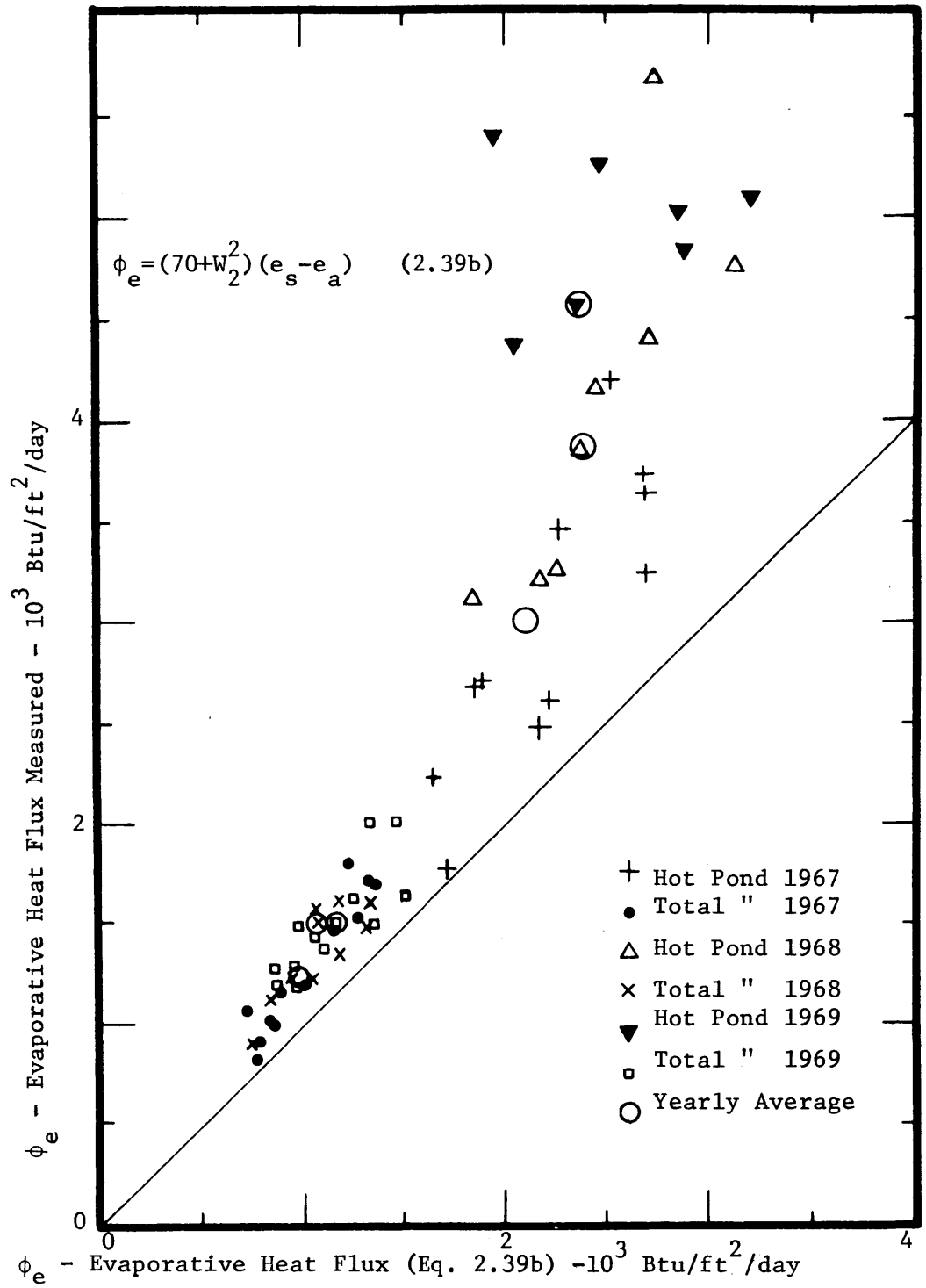

Figure 2-16 Comparison of Brady Formula with Hazelwood Data

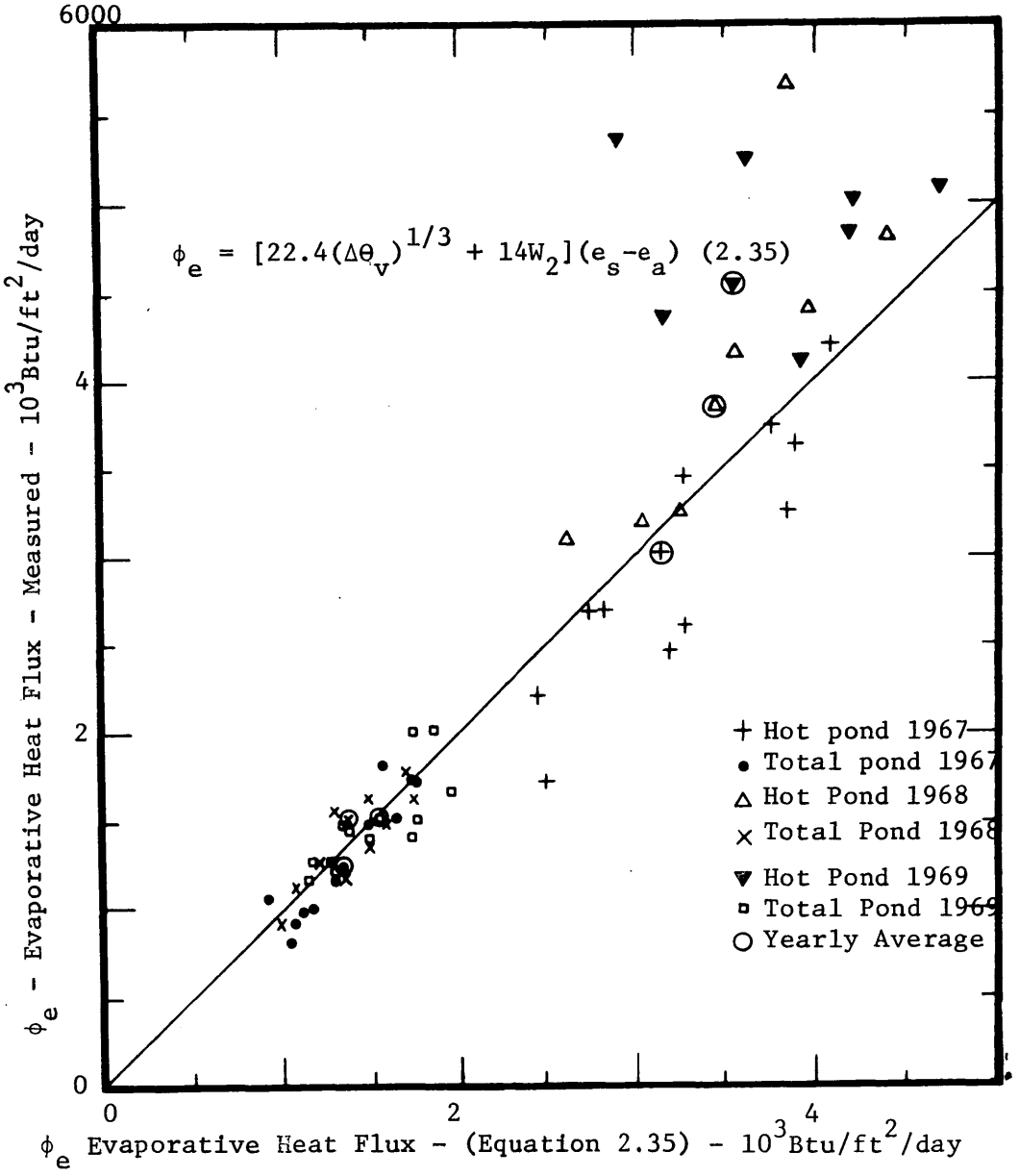

Figure 2-17 Comparison of Proposed Formula with Hazelwood Data

quite a good fit for both total pond and hot pond, although it may be somewhat conservative at very high $\Delta\theta_v$.

The overall performance of the proposed formula, Equation 2.35, a modified version of Shulyakovskiy's formula, over a wide range of heat loading (0.2-0.8 MW_e (nuclear)/acre) has been quite satisfactory. The formula also gave reasonable results when checked against the Hazelwood hot pond data which involved virtual temperature differences as high as $\Delta\theta_v = 45°F$. This formula (Equation 2.35) will be incorporated in the mathematical model developed in this study.

2.4.3 Conclusions

a) Five evaporation formulae for a natural water surface were considered. When reduced to a common measurement height, and allowance made for pan versus lake evaporation, reasonably good agreement was obtained in the 5-15 mph windspeed range. The Lake Hefner formula, Equation 2.18, has the best data base and has performed well at other sites such as Lake Mead(138), Lake Eucumbene (141)and Russian Lakes (18).

b) A formula, Equation 2.35, which gives good results for the evaporative heat flux from a heated water surface both in the laboratory (zero windspeed), and in the field, has been developed. The formula is a modified version of that proposed by Shulyakovskiy (1969). The basis of the formula is the explicit recognition of the importance of free convection in the evaporative heat flux from highly loaded cooling ponds.

2.5 Conduction (Sensible) Heat Flux, ϕ_c

Heat fluxes by conduction have received relatively little attention. One reason for this is that these fluxes are usually small compared to evaporative fluxes. Bowen (1926) suggested that conduction could be directly related to evaporative fluxes by assuming that eddy diffusivities of heat and mass are identical. This leads directly to the Bowen ratio concept.

$$E = K_m \frac{\partial \rho_v}{\partial z} = A K_m \frac{\partial e}{\partial z} \qquad (2.43)$$

where

ρ_v = vapor density

A = constant

and

$$\phi_c = \rho c K_h \frac{\partial T}{\partial z}$$

but

$$K_h = K_m = \frac{E}{A \frac{\partial e}{\partial z}}$$

therefore

$$\phi_c = B \frac{E}{\partial e/\partial z} \frac{\partial T}{\partial z} = B \frac{\partial T/\partial z}{\partial e/\partial z} E \qquad (2.44)$$

where B = constant.

Choosing some convenient height z (say 2 m. (6.5 ft)) one can write

$$\phi_c = R\phi_e \qquad (2.45)$$

where $R = C_l \left| \frac{T_s - T_z}{e_s - e_z} \right|$ = Bowen Ratio

For the units of °F, mm Hg, C_l = .255 mm Hg/°F.

The primary assumption is the equivalence of K_h and K_m. There is general agreement that in a near neutral and slightly stable atmosphere, this assumption is reasonable, and, as discussed in Sec. 2.4.2.1 all evidence points to K_h/K_m equal to unity under unstable conditions, also. Anderson (1954) points out, however, that as $e_s \rightarrow e_a$, and the Bowen ratio becomes very large, this approach is less reliable.

In conclusion, the Bowen ratio is a convenient method for calculating conductive heat flux. Its validity has been demonstrated for natural water surfaces (3), and it should be valid for artificially heated water surfaces as well. Certainly, the approach is the best available. Some recent attempts to abandon the Bowen ratio approach in favor of heat-momentum ratio approach are not recommended, because of uncertainty about momentum transfer over a limited fetch, and also the considerable uncertainty about the relationship between heat and momentum transfer under non-neutral conditions.

2.6 Effect of Averaging on Evaporative and Conductive Fluxes

It is sometimes suggested that one of the reasons for the lack of agreement among the various evaporation formulae is the widely differing periods of time over which the basic data is averaged. Typical time scales vary from 3 hours to 1 month. Since the rate of evaporation at any instant is $(e_s - e_a) \cdot f(W)$, best results should be obtained when long-term evaporation is related to the average value of $(e_s - e_a) \cdot f(W)$, rather than long-term averages of e_s, e_a and $f(W)$. This problem was

examined by Kohler (1954) and Jobson (1972). Both used the Lake Hefner data, and found that averaging short term data (30 mins., 3 hrs.) for periods of up to 1 day had no significant effect. Averaging over a period of 1 month introduced a systematic positive error. In 11 cases out of 13, this error was $\leq$ 5% and therefore, in view of the general level of accuracy involved, can hardly be called significant.

Webb (1960) considered the problem of the effect of a fluctuating Bowen ratio on the accuracy of the heat budget approach to evaporation estimation, and showed that averaging 3 hr. values for periods from 3-4 weeks could lead to underestimation of the evaporative loss by up to 5%. Since conduction losses may be as low as 10% of evaporation losses, this is a serious error, although in terms of the overall heat budget it is not so significant.

Since for design purposes it is generally necessary to use long term average data, it is reasonable to develop formulae on the same basis.

2.7 Effect of Measurement Height

One of the problems with comparison of different evaporation formulae is due to the different measurement heights used in obtaining the basic data. Both windspeed and vapor pressure are functions of the height above the water surface. In this study a consistent height of 2 m. (6.5 ft) is used for both variables. The 2 meter windspeed height has the advantage of including, at least to some extent, the effect of local topography. Unfortunately, in some references, the measurement heights are not given, but where possible data has been reduced to the

2 meter level using the following formulae

$$\frac{W_z}{W_{z_1}} = \frac{\ln \frac{z}{z_o}}{\ln \frac{z_1}{z_o}} \tag{2.46}$$

$$\frac{e_z - e_o}{e_{z_1} - e_o} = \frac{\ln \frac{z}{z'}}{\ln \frac{z_1}{z'}} \tag{2.47}$$

where

z_o = roughness height for wind profile

z' = roughness height for vapor pressure profile

Values of z_o and z' have been obtained by back fitting measured wind and vapor pressure profiles,(137), (138), (141) Values of z_o range from 0.0005 ft. at Lake Mead (138) to 0.015-0.03 ft. at Lake Hefner (137). Webb (1960) found z_o to vary from 0.001-0.015 ft. Values for z' are much smaller than z_o and are given as .0002 ft. (137), and .00001 ft. (138). Normalized wind and vapor pressure profiles are shown in Figure 2-18, demonstrating that the use of 8 m. (26 ft) instead of 2 m. (6.5 ft) measurement heights involves differences of 20% in windspeed, and 10% in vapor pressure. In this study z_o is taken to be .003 ft (.001 m) for windspeeds less than 5 mph, and 0.015 ft (.005 m) for higher windspeeds. The Lake Hefner value of z' (0.0002 ft or 0.000067 m.) is also used.

2.8 Summary of Heat Transfer Formulae

The net heat input, ϕ_n, to a water body may be defined in terms of the components of surface heat transfer as defined in the previous

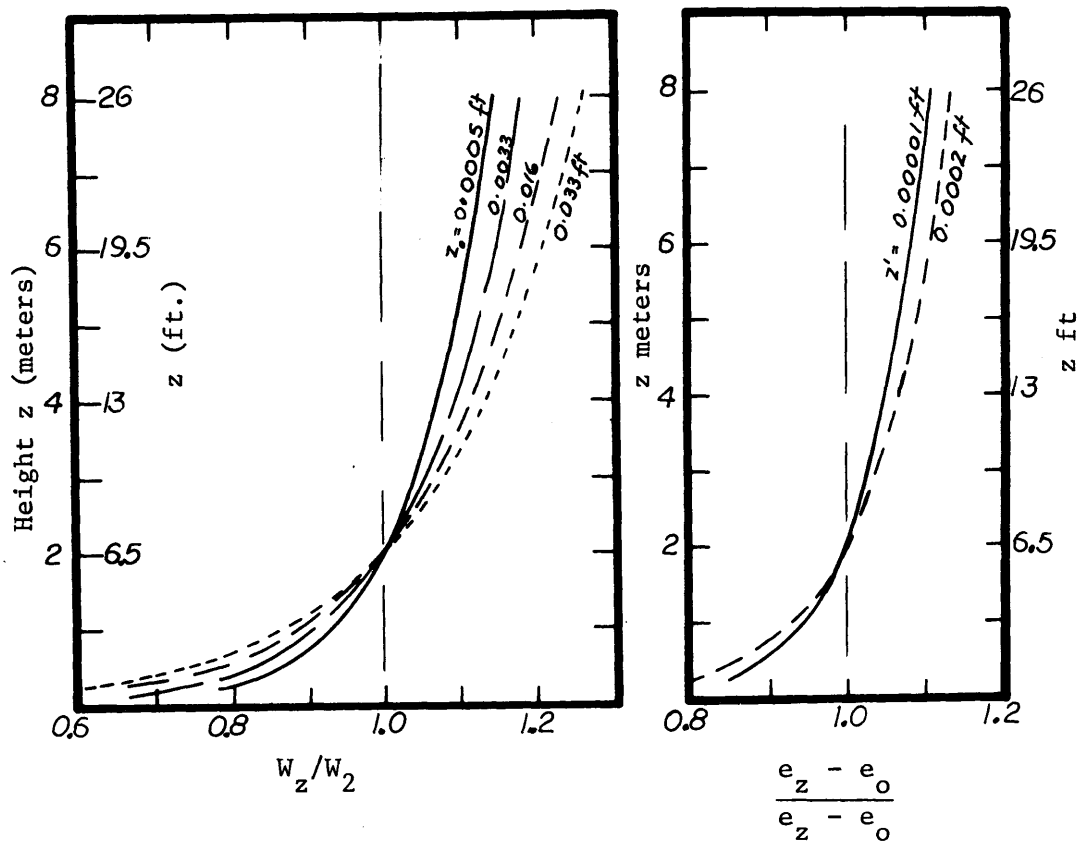

Figure 2-18 Wind Speed and Vapor Pressure Profiles

sections.

$$\phi_n = \phi_s - \phi_{sr} + \phi_a - \phi_{ar} - \phi_{br} - \phi_e - \phi_c \qquad (2.48)$$

If all the incident and reflected short and long wave radiation terms are grouped in a net radiation term ϕ_r, and using Equation (2.10)

$$\phi_r = \phi_s - \phi_{sr} + \phi_a - \phi_{ar} \equiv \phi_{sn} + \phi_{an} \qquad (2.49)$$

$$= \phi_{sn} + 1.16\text{x}10^{-13}(460 + T_a)^6(1 + 0.17C^2) \qquad (2.50)$$

then

$$\phi_n = \phi_r - (\phi_{br} + \phi_e + \phi_c) \qquad (2.51)$$

in which ϕ_r is a function of meteorological variables and the quantity $\phi_{br} + \phi_e + \phi_c$ depends in part upon the water surface temperature. Using formulas from the previous section (Equations (2.12), (2.16) and (2.45))

$$\phi_n = \phi_r - [4\text{x}10^{-8}\ (T_s + 460)^4 + f(W)\ [(e_s - e_a)$$

$$+ .255(T_s - T_a)]] \qquad (2.52)$$

where

$$f(W_2) = 17\ W_2 \qquad (2.18b)$$

for a natural water surface and

$$f(W_2) = 22.4\ (\Delta\Theta_v)^{1/3} + 14\ W_2 \qquad (2.35)$$

for an artificially heated water surface.

It should be noted that the evaporation terms in the above equation are only valid for $e_s > e_a$, that is when the evaporative heat transfer is out of the water. When $e_a > e_s$ condensation may occur, as discussed by Wunderlich (1972). At present very little appears to be known about the transfer coefficients in this situation, and in this study, when $e_a > e_s$, evaporation is set equal to zero. Similarly the Bowen ratio is not defined in this situation, but the conduction terms in Equation (2.52) are retained as the best available. Fortunately $e_a > e_s$ is rare even above a natural water surface, so the problem of heat transfer by condensation is not a significant one for a heated surface. The following section is a result of a collaboration with Dr. K.D. Stolzenbach (108).

2.9 Linearization of Heat Transfer Equations

The preceding section presents methods for estimating the magnitudes of the various components of heat transfer through the water surface. Several of these components are nonlinear functions of water surface temperature. A linearized approach to heat transfer has been developed by Edinger and Geyer (1965). This approach involves two concepts, that of equilibrium temperature, T_E, and surface heat exchange, K, and ϕ_n can now be written as

$$\phi_n = K(T_s - T_E) \qquad (2.53)$$

The equilibrium temperature, T_E, is defined as that water surface temperature which, for a given set of meteorological conditions, makes the back radiation, evaporation, and conduction losses exactly equal

to the radiation inputs, that is, the net heat exchange ϕ_n is zero (see Equation (2.51)). The surface heat exchange coefficient, K, is defined to give the incremental change of net heat exchange induced by an incremental change of water surface temperature. These concepts may be used separately or together in a variety of applications, especially to heated power plant discharges.

2.9.1 Equilibrium Temperature

The equilibrium temperature, T_E, is useful because it is dependent solely upon meteorological variables at a given site, although it is the temperature toward which every water body at the site will tend. A water body at a surface temperature, T_s, less than T_E, will have a net heat input and thus will tend to increase its temperature. The opposite is true if $T_s > T_E$. Thus, the equilibrium temperature embodies all the external influences upon ambient temperatures. T_E can be calculated by setting $\phi_n = 0$ and $T_s = T_E$ in Equation (2.52)

$$\phi_r = 4 \times 10^{-8} (T_E + 460)^4 + f(W) [(e_E - e_a) + .255(T_E - T_a)] \quad (2.54)$$

For a given net radiation term, ϕ_r, wind function, f(W), air vapour pressure, e_a, and air temperature, T_a, the equilibrium temperature T_E may be calculated by trial and error from the above equation. Note that T_E is usually close to the natural water surface temperature and therefore f(W) for a natural water surface should be used.

An approximate formula for obtaining T_E may be derived by neglecting certain terms in Equation (2.54) thus permitting an explicit solution for T_E. It is necessary to express the vapour pressure

difference $(e_s - e_a)$ in terms of temperature:

$$e_s - e_a = \beta(T_s - T_d) \tag{2.55}$$

where T_d is the dew point temperature of the air, measured at the same elevation as the air temperature. The proportionality factor β is a function of temperature. Assuming that a representative average temperature is

$$T^* = \frac{1}{2}(T_s + T_d) \tag{2.56}$$

$$\beta = .255 - .0085\ T^* + .000204T^{*2}\ \left[\frac{\text{mm Hg}}{^\circ\text{F}}\right] \tag{2.57}$$

or

$$\beta = 25.4 \cdot \frac{9500}{(T^* + 460)^2} \exp\left[17.62 - \frac{9500}{T^* + 460}\right] \left[\frac{\text{mm Hg}}{^\circ\text{F}}\right] \tag{2.58}$$

The back radiation term may be simplified by noting that

$$4 \times 10^{-8}(T_s + 460)^4 \simeq 1600 + 23T_s \tag{2.59}$$

Using these approximations the equilibrium temperature is given by:

$$T_E = \frac{\phi_r + f(W)\ [\beta T_d + .255\ T_a] - 1600}{23 + f(W)\ (\beta + .255)} \tag{2.60}$$

The above expression must be used by assuming a value of T_E, calculating T^* and β, and then checking to see if the resulting value of T_E is close to the assumed value. If not, a new calculation is made with an improved estimate. A separate calculation must be made for each set of atmospheric parameters ϕ_r, $f(W)$, T_d, and T_a.

Brady (1969) has shown that an even simpler expression yields fairly accurate results:

$$T_E = \frac{\phi_{sn}}{23 + f(W)\ (\beta + .255)} + T_d \qquad (2.61)$$

where ϕ_{sn} is the net incident solar radiation as previously discussed. This expression implies that many of the components of the numerator in Equation (2.60) cancel each other. In the laboratory it was found that using $f(W) = a = 75$ Btu/ft^2/day/mm Hg gave T_E within ±1°F of its measured value. Equation (2.33) applies only to a heated water surface and cannot be used to calculate T_E. Table 2-3 gives T_E in the laboratory as a function of air temperature and relative humidity.

2.9.2 Surface Heat Exchange Coefficient

The surface heat exchange coefficient, K, relates the net heat transfer rate to changes in water surface temperature. Figure 2-19 shows a typical plot of the net heat transfer vs. water surface temperature. As previously stated, the equilibrium temperature T_E is the value of T_s at which $\phi_n = 0$. The surface heat loss coefficient is defined as the inverse of the slope of the $\phi_n - T_s$ curve:

$$K = -\frac{\partial \phi_n}{\partial T_s} \qquad (2.62)$$

Note that the slope may be defined at any value of T_s, above or below the equilibrium temperature.

Table 2-3 Equilibrium Temperature - T_E - Laboratory

Air Temperature ^{o}F

Relative Humidity (%)	60	61	62	63	64	65	66	67	68	69	70	71	72	73	74	75	76	77	78	79
40	51.66	52.48	53.3	54.13	54.95	55.77	56.59	57.4	58.22	59.04	59.85	60.67	61.48	62.29	63.09	63.9	64.71	65.51	66.32	67.12
42	51.95	52.79	53.62	54.45	55.28	56.1	56.93	57.75	58.58	59.4	60.22	61.04	61.86	62.68	63.49	64.31	65.12	65.94	66.75	67.56
44	52.25	53.09	53.93	54.76	55.6	56.43	57.27	58.1	58.93	59.76	60.59	61.41	62.24	63.07	63.89	64.71	65.54	66.36	67.18	68.0
46	52.54	53.39	54.23	55.08	55.92	56.76	57.6	58.44	59.28	60.11	60.95	61.79	62.62	63.45	64.28	65.11	65.95	66.77	67.6	68.43
48	52.84	53.69	54.54	55.39	56.24	57.09	57.93	58.78	59.63	60.47	61.31	62.15	62.99	63.84	64.67	65.51	66.35	67.19	68.03	68.86
50	53.13	53.99	54.84	55.7	56.56	57.41	58.27	59.12	59.97	60.82	61.67	62.52	63.37	64.22	65.06	65.91	66.75	67.6	68.44	69.29
52	53.42	54.28	55.15	56.01	56.87	57.73	58.6	59.45	60.31	61.17	62.03	62.88	63.74	64.59	65.45	66.3	67.16	68.01	68.86	69.71
54	53.7	54.58	55.45	56.32	57.19	58.06	58.92	59.79	60.65	61.52	62.38	63.25	64.11	64.97	65.83	66.69	67.55	68.41	69.27	70.13
56	53.99	54.87	55.75	56.63	57.5	58.37	59.25	60.12	60.99	61.87	62.74	63.6	64.48	65.34	66.21	67.08	67.95	68.81	69.68	70.55
58	54.28	55.16	56.05	56.93	57.81	58.69	59.57	60.45	61.33	62.21	63.09	63.96	64.84	65.72	66.59	67.47	68.34	69.21	70.09	70.96
60	54.56	55.45	56.34	57.23	58.12	59.0	59.9	60.78	61.67	62.55	63.44	64.32	65.2	66.08	66.97	67.85	68.73	69.61	70.49	71.37
62	54.85	55.74	56.64	57.54	58.43	59.32	60.22	61.1	62	62.89	63.78	64.67	65.56	66.45	67.34	68.23	69.12	70.0	70.89	71.78
64	55.13	56.03	56.93	57.84	58.74	59.64	60.53	61.43	62.33	63.23	64.13	65.02	65.92	66.82	67.71	68.6	69.5	70.4	71.29	72.18
66	55.41	56.32	57.23	58.13	59.04	59.95	60.85	61.76	62.66	63.57	64.47	65.37	66.27	67.18	68.08	68.98	69.88	70.78	71.68	72.59
68	55.69	56.6	57.52	58.43	59.34	60.26	61.17	62.08	62.99	63.9	64.81	65.72	66.63	67.54	68.45	69.35	70.26	71.17	72.08	72.98
70	55.97	56.89	57.8	58.73	59.65	60.56	61.48	62.4	63.32	64.23	65.15	66.06	66.98	67.89	68.81	69.72	70.64	71.55	72.47	73.38
72	56.25	57.17	58.1	59.02	59.95	60.87	61.79	62.72	63.64	64.56	65.48	66.4	67.33	68.25	69.17	70.09	71.01	71.93	72.85	73.77
74	56.52	57.45	58.38	59.32	60.25	61.18	62.1	63.03	63.96	64.89	65.82	66.75	67.67	68.6	69.53	70.46	71.38	72.31	73.24	74.16
76	56.8	57.73	58.67	59.6	60.54	61.48	62.41	63.35	64.28	65.22	66.15	67.09	68.02	68.95	69.89	70.82	71.75	72.69	73.62	74.55
78	57.07	58.01	58.96	59.9	60.84	61.78	62.72	63.66	64.6	65.54	66.48	67.42	68.36	69.3	70.24	71.18	72.12	73.06	74.0	74.94

Note: This table is based on two assumptions

a) The interior of the laboratory radiates as a greybody, $\varepsilon = .97$.

b) Evaporation is given by $\phi_e = a(e_w - e_a)$ where $a = 75$ Btu/ft^2/day/mm.Hg. and was obtained experimentally. The probable error in T_E is $\pm 1^{o}F$.

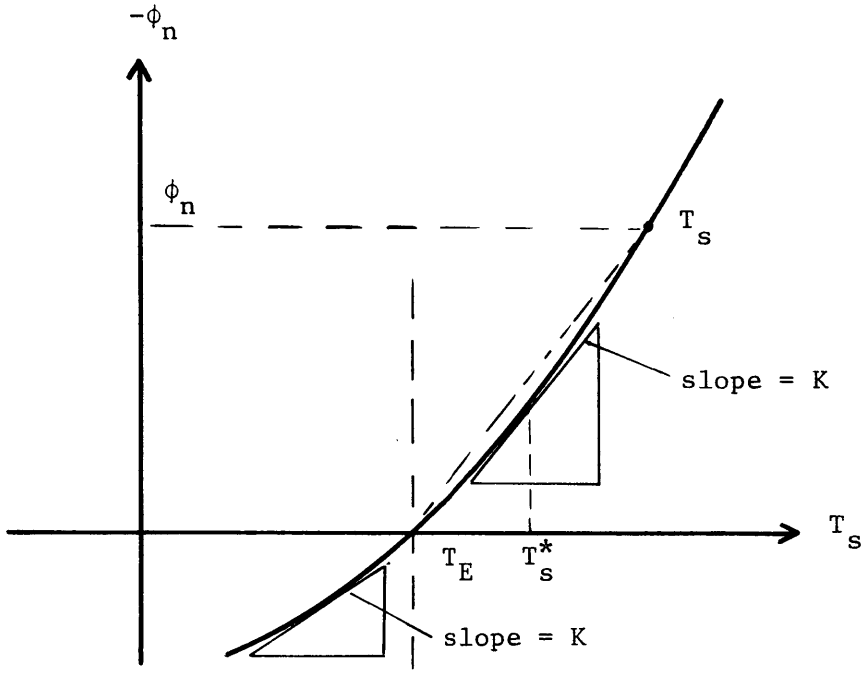

Figure 2-19 Variation of Heat Transfer Coefficient K with Water Surface Temperature T_s

Using Equations (2.52) and (2.59)

$$K = 23 + \frac{d}{dT_s}\left[f(W)\right](e_s - e_a) + .255(T_s - T_a)]] \qquad (2.63)$$

Note that the definition of β (Equation 2.55) implies:

$$\frac{\partial e_s}{\partial T_s} = \beta_s \qquad (2.64)$$

where β_s is evaluated at T_s using Equations (2.57) or (2.58). The following approximate form for K is obtained

$$K = 23 + f(W)\ (\beta_s + .255) + [(e_s - e_a) + .255(T_s - T_a)]\ \frac{df(W)}{dT_s} \qquad (2.65)$$

For a natural water surface we have

$$f(W) = 17W_2 \tag{2.18b}$$

$$K = 23 + (\beta_s + .255)\ 17W_2 \tag{2.66}$$

where W_2 is wind speed at 2m. (6.5 ft) elevation in mph. For an artificially heated water surface we have

$$f(W) = 22.4\ (\Delta\Theta_v)^{1/3} + 14W_2 \tag{2.35}$$

$$K = 23.0 + [14W_2 + 22.4\ (\Delta\Theta_v)^{1/3}]\ (\beta_s + .255)$$

$$+ 7.5(\Delta\Theta_v)^{-2/3}\ [e_s - e_a + .255(T_s - T_a)] \tag{2.67}$$

2.9.3 Evaluation of K

The surface heat exchange coefficient, K, (Eq. 2.67) is a function of water surface temperature, T_s. Generally the interest is not in K per se, but in the total heat transfer, ϕ_n, and K must be evaluated in such a way as to give the correct value of ϕ_n via Equation (2.53). From Figure 2-19 it can be seen that for a water surface at a uniform temperature T_s, and corresponding heat loss ϕ_n, K must be evaluated at T_s^* which lies between T_E and T_s. Over a range of T_s, the best results were obtained for

$$T_s^* = 0.55\ T_s + 0.45\ T_E \tag{2.68}$$

but the more obvious choice of

$$T_s^* = (T_s + T_E)/2 \tag{2.69}$$

gave quite reasonable results and this form will generally be used.

For the case where the water surface temperature, T_s, varies over the range T_{s0} to T_{s1}, a representative water temperature $\bar{T}_s$ is first defined e.g.

$$\bar{T}_s = \frac{T_{s0} + T_{s1}}{2} \tag{2.70}$$

and then

$$T_s^* = \left(\frac{T_{s0} + T_{s1}}{2} + T_E \right)/2 \tag{2.71}$$

Note that the method given by Brady et al is not correct for a heated water surface. They evaluate K at T^* where

$$T^* = \frac{\bar{T}_s + T_d}{2} \tag{2.72}$$

which is correct only for the determination of T_E. The problem arises from their implicit assumption of $\partial\beta/\partial T_s = 0$ when obtaining the formula for K.

Design charts giving K as a function of a water surface temperature, and windspeed for a $\Delta\Theta = T_s - T_a$ of 10, 20 and 40°F are given by Ryan and Stolzenbach (1972), and are shown in Figures 2-20 to 2-22. A relative humidity of 75% is assumed, which introduces a maximum error of 7% for an error of 25% in relative humidity.

When temperature rises above ambient are the only consideration, the ambient temperature T_{Am} can be substituted for T_E in Equations (2.69) and (2.71) for T_s^* (108). An example will now be given which will both demonstrate the magnitude of error involved in evaluating K at the wrong temperature, and will provide further support for

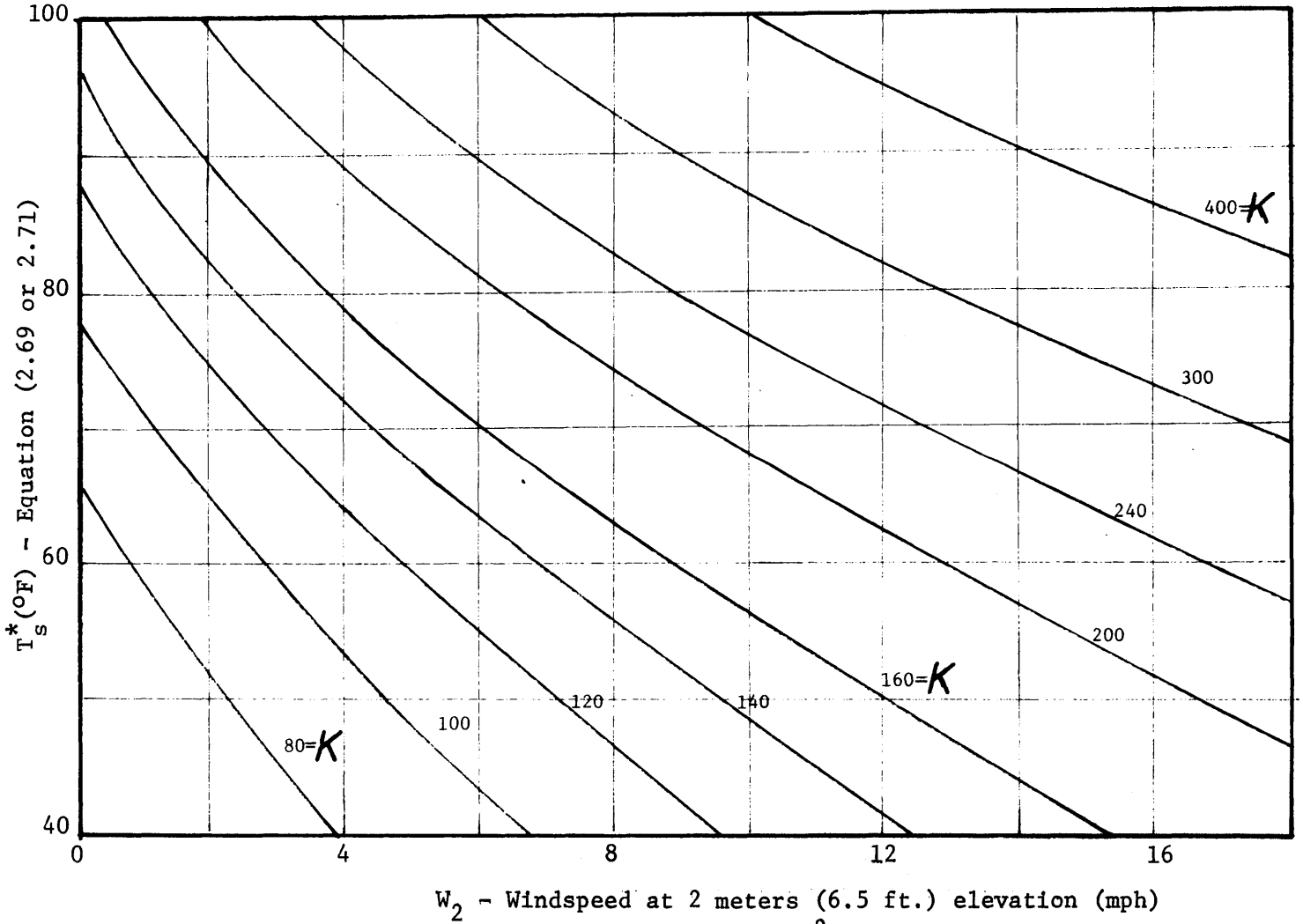

Figure 2-20 Heat Exchange Coefficient - K - (Btu/ft^2/day/°F) for a Heated Water Surface (T_s-T_a = 10°F)

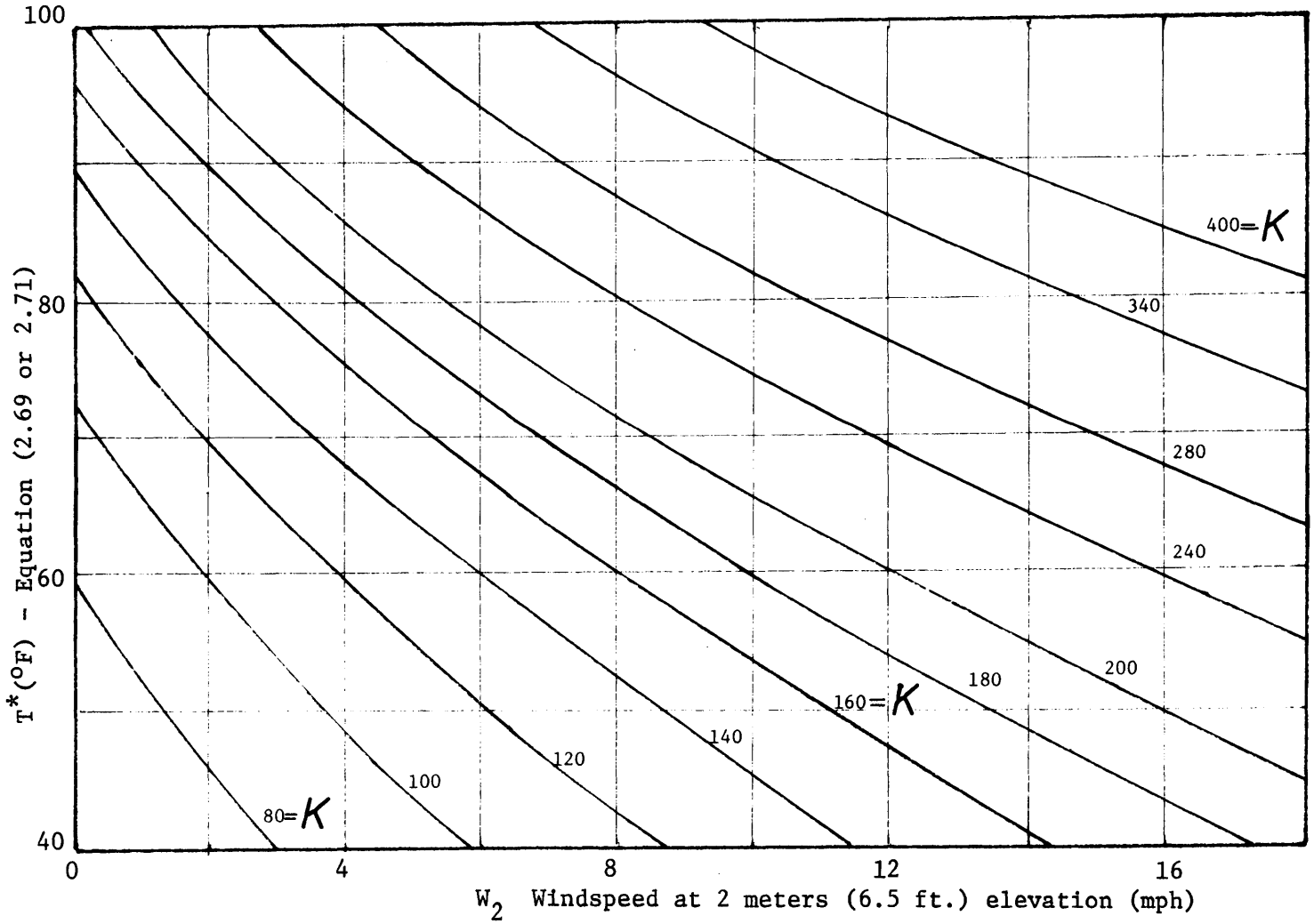

Figure 2-21 Heat Exchange Coefficient - K - (Btu/ft^2/day/°F) for a Heated Water Surface (T_s-T_a=20°F)

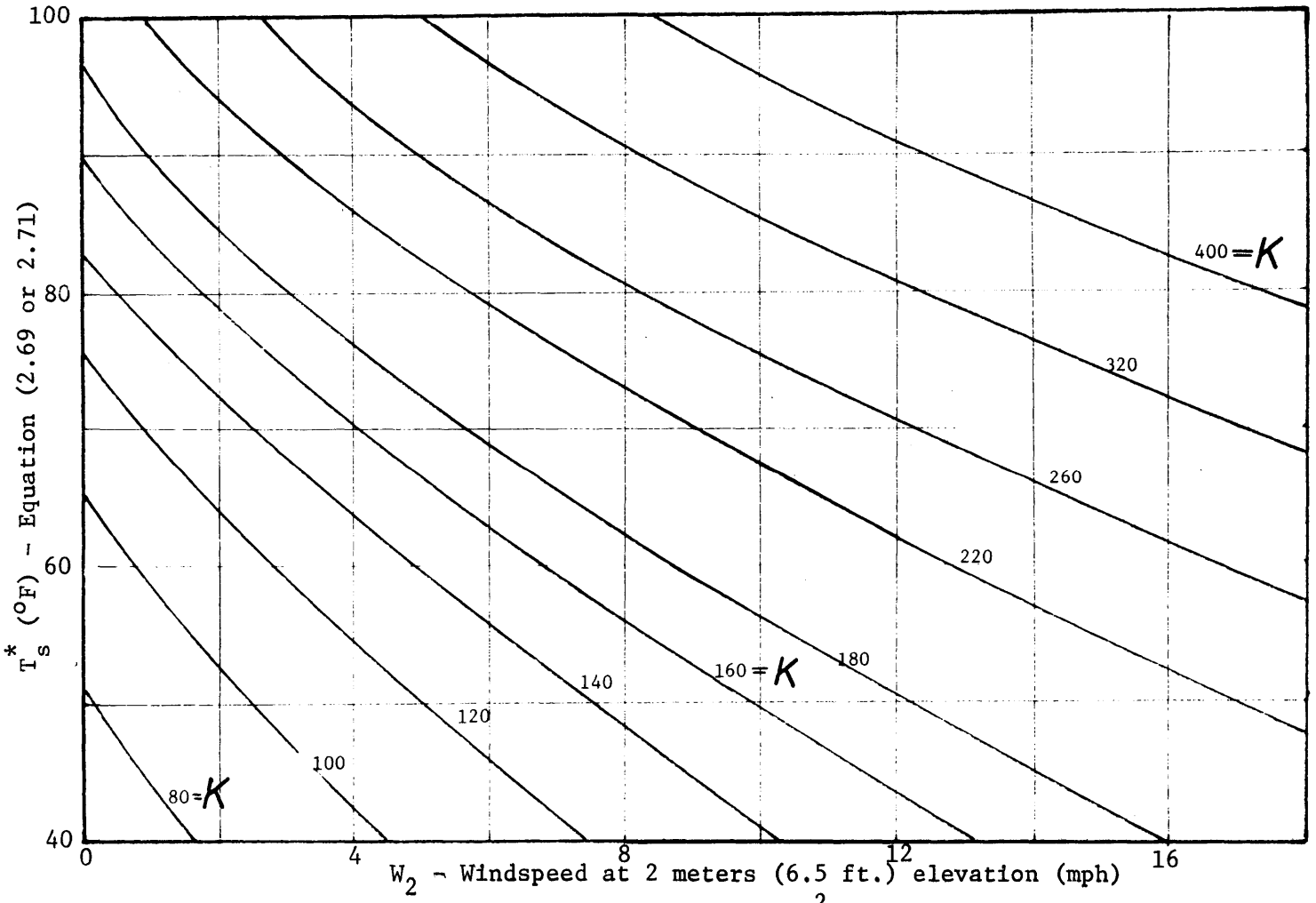

Figure 2-22 Heat Exchange Coefficient - K - (Btu/ft^2/day/°F) for a Heated Water Surface ($T_s - T_a = 40°F$)

the proposed evaporation Equation (2.35).

2.9.4 Case: Shawville Power Plant

SEE ERRATA

The Shawville plant is located on the West Brancy of the Susquehanna River below Shawville, Pennsylvania. Temperatures were measured over a 24 hour period at four sections downstream and one section upstream of the power plant as shown in Figure 2-23a (83). Windspeed, air temperatures, vapor pressure and total radiation were also measured. During the 24 hour period the plant was operating at constant load of 600 MW_e and the river discharge was 370 cfs. The effect of the power plant was to heat the whole stream by approximately 27°F. Stream temperatures in the 5 mile reach below the plant, averaged over the 24 hour period, are shown in Figure 2-23b. The average width in this reach is 270 ft. An attempt by Messinger (1963) to account for the heat loss using the Lake Hefner formula resulted in the predicted heat loss rate being about two thirds of that observed. Subsequently Garrison and Elder (1965) obtained almost perfect agreement using Throne's formula. Both Messinger (1963) and Garrison and Elder (1965) used the non-linear heat transfer equations, and divided the river into a series of relatively short reaches. Harleman (1971) showed that using the linearized approach to heat transfer in the one-dimenionsal heat transport equation

$$\Delta T = \frac{[H_p]}{\gamma Q} \exp - \left[\frac{x\,K}{\rho c h U} \right] \qquad (2.73)$$

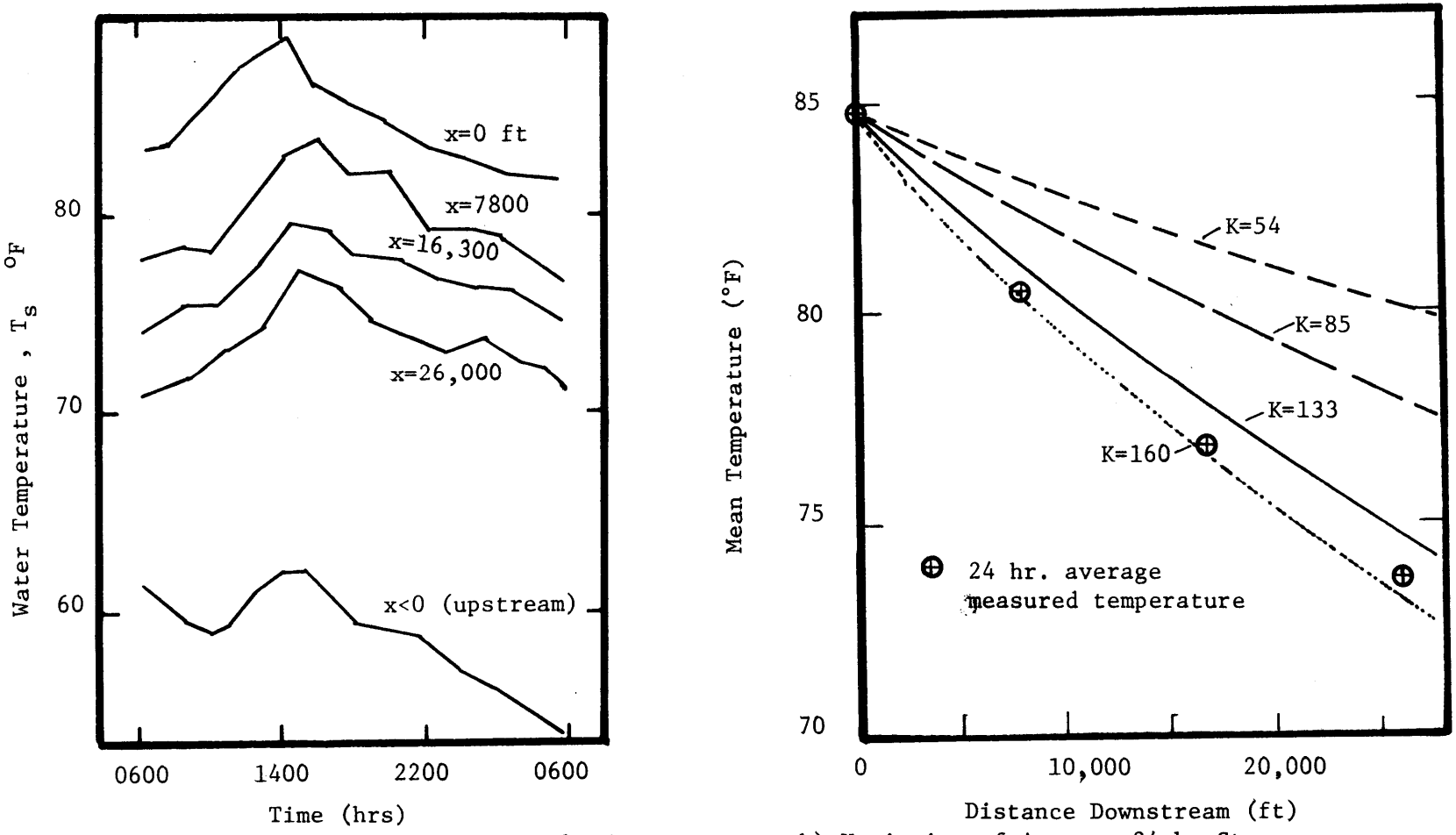

a) Variation of Stream Temperature with Time

b) Variation of Average 24 hr Stream Temperature with Distance Downstream

Figure 2-23 Predicted and Measured Temperatures in Susquehanna River

where

ΔT = temperature rise above ambient at distance x from the plant

SEE ERRATA

H_p = heat reflected by plant (Btu/day)

Q = flow rate

h = average depth of river

U = average velocity of river

gave excellent results for K = 160 Btu/ft^2/day/°F. Only 48 hour average data has been available for windspeed (3 mph), air temperature (59.4°F), and relative humidity (11%). Over a distance of five miles the maximum temperature T_{s0}, is 84.8°F and the minimum T_{s1} is 73.8°. K will be calculated in three ways.

a) Using Brady's design chart and his method of evaluating K, T_d is approximately equal to 5°F and T^* = 42°F (Eq. 2.56) leading to K = 54 Btu/ft^2/day/°F.

b) Using Brady's design chart but evaluating K at T_s^* given by

$$T_s^* = \left(\frac{T_{s0} + T_{s1}}{2} + T_{Am} \right)/2$$

where T_{Am} = ambient river temperature upstream of plant

= 59°F

T_s^* = 69.2°F

K = 85 Btu/ft^2/day/°F

c) Using Equations (2.67) and (2.57)

T_s^* = 69.2°F

$\Delta\theta_v$ = 14.3°F, Eq. (2.30b)

β_s = .635 mm Hg/°F, Eq. (2.64)

$$K = \underline{133}\ \text{Btu/ft}^2\text{/day/°F}$$

Using the above values of K and an initial temperature rise of 27°F ($[H_p]/\gamma Q = 27$) we obtain the curves shown in Figure 2-23b. The results for case a) are very poor, with the predicted heat flux less than half the observed loss. Evaluating K at a more correct temperature increases the heat flux significantly, but results are still poor. Case c), involving the proposed evaporation Equation (2.35) gives quite good results.

2.10 Summary

The various components of heat transfer at a water surface have been discussed, and where possible existing empirical formulae have been selected for use in this study. Existing formulae for predicting evaporative flux from an artificially heated water surface were found to be unsatisfactory, and a new formula (Equation 2.35) has been proposed. The proposed formula, a modified form of that given by Shulyakovskiy (1969), explicitly accounts for mass transfer due to free convection, which can be very significant at low windspeeds. The formula has been tested against laboratory and a wide range of field data, and given consistently good results. A linear version of the selected formulae has been described and tested against some additional field data.

III. Simple Steady State Analytical Models

3.1 Introduction

Most existing analytical models for cooling ponds are based on the steady state plug flow or fully mixed concepts. Plug flow requires that there is no mixing between the heated discharge and the receiving water and surface temperatures decrease approximately exponentially from outlet to intake. In contrast, the fully mixed situation requires uniform temperatures throughout the pond, and hence a high degree of mixing. In most cases, neither of these extremes is realistic, and usually it is necessary to compensate for the assumed flow pattern. Plug flow, by maintaining surface temperatures as high as possible, tends to overestimate heat loss. Usually this has been compensated by introducing an "effective area", which is defined as the area of a plug flow pond with the same performance. On the other hand the fully mixed concept, by assuming all temperatures are as low as the intake temperature, underestimates heat loss, and this has been compensated by using optimistic surface heat loss formulae e.g. Throne (1951).

In chemical or sanitary engineering it is common practice (Levenspiel (1963)) to treat cases between the plug flow and fully mixed situation by use of a longitudinal dispersion coefficient, but in a situation such as a pond or a stream it has been shown (50) that use of physically realistic values for a longitudinal dispersion coefficient does not cause significant departure from the steady state plug flow solution. Hence while it is possible to reproduce the behaviour of a cooling pond by backfitting measured results to obtain the re-

quired dispersion coefficient, the resulting analytical model cannot be called predictive. The departure from the ideal plug flow case is due usually to entrance mixing, i.e. mixing by jet induced turbulence at the entrance to the cooling pond. As part of this study, two simple, idealized, steady state, analytical models were developed which clearly demonstrate the important effect of entrance mixing. It can be shown that the plug flow and fully mixed ponds are simply special cases of either of these entrance mixing models. These models, plus a simple two-stage model will be presented, and some other simple analytical models will be discussed.

3.2 Entrance Mixing Models

In considering the effect of entrance mixing, the purpose is not to introduce another fitting parameter, and hence entrance mixing must be defined in such a way that its value can be predicted on the basis of known parameters of the pond. The mixing between a heated discharge and the receiving water does not take place completely at the point of entry, but is a continuous process over a large area. However, at a relatively short distance from the outlet, the mixing induced by the outlet jet becomes rather small, and a stable plateau is usually observed. This behaviour is shown in Figure 3-1a both in terms of the dilution D and the relative centerline temperature rise $\Delta T_c/\Delta T_o$. The entrance mixing will be defined by the dilution D_s that has occured at the stable region, and Figure 3-1b shows the relationship between this dilution D_s, and the discharge densimetric Froude Number F_D, and the outlet aspect ratio A_D. This relationship was

obtained by Stolzenbach, Adams and Harleman (1972) using a mathematical model of a heated discharge. The parameters D_s, F_D and A_D are defined as follows for a rectangular channel of width $2b_o$.

$$D_s = \frac{Q_s}{Q_o}$$

$$F_D = \frac{Q_o/(2h_o^* b_o)}{\sqrt{g \frac{\Delta\rho}{\rho} h_o^*}}$$

$$A_D = h_o^*/b_o$$

where

Q_s = total flow rate at the stable region (i.e. the sum of the outlet flow plus the entrained flow)

Q_o = outlet flow rate

h_o^* = depth of heated layer at outlet

$\Delta\rho$ = initial density difference between the heated discharge and the receiving water

Figure 3-1b shows that the dilution (entrance mixing) is a minimum for F_D equal to unity and A_D small. When $F_D = 1$ a cold wedge may be present in the outlet channel, and hence h_o^* is not necessarily equal to the depth h_o of the outlet channel, but may have to be calculated on the basis of the critical depth of the warm layer as shown in Figure 3-2.

The general case of a cooling pond with both vertical and

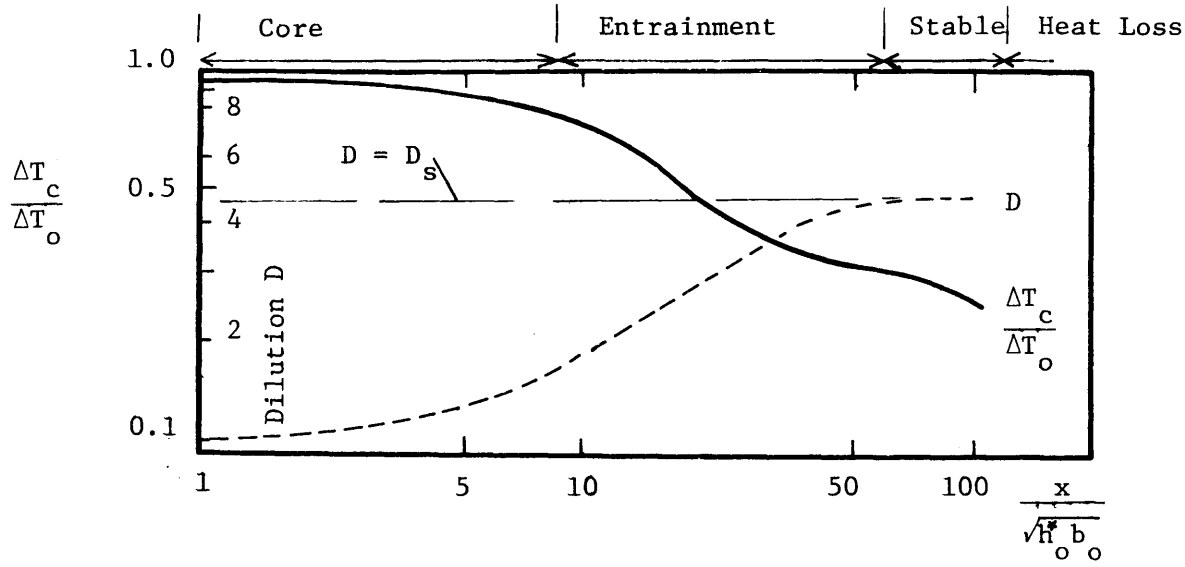

a) Typical Behaviour of a Heated Discharge

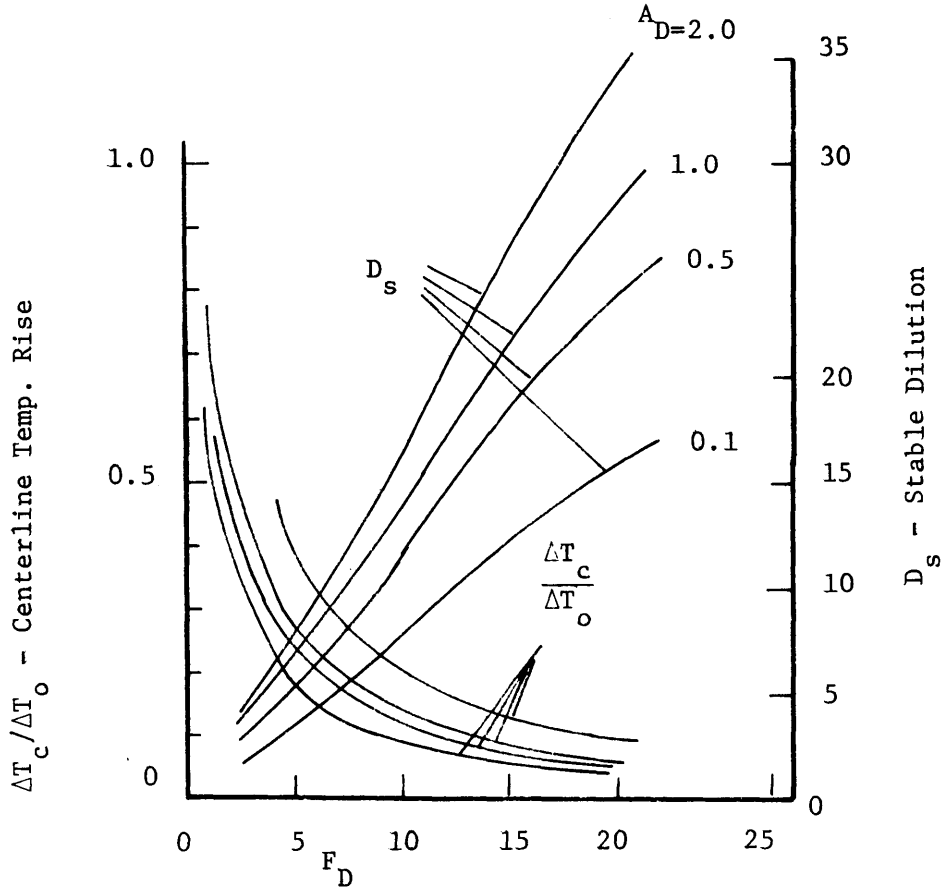

b) Centerline Temp. Rise and Dilution in the Stable Region

Figure 3-1 Heated Discharge Behaviour (Stolzenbach, Adams and Harleman, (1972))

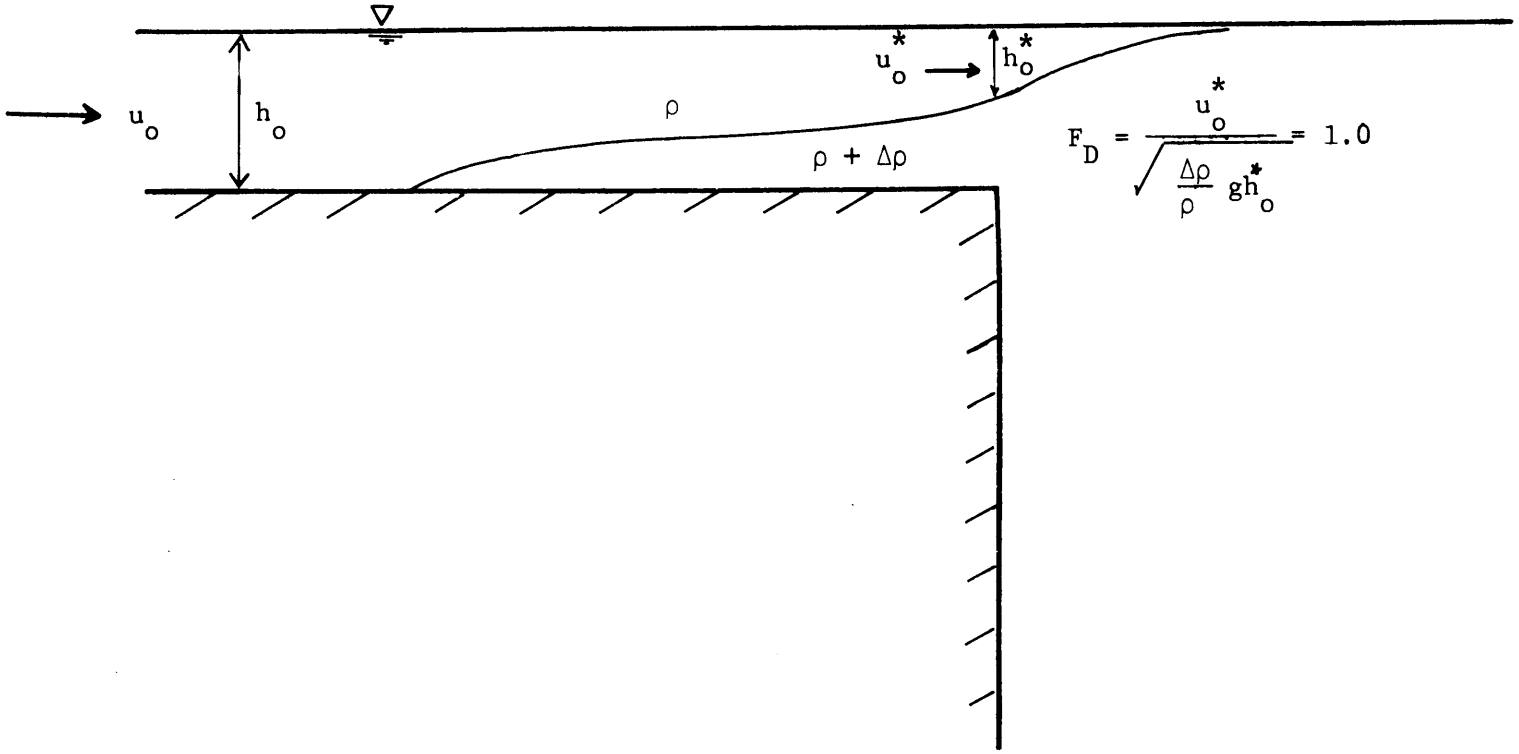

Figure 3-2 Outlet Conditions for Two Layer Flow in a Discharge Channel

horizontal circulations is shown in Figure 3-3.

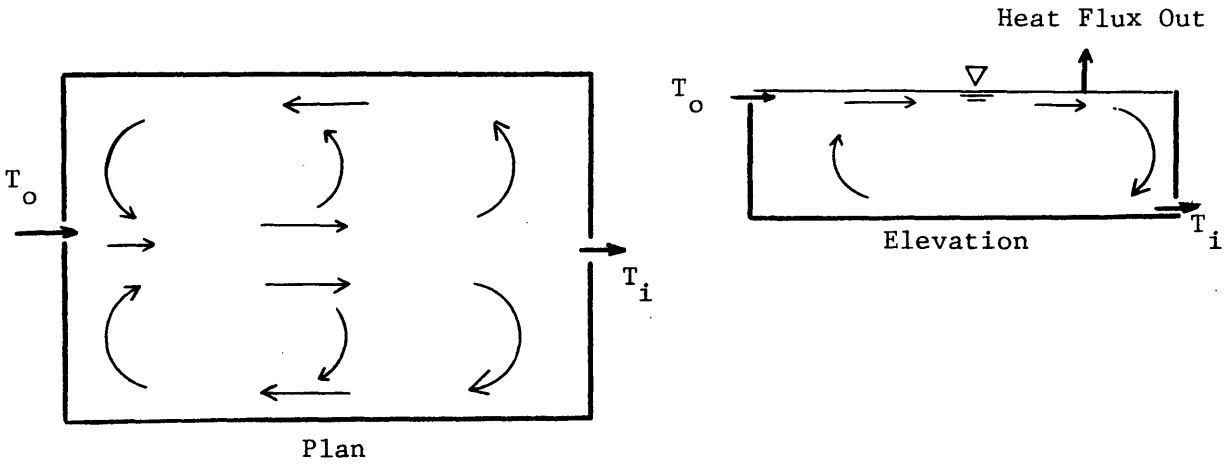

Figure 3-3 Cooling Pond Circulation

The case is rather difficult to solve analytically, and some simplifying assumptions will be made. Two cases will be treated separately, and the case where lateral mixing dominates (e.g. a shallow pond), and the case where vertical mixing dominates (a deep, narrow pond).

SEE ERRATA

In both cases the near field area enclosed by the stable region is assumed to be insignificant in comparison with the total pond area.

3.2.1 Entrance Mixing Model for Shallow Ponds

Consider the following assumptions:

a) Assume that the lateral mixing is very much greater than the vertical mixing. This will be a reasonable assumption in many cases since the vertical mixing is inhibited by density differences between the inflow and the receiving water. Let the dilution due to

lateral mixing be D_s where D_s = 1 represents no mixing.

b) Assume that the pond can be schematized as shown in Figure 3-4 i.e. the mixed flow $D_s Q_o$ (where Q_o is the pumping rate) goes through the pond as a plug flow, and that the return flow $(D_s-1)Q_o$ comes back to the outlet end also as a plug flow. Assume that the areas of the mixed flow zone and the return flow zones are proportional to their respective flow rates. Note that this assumption is not valid for a skimmer wall type intake, since in this case only the coolest water in the surface layer can be removed through such an intake.

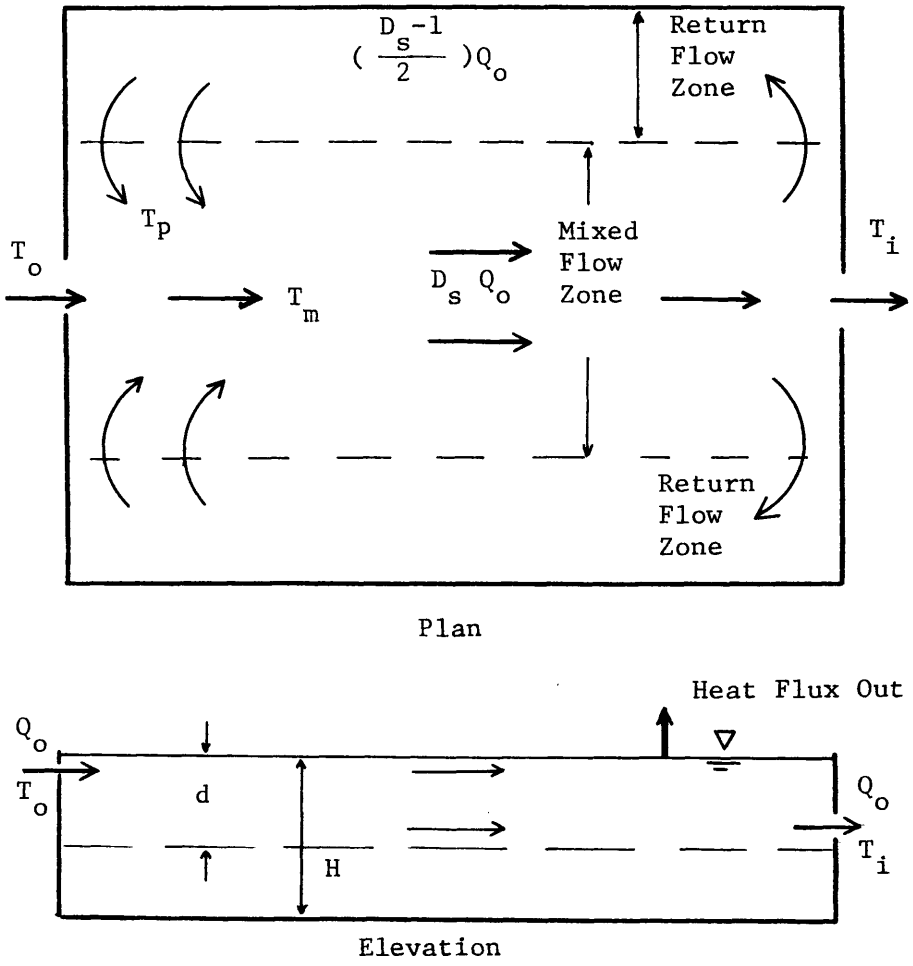

Figure 3-4 Shallow Cooling Pond - Horizontal Circulation Only

c) Assume that the total surface area of the pond (A_p) plays an active part in the heat dissipation, but that only depth d of the total depth H is affected.

d) Complete vertical mixing exists in the surface layer, depth d.

Let T_o = outlet temperature

T_p = temperature of the mixing water

T_m = temperature of the mixed discharge

T_i = intake temperature

Q_o = pumping rate

A_p = total surface area of pond

ρ = density

c = specific heat

d = depth of active layer

Therefore

$$T_m = \frac{Q_o T_o + (D_s - 1)Q_o T_p}{D_s Q_o} = \frac{T_o + (D_s - 1)T_p}{D_s} \qquad (3\text{-}1)$$

Consider the heat loss in the mixed flow zone of area A_1 where

$$A_1 = \frac{D_s}{2D_s - 1} \cdot A_p$$

For steady state the basic 1 - D heat transport equation (neglecting longitudinal dispersion) is

$$\frac{\partial}{\partial x}(u\, T_s) = \frac{K}{\rho c d}(T_s - T_E) \qquad (3.2)$$

where u = velocity in the x direction. Assuming the width of the mixed flow zone is equal to a constant b_1, u is given by

$$u = \frac{D_s Q_o}{b_1 d} \tag{3.2a}$$

Thus

$$\frac{DQ_o}{b_1 d} \frac{\partial T_s}{\partial x} = \frac{K}{\rho c d} (T_s - T_E) \tag{3.3}$$

Eliminating d and noting that $b_1 dx = dA$ leads to

$$\frac{dT_s}{dA} = \frac{K}{\rho c D_s Q_o} \tag{3.4}$$

This is the familiar steady state decay equation which has the solution

$$\frac{T_i - T_E}{T_m - T_E} = e^{-r_1} \tag{3.5}$$

where

$$r_1 = \frac{KA_1}{\rho c D_s Q_o} = \frac{KA_p \frac{D_s}{2D_s - 1}}{\rho c D_s Q_o} = \frac{KA_p}{\rho c (2D_s - 1) Q_o} \tag{3.5}$$

Note that neither the active depth d, nor the total depth, H, appear in the solution.

In a similar fashion to the mixed flow, the temperature in the return flow is given by

$$\frac{T_p - T_E}{T_i - T_E} = e^{-r_2} \tag{3.6}$$

where

$$r_2 = \frac{KA_2}{\rho c(D_s - 1)Q_o} = \frac{KA\,\frac{(D_s - 1)}{(2D_s - 1)}}{\rho c(D_s - 1)Q_o}$$

$$= \frac{KA}{\rho c(2D_s - 1)Q_o} = r_1$$

After some manipulation of Equations (3.1), (3.5) and (3.6) it is found that

$$\frac{T_i - T_E}{T_o - T_E} = \frac{e^{-r(2D_s-1)}}{D_s - (D_s - 1)e^{-2r/(2D_s-1)}} \qquad (3.7)$$

where

$$r = \frac{KA_p}{\rho c Q_o}$$

The intake temperature T_i represents a weekly or a monthly average depending on the data used to determine the surface exchange coefficient K, and the equilibrium temperature T_E.

The solutions are plotted in Figure 3-5 and the marked effect of entrance mixing on pond performance is clearly seen. It will be shown that the curves for no mixing ($D_s = 1$) and for high mixing ($D_s >> 1$) are identical to the curves for plug flow and for the fully mixed case respectively. The circulation pattern assumed here may not be very realistic, and the principal value of this model may be to indicate the importance of entrance mixing.

3.2.2 Entrance Mixing Model for Deep Ponds

For a deep, relatively narrow pond, lateral mixing may be

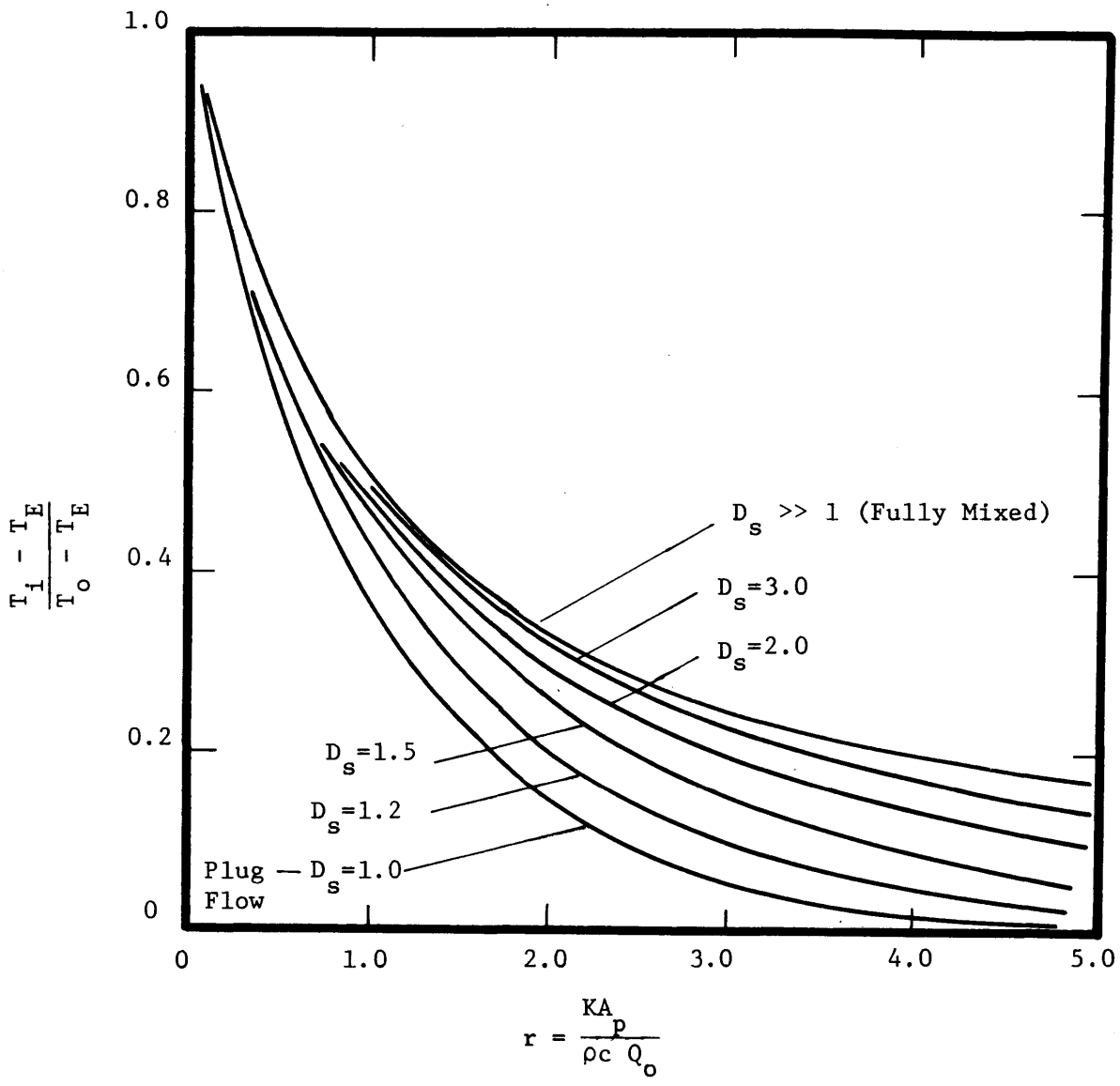

Figure 3-5 Intake Temperatures for a Shallow Pond with Entrance Mixing

suppressed by the pond boundaries. A different schematization to that for a shallow pond is required, and the following assumptions are made:

a) It is assumed that the pond can be schematized as shown in Figure 3-6. The heated discharge (flow rate Q_o, temperature T_o) is mixed with the pond water (dilution D_s), and the mixed flow ($D_s Q_o$) proceeds to the end of the pond as a plug flow, sweeping through the full area of the pond surface. The return flow $(D_s - 1)Q_o$ comes back under the surface to the outlet where it is re-entrained, while the flow, Q_o, proceeds under the surface to the intake. In contrast to the shallow pond, the intake temperature is now equal to the lowest surface temperature, and the mixing flow does not return at the pond surface.

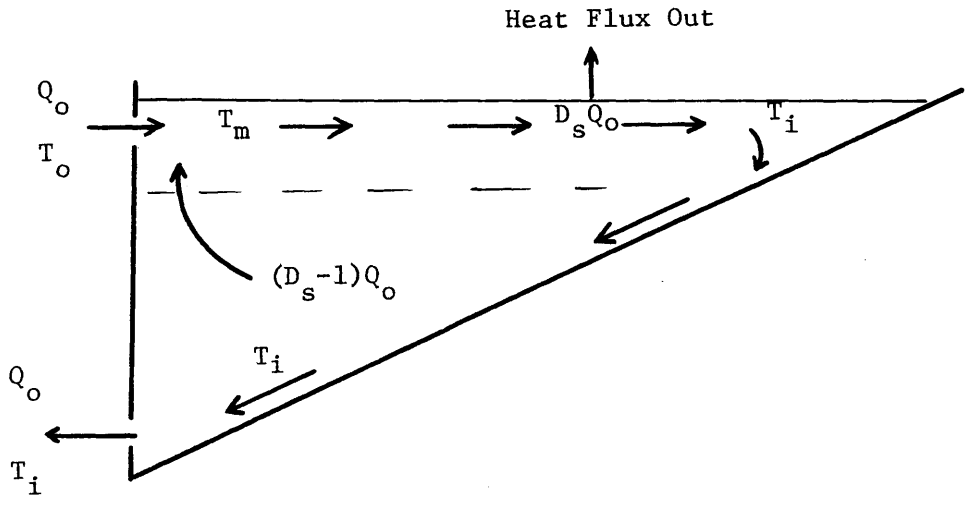

Figure 3-6 Schematization of a Deep Pond

b) The temperature of the entrained flow is assumed equal to the intake temperature. One way of achieving this is for lateral mixing to be completely inhibited.

c) The total surface area of the pond is assumed to be effective in dissipating heat.

Using the same symbols as for the shallow pond, the following equations are obtained:

$$T_m = \frac{T_o + (D_s - 1)T_i}{D_s} \tag{3.8}$$

$$\frac{T_i - E}{T_m - E} = e^{-r_3} \tag{3.9}$$

where

$$r_3 = \frac{KA_p}{\rho c D_s Q_o}$$

From Equations (3.8) and (3.9) one obtains, after some manipulation, the following equation

$$\frac{T_i - T_E}{T_o - T_E} = \frac{e^{-r/D_s}}{D_s - (D_s - 1)e^{-r/D_s}} \tag{3.10}$$

The results are plotted in Figure 3-7. Comparison with Figure 3-5 shows that mixing has conisderably less effect in a deep pond than in a shallow one, where the return flow takes place at the surface, i.e. where large horizontal eddies are induced.

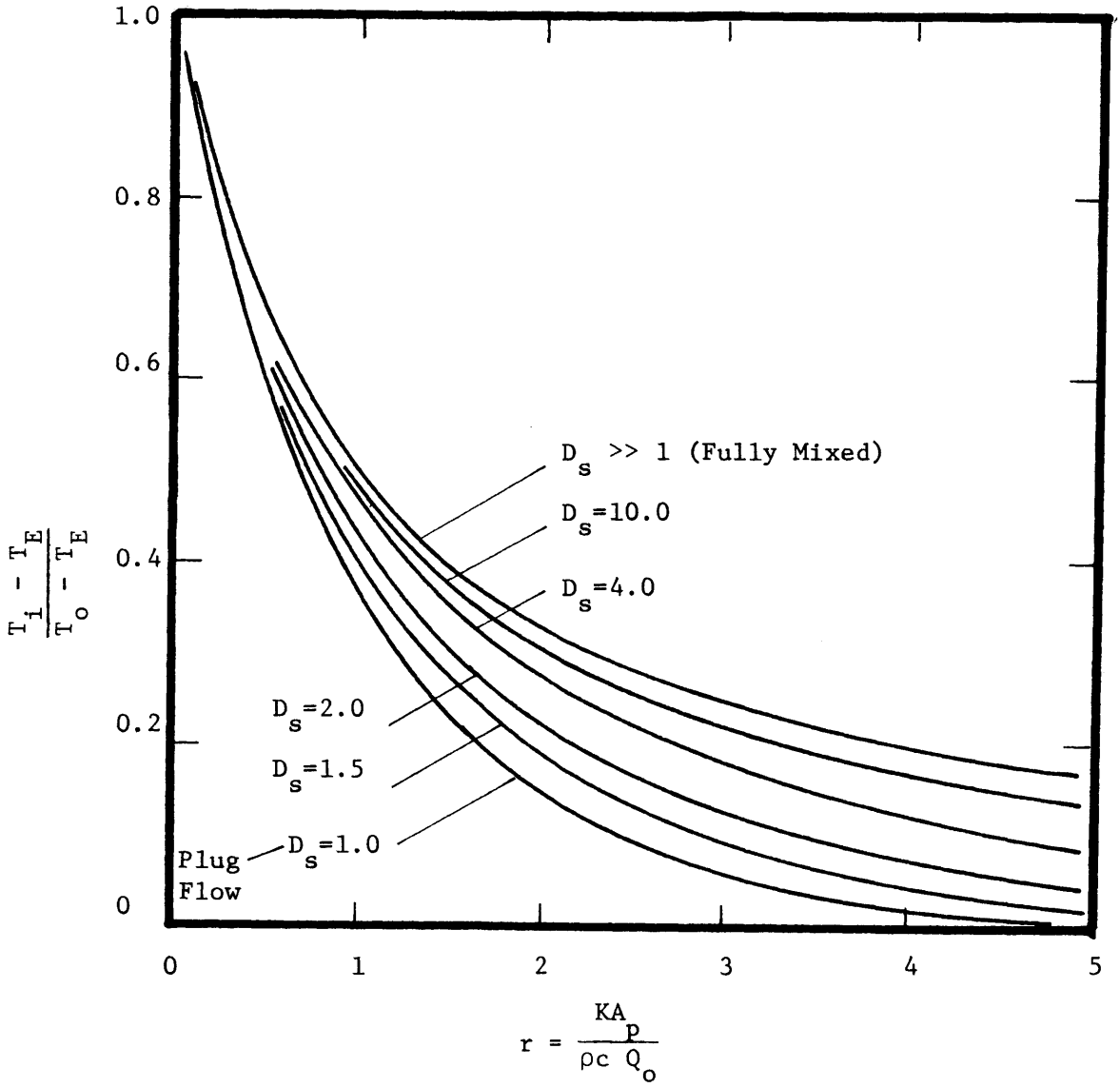

Figure 3-7 Intake Temperature of a Deep Cooling Pond with Entrance Mixing

Note that this model is very close to the ideal pond configuration discussed in Chapter 1. The assumption that the temperature of the entrained water is equal to the intake temperature is not unrealistic. In the laboratory cooling pond, a deep, stratified pond with a low intake, significant lateral mixing took place, but nevertheless it was observed that the temperature of the entrained water was not markedly different from the coolest surface temperatures (i.e. intake temperatures at steady state).

It can be seen that the limiting cases of no mixing ($D_s = 1$) and high mixing ($D_s >> 1$) give the same curves as for the shallow pond, but the intermediate curves are markedly different, and a dilution of 4 in the deep pond has less effect than a dilution of 2 in the shallow pond.

The plug flow and the fully mixed ponds are special cases of either of the more general entrance mixing models and these will now be discussed.

3.3 Plug Flow Models

The equation for a plug flow pond can be obtained from Equation (3.7) or (3.10) by setting $D_s = 1$, giving

$$\frac{T_i - T_E}{T_o - T_E} = e^{-r} \qquad (3.11)$$

the same equation as that given by Edinger and Geyer (1965). From Figure 3-7 it can be seen that the plug flow pond is the most efficient type of pond, but unless the cooling pond is a narrow channel, the plug flow requirement of zero mixing is almost impossible to

obtain, and $D_s = 1.5$ is a practical minimum. Langhaar (1953) used the plug flow configuration as the basis for his design nomographs, and Hogan et al (1970) based some of their models on this concept. The only significant difference between the Edinger and Geyer model and the models of Hogan et al. is the introduction by the latter of a linear vertical temperature gradient. A mean vertical temperature gradient does exist, due primarily to selective absorption of solar radiation. Note, however, that this gradient must be intermittent as otherwise there would be no mechanism to replenish the cooler bottom waters.

3.4 Fully Mixed Ponds

For the case of high mixing it can be shown that both of the general cases approach the fully mixed case of Edinger and Geyer (1965).

For $D_s >> 1$, $\quad e^{-r/D_s} \simeq 1 - r/D_s$

From Equation (3.10)

$$\frac{T_i - T_E}{T_o - T_E} \simeq \frac{1 - r/D_s}{D_s - (D_s - 1)(1 - r/D_s)} = \frac{1 - r/D_s}{1 + r - r/D_s}$$

and

$$\frac{T_i - T_E}{T_o - T_E} \simeq \frac{1}{1 + r} \qquad (3.12)$$

the same equation as in (29). Equation (3.12) could have been obtained directly by assuming that the surface temperature is uniform and equal to the intake temperature. The fully mixed curve is shown in

Figure 3-7 and it is readily seen that this type of pond is the least efficient.

The fully mixed concept has been used by Lima (1931) as a basis for his design curves, and has also been used by Hogan et al (1970). A modification to the fully mixed concept, which involves complete horizontal mixing but some vertical stratification, has been used by Throne (1951) and Hogan et al (1970). Throne's model is of particular interest, both because of its simplicity and because it is based on very extensive field data, and this model will be discussed in some detail.

3.4.1 Throne Model

Throne (1951) based his model on 25 years of records from a small (120-210 acre) moderately loaded (35-140 Btu/ft^2/hr) lake in Colorado. It was observed that the surface temperature was approximately constant over the area, and was about 2°F warmer than the intake temperature. A schematic view of Throne's model is shown in Figure 3-8.

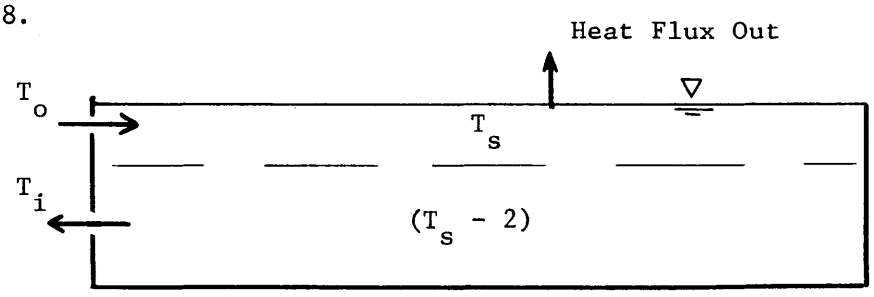

Figure 3-8 Throne's Model (1951)

For the steady state case the heat rejected by the power plant

H_p is dissipated from the pond surface, therefore $H_p = KA(T_s - E)$ which leads to $T_s = H_p/KA + E$, which is identical with the fully mixed case. However, the intake temperature and hence the outlet temperature is 2°F below that in the fully mixed case.

Throne claims that of the 298 months in the study, 98.6% of the predicted average monthly temperatures fell within ±5°F and 87.8% within ±3°F. This is quite impressive, but it should be pointed out that the physical model proposed by Throne is incorrect. He assumes that the discharged water forms a thin film, approximately .003 ft. thick on the lake surface, but this is not feasible as velocities of the order of 100 ft/sec in this top layer would result. The probable cause for the observed behaviour is the direct absorption of short wave radiation setting up temperature gradients during the day (when measurements are normally taken). Even if these vertical gradients are destroyed each night, the average surface temperature is a few degrees Fahrenheit higher than the fully mixed temperature. The uniform surface temperature is probably due to high entrance mixing. Throne's idea of treating the surface temperature as a few degrees higher on the average than the fully mixed temperature is probably a good one, even if the mechanism suggested by him is incorrect. Lamb (1958) criticizes Throne's work on the grounds that he measured wind speed at 5 ft. instead of 1 ft. above the water surface, which is incorrect since Rohwer's evaporation formula was used. In effect Throne proposed a new evaporation formula. This has been previously discussed in Chapter 2, where it was seen that Throne's formula tended to be somewhat high.

3.5 Comparison of Plug Flow and Fully Mixed Models

An interesting comparison was made by Edinger and Geyer (1965) of the relative area required by plug flow and fully mixed ponds to achieve a specified amount of cooling. From Equation (3.11) and (3.12) one obtains for the same pond surface area A_p

$$\frac{(T_i - T_E)_m}{(T_i - T_E)_p} = \frac{e^r}{1 + r} \tag{3.13}$$

where the subscripts (m) and (p) refer to the fully mixed and plug flow case respectively. The advantage of the plug flow pond, particularly for cases where $T_i \to T_E$ (i.e. r is large) is clearly illustrated in Table 3-1.

Table 3-1

Ratio of Area Required for Completely Mixed Pond to that of a Plug Flow Pond to Produce the Same Temperature Excess under Similar Loading and Cooling Conditions (29)

Temperature Excess Ratio $\frac{T_i - E}{T_o - E}$	Ratio of Areas A_{p_m}/A_{p_p}
0.8	1.12
0.7	1.20
0.6	1.30
0.5	1.44
0.4	1.64
0.3	1.95
0.2	2.47
0.1	3.87

3.6 Two Stage Model

A model which is more realistic than a plug flow or fully mixed model is a two stage model consisting of a fully mixed initial area followed by a plug flow area. Such a model is applicable when the shape of the pond confines eddies, generated by the inflow, to a limited area, as in Figure 3-9.

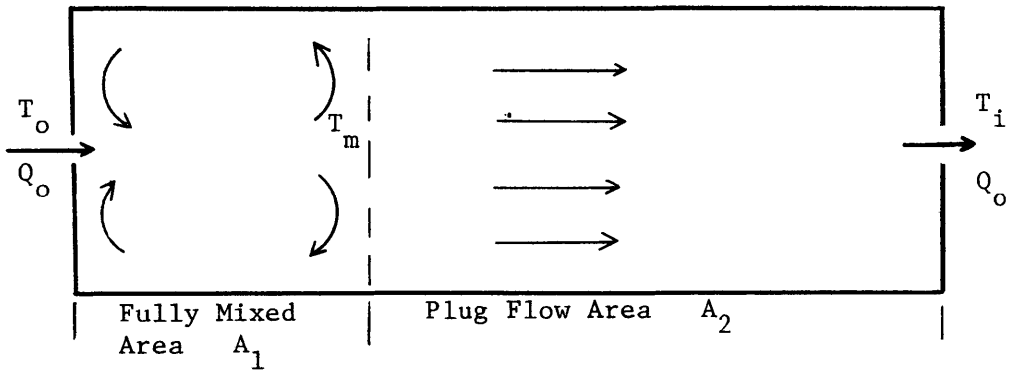

Figure 3-9 Two Stage Pond

Let

A_1 = area of fully mixed pond

A_2 = area of plug flow pond

A_p = total pond area

T_m = temperature of fully mixed pond

$p = A_1/A_p$

$r = KA_p/\rho cQ_o$

In the fully mixed region Equation (3.12) gives

$$\frac{T_m - T_E}{T_o - T_E} = \frac{1}{1 + pr} \tag{3.14}$$

In the plug flow region Equation (3.11) gives

$$\frac{T_i - T_E}{T_m - T_E} = e^{-(1-p)r} \qquad (3.15)$$

From Equations (3.14) and (3.15)

$$\frac{T_i - T_E}{T_o - T_E} = \frac{e^{-(1-p)r}}{1 + pr} \qquad (3.16)$$

which reverts to the equation for a fully mixed or plug flow pond for p = 1 or zero respectively. Figure 3-10 shows the effect of increasing the fully mixed area on pond efficiency, and compares the effect of limiting the fully mixed area, with the effect of limiting the entrance mixing itself. Surprisingly, it is just as effective to limit the area of the fully mixed region to 50% of the total area, as it is to limit the entrance mixing to the rather low value of $D_s = 1.5$.

3.7 Concept of Effective Area

As mentioned in Section 3.1 the limitation of the plug flow assumption has often been compensated by the introduction of an "effective" surface area which is less than the actual area. The basic assumption is that areas such as eddies, backwaters, etc., do not play an active role in heat dissipation. In some cases this may be true, and several methods have been proposed for estimating the "effective" area" or "area of the active zone" which is defined by Berman (1961) as the area of a perfect plug flow pond with equivalent performance. These methods, by Berman (1961) and Edinger (1971) will be briefly discussed.

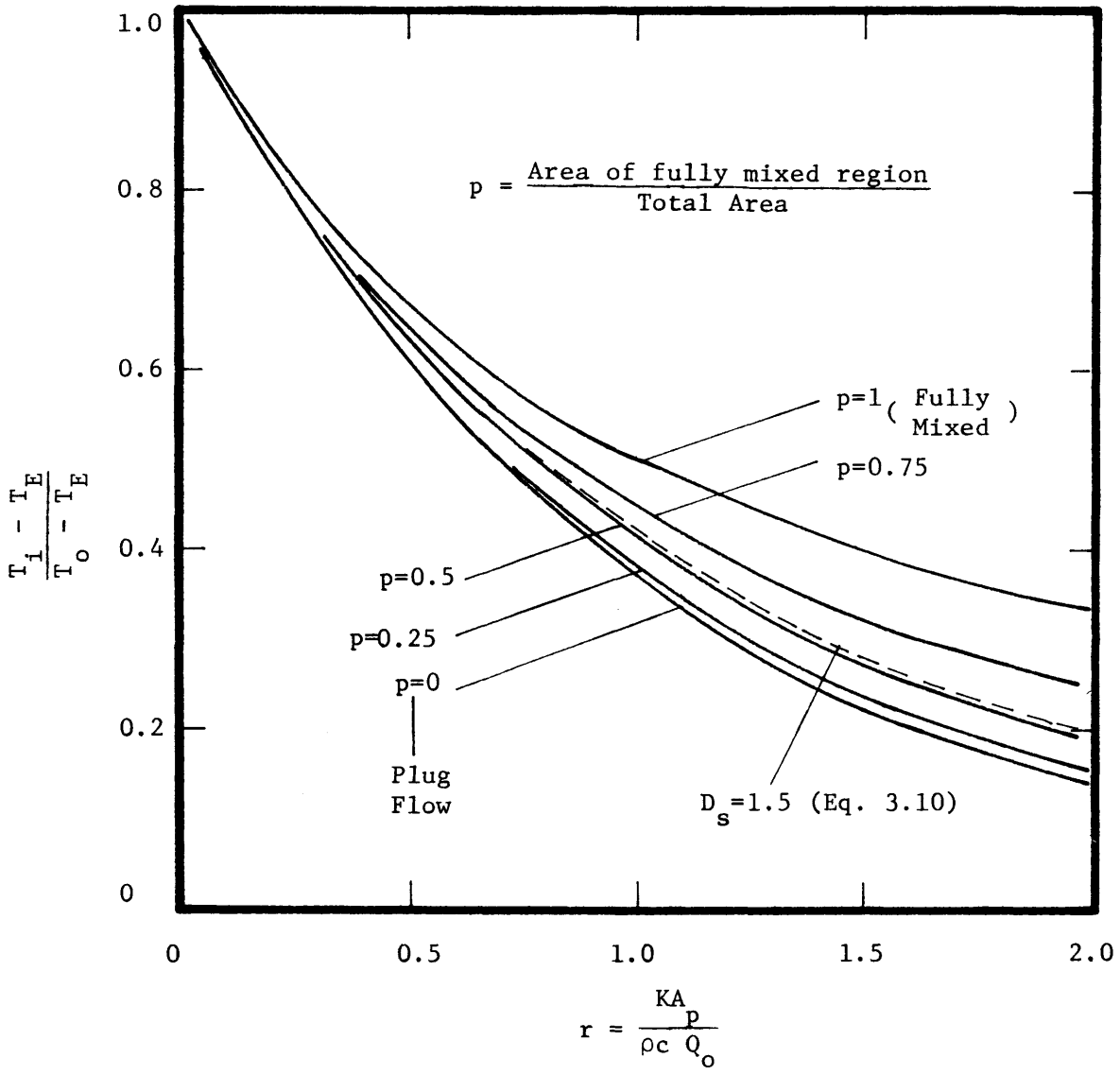

Figure 3-10 Intake Temperatures for Two Stage Pond

a) Berman's Method

Berman gives an approximate method for calculating the area of the active zone A_f. The flow plan must first be obtained on the basis of calculations or by experiments. The areas of the flow-through zone A_{th} and the area of the eddy zones a_e are obtained.

$$A_f = k_{th} A_{th} + \Sigma k_e a_e \qquad (3.17)$$

where

k_{th} = coefficient of through flow utilization

= 0.8 - 0.9 -- long narrow ponds

= 0.5 - 0.7 -- circular ponds

k_e = coefficient of eddy utilization

where for

a_e/A_{th} =	0	1	2	3	5	10
k_e =	1	.6	.4	.3	.2	.1

The ratio of the "area of the active zone" A_f to the total area A_p is called the "coefficient of utilization", or "effective area" ratio k_u. For long narrow ponds or those with effective stream guiding and distributing equipment, Berman gives k_u = 0.8 - 0.9, but for ponds with circular, or very irregular shapes, without stream guiding equipment, k_u may be as low as 0.4 - 0.5. Mean values for badly shaped ponds are given as 0.60 - 0.75.

b) Edinger's Method

A more sophisticated method, which is applicable to vertically mixed ponds, has been proposed by Edinger (1971). The pond is divided

into a main flow arm and side arms as shown in Figure 3-11. Plug flow

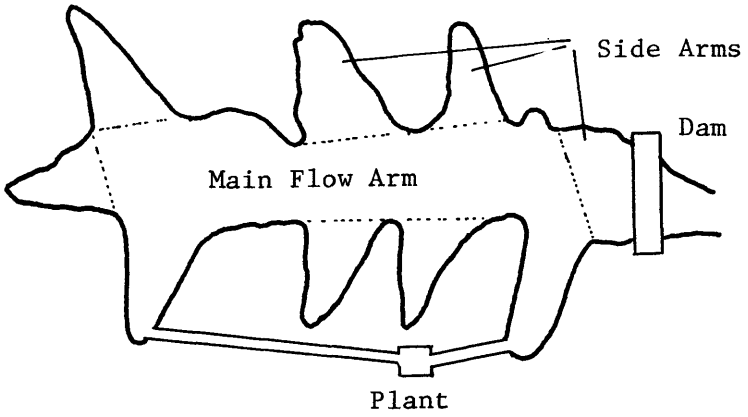

Figure 3-11 Edinger's Model (1971)

is allowed to take place along the main arm, and heat is allowed to diffuse into the side arm areas. An approximate value of the diffusion coefficient is assumed. An analytical expression is obtained for the intake temperature, and from this the effective area is easily obtained.

Neither of the above methods is particularly convincing. Berman's method requires knowledge of the pond circulation pattern, which he implies can be obtained on the basis of potential flow calculations or by use of hydraulic models. However, prototype Reynolds numbers ($\sim 10^5$) are somewhat low for potential flow calculations, and density effects even if not dominant, complicate matters. The use of hydraulic models has very severe limitations as discussed in Section 5.8. Edinger's assumption of diffusion of heat into the side arms of the pond is rarely valid since this is primarily an advective process. A second weakness is that entrance mixing is accounted for incorrectly. Nevertheless, Edinger's approach may be useful for comparing different

intake-outlet locations in a shallow pond.

3.8 Conclusion

Existing analytical models are steady state, one-dimensional, and based on the extreme concepts of plug flow or complete mixing. These models are usually not predictive and require a fitting parameter such as "effective area" to match observed results. The concept of "effective area" and some methods for its determination have been discussed.

Some simple analytical models have been proposed which consider the effect of entrance mixing, and these models include the plug flow and fully mixed ponds as special cases. The entrance mixing factor can be determined a priori from known pond parameters, and thus these proposed models, although highly idealized, and limited to the steady state case, are predictive. In the next chapter the observed behaviour of cooling ponds, both in the laboratory and the field will be considered, and in Chapter 5, the performance of the above models, plus that of existing transient models will be discussed.

IV. Observed Cooling Pond Behaviour

4.1 Introduction

Before the limitations of existing cooling pond models can be properly discussed, it is necessary to examine what is known of cooling pond behaviour. The models can then be discussed in terms of how effectively they simulate the more important observed characteristics. As mentioned in Chapter 1, the primary objective of this study is to determine the most effective types of cooling ponds. These exhibit vertical stratification, and thus in this section the emphasis will be on the behaviour of stratified ponds. The criteria for stratification to occur, and some reasons for the increased effectiveness of stratified ponds,will be discussed later in this chapter.

4.2 Data Sources

Observations on cooling pond behaviour are available both for laboratory and field situations. As part of this study, an intensive series of tests were carried out in the Ralph M. Parsons laboratory at M.I.T. in an attempt to learn more about the behaviour of cooling ponds. Particular attention was paid to the effect of entrance mixing and density currents on overall pond performance. The laboratory pond is 42' x 22' x 1'. Approximately 100 temperature probes were used, about 60 of these in one horizontal plane, which could be adjusted vertically to give the three-dimensional temperature structure. The pond geometry is shown in Fig. 4-1. The geometry of the discharge channel could be adjusted and inflow and outflow rates were varied from 5 to 20 gpm. The densimetric Froude Numbers at the outlet (based on channel

depth) varied from 0.2 to 6. Outlet temperatures were ∿ 112°F while intake temperatures varied from 80-97°F. Complete details of the experiments are given in Chapter 7.

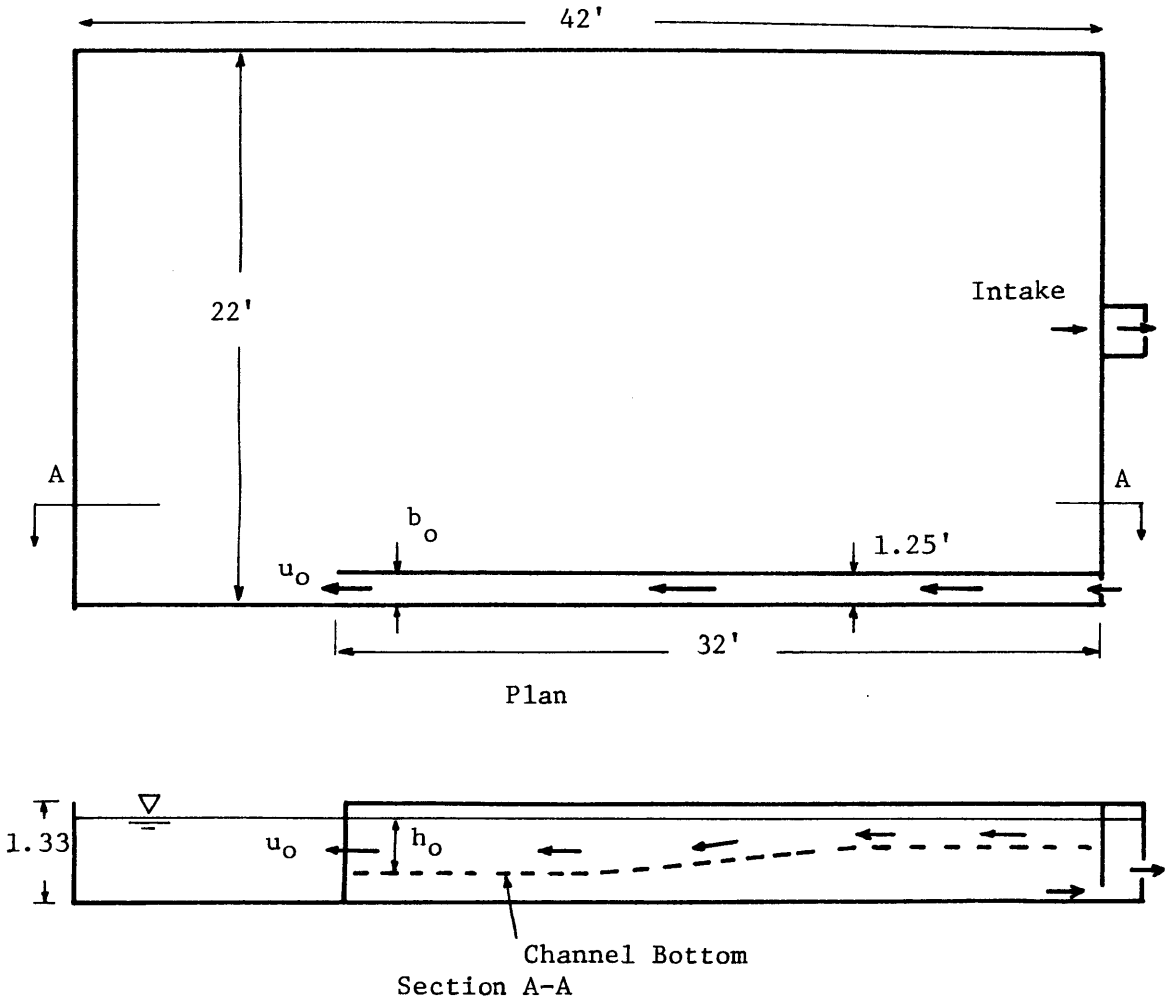

Figure 4-1 Laboratory Cooling Pond

Where possible the laboratory observations have been supplemented by field data. Unfortunately, the latter are rather scarce. Field observations were taken in the Hazelwood cooling pond (Aust.), 1250 acres, 1600 Mw, average depth 20 ft.; the Maitland pond (Aust.), 40 acres, 20 Mw, average depth 20 ft.; Lake Trawsfynydd (U.K.), 1350 acres,

500 Mw (nuclear) average depth 20 ft.; and Lake Norman (N.C.), 32,000 acres, 2200 Mw, Max. depth 120 ft. Tracer tests using dye and radioactive iodine were carried out in the Maitland pond, and extensive temperature surveys were made in all the ponds.

Cooling pond behaviour will be discussed under the following headings:

a) thermal structure

b) circulation patterns including density currents and their effects

c) entrance mixing and its effects

d) transient pond response

e) wind effects

4.3 Thermal Structure

4.3.1 Laboratory Pond

The temperature structure exhibited by the laboratory pond was quite complex, temperature gradients existed in both the horizontal and vertical planes. However, there is one unique aspect to the structure which should be noted, as it determines the choice of the mathematical model in Chapter 6. The horizontal gradients tend to occur only in a relatively thin surface layer (~0.1 ft). Underneath the surface layer, temperature variations occur only in the vertical direction, as in a deep reservoir (57). Figure 4-2 illustrates this type of structure. The thickness of the surface layer is determined primarily by the design of the outlet structure. The heated water moves away from the point of discharge, cooling both by entrainment of the receiving

Isotherms in Laboratory Cooling Pond ($t^* = 0.9$)

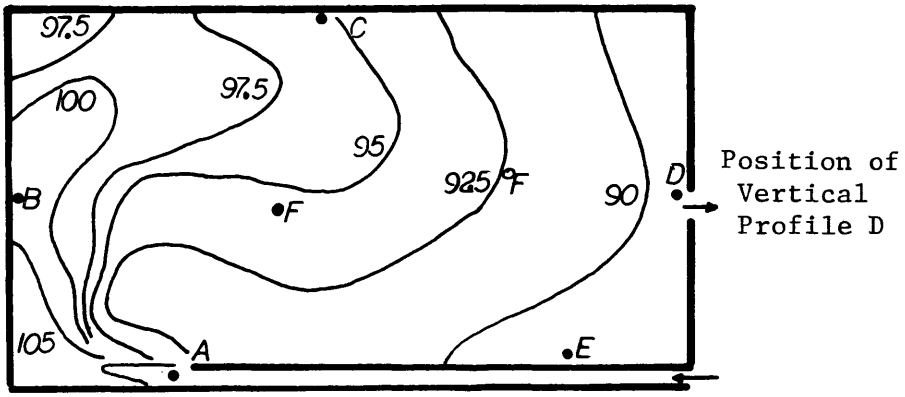

Temperature °F

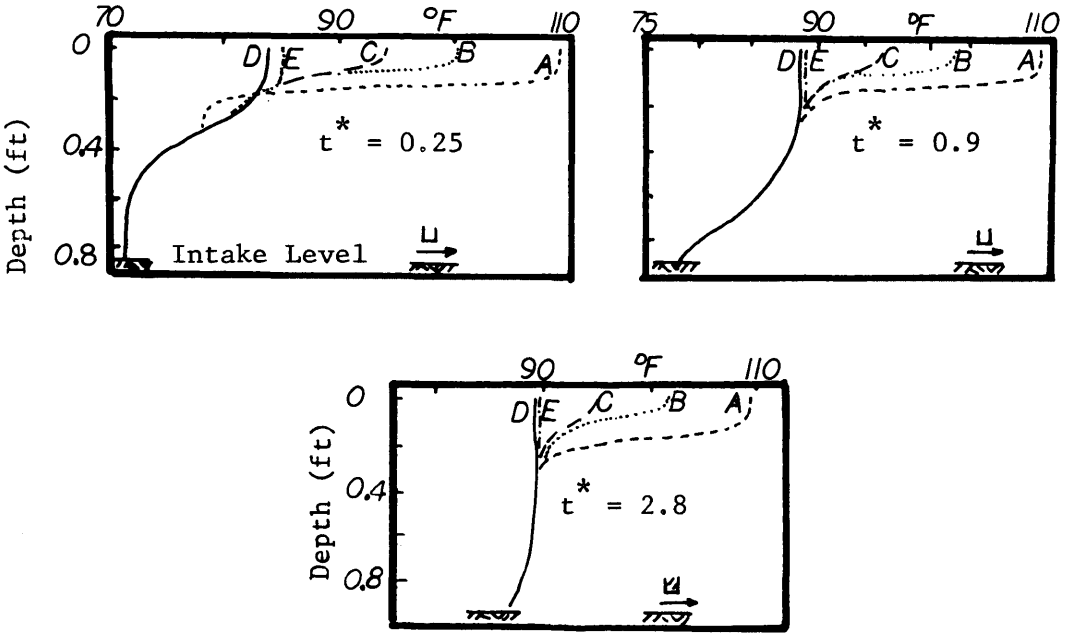

Figure 4-2 Thermal Structure in Laboratory Cooling Pond Under Transient Conditions

waters and by surface heat loss. After a relatively short distance, entrainment ceases to be important. The discharge continues to spread and to cool until it reaches the pond boundaries. The various zones are illustrated by the observed surface temperature distribution in Figure 4-3. At the boundaries the cooled water is forced to move downwards and forms a layer just underneath the surface layer. This cooled water is advected downwards towards the intake level. Figure 4-2 shows this process for the case of a pond after an increase in loading. The non-dimensional time $t^* = (t/\hat{t})$ where t is the time after increase in loading, and $\hat{t}$ is the fully-mixed pond residence time and is given by $\hat{t} = (\forall/Q)$ where $\forall$ is the pond volume and Q is the flow-through rate. At steady state all the lower layers should reach the same temperature as the coolest areas at the surface, and these areas, usually those farthest from the discharge point, may be neutrally stable. Any load decrease, after a period of steady state, will cause complete vertical mixing over the full depth in these areas. In the laboratory cooling pond there was always some heat loss through the concrete floor. This heat loss was monitored, and it was found that the gradients near the bottom corresponded to molecular diffusion of heat in this region.

4.3.2 Field Cooling Ponds

Figure 4-4 shows that field cooling ponds exhibit a similar type of structure. It was noted that the warm surface layer in Figure 4-4 can be disrupted by winds of more than 15 mph. Similar behaviour was reported by McMillan (1971) in Lake Trawsfynydd.

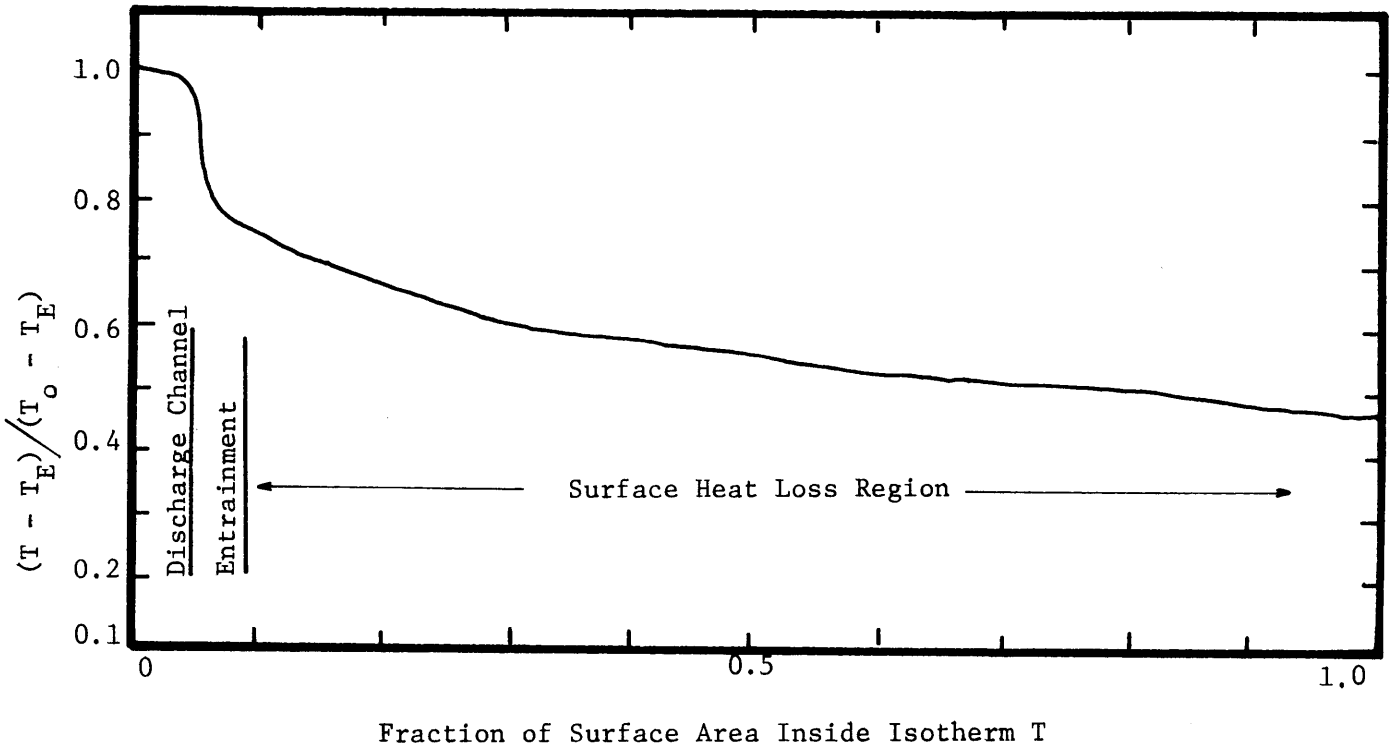

Figure 4-3 Zones of Temperature Decrease in a Cooling Pond

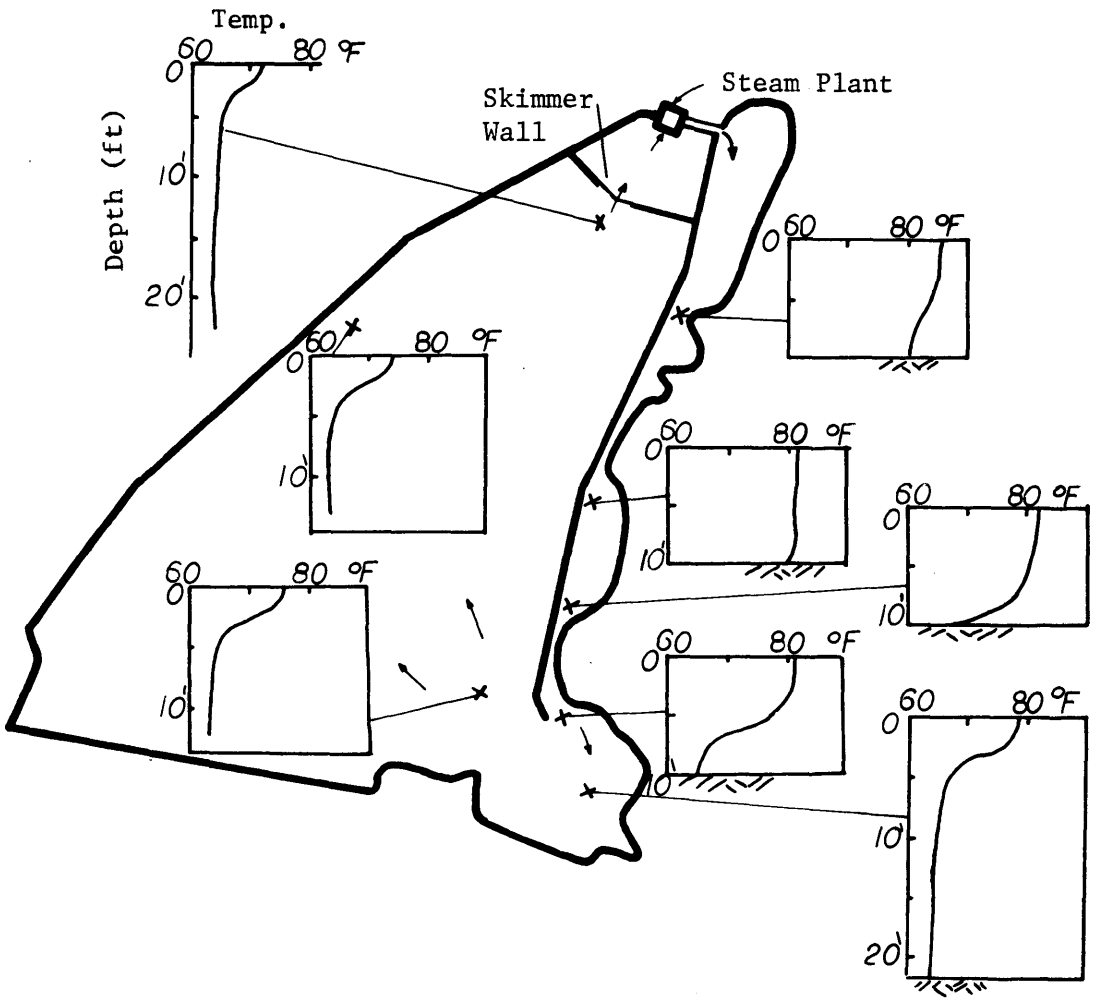

Figure 4-4 Temperature Structure in Hazelwood Cooling Pond (130,D3)

The temperature structure in a deep, lightly loaded reservoir is shown in Fig. 4-5. Here the area in which horizontal gradients are important is considerably smaller than the total area.

The diurnal fluctuations discussed in Chapter 6 will be superimposed on the type of temperature structure shown for the laboratory case, and this complicates matters further for the field case. For example the temperature profile in front of the skimmer wall in Figure 4-4 is due to unsteady conditions, probably diurnal effects.

4.4 Circulation Patterns in Cooling Ponds

Currents in cooling ponds are a result of three mechanisms, pumping (i.e. inflow-outflow), density differences and wind stresses. Previous approaches to cooling pond design have tended to neglect the latter two mechanisms, e.g. hydraulic models of cooling ponds under isothermal conditions have been used as design aids. However, McMillan notes that field observations in Lake Trawsfynydd showed that wind induced currents were an order of magnitude higher than density currents. While it may be reasonable to neglect wind effects on the grounds that critical heat loss conditions will occur under low winds, density currents may not be neglected. Observations, both in the laboratory and the field have tended to support the conclusion. Averkiev, et al (1971) note that density currents govern cooling pond behaviour both in the laboratory and the field.

SEE ERRATA

4.4.1 Density Currents in the Laboratory Pond

A series of tests were carried out in the M.I.T. laboratory pond with specific objective of determining the magnitude of density

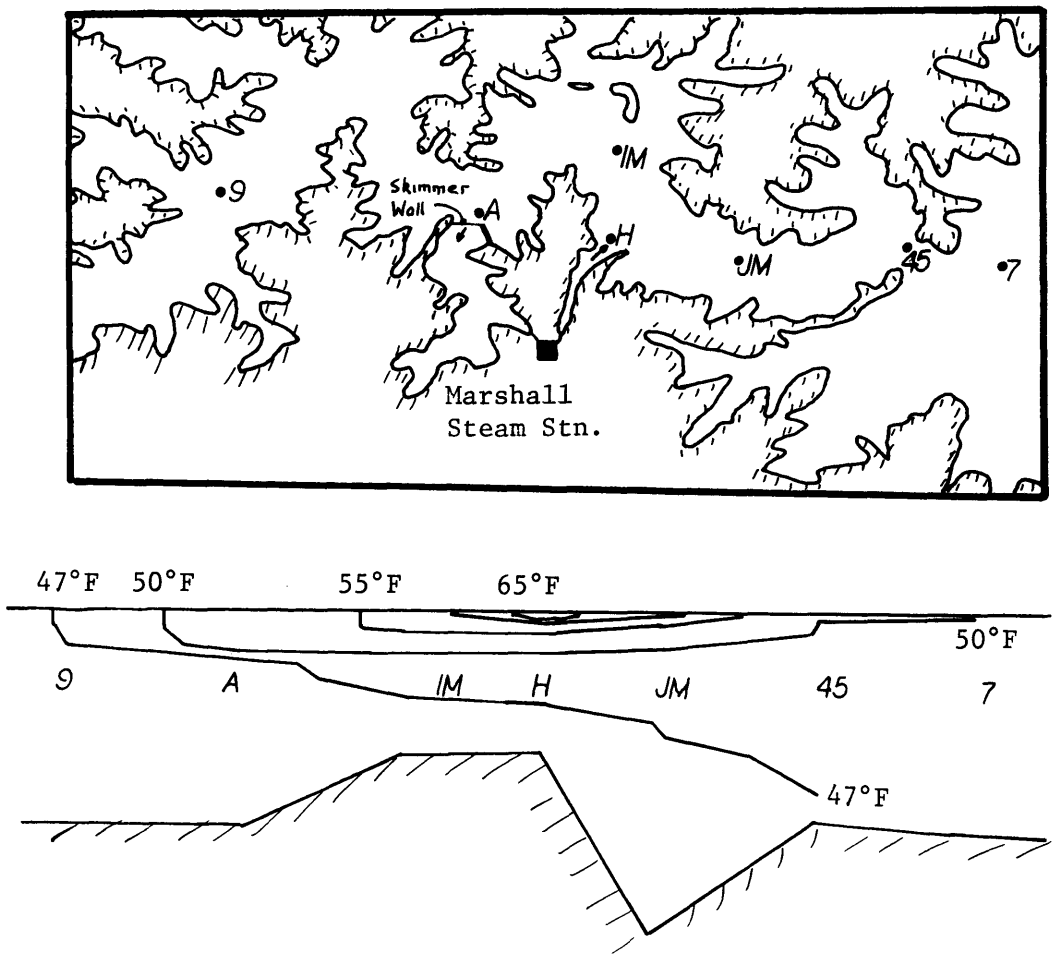

Figure 4-5 Vertical Isotherms - Lake Norman, North Carolina

currents and their overall effects. Baffles were inserted in the pond as shown in Figure 4-6.

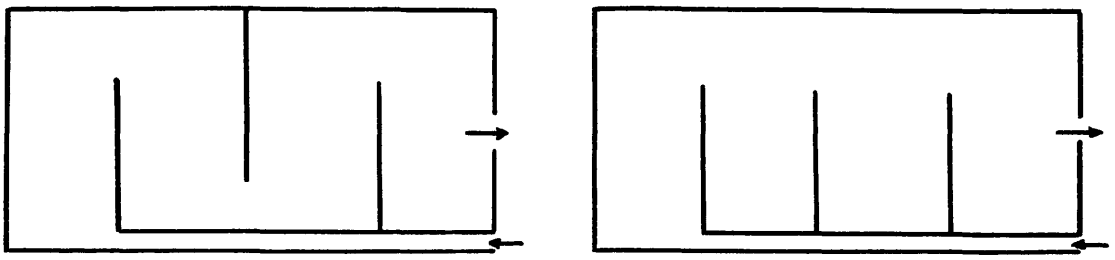

Pond A - Flow Through Pond B - Backwater

Figure 4-6 Pond Geometry to Test Density Current Behaviour

It can be seen that pond geometry A should result in a highly effective pond, whereas pond geometry B, with a high percentage of backwater areas should be ineffective, unless strong density currents are present. In pond A a mixing region is followed by a long narrow plug flow region. The heated discharge moves more or less directly from outlet to intake and pond A will be referred to as a flow-through pond. The flow-through pond is similar to the two-stage pond discussed in Chapter 3 except for the fact that the initial region need not be fully mixed. In contrast pond B will be referred to as a backwater pond. Discharge and intake conditions were identical for the two cases. Tests were carried out for a variety of depths and outlet conditions. For the majority of tests a high inflow-outflow rate was used, since this tends to lower the importance of density currents in two ways, be increasing the pumping currents, and reducing temperature and hence density differences. Depths varied from 0.17 to 0.9 ft. Entrance mixing varied from a practical minimum of 50% to about 1000%. A bottom (skimmer wall) intake was used for all runs. Comparisons of

behaviour were made by means of dye tests, surface temperature distribution, measurement of steady state intake temperatures, and examination of vertical velocity profiles. Some results for a case with low entrance mixing and moderate depth are shown in Figures 4-7 to 4-10.

Figure 4-7 shows the movement of dye fronts in the two ponds. It is immediately obvious that the currents into the backwater areas (Fig. 4-7b) are as large as those in the flow-through case (Fig. 4-7a). Figure 4-8 shows the vertical velocity profiles at point X for both geometries. Note the thinner surface layer and larger subsurface return flow for pond geometry B. Figure 4-9 shows the steady state surface temperature distribution for similar test runs for both geometries. Figure 4-10 shows the overall pond performance as reflected in the steady state intake temperatures for both geometries. Here the experiment was run to steady state for the flow-through pond, and then the geometry was changed to that of the backwater pond, with no apparent effect on the intake temperature.

The above results show very conclusively that density currents can be a dominating factor in determining cooling pond performance, at least for cases with low entrance mixing, moderate depth, and a bottom intake.

4.4.2 Density Currents in the Field

The available data is limited, but most of that which is available tends to support the previous conclusions. Figure 4-11a shows an isotherm plot in the Maitland pond which indicates that treated water is being distributed to the South-West corner despite the wind. (68)

SEE ERRATA

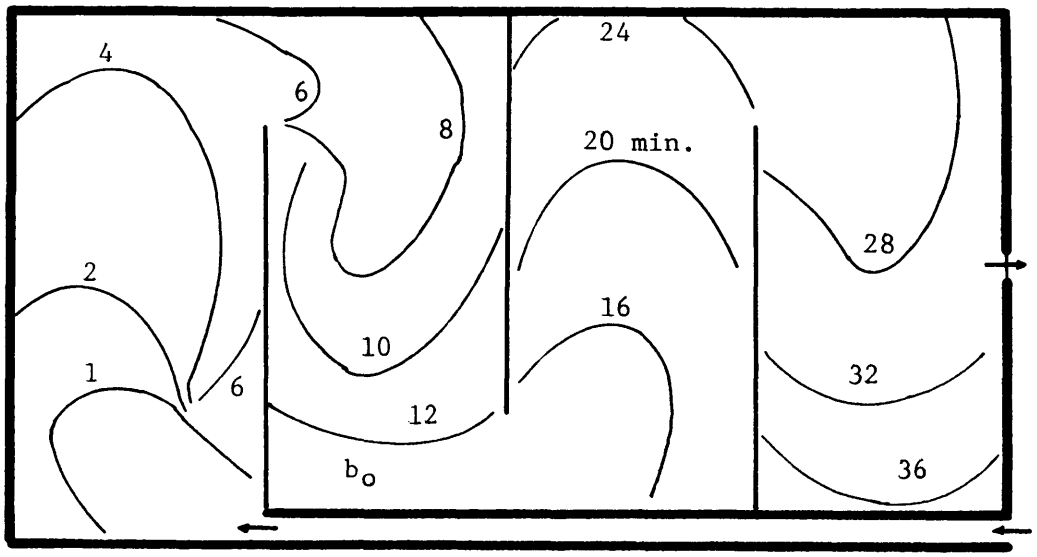

a) Position of Dye Front with Time (mins) - Flow Through Geometry A

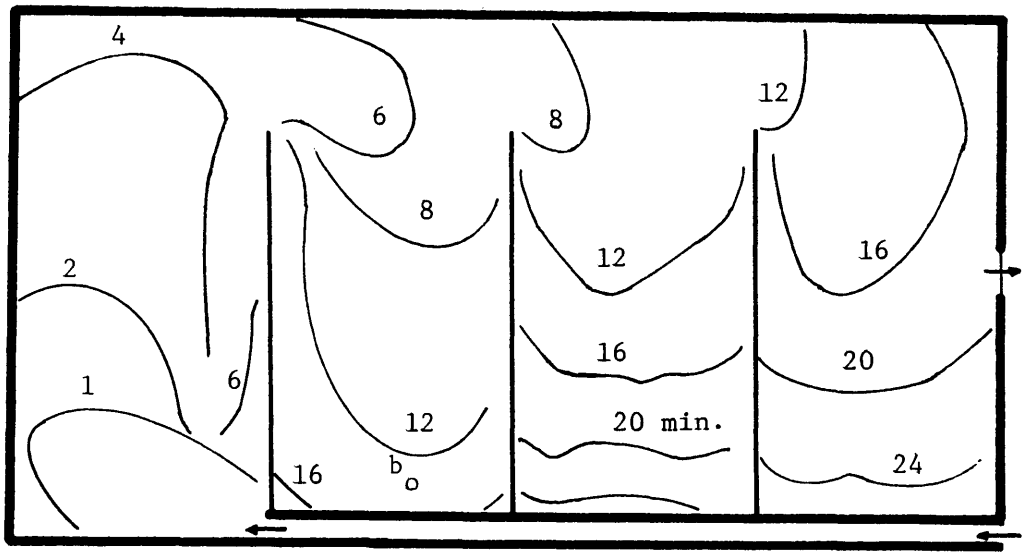

b) Position of Dye Front with Time (mins) - Backwater Geometry B

Figure 4-7 Effect of Geometry on Dye Movement
(Q=20 gpm, Depth=0.51, b_o=1.25')

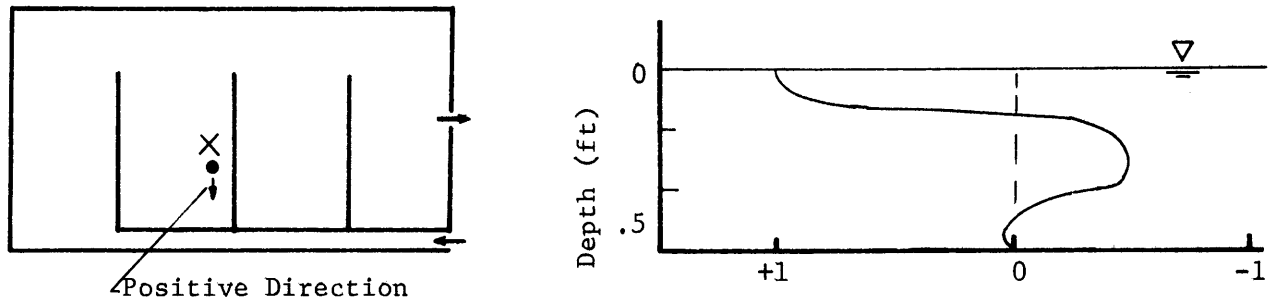

a) Backwater Pond

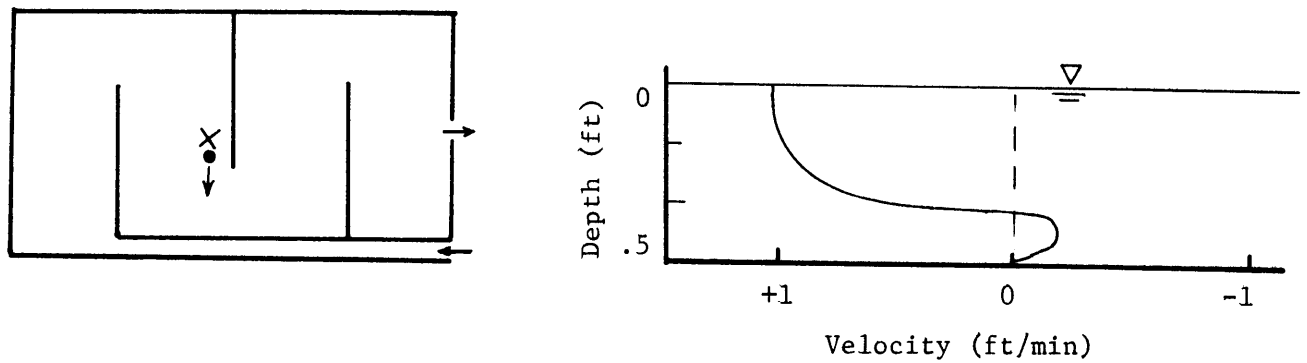

b) Flow Through Pond

Figure 4-8 Vertical Velocity Profiles at Point x for Different Pond Geometries

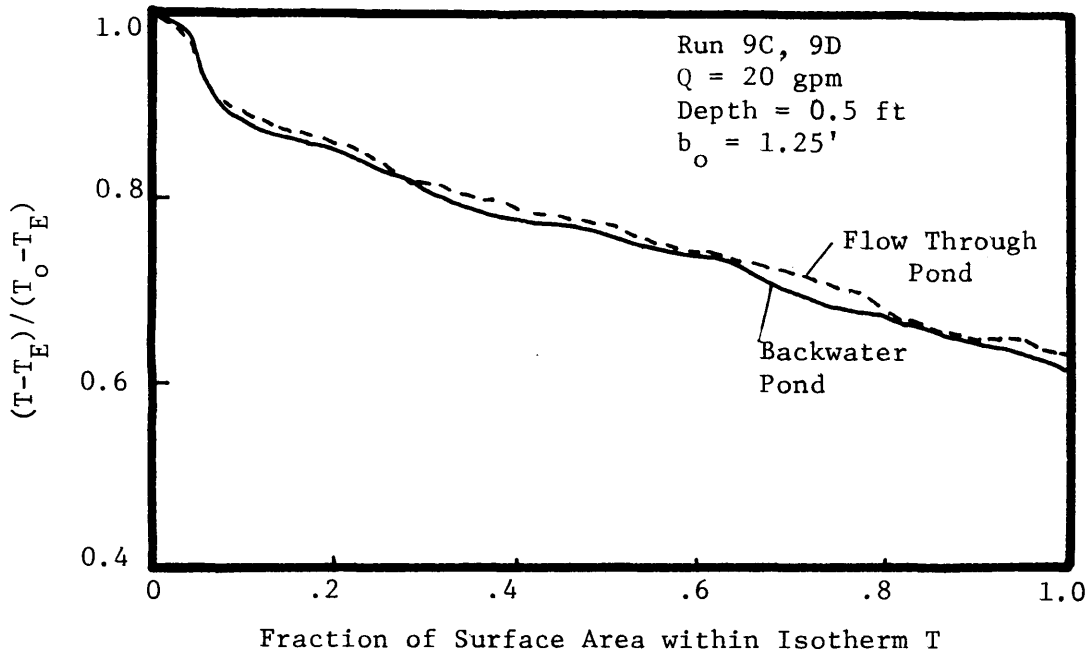

a) Comparison of Area-Temperature Distribution

b) Surface Isotherms Flow Through Pond

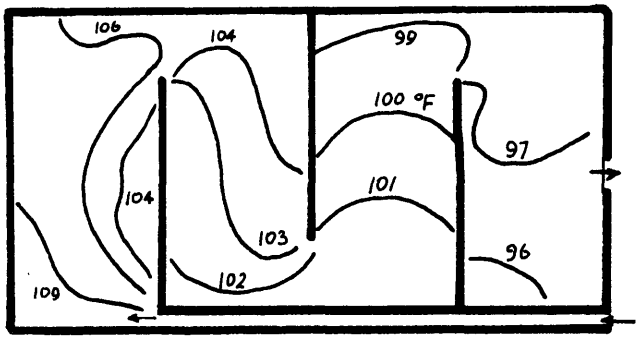

c) Surface Isotherms Backwater Pond

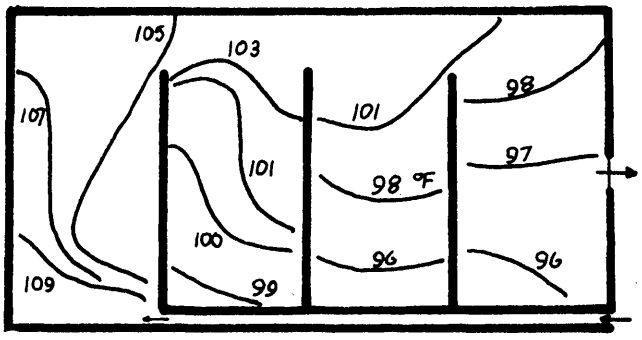

Figure 4-9 Effect of Pond Geometry on Temperature Distribution

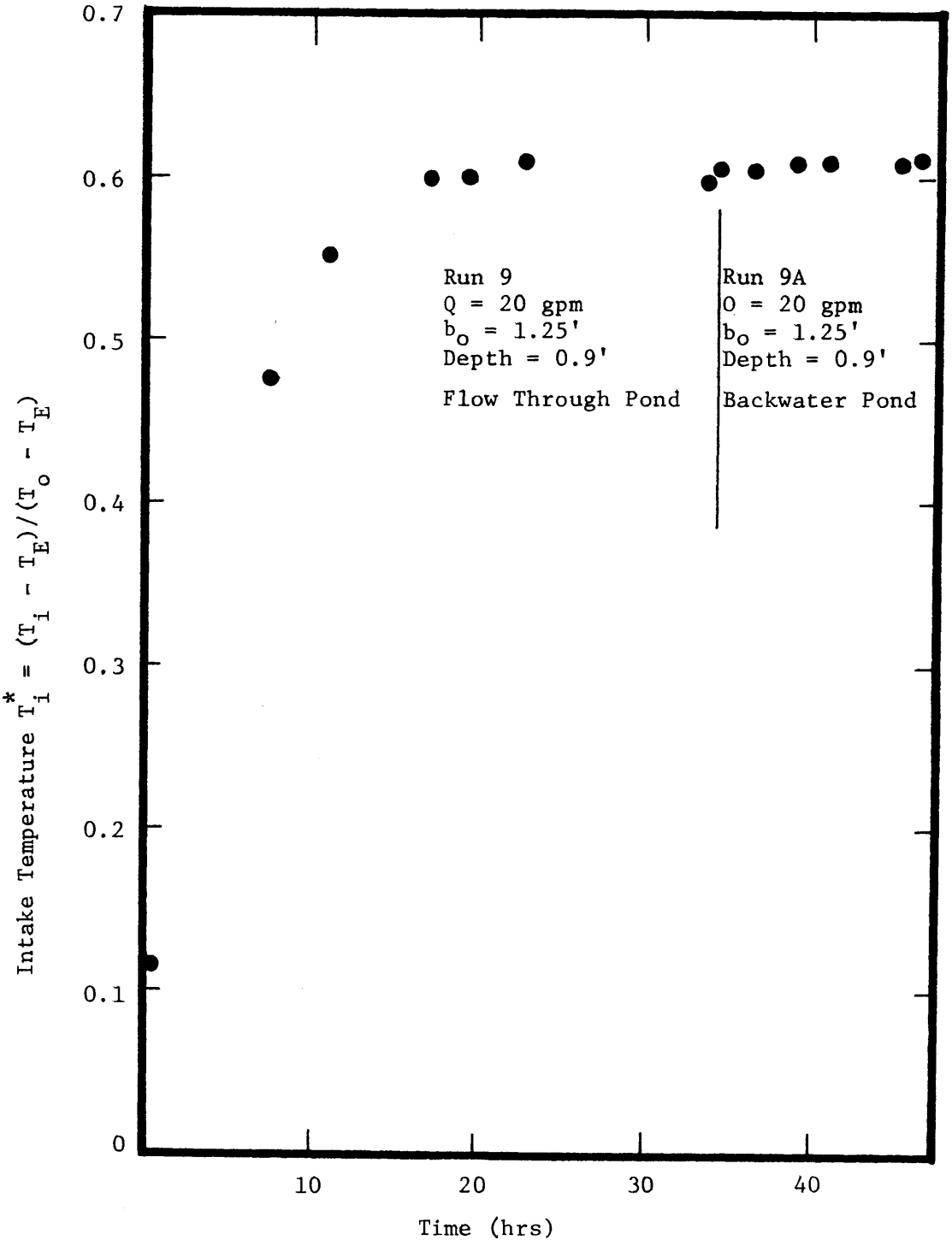

Figure 4-10 Effect of Pond Geometry on Intake Temperature

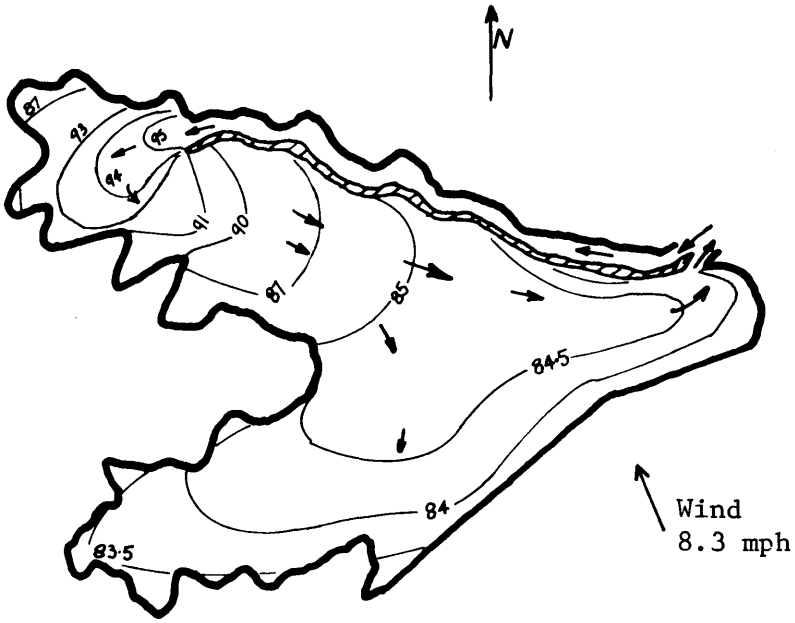

a) Isotherms - Load 56 Btu/ft^2/hr, T_E = 75.5°F

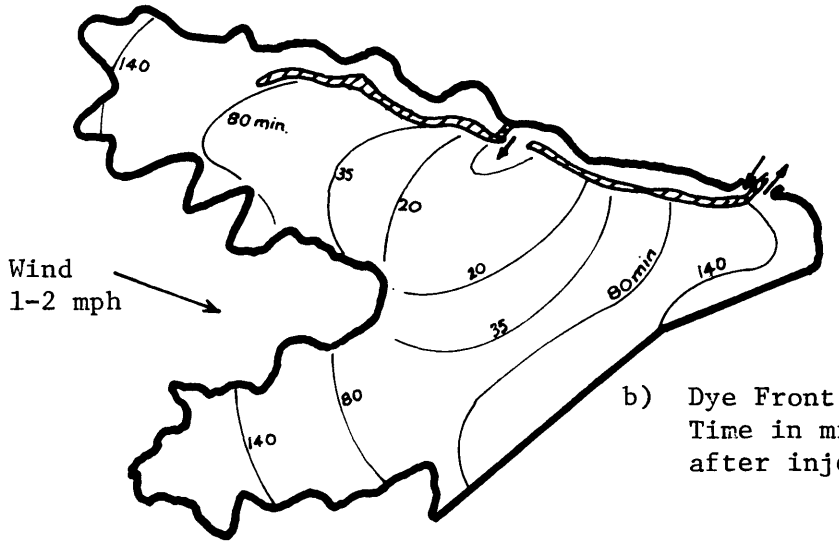

b) Dye Front Position
Time in minutes
after injection

Figure 4-11 Dye Front and Isotherms in the Maitland Cooling Pond, Showing Effect of Density Currents

Figure 4-11b shows the results of a dye test in the same pond with the outlet location changed. The important fact is that the dye spreads to all corners of the pond at an equal rate (68).

Similar results for the same pond were obtained using radioactive iodine as a tracer. Under calm conditions a shallow layer (1 - 2 feet deep) spread over the entire pond, although some channelling towards the surface intake was apparent (34). Later tests were carried out for a low intake (35). The low intake was not designed as a skimmer wall, however, and lowering the intake had very little effect. Considerable evidence exists of density current behaviour in the field for situations other than cooling ponds. Examples are upstream flows in warm wedges in rivers (see Figure 4.12) and density flows in reservoirs (144). Some field data which conflicts with the above evidence is given by Georgiev and Monev (1972) who carried out a radioactive tracer test on a 1200 acre cooling pond, with a surface intake, and found that although a shallow surface density current (approximately 1 ft. thick) did exist, it spread only over a very small fraction of the total pond area (see Figure 4-13). This type of flow pattern looks very similar to that caused by wind effects (see Figure 4-18). No wind data was given in the reference, however, and further evidence is needed before one can be certain of the role of density currents in a pond with a surface intake.

4.4.3 Effect of Depth on Density Currents

In a very deep pond, the strength of the density current is controlled by the heat (buoyancy) flux through the surface, and the

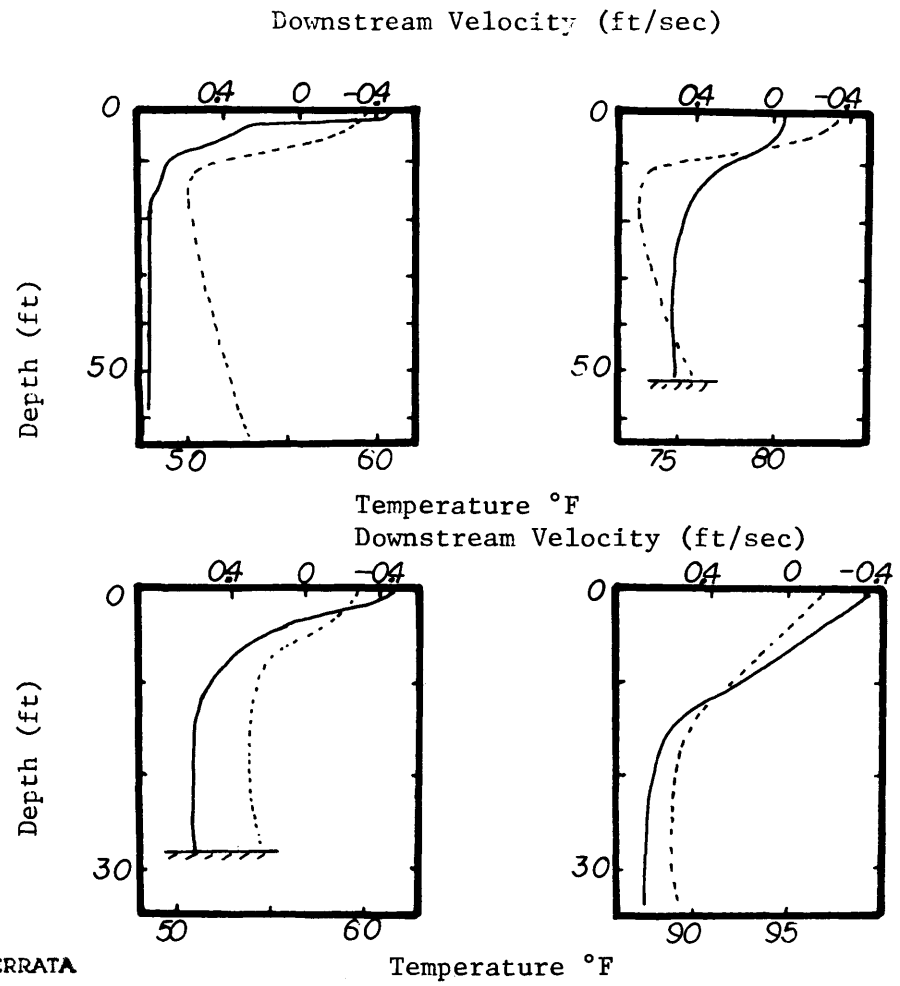

SEE ERRATA

Figure 4-12 Velocity and Temperature Distribution in Warm Wedges in Streams (149)

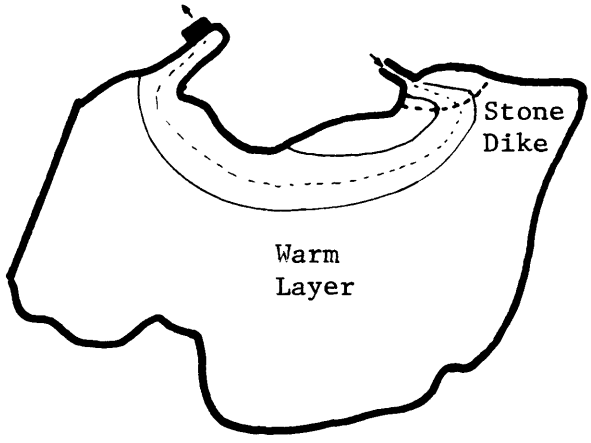

Figure 4-13 Observed Short Circuiting of the Warm Surface Layer (Georgiev and Monev, 1972)

interfacial stress. A typical velocity profile of a density flow into a deep backwater region is shown in Figure 4-14.

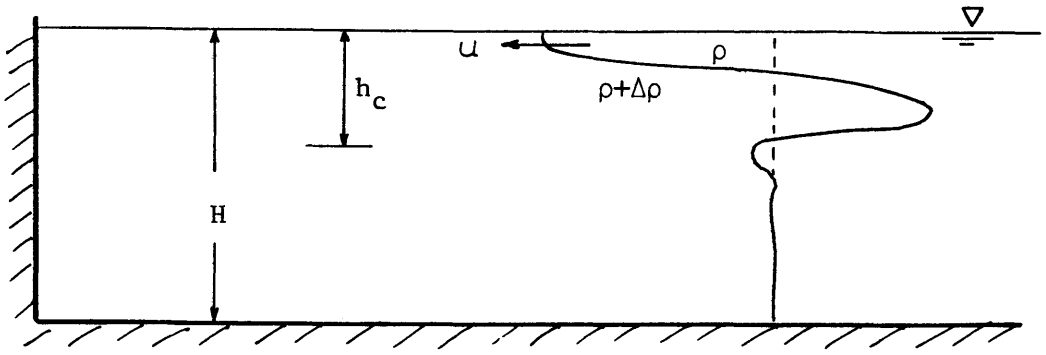

Figure 4-14 Density Current in Backwater Area

As long as the pond depth H is greater than the flow depth h_c, then the effect of pond depth, H, on the density current is minimal. The critical depth, h_c, can be defined in terms of a critical densimetric Froude Number F_c, defined as

$$F_c = \frac{u}{\sqrt{g \frac{\Delta\rho}{\rho} h_c}} \qquad (4\text{-}1)$$

where the symbols are as shown in Figure 4-14. Rigter (1970) has shown theoretically that for a steady state system, with equal but opposite flows in each layer, F_c has an upper limit of 0.25. This upper limit is reached when the flow takes place through a very short channel connecting two large reservoirs. As the channel length is increased, interfacial friction becomes important, the flow rate decreases, and thus F_c becomes smaller. No reliable laboratory data or field data on steady opposing density flows is available to test this theory

SEE ERRATA

but supporting evidence is available from other sources. Eleven velocity profiles were taken in the laboratory cooling pond (see Figure 4-8a). F_c varied from 0.16 to 0.38 with a mean of 0.26. For the density flows in rivers (see Figure 4.12) F_c varies from 0.22 to 0.5 with a mean of 0.375, where h_c is taken as twice the depth of the moving layer. Yih's (1958) theoretical value of F_c for selective withdrawal is $1/\sqrt{2\pi}$ (= 0.225) and Debler's (1959) experimental value is 0.2. Perhaps the strongest evidence in support of $F_c \leq 0.25$ comes from measurements of density currents in TVA reservoirs (Elder and Wunderlich, 1972) where F_c was found to be consistently of the order of 0.2. Thus it seems likely that there will be no inhibition of density currents for $F_c \leq 0.2$, but it is not clear at what stage the actual performance of the pond will be significantly affected. Figure 4-15 shows the effect of reduction in depth on the surface temperature distribution in the laboratory pond, and it is readily seen that it is not until the depth is reduced below 0.2 ft. (Figure 4-15d) that there is any significant difference in heat transfer efficiency of the flow-through and backwater type ponds. If the backwater areas in the laboratory pond are to play a full role in heat dissipation, about one-third of the through flow must move into each backwater area as a density current. For a depth of 0.18 ft., a through flow of 20 gpm, and a typical temperature decrease in each backwater area of approximately 3°F, F_c is found to be ~ 0.4, and hence some loss of efficiency should be expected. The corresponding depth for $F_c = 0.2$ is 0.27 ft.

In conclusion, it seems reasonable to state that density

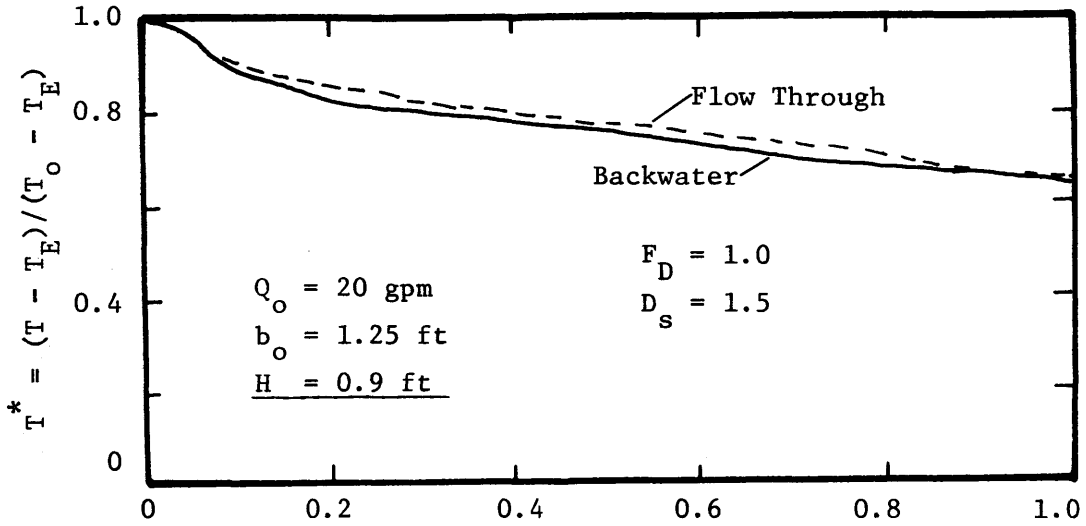

(a) Fraction of Area inside Isotherm T

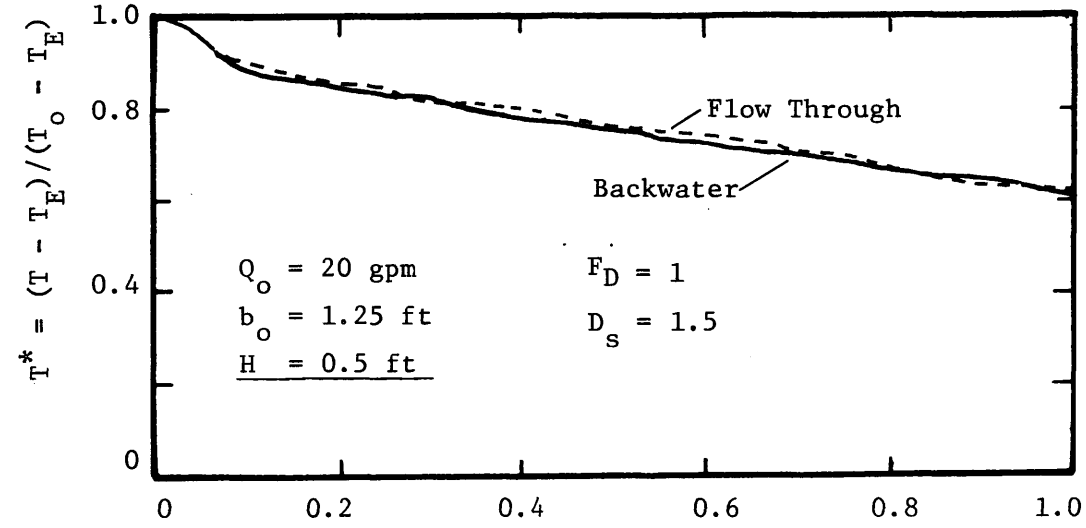

(b) Fraction of Area inside Isotherm T

Figure 4-15 Effect of Depth on the Significance of Density Currents in Backwater Areas

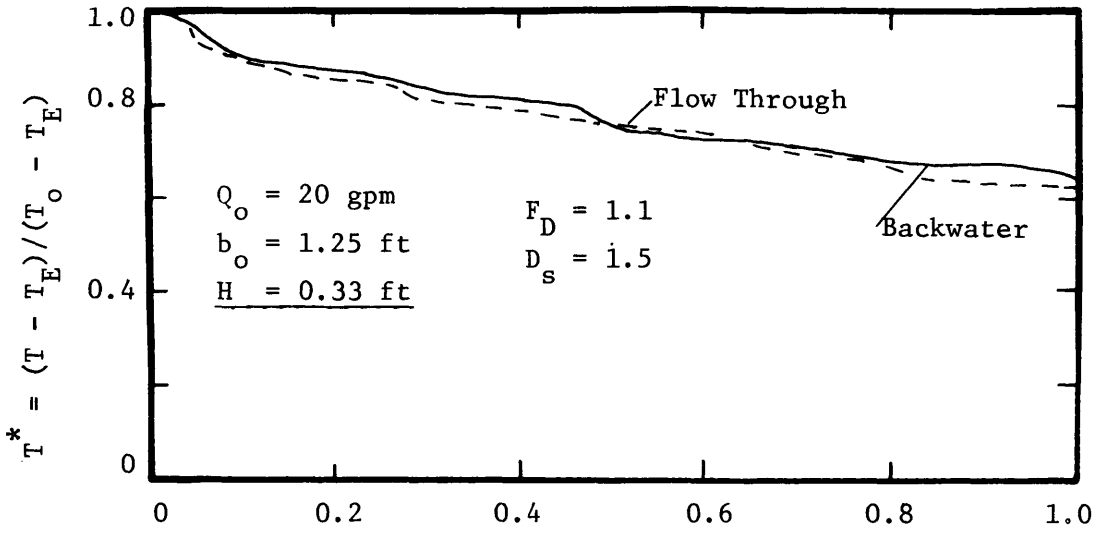

(c) Fraction of Area inside Isotherm T

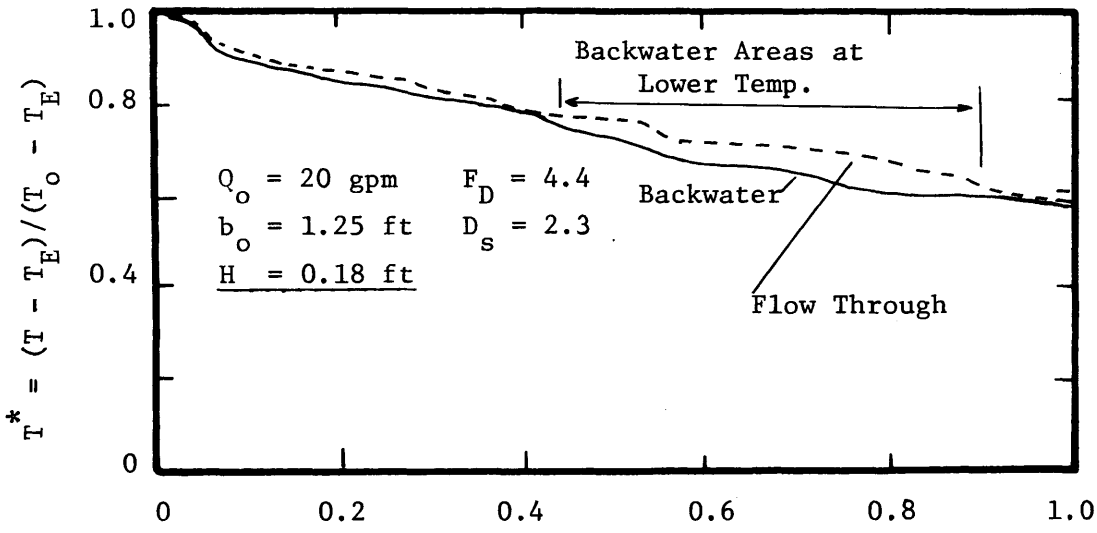

(d) Fraction of Area inside Isotherm T

Figure 4-15 Effect of Depth on the Significance of Density Currents in Backwater Areas

currents are independent of depth, H, when the internal densimetric Froude Number, defined as $F_i = u/\sqrt{g \frac{\Delta\rho}{\rho} H}$ is less than F_c (~ 0.2). Thus, for $F_i < 0.2$, pond performance is independent of pond shape.

4.4.4 Effect of Entrance Mixing on Density Currents

High entrance mixing reduces temperature changes throughout the main body of the pond and tends to destroy stratification. Thus, one would expect density currents to be less effective when high entrance mixing occurs. Figure 4-16 shows the surface temperature distributions for the flow-through and backwater geometries for two cases with high entrance mixing. Figure 4-16a shows that at large depths the density currents are completely effective. However, at low depths, (Figure 4-16b) the flow-through case seems to have a better performance. Note that for the same flow rate and depth as for 4-16b, but low entrance mixing (Figure 4-15c) the density currents are completely effective.

4.4.5 Effect of Intake Elevation on Density Currents

The ideal type of intake is a bottom intake which acts as a skimmer wall. Since cold water moves downward more easily than warm water, the cooler areas on the pond surface act as sinks, and density flows into these areas are enhanced. However, as shown in Figure 4-11, density currents may still be effective for a surface intake which withdraws over the entire depth. This observation is supported by results from the laboratory pond, such as in Figure 4-15c, where, although the intake was on the bottom, withdrawal took place from all depths. Thus, while a low skimmer type intake will enhance density

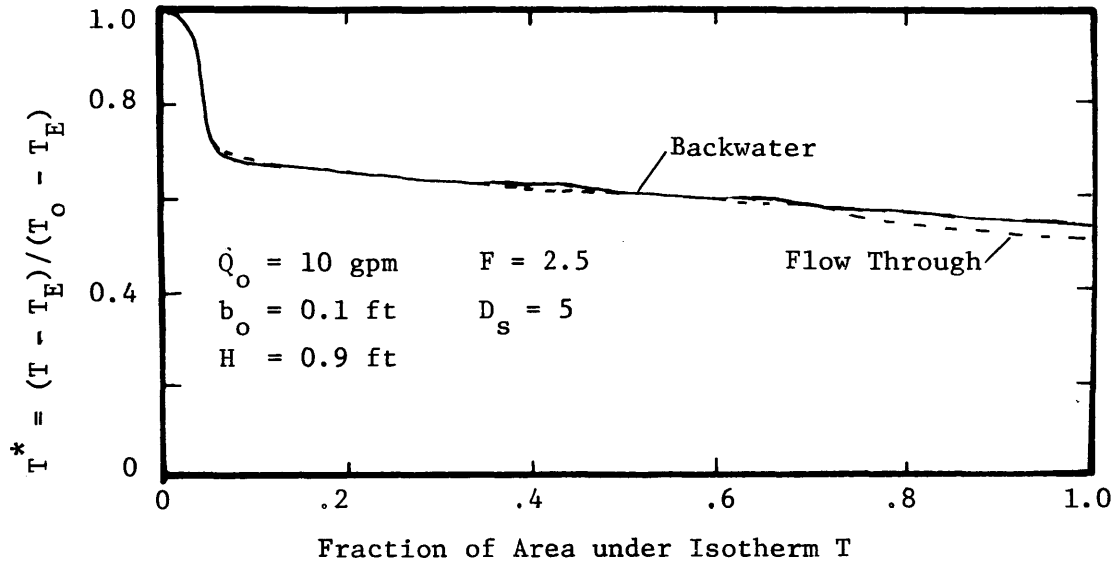

(a)

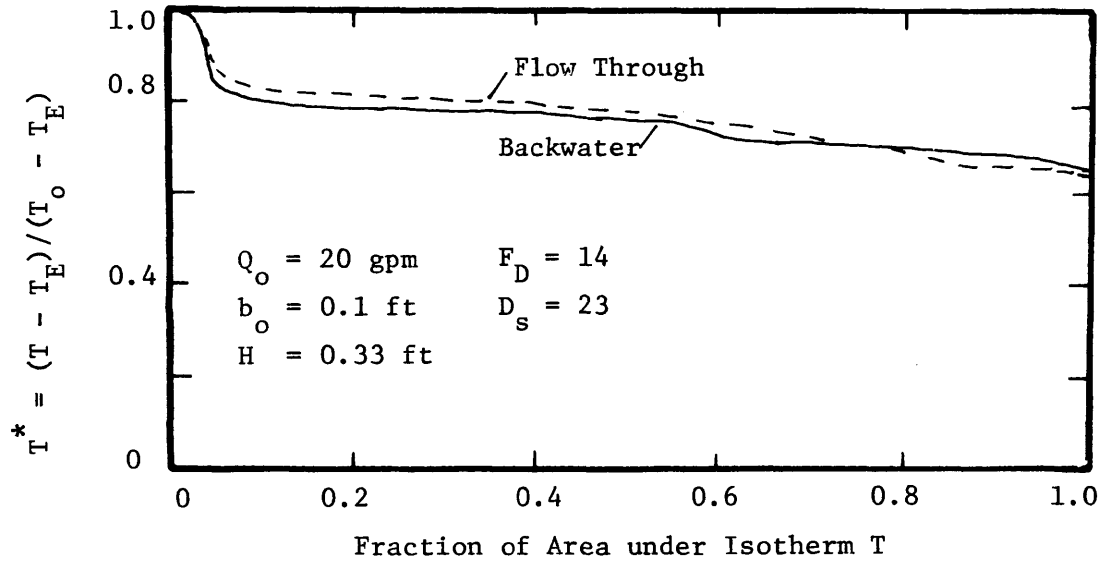

(b)

Figure 4-16 Effect of Entrance Mixing on Density Currents

currents, it is not essential to their formation. The prime purpose of a skimmer wall type intake is to stop short circuiting (as in Figure 4-13) and to improve transient behaviour by minimizing diurnal effects and forcing the whole pond volume to be active.

4.4.6 Wind Induced Currents

McMillan (1971) in Lake Trawsfynydd observed that wind induced currents were considerably larger than density or pumping currents. These observations were supported by measurements taken by Ellis, et al (1961) in the Maitland pond. Figure 4-17 shows the movement of a tracer in this pond with the wind tending to oppose the normal water movement away from the outlet. Figure 4-18 shows the effect of wind on the surface isotherms. In this case it is apparent that the active area of the pond is considerably reduced. At present the trade off between increase in heat loss with increased wind, and the decreased active area is not clear. The wind stress also tends to tilt the warm-cool interface downwards at the leeward end of the pond. If the wind is blowing towards the intake this can cause the warm water to be withdrawn, even through a low skimmer wall intake.

4.4.7 Effect of Pond Shape on Circulation

Traditionally the pond shape has been the major design variable for a cooling pond. Pond efficiency has usually been given as the "effective area" ratio, k_u, of the pond, where the "effective area" of a pond is the area of a plug flow pond with the same performance, i.e. the same intake and outlet temperatures for the same heat loading. Berman (1961) gives the effective area ratio primarily as a function of

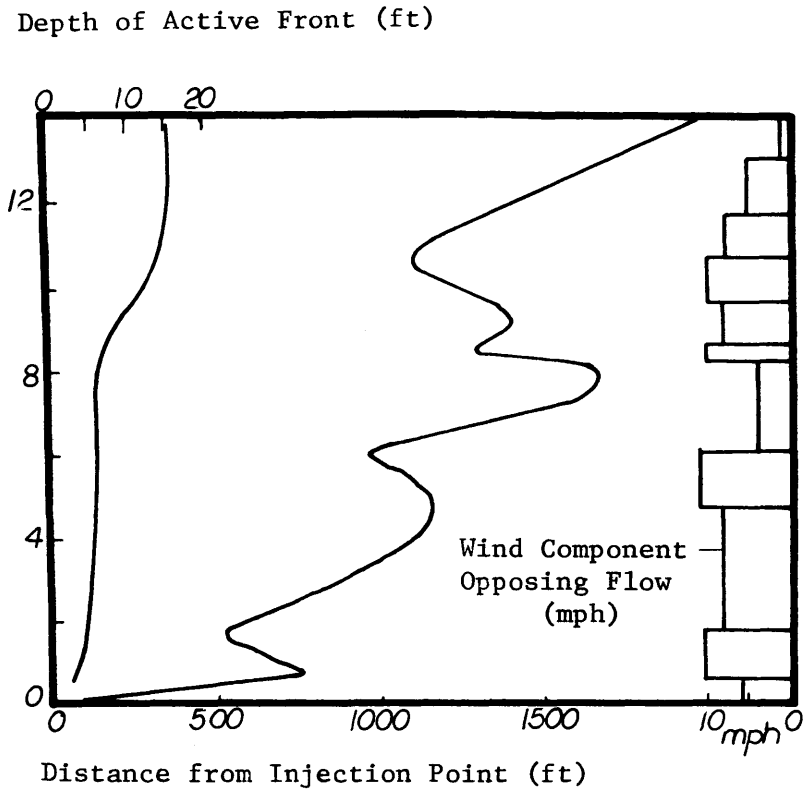

Figure 4-17 Effect of Wind on Radioactive Tracer Movement in a Cooling Pond

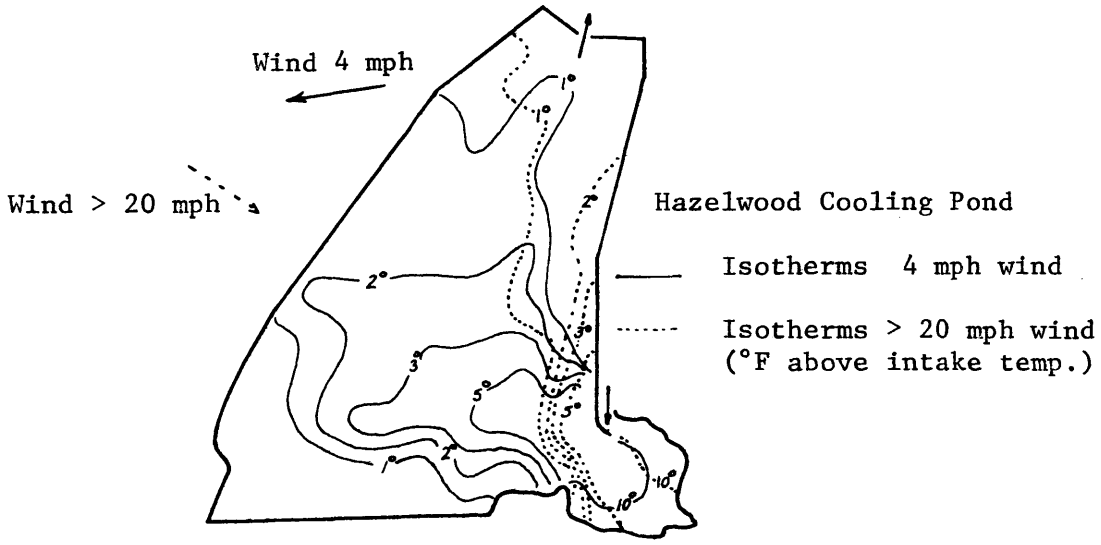

Figure 4-18 Effect of Wind on Isotherms

shape, with a favorable shape, long and narrow, having a k_u of 0.8 to 1.0 and a poor shape, circular, having a k_u of 0.4 to 0.6. However, it is now seen that a deep stratified pond has an effective area of unity, regardless of shape. Pond shape can be important, however, in two ways. A long narrow pond dereases the importance of entrance mixing because the entrained water tends to be closer to the discharge temperature, and a smaller temperature decrease results. This shape also prevents short circuiting induced either by pumping or wind currents. Both these effects can be accounted for, however, by correct design and location of the outlet and intake structures. The use of an effective area ratio has often represented merely a lack of knowledge of entrance mixing effects, and inaccuracies in surface heat transfer.

4.5 Wind Effects

Apart from the wind induced currents discussed previously, wind can have several other important effects on cooling pond behaviour.

a) The most important effect of wind is to increase the surface heat transfer coefficient, as discussed in Chapter 2. A change of wind speed from 5 to 10 mph will increase the heat transfer coefficient by 30-50%.

b) Wind generated waves can cause mixing in the surface layers. The direct mixing of a warm front has been observed by Smith (1965). The direct vertical mixing is probably only significant for very shallow warm layers, or when the overall pond depth is small. Kirkwood, et al. (1964) found that even when reversal of flow was

caused by the wind, significant vertical mixing did not occur (for an interface 7-10' deep). Both McMillan (1971) and Thompson (1971) noted that wind speeds of the order of 15 mph were necessary to disrupt warm surface layers.

4.6 Entrance Mixing

The effect of entrance mixing on pond performance is obvious. If the heated discharge mixes extensively with the receiving waters, temperature excess above equilibrium is reduced, and the rate of surface heat loss is decreased. The large difference in area requirements for the same intake temperature, between a plug flow (no entrance mixing) and a fully mixed cooling pond is known (see Table 3-1, Chapter 3). The amount of entrance mixing is affected by many factors including the design of the discharge structure, the densimetric Froude Number of the discharge, F_D and the hydrography in the vicinity of the outlet (116,118).

A series of tests were carried out in the laboratory to check the effect of discharge channel geometry and densimetric Froude Number on the overall pond performance. Basically these tests consisted of maintaining steady state heat loss and discharge conditions as closely as possible, and changing the discharge channel geometry so as to increase the discharge densimetric Froude Number, F_D, and the aspect ratio (h_o^*/b_o), thus increasing entrance mixing (116, 118). The increase in entrance mixing had three major effects on pond behaviour.

a) The pond performance suffered as shown by the increase in intake temperature in Table 4-1.

Q_o gpm	h_o ft	b_o ft	h_o/b_o	F_D (based on Channel Depth)	Steady State Intake Temperature $T_i^*=(T_i-T_E)/(T_o-T_E)$
5	.22	1.25	.18	0.19	.332
5	.21	0.25	.84	0.95	.357
5	.20	0.1	2.06	2.5	.375
10	.36	1.25	.29	.21	.478
10	.36	0.25	1.44	1.07	.491
10	.36	0.1	3.60	2.7	.519
20	.28	1.25	.22	.76	.630
20	.28	0.25	1.12	3.8	.650
20	.28	0.1	2.8	9.7	.666

Table 4-1 Effect of Outlet Geometry and Densimetric Froude Number on Pond Performance

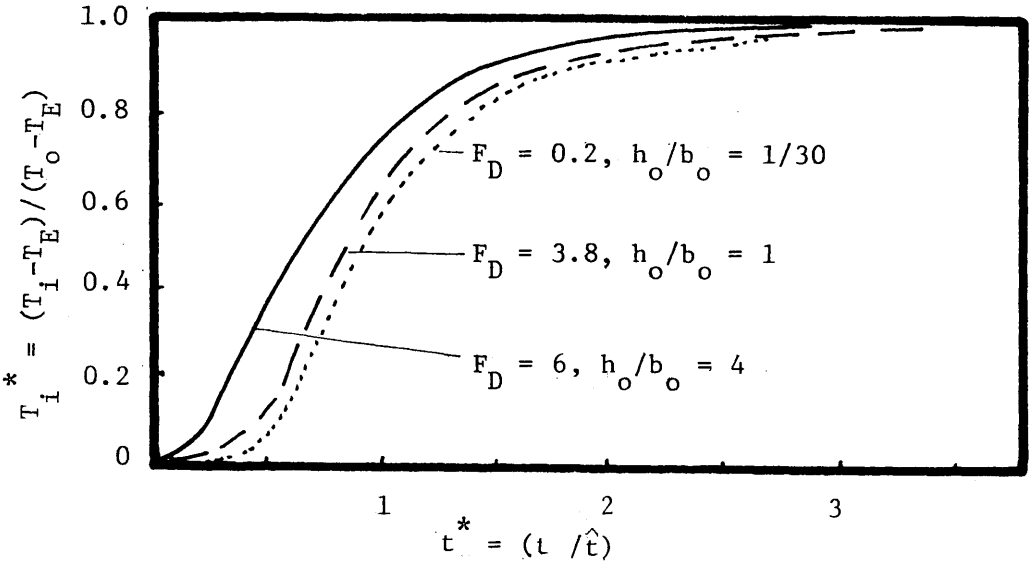

Figure 4-19 Effect of Outlet Geometry and F_D on Pond Response

b) The thickness of the surface layer increased.

c) The response time for the pond decreased as might be expected (see Figure 4-19). This means that an increase in pond loading will more quickly affect the intake temperature, an undesirable effect.

4.6.1 Eddy Formation

One effect of entrance mixing is to induce an eddy in the vicinity of the discharge area. Examples of this type of eddy formation are shown in Figures 4-20 for both the laboratory (Rouse, 1969) and the field. Eddies have always been anethema to cooling pond designers on the grounds that eddy areas did not participate fully in heat dissipation, and extensive model tests were often carried out to eliminate them. Apart from the considerable difficulties in correctly modeling a cooling pond (see Section 5.8) it was observed in the laboratory that density currents tended to override the eddies and carry warm water into the area. However, in some cases a cool spot did persist at the center of the eddy. It would seem that the best way to inhibit eddy formation is to minimize entrance mixing, which will certainly enhance pond performance.

4.7 Response

One of the major advantages of cooling ponds over other closed cycle methods of cooling is their relatively large thermal inertia. This ensures that intake temperatures (for a low skimmer type intake) do not reflect short term (e.g. diurnal) fluctuations in meteorological conditions, and respond slowly to changes in loading. A convenient time scale, $\hat{t}$, for a cooling pond is $(\forall/Q)$ where $\forall$ is the volume of the

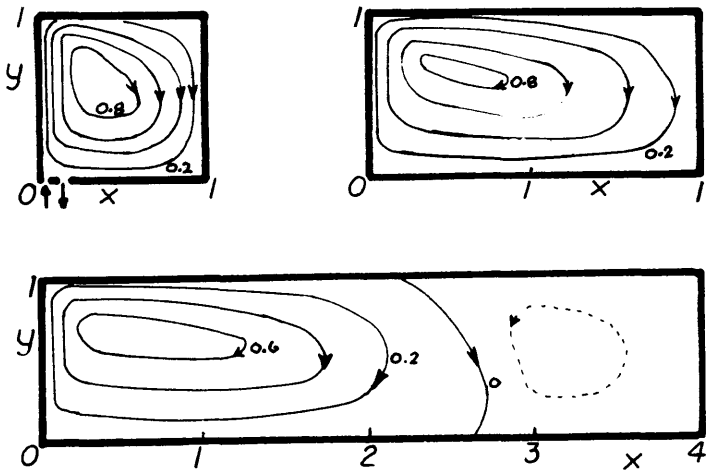

a) Laboratory Case (Rouse, 1969)

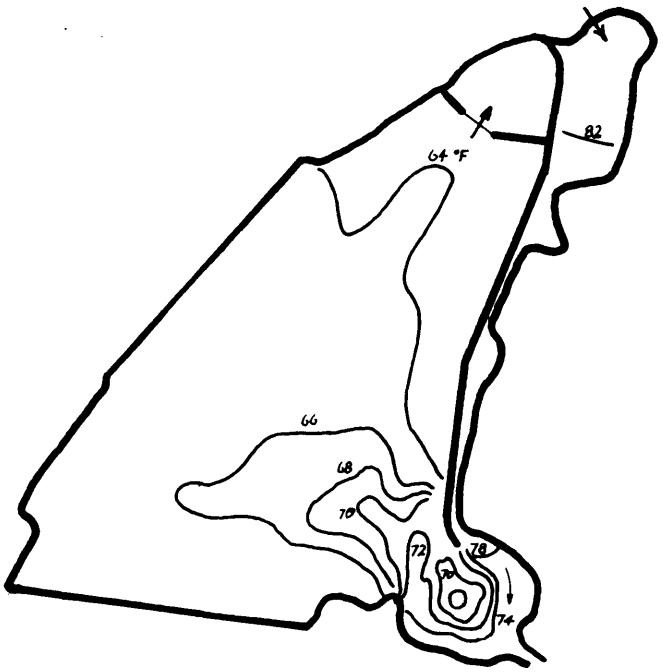

b) Field Case - Hazelwood (D3)

Figure 4-20 Eddies caused by Jet Entrainment

pond, and Q is the condenser flow rate. Thus, for a moderately loaded pond, 1 acre/Mw, and a typical flow rate of 1 cfs/Mw, $\hat{t}$ is equal to $(\bar{h}/2)$ days where $\bar{h}$ is the mean depth of the pond in feet. This means that time scales are usually of the order of a week or more. In the laboratory pond, time scales of 5 to 20 hours were standard. The response of the laboratory pond to the application of a heat load to an isothermal pond, and the response to a change in heat loading is shown in Figure 4-21. The response of a prototype cooling pond is shown in Figure 4.22. In general it can be said that at $t = \hat{t}$ about 60% or greater of the final response has occured. High entrance mixing tends to increase the response rate.

4.8 Conclusions

From laboratory and field observations of cooling pond behaviour certain conclusions can be drawn. These apply particularly to well-designed cooling ponds which require small entrance mixing and thus a low discharge Froude Number (preferably < 1), a low skimmer wall intake and a reasonable depth (average > 15').

a) Horizontal temperature gradients are generally limited to a relatively thin surface layer (< 10'). The thickness of this layer is governed primarily by the discharge conditions. Under the surface layer, temperature gradients exist only in the vertical direction.

b) Entrance mixing has a significant effect on pond performance, the smaller the mixing, the more efficient the pond. This applies to all ponds regardless of depth.

c) Density currents are of paramount importance in the distri-

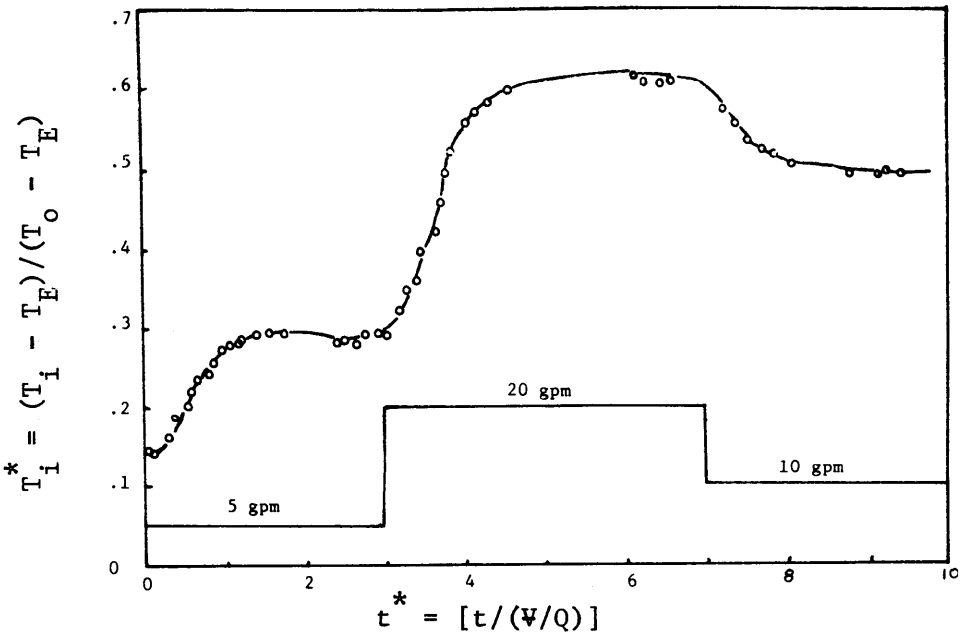

Figure 4-21 Response of Pond to Loading Changes (Laboratory)

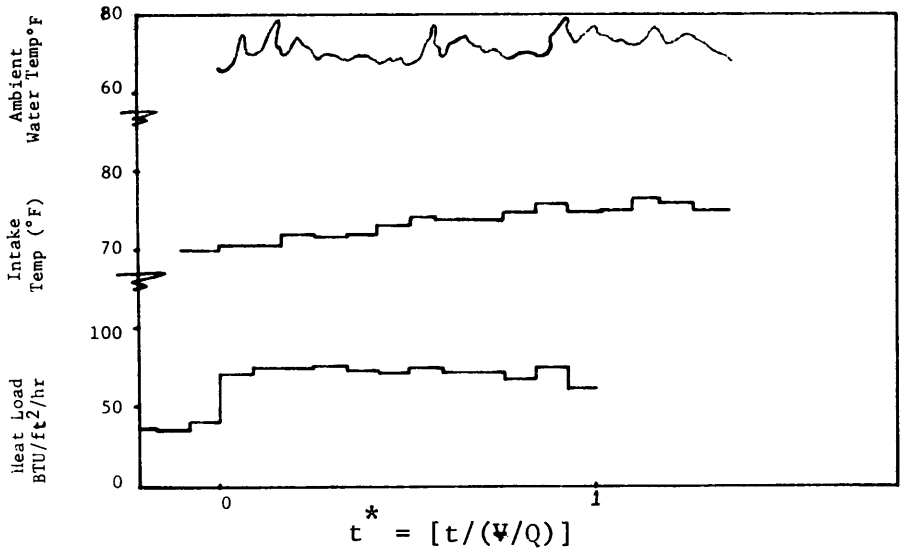

Figure 4-22 Response of Hazelwood Pond to Load Change

bution of heated water into the backwater areas of the pond. As long as the internal densimetric Froude Number ($F_i = \frac{2q}{H} / \sqrt{g \frac{\Delta\rho}{\rho} H}$ where q = flow/unit width) of the flow in these areas is less than 0.2, the effective area ratio of the pond will be close to unity.

d) The shape of a deep pond is important primarily from the point of view of entrance mixing effects and shortcircuiting, and both these effects can be minimized by good design.

e) A deep, skimmer type intake can prevent shortcircuiting, except under unfavorable wind conditions. It also improves the transient response of the pond and enhances the effects of density currents.

f) The response of a pond can be approximately described by a time constant $\hat{t} = \forall/Q$.

g) Wind effects are important from the point of view of the heat transfer coefficient, inhibition of density currents by vertical mixing, reduction in active area and possible short circuiting.

h) Internal diking may be necessary to prevent short circuiting, particularly under unfavorable wind conditions, but some disadvantages may also be present, and these should be recognised. For example, internal diking narrows the flow path, and thus increases the internal densimetric Froude Number, with possible inhibition of density current effects. Furthermore, constrictions, caused by the diking, may promote internal mixing.

V. Performance of Existing Models

5.1 Introduction

In this chapter the performance of the simple analytical models, discussed in Chapter 3, will be tested against laboratory and field data. The basic structure of more complex mathematical models will be discussed, and where possible their performance against field data will be assessed. It will be shown that no realistic predictive model exists for the ideal type of pond (i.e. deep, stratified with low entrance mixing and a deep skimmer-type intake). It will also be shown that the use of physical models of cooling ponds entails severe limitations, and hence that a realistic transient mathematical model is required for the prediction of cooling pond performance.

5.2 Simple Analytical Models

The performance of the entrance mixing models proposed in Chapter 3 was tested against both laboratory and field data, and compared with the performance of the simple plug flow and fully mixed models. These steady state models are described by Equations (3.7),(3.10), (3.11), and (3.12) and are as follows:

Entrance Mixing Model - Shallow Pond

$$\frac{T_i - T_E}{T_o - T_E} = \frac{e^{-r/(2D_s-1)}}{D_s - (D_s - 1)e^{-2r/(2D_s-1)}} \qquad (5.1)$$

Entrance Mixing Model - Deep Pond

$$\frac{T_i - T_E}{T_o - T_E} = \frac{e^{-r/D_s}}{D_s - (D_s - 1)e^{-r/D_s}} \qquad (5.2)$$

Plug Flow Pond

$$\frac{T_i - T_E}{T_o - T_E} = e^{-r} \tag{5.3}$$

Fully Mixed Pond

$$\frac{T_i - T_E}{T_o - T_E} = \frac{1}{1 + r} \tag{5.4}$$

where

$r = KA_p/\rho c\, Q_o$

K = Surface heat transfer coefficient

A_p = Surface area

Q_o = Condenser flowrate

D_s = Initial dilution due to entrance mixing

T_i = Steady state intake temperature

T_o = Steady state discharge temperature

T_E = Equilibrium temperature

For the laboratory case the surface heat transfer coefficient K, was determined by the methods outlined in Chapter 2, and was then modified to include the heat loss through the concrete floor. The dilution D_s was determined using the model of Stolzenbach and Harleman (1971) as outlined in section 6.5. Figure 5-1 compares the measured steady state intake temperatures in the M.I.T. laboratory pond with the four models. It is seen that over a wide range of entrance mixing (D = 1.5 - 18.7), the entrance mixing models give more consistent results than either the plug flow or the fully mixed model.

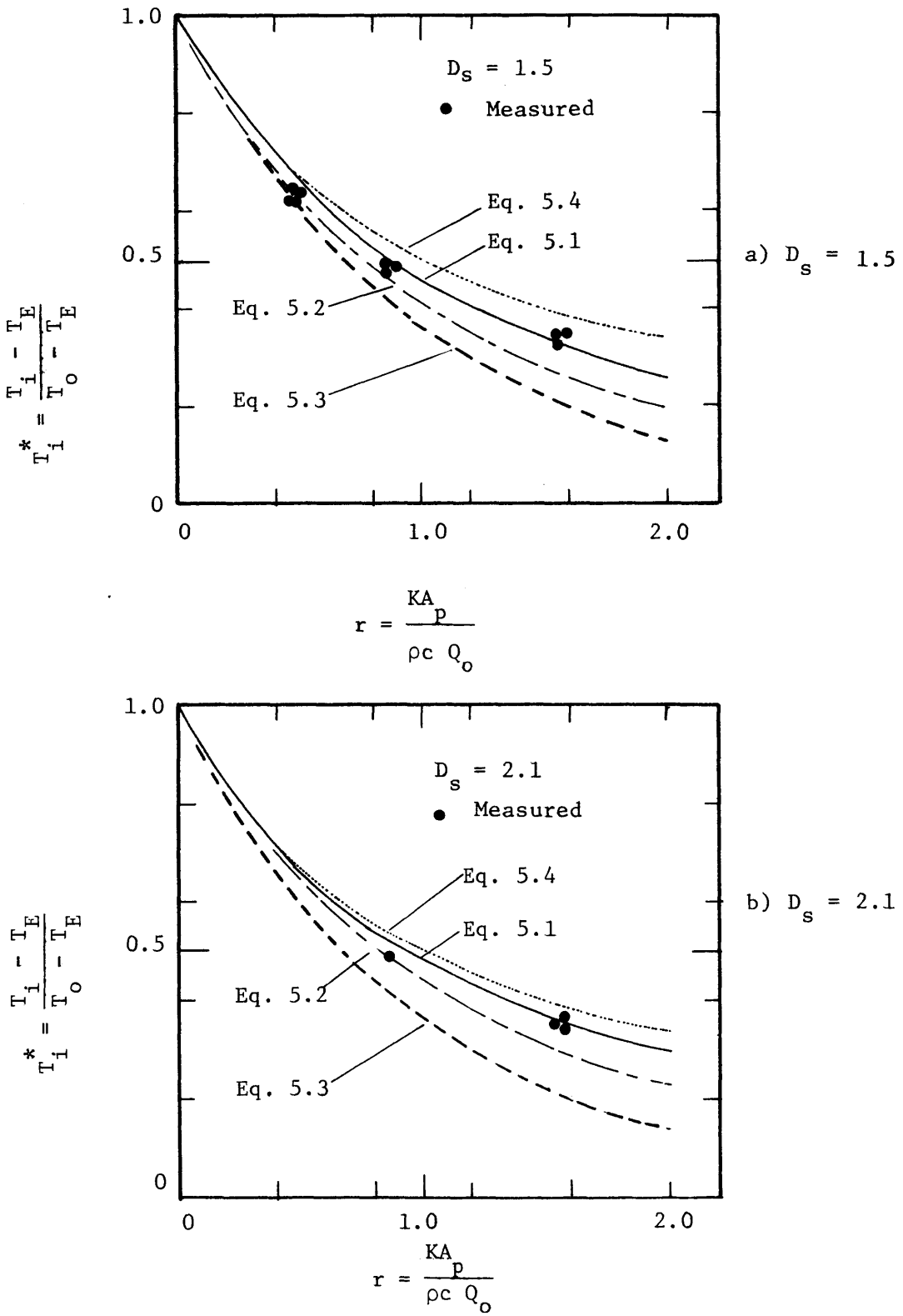

Figure 5-1 Predicted vs. Measured Laboratory Cooling Pond Intake Temperatures (D_s = 1.5, 2.1)

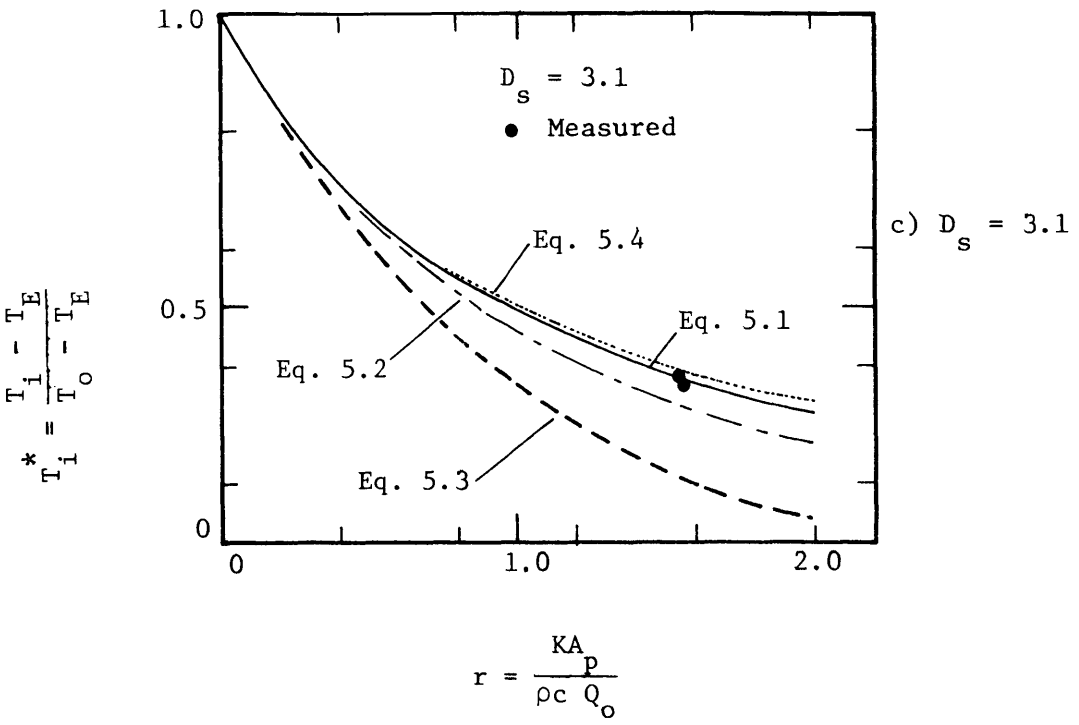

c) D_s = 3.1

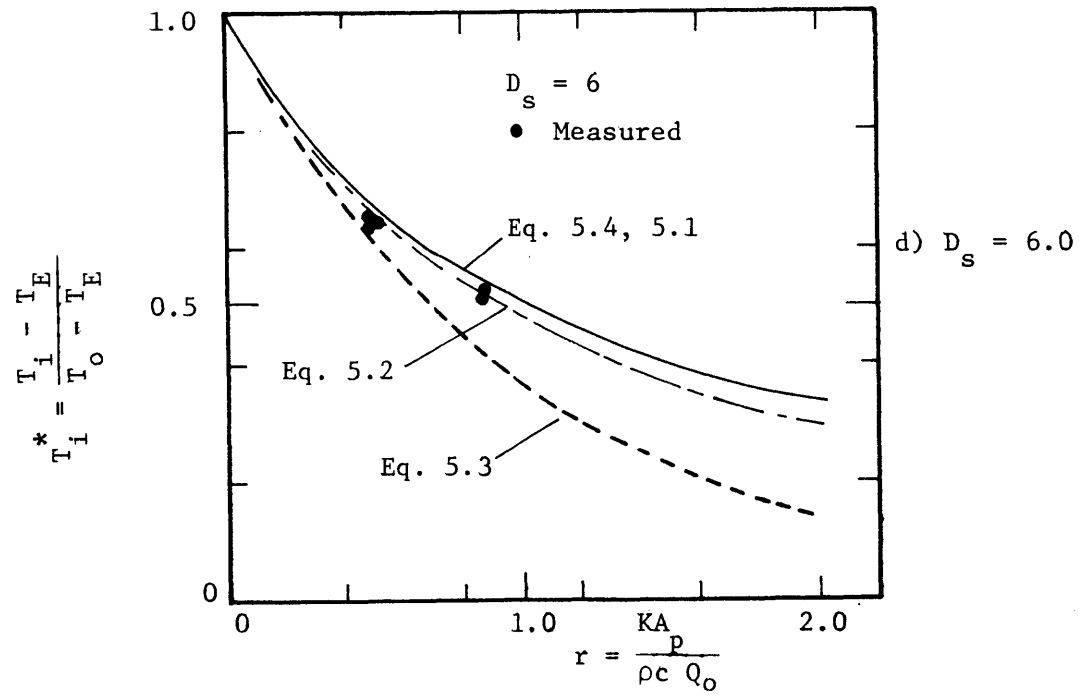

d) D_s = 6.0

Figure 5-1 Predicted vs. Measured Laboratory Cooling Pond Intake Temperatures (D_s = 3.1, 6.0)

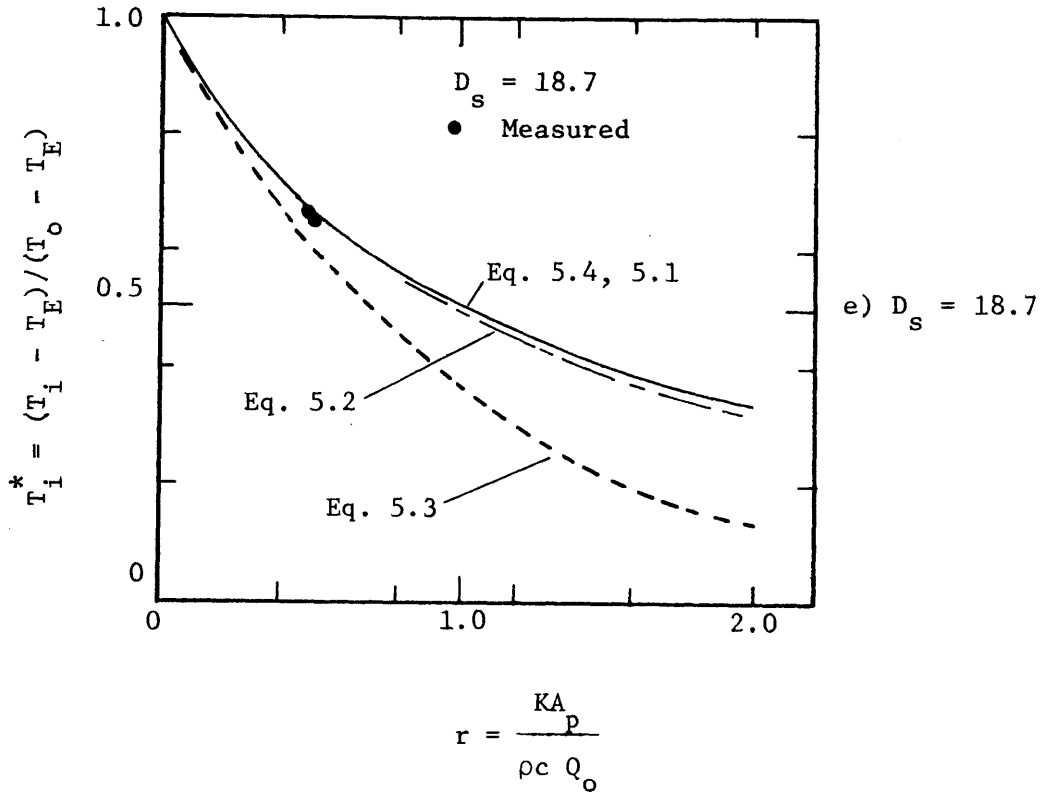

Figure 5-1 Predicted vs. Measured Laboratory Cooling Pond Intake Temperatures (D_s = 18.7)

Figure 5-2 compares the measured monthly average intake temperature for the Hazelwood cooling pond (D3) against the steady state intake temperatures predicted by the above four models. K was determined from monthly average data as outlined in Chapter 2, and D_s was calculated as given in section 6.5. It can be seen that again the entrance mixing models are more consistent than the plug flow or fully mixed cases.

It should be noted that both in the laboratory and the field the heat loss for a wide range of surface temperatures (20 - 30°F) are represented by one value of K, and errors of ±10% are likely. For this reason one cannot use the above results to choose one entrance mixing model over the other, although, as pointed out in Chapter 3, on the basis of observed behaviour, the deep entrance mixing model seems preferable.

5.3 Littleton Models

Hogan et al (1970) developed a series of models based on the plug flow and fully mixed concepts. The heat balance was extended to include the effect of make-up water, seepage and precipitation. A mass balance and a linear vertical temperature gradient were also included. None of these modifications is particularly significant, as the basic extreme character of the model is unchanged. Both steady state and transient models were considered. The models were tested against field data from five steam plants. The pertinent data is listed in Table 5-1 and four of the ponds are shown in Figure 5-3.

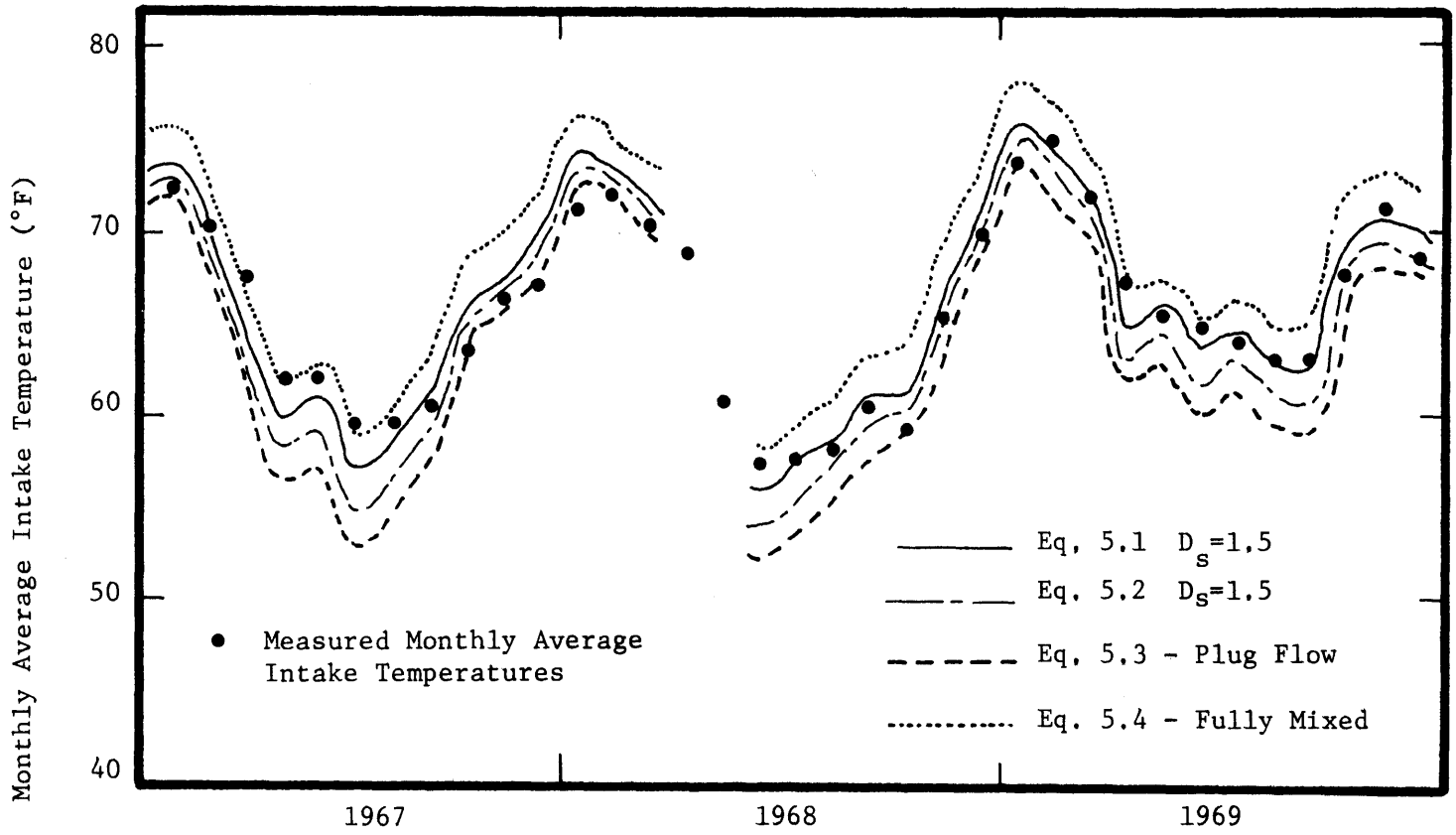

Figure 5-2 Predicted vs. Measured Monthly Average Intake Temperatures for Hazelwood Cooling Pond

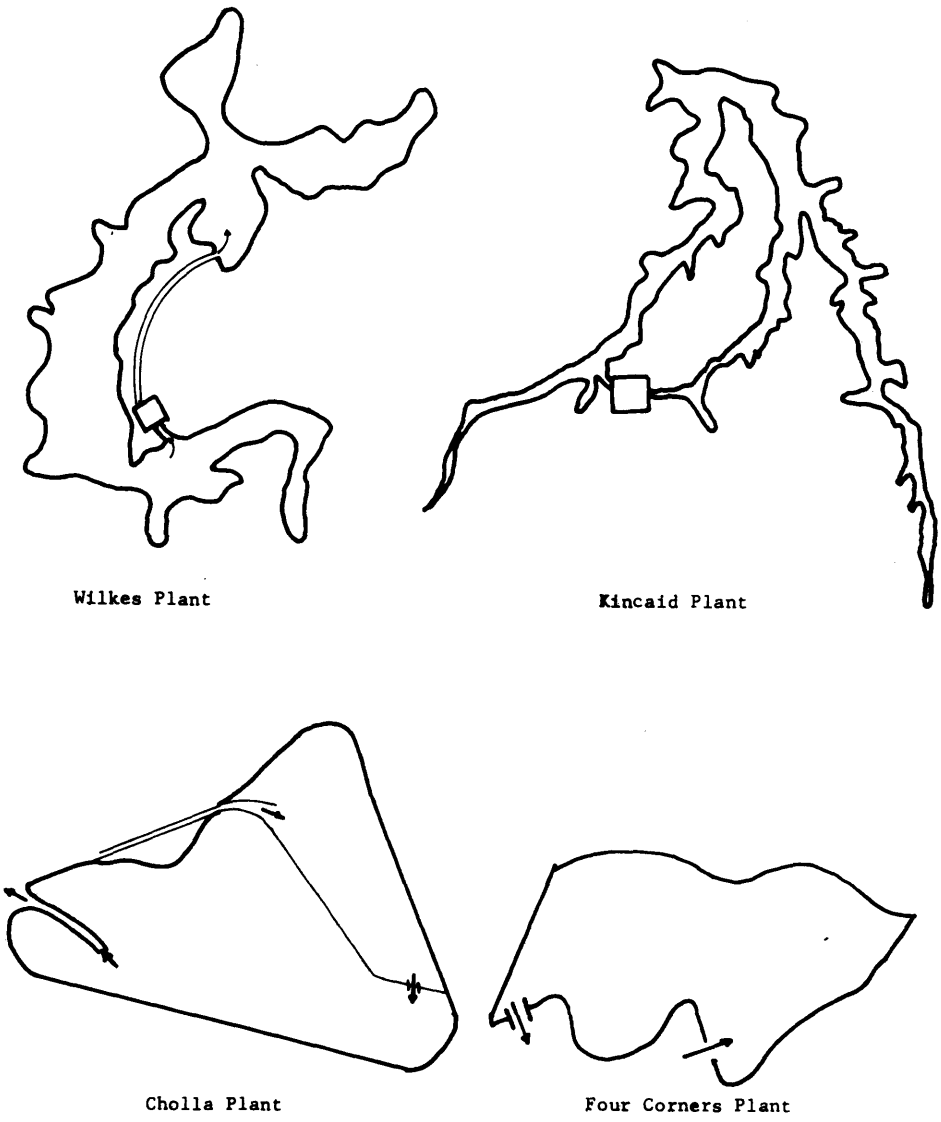

Figure 5-3 Cooling Ponds (53)

Table 5-1

Power Plant	Average Depth(ft)	Residence Time (days)	Acres/Mw	Effective Area Ratio k_u	Remarks
Wilkes	15	46	$\approx$ 4	1	
Kincaid	10	9	$\approx$ 2.7	0.6	The area ratio was estimated from the map. See Figure 5-3
Cholla	4.5	8	$\approx$ 3	0.33	The area ratio chosen on the basis of best fit.
Mt. Storm	40	22	~ 1	1	
Four Corners	40	35	$\approx$ 2	1	

The assumed effective area ratios are of particular interest. These seem to have been chosen on the basis of the best fit with the field data and as such the models are not truly predictive. The discrepancy between the effective area ratio, k_u, used for Cholla ($k_u = \frac{1}{3}$) and for Four Corners ($k_u = 1$) is disturbing since their overall shape is similar and in fact an attempt has been made to improve the flow behaviour at Cholla by constructing a hot pond. The explanation may lie in the very shallow depth at Cholla, which may limit the effectiveness of density currents. Note also that the "effective area" concept is here applied to fully mixed as well as the plug flow case, although it is defined in terms of the latter.

Average monthly data was used to generate all the curves

shown. Steady state conditions were assumed for the Wilkes, Kincaid and Cholla ponds. This assumption is reasonable since Kincaid and Cholla both have short residence times, and Wilkes is so lightly loaded that it is always close to equilibrium temperature. For the Mt. Storm and Four Corners ponds a transient effect was introduced to account for the residence time in the pond, although monthly average meteorological data was used. The results are shown in Figures 5.4 to 5.8 and it is seen that relatively good agreement (±5°F) is obtained. The almost perfect agreement between the measured intake temperature for the Mt. Storm pond and the intake temperatures predicted by the plug flow model is surprising since field data show that a large amount of entrance mixing takes place ($D_s \simeq 5$), and hence the plug flow assumption is not valid.

In conclusion, the Littleton models provide no new insight into pond behaviour. Reasonable agreement with measured data is obtained, but this is at least partly due to judicious choice of "effective area" ratios. Only the extreme cases of plug flow and complete mixing are considered.

5.4 Curtis Model

Curtis (1966) took the unprecedented step of studying the behaviour of a field cooling pond (the Hazelwood pond, see Figure 4-4) and developing a model which included the significant characteristics which he had observed. This is in contrast to most other models which use idealized, and usually unrealistic, flow patterns, and obtain reasonable results by use of fitting parameters. Curtis noted the in-

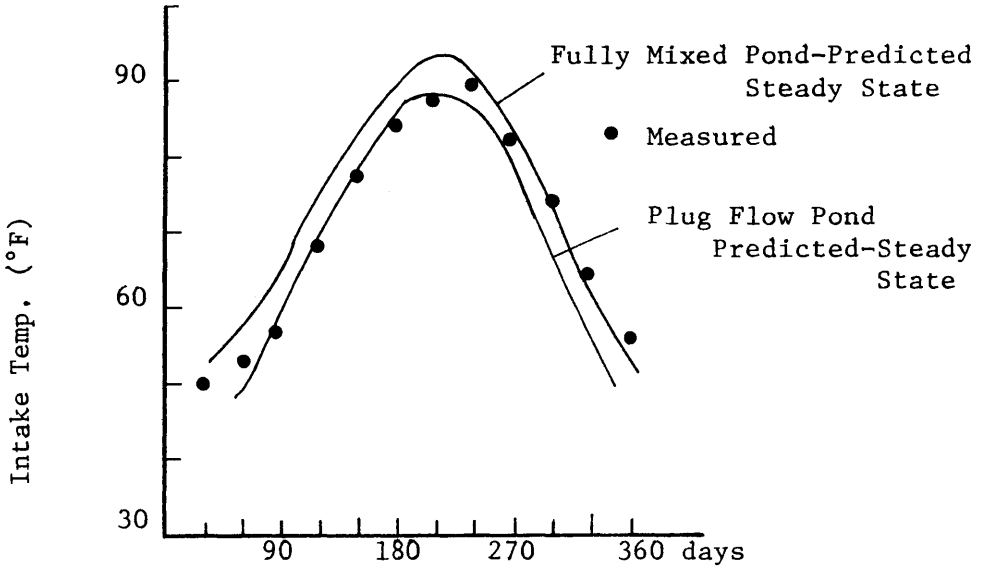

Figure 5-4 Monthly Average Intake Temperatures - Wilkes Plant (53)

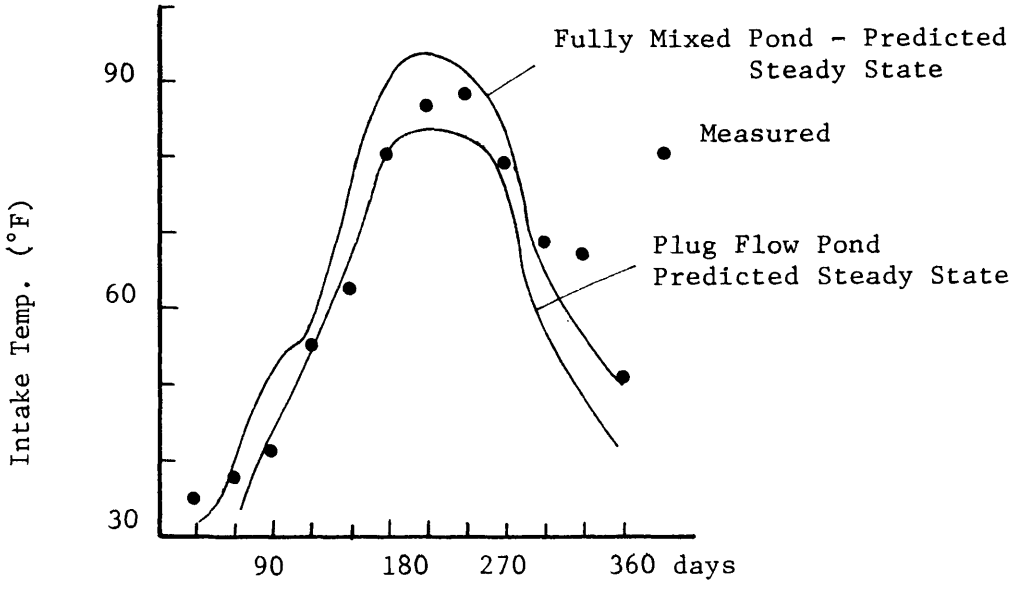

Figure 5-5 Monthly Average Intake Temperatures - Kincaid Plant (53)

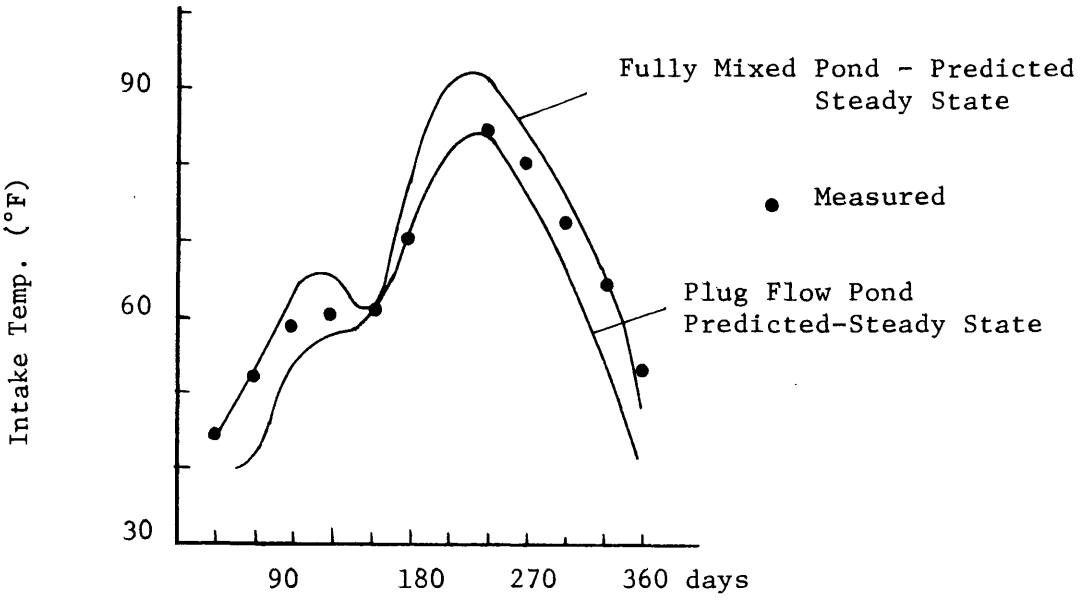

Figure 5-6 Monthly Average Intake Temperatures - Cholla Plant (53)

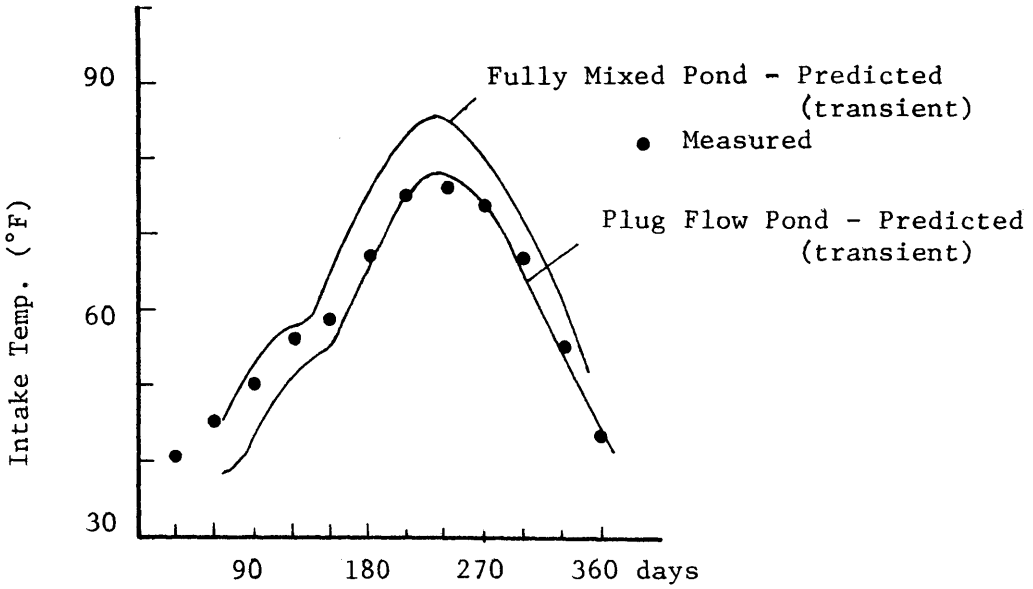

Figure 5-7 Monthly Average Intake Temperatures-Four Corners Plant (53)

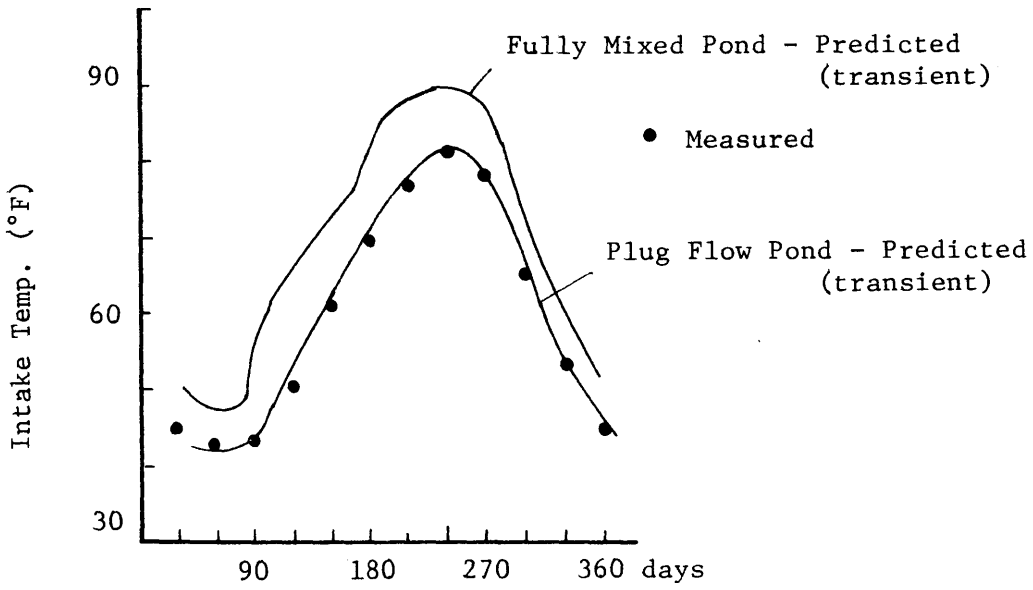

Figure 5-8 Monthly Average Intake Temperatures - Mt. Storm Plant (53)

trusion of a cold wedge in the discharge canal, and the steep horizontal temperature gradients at the end of the canal due to entrance mixing. He recognized the intermittent nature of stratification in front of the deep intake, and the effect of the intake pond on diurnal fluctuations in the intake temperature. He also discusses the effect of wind on pond behaviour. The model, which is applicable only to Hazelwood, considers the pond as nine segments, each with its own characteristics. The segments are as follows (see Figure 4-4 for reference).

Segment 1: The top end of the discharge canal where only surface heat loss is significant.

Segment 2: The discharge canal where a cold wedge is present. Interfacial entrainment of the cold water by the warm layer is accounted for using the approach of Keulegan (1966).

Segments 3,4,5,6,7: These segments all have areas of about 4% of the pond surface. Entrance mixing is allowed to take place by vertical entrainment. A velocity distribution is assumed, based on critical depth, and entrainment calculated using Keulegan's approach. Since the entering jet is very wide and shallow, the assumption of no lateral entrainment is reasonable.

Segment 8: The rest of the pond in front of the skimmer wall is considered as a heat loss region, with a linear, horizontal temperature gradient.

Segment 9: The intake pond is assumed to be fully mixed.

Throne's evaporation formula was used to determine surface heat dissipation. It appears that the Curtis model has been used only in a steady-state form and some results are shown in Figures 5-9 and 5-10.

Figure 5-9 shows that the model predicts too much cooling. This has rectified by using an effective area ratio, k_u, of 0.9. (130). However, as shown in Chapter 2, Throne's evaporation formula tends to be somewhat high, and the problem could be due to too much surface heat loss rather than ineffective surface areas. Also, neglect of lateral entrainment may lead to low entrance mixing and hence higher pond efficiency than is actually the case.

In conclusion, it must be said that the Curtis model represents the best attempt so far to simulate the behaviour of an artificial cooling pond. The model is limited by being steady state, and designed only for Hazelwood.

5.5 Slotta and Dyke's Deep Reservoir Model

In many lakes and reservoirs in which natural thermal stratification occurs, the discharge of heated water into the upper layers serves mainly to reinforce the natural stratification. Temperature standards which seek to minimize the area of heated water, lead to diffuser type outfalls which will give large dilution ratios. The concept of complete horizontal mixing is thus reasonable valid here, and the temperature prediction model for a vertically stratified reservoir, detailed in Chapter 6, can be used. It is important that the entrainment of the pond water by the heated discharge be treated correctly, as the

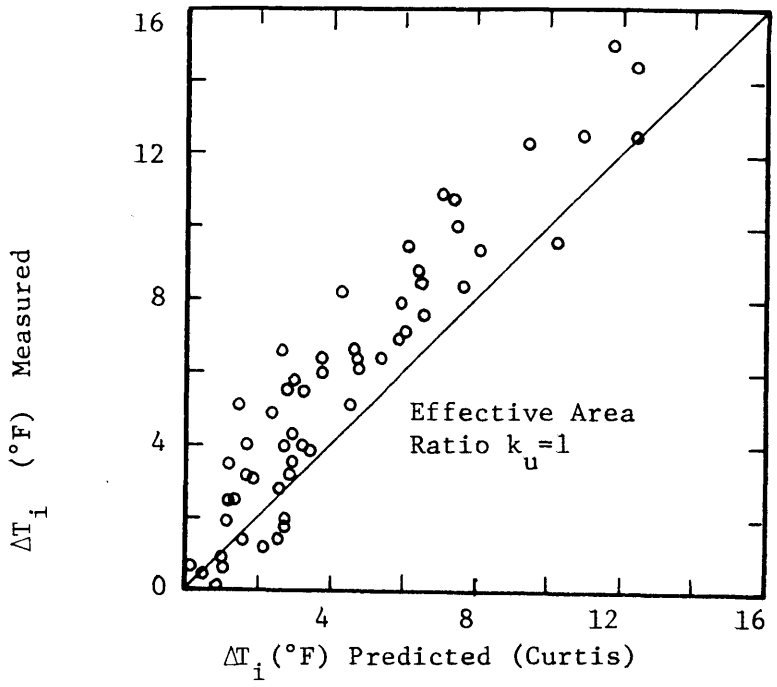

Figure 5-9 Measured vs. Predicted Monthly Average Intake Temperature Elevation Above Natural Surface Temperature

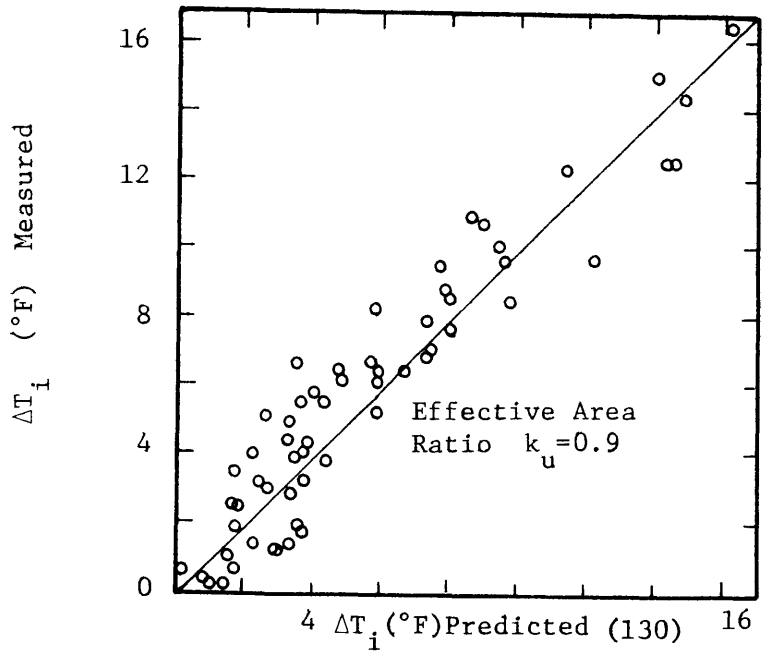

Figure 5-10 Measured vs. Predicted Monthly Average Intake Temperature Elevation above Natural Surface Temperature

temperature prediction model is sensitive to this factor. Correct vertical distribution of entrainment velocities would also be useful, but is not so important. The results of the application of the M.I.T. deep reservoir model(57,107) to Lake Norman by Slotta and Dyke (1970) are given in Figure 5-11. The details of the lake and of Marshall Steam Station are given in Chapter 8. Condenser SEE ERRATA was withdrawn from 60-70 ft. depth, and an entrance mixing of 400% (D_s = 5) was assumed. Good results were obtained, but a closer examination of the discharge canal showed that this degree of entrance mixing was extremely unlikely, due to the fact that the discharge entered the main lake with densimetric Froude Number of unity (cold wedge in discharge channel) and a low aspect ratio ($h_o^*/b_o \sim 1/50$). Also the heated discharge was combined in the model with the colder river inflows. These factors make it unlikely that the good results obtained mean much except that entrance mixing can be a useful fitting parameter.

It must be stressed that one dimensional (vertical) models can only be used if the initial dilution of the heated discharge with the reservoir water is large enough so that the surface heat loss may be adequately described by a single surface temperature (i.e. the mixing zone must be small in comparison with the reservoir surface area, and the temperatures on the edge of the mixing zone must approach background temperatures. If a large amount of mixing does not take place, the one-dimensional model is at a disadvantage, since it becomes impossible to simulate correctly the far field surface temperatures, the surface heat loss and the entrance mixing itself, all of which have

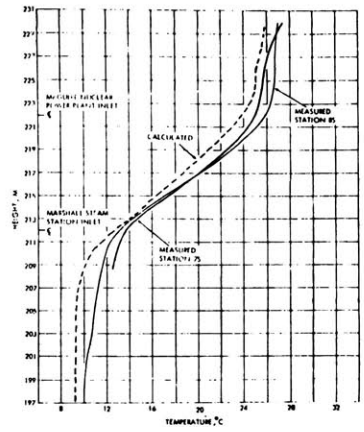

a) Predicted vs. Measured Temperature Profiles 8/6/69

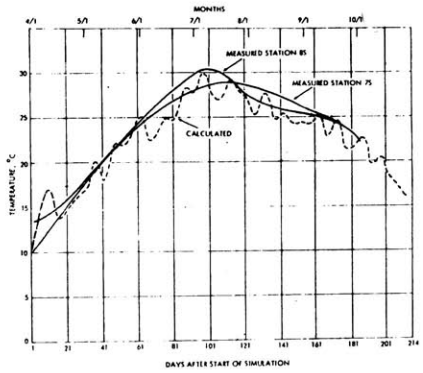

b) Predicted and Measured Surface Temperatures 8/6/69

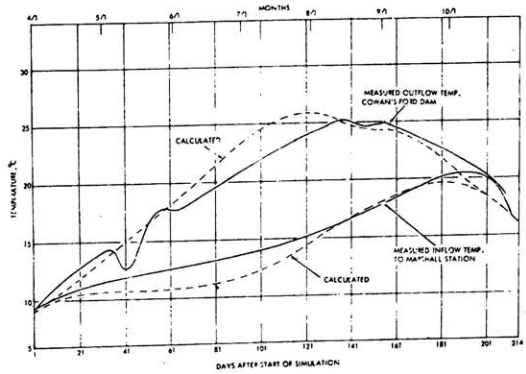

c) Predicted and Measured Dam Outflow and Plant Intake Temperatures 1969

Figure 5-11 Predicted and Measured Temperatures (Slotta and Dyke, 1970)

an important effect on the final thermal structure. For example, if the correct surface temperature is obtained by overestimating the entrance mixing, the net effect is to underestimate the surface heat loss, and propagate too much heat into the body of the lake. Alternatively, adjusting the mixing to give the correct heat loss would give too high surface temperatures, while use of the correct entrance mixing will lead to overestimation of the heat loss. There appears to be no way that a one-dimensional model will simultaneously satisfy the three important parameters given above, unless large initial dilution is present.

5.6 Sundaram Deep Lake Models

Recently a series of deep lake models have been proposed by Sundaram and his co-workers(121,122).The basis for these models is that the thermal structure of a lake is determined by a balance between wind mixing forces and buoyancy forces due to both natural and artificial heat inputs. Many simplifying assumptions are made which tend to limit the validity of the model. These assumptions are as follows:

a) Solar radiation is absorbed at the surface. This will be shown to be a poor assumption is some natural lakes.

b) Surface heat flux is described by the familiar form $K(T_s - T_E)$, but K is assumed constant over a year (a very poor assumption) and T_E is given a sinusoidal form.

c) The heated discharge is introduced below the surface without mixing.

d) The balance between wind mixing and buoyancy forces is described by use of an eddy diffusion coefficient, K_z, of the form used by Munk and Anderson (1948)

$$K_z = K_o(1 + \sigma_1 R_i)^{-1} \qquad (5.5)$$

where

K_o = diffusion coefficient for the homogeneous case

σ_1 = constant

R_i = Richardson's Number

Sundaram has not tested his models against field or laboratory data and hence it is rather difficult to judge their performance. However, one interesting analogy is made between the length scale for the atmospheric boundary layer formulated by Monin and Obukhov (1954), and the depth of the thermocline. Sundaram gives the length scale for lakes as

$$L^* = \frac{u_*^3}{\beta\, \alpha_v\, g\, \frac{\phi_n}{\rho c}} \qquad (5.6)$$

where

$u_* = \sqrt{\tau_w/\rho}$

τ_w = wind induced shear stress

β = constant

α_v = volumetric expansion coefficient for water

It is felt that this analogy is questionable on two grounds. Firstly, the Monin-Obukhov length was developed for a system which has the property of horizontal homogeneity, whereas many lakes have a fetch limited field. Also Mortimer (1952) showed that the limited horizontal

length scale can be of great importance, since wind stress may cause the thermocline to reach the surface at the windward end of the lake, causing direct mixing across the interface. The second point is that the density stratification in a lake is a function of the previous history of the lake, so that use of the term ($\alpha_v \frac{\phi_n}{\rho c}$) to denote a density difference is meaningless.

5.7 Ljatkher's Model

An interesting Lagrangian model which can be applied to both vertically mixed and stratified ponds has been developed by Ljatkher (1972). The basis for the model is the assumption that a unique probability or distribution function can be developed for the detention time of a water particle in both the upper (cooling) layer and lower (passive) layer. The probability that the detention time of a particle in the upper layer is t_1 is given by $P_1(t_1)$ where

$$\int_0^\infty P_1(t_1) = 1 \tag{5.7}$$

and

$$\int_0^\infty P_1(t_1)\ t_1 = \frac{\forall_u}{Q} \tag{5.8}$$

where $\forall_u$ = volume of upper layer. The temperature of a water particle T_1 with detention time t_1, exiting from the upper layer at time τ_1 is

$$T_1(\tau_1) = T_E(\tau_1) + (T_o - T_E)_{\tau_o} \exp\left[-\int_{\tau_o}^{\tau} \frac{K}{\rho c d_u}\ dt \right] \tag{5.9}$$

where

$\tau_o = \tau_1 - t_1$

d_u = depth of upper layer

The intake temperature is taken as the mean temperature of the bottom passive layer. If the detention time in the bottom passive layer is t_2, the intake temperature T_i at time τ is given as

$$(T_i - T_E) = \int_0 (T_o - T_E)_{\tau - t_1 - t_2} \exp\left[- \int_{\tau - t_1 - t_2}^{\tau - t_2} \frac{K\, dt}{\rho c\, d_u} \right] P_1(t_1) dt_1 \qquad (5.10)$$

Note that the detention time t_2 in the passive layer may also be described by a distribution function $P_2(t_2)$. The distribution functions $P_1(t_1)$ and $P_2(t_2)$ may be obtained from tracer tests on hydrothermal models. Ljatkher noted that agreement between model measurements and those predicted by Equation (5.10) is within 2-3 percent.

The interesting point is that this model, despite its apparent sophistication, is really no better than the familiar "effective area" type model. Both models rely on data from a hydraulic model to obtain a function which is then applied to the prototype. The problems in physically modelling a cooling pond have already been briefly mentioned and will be discussed in detail in the next section. Ljatkher's method may be of some value in comparing different flow patterns, but for comparative purposes whether one uses a detention time probability function, or a dispersion coefficient, or an effective area ratio, is really of little significance.

5.8 Physical Modelling of Cooling Ponds

5.8.1 Introduction

Several of the mathematical models, previously discussed, require information from a physical model, e.g. Berman's "effective areas" or Litkher's distributions functions. These models can only be as realistic as the physical model itself. Since modern power stations are now so large and expensive, it could be argued that, if physical models were valid, the problems of time and expense usually associated with their use would not be a serious obstacle. Unfortunately, there are severe limitations on the validity of a physical cooling pond model. These limitations are due to the fact that a cooling pond can have a number of flow regions each with its own similarity requirement. These regions are as follows:

SEE ERRATA

a) The Discharge Canal: Two layer flow may exist and is some cases heat loss may be significant. In many cases, however, this is not a region of great importance.

b) Jet Mixing Region: The expansion from the discharge canal into the main pond is often accompanied by considerable mixing. This mixing must be simulated in the model.

c) Heat Loss Region: The discharge canal and jet mixing region usually take up only a small percentage of the pond surface. Over the remainder of the pond, surface heat loss is dominant. In this region it is important to simulate both the surface heat loss and the flow field correctly. Density currents are a significant factor in determining the flow field, and thus the similarity requirements for strati-

fied flow apply.

d) Intake Region: The performance of the intake, in selectively withdrawing water from a limited depth, or uniformly withdrawing over the full depth, affects the pond behaviour, and must be simulated in the model.

The modelling requirements for heated discharges, stratified flows including selective withdrawal, and surface heat loss will now be considered. It is usually impossible to simultaneously satisfy all these similarity requirements.

5.8.2 Similarity Requirements for Heated Discharges

The jet induced entrainment and temperature distribution in the immediate vicinity of the outlet are found to be functions of the discharge densimetric Froude No. F_D, and geometric parameters such as aspect ratio (h_o^*/b_o) and bottom slope. F_o, h_o^* and b_o have been defined in section 3.2. It is well known (1, 117) that all types of turbulent jets must be modelled with undistorted scales, because the turbulent mixing region will not be distorted regardless of geometrical distortion. The effect of distortion is illustrated by Figure 3-1b, where it is seen that the stable dilution, D_s, increases with F_D and (h_o^*/b_o). For a vertically distorted Froude model

$$F_{D_r} = 1 \qquad (5.11)$$

but

$$(h_o^*/b_o)_r = \frac{L_{z_r}}{L_{x_r}} > 1 \text{ (distorted model)} \qquad (5.11a)$$

where

L_{z_r} = vertical length scale ratio

L_{x_r} = horizontal length scale ratio

Thus $D_{s_r} > 1$ for a distorted model

5.8.3 Similarity Requirements for Stratified Flows

The similarity requirements for stratified flows have been obtained by Stolzenbach and Harleman (1967) from an examination of the equations for one dimensional two-layer flows. Treating the upper and lower layer flows as one dimensional, the following differential equation is obtained describing the change in layer thickness in a horizontal open channel

$$\frac{dh_2}{dn} = -\frac{dh_1}{dx} = \frac{\frac{f}{8}(1-\eta')^3 \frac{|q_2|q_2}{q_1^2} - \frac{f_i}{8}\left|\eta' - \frac{q_2}{q_1}(1-\eta')\right|\left(\eta' - \frac{q_2}{q_1}(1-\eta')\right)}{-\frac{1}{F^2}(1-\eta')^3\eta'^3 + \eta'^3 + (1-\eta')^3\left(\frac{q_2}{q_1}\right)^2} \qquad (5.12)$$

where $F^2 = \dfrac{q_1^2}{g\frac{\Delta\rho}{\rho}(h_1+h_2)^3}$

and

q_1 = flow/unit width in upper layer

q_2 = flow/unit width in lower layer

h_1 = depth of upper layer

h_2 = depth of lower layer

$\eta' = h_2/(h_1 + h_2)$

f = bottom friction coefficient

f_i = interfacial friction coefficient

For no flow in the lower layer ($q_2 = 0$), as in the case of a stagnant cold wedge in the discharge canal, Equation (5.12) reduces to

$$\frac{dh_2}{dx} = - \frac{- f_i/8}{- \frac{1}{F^2} (1 - \eta')^3 \eta' + \eta'} \tag{5.13}$$

Stolzenbach and Harleman point out that while strictly speaking a model should be undistorted with $f_r = f_{i_r} = F_r = 1$, it is possible to balance the effects of distortion and friction, using Equation (5.13). This gives the similarity requirement for stratified flows as

$$\frac{L_{z_r}}{L_{x_r}} = N_r \tag{5.14}$$

where N = right hand side of Equation (5.12). Note that if $F_r = 1$ as will usually be the case, then for $q_2 = 0$ (stagnant wedge) Equation (5.14) reduces to

$$\left(\frac{L_z}{L_x} \right)_r = f_{i_r} \tag{5.15}$$

Typical values of f_i for the model are 0.05 - 0.1 while for the prototype $f_i \rightarrow 0.01$. Thus a vertical distortion of 5 - 10 may be necessary

to balance the effects of friction on density currents.

When the interest in the interface position is restricted to a local phenomena such as selective withdrawal drawdown in the vicinity of the intake structure, the densimetric Froude similarity alone is sufficient (117).

5.8.4 Similarity Requirements for Surface Heat Loss

The modelling law for surface heat loss can be obtained quite simply from the one dimensional equation for heat transport. Using the linear form for heat loss, the following equation applies for steady state plug flow

$$\frac{T_x - T_E}{T_o - T_E} = \exp\left(- \frac{Bx}{Q} \frac{K}{\rho c} \right) \qquad (5.16)$$

For similarity, assuming the same fluid in model and prototype,

$$\frac{L_{x_r}^2}{Q_r} K_r = 1 \qquad (5.17)$$

The Froude criteria still applies and therefore Q_r is given by

$$Q_r = L_{z_r}^{3/2} L_{x_r} \qquad (5.18)$$

thus

$$\left(\frac{L_z}{L_x} \right)_r = \frac{K_r}{(L_{z_r})^{1/2}} \qquad (5.19)$$

Since $K_r \tilde{\sim} 0.5$ and L_{z_r} is of the order of 1/25 to 1/100, the similarity of heat transfer requires a distortion of $2\frac{1}{2}$ to 5.

5.8.5 Reynolds Criteria

Reynolds numbers in a field cooling pond are relatively low, of the order $5 \times 10^5 - 10^6$, where the Reynolds Number, R, is defined as $(4q/\nu)$ and q is the flow per unit width. In a distorted Froude model the Reynolds number ratio between model and prototype $R_r = L_{z_r}^{3/2}$. For turbulent flow in the model, Reynolds numbers greater than 2500 are required, and thus L_{z_r} cannot be less than about 1/40. Since length scales of large ponds are now 10,000 - 20,000 ft., satisfaction of Reynolds criteria may require a distortion of 5 to 15.

5.8.6 Conclusions on Physical Modelling

Accurate modelling of cooling pond behaviour requires that similarity requirements for jet mixing, stratified flows, and surface heat loss all be satisfied along with the Froude and Reynolds criteria. It has been shown that each similarity requirement imposes its own distortion ratio, which ranges from no distortion for jet mixing, to $2\frac{1}{2}$ to 5 for surface heat loss, to 5 - 10 for stratified flow, to 5 - 15 for Reynolds effects. Obviously a problem exists as it is impossible to satisfy all these criteria simultaneously, and the possibility of finding a reasonable compromise must be evaluated on a case by case basis.

5.9 Conclusions

Existing analytical models, plus some simple proposed models have been tested against laboratory and field data. The proposed models which include the effect of entrance mixing, performed somewhat better than the usual plug flow or fully mixed models. Existing

models, which are based on the plug flow or fully mixed concept often require the use of a fitting parameter such as the "effective area ratio" to give acceptable results. It was noted that one can also use entrance mixing as a fitting parameter, and the severe consequences of this approach were discussed. Some analytical models require input information from physical models, and the severe limitations on physical modelling make this approach suspect. All existing models are one dimensional, with temperature variations either in the horizontal plane only, or vertical plane only. The ideal cooling pond, defined in Chapter 1 as a deep stratified pond, with low entrance mixing, and a deep skimmer type intake, was shown in Chapter 4 to have temperature variations both in the horizontal and vertical plane. A realistic model of this type of pond must include horizontal variations in order to simulate heat loss correctly, and must include vertical variations in order to reproduce the transient response of the pond i.e. a <u>three dimensional model is required</u>. It has been shown that a physical model cannot simulate the behaviour of the ideal type of cooling pond and hence a mathematical model is required. Fortunately, the significant role of density currents in an ideal cooling pond makes possible the use of some assumptions which greatly simplify the necessary mathematical model. The development of the mathematical model will be given in the next chapter.

VI. Mathematical Model of a Two-Dimensional Stratified Cooling Pond

6.1 Introduction

In the previous chapters it has been shown that an ideal cooling pond is a deep, stratified pond with an effective skimmer type intake, and minimal entrance mixing. It was also shown that no mathematical model exists for this type of pond. The required model must include temperature variations in both the horizontal and vertical planes, and must account for both entrance mixing and selective withdrawal. Heat transport within the pond by advection, diffusion and absorption of transmitted radiation, surface heat transfer to the atmosphere, and other boundary heat fluxes should all be treated as realistically and accurately as possible. In this chapter the assumptions and geometrical simplifications leading to the development of the mathematical model will be presented, and the equations governing the temperature distribution within the pond will be derived. The important regions within a stratified pond will be discussed separately, and finally the numerical technique, used to solve the equations, will be presented.

The emphasis will be on the development of a predictive model, which does not require input from field measurements (other than meteorological), satisfies the above requirements, and is as simple as possible.

6.2 Development of Governing Equations

The general equations for the temperature distribution within a non-homogeneous water body are presented in this section. Following the mathematical statement of the problem, the difficulties of the

three-dimensional approach will be discussed. A simplification, which reduces the three-dimensional equations to two sets of weakly coupled one-dimensional equations, while retaining the important characteristics of an ideal cooling pond, will be presented. Finally, the governing equations are developed from finite control volumes. The approach here follows that of Huber and Harleman (1968).

6.2.1 General Equations

In the determination of the temperature distribution in a body of water with inflows and outflows there are four unknowns to be determined; all are functions of space and time: (1) the temperature, T; (2) the vector velocity, $\overline{V}$; (3) the pressure, p; and (4) the density, ρ. The complete mathematical statement requires four equations. The first equation is the fundamental differential equation governing the distribution of heat (temperature) in a fluid, the conservation of heat equation. In vector notation (Bird, et al., 1965), this equation is:

$$\frac{\partial T}{\partial t} + \overline{V}\cdot\nabla T = \nabla\cdot E\nabla T + D_m\nabla^2 T + \frac{H_v}{\rho c} \qquad (6\text{-}1)$$

where T = temperature = f(space, time),

t = time,

$\overline{V}$ = velocity vector = f(space, time),

E = turbulent diffusivity of heat = f(space, time),

D_m = molecular diffusivity of heat,

H_v = rate of heat generation or dissipation per unit volume (energy/time-volume) = f(space, time),

ρ = fluid density = f(temperature),

c = fluid specific heat = f(temperature).

The molecular diffusivity, D_m, is usually small in comparison with the turbulent diffusivity, E, and is often neglected. It is retained here because it may be important in the laboratory case.

The second equation is the momentum equation, or equation of motion, given in vector notation as:

$$\frac{\partial \overline{V}}{\partial t} + (\overline{V}\cdot\nabla)\overline{V} = \overline{g} - \frac{1}{\rho}\nabla p + \nu\nabla^2\overline{V} + \nabla\cdot E\nabla\overline{V} \qquad (6\text{-}2)$$

in which $\overline{g}$ = gravitational acceleration vector,

ν = kinematic viscosity,

and E is the turbulent diffusivity which is assumed to be the same for both heat and momentum transfer in the fluid. Equation 6-2 is the Reynold's equation, or the turbulent form of the Navier-Stokes equation.

The third equation is the continuity equation for an incompressible fluid:

$$\nabla\cdot\overline{V} = 0 \qquad (6\text{-}3)$$

The fourth equation is an equation of state relating temperature, density, and pressure. For an incompressible fluid, the density and temperature are independent of pressure but depend on each other. Thus

$$\rho = f(T) \qquad (6\text{-}4)$$

is the equation of state.

In principle, it should be possible to solve the four equations: (1) conservation of heat, (2) momentum, (3) continuity, and (4) state, simultaneously for the four unknowns: temperature, velocity, density, and pressure. In practice this is seldom the case except in certain special situations. The difficulty lies in the non-linearity of Equations 6-1 and 6-2 and in the statement of boundary and initial conditions. Except for the simplest of geometries, the boundary conditions on temperature and velocity for Equations 6-1 and 6-2 are very difficult to specify, especially for conditions resembling those in the field. Consequently a method is required for simplifying the general problem to one amenable to solution by present mathematical means.

6.2.2 Geometric Schematization as a Means of Solving the Conservation of Heat Equation

Since a solution of the equations described in Section 6.2.1 is not possible for the most general three-dimensional case, simplifications in geometry are commonly employed. It will be useful to view the two-dimensional form of Equation 6-1 to examine the effects of some geometric simplifications. Equation 6-1 can be written in two-dimensions as

$$\frac{\partial T}{\partial t} + u\frac{\partial T}{\partial x} + v\frac{\partial T}{\partial z} = \frac{\partial}{\partial x}\left[(E_x+D_m)\frac{\partial T}{\partial x}\right] + \frac{\partial}{\partial z}\left[(E_z+D_m)\frac{\partial T}{\partial z}\right] + \frac{H_v}{\rho c} \qquad (6\text{-}5)$$

where x and z are the horizontal and vertical coordinates, as shown in Figure 6-1a for an idealized pond, u and v are the horizontal and vertical advective velocities respectively, and E_x and E_z are the

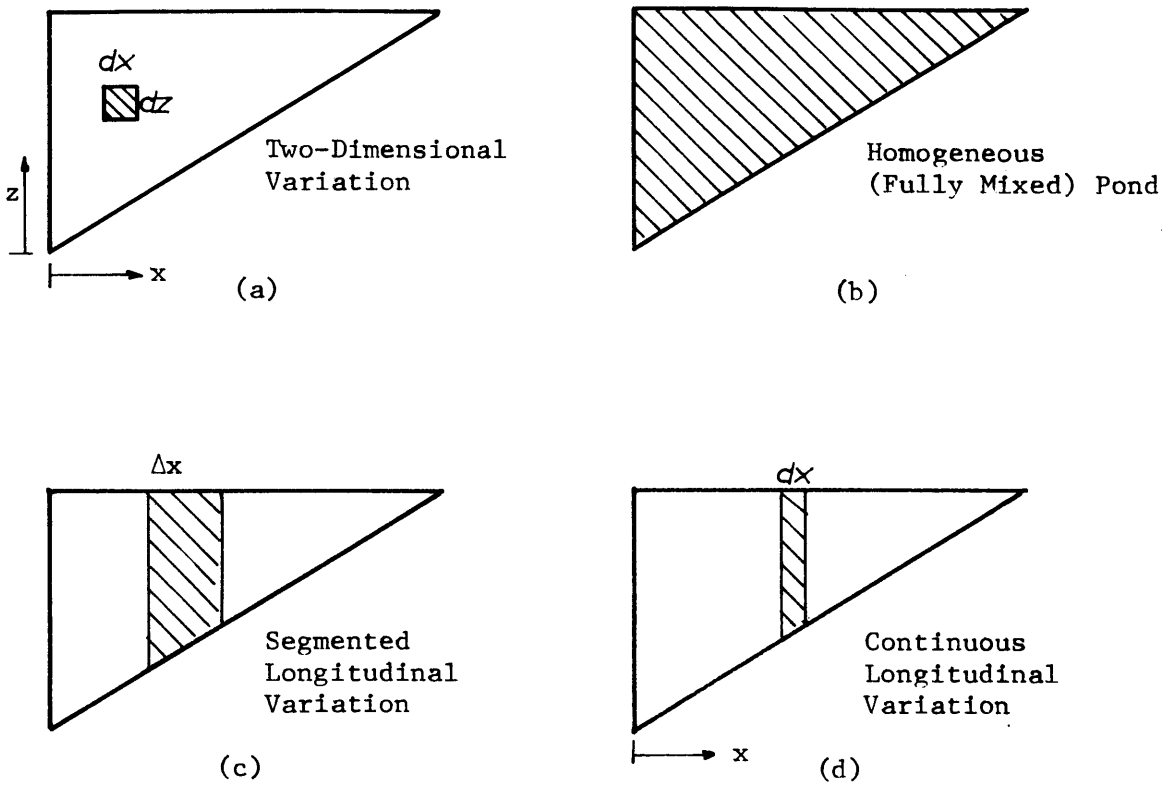

Figure 6-1 Possible Geometric Schematizations of a Two Dimensional Cooling Pond

horizontal and vertical turbulent diffusivities. Other variables are as previously defined.

Equation 6-5 applies to the elemental fluid particle shown in Figure 6-1a. The source term, H_v, will refer only to internal absorption of penetrating solar radiation since other sources or sinks of heat will be accounted for by boundary conditions.

An additional simplification is frequently obtained by eliminating the dependence of temperature on one or both coordinates by, in effect, the spatial integration of Equation 6-5. This can be done in a variety of ways. The simplest case results in the mathematical model for the fully mixed pond discussed in Chapter 3. This is shown schematically in Figure 6-1b. All spatial dependence of temperature is removed, and the resulting equation is of the form:

$$\frac{\partial T}{\partial t} = \frac{H_v}{\rho c} \tag{6-6}$$

in which H_v now includes any heat additions or losses through the boundaries.

If Equation 6-5 were integrated in the vertical direction, but only over a portion of the horizontal direction, the schematization of Figure 6-1c would result, in which an equation of the form 6-6 would apply over each segment of length Δx. Such a segmentation assumes some variations in temperature in the horizontal direction. The limiting case of this type of segmentation is one in which a continuous horizontal temperature variation is assumed. The limiting case of Figure 6-1c is shown in Figure 6-1d which is governed by the equation:

$$\frac{\partial T}{\partial t} + u \frac{\partial T}{\partial x} = \frac{\partial}{\partial x}\left[(E_x + D_m) \frac{\partial T}{\partial x} \right] + \frac{H_v}{\rho c} \qquad (6\text{-}7)$$

Here, u is the average horizontal velocity across any vertical section, and H_v includes any heat sources or sinks along the horizontal boundaries, such as the surface. Note that Figure 6-1d represents a vertically mixed plug flow pond, and Equation 6-7 is the basic equation for this type of pond.

If Equation 6-5 is integrated in the horizontal plane but some vertical variation of temperature is retained, the layered system shown in Figure 6-1e is developed. Again, an equation of the type of 6-6 governs each horizontal layer. In an analogous manner to the situation of the previous paragraph, the limiting case of Figure 6-1e arises when a continuous variation in the vertical direction is retained and only the horizontal temperature variation is ignored, as shown in Figure 6-1f. This type of schematization is governed by an equation of the form

$$\frac{\partial T}{\partial t} + v \frac{\partial T}{\partial z} = \frac{\partial}{\partial z}\left[(E_z + D_m) \frac{\partial T}{\partial z} \right] + \frac{H_v}{\rho c} \qquad (6\text{-}8)$$

in which v is the average vertical velocity across a horizontal section, and H_v includes any heat sources or sinks along vertical boundaries, such as those due to the inflow and outflow of the cooling pond.

None of the schematizations presented above is suitable for an ideal cooling pond where temperature variations in both the horizontal and vertical directions are important. It is necessary to retain the

horizontal variations in order to correctly account for surface heat transfer, and vertical variations are essential for simulating the pond transient response. However, both the schematized form of an ideal pond, (Figure 1-6) and the observed temperature structure in the laboratory and the field (Figures 4-2 and 4-4) suggest a simple solution. The solution is to divide the pond into two regions, a vertically mixed surface region where only horizontal temperature variations are considered, and a horizontally mixed lower region, where only vertical temperature variations are present. The depth of the surface layer is controlled by inflow conditions. The suggested schematization is shown in Figure 6-2

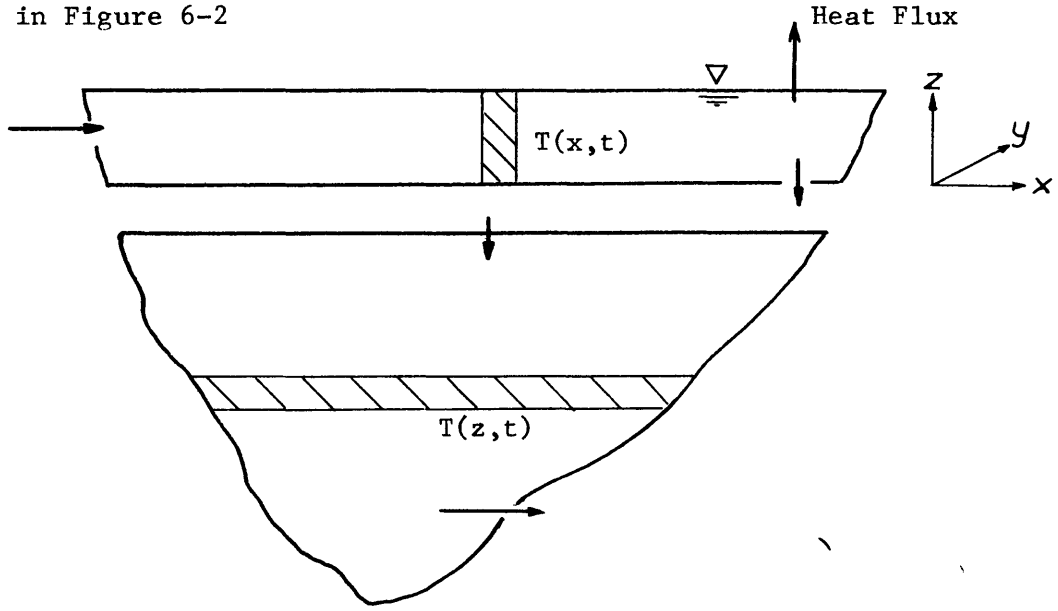

Figure 6-2 Geometric Schematization of an Ideal Cooling Pond

Note that the temperature of the surface layer is given as a function of x only, although as seen in Figure 4-2, pronounced gradients exist in the lateral (y) direction. This schematization is

acceptable because the shape of a deep, statrified pond does not affect the areal temperature distribution as was shown in Chapter 4. Laboratory experiments showed that surface temperature for a ideal pond is a function only of area and time i.e. $T = T(A_x,t)$ where A_x is the area swept out by the heated discharge. Since pond shape does not matter, except in its effect on entrance mixing, the surface layer can be schematized as a long, narrow, constant width strip in the x direction, and hence T can be described either as $T(x,t)$ or $T(A_x, t)$. In reducing the surface layer to one dimension, the problem is simplified enormously, but a certain amount of information is lost, since the temperature at a specified point (x,y,z) within the pond is not given. However, the area and volume under any specified isotherm is available, and legislated thermal criteria are generally given in these terms, and not in terms of point temperature. For certain simplified geometries, a good approximation of point temperatures may be obtained from a knowledge of $T(A_x,t)$. The linear description of surface temperature $T(x,t)$ is useful in the development of the governing equations, but will then be discarded.

The governing equation for each region will now be developed.

6.2.3 Governing Equation for the Surface Layer

The governing equation for a surface layer can be obtained by considering the conservation of mass and heat in the finite control volume shown in Figure 6-3. The depth of the surface layer, d_s, is a function of space and time, and is controlled primarily by the flow conditions at the outlet i.e. the point where the heated discharge

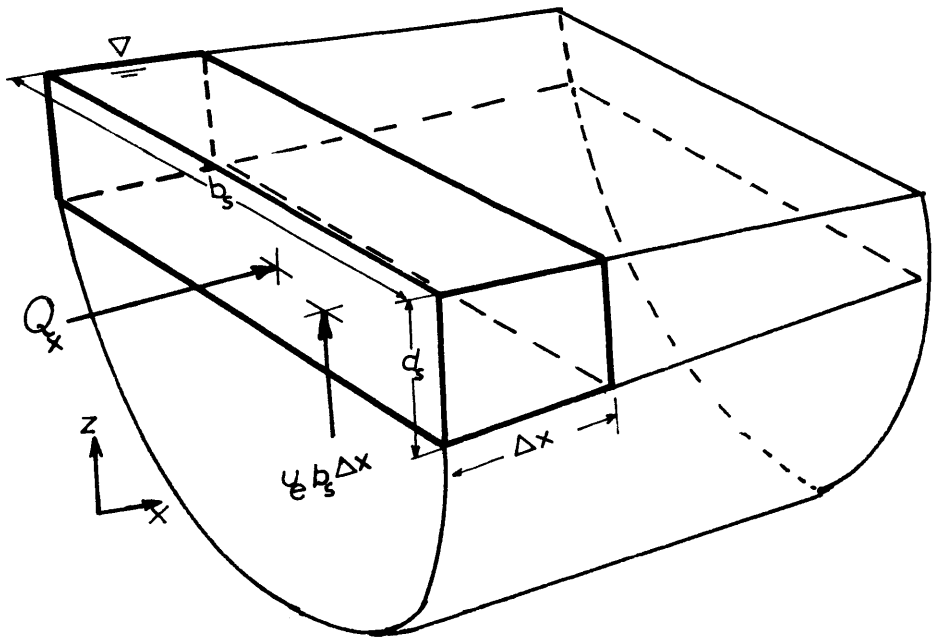

a) Control Volume Illustrating Mass Concentration

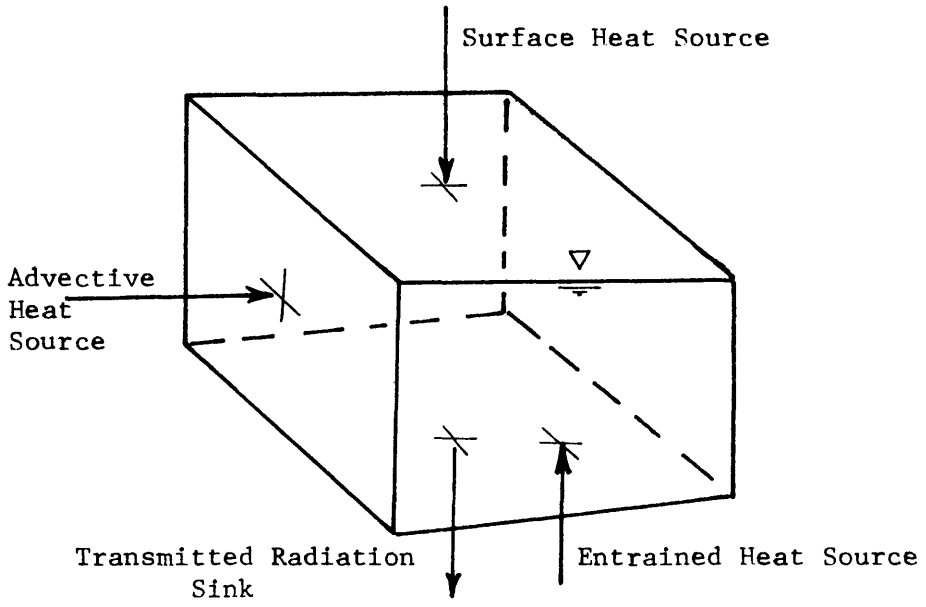

b) Control Volume Illustrating Heat Conservation

Figure 6-3 Control Volume in Surface Layer

enters the main cooling pond. Two assumptions are made which simplify the final equation. These assumptions are:

a) The temperature of the entrained flow is constant in space. This is not strictly true, but it was observed in the laboratory that temperature of the water entrained laterally within the surface layer was approximately equal to that entrained vertically from the layer underneath the surface layer. It is assumed in the model that all entrained flow comes from the uppermost layer in the lower region.

b) Heat transport by diffusion and dispersion is neglected. This applies both to longitudinal dispersion within the surface layer, and vertical diffusion downward from the surface layer to the underlying region. It is common to neglect longitudinal dispersion, this is typically done in determining steady state temperature distributions in rivers and is justified on the grounds that the curvature of the longitudinal temperature profile is small. This is also true for cooling ponds except for a relatively small area near the outlet. Neglect of diffusion in the transient case is justified on the grounds that the time scale of the motion in the horizontal layer is often an order smaller than the time scale of interest, which is defined as the residence time of the pond, and hence no attempt is made to accurately simulate the transient behavior of the surface layer e.g. the horizontal motion of a warm front. Note that although dispersion is explicitly neglected, the numerical treatment of advective terms introduces an effective dispersion, and it will be shown that this effective dispersion is of the same order as the Taylor dispersion in a narrow stream.

Vertical diffusion will be discussed in detail in Section 6.7.7

Using the control volume in Figure 6.3a, conservation of mass gives

$$(Q_x + \frac{\partial Q_x}{\partial x} \cdot \Delta x) - Q_x = u_e b_s \Delta x$$

which reduces to

$$\frac{\partial}{\partial x}(Q_x) = b_s u_e \qquad (6.10)$$

where Q_x = volume flow rate in the x direction

$u_e = u_e(x,t)$ = entrained inflow rate per unit horizontal area

b_s = width of the surface layer

The specification of u_e is a critical part of the proposed model and is discussed in detail in Section 6.5.

The conservation of heat equation is derived by equating the time rate of change of heat stored in the control volume of Figure 6.3b to the heat flux through the control volume.

The advective heat flux entering the control volume in the horizontal direction is

$$\rho c Q_x(x,t) \quad T(x,t)$$

The heat flux from the entrained inflow is

$$\rho c u_e(x,t) \quad T_e b_s \Delta x$$

where T_e = temperature of entrained water

Δx = horizontal thickness of control volume

The heat flux, per unit area, through the surface is ϕ_n. All components of the surface heat flux, except the short wave radiation, are either absorbed in, or originate from the top millimeter (.003 ft) of water. Some of the short wave radiation will be transmitted through the surface layer, and a reasonable estimate of this flux (see Section 6.7.8) is

$$\phi_{sn}(1-\beta^*)e^{-\eta d_s}$$

where ϕ_{sn} = net incident short wave radiation

β^* = Fraction of short wave radiation absorbed at the water surface

η = extinction coefficient of water

d_s = thickness of surface layer

Assuming that density and specific heat are constant over the range of temperatures considered, the following equation is obtained

$$\rho c b_s \Delta x d_s \frac{\partial T}{\partial t} = \rho c Q_x T - \left[\rho c Q_x T + \left(\frac{\partial}{\partial x} \rho c Q_x T\right)\Delta x \right] + \rho c u_e T_e b_s \Delta x + b_s \Delta x \left[\phi_n - \phi_{sn}(1-\beta^*)e^{-\eta d_s} \right] \quad (6.11)$$

which reduces to

$$\frac{\partial T}{\partial t} + \frac{1}{b_s d_s} \frac{\partial}{\partial x} (Q_x T) = \frac{u_e T_e}{d_s} + \frac{1}{\rho c d_s} \left[\phi_n - \phi_{sn} (1-\beta^*) e^{-\eta d_s} \right] \tag{6.12}$$

Since the width of the surface layer can be assumed constant, the advective term can be written as

$$\frac{1}{b_s d_s} \frac{\partial}{\partial x} (Q_x T) = \frac{1}{d_s} \frac{\partial}{\partial (b_s X)} (Q_x T) = \frac{1}{d_s} \frac{\partial}{\partial A_x} (Q_x T) \tag{6.13}$$

where $A_x = b_s x$

Equation 6.12 now becomes

$$\frac{\partial T}{\partial t} + \frac{1}{d_s} \frac{\partial}{\partial A_x} (Q_x T) = \frac{u_e T_e}{d_s} + \frac{1}{\rho c d_s} \left[\phi_n - \phi_{sn} (1-\beta^*) e^{-\eta d_s} \right] \tag{6.14}$$

Equation (6.14) requires one initial and one boundary condition for its solution. The initial condition is supplied by specifying an initial temperature distribution

$$T(A_x, 0) = T_1(A_x) \quad \text{for all } A_x \tag{6.14a}$$

where $T_1(A_x)$ is a constant or a known function of A_x. The boundary condition is obtained by setting the temperature at the power plant end of the surface layer equal to the discharge temperature

$$T(0,t) = T_o(t) \quad \text{for all } t \tag{6.14b}$$

where

$T_o(t)$ = plant discharge temperature

6.2.4 Governing Equation for Subsurface Region

The fundamental assumption for this region is that isotherms are horizontal. This assumption was strongly supported by observations in the laboratory and field (see Figure 4-2, 4-4, 4-5). The governing differential equation will be formulated with respect to a finite control volume, taken as a horizontal slice of a deep reservoir as shown in Figure 6.4. The subsurface region is considered here as part of a deep multi-purpose reservoir, with multiple inflows and outflows, since this provides a more general equation than an artificial cooling pond with essentially one inflow and outflow. The control volume has a thickness Δz, and a horizontal surface area A(z). A portion of a river inflow ΔQ_{in} enters the slice at the upstream end, and a portion of the outflow through the dam, ΔQ_{os}, leaves the slice at the downstream end. The vertical flow rate is Q_v.

Conservation of mass for the control volume shown in Figure 6-4a gives

$$\Delta Q_{os} - \Delta Q_{in} = Q_v - (Q_v + \frac{\partial Q_v}{\partial z} \Delta z) \tag{6.15}$$

which reduces to

$$\frac{\partial Q_v}{\partial z} = \frac{\Delta Q_{in} - \Delta Q_{os}}{\Delta z} \tag{6.16}$$

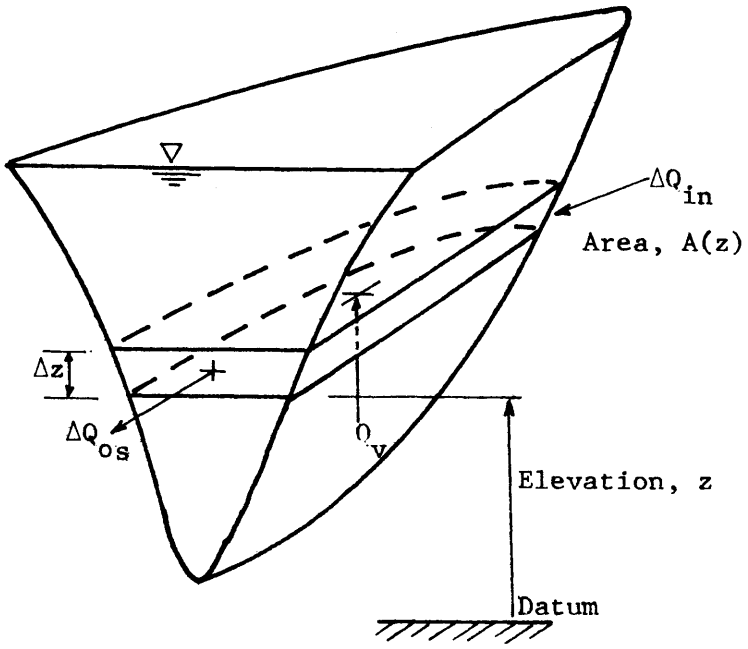

a) Sub-Surface Control Volume Illustrating Mass Continuity

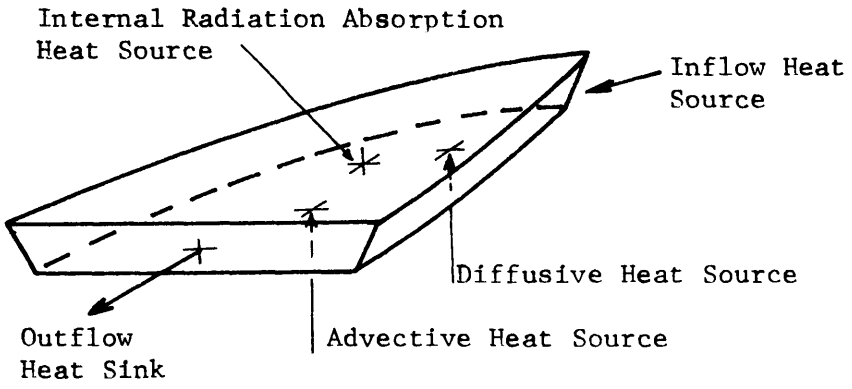

b) Sub-Surface Control Volume Illustrating Heat Conservation

Figure 6-4 Schematization and Control Volume for Sub-Surface Region

If q_{in} and q_{os} are defined as the inflow and outflow rate per unit vertical distance, respectively, then Equation (6.15) becomes

$$\frac{\partial Q_v}{\partial z} = q_{in}-q_{os} \tag{6.17}$$

The vertical flow rate, Q_v, at any elevation z, can be found by integrating Equation (6.17)

$$\begin{aligned} Q_v(z,t) &= \int_o^z [q_{in}(z_1,t)-q_{os}(z_1,t)]dz_1 \\ &= Q_{in}(z,t)-Q_{os}(z,t) \end{aligned} \tag{6.18}$$

where $Q_{in}(z,t)$ and $Q_{os}(z,t)$ represent the total inflow and outflow from the control volume below elevation z. The determination of $Q_v(z,t)$ can be seen to depend upon the proper representation of the vertical distribution of inflow and outflow from the reservoir.

The conservation of heat equation is derived by equating the time of change of heat stored in the control volume of Figure 6-4b to the heat flux through the control volume.

The advective heat flux entering the control volume in the vertical direction is

$$\rho c Q_v T$$

where Q_v = $Q_v(z,t)$ = volume flow rate crossing elevation z (positive upward)

ρ = density of water

c = specific heat of water

T = $T(z,t)$ = reservoir water temperature

The diffusive heat flux is

$$-\rho c A_z (D_m + E_z) \frac{\partial T}{\partial z}$$

where A_z = $A_z(z)$ = reservoir horizontal cross sectional area normal to the vertical axis

D_m = molecular diffusivity of heat

E_z = $E(z,t)$ = turbulent diffusivity of heat in the vertical direction

and the negative sign indicates positive diffusive heat transport in the direction of the negative temperature gradient.

The heat flux from the inflow source is

$$\rho c q_{in} T_{in} \Delta z$$

where q_{in} = $q_{in}(z,t)$ = inflow rate per unit vertical distance

T_{in} = $T_{in}(t)$ = inflow temperature

Δz = control volume thickness

The heat flux from the outflow sink is

$$\rho c q_{os} T \Delta z$$

where q_{os} = $q_{os}(z,t)$ = outflow rate per unit vertical distance

The heat flux per unit area due to internal absorption of radiation

$$\phi_b = \phi_b(z,t) = (1-\overset{*}{\beta})\phi_{sn} e^{-\eta(z_s-z)} \tag{6.19}$$

where $\overset{*}{\beta}$ = fraction of radiation absorbed at water surface

η = solar radiation absorption coefficient

$\phi_{sn} = \phi_{sn}(t)$ = net solar radiation reaching water surface

$z_s = z_s(t)$ = water surface elevation

The conservation of heat equation is formulated using the heat fluxes derived, assuming that the density and specific heat are constant over the range of temperature considered.

$$\rho c A_z \Delta z \frac{\partial T}{\partial t} = \rho c Q_v T - \left[\rho c Q_v T + \frac{\partial}{\partial z} \left[(\rho c Q_v T) \right] \Delta z \right]$$

$$-\rho c A_z (D_m + E_z) \frac{\partial T}{\partial z} - \left[-\rho c A_z (D_m + E_z) \frac{\partial T}{\partial z} - \frac{\partial}{\partial z} \left[\rho c A_z (D_m + E_z) \frac{\partial T}{\partial z} \right] \Delta z \right]$$

$$+\rho c q_{in} T_{in} \Delta z - \rho c q_{os} T \Delta z$$

$$+A_z \phi_b - \left[A_z \phi_b + \frac{\partial}{\partial z} (A_z \phi_b) \Delta z \right] \tag{6.20}$$

In Equation (6.20) heat sources due to absorption of short wave radiation by the sides of the reservoir are included.

Simplifying Equation (6.20) and dividing by $\rho c A_z \Delta z$ gives

$$\frac{\partial T}{\partial t} + \frac{1}{A_z} \frac{\partial}{\partial z} (Q_v T) = \frac{1}{A_z} \frac{\partial}{\partial z}\left[A_z (D_m + E_z) \frac{\partial T}{\partial z} \right] + \frac{q_{in} T_{in}}{A_z}$$

$$- \frac{q_{os} T}{A_z} - \frac{1}{\rho c A_z} \frac{\partial}{\partial z} (A_z \phi_b) \qquad (6.21)$$

It is possible to further simplify this equation by expanding the advective term $\frac{1}{A_z} \frac{\partial}{\partial z} (Q_v T)$. However, expanding advective terms often results in a non-conservative form of the resulting finite difference equation, and where possible should be avoided.

Equation (6.21) requires one initial and two boundary conditions. The initial condition is provided by specifying the temperature distribution in the pond at time $t = 0$.

$$T = T_f(z) \quad \text{for all } z \text{ at } t = 0 \qquad (6.22)$$

The upper boundary condition is obtained by setting the temperature at the upper boundary equal to the lowest temperature in the surface layer

$$T(z_s - d_s, t) = T(A_p, t) \quad \text{for all } t \qquad (6.23)$$

where A_p = total area of surface

The bottom boundary condition for the field cooling pond is obtained by assuming no heat flux across the boundary, a reasonable assumption since the thermal diffusivity of mud is approximately equal

to the molecular thermal diffusivity of water (Johnson and Likens (1967)). Thus the bottom boundary condition is

$$\left.\frac{\partial T}{\partial z}\right|_{z=0} = 0 \quad \text{for all } t \tag{6.24}$$

For the laboratory cooling pond considerable heat loss takes place through the bottom boundary, a concrete floor, and it was necessary to include the concrete floor as part of the cooling pond and apply the bottom boundary condition on the underside of the floor. Heat transfer by radiation only was assumed and the boundary condition becomes

$$\rho_f c_f D_f \left.\frac{\partial T}{\partial z}\right|_{z=-d_f} = \phi_R \tag{6.25}$$

where

ϕ_R = net radiation from floor

ρ_f = density of concrete

c_f = specific heat of concrete

D_f = thermal diffusivity of concrete

d_f = thickness of floor

So far the cooling pond has been considered as two regions, a surface and a subsurface region, and governing equations have been developed for each region. The surface region can be divided into three subregions, all governed by equation (6.14), but with different flow characteristics. A separate region, a simple fully mixed region, representing the intake pond must also be considered. A detailed outline

of the model is now given, and then each sub-region will be considered separately.

6.3 Outline of Model

A cooling pond may have up to five (5) flow regions, each with distinctive heat loss and flow characteristics. These regions are as follows:

a) Discharge (Outlet) Channel Region

b) Entrance Mixing Region

c) Heat Loss Region

d) Subsurface (Deep Reservoir) Region

e) Intake Pond Region

The characteristics of each region for an artificial pond are listed in Table 6-1. A natural pond, with multiple inflows and outflows is somewhat more complicated. A particle moving from outlet to intake proceeds from region 1 to region 5. A schematic of a model for a natural pond is shown in Figure 6-5.

6.4 Discharge Channel

6.4.1 Introduction

In order to minimize short circuiting of the heated discharge, it is common practice to discharge the heated water through a long narrow channel, which may be several miles in length, and may have an area of 10-100 acres. Minimal mixing at the point of entry into the main pond demands that the channel exit be designed so that a cold

Region Name	Region Number	Heat Loss	Entrainment	Type of Flow	Flow, Temperature at Start of Region	Flow, Temperature at End of Region	Remarks
Discharge (Outlet) Channel	1	Important	Present, but usually not significant (Q_{e_c} small)	Horizontal flow - possibly two-layer	Q_o T_o	Q_1 T_1	Sometimes this region is not present, and usually it is not important
Entrance Mixing Region	2	Usually unimportant	Dominant $Q_{e_p} >> Q_o$	Three-Dimensional	Q_1 T_1	Q_2 T_2	Very important region - may determine pond performance
Heat Loss Region	3	Dominant	Usually insignificant	Horizontal density flow	Q_2 T_2	$Q_3=Q_2$ T_3	Very important region. Most heat dissipation occurs here
Subsurface (Deep Reservoir) Region	4	Absent in field case. Present in laboratory	Entrained flow at outlet comes from this region	Net vertical motion	Q_3 T_3	$Q_4=Q_o$ T_4	Important from transient response point of view
Intake Pond	5	Present-may be positive or negative	Absent	Assumed fully mixed	Q_4 T_4	$Q_5=Q_o$ T_5	May be detrimental to pond performance if too large

Table 6-1. Characteristic Regions in a Closed Cooling Pond

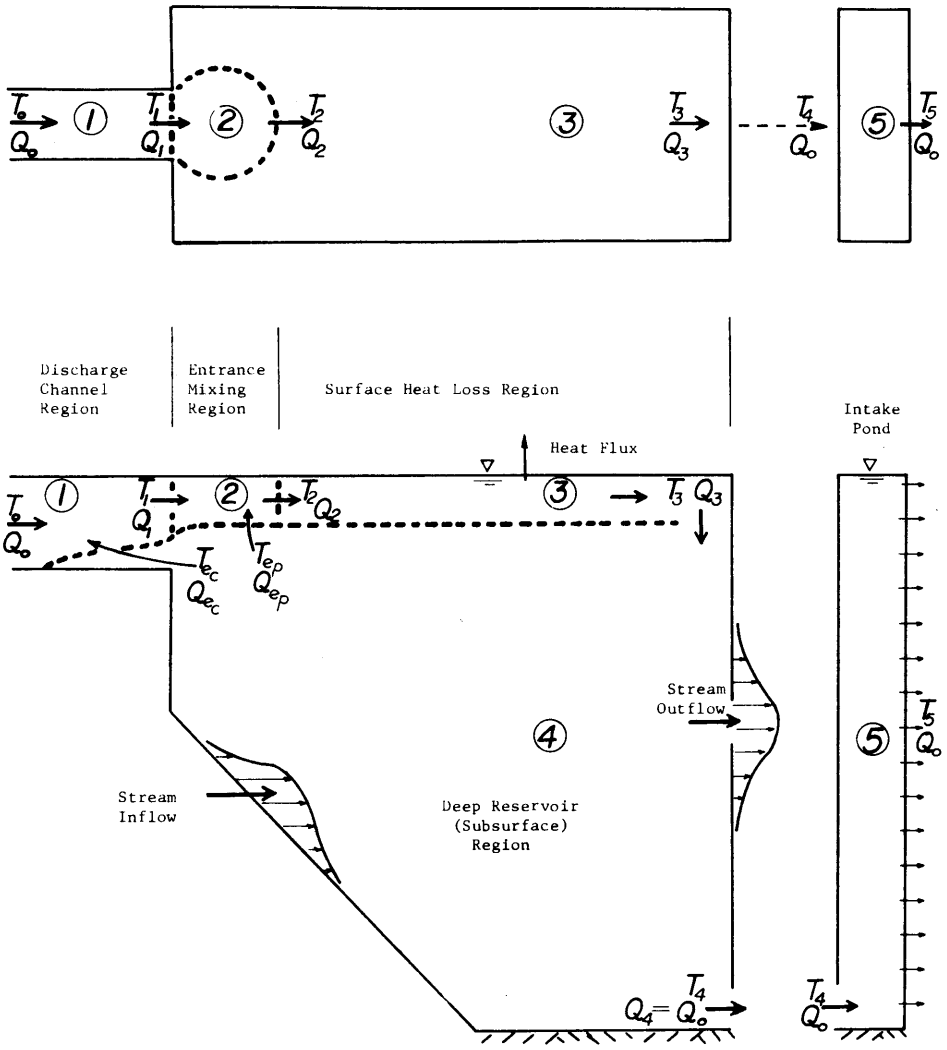

Figure 6-5 Schematic of Proposed Model for a Natural Cooling Pond

wedge intrudes into the channel. Thus in a well designed discharge channel, two layer flow will exist over part of the length. The depth, d_s, of the surface layer will vary along the channel, and some interfacial entrainment will occur. Equation (6.14) is the governing equation and is

SEE ERRATA

$$\frac{\partial T}{\partial t} + \frac{1}{d_s}\frac{\partial}{\partial A_x}(Q_x T) = \frac{u_e T_e}{d_s} + \frac{1}{\rho c d_s}(\phi_n - \phi_{sn}(1-\beta^*)e^{-nd_s}) \qquad (6.14)$$

The solution to Equation (6.14) requires that d_s and u_e be specified. u_e is usually given as a function of the local densimetric Froude number, which depends on d_s. To obtain $d_s = d_s(x,t)$ involves solving the equations of motion for a two layer flow. Solutions exist for the simplified case of a uniform channel with constant depth, and for two reasons it is sufficient to schematize the channel in this way. The reasons are:

a) The amount of entrainment tends to be small e.g. Curtis (1966) estimates that at Hazelwood, for an intrusion length of approximately 6000 ft., the maximum entrained flow was $\sim$ 6% of the condenser flow.

b) The entrainment function relating the entrained flow to the other flow parameters is not known accurately.

6.4.2 Two Layer Flow

Consider the flow of two layers of different density in a wide rectangular open channel: Figure 6.6.

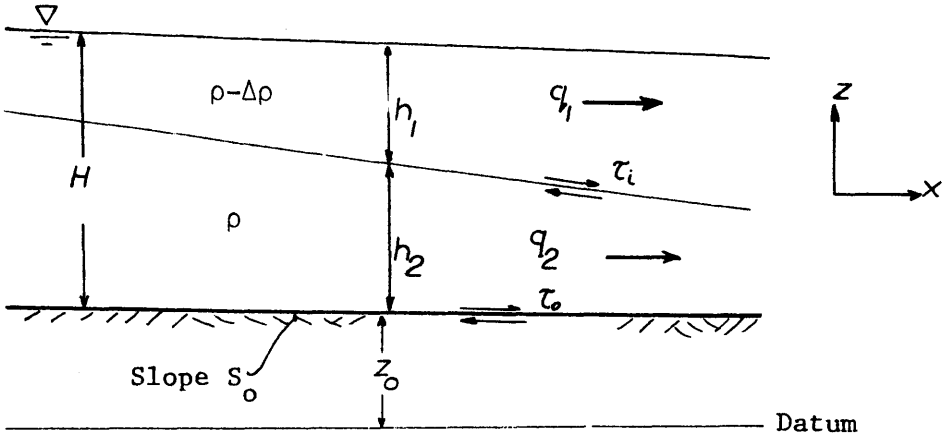

Figure 6-6 Two Layer Flow

The following assumptions are made:

a) One dimensional flow in each layer

b) Uniform density in each layer

c) Constant total depth H.

Schiff and Schonfield (1953) give an equation of the following form to describe the interface

$$\frac{dh_2}{dx} = -\frac{dh_1}{dx} = \frac{\frac{f}{8}(1-\eta')^3 \frac{|q_2|q_2}{q_1^2} - \frac{f_i}{8}\left|\eta' - \frac{q_2}{q_1}(1-\eta')\right|\left(\eta' - \frac{q_2}{q_1}(1-\eta')\right)}{-\frac{1}{F^2}(1-\eta')^3\eta'^3 + \eta'^3 + (1-\eta')^3\left(\frac{q_2}{q_1}\right)^2} \qquad (6.26)$$

where q_1 = flow unit width in the upper layer in x direction

q_2 = flow unit width in the lower layer in x direction

h_1 = depth of upper layer

h_2 = depth of lower layer

H = total depth = $h_1 + h_2$

$\eta' = \frac{h_2}{H}$

$$F^2 = \frac{q_1^2}{g \frac{\Delta\rho}{\rho} H^3}$$

f = friction factor at the bottom

f_i = friction factor at the interface

Since the entrained flow tends to be small, it is reasonable to put $q_2 = 0$ and Equation (6.26) now becomes

$$\frac{dh_2}{dx} = \frac{-\frac{f_i}{8}}{\frac{-1}{F^2}(1-\eta)^3\eta' + \eta'} \tag{6.27}$$

Assuming critical depth in the upper layer at the end of the channel, Equation (6.27) can be integrated to give the wedge length L_w as follows:

$$L_w = \frac{2H}{f_i}\left[\frac{1}{5}\frac{1}{F^2} - 2 + 3F^{2/3} - \frac{6}{5}F^{4/3}\right] \tag{6.28}$$

From Equation (6.28) it is seen that for $F = 1$ the cold wedge is swept from the channel. Actually, as $F \to 1$, one of the assumptions necessary for the solution ($\frac{dh_2}{dx} \simeq 0$) is violated, and it appears that a cold wedge actually exists only for $F \leq 0.7$.

The shape of the wedge can be obtained either from a solution to Equation (6.27), or using the affine shape for an arrested wedge given by Keulegan (1966). In fact it was found that calculating the entrainment based on an average depth of the upper layer gave almost identical results to the above more complicated approaches.

An important parameter in determining the length of the wedge is the interfacial friction coefficient f_i. Stolzenbach and Harleman (1972) show that reasonable values of f_i can be determined on the basis of smooth turbulent flow, and give f_i as a function of the Reynolds number as in Figure 6-7. For the laboratory case, Reynolds Numbers, based on flow depth ranged from $2 - 4\times10^3$, and thus f_i is approximately 0.03. Wedge lengths in the laboratory, calculated from Equation (6.28) agree reasonably well with those observed (Figure 6-8). Curtis (1966) used Equation (6.28) to estimate wedge lengths in the Hazelwood pond. He used $f_i = 0.0086$, based on measured velocity profiles, and obtained reasonable agreement with observed intrusions. Reynolds numbers in the Hazelwood canal were $\sim 10^6$, and thus Figure 6-7 gives $f_i \sim .012$ which is somewhat higher than Curtis' value, but is nevertheless reasonable.

When the geometry of the wedge is known, the entrained flow can be calculated.

6.4.3 Interfacial Entrainment

Interfacial entrainment between two layers of different density depends on the tendency of small disturbances at the interface to be damped or amplified. The interface stability is controlled by a balance of inertial, gravitational and viscous effects, and hence the local densimetric Froude number, F, and the Reynolds number, R, are the significant parameters. Keulegan (1966) proposes $\theta = \frac{1}{F^2R}$ as an indication of incipient mixing. For $\theta < \theta_c$ the interface will become unstable and mixing will occur. However, Ippen and Harleman have shown that

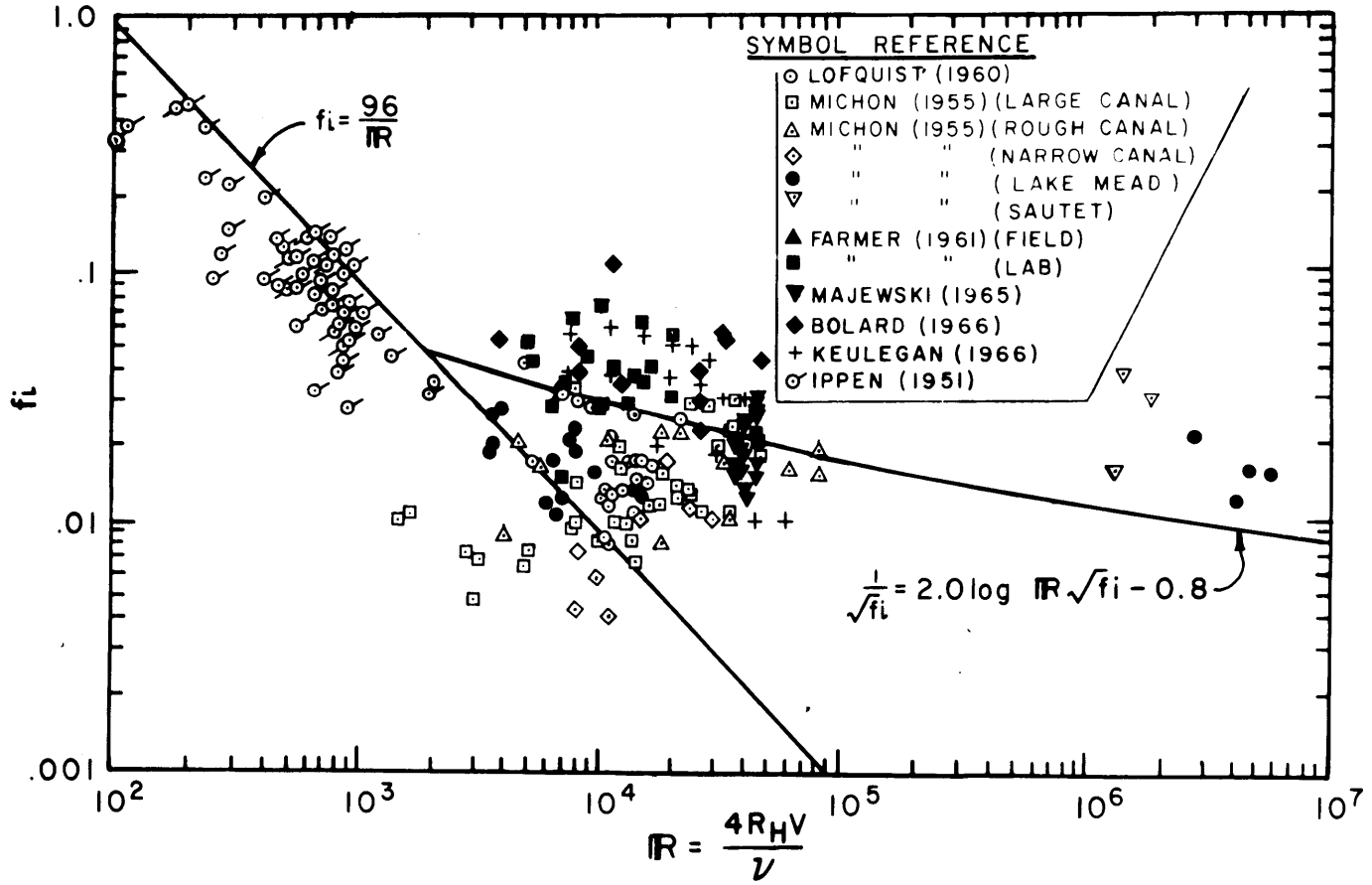

Figure 6-7 **Interfacial friction factor vs Reynolds Number** (117)

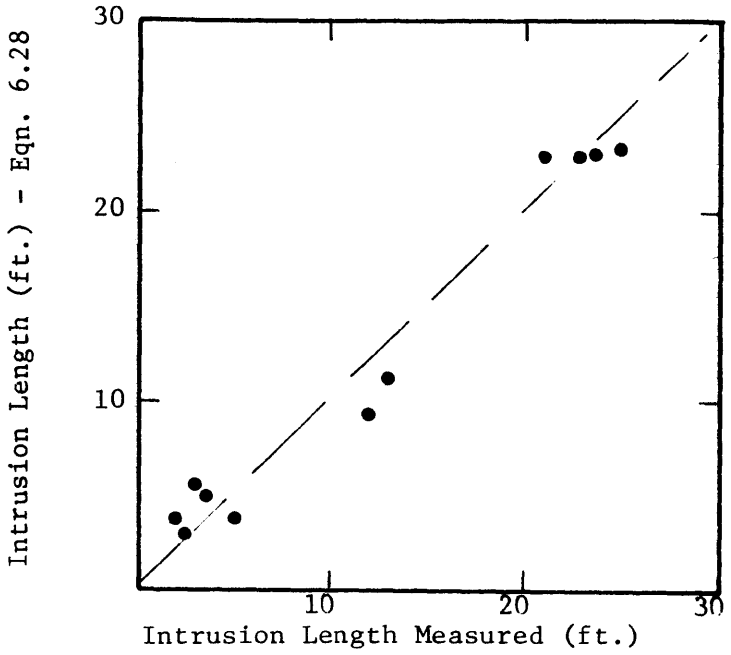

Figure 6-8 Intrusion of Cold Wedge in Laboratory Discharge Channel

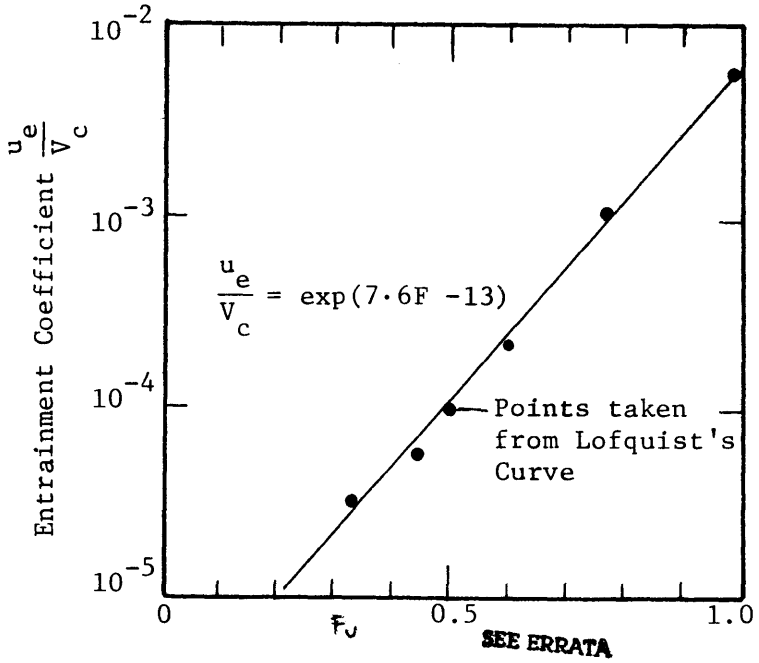

Figure 6-9 Entrainment in Two Layer Flows(F_u<1)

in the laminar range instability occurs only when $F > 1.0$. Ellison and Turner (1959), and Lofquist (1960), working in the turbulent range of R, showed that even for an "unstable" interface entrainment and mixing is small for $F < 1$, and this is supported by the work of Lean and Whillock (1965). However, as shown in the previous section, in a discharge channel with two layer flow, $F < 0.7$ and hence it is expected that the entrainment rate will be low, but in a long channel it is possible that the entrained flow will not be negligible. The results of Lofquist are the only ones of interest in the range of $F < 1$. An approximate curve which describes his results is shown in Figure 6-9, and it is seen that u_e can be described as

$$\frac{u_e}{V_c} = \exp\ (7.6\ F_u - 13) \tag{6.29}$$

where V_c = relative velocity between the two layers

$$F_u = \frac{V_c}{\sqrt{g\ \frac{\Delta\rho}{\rho}\ h_r}}$$

h_r = hydraulic radius of moving layer.

The total entrained flow in the discharge channel, Q_{e_c}, is given by

$$Q_{e_c} = \int_0^{L_w} u_e b_i dx \tag{6.30}$$

where b_i = interfacial width.

Using Equations (6.28), (6.29), (6.30), entrained flows in the laboratory discharge channel were found to be always < 1% of the condenser flow i.e. insignificant. In the Hazelwood case, with a highly non uniform channel, the entrained flow depends on the way in which the

channel is schematized. However, the above equations give a maximum entrained flow of about 6% of the condenser flow (i.e. similar to that observed by Curtis (1966), for a reasonable schematization. A simple mathematical model for the discharge channel will now be presented.

6.4.4 Mathematical Model of Discharge Channel

The discharge channel is schematized as a uniform channel, length L, depth h_o, width B, as shown in Figure 6-10.

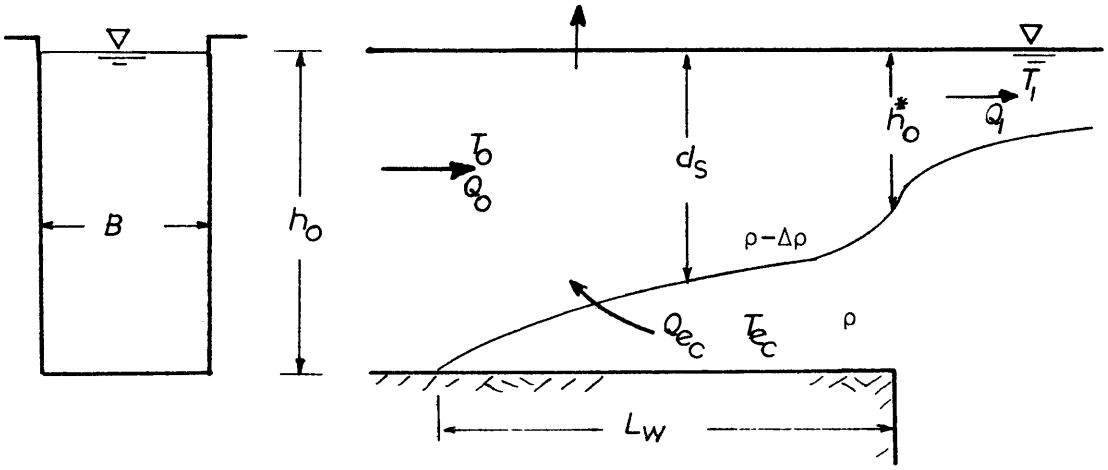

Figure 6-10 Schematization of Discharge Canal

For a given condenser flow rate and temperature, and given meteorological conditions, steady state conditions are assumed in the channel, a reasonable assumption since the residence time in the channel is only of the order of hours. Transmitted short wave radiation through the interface is assumed zero. The governing equation now becomes:

$$\frac{1}{d_s}\frac{\partial}{\partial A_x}(Q_x T) = \frac{u_e T_e}{d_s} + \frac{\phi_n}{\rho c d_s} \tag{6.31}$$

Equation (6.31) is solved by dividing the channel into segments and using a simple algorithm. The algorithm is as follows:

a) Calculate T_1 assuming $u_e = 0$. Use the correct surface area when calculating heat loss

b) Calculate the densimetric Froude number F_D at the channel exit, the wedge length L_w, the average depth of the upper flow d_s, and the entrainment velocity u_e

c) Calculate the entrained flow Q_{e_c} and hence a new T_1 and Q_1. Iterate until there is no significant change in T_1 and Q_1.

This very simple approach was found to give results indistinguishable from those of a more sophisticated model which included the correct shape of the wedge and solved Equation (6.31) in each segment.

6.4.5 Conclusion

A simple model of the discharge canal which includes the effects of surface heat loss and interfacial entrainment has been developed. The model assumes a uniform channel and steady state conditions. The wedge length is calculated using Equation (6.28). The entrained flow is calculated using an average value of upper layer depth d_s, and an empirical equation (6.29) based on Lofquist's experiment. A simple algorithm is used to couple the effects of heat loss and entrainment. No advantage is seen in using a more complicated model.

6.5 Entrance Mixing Region

6.5.1 Introduction

The exit from the discharge channel into the main pond usually involves a sudden lateral, and sometimes a vertical expansion. Considerable mixing of the heated discharge with the main pond water may result. This entrance mixing has been shown to have detrimental effects on the pond performance in three ways, by reducing the temperature of the discharge, and hence the surface heat loss rate, by inhibiting the role of density currents, and thus possibly reducing the effective area of the pond, and finally by reducing the response time of the pond. An accurate predictive model of cooling pond behavior must include an adequate description of entrance mixing effects. It is necessary to predict the amount and areal distribution of the entrained flow Q_{e_p} (see Figure 6-5), and also the area and depth at the edge of the entrance mixing region (Region 2 in Figure 6-5).

Along the centerline of a buoyant surface jet the following behavior is usually observed. First there is a core region, with little change in centerline temperature or velocity. Then follows a dilution region in which entrainment of the receiving fluid causes a quick reduction in both centerline temperature and velocity. Lateral spreading is much more pronounced than vertical spreading. The dilution region is followed by a stable region where the jet continues to spread, and the centerline velocity decreases, but vertical stability inhibits vertical entrainment, and the lower velocities and small jet depths reduce lateral entrainment. Dilution and centerline temperature

remain approximately constant in this region. At the end of the stable region heat loss starts to become important. The regions are shown in Figure 6-11, where h_o and b_o are the initial depth and half width of the jet, and ΔT_o is the initial temperature difference.

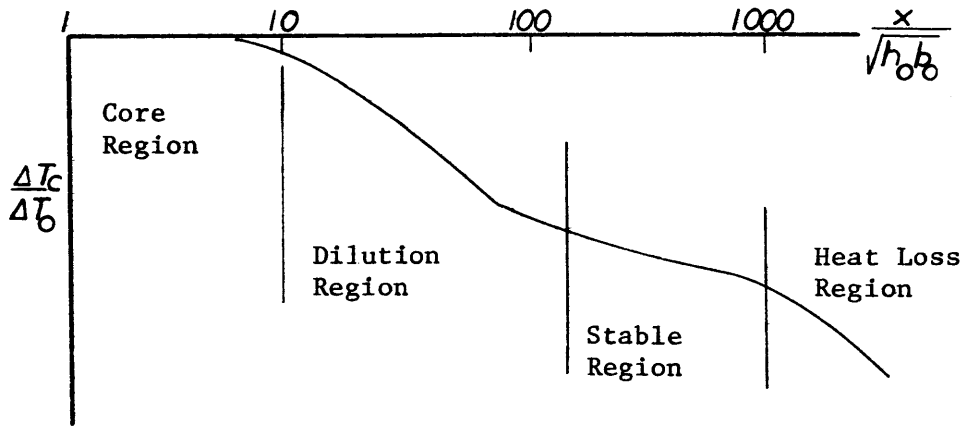

Figure 6-11 Regions in a Buoyant Surface Jet

The entrance mixing region is assumed to end at the stable region, and usually covers a relatively small area in comparison with the area of a cooling pond (< 10%).

Analytical models of heated discharges are rather plentiful, and sixteen of them were recently reviewed by Policastro and Tokar (1972). The necessary requirements of an entrance mixing model, for inclusion in the cooling pond model, will now be considered, and a suitable model selected.

6.5.2 Selection of Entrance Mixing Model

The requirements for an analytical model of entrance mixing

are as follows:

a) The model should have a sound theoretical basis. It is felt that present field data on heated discharges is of too low a standard, and covers too limited a range, to provide an adequate basis for phenomenological models.

b) Since mixing due to jet induced turbulence, and not ambient turbulence is of primary interest, a near field or jet-type model is required.

c) Since low Froude No. discharges are of primary interest, buoyancy effects will be important, and the effects of buoyancy on lateral spreading and vertical mixing should be included. The effects of outlet geometry must be considered.

d) The model must give information on the temperature distribution within the mixing region as a function of area, and on the temperature, flow rate (dilution), depth and areal extent at the end of the entrance mixing region.

e) A steady state model is sufficient, and the effects of bottom slope and ambient current are not considered to be too important for a deep, stratified pond. However a model which includes the effect of a stratified receiving water body would be preferable.

f) The model should be relatively simple so that it does not further complicate an already rather complex situation.

Restricting the model to a semi-empirical jet-type model reduces the number of suitable models to six, including those of Hoopes (1967), Carter (1969), Molz and Benedict (1970), Stolzenbach and

Harleman (1971), Pritchard (1969) and Sundaram (1969). Inclusion of buoyancy effects, and the requirement that the model predict the depth of the surface layer at the end of the mixing region, eliminate all models but the Stolzenbach-Harleman model. Policastro and Tokar (1972) note that the latter model has been carefully developed, is easily applied and is unique among existing jet models in that it considers all major factors. Thus the Stolzenbach-Harleman model has been selected although it does not meet some of the above criteria, in that it cannot handle a stratified receiving water, and it is a rather complex model. A brief description of the model follows.

6.5.3 Stolzenbach-Harleman Heated Discharge Model

Stolzenbach and Harleman (1971) developed a three dimensional model for the horizontal surface discharge, Q_D, of heated water from a rectangular channel into a large homogeneous receiving water body (see Figure 6-12). The model can handle a bottom slope, and an ambient cross flow. Surface heat loss effects are included. The mathematical model predicts the distribution of temperature and velocity within a completely determined jet structure, for a near field region defined by the predominance of jet induced turbulence over ambient turbulence. A dimensionless formulation of the heated discharge is

$$\frac{T - T_e}{T_D - T_e} = \text{function}\left[F_D, h_o^*/b_o, \frac{K}{\rho c u_D}, \theta, S_x, \frac{V_a}{u_D}, \frac{x}{\sqrt{h_o^* b_o}}\right] \qquad (6.32)$$

where

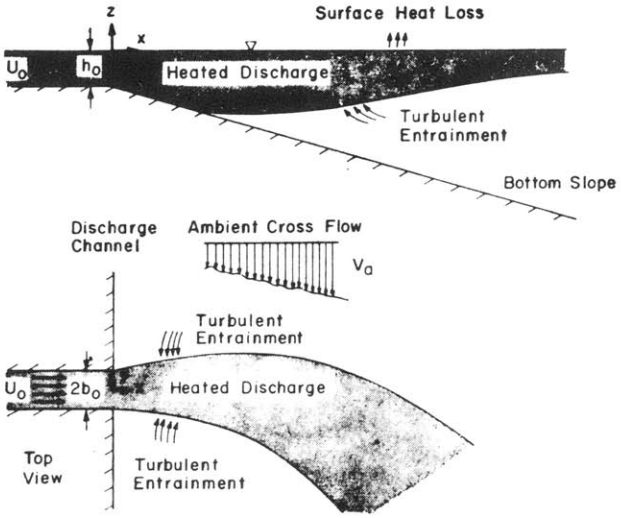

Figure 6-12 Surface discharge of heated water from a rectangular discharge channel.

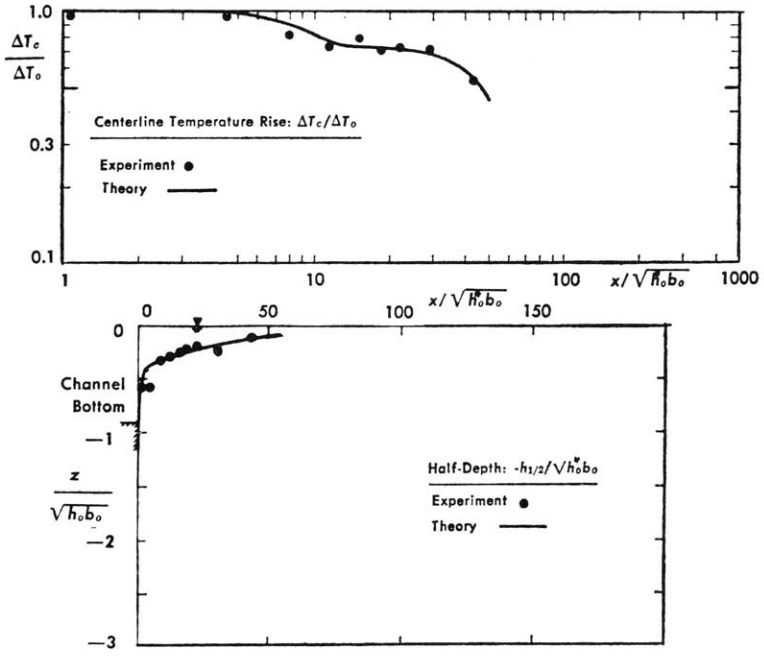

Figure 6-13 Comparison of Theory and Experiment for a Heated Discharge for $F_D = 1.03$, $h_o^*/b_o = 0.85$. (Stolzenbach and Harleman, 1971)

$F_D = \frac{u_D}{\sqrt{\frac{\Delta\rho}{\rho} g\, h_o^*}}$ = discharge densimetric Froude number SEE ERRATA

h_o^* = depth of discharge layer

b_o = half width of discharge channel

u_D = discharge velocity = $Q_d/2h_o^* b_o$

K = surface heat transfer coefficient

T_e = temperature of receiving water

T_D = discharge temperature

S_x = bottom slope

V_a = cross current velocity

θ = angle between centerline of discharge, and normal to shoreline

x = distance from exit in direction normal to the shoreline

The temperature and velocity distributions are assumed to be structured as in a classical non-buoyant jet. The authors assume an initial core region void of shear, followed by a turbulent shearing region, in which the temperature and velocity distributions are described by similarity functions. Horizontal entrainment of ambient fluid is assumed to be the same as for a non-buoyant jet; vertical entrainment is related to the local densimetric Froude number using the results of Ellison and Turner (1959), and is chosen to reduce to the non-buoyant value when no density gradients are present. Buoyant convection is incorporated through the pressure gradient terms in the equations of motion. The model is developed from the steady, time averaged

differential equations of continuity, momentum and conservation of heat energy. The equations are reduced to a set of simultaneous, first order, non linear ordinary differential equations, in a single variable x, and solved numerically. No fitting of the model to data is necessary, since the model is basically a synthesis of known results. A series of laboratory experiments were carried out to test the model, and good agreement was obtained. Figure 6-13 shows the agreement for the case of a low Froude number discharge. Note that all lengths are scaled against the characteristic length of the outfall, $\sqrt{h_o^* b_o}$.

6.5.4 Use of Stolzenbach-Harleman Model

The input information for the Stolzenbach-Harleman model is rather low, requiring only the discharge densimetric Froude Number, F_D, the discharge channel aspect ratio ($A_D = h_o^*/b_o$), the surface heat loss parameter ($K/\rho c u_D$ where u_D is the initial discharge velocity), the angle of discharge and the ambient current characteristics. The output information includes centerline temperatures and velocities, jet widths, depths and flow rate (dilution). Using the output information and the assumed similarity forms for the jet structure, one can easily calculate isotherm areas.

The above model requires the solution by computer of a set of simultaneous, first order, ordinary differential equations. The computer program could have been incorporated directly in the cooling pond model. This was not done for two reasons. The first reason is that the cooling pond model is a transient model, so the receiving water temperature is constantly changing and hence the discharge Froude

Number F_D defined with respect to the receiving water temperature, changes also. Changes in depth of the receiving water cause changes in the aspect ratio h_o^*/b_o . The continual use of the Stolzenbach-Harleman model to re-calculate the dilution would be prohibitively expensive. The second reason is that the model may fail to generate a solution for particular values of F_D, h_o^*/b_o . Reasons for this behavior are discussed by Stolzenbach, Adams and Harleman (1972). This anomalous behavior occurs frequently for F_D less than 2, and h_o^*/b_o less than 0.5, conditions which are often present for a well designed cooling pond. Hence it was decided to replace the computer model by a set of empirical formulae which fit the results of the computer model.

6.5.5 Development of Empirical Formulae

Equation (6.32) indicates that the temperature of the heated jet is a function of seven dimensionless variables. The problem can be immediately simplified by considering a jet normal to the shoreline, and then by eliminating the effects of bottom slope and cross current, both very reasonable assumptions for a deep cooling pond. Since the effects of surface heat loss are not really significant until after the end of the dilution (entrance mixing) region, it seems reasonable to develop empirical equations based on zero heat loss, and later include the heat loss effect through the governing equation (6.14). This reduces the required function to one dependent on three dimensionless parameters, F_D, h_o^*/b_o, $\frac{x}{\sqrt{h_o^* b_o}}$. Empirical formulae are required which give the dilution as a function of area out to the limit of the entrance mixing

region, plus the areal extent of the mixing zone and the depth of the surface layer at the edge of the zone. The following approach was used to obtain the required formulae.

a) Using the computer program for the Stolzenbach-Harleman model, a large number of solutions giving $\Delta T_c/\Delta T_o$ vs $x/\sqrt{h_o^* b_o}$ for a wide range of F_D, h_o^*/b_o was generated.

b) An empirical formula was obtained relating the dilution at the stable region, D_s, to F_D and h_o^*/b_o. Figure 6-14 shows that the expression

$$D_s = 1.4 \sqrt{1+F_D^2}\,(h_o^*/b_o)^{1/4} \tag{6.33}$$

gives good agreement over a wide range of F_D (1-20) and h_o^*/b_o (0.05-4). The Stolzenbach-Harleman model does not give consistent results below $D_s = 2$, while Equation (6.33) can give meaningless values of $D_s < 1$ for low values of F_D and h_o^*/b_o. Based on experimental data (see Chapter 7) a lower limit of 1·5 was set for D_s. This is also consistent with Equation (5.4) in reference (116).

c) An empirical formula was obtained relating the area of the entrance mixing region, A_M to F_D and h_o^*/b_o. A_M is defined as the area swept out by the plume at the stable region, and Figure 6-15 shows that a good fit is given by the equation

$$\frac{A_M}{h_o^* b_o} = 550\ (1+F_D^2)(h_o^*/b_o)^{1/2} \tag{6.34}$$

d) A dilution area curve was obtained, giving the dilution D_x,

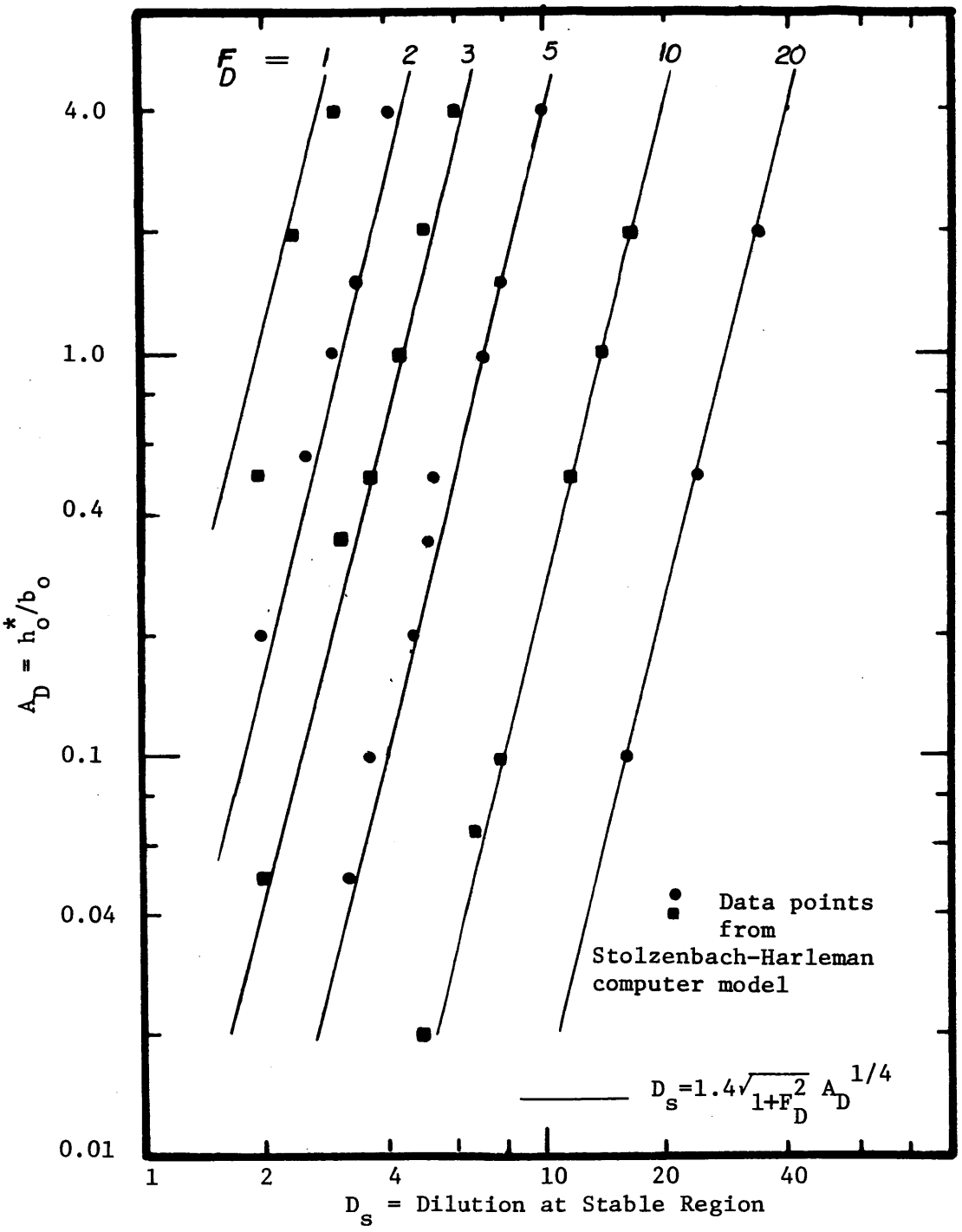

Figure 6-14 Stable Dilution vs. F_D and A_D

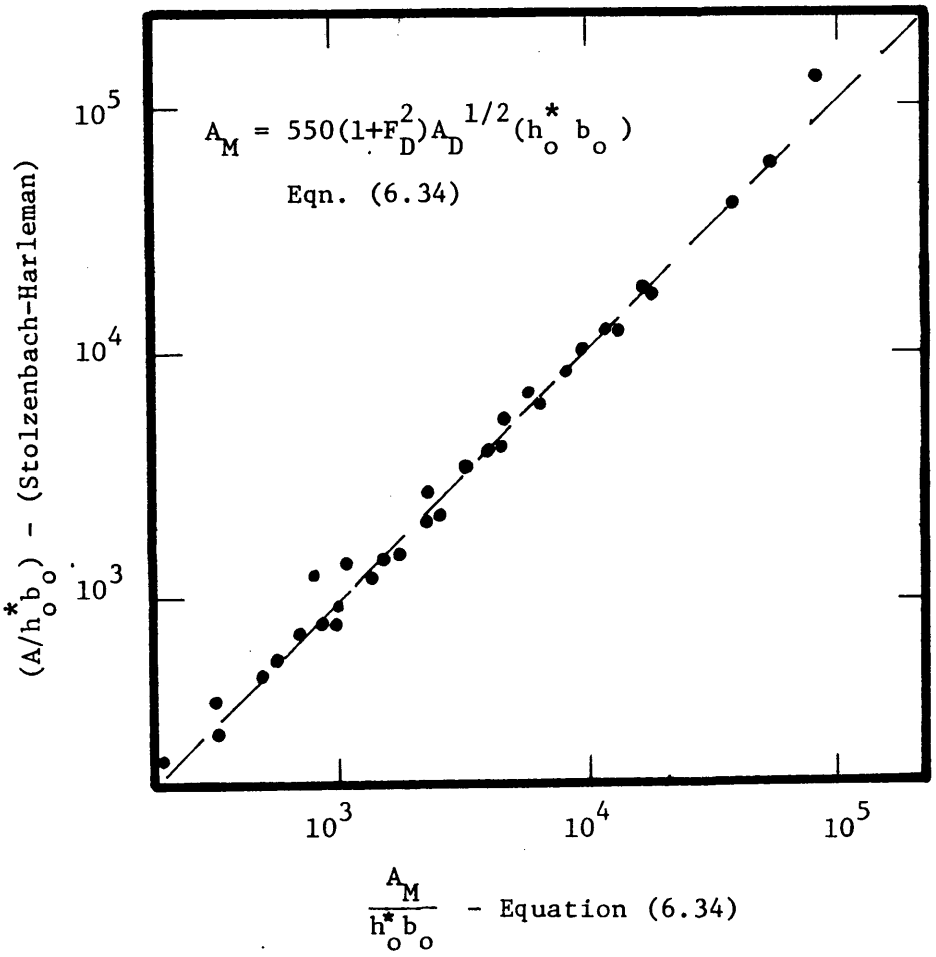

Figure 6.15 Comparison of Areas of the Entrance Mixing Region, A_M, predicted by the Stolzenbach-Harleman Model, and Empirical Formulae.

corresponding to the area A_x, as follows

$$\frac{D_x}{D_s} = \left(\frac{A_x}{A_M}\right)^{1/5} \tag{6.35}$$

Figure 6-16 shows an example of the agreement between the empirical equation (6.35) and the Stolzenbach-Harleman results.

e) Finally an empirical expression was obtained relating the depth at the stable region d_M to F_D and h_o^*/b_o . The depth, d_M, determines the thickness of the heat loss region (Region 3 in Figure 6-5) and thus is an important parameter. A good fit to the Stolzenbach-Harleman results was given by

$$\frac{d_M}{\sqrt{h_o^* b_o}} = \frac{3}{8}\sqrt{1+F^2}\ (h_o^*/b_o)^{1/4} \tag{6.36}$$

Figure 6-17 shows the agreement obtained.

6.5.6 Summary

The computer model of Stolzenbach and Harleman (1971) was used to generate solutions to the problem of a heated surface discharge over a wide range of the dimensionless parameters F_D and h_o^*/b_o . Using these results empirical formulae were obtained relating the dilution at the stable region, D_s, the area of the entrance mixing region, A_M, and the depth at the end of the entrance mixing region, d_M, to the dimensionless parameters F_D and h_o^*/b_o . A relationship between dilution, D, and area swept out by the jet, A_x, was also obtained. The formulae are as follows:

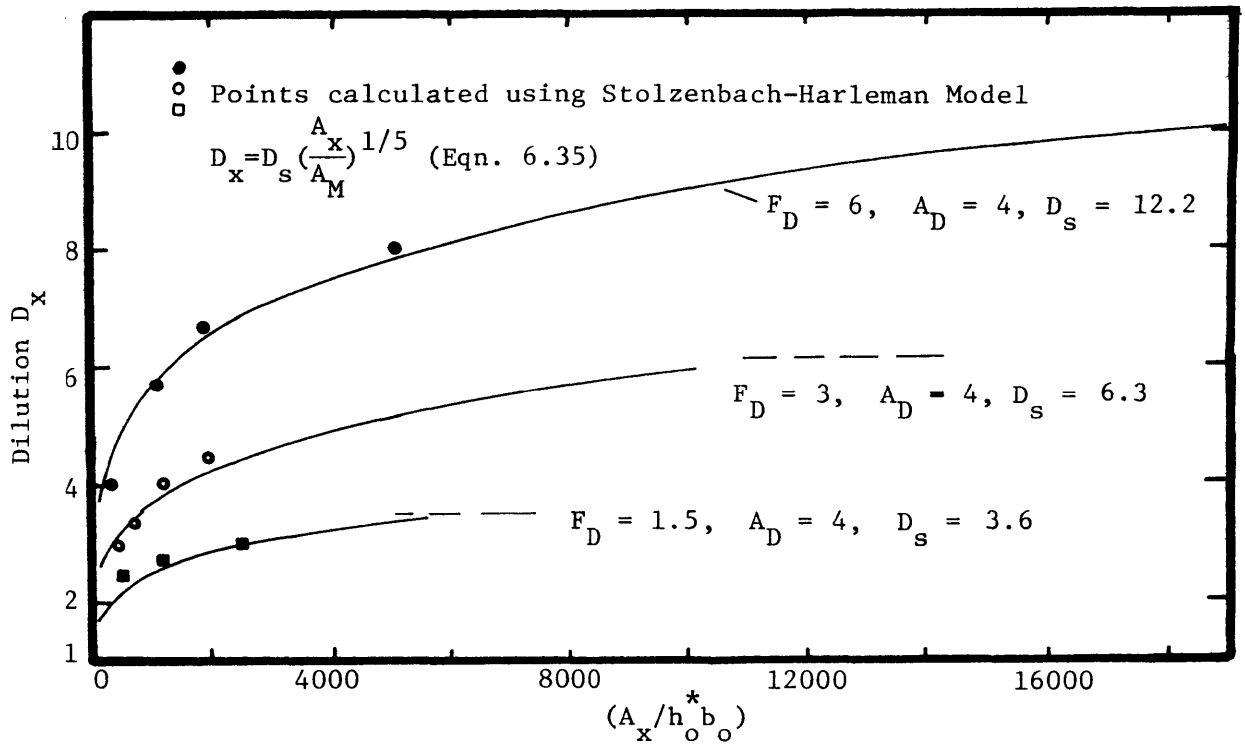

Figure 6-16 Comparison of Dilution-Area Curves predicted by Stolzenbach-Harleman Model and Empirical Formulae (Eqns. 6.37-6.40)

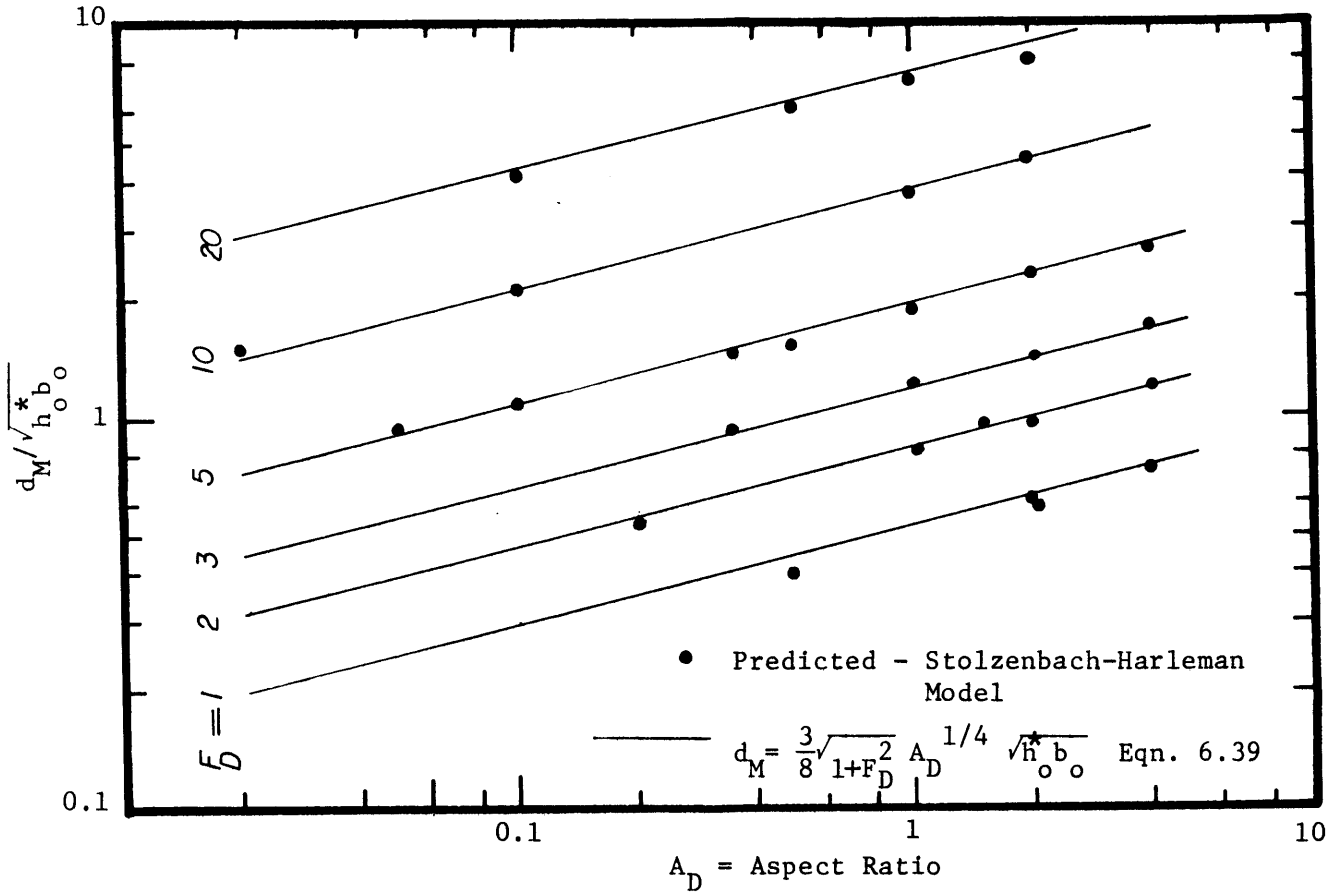

Figure 6-17 Comparison of Depth at the Start of the Stable Region Predicted by Stolzenbach-Harleman Model and Empirical Formulae

$$D_s = 1.4 \sqrt{1+F_D^2}\, A_D^{1/4} \tag{6.37}$$

$$A_M = 550(1+F_D^2)\, A_D^{1/2}\, h_o^* b_o \tag{6.38}$$

$$d_M = \frac{3}{8}\sqrt{1+F_D^2}\, A_D^{1/4} \sqrt{h_o^* b_o} \tag{6.39}$$

$$D_x = D_s \left(\frac{A_x}{A_M}\right)^{1/5} \tag{6.40}$$

6.5.7 Mathematical Model of Entrance Mixing Region

A jet mixing model has been selected, and using some simplifying assumptions has been reduced to a set of simple equations (6.37 - 6.40). An important assumption in this process was the neglect of surface heat loss. The heat loss effect is now re-introduced by incorporating the jet mixing equations in an overall model of the entrance mixing region. In section 6.2.3 an important simplification was introduced by assuming that the receiving water in the vicinity of the jet was homogeneous, and hence there is no necessity to distinguish between lateral and vertical entrainment. The entrance mixing region can therefore be schematized as shown in Figure 6-18. Note that the discharge depth, h_o^*, and the discharge Froude number, F_D, are defined in terms of the layer depth, and not the channel depth, h_o.

The governing equation for the above entrance mixing region is Equation (6.14). During any time increment Δt, the entrance mixing region is assumed to be at steady state, and the governing equation reduces to

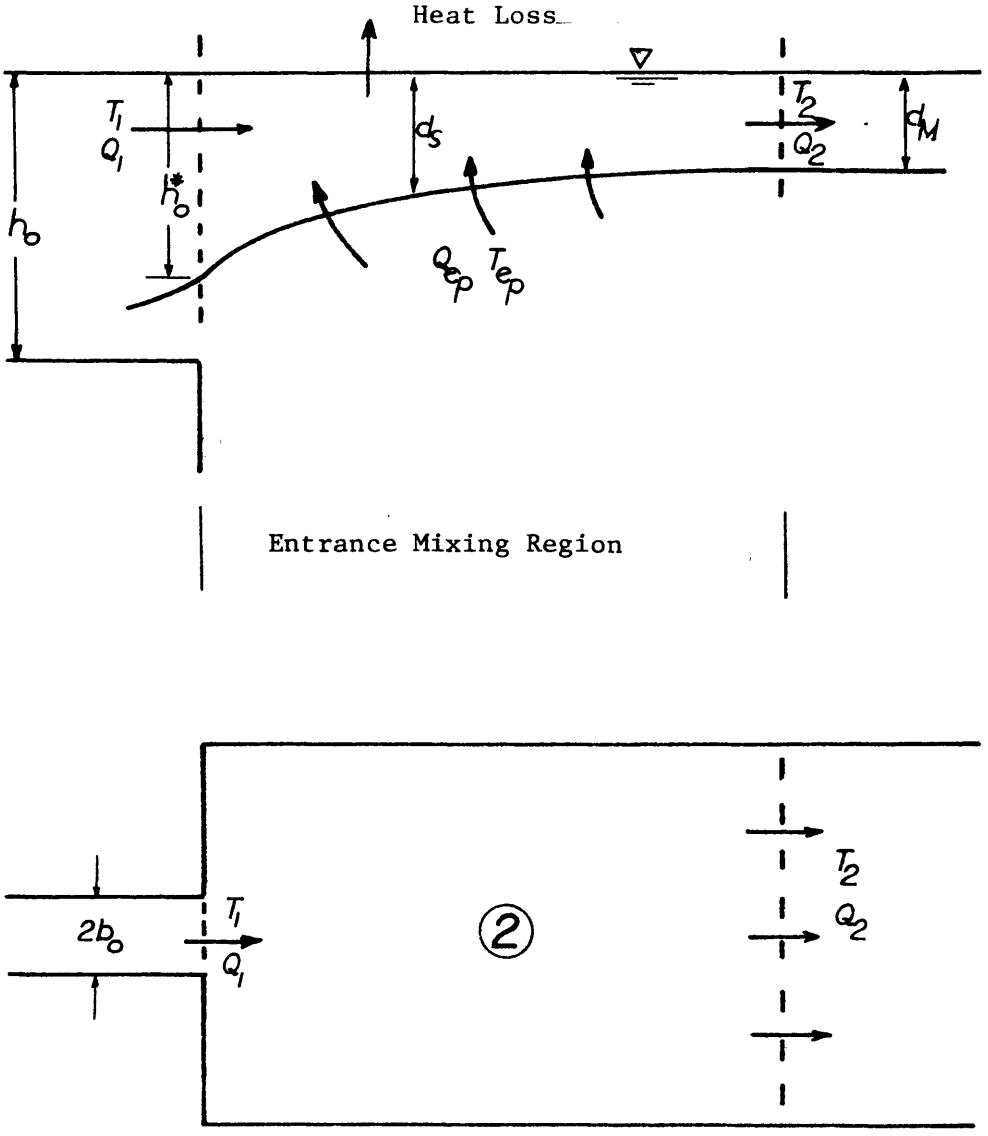

Figure 6-18 Geometric Schematization of Entrance Mixing Region

$$\frac{1}{d_s}\frac{\partial}{\partial A_x}(Q_x T) = \frac{u_e T_e}{d_s} + \frac{1}{\rho c d_s}\left[\phi_n - \phi_{sn}(1-\beta^*)e^{-\eta d_s}\right] \tag{6.41}$$

$$\frac{\partial}{\partial A_x}(Q_x T) = u_e T_e + \frac{1}{\rho c}\left[\phi_n - \phi_{sn}(1-\beta^*)e^{-\eta d_s}\right] \tag{6.42}$$

The previous sections, 6.5.2 to 6.5.7, have been devoted to determining the depth of the surface layer, d_s, and the entrained flow per unit area, u_e. Equation (6.42) shows that the only effect of d_s is in determining how much short wave radiation is transmitted through the surface layer. Usually this heat flux is small, and very little error is introduced by putting

$$d_s = \frac{1}{2}(h_o^* + d_M) \tag{6.43}$$

The entrained flow per unit area, u_e, is given by

$$u_e = \frac{d}{dA_x}(Q_1 D_x) \tag{6.44}$$

$$u_e = \frac{1}{5}\frac{D_s Q_1}{A_x}\left(\frac{A_x}{A_M}\right)^{1/5} \tag{6.45}$$

Equation (6.42) can now be solved by simple numerical methods by dividing the mixing region into segments, and using the exit conditions for the discharge channel, (Region 1), as the required upstream boundary condition. Note that surface heat loss, neglected in the determination of u_e, is now included through the governing equation.

As mentioned previously, an accurate representation of the

entrance mixing region is essential if an effective model is to be developed. A set of experiments was carried out in the laboratory cooling pond to test the accuracy of the approach outlined above. Good results were obtained, and these will be discussed in the next chapter.

The specification of the depth, d_M, and the dilution, D_s, at the end of the entrance mixing region, and the solution of Equation (6.42), gives the depth, flow rate, and temperature (i.e. the required boundary conditions) at the start of the heat loss region. This region will now be discussed.

6.6 Heat Loss Region

In this region surface heat loss is the dominant factor. Mixing due to jet induced turbulence is limited (by definition) to the entrance mixing region. Mixing due to ambient turbulence is assumed to be insignificant, and the effect of this assumption will be checked. Laboratory experiments, supported by field data (see Chapter 4) strongly suggest that in a deep, stratified cooling pond, density currents are of great importance, and the effect of pond shape is minimal. Therefore the heat loss region can be schematized in a convenient fashion e.g. a rectangle. The depth of the surface layer in this region is assumed constant and equal to d_M (Figure 6-18). This is not strictly a valid assumption as the layer thickness tends to decrease while lateral spreading continues, and then to increase when the flow is laterally confined (Koh, 1971). However, the assumption is a convenient one, and has very little effect on the temperature decrease. The heat loss region may be schematized as shown in Figure 6-19.

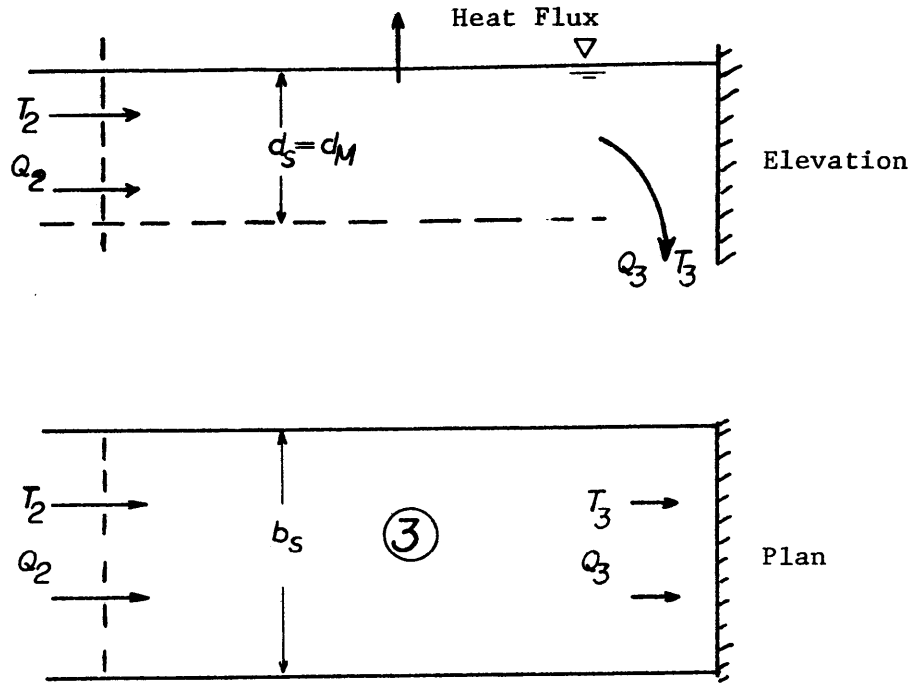

Figure 6-19 Geometric Schematization of Heat Loss Region (Region 3)

Residence time in the heat loss region may be of the order of days, instead of hours as in the previous two regions, and a transient solution will be sought. The governing equation (6.14), neglecting the entrained flow (u_e=0) becomes

$$\frac{\partial T}{\partial t} + \frac{1}{d_s}\frac{\partial}{\partial A_x}(Q_x T) = \frac{1}{\rho c d_s}\left[\phi_n - \phi_{sn}(1-\beta^*)e^{-\eta d_s}\right] \qquad (6.46)$$

The boundary condition is obtained from the flow conditions at the end of the entrance mixing region. An initial condition $T = T(A_x,0)$ must

be specified at time t = 0.

Two assumptions have been made for the heat loss region, the assumption of constant depth, and of negligible mixing. These will be briefly examined. The assumption of constant depth is an essential one since the lower boundary of the heat loss region provides the top boundary to the deep reservoir region, and the latter must be horizontal. The solution to the steady state form of Equation (6.46) gives information about the effect of the depth of the surface layer. Using the linear form of $\phi_n[=K(T-T_E)]$, and the boundary conditions shown in Figure 6-19, and neglecting the transmitted short wave radiation the following solution is obtained

$$\frac{T-T_E}{T_2-T_E} = \exp\left(-\frac{KA_x}{\rho c Q_2}\right) \tag{6.47}$$

where Q_2 = flow rate at start of heat loss region

T_2 = temperature at start of heat loss region

K = heat loss coefficient

T_E = equilibrium temperature

A_x = area swept out by flow in heat loss region

Note that the surface layer depth does not enter into the steady state solution. The depth does influence the transient behavior of the surface layer, and in clear water (low extinction coefficient, η), the transmitted radiation term $(\phi_{sn}(1-\beta^*)e^{-\eta d_s})$ may be significant, but both these factors will not be seriously affected by the use of a mean depth instead of a slowly varying one.

The assumption of no further mixing in the heat loss region is relatively important, as even if it is not necessary to accurately reproduce the transient behavior of the surface layer, mixing can influence the steady state temperature distribution. It has been shown (50) that longitudinal dispersion has little effect, and the importance of vertical mixing will be examined. Theory and experience both indicate that local densimetric Froude Numbers, F_L, of surface currents in the heat loss region have a value of approximately 0.25 (see section 4.4.3). Assuming that the Froude number of the surface layer was actually unity, a very conservative assumption, and using Equation (6.29) to calculate entrainment, the surface temperature distribution was calculated for the cases of both high and low entrance mixing. The effect of vertical mixing in the heat loss region was negligible for the high entrance mixing case, and very small for the low entrance mixing case (see Figure 6-20).

Equation (6.46) can be solved very simply by numerical means, and the flow rate, Q_3, and temperature, T_3, at the end of the heat loss region provide the boundary condition to the deep reservoir region (Region No. 4). The deep reservoir region will be considered in the next section.

6.7 Deep Reservoir Region

6.7.1 Introduction

The deep reservoir region is a zone that is usually neglected in cooling pond analysis since it is not concerned with steady state intake temperatures. This region controls the transient response of

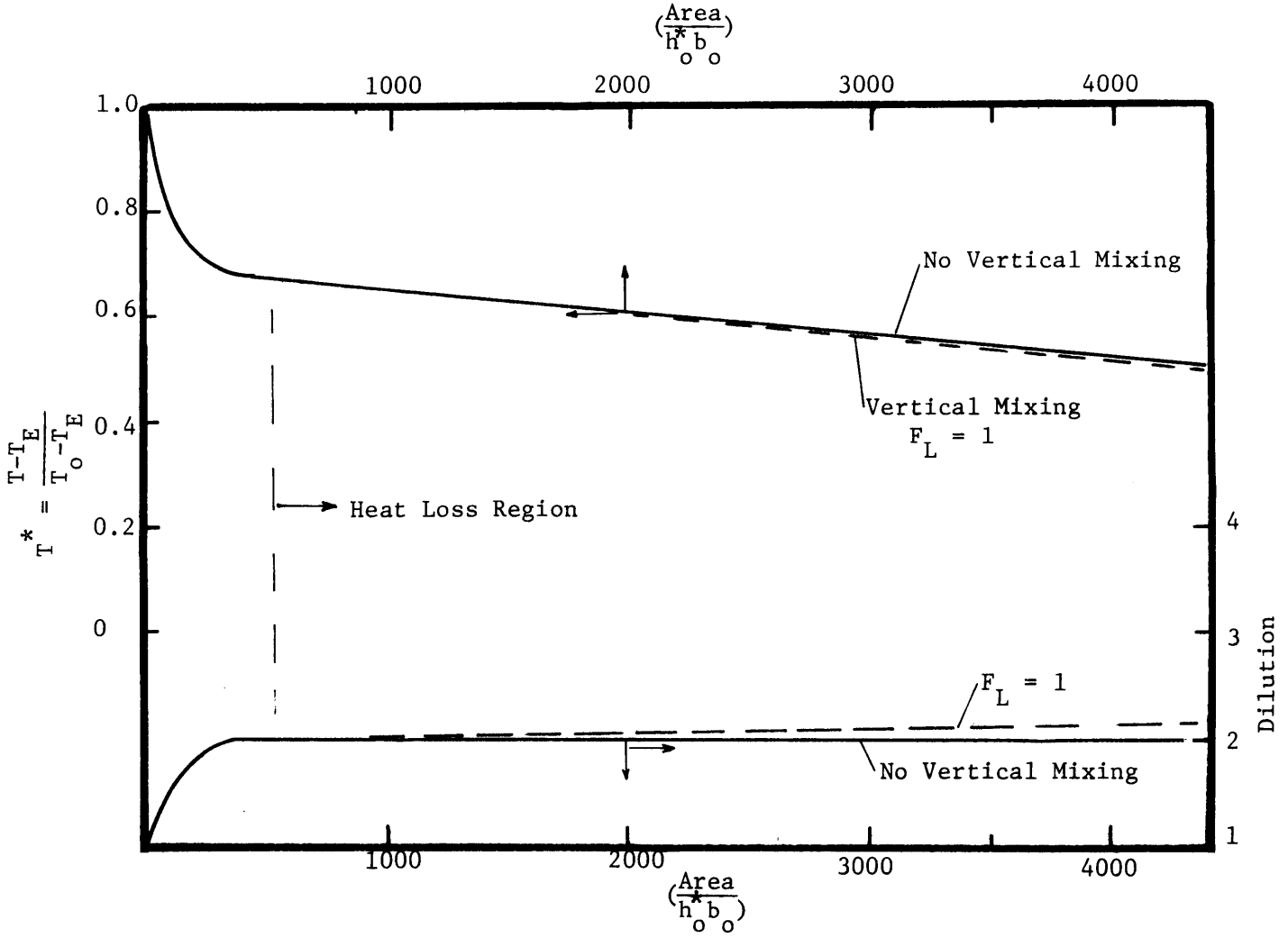

Figure 6-20 Effect of Vertical Mixing in Heat Loss Region

the pond to both short term (diurnal), and long term (seasonal) fluctuations. In an artificial pond, with a residence time of the order of a week, the short term fluctuations are of major interest, and elimination of the effect of diurnal meteorological or operating fluctuations is a realistic goal. In a natural pond (multi-purpose reservoir) the response to seasonal effects can be of enormous importance, as will be shown in Chapter 8 in a case study on Lake Norman, North Carolina.

The basic assumption for this region is that isotherms are horizontal, a property of deep reservoirs that has been widely observed in the field (Hutchinson (1957)), and also in the laboratory (Huber and Harleman (1968)). In the M.I.T. laboratory cooling pond, the horizontal homogeneity in the region under the surface layer was very striking (see Figure 4-2), and this type of structure was also observed in the Hazelwood pond (see Figure 4-4). Note that the term "deep reservoir" is relative (e.g. Hazelwood pond has a maximum depth of only 40 ft.), and means that the subsurface region has a volume at least several times that of the surface layer.

The approach will be to consider the deep reservoir region initially as if it were a typical vertically stratified reservoir. A mathematical model for this type of reservoir (the M.I.T. Deep Reservoir Model (57 ,107)) is available, and will be used to describe the behavior of this region. The mathematical model has been verified against data from a laboratory reservoir and a wide variety of field data. The laboratory deep reservoir, a plexiglas flume 40 ft. long, 1 ft. thick, and 4 feet deep, with the capacity for variable

insolation and through-flow is described in detail by Huber and Harleman (1968). Considerable information on the behavior of a vertically stratified reservoir was obtained through observations on this laboratory system, and some of the more significant observations will be presented here. Some changes in the boundary conditions for the M.I.T. deep reservoir model are necessary for it to be used as a component of the cooling pond model. These changes will be discussed after presentation of the important aspects of the deep reservoir model.

6.7.2 Schematization of Deep Reservoir Region

The region is schematized as shown in Figures 6-21 a,b,c, by considering it as a series of horizontal elements similar to the control volume in Figure 6-4 which was used to derive the governing equation (6.21) for the region. The solution of the governing equation

$$\frac{\partial T}{\partial t} + \frac{1}{A_z}\frac{\partial}{\partial z}(Q_v T) = \frac{1}{A_z}\frac{\partial}{\partial z}\left[A_z(D_m+E_z)\frac{\partial T}{\partial z}\right] + \frac{q_{in}T_{in}}{A_z}$$

$$- \frac{q_{os}T}{A_z} - \frac{1}{\rho c A_z}\frac{\partial}{\partial z}(A_z\phi_b) \qquad (6.21)$$

is dependent on the specification of the vertical and horizontal advection terms $Q_v(z,t)$, $q_{in}(z,t)$ and $q_{os}(z,t)$, and on the short wave radiation transmission term, ϕ_b. The advection terms will be considered in the following section.

6.7.3 Advection Terms in Deep Reservoir Region

The velocity distribution within the deep reservoir region

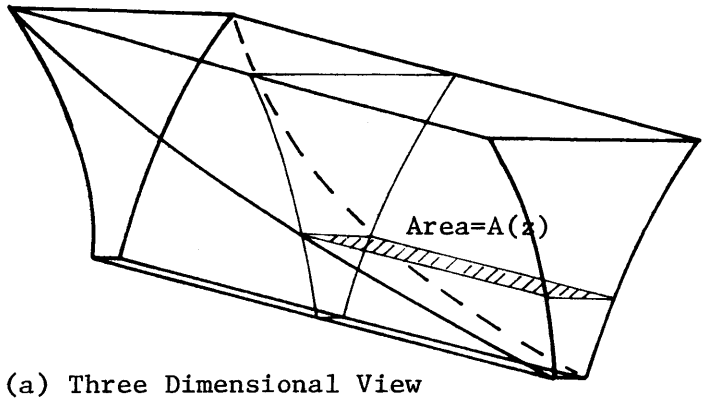

(a) Three Dimensional View

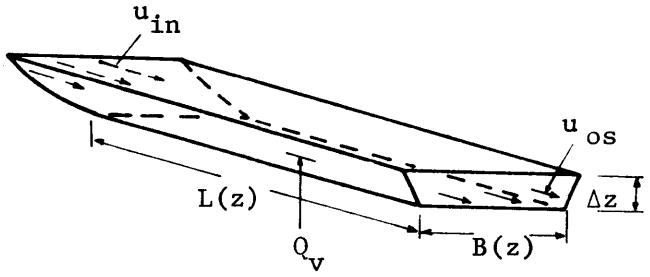

(b) Control Volume Slice

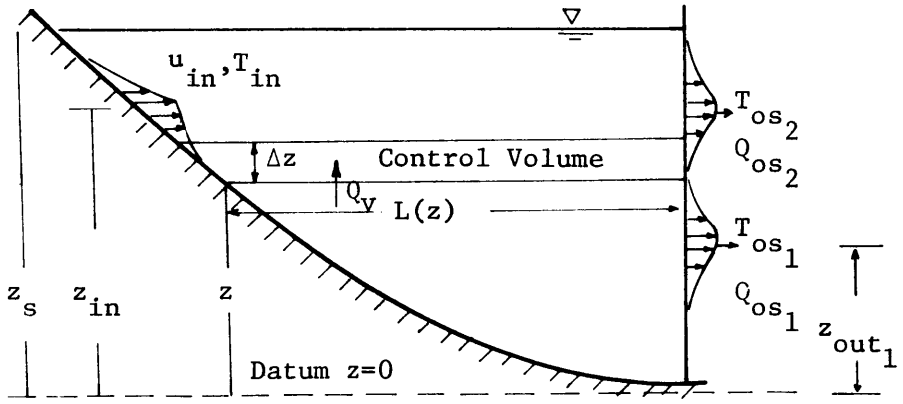

(c) Side Elevation

Figure 6-21 Control Volume and Schematization for Deep Reservoir Region

may be extremely complex, since it is influenced by density distribution and by inflow and outflow conditions. Figure 6-22 shows the currents in the M.I.T. laboratory deep reservoir for two types of inflow, and Figure 6-23 shows that similar current distributions exist in prototype reservoirs. Since isotherms are horizontal in this region, the horizontal currents have little effect on temperature distribution. In contrast the net vertical current, which has a velocity about three orders smaller than the horizontal motion, can have a very significant effect. The vertical flow rate is obtained from Equation (6.18)

$$Q_v(z,t) = \int_o^z [q_{in}(z_1,t)-q_{os}(z_1,t)]dz_1 \qquad (6.18)$$

and hence $Q_v(z,t)$ is a function both of the magnitude and location of the inflows and outflows. The significance of $Q_v(z,t)$ was demonstrated in the M.I.T. laboratory deep reservoir. Figure 6-24a shows the effect of varying the inflow-outflow rate, while Figure 6-24b shows the effect of varying the outlet location. Note that initially a warm interface moves downward with a velocity approximately proportional to the inflow-outflow rate, but does not penetrate far past the outlet. The reason for this is that when the interface is opposite the outlet, the presence of the strong temperature gradient results in a very narrow withdrawal layer, and thus cool water below the outlet tends to remain there as a stagnant wedge. It is apparent that the temperature distribution in a deep reservoir is controlled by the vertical advection terms. Determination of $Q_v(z,t)$ requires the specification of the

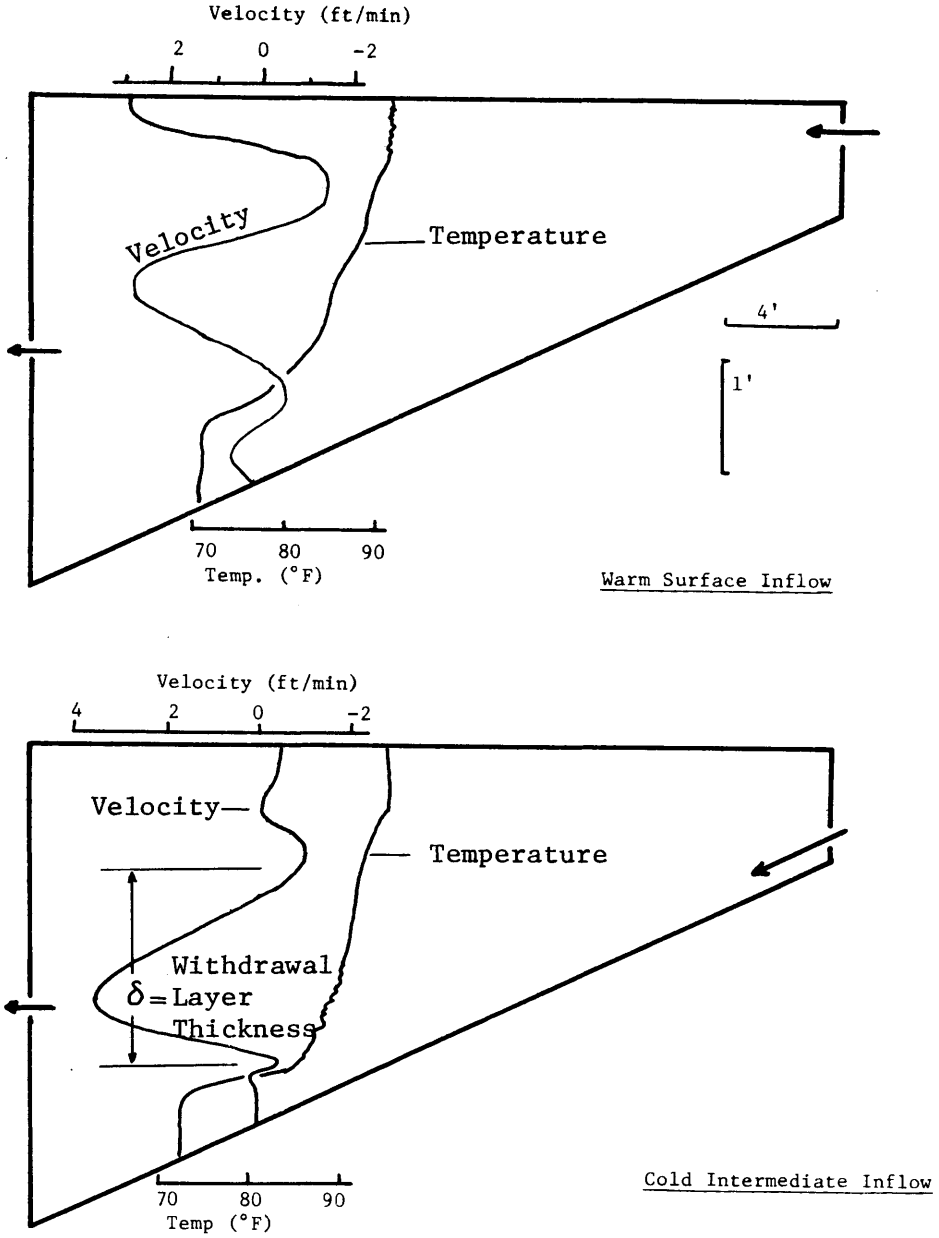

Figure 6-22 Velocity and Temperature Profiles in a Laboratory Reservoir

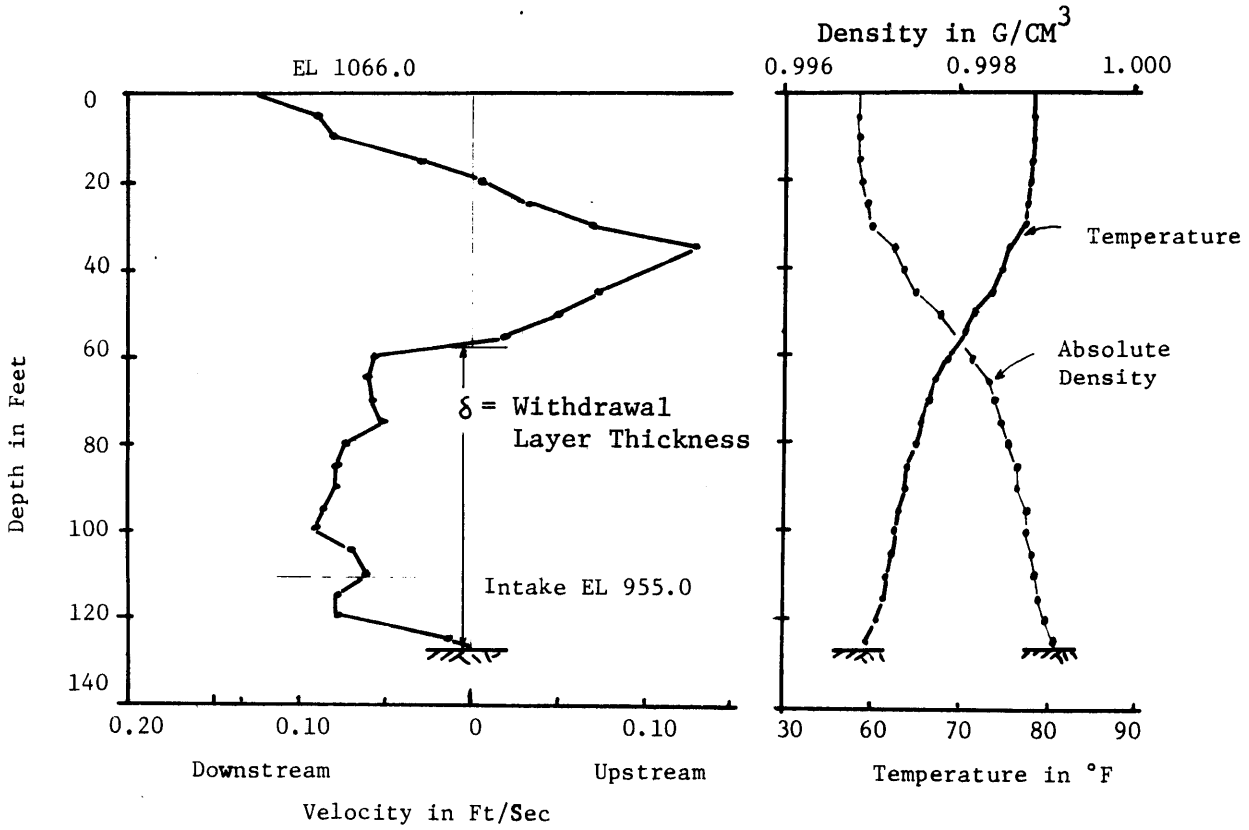

Figure 6-23 Velocity and Temperature Profiles in Cherokee Reservoir

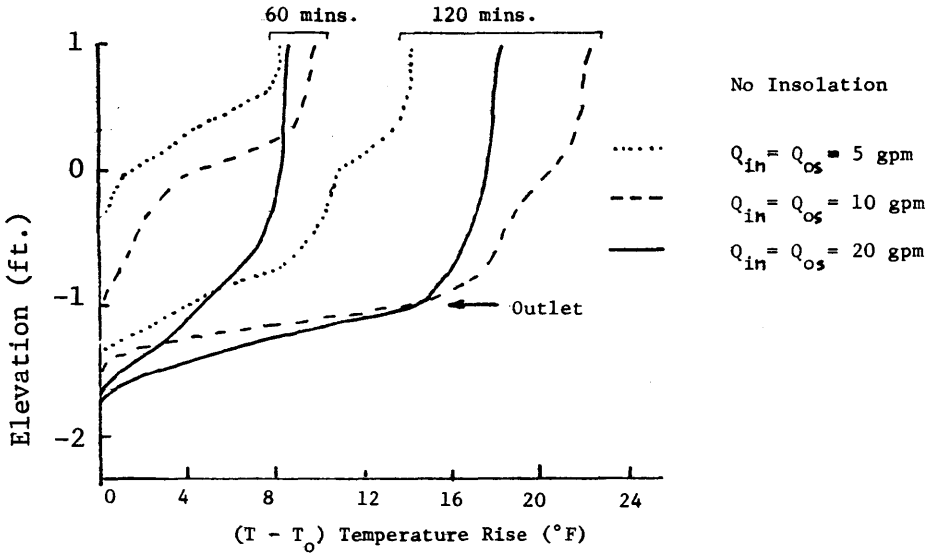

a) Effect of Flow rate on Temperature Distribution

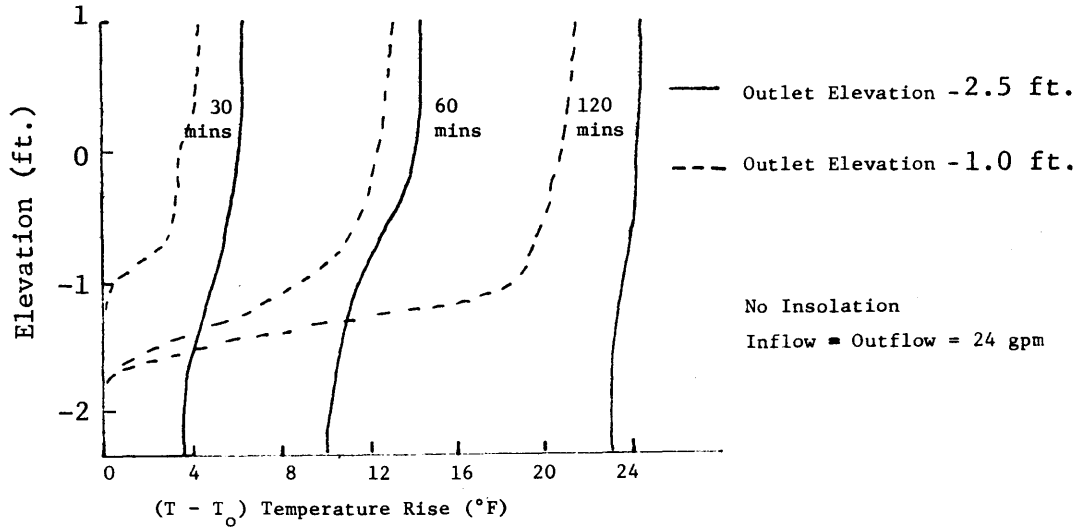

b) Effect of Outlet Elevation on Temperature Distribution

Figure 6-24 Effect of Flowrate and Outlet Elevation on the Temperature Distribution in the Laboratory Deep Reservoir.

inflow and outflow velocity distributions, and this is discussed in the following section.

6.7.4 Inflow Velocity Distribution

Little is known about the behavior of a stream when it enters a reservoir. In general streams enter reservoirs through slowly expanding channels, there is no well defined entry point, and the reservoir water tends to form a warm or cold wedge with respect to the stream. Entrance entrainment may be small in comparison with that usually associated with heated discharges. The fact that warm inflows flow directly over the surface and dense inflows (cold or sediment laden) flow along the bottom is accepted in the literature on reservoir flows (Howard (1953), Goda (1959)). However, the evidence for flows at intermediate depth is sparse. Elder and Wunderlich (1968) give the results of dye tests in Fontana Reservoir (see Figure 6-25). These dye profiles also show that the inflow velocity profile may be approximated by a Gaussian curve. It is assumed that

$$u_{in}(z) = u_{in_{max}}(t)\ e^{-\frac{(z-z_{in}(t))^2}{2\sigma_i^2}} \qquad (6.48)$$

where

$u_{in}(z)$ = inflow velocity at elevation z

$u_{in_{max}}(t)$ = maximum value of the inflow velocity at time t

$z_{in}(t)$ = elevation of inflow at time t

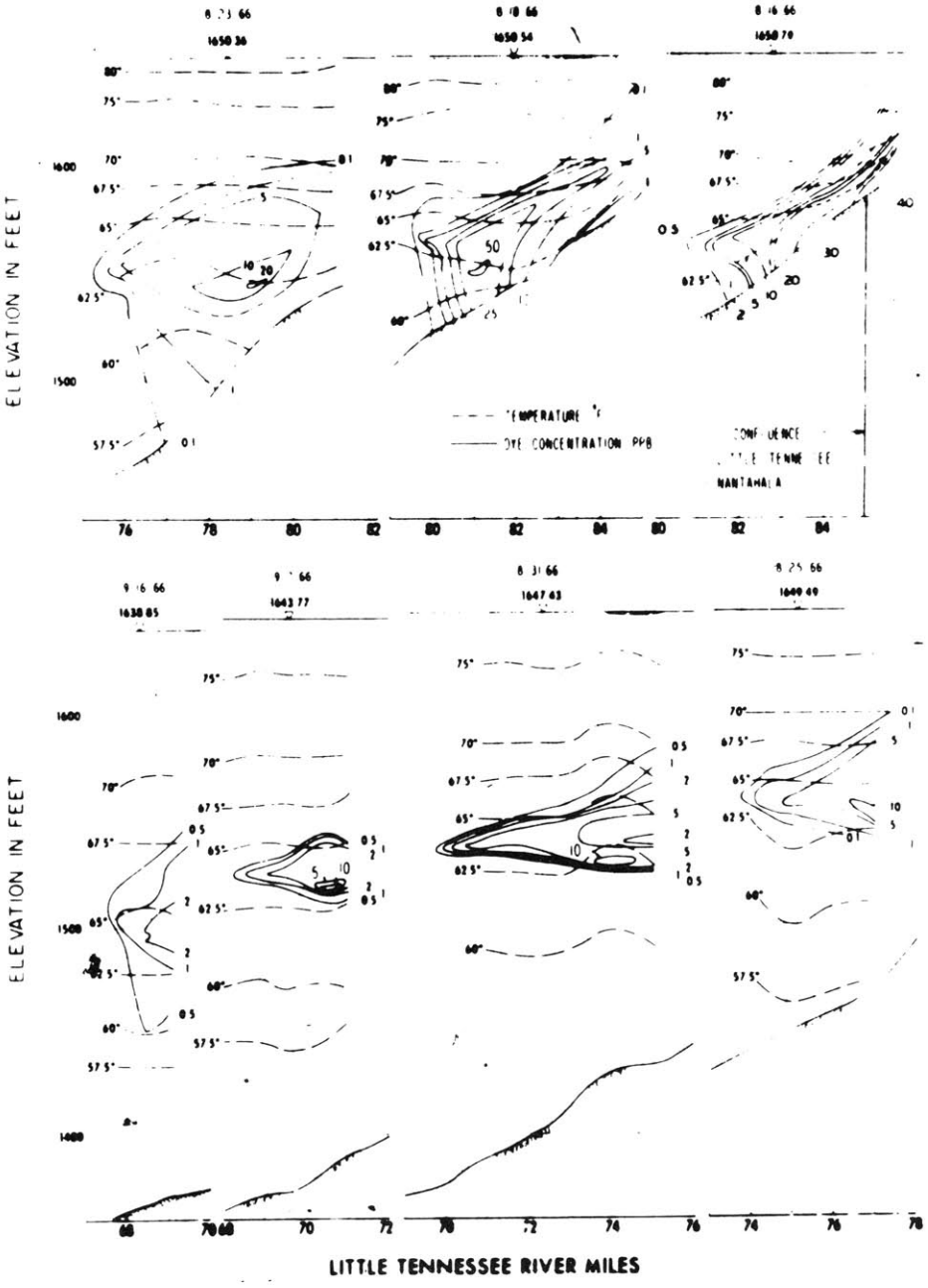

Figure 6-25 Dye Concentration Profiles in Tributary of Fontana Reservoir

σ_i = inflow standard deviation

Little is known about the value of σ_i. Since in general the concern is with flow in a slowly expanding channel, no control point exists, and hence one cannot set F_L equal to unity and thus obtain a value for σ_i. Data from TVA reservoirs indicates that the densimetric Froude No. for the moving layer tends to be $\sim \frac{1}{4}$, regardless of whether the flow is at the surface, bottom or an intermediate height. As Elder and Wunderlich (1972) point out, this is in agreement with Yih's (1958) theoretical and Debler's (1959) experimental results for a density current in the presence of stagnant layers. Until more experimental evidence is available, it seems reasonable to set E_L for the moving layer equal to 0.25, and obtain σ_i by assuming that 95% of the inflow is contained within the calculated layer thickness.

6.7.4.1 Entrance Mixing

When a river enters a reservoir it will entrain some of the reservoir water. Recent field measurements indicate that the entrance mixing is rather low with dilutions of 1.1 to 1.5 (32). Measurements in the laboratory deep reservoir indicate dilutions of 1.1 to 3, with the higher values occurring for dense underflows (107). It has been shown that entrance mixing has a considerable effect on computed behavior (57 , 107) and Figure 6-26 shows the effect of a dilution of 2 on the computed outflow temperature in Fontana Reservoir.

Entrance mixing is simulated in the mathematical model by withdrawal of a specified amount of water from a selected depth, d_m,

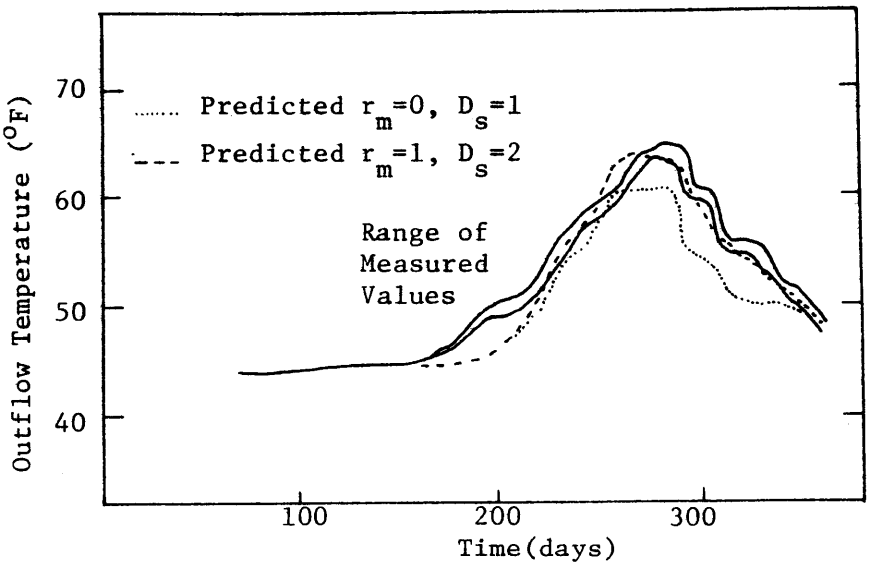

Figure 6-26 Effect of Entrance Mixing on Outflow Temperatures, Fontana Reservoir, 1966

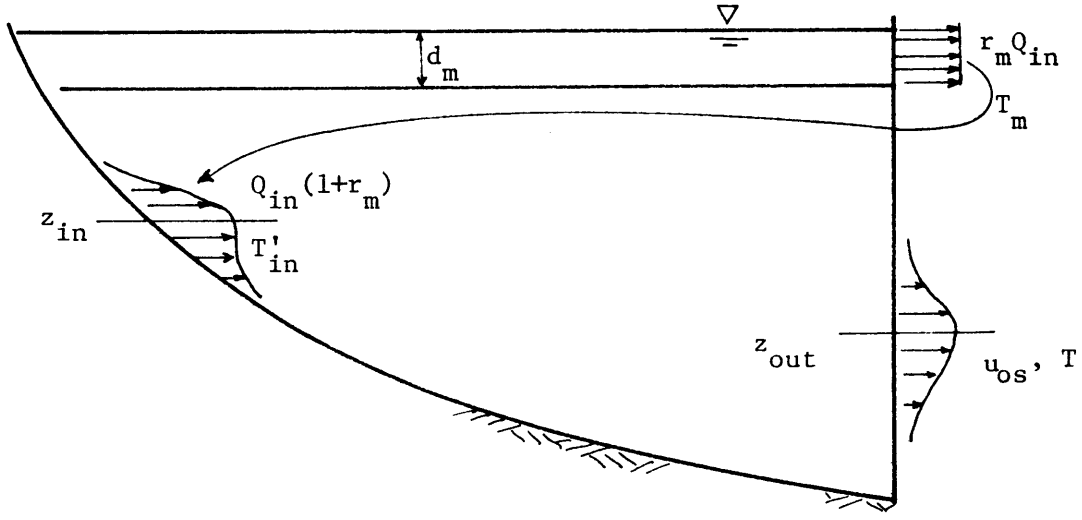

Figure 6-27 Schematic Representation of Entrance Mixing

and mixing this with the inflow (see Figure 6-27). It was observed in the laboratory reservoir that only the upper layers contributed to the entrance mixing, and d_m was put equal to the depth of the entering stream. The ratio of entrained flow to inflow is denoted by r_m. The mixing temperature T_m was taken to be the average over the depth, d_m, and hence the mixed inflow temperature, T'_{in}, is given by

$$T'_{in} = \frac{(T_{in}+r_m T_m)}{(1+r_m)} \tag{6.49}$$

In this model multiple stream inflows can be considered. Each inflow is considered separately, in contrast to the previous M.I.T. deep reservoir models where all inflows were lumped together.

6.7.5 Outflow Velocity Distribution

The problem of withdrawal from a stratified reservoir is treated rather extensively in the literature. The solutions have been summarized by Brooks and Koh (1968). Due to density differences, selective withdrawal may occur (i.e. the withdrawal layer thickness may be less than the total depth). The basic criterion was given by Yih (1958) who showed theoretically that no stagnant layers can exist when the densimetric Froude number, F, for a linearly stratified two dimensional channel is greater than $\frac{1}{\pi}$.

$$F = (q/d^2)/\sqrt{g\varepsilon} > 1/\pi \tag{6.50}$$

where

q = flow per unit width

d = depth of the channel

ε = normalized density gradient = $\frac{1}{\rho}\frac{\partial \rho}{\partial z}$

Kao (1965) showed that for a line sink at the bottom of a linearly stratified uniform channel the withdrawal layer thickness (δ) would grow until the densimetric Froude number of the withdrawal layer reaches a critical value, F^1.

$$F^1 = (q/\delta^2)/\sqrt{g\varepsilon} \tag{6.51}$$

therefore

$$\delta = \left(\frac{1}{F^1}\right)^{1/2} \cdot \left(\frac{q^2}{g\varepsilon}\right)^{1/4} \tag{6.52}$$

Kao found F^1 to be 0.33, close to Debler's (1959) experimental result of 0.28.

In a prototype reservoir flow may <u>not be two-dimensional</u>, and the density gradient is usually <u>not linear</u>. Thus F^1 is unknown, but is assumed constant. Brooks and Koh (1968) give the following expressions

Bottom or Surface Outlet: $$\delta = a_1\left(\frac{q^2}{g\varepsilon}\right)^{1/4} \tag{6.53a}$$

Intermediate Outlet: $$\delta = \sqrt{2}.a_1.\left(\frac{q^2}{g\varepsilon}\right)^{1/4} \tag{6.53b}$$

where a_1 = constant.

Wunderlich and Elder (1971), from a study of ten TVA reservoirs, found "a_1" to be approximately 4.5. Thus reasonable formulae

for withdrawal layer thicknesses in stratified prototype reservoirs are:

Surface or Bottom Outlet: $$\delta = 4.5 \left(\frac{q^2}{g\varepsilon}\right)^{1/4} \tag{6.54a}$$

Intermediate Outlet $$\delta = 6.4 \left(\frac{q^2}{g\varepsilon}\right)^{1/4} \tag{6.54b}$$

In the laboratory, Kao's assumption of inviscid flow is unrealistic and Koh's (1964) formula which includes the effect of viscosity and diffusion is applicable. δ is given by

$$\delta = \frac{7.14\ x^{1/3}}{(\varepsilon g / b_m \nu)^{1/6}} \tag{6.55}$$

where ν = kinematic viscosity of water

x = distance from outlet

The above formulae have all been developed for a two dimensional reservoir, and while the constant a_1 includes some three dimensional effects, these formulae will work best on deep field reservoirs which are often markedly two dimensional in character. For a typical artificial cooling pond with a skimmer wall intake, the simple two layer model of Harleman and Elder (1965) is more appropriate. In this model it is assumed that only the lower layer is withdrawn, that velocities in the main channel are negligible compared with those at the skimmer wall, and that curvature effects are negligible. Writing an energy equation between section 1 and 2 in Figure 6-28 we obtain

$$h_2 = d_{si} + \frac{1}{\frac{2\Delta\rho g}{\rho}} \left(\frac{Q_o}{b_{si} d_{si}}\right)^2 \tag{6.55a}$$

The symbols are defined in Figure 6-28.

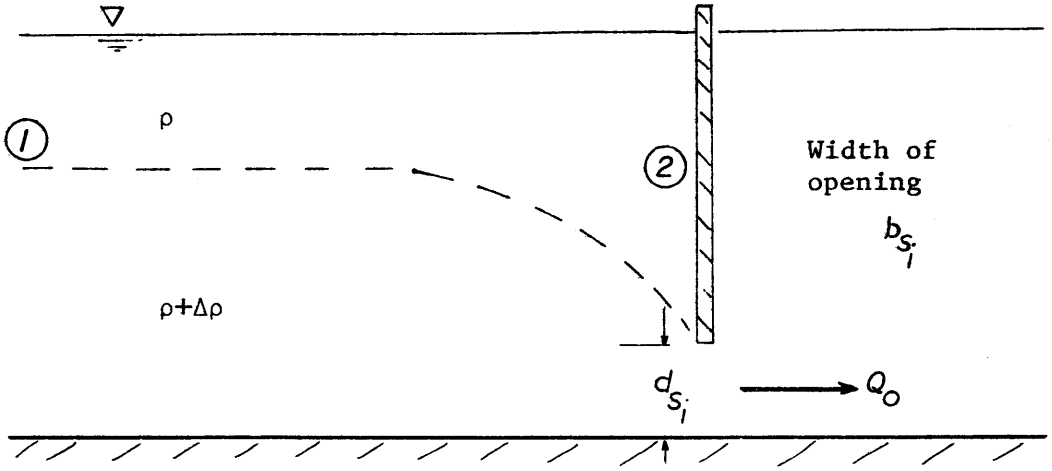

Figure 6-28 Skimmer Wall Intake

The outflow standard deviation σ_o is calculated on the basis that 95% of the outflow comes from the calculated withdrawal layer, which is assumed to have a gaussian velocity distribution. Thus

$$u_{os}(z) = u_{os_{max}} e^{-\frac{(z-z_{out})^2}{2\sigma_o^2}} \tag{6.56}$$

where

$u_{os_{max}} = u_{os_{max}}(t)$ = velocity at $z = z_{out}$

z_{out} = elevation of reservoir outlet centerline.

In the model calculations a density gradient is determined from the temperature gradient at the outlet. However, vertical temperature profiles tend to be roughly non-linear and it is sometimes necessary to specify a cut-off temperature gradient to stop unrealistic behavior, such as withdrawal of a warm surface layer when sub-surface layers are at a uniform lower temperature.

In many reservoirs, withdrawal can take place from several levels. This facility has been included in the mathematical model. The number of outlets, the level of each outlet and the individual outflow rates, are specified in the input data. Withdrawal may take place from one or all outlets at any time. The velocity field of each outlet is calculated as above, and superimposed on one another. No field verification has been carried out for the multiple outlet case, but the comparison with laboratory results is quite promising (see Figure 6-34).

The outflow temperature at any outlet, $\underline{k}$, is given by

$$T_{os_k} = \frac{\int_{z_b}^{z_s} B(z)u_{os_k}(z,t)\ T(z,t)\ dz}{\int_{z_b}^{z_s} B(z)u_{os_k}(z,t)\ dz}$$

$$= \frac{1}{Q_{os_k}} \int_{z_b}^{z_s} B(z)u_{os_k}(z,t)\ T(z,t)\ dz \qquad (6.57)$$

where z_s = elevation of water surface

z_b = elevation of pond bottom

$u_{os_k}(z,t)$ = outflow velocity at elevation z caused by outlet k

Q_{os_k} = discharge at outlet k

6.7.6 Calculation of Vertical Flow rate

The vertical flow rate $Q_v(z,t)$ is obtained by requiring that the continuity equation is satisfied at each level. Starting at the bottom element of the region and setting the flow rate across the bottom equal to zero, each element is considered in turn and the vertical flow rate calculated (see Figure 6-29).

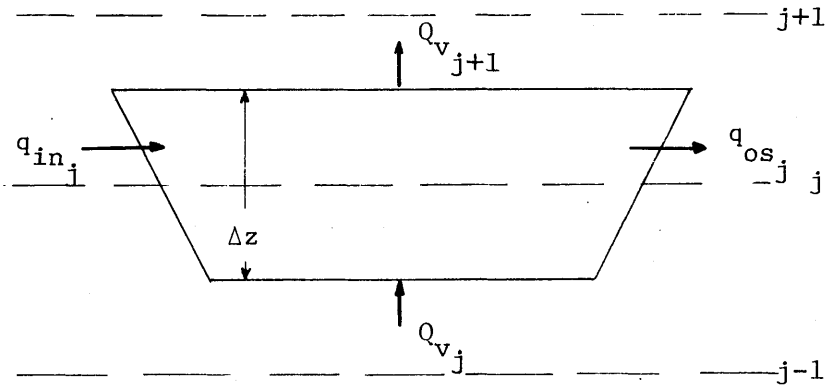

Figure 6-29 Calculation of Vertical Flow Rate

$$Q_{v_{j+1}} = Q_{v_j} + q_{in_j} - q_{os_j} = Q_{v_j} + B_j \Delta z (u_{in_j} - u_{os_j}) \qquad (6.58)$$

where B_j = width of element j.

6.7.7 Role of Diffusion in Deep Reservoir Region

The significance of vertical diffusive heat transport in a

deep reservoir is the subject of some controversy. Many existing mathematical models for thermal stratification in lakes and reservoirs have included turbulent diffusion coefficients for heat at important parameters (94 ,121). In general, these diffusion coefficients are functions of depth and time, and since these functional relations cannot be specified a priori, such mathematical models tend to lose their predictive value. For any given model it is always possible to find turbulent diffusion coefficients which will match field data. However, it is difficult to determine to what extent these coefficients represent diffusion or merely the effect of simplifications or inaccuracies in the basic formulation of the mathematical model. The approach used in this study follows that of the M.I.T. deep reservoir models (57 ,107) which assume that diffusive transport is only significant in the surface layers. The mechanics of this approach, and the reasoning on which it is based, are discussed in the following section.

The fundamental idea behind the following treatment of heat transport by turbulent diffusion is that a temperature prediction model should not require assigned values for turbulent diffusion coefficients. Whenever the temperature profile in the epilimnion develops an unstable density gradient, vertical mixing is induced to produce a surface layer of uniform temperature. Thus, even though turbulence may exist in the surface layer due to wind shear and wave motion, the heat transfer will be dominated by convection currents and surface cooling effects. These currents tend to eliminate near surface temperature gradient, and nullify the role of turbulent diffusive heat transport.

In the hypolimnion region vertical temperature gradients are

small and diffusive heat transport will not be significant even if turbulence does exist. In the thermocline region, the density stratification will tend to inhibit turbulence, although it will not necessarily remove it altogether. Attempts have been made to relate thermal diffusivity in the thermocline region to the local Richardson number, or the local stability, but with very limited success. The accurate determination of either the local Richardson number or the thermal diffusivity itself is very difficult. The former requires accurate velocity profiles. The best velocity profiles available have been obtained by TVA (1971) and Figure 6-30 shows the local Richardson number calculated using one of these profiles. Figure 6-31 demonstrates the limited success in relating thermal diffusivity to the local stability (143). Thermal diffusivity itself is usually calculated in one of two indirect ways, the heat budget approach, or the eddy diffusivity approach. The heat budget approach is only reliable when all other methods of heat transport such as advection and direct absorption are accurately known. Often the thermal diffusivity, calculated by this method, represents ignorance of reservoir behavior than an actual physical process. The eddy diffusivity approach used by Wunderlich and Fan (1971) calculates momentum diffusivity from velocity profiles, and assumes a relation between heat and momentum diffusivities. Problems arise here due to lack of accuracy both in the velocity profiles and in the ratio of heat and momentum transfer at high Richardson numbers. Nevertheless, Wunderlich and Fan obtained satisfactory agreement between thermal diffusivities calculated by the two methods. Table 6-2

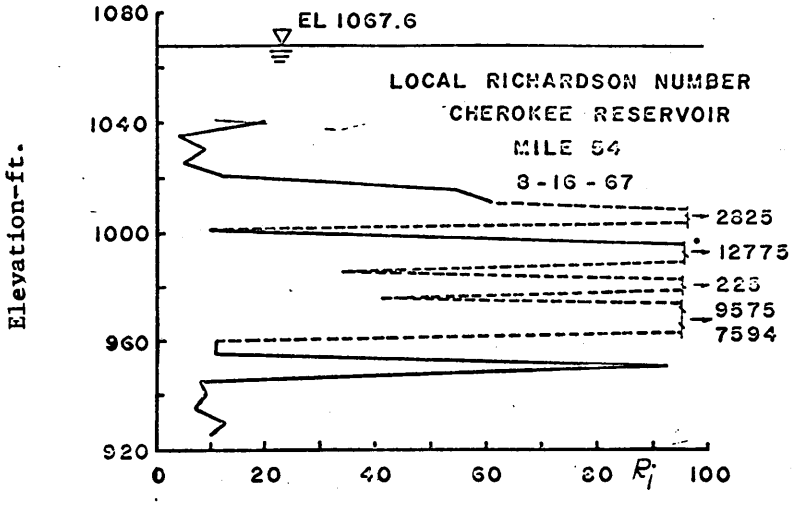

Figure 6-30 Local Richardson Numbers, Ri, in Cherokee Reservoir. From (143)

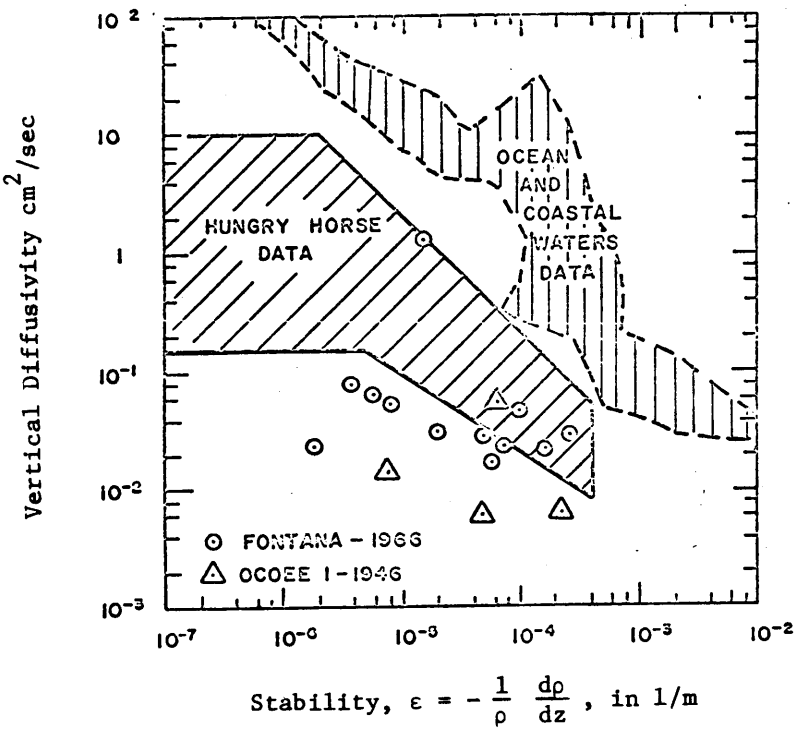

Figure 6-31 Comparison of Vertical Diffusivities in Reservoirs, the Ocean and Coastal Areas From (143)

shows calculated values of thermal diffusivities in the thermocline region of lakes and reservoirs. These values were obtained using a heat budget approach.

Table 6-2

Vertical Diffusivities in Lakes and Reservoirs

Molecular Diffusivity of Heat (D_m=0.133 ft^2/dam)

SEE ERRATA

Lake or Reservoir	Thermal Diffusivity ft^2/day	Thermal Diffusivity Molecular Diffusivity	Reference
Sodon	.65	5	(58)
Linsley Pond	.31	2.3	(58)
Mendota	2.32	17	(58)
Castle Lake	1.85	14	(93)
Ontario (seasonal average)	2-7	14-50	(127)
Fontana	2-13	14-90(mean 32)	(143)
Ocoee	.6-5	4-38(mean 14)	(143)

It has been found (107) that the "numerical diffusion" coefficient arising from the advective terms is of the same order as the thermal diffusivities in Table 6-2,and it was shown that the only significance of this term is on the smoothing of the temperature profile, and that this term is not a significant source of heat transport.

A reasonable approach is then to neglect turbulent diffusion as a first approximation, and to take all other known forms of heat transport into account as accurately as possible. If marked discrepancies occur, which cannot be explained by other factors, e.g., mixing of the inflow as it enters the reservoir, then allowance should be made

for turbulent diffusive transport. However, in both laboratory and field reservoirs (57), (106), (107) good agreement has been obtained between predicted and measured temperatures, and thus it appears that this approach is justified.

Since turbulent diffusion is neglected, it would seem only reasonable to neglect molecular diffusion as well, however this process may be included for three reasons: 1) Molecular diffusion may be significant in the laboratory case; 2) If accurate values of vertical turbulent diffusivity become available, they may be included in the model at a later date; 3) A numerical solution to the heat transport equation will be presented, and numerical schemes, regardless of type, behave better when diffusion is present.

A small amount of numerical diffusion ($\sim 20D_m$) is useful as it smooths the temperature profile without significantly altering it, and this amount of diffusion is probably present in the prototype anyway. If a numerical scheme, which minimizes numerical diffusion (e.g. Stone-Brian (1963)) is used, then it may be wise to use a small arbitrary value of E_z(e.g. $20D_m$). If an explicit forward difference scheme, such as in (107) is used, E_z may be put equal to zero.

6.7.8 Internal Absorption and Transmission of Short Wave Radiation

The depth of influence of the various surface heat fluxes is shown in Figure 6-32. The only flux which directly acts on the fluid below a depth of 1 mm. is the short-wave (solar) radiative flux, which can be transmitted to depths of the order of 10-100 ft. (see Figure

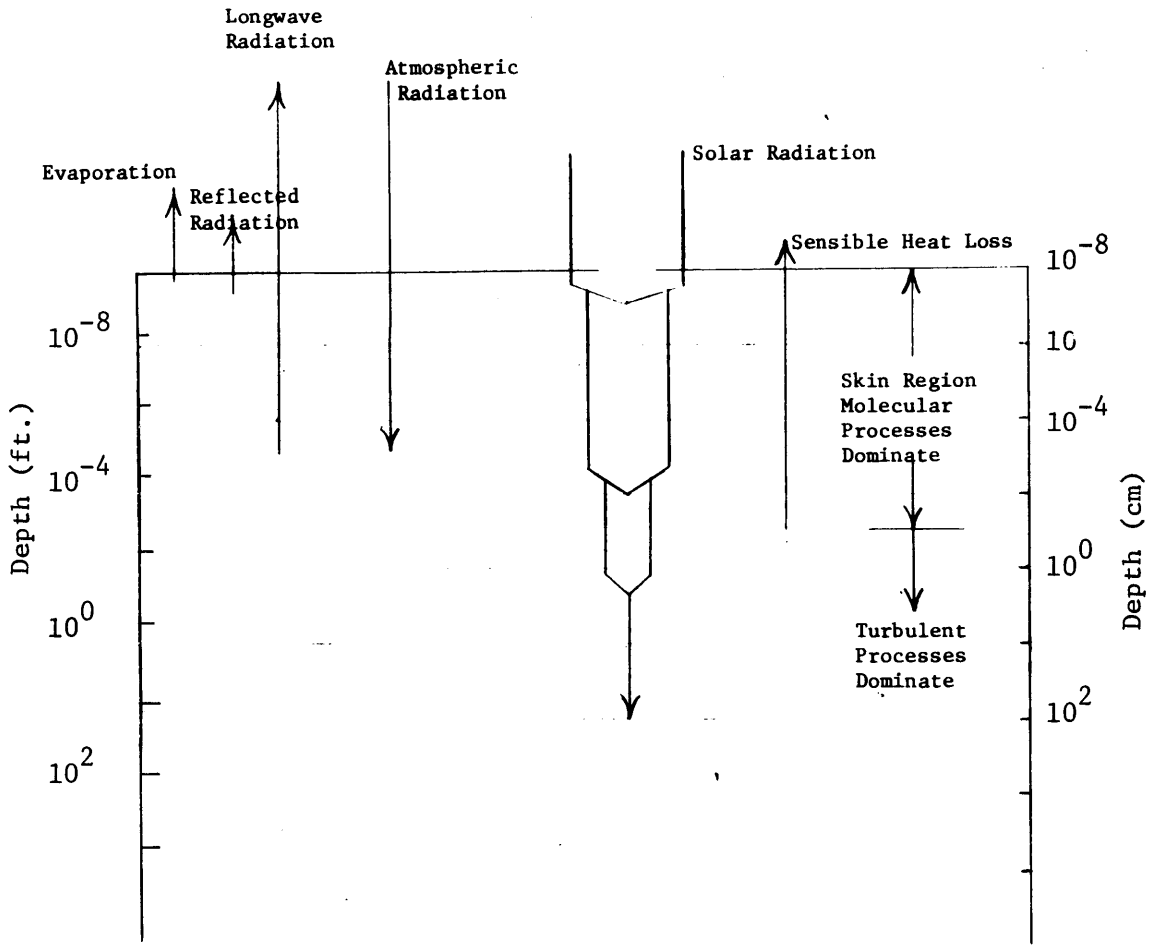

Figure 6-32 Surface Heat Fluxes and their Region of Influence

6-32 and 6-33). The long-wave content of solar radiation (above approximately 1 micron) is absorbed very near the surface while the short-wave content is absorbed exponentially with depth. Early investigations of thermal stratification in lakes and reservoirs usually assumed either complete surface absorption of solar radiation or complete internal absorption. Dake and Harleman (1969) have shown that the insolation penetrating the water surface can conveniently be separated into a fraction, β^*, representing the long-wave content, absorbed at the surface, and a fraction $(1-\beta^*)$ distributed exponentially throughout the depth of the body of water and absorbed internally. Thus it is unnecessary to resort to either of the gross assumptions given above. This approximation is shown in Figure 6-33b where the ratio ϕ_b/ϕ_{sn} is plotted versus depth. ϕ_b is the solar radiation at any depth z and is described by the equation

$$\phi_b = (1-\beta^*)\ \phi_{sn}\ e^{-\eta(z-z_s)} \tag{6.59}$$

where η is the extinction coefficient for solar radiation in the water. The value of η increases with increasing turbidity of the water. For very clear lakes, Equation (6.59) is not really accurate close to the surface (depth < $1/3\eta$), but most cooling ponds tend to be somewhat turbid and Equation (6.59) is quite adequate. Values of η and β can be obtained from field measurements, either using a submerged photo cell as was done by Elder and Wunderlich (1968) (see Figure 6-33b) or a Seechi disk (Tyler, 1968). η can be related to the Seechi disk depth, d_D, by a simple formula

SEE ERRATA

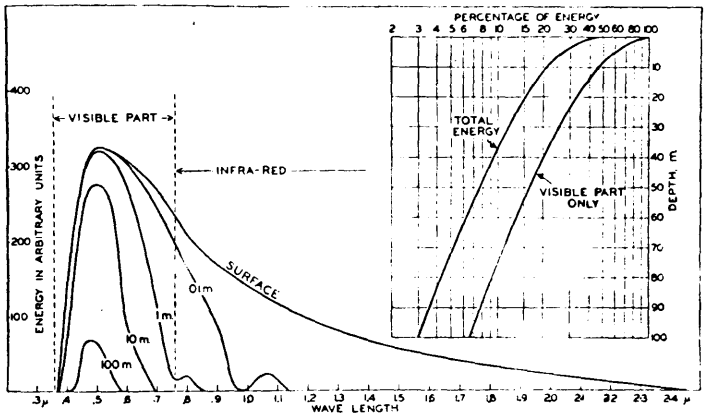

a) Absorption of Solar Radiation in Water (126)

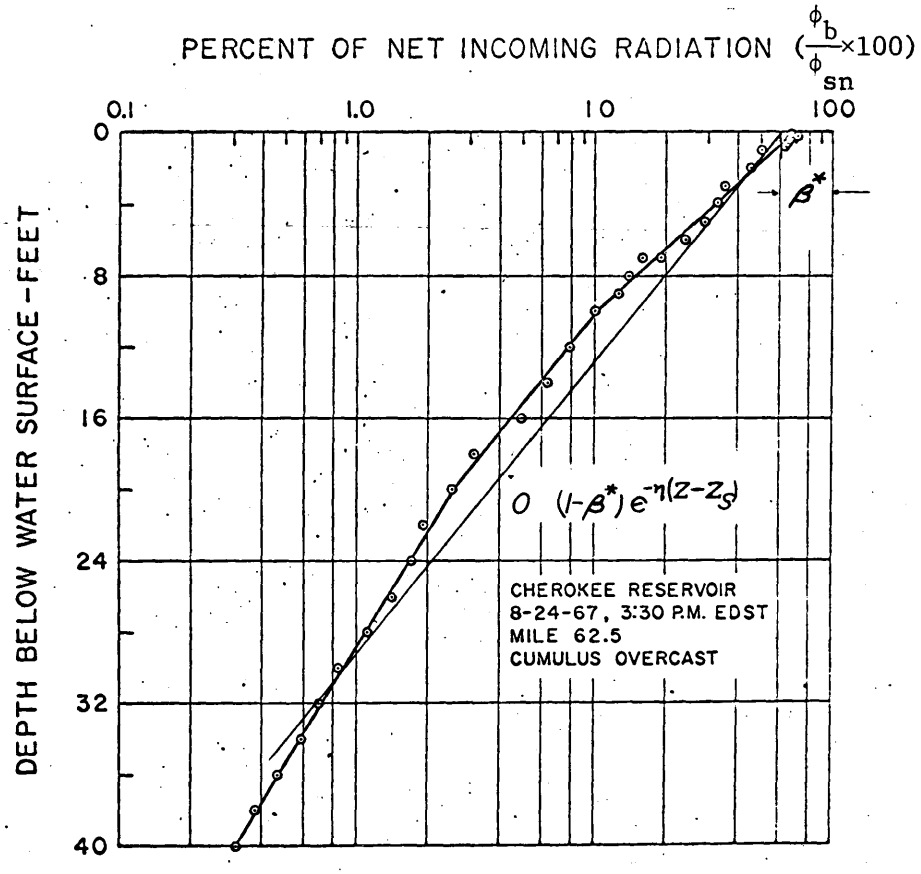

b) Field Measurement of Solar Radiation Absorption with Depth (D6)

Figure 6-33 Absorption of Solar Radiation in Water

$$\eta = 1.7/d_D \tag{6.60}$$

Equation (6.60) was used to determine the extinction coefficient η for use in the Lake Norman case study in Chapter 8.

The M.I.T. Deep Reservoir Model has been tested against both laboratory and field data, including data from both lakes and reservoirs, and over both diurnal and seasonal time scales. Some results obtained by the mathematical model will now be presented.

6.7.9 Verification of M.I.T. Deep Reservoir Model

The M.I.T. Deep Reservoir Model has been verified both in the laboratory and the field. Some results for the M.I.T. laboratory deep reservoir are shown in Figure 6-34. Equivalent results for a deep field reservoir (Fontana) are shown in Figure 6-35. The model has been checked against profiles in lakes and Figure 6-36 shows the results for Lake Tahoe and Castle Lake. For the lake situations, inflow and outflow are negligible, and the temperature profiles result from the interaction between internal absorption of short wave radiation and surface cooling effects. Figure 6-37 shows that the model is also reasonably successful in predicting diurnal temperature fluctuations.

The good results obtained for a wide variety of situations indicate that the basic assumptions, used in the deep reservoir model, are reasonable. The application of this model to the deep reservoir region in the cooling pond entails some changes in the upper boundary condition, and in the way that convective mixing is handled. These changes are discussed in the following section.

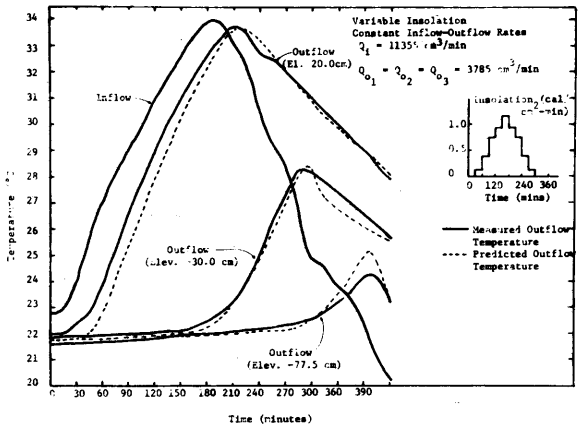

a) Outflow Temperatures - Simultaneous Withdrawal from Multiple Outlets - Laboratory

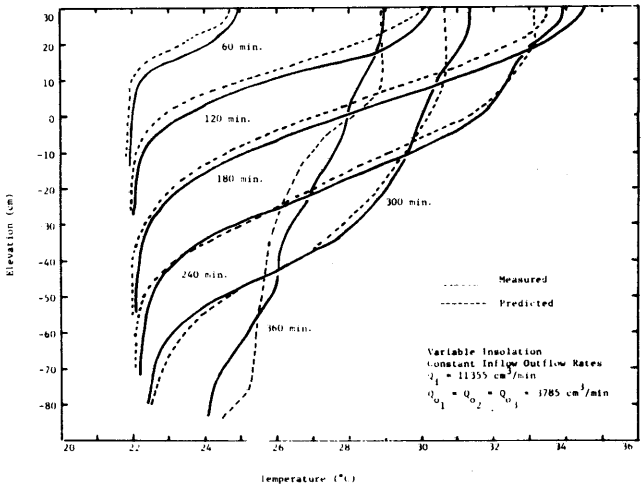

b) Temperature Profiles - Simultaneous Withdrawals from Multiple Outlets - Laboratory

Figure 6-34 Predicted vs. Measured Behavior in Laboratory Deep Reservoir (Ryan and Harleman, 1971)

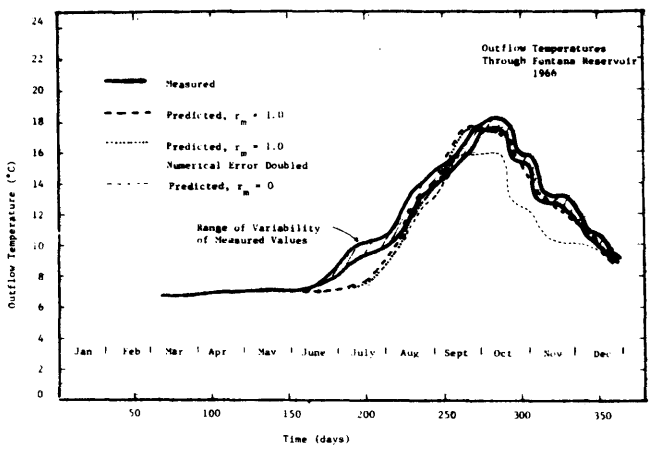

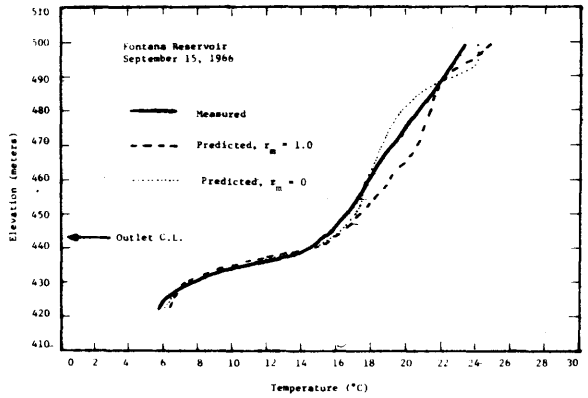

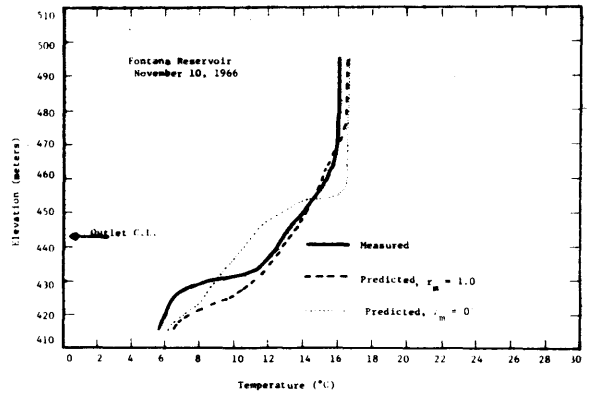

Figure 6-35 Predicted vs. Measured Outflow Temperatures and Temperature Profiles in Fontana Reservoir (Ryan and Harleman, 1971)

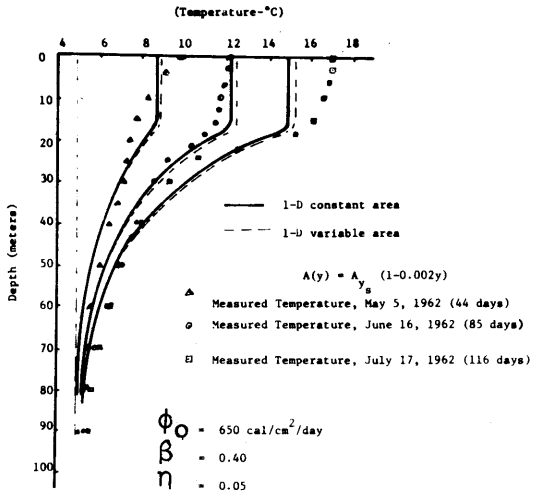

a) Measured and Predicted Temperatures - Lake Tahoe (D2)

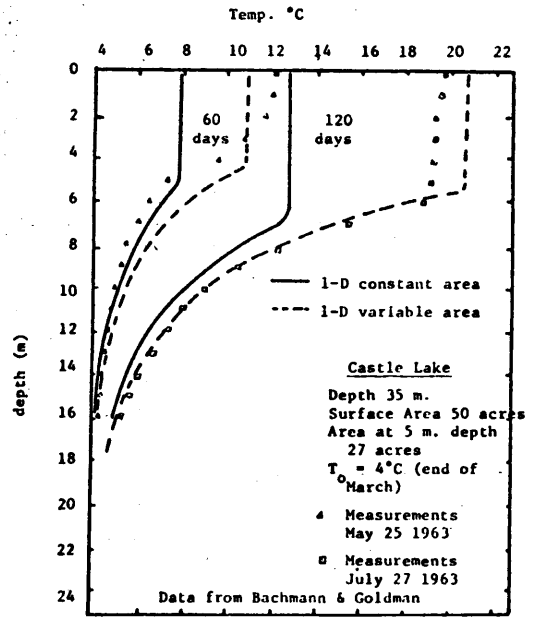

b) Measured and Predicted Temperatures - Castle Lake

Figure 6-36 Predicted vs. Measured Lake Behavior (Ryan, 1968)

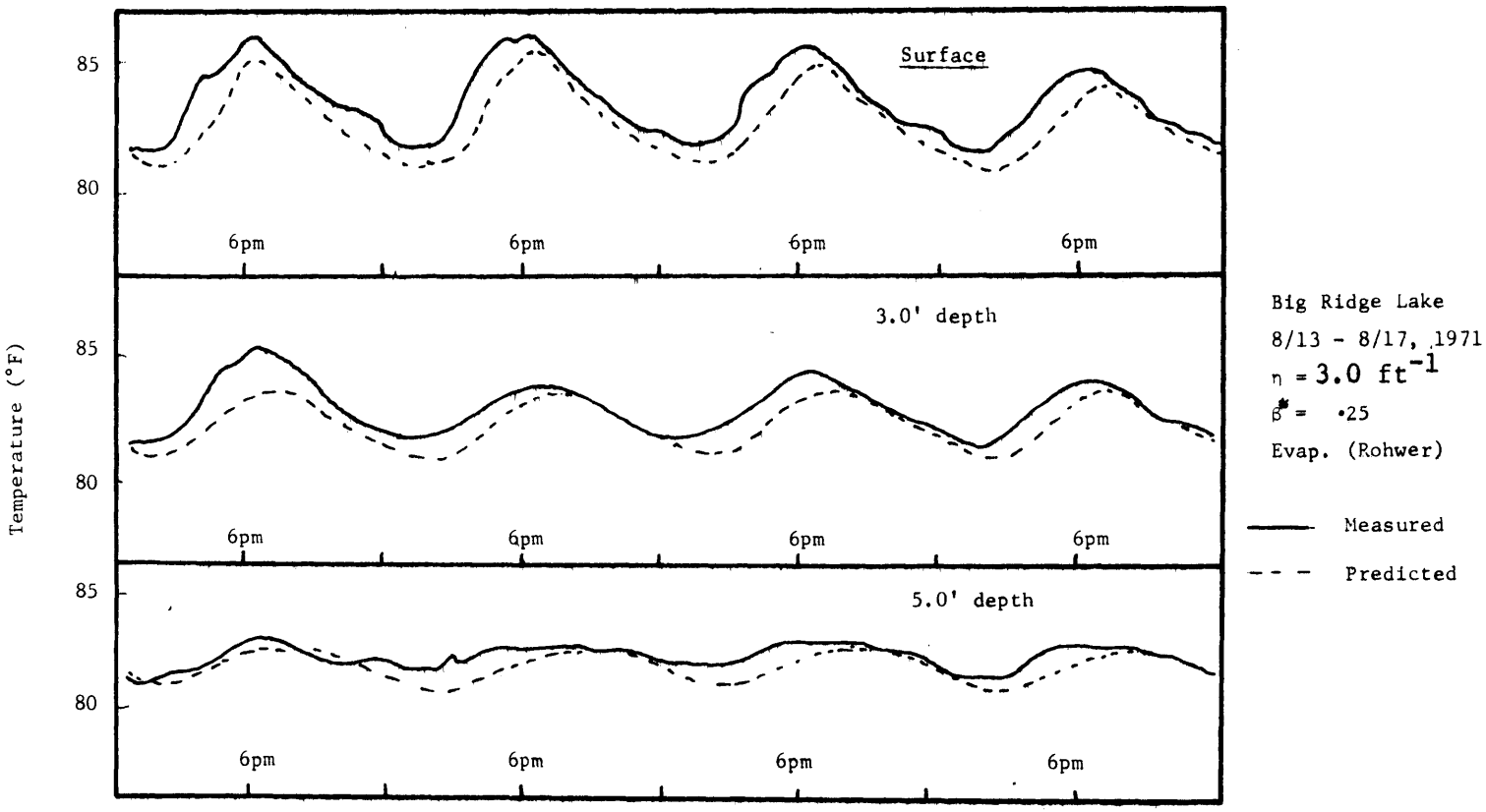

Figure 6-37 Predicted and Measured Diurnal Temperature Fluctuations

6.7.10 Modifications to M.I.T. Deep Reservoir Model

Two important changes were made to the deep reservoir model to adapt it as a component of the cooling pond model. The upper boundary condition for the deep reservoir region is no longer the heat flux at the surface, as in a deep reservoir model. The new heat flux boundary condition is obtained from the conditions at the downstream end of the surface layer (see Figure 6-38).

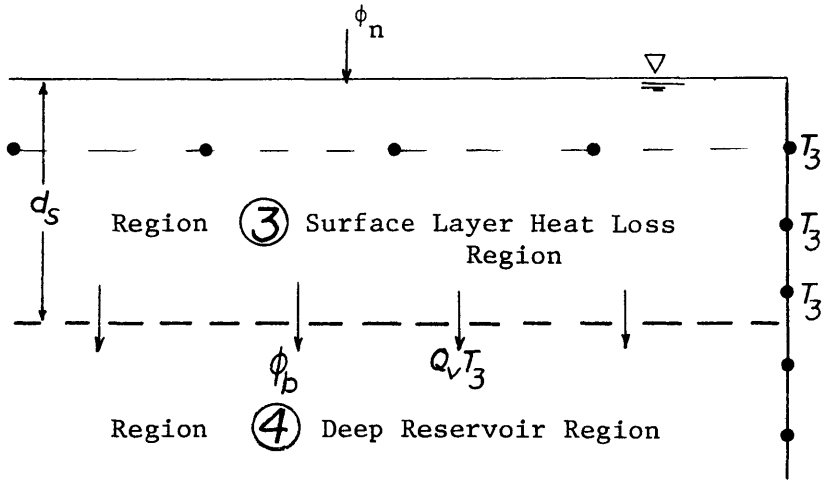

Figure 6-38 Junction of Surface Heat Loss Region and Deep Reservoir Region

When the temperature at the end of the surface heat loss region is less than the top temperature in the deep reservoir region, vertical mixing is allowed to take place until all areas in the cooling pond are stable. Note that only a portion of the surface layer (heat loss region) may be involved in this vertical mixing, as only that portion of the surface area where instability is present takes part in the vertical mixing. Heat energy is conserved so that the mixed temperature is given by

$$T_m(t) = \frac{\int_{A_s}^{A_p} d_s\, T(A,t)dA + \int_{z_\ell}^{z_s-d_s} A(z)\, T(z,t)\, dz}{(A_p-A_s)d_s + \int_{z_\ell}^{z_s-d_s} A(z)\, dz} \qquad (6.61)$$

where A_p = total pond surface area

A_s = stable portion of pond surface area

z_s = pond surface elevation

z_ℓ = elevation of bottom of mixed layer

d_s = depth of heat loss region

(see Figure 6-39).

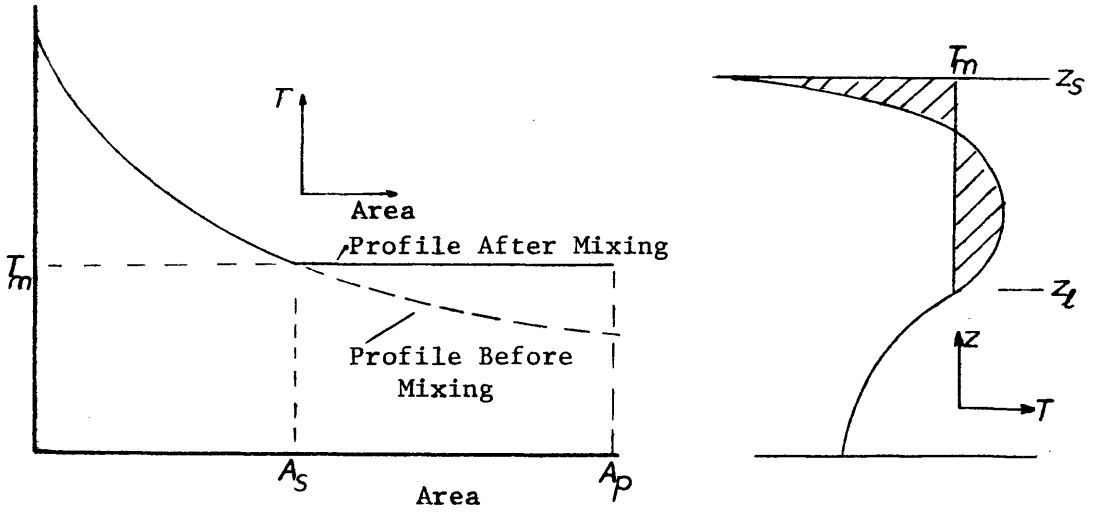

Figure 6-39 Convective Mixing Near Surface

6.8 Intake Pond - Region 5

In many cooling ponds the topography is such that it is necessary to have the intake structure at some distance from the skimmer

wall e.g. to be effective a skimmer wall must be located in relatively deep water, and thus may be constructed at some distance from the shoreline. Examples of cooling ponds with large intake ponds are Lake Norman (Figure 4-5 and Hazelwood (Figure 4-4). The area of the Lake Norman intake pond is ~ 200 acres, and the Hazelwood intake pond is approximately 50 acres. A typical intake pond is shown in Figure 6-40.

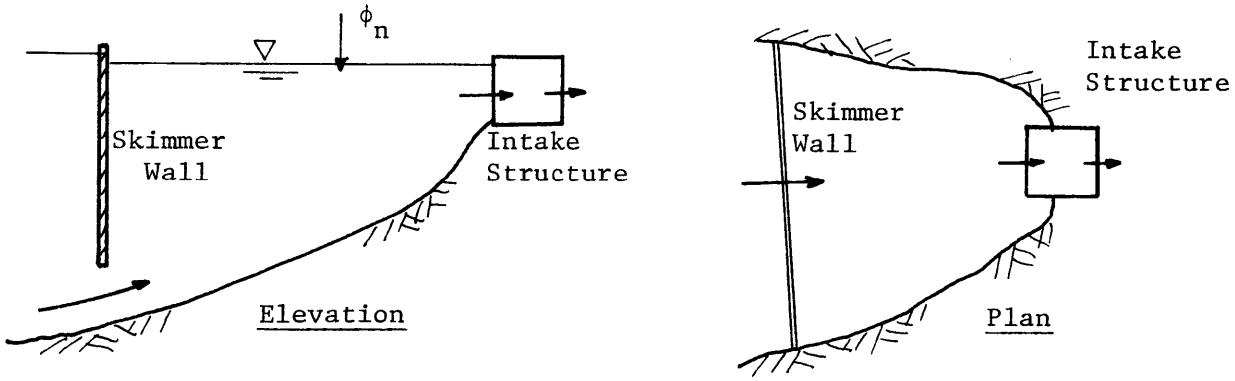

Figure 6-40 Intake Pond

An intake pond may have two detrimental effects on pond performance. Unless the intake structure is carefully designed as a skimmer wall it will withdraw over the full depth and this may result in diurnal fluctuations in the intake water, even though the flow under the skimmer wall has a constant temperature. In the case of a natural pond, e.g. Lake Norman, the water temperature at the skimmer wall opening may be below equilibrium temperature, and an overall temperature rise of several degrees (F) may occur between the skimmer wall and the intake due to surface heat transfer in the intake pond.

The most accurate way to treat the intake pond is as a deep reservoir, allowing vertical stratification to occur. However, this degree

of sophistication may not be justified in view of the short residence time, and in this model a fully mixed system has been assumed. The region is schematized as shown in Figure 6-41.

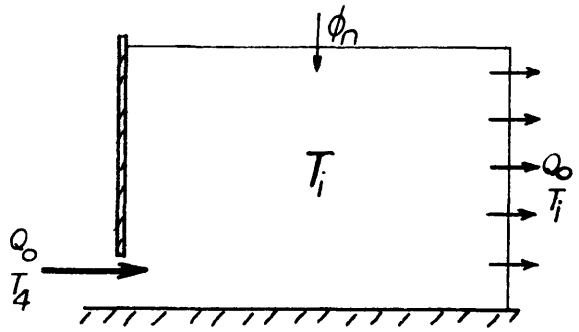

Figure 6-41 Geometric Schematization of Intake Pond

The governing equation is Equation (6.6):

$$\frac{\partial T}{\partial t} = \frac{H_v}{\rho c} \tag{6.6}$$

where

$$H_v = \frac{1}{\forall_{IP}} \left[\phi_n A_{IP} + \rho c Q_o (T_4 - T_i)\right] \tag{6.62}$$

A_{IP} = surface area of intake pond

$\forall_{IP}$ = volume of intake pond

An initial condition, specifying T_i at zero time, is all that is required to solve Equation 6.62.

The numerical solution to the main governing equations is discussed in the following section.

6.9 Numerical Solution of the Governing Equations

6.9.1 Choice of Scheme

Since it is not possible to obtain an analytical solution to the governing equations, 6.14 and 6.21, a finite difference method is used. The simplest possible solution which is consistent with certain requirements for accuracy and cost is sought. Three basic finite difference methods are applicable to the convective-diffusion equation under consideration: (1) an explicit or forward difference scheme, (2) an implicit or backward difference scheme, (3) a combination of the first two which also results in an implicit method. An explicit scheme specifies the value of an unknown variable in terms of known parameters only e.g. the value of an unknown variable (temperature) at time step n+1 is specified in terms of known variables including values of temperature at time step n. Explicit schemes are easy to formulate, particularly in regard to their boundary conditions. The computer time required for a given time step is less than that required by an implicit solution by a factor of approximately $(1.5)^n$, where n is the number of spatial dimensions. There are, however, several disadvantages. Explicit schemes may be subject to stability requirements which can restrict the size of the time step to such an extent that the scheme becomes impractical. Also simple explicit schemes, which are generally not time centered, may introduce a numerical damping effect which is not present in time-centered implicit schemes. Implicit schemes, which specify the unknown variable at time step n+1 in terms of known and unknown variables at time steps n and n+1, are usually unconditionally stable, and avoid the effects of numerical damping. However, implicit methods are more difficult to formulate, use more computer

time per time step, and are subject, along with explicit schemes to the problem of numerical dispersion. Note that numerical damping and numerical dispersion are not the same, as is sometimes implied. Numerical damping acts in exactly the same fashion as a diffusion coefficient, and reduces the amplitude of the frequencies in the solution, particularly the high frequencies, i.e. numerical damping tends to smooth out a sharp interface. Numerical dispersion, on the other hand, results from the fact that different frequencies are propagated with different velocities. Again the effect is largest for the high frequencies, and large oscillations may appear at a sharp interface. See Figure 6-42 .

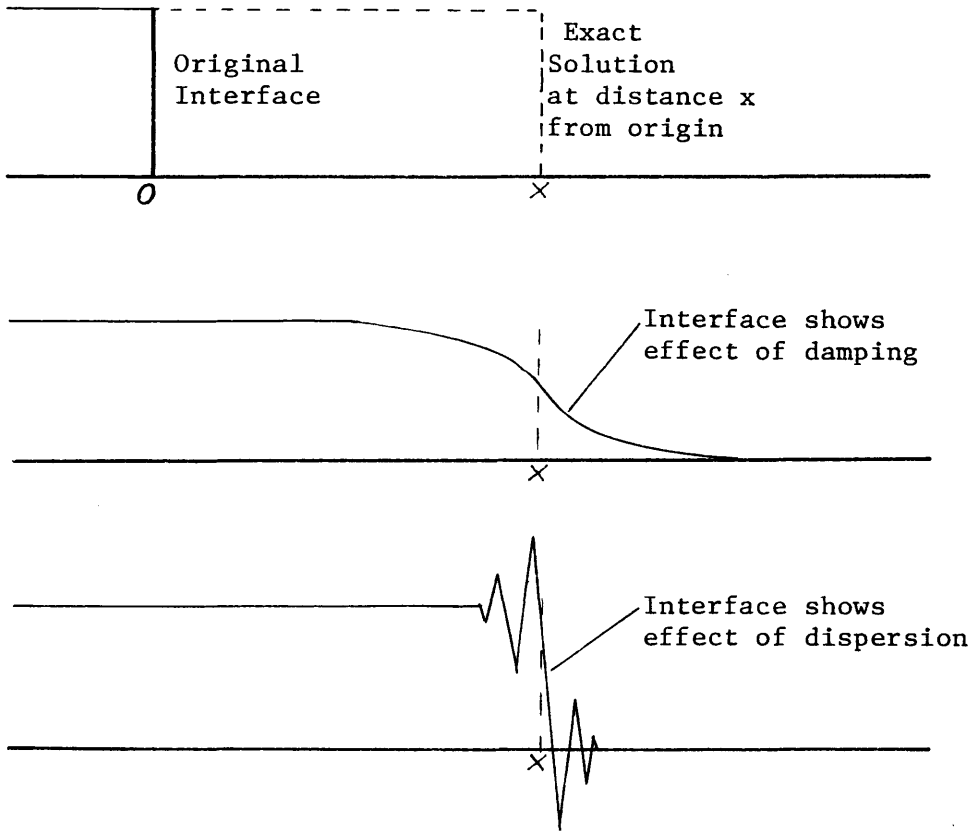

Figure 6-42 Numerical Damping and Dispersion

The problem of numerical dispersion can be minimized by suitable choice of scheme e.g. Stone and Brian's (1963) implicit, six-point scheme in one-dimensional problems. Note that if a large amount of diffusion is present (either physical diffusion or numerical damping) the numerical dispersion effects are minimized, since the diffusion eliminates high frequencies before they can be propagated incorrectly.

In choosing a numerical scheme it is essential to fit the scheme to the problem. For example if high frequencies are absent, it is a waste of effort to choose a complicated scheme which minimizes damping and dispersion effects. Alternatively, if the crux of the problem is the correct propagation of a sharp interface or a pulse, then one must choose a scheme which minimizes damping and dispersion. It has already been stated that in this model there is no interest in accurately simulating the horizontal movement of a warm interface in the surface layer, and vertical temperature profiles tend to be relatively smooth, and thus it seems likely that a simple explicit scheme may suffice. The stability criteria for such a scheme will be given, and it will be shown that these are not unduly restrictive.

6.9.2 Limitations on a Simple Explicit Scheme

The use of a simple explicit finite difference scheme entails some limitations of numerical stability is to be maintained. The stability criteria for both the surface layer and the deep reservoir region are given below

Surface Layer

$$\frac{Q\,\Delta t}{d_s\,\Delta A} \leq 1 \qquad (6.63)$$

Deep Reservoir Region

$$\frac{V\Delta t}{\Delta z} \leq 1 \tag{6.64}$$

$$(E_z+D_m)\frac{\Delta t}{(\Delta z)^2} \leq \frac{1}{2} \tag{6.65}$$

where Δt = time increment

ΔA = area increment in the surface layer

Q = horizontal flow rate in the surface layer

d_s = depth of the surface layer

Δz = vertical length increment in the deep reservoir region

V = vertical velocity in the deep reservoir region

(E_z+D_m) = vertical diffusion coefficient = 0.133 ft^2/day for $E_z = 0$

As long as turbulent diffusion is neglected, Equation 6.65 is not at all restrictive. Equations (6.63) and (6.64) may lead to a rather small Δt because of inflow conditions which occur over a small period of time, or which occur in only one of the five regions. This is accounted for by allowing Δt to vary, both in time and from region to region. Note that Equation (6.63) or (6.64) is often applied to implicit schemes on the grounds of accuracy. The following table (Table 6-3) shows the typical length (area) and velocity (discharge) scales, and the resulting maximum time increments for the field case.

Table 6-3

Region	ΔA	d_s	Δz	Q	V	Δt_{max}
Surface Heat Loss Region	2×10^6 ft^2	5 ft		10^8 ft^3/day		0.1 days
Deep Reservoir Region			2 ft		2 ft/day	1.0 days

A time increment of 0.1 days may seem somewhat small in relation to the usual time scale of one year, but it was found that the solution for the whole surface region, which was divided into 20 area increments, for one year took only ∿ 20 secs. of computation time on an IBM 370/155, and hence the stability requirements cannot be called restrictive.

6.9.3 Description of Proposed Scheme

The scheme used is one of the simplest available, a three point (donor cell) forward differences scheme as shown in Figure 6.43

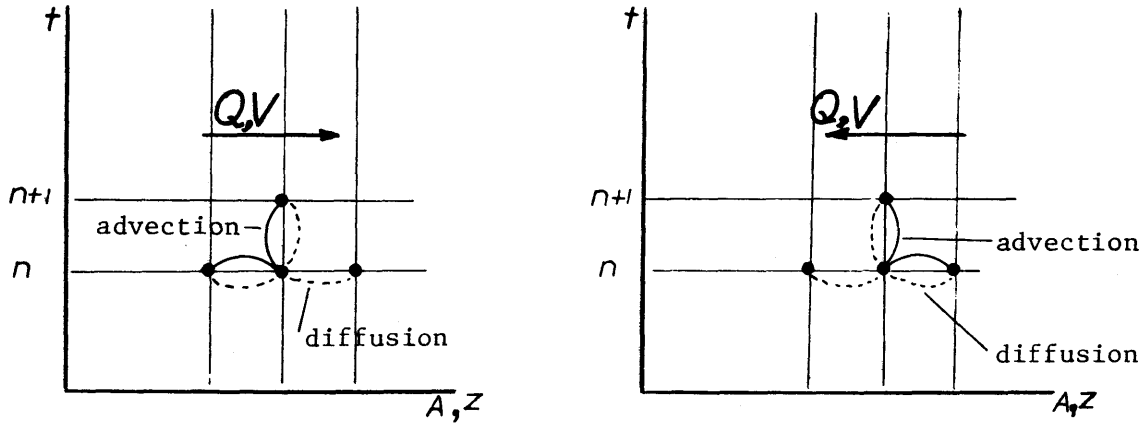

Figure 6.43 Explicit Scheme Used in Both Horizontal and Vertical Direction

This scheme is easily formulated in a conservative form i.e. the finite difference equation is written as the difference between fluxes. The conservative form of the finite difference equations has the advantage of conserving the transported quality (mass, heat, DO etc.). A significant advantage of the above scheme is that local oscillations never appear, and in a vertical temperature profile where a negative $\frac{\partial T}{\partial z}$ is immediately followed by convective mixing, and where inflow and outflow widths depend on local temperature gradients, this can be an important factor.

The magnitude of the numerical damping in the surface layer is given by Bella (1968) as $\frac{Q\Delta A}{4d_s(b_s)^2}$ where b_s is the width of the surface layer. For a typical b_s of $2x10^3$ ft this gives a damping coefficient of $\sim 6x10^5$ ft^2/day (approximately 7 ft^2/sec) which is the same order as longitudinal dispersion in a narrow river. For the deep reservoir region the expression is $(\frac{V\Delta z}{4})$ and this leads to a maximum damping coefficient of 1.0 ft^2/day. This is only about 8 times the molecular value and is of the same order as the actual diffusivity calculated from field data (see Table 6-2). Thus it seems unlikely that the numerical damping, introduced as a result of the simple explicit scheme, will cause significant problems.

The scheme is formulated by applying the heat balance approach to the same control volumes through which the governing differential equations were developed. Figure 6.44 shows the array of grid points used for the first four regions in the scheme. The finite difference equations for the proposed simple explicit scheme are well known and

will not be discussed.

The length increment, Δz, and the area increment, ΔA, are chosen on the basis of the required resolution, and the allowable computation time. An initial Δt is chosen using Equations (6.63) to (6.65), although automatic safeguards are included in the computer program which prevent violations of the stability requirements. The magnitude of the numerical damping is checked using the expressions obtained from Bella (1968) to ensure that numerical errors are not excessive.

The initial condition is usually given as an isothermal one, but sometimes (e.g. in the Lake Normal case) an initial vertical profile may be specified.

6.9.4 Review of Mathematical Model

The mathematical model developed in this chapter predicts the surface temperature distributed as a function of area and time, $T(A_x,t)$, the vertical temperature profile $T(z,t)$ and the intake temperature $T_i(t)$, for a deep stratified cooling pond. The model includes the effects of surface heat transfer and entrance mixing, as well as advective inflows and outflows, internal radiation absorption, diffusion, convective mixing and selective withdrawal. The model can handle multiple inflows and outflows, and thus can be applied to both natural and artificial cooling ponds. In the next chapter, the mathematical model will be applied to physical situations, first an idealized laboratory cooling pond, and then to two prototype cooling ponds, the Hazelwood pond (artifical type) and the Lake Norman Reservoir

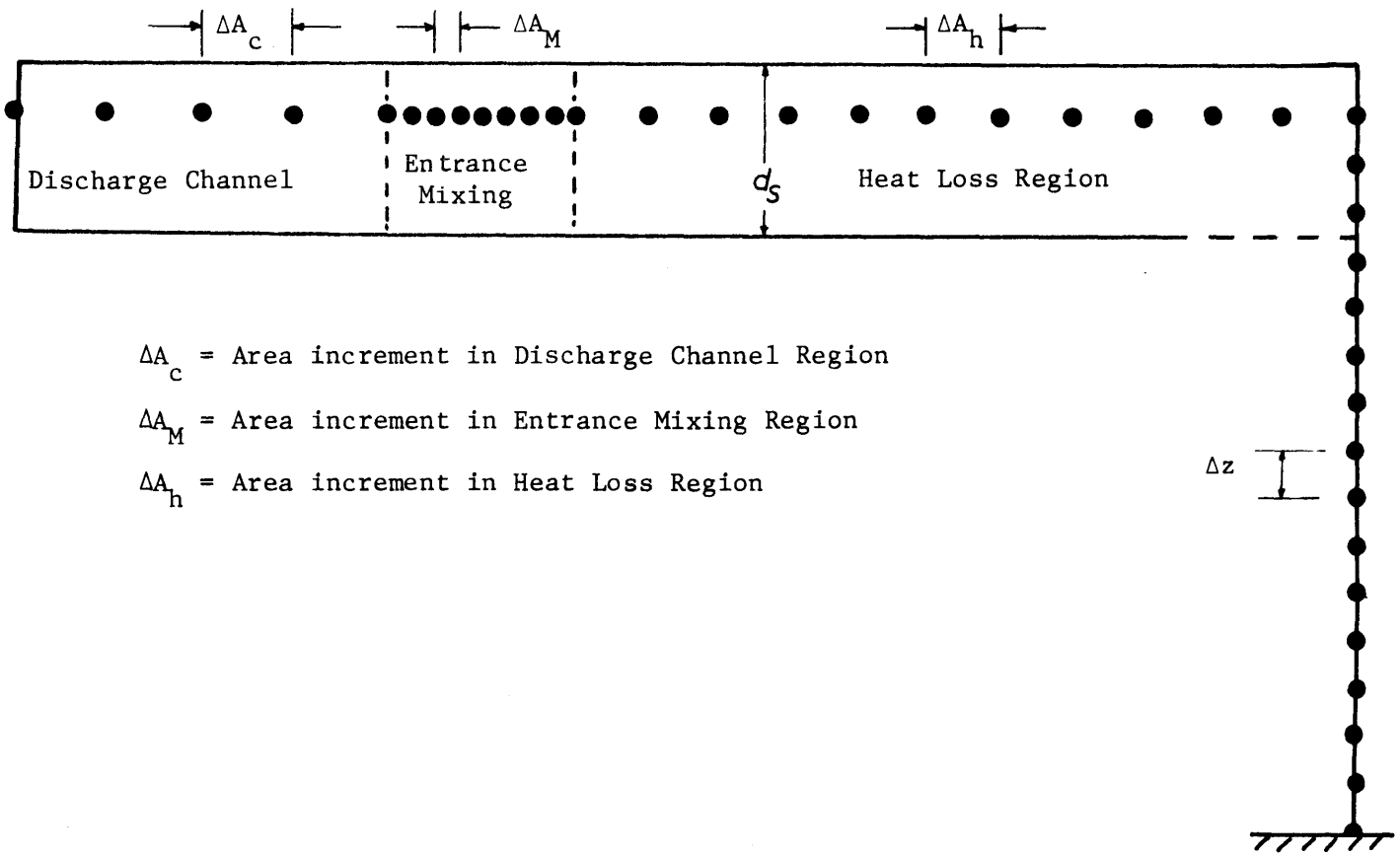

ΔA_c = Area increment in Discharge Channel Region

ΔA_M = Area increment in Entrance Mixing Region

ΔA_h = Area increment in Heat Loss Region

Figure 6-44 Grid Point Arrangement

(a natural type). These trials should test the validity of the assumptions involved in the development of the theory, and the applicability of the model to the prediction of transient cooling pond performance.

VII. Laboratory Experiments on a Three-Dimensional Cooling Pond

7.1 Laboratory Equipment

Laboratory experiments were carried out on an idealized cooling pond constructed in the Ralph M. Parsons Laboratory for Water Resources and Hydrodynamics at MIT. This facility was not intended as a scaled model of a particular prototype cooling pond, rather it has been used primarily as a physical system on which observations on the behavior of cooling ponds could be made, and as an aid to the development and verification of analytical methods. Many of the factors affecting cooling pond performance such as shape, outlet design, flow rate, depth, etc. could be varied over a wide range. This system has the obvious advantage of control of variables, ease of measurement, and a time scale measured in hours rather than days.

Figure 7-1 shows the basic arrangement of the experimental equipment. The basin within which the cooling pond was constructed is 46'x28'x1.5'. The overall dimensions of the pond itself were 40.5'x21.75'x1.2'. The bottom of the pond is a 0.6 ft thick concrete floor. The external geometry of the pond, including the discharge channel was kept constant for all the experimental runs. All walls within the basin, including the discharge channel, and internal baffles, are constructed of 3/4"-1" thick marine plywood. Leakage between the pond and the rest of the basin was minimized by sealing all joints with a sealing compound and water proof tape. The probe platform rests on four leveling jacks which may be reached from the sides of the basin. Depth gauges at each corner of the platform assure accurate control of

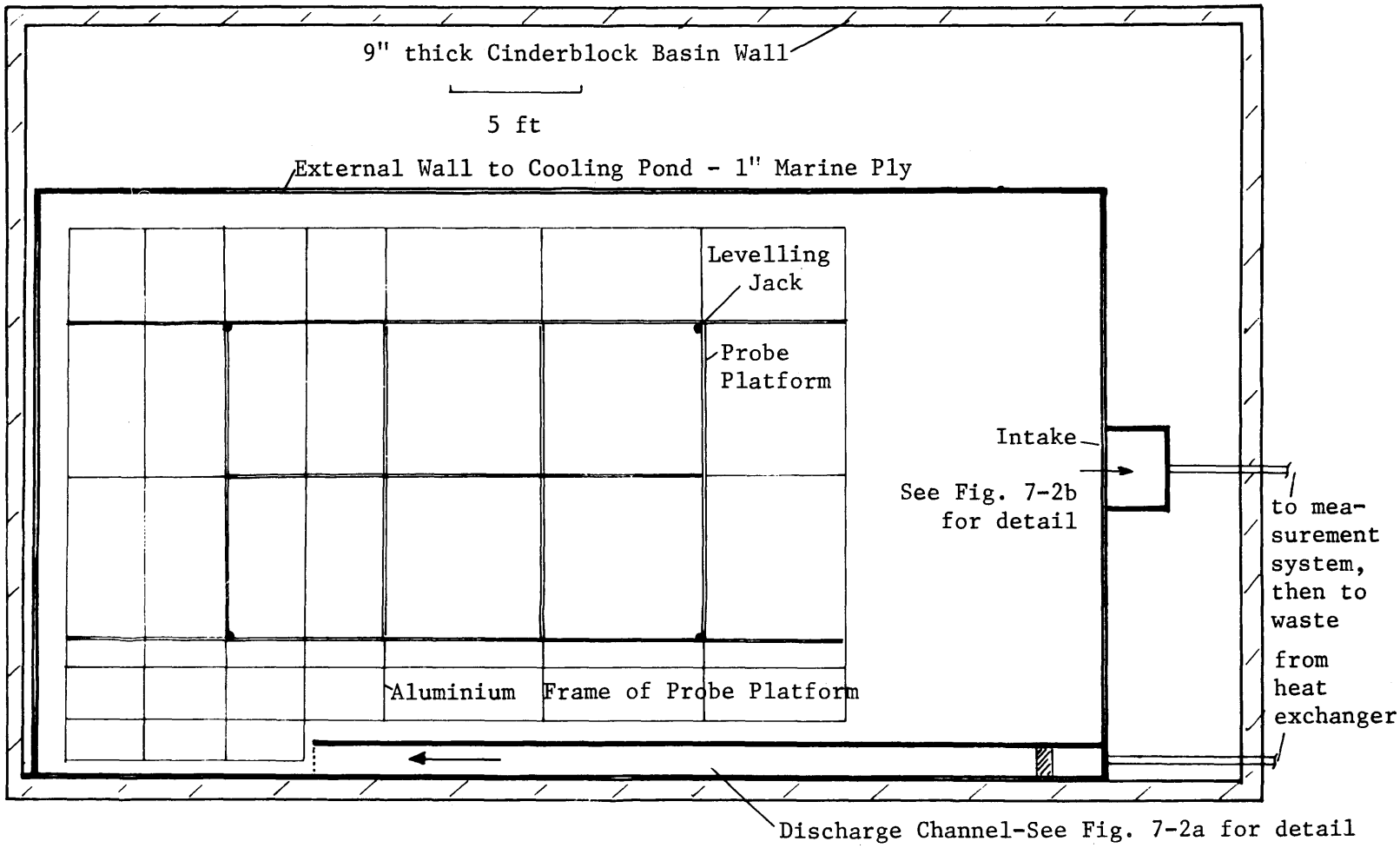

Figure 7-1 Basic Arrangement of Laboratory Cooling Pond

the platform level. The water level in the basin was monitored by a fixed point gauge.

The heated discharge is supplied from a steam heat exchanger capable of delivering up to 60 gallons per minute of water at a constant temperature up to 150°F. The flow is introduced into the discharge channel through a horsehair filter to ensure a uniform velocity distribution in the channel. The design of the discharge channel is shown in Figure 7-2a. The sloping bottom at the upstream end of the channel was designed to ensure that a cold wedge never penetrated up to the filter as direct mixing can result. Channel geometry was varied using adjustable internal walls over the full length of the channel.

The intake is designed as a skimmer wall as shown in Figure 7-2b. The dimensions of the opening are 3'x0.15'. For a typical density difference $(\frac{\Delta\rho}{\rho})$ of 10^{-3}, the critical flow rate at which drawdown of the warm upper layer occurs is approximately 30 gpm. A 1.5 horsepower centrifugal pump is used to provide a steady withdrawal rate. Inflow and outflow were monitored by Brooks rotameter flowmeters, and it was usually possible to maintain the water level within ±.01 ft with a minimal amount of adjustment.

The water temperature measurement system consists of 92 YSI #401 thermistor probes. 56 probes are mounted on the probe platform in one horizontal plane which can be moved vertically using the platform leveling jacks. Three sets of 7 probes are used to define vertical profiles in the inaccessible areas of the pond. Six (6) probes are mounted on depth gauges, one of which was motor driven, the rest

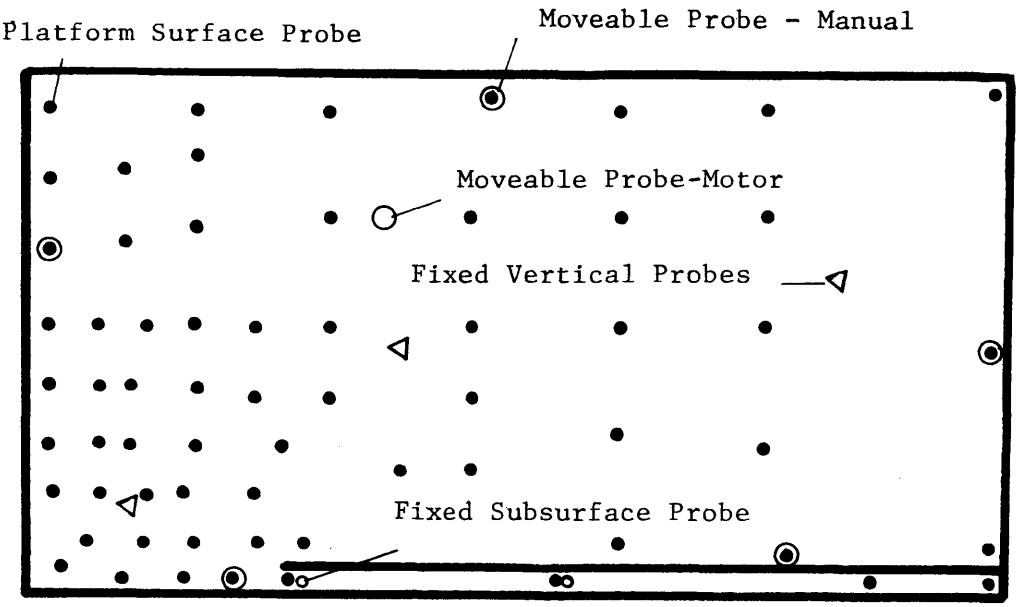

a) Typical Probe Location

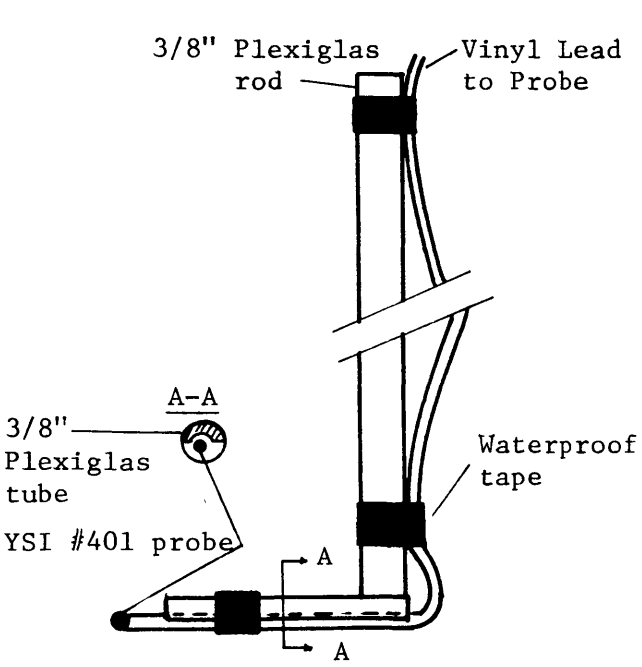

b) Probe Holder on Platform

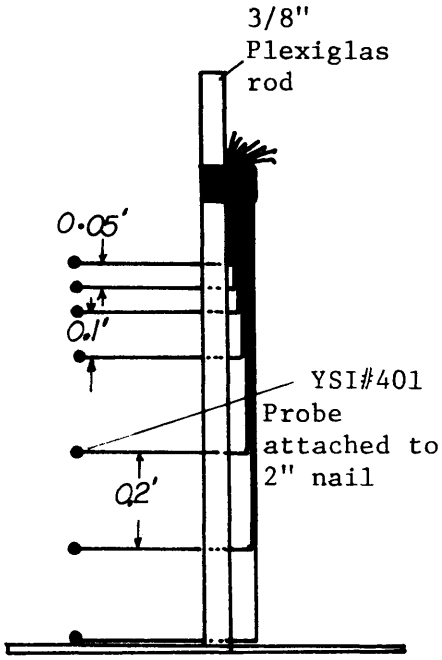

c) Fixed Vertical Probes

Figure 7-3 Probe Location and Details

made of $\frac{3"}{8}$ thick marine plywood surrounded by 3 inches of fibreglass insulation (see Figure 7-4). The depth of water in the tank was usually $\frac{1}{2}$ - 1" giving a lag time for the equilibrium temperature of 30-60 minutes. This tank was also used for separate heat loss runs to determine evaporation under laboratory conditions.

Heat loss through the concrete floor was monitored using 3 YSI #401 thermistor probes. One of these was held against the underside of the floor using a 3" cube of styrofoam taped to the concrete, while two probes were held with a packing of modelling clay in $\frac{1"}{2}$ deep, $\frac{1"}{4}$ diameter holes drilled in the underside of the floor. The YSI #401 probes for both air and concrete temperatures were read using a Digitec (United Systems) Digital Thermometer, Model No. 500-1N. Key temperature probes e.g. inflow and outflow probes, were checked periodically using a Kessler R21024 - 76mm Immersion mercury thermometer.

7.2 Experimental Procedure

Three basic types of experiments were conducted:

a) Boundary Condition Experiments. The primary objective of these experiments was to determine the boundary conditions applicable in the laboratory, including surface heat loss, bottom heat loss, and entrance mixing. Parameters, necessary for inclusion in the mathematical model, were determined from,or tested against, data from these experiments.

b) Steady State Experiments. The primary objective of these experiments is to examine the effect on pond performance of changes in

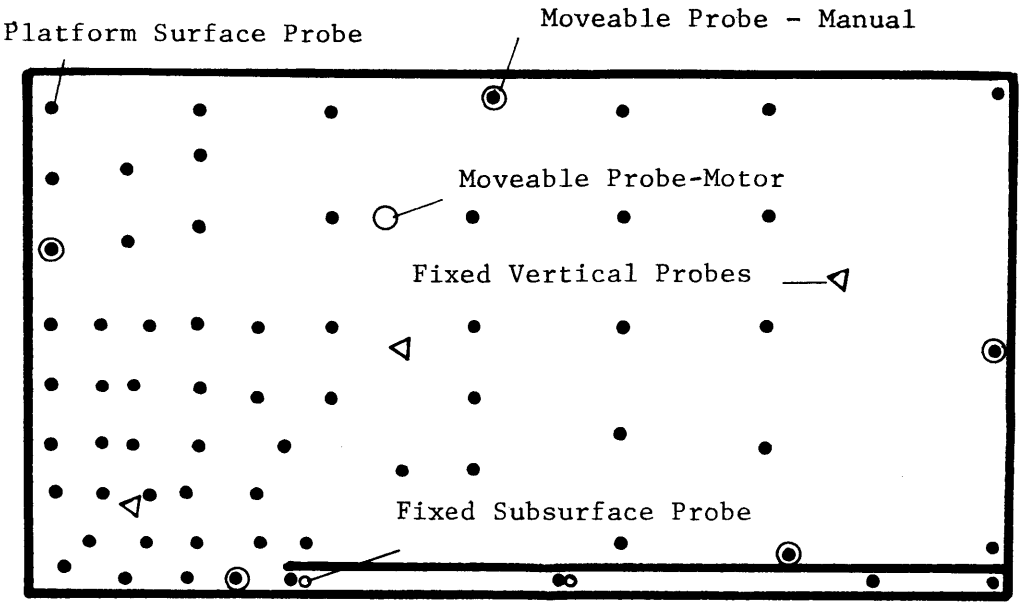

a) Typical Probe Location

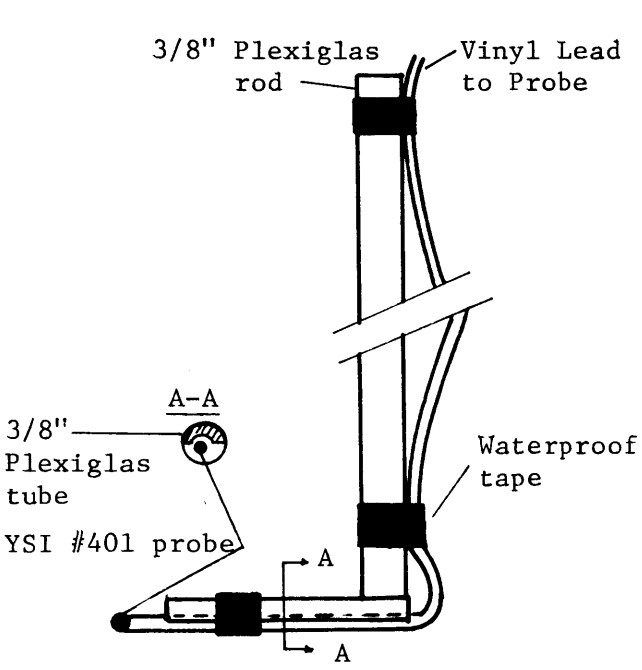

b) Probe Holder on Platform

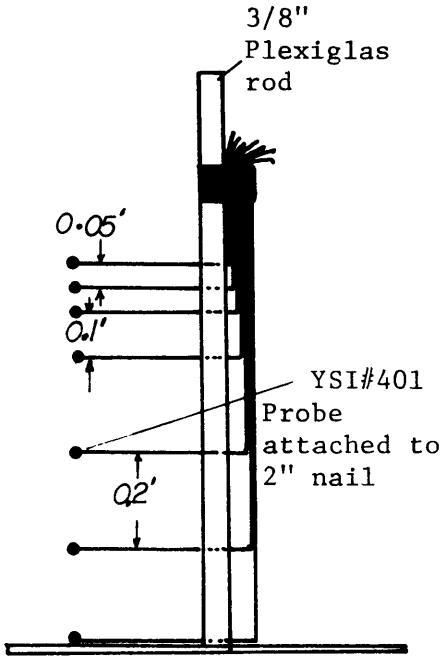

c) Fixed Vertical Probes

Figure 7-3 Probe Location and Details

made of $\frac{3"}{8}$ thick marine plywood surrounded by 3 inches of fibreglass insulation (see Figure 7-4). The depth of water in the tank was usually $\frac{1}{2}$ - 1" giving a lag time for the equilibrium temperature of 30-60 minutes. This tank was also used for separate heat loss runs to determine evaporation under laboratory conditions.

Heat loss through the concrete floor was monitored using 3 YSI #401 thermistor probes. One of these was held against the underside of the floor using a 3" cube of styrofoam taped to the concrete, while two probes were held with a packing of modelling clay in $\frac{1"}{2}$ deep, $\frac{1"}{4}$ diameter holes drilled in the underside of the floor. The YSI #401 probes for both air and concrete temperatures were read using a Digitec (United Systems) Digital Thermometer, Model No. 500-1N. Key temperature probes e.g. inflow and outflow probes, were checked periodically using a Kessler R21024 - 76mm Immersion mercury thermometer.

7.2 Experimental Procedure

Three basic types of experiments were conducted:

a) Boundary Condition Experiments. The primary objective of these experiments was to determine the boundary conditions applicable in the laboratory, including surface heat loss, bottom heat loss, and entrance mixing. Parameters, necessary for inclusion in the mathematical model, were determined from,or tested against, data from these experiments.

b) Steady State Experiments. The primary objective of these experiments is to examine the effect on pond performance of changes in

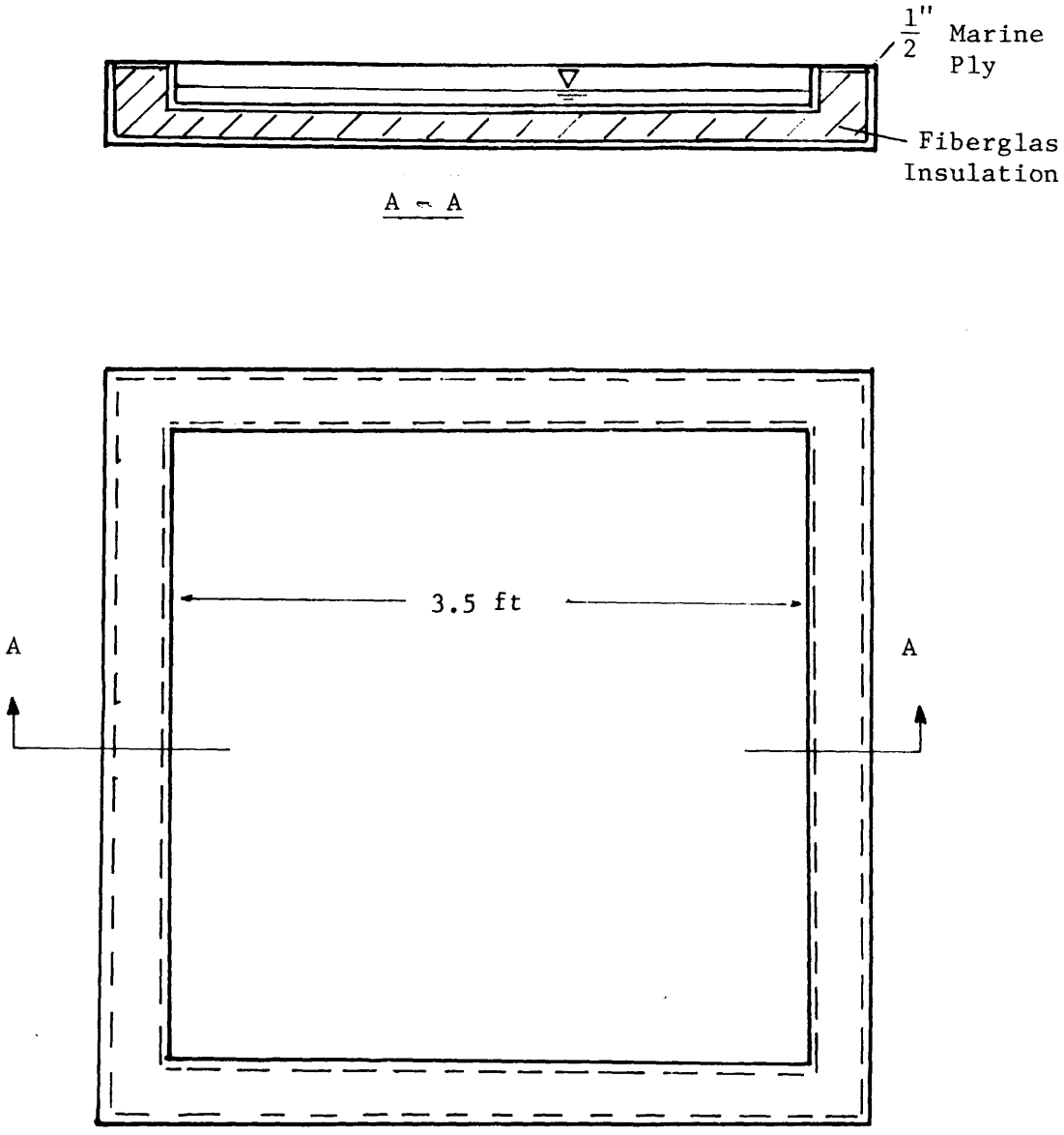

Figure 7-4 Equilibrium Temperature Tank
(Scale 1" = 1 ft)

certain boundary conditions such as shape, depth and outlet design. The results of these tests were used to help postulate a viable mathematical model.

c) Transient Experiments. The primary objective of these experiments is to provide a verification of the transient mathematical model under laboratory conditions.

The experimental procedure for each of these types of experiments is discussed below.

7.2.1 Boundary Condition Experiments

Three types of boundary condition experiments were carried out, surface heat loss, bottom heat loss and entrance mixing. Each of these will be considered in turn.

7.2.1.1 Surface Heat Loss

Surface heat loss experiments were carried out both in the laboratory cooling pond and in the small insulated tank. The procedure was simple for both cases. The small insulated tank was filled with hot water at about 120^{o}F and allowed to stand for approximately half an hour. This water was then removed and 100 lbs of hot water at 120 - 140^{o}F placed in the tank, and allowed to cool. Temperature readings were taken using 3 YSI #401 thermistor probes, and a mercury thermometer. Readings were commenced 5 minutes after the water was put in the tank and initially were taken at 5 minute intervals, and later at intervals of as much as 30 minutes. The water was stirred before each reading. Air temperatures were taken at 1 ft and 8 ft elevations. Relative

humidity was measured alongside the tank, and dewpoint temperature was measured at the 8 ft elevation. These latter readings were generally taken at 30 minute intervals. At the end of the experiment, which lasted up to 5 hours, the water remaining in the tank was reweighed. The thermal capacity of the insulated tank is approximately 10 Btu/^{o}F. No temperature increase was observed at the exterior of the insulation, and hence the maximum average temperature increase in the tank materials is half that of the water, and heat flux from the bottom and sides of the tank is negligible. Since the thermal capacity of the water is 100 Btu/^{o}F, neglect of the effect of heat storage of the tank itself amounts to an error of less than 5 percent. The heat loss experiments using the cooling pond itself were usually done at the end of a transient run so that the concrete floor had reached equilibrium. The water temperature in the basin outside the actual cooling pond area was first increased to minimize heat losses through the sides of the cooling pond. The water in the cooling pond was then thoroughly mixed by manual methods, and readings commenced. The mean water temperature was obtained by averaging 88 probes (probes in the inflow and outflow pipes were ignored). The pond was continually mixed throughout the test by circulating the water through the 1.5 HP centrifugal pump, and the heat input from the pump was included in the energy budget. The temperature of the concrete floor was monitored throughout the run. Temperature readings, including water, air, dewpoint and concrete temperatures were taken every thirty minutes initially, and later at intervals of up to 3 hours. The duration of runs varied from 6 to 24 hours. Air temperature in the laboratory showed some horizontal variation ($\sim$2^{o}F) but no

apparent vertical stratification. Air temperatures were taken at three locations 2 ft above the water surface, and also at one location 8 ft above the center of the pond. Relative humidity was measured 2 ft above the water surface and dewpoint temperature at 8 ft.

7.2.1.2 Bottom Heat Loss

A simple transient experiment was run to check the heat loss through the bottom boundary. Approximately 0.1 ft of water was allowed to stand in the cooling pond for a period of 36 hours to establish a known initial condition for the concrete floor. The temperature of the water was then increased as quickly as possible by approximately $25^{o}F$, kept constant for a considerable period, and then allowed to cool. The temperature of the underside of the floor, plus the air temperature on the underside of the floor were monitored over a period of 44 hours, and the transient behavior of the floor observed. This behavior was then compared against the behavior predicted by the simple theory for heat conduction in solids, using values for density, specific heat capacity and thermal conductivity taken from the CRC Handbook by Bolz and Tuve (1970).

7.2.1.3 Entrance Mixing

A separate series of experiments were run to check that the empirical formulae developed from the Stolzenbach-Harleman heated discharge model were applicable to a typical cooling pond discharge configuration, where entrainment is restricted to one side of the jet, and forward motion of the jet is blocked at a relatively short distance

from the outlet (see Figure 7-5).

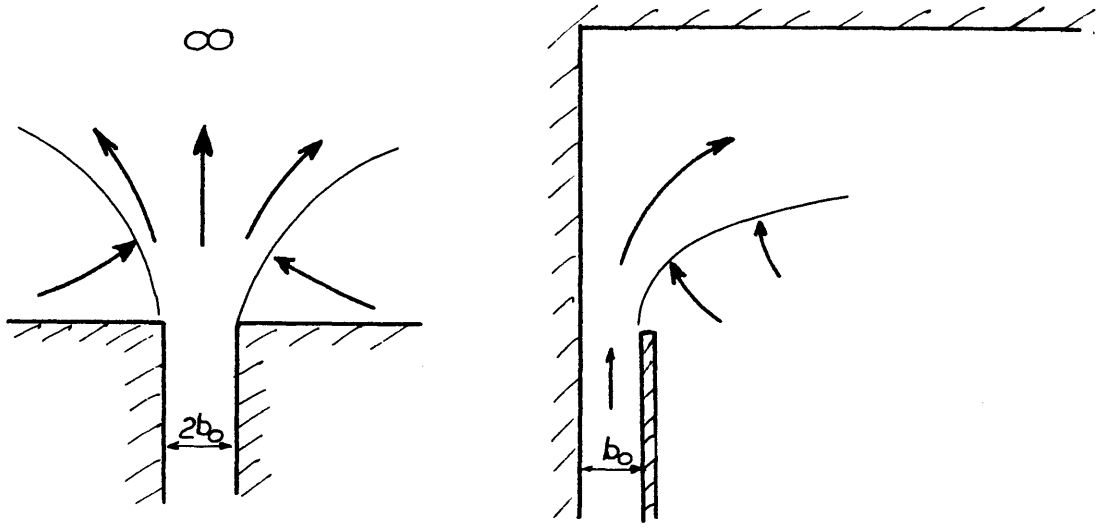

a) Normal Surface Jet Configuration

b) Typical Cooling Pond Outlet Configuration

Figure 7.5 Outlet Configurations

For these experiments, temperature probes were concentrated in the outlet area as shown in Figure 7.6. The outlet channel was designed so that the vertical profile of the heated discharge could be viewed directly (see Figure 7.6). Before each run the water in the cooling pond was mixed and the probe platform leveled. Readings were commenced approximately 1 hour after the start of the heated discharge, and the following measurements were taken:

a) 5 vertical temperature profiles along the centerline of the jet and 3 vertical temperature profiles within the discharge channel

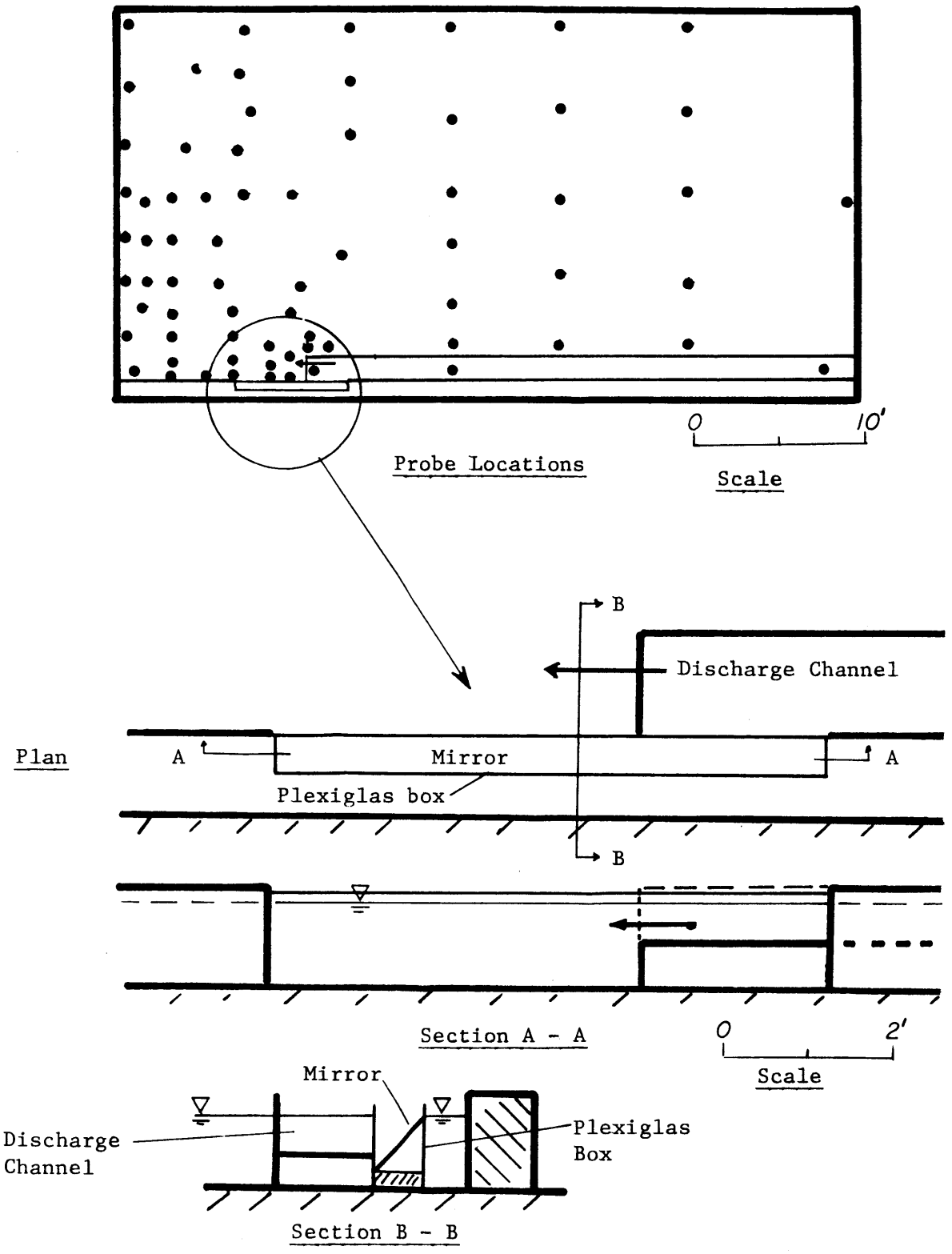

Figure 7-6 Probe Location & Outlet Geometry for Entrance Mixing Experiments

(if a cold wedge was present).

b) Temperatures were taken via the probe platform at (7) depths, with particular emphasis on the near surface readings. These readings defined the three-dimensional temperature field.

c) Dye tests were used to determine visually the vertical and horizontal spread of the jet.

d) Inflow temperature and depth, air temperatures and vapor pressures were monitored throughout the run. Typical run durations were approximately 1 hour. Table 7-1 shows the significant parameters for each run.

7.2.2 Steady State Experiments

A large number of experimental runs were done to examine the effect of certain boundary conditions on cooling pond performance. The procedure for these runs was quite straightforward. A run with a particular set of boundary conditions would be allowed to proceed to steady state, with discharge and intake flowrates and discharge temperatures held constant. Intake temperatures, air temperatures, equilibrium temperatures and vapor pressures are monitored. Steady state was determined on the basis of intake temperatures, and usually occurred after $t = 3\hat{t}$ where $\hat{t}$ is the residence time. Once steady state was reached, the three-dimensional temperature structure was defined with particular emphasis on near surface temperatures, and dye tests were carried out showing the motion of a dye front in the surface layer. The position of the dye front was determined visually using a 3 ft square grid on the floor of the pond as a frame of reference. Velocities

Run No.	h_o ft	b_o ft	Q_o gpm	ΔT_o	T_{Am}	$\frac{\Delta\rho}{\rho} \times 10^3$	h_o^*	u_o^*	R_e	F_D	$A_p = \frac{h_o^*}{b_o}$
DR 1	.38	.25	5	23.8	85.4	4.86	.23	.19	6200	1 (.58)	.93
DR 2	.38	.25	10	24.3	87.0	4.87	.38	.23	8800	1 (.96)	1.5
DR 3	.38	.25	20	14.5	98.5	3.13	.38	.47	17600	2.4	1.5
DR 4	.38	.1	20	14.6	99.0	3.15	.38	1.17	20700	6.0	3.8
DR 5	.37	.1	10	18.8	93.0	3.89	.37	.60	10600	2.8	3.7
DR 6	.37	.1	5	21.6	88.5	4.33	.37	.30	5300	1.32	3.7
DR 7	.38	1.25	5	22.6	86.4	4.46	.082	.11	3150	1 (.10)	.065
DR 8	.37	1.25	10	22.7	89.2	4.57	.13	.14	5900	1 (.20)	.1
DR 9	.37	1.25	20	15.6	98.0	3.33	.23	.16	10400	1 (.48)	.18
DR 10	.25	1.25	20	14.9	98.0	3.16	.25	.14	10200	1 (.90)	.2
DR 11	.125	1.25	20	15	98.0	3.21	.125	.28	11800	2.5	.1
DR 12	.062	1.25	20	19.8	95.0	4.21	.062	.57	13000	6.3	.05

Note: a) Figures in parentheses are densimetric Froude No's based on channel depth

b) Reynolds No. $R_e = \frac{u_o^* h_r}{\nu}$ where $h_r = (h_o^* b_o / (b_o + 2h_o^*)$

Table 7-1 Summary of Experimental Runs for Entrance Mixing

were usually of the order of 1-2 ft/min and the location of the dye front is accurate only to ±1 ft. Vertical velocity profiles were also taken for some runs. The method consisted of using the plexiglas box plus mirror shown in Figure 7-6, as part of the internal baffles. Initially photographic methods were used to determine the velocity profiles. These proved unsuccessful due to the lack of a definitive background, and finally the profiles were taken visually using a scale and a stop watch. The accuracy would be ±0.2 ft/min for the horizontal velocity, and ± .03 ft for the vertical position. The location of the plexiglas box is shown in Figure 7-7.

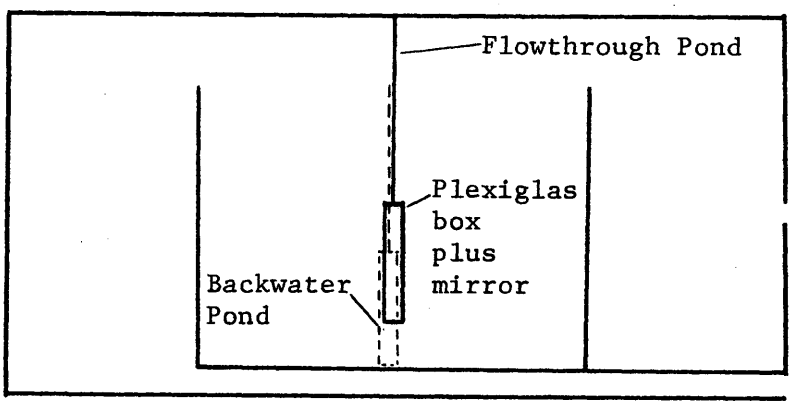

Figure 7-7 Location of 6'x0.5'x1' Plexiglas Box Plus Mirror

Once steady state conditions have been reached for one set of boundary conditions, the effect of a series of changes in the boundary conditions can be evaluated relatively quickly i.e. in time increments of 1-2 times the residence time. Five major experimental runs were carried out, and each of these runs consisted of 4-14 minor runs each

with a specified set of boundary conditions. Table 7-2 shows the important parameters for each run. Outlet temperatures were kept relatively constant over all runs, 110 - 114°F.

7.2.3 Transient Experiments

A series of experiments were run with the prime objectives of examining the transient behavior and thermal structure of a stratified cooling pond, and data from these experiments has been used to verify the mathematical model. The procedure during these runs was straightforward. The basin was filled to the required level with water at about room temperature. Usually the basin was then allowed to stand overnight. Before the start of the run the basin temperatures were checked to ensure initial homogeneity. After the start of the heated discharge, temperature readings for the discharge, intake, air, dewpoint and equilibrium tank were taken every 30 minutes. Initially surface temperatures and vertical profiles were taken hourly, and later at less frequent intervals. Dye tests were done in some cases to examine the velocity distribution. In early runs the movements of small styrofoam floats were plotted, but it was found that this process was highly misleading due to the formation of some type of surface skin which hampered the motion of the floats. The important run parameters are shown in Table 7-3. No internal baffles were used and all runs were taken from approximately room temperature ($\sim$70°F) to steady state, at which the intake temperature ranged from 80 - 97°F depending on the flow rate. In the last two runs (No. 6, 7) the emphasis was on transient response, and flow rates and outlet conditions were varied. The water in the

Tabel 7-2 Parameters for Steady State Runs

Run No.	Outlet Depth h_o ft.	Outlet Width b_o ft	Flowrate Q_o gpm	Depth of Pond ft.	Internal Baffles	Boundary Conditions of Particular Interest
8	.35	1.25	10	.92		Shape, Entrance Mixing
8A	.35	.1	10	.92		Shape, Entrance Mixing
8B	.35	.1	10	.92		Shape, Entrance Mixing
8C	.35	1.25	10	.92		Shape, Entrance Mixing
9	.75	1.25	20	.92		Shape, Depth
9A	.75	1.25	20	.92		Shape, Depth
9B	.53	1.25	20	.7		Shape, Depth
9C	.33	1.25	20	.5		Shape, Depth
9D	.33	1.25	20	.5		Shape, Depth
10	.16	1.25	20	.33		Shape, Depth
10A	.16	1.25	20	.33		Shape, Depth
10B	.16	1.25	20	.33		Area Reduction
10C	.16	.25	20	.33		Shape, Entrance Mixing
10D	.16	.1	20	.33		Shape, Entrance Mixing
10E	.16	.1	20	.33		Shape, Depth, Entrance Mixing
10F	.16	.1	20	.33		Shape, Depth, Entrance Mixing
11	.05	.1	20	.22		Shape, Depth, Ent. Mixing
11A	.05	1.25	20	.22		Shape, Depth, Ent. Mixing
11B	.05	1.25	20	.22		Shape, Depth, Ent. Mixing
11C	.05	1.25	20	.22		Shape, Depth, Ent. Mixing
11D	.05	.25	20	.22		Shape, Depth, Ent. Mixing
11E	.05	.25	20	.22		Shape, Depth, Ent. Mixing
11F	.25	.25	20	.42		Shape, Depth, Ent. Mixing
11G	.25	.25	20	.42		Entrance Mixing
11H	.25	1.25	20	.42		Entrance Mixing
11I	.25	.1	20	.42		Entrance Mixing
11J	.51	1.25	20	.58		Entrance Mixing
11K	.51	.25	20	.58		Entrance Mixing
11L	.41	.1	20	.58		Entrance Mixing
11M	.41	1.25	20	.58		Entrance Mixing
12	.33	1.25	20	.5		Entrance Mixing
12A	.33	1.25	10	.5		Entrance Mixing
12B	.33	.25	10	.5		Entrance Mixing
12C	.33	.1	10	.5		Entrance Mixing
12D	.16	1.25	5	.33		Entrance Mixing
12E	.16	.25	5	.33		Entrance Mixing
12F	.16	.1	5	.33		Entrance Mixing
12G	.16	1.25	5	.33		Entrance Mixing

Table 7-3 Transient Runs

Run No.	b_o ft.	h_o ft.	Q_o gpm	Run Duration $t^* = t/\hat{t}$	Remarks
3	1.25	.35	10	2.8	$IF_D = 1$. Straightforward run from initial condition to steady state
4	1.25	.35	20	3.8	Same as for Run 3
5	.25	.35	20	3.8	IF = 2.5. Otherwise as for Run 3
6	.25 .25 .25	.35 .35 .35	5 10 5	3.3 4.2* 4.8*	IF = 1-1.1. Run from initial condition to steady state at 5 gpm, then include effect of load increase and decrease
7	1.25 0.1 0.1	.35 .35 .35	5 20 10	2.8 3.75* 6.2*	IF = 1-7. Run from initial condition to steady state, then change flowrate and outlet conditions and look at transient behavior

*Residence times calculated on the basis of a flowrate of 5 gpm.

small insulated tank, used to obtain approximate equilibrium temperatures, was weighed before and after each run, to determine the natural evaporative loss in the laboratory.

7.3 Data Reduction

7.3.1 Heat Loss Experiments

The data from each experiment consists of a set of water temperatures, air temperatures, relative humidity and/or dewpoint temperatures, and in some cases concrete temperatures and mass differences. Heat flux from the water surface, ϕ_n, is obtained using water temperatures, time increments, water mass and surface areas. For the basin, the heat flux radiated from the underside of the basin, ϕ_R, is calculated assuming an emmissivity of 0.97. The change in heat stored in per unit area in the concrete floor ΔH_f, is calculated from

$$\Delta H_f = \rho_f c_f d_f \frac{(\Delta T_s + \Delta T_f)}{2}$$

where

ΔT_s = change in water temperature

ΔT_f = change in temperature of underside of floor

d_f = thickness of the floor

The net heat flux, ϕ_n from the basin is given by

$$\phi_n = \frac{1}{\Delta t} (\rho c d_b \Delta T_s + \Delta H_f) - \phi_R$$

where

d_b = mean depth of water in the basin

Δt = time increment

From Chapter 2, Equation 2.51 gives

$$\phi_n = \phi_r - (\phi_e + \phi_c + \phi_{br})$$

For the laboratory, ϕ_r is assumed as

$$\phi_r = 0.97\sigma (T_a + 460)^4$$

thus

$$\phi_e = \frac{-1}{(1+R)} (\phi_n - \phi_r + \phi_{br})$$

R, the Bowen ratio is a function of T_s, T_a, e_s, e_a, all of which are known or are tabulated functions of known parameters. Thus the measured value of evaporative heat flux, ϕ_e, is obtained. The directly measured mass loss, when available, is used simply as an overall check on the energy budget approach.

7.3.2 Cooling Pond Experiments

The amount of data from a cooling pond experiment was very large, with 1000-2000 pieces of data per set of boundary conditions. For comparative purposes, the data was presented in three ways

a) $T_s^* (A^*, t^*)$ vs. A^*

b) $T_i^* (t^*)$ vs. t^*

c) $T(z, t^*)$ vs. z

where

$T_s^* (A^*, t^*)$ = the normalized surface temperature

$T_i^* (t^*)$ = normalized intake temperature

$T(z,t^*)$ = temperature at elevation z

A^* = normalized surface area = A/A_p

t^* = normalized time = $t/\hat{t}$

In obtaining $T_s^*(A^*,t^*)$ the following procedure was programmed on a HP 2114B computer.

a) Apply calibration corrections to each probe.

b) Assign a surface area to each probe.

c) Subdivide the range of surface temperatures into forty (40) increments, and calculate the area in the pond with a temperature lower than each of the 39 intermediate temperatures.

d) Normalize each of the 41 temperatures T by

$$T^* = \frac{T - T_E}{T_o - T_E}$$

where T_E = equilibrium temperature (Table 2-3) calculated at time t

T_o = outlet temperature at time t

e) Normalize the area associated with each T^* against the total pond area.

In obtaining T_i^* an average equilibrium temperature over the time increment $t - \hat{t}$ to t was used, as it was felt that an instantaneous T_E would not give consistent results. Figure 7-8 shows an example of the original data for surface temperatures and the final $T_s(A^*,t^*)$ vs. A^* curve. Figure 4-2 gives an example of the vertical profiles produced.

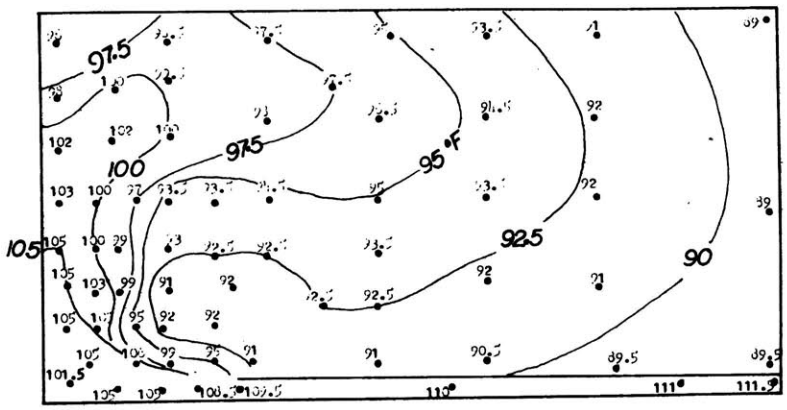

a) Original Data Plus Isotherms

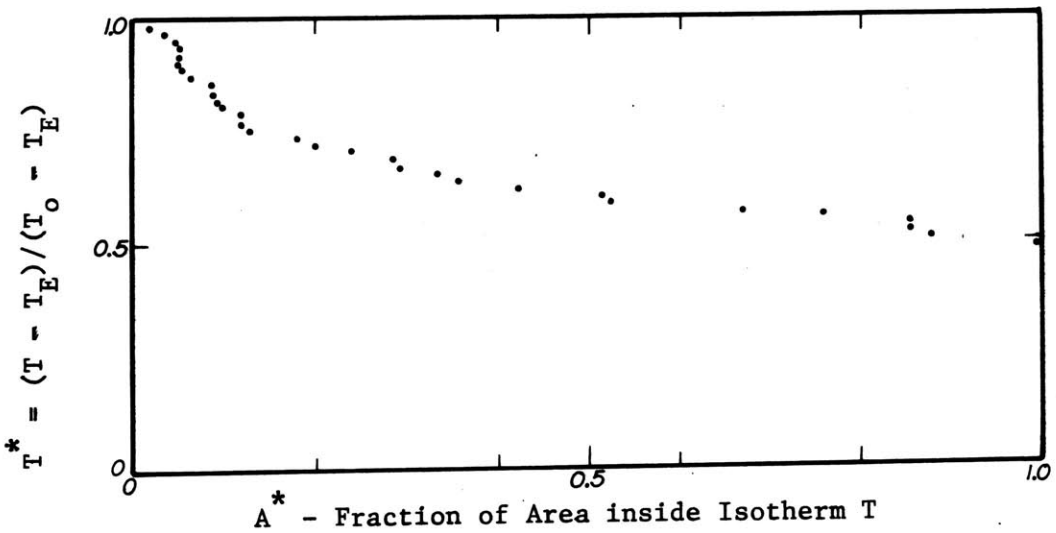

b) Temperature Area Curve

Figure 7-8 Example of Original and Reduced Data for Cooling Pond Experiments

7.4 Evaluation of Parameters for Computation

Many of the necessary parameters used in the mathematical model are measured directly and require no evaluation. These are

1. Cooling pond geometry including details of the discharge channel, elevation of the intake, etc.
2. Initial temperature.
3. Outlet and intake flow rates.

Some parameters such as air temperature, relative humidity, and discharge temperatures which were measured directly, were first plotted and mean hourly values extracted. These hourly means were used as input data.

Values of molecular diffusivity, D_m, density, ρ, and specific heat, c, were assumed to be

$$D_m = .133 \text{ ft}^2/\text{day (suitable for range 70-100°F)}$$

$$\rho = 62.4 \text{ lbm/ft}^3$$

$$c = 1 \text{ BTU/lbm}$$

The parameters for the concrete floor were taken from the CRC Handbook by Bolz and Tuve (1970), Table 1-85. They are

$$\rho_f = 137 \text{ lbm/ft}^3$$

$$c_f = 0.18 \text{ BTU/lb}_m$$

$$k_f = \rho_f c_f D_f = 24 \text{ BTU/day/ft/°F}$$

The initial temperature of the concrete floor is usually assumed equal to the initial water temperature, except for the case where the response of the floor itself was of prime interest, and here a linear temperature profile was assumed.

Calculations of $\frac{\Delta\rho}{\rho}$, where large temperature differences were involved, used the Thiesen-Scheel-Diesselhorst equation after Tilton and Taylor (1937).

$$\rho = .999973\left[1 - \frac{\theta-(3.9863)^2}{508929.2} \cdot \frac{\theta+288.9414}{\theta+68.12963}\right] \qquad (7.1)$$

SEE ERRATA

where

ρ = density of water in gm/cm^3

θ = temperature of water in °C.

Where temperature differences were relatively small an expression developed by Huber and Harleman (1968) was deemed sufficient:

$$\rho = (1-.00000205\ (T_s - 39)^2)\ \ gm/cm^3 \qquad (7.2)$$

Saturated vapor pressure at a water surface was calculated using the expression developed by Thackston and Parker (1971)

$$e_s = 25.4 \exp\left[17.62 - \frac{9500.8}{T_s + 460}\right] \ \text{mm Hg} \qquad (7.3)$$

where T_s is the water temperature in °F.

Determination of the withdrawal layer thickness, δ, requires some comment. δ is defined as in Figure 6.22. For the laboratory case, Koh's solution for a viscous diffusive flow seemed most appropriate, and the withdrawal layer thickness for a line slot is

$$\delta = \frac{3.57x^{1/3}}{\beta_o} \qquad (7.4)$$

where

SEE ERRATA

$$\beta_o = \frac{\varepsilon g}{D_m \nu}^{1/6}$$

and

$$\varepsilon = \frac{1}{\rho} \frac{\partial \rho}{\partial z}$$

ν = kinematic viscosity

The solution is restricted to $\frac{q}{D_m \beta_o x^{2/3}} << 1$

where q = flow per unit width.

In the cooling pond $q_{max} \simeq 1$ gpm/ft = 192 ft^2/day. $\varepsilon \simeq 10^{-3}$ ft.$^{-1}$, and x is taken as the quarter length of the pond (10 ft.) leading to

$$\frac{q}{D_m \beta_o x^{2/3}} \simeq 8 \tag{7.5}$$

and thus the extension to Koh's formula must be used. The extended solution is

$$\delta = \frac{3.57 x^{1/3}}{\beta} \tag{7.6}$$

where $\beta = \beta_o \left[3.5 \frac{q}{D_m \beta_o x^{2/3}} \right]^{-0.133}$ for $0.3 \leq \frac{q}{D_m \beta_o x^{2/3}} \leq 25$

This solution gave results which agreed qualitatively with observed behavior during the dye tests, and it was found that the specification of the intake velocity did not have a major effect on the transient intake temperature.

7.5 Experimental Results

Experimental results for the surface heat loss experiments

have already been presented in Chapter 2, and results for the steady state cooling pond experiments have been presented in qualitative form in Chapter 4, and in quantitative form in Chapter 5. The experimental results that will be discussed here are first those for the entrance mixing and bottom heat loss boundary conditions, where the emphasis is on ensuring that these boundary conditions are described adequately in the mathematical model. The results for the transient runs will then be presented and compared with the behavior predicted by the mathematical model developed in Chapter 6.

7.5.1 Entrance Mixing Experiments

A separate series of experimental runs was carried out to check on the validity of the Stolzenbach-Harleman model when applied to entrance mixing in the cooling pond case. It was noted that for discharge densimetric Froude numbers of unity ($F_D = 1$) and low aspect ratios ($A_D < 1$), the computer solution for the above model was not available, and that the empirical formulae for $F_D = 1$ and $A_D << 1$ gave meaningless results, and thus it was necessary to impose a minimum value on the stable dilution D_s. This minimum value was determined on the basis of these experiments, plus some results from the transient runs. Figures 7-9 to 7-11 show the agreement between measured surface temperature distributions and the distribution predicted by the solution to Equation 6.42 using the empirical equations 6.37 to 6.40 to determine entrainment.

Only those runs are shown for which the predicted dilution (Equation 6.37) is greater than 2 (the lower limit of the Stolzenbach-Harleman model). For these runs the temperature of the receiving water

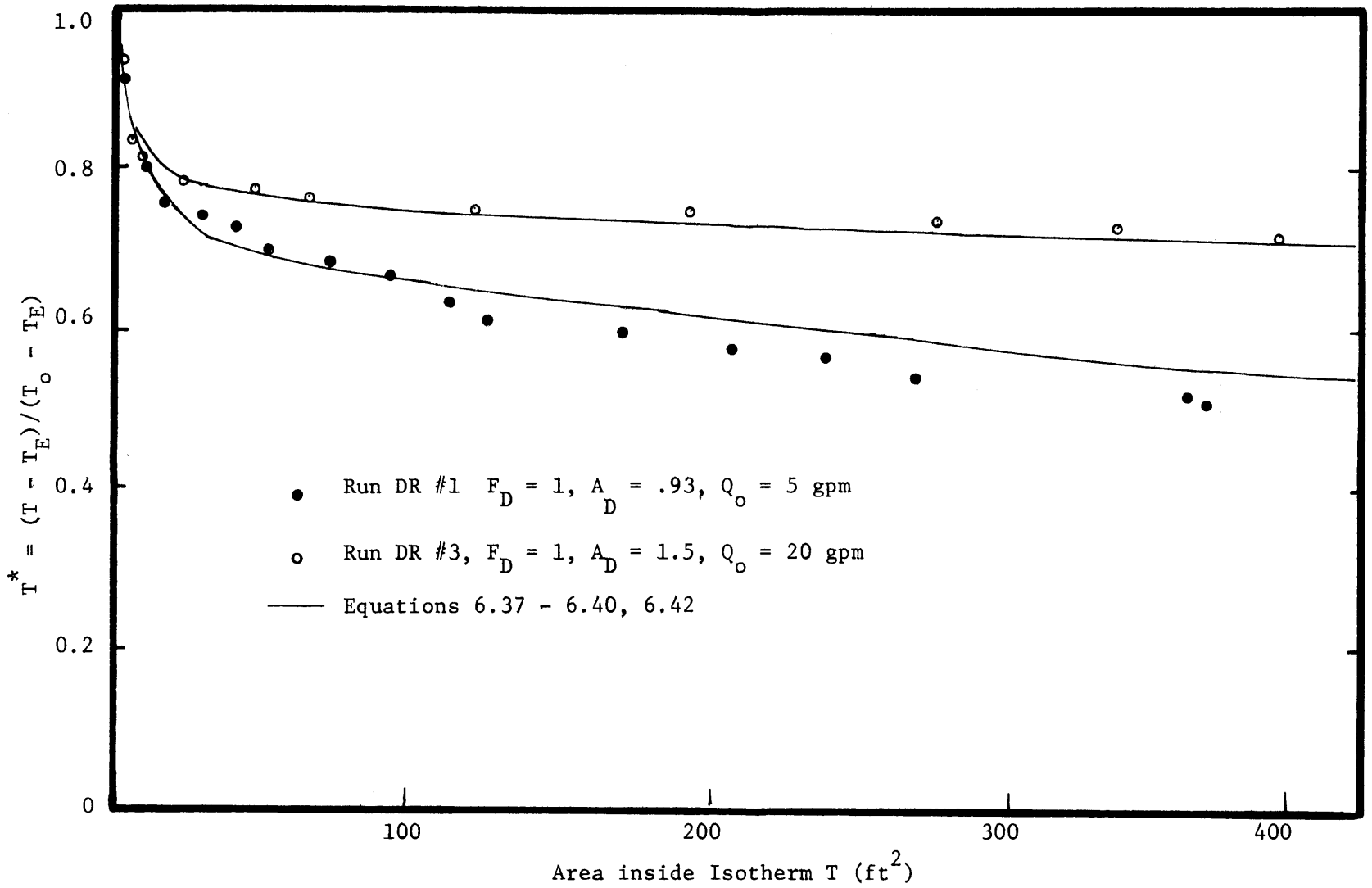

Figure 7-9 Surface Temperature Distribution Near Outlet (b_o = .25)

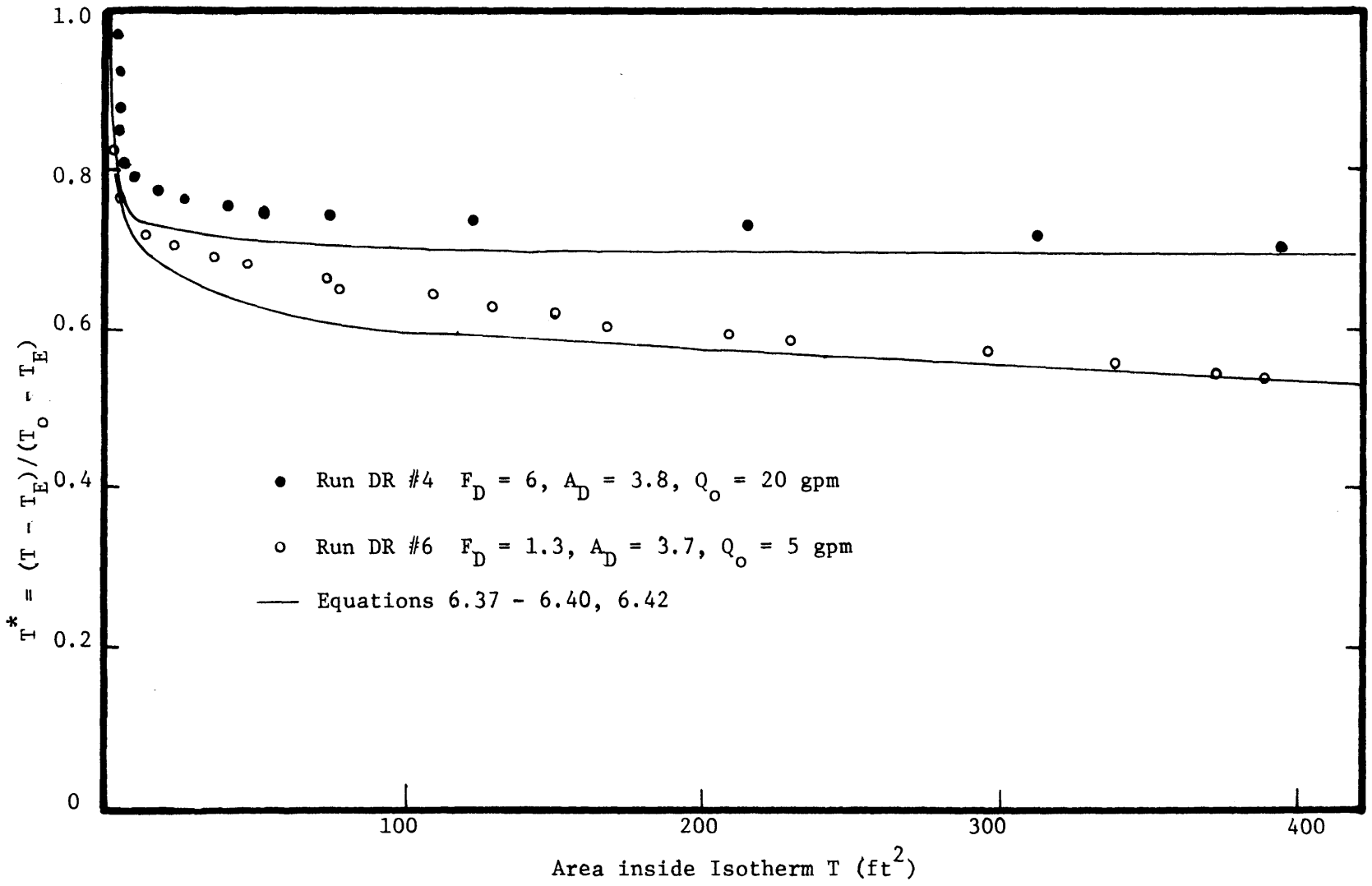

Figure 7-10 Surface Temperature Distribution near Outlet (b_o = 0.1)

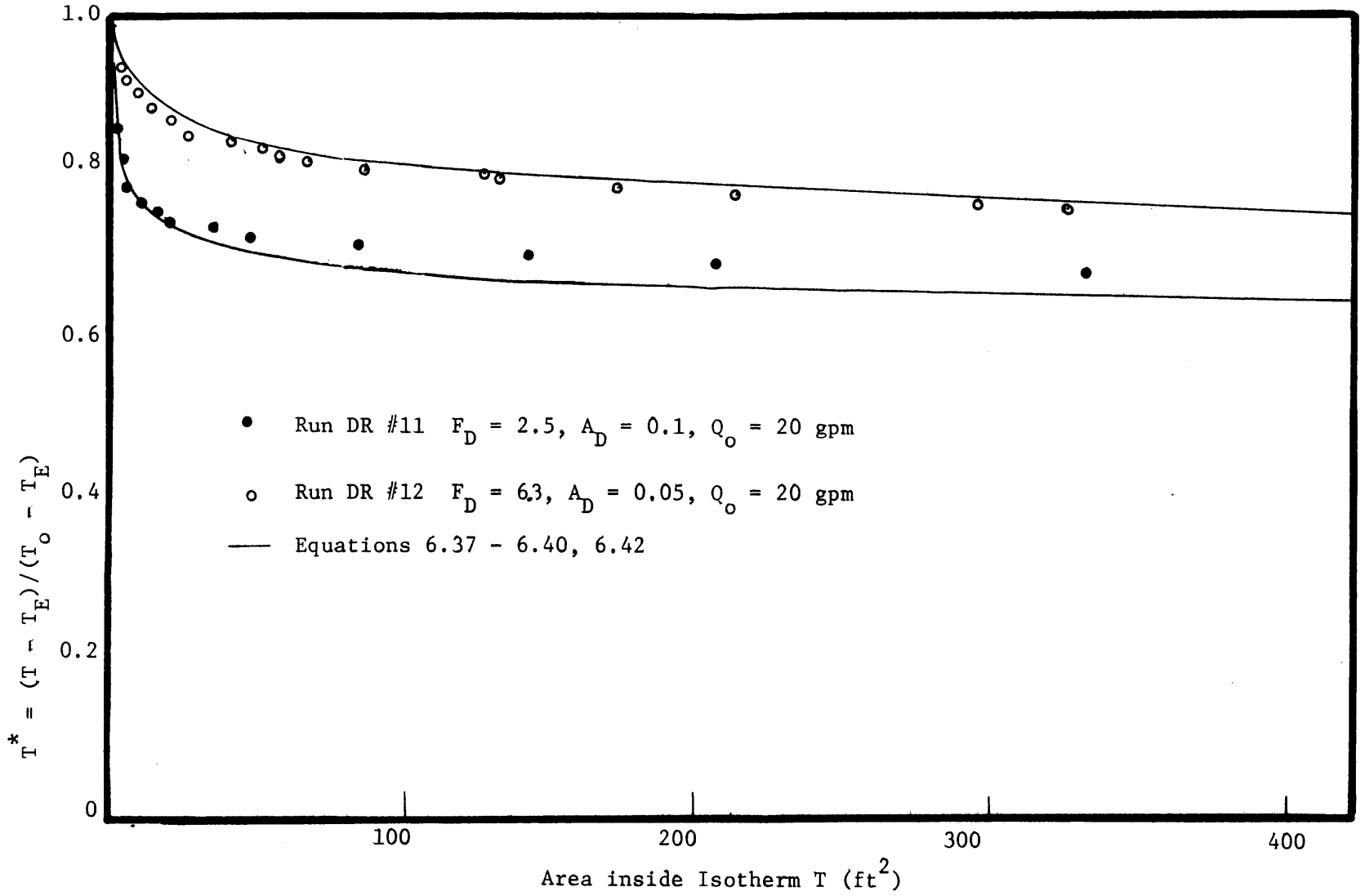

Figure 7-11 Surface Temperature Distribution near Outlet (b_o = 1.25)

is taken from measurements of the water temperature just underneath the heated discharge layer. Note that the surface temperature has been normalized using the equilibrium temperature, and not the receiving water temperature as is usual for jet dilution studies. It is seen that good agreement is obtained except for the extreme cases of very high mixing (Figure 7-10). The high mixing case is not of particular interest, and no attempt will be made to improve the agreement. The case of low entrance mixing (i.e. $D_s < 2$) will be examined in some detail. From the equation for stable dilution

$$D_s = 1.4\sqrt{1 + F_D^2}\, A_D^{1/4} \tag{7.7}$$

it is seen that for $F_D = 1$, D_s is significantly less than 2 only when $A_D << 1$, which occurs in the laboratory pond only when a channel width of 1.25 ft. is used (see runs DR 7-9 in Table 7-1, and runs 3, 4, and 7 in the Table 7-3). Figures 7-12 to 7-14 show the surface temperature distribution for the above runs. Note that the vertical scale is enlarged by comparison with the previous figures. Theoretical curves are given for a minimum dilution limit ($D_{s_{min}}$) of 1.5, and for the case of no mixing. The results demonstrate that although the use of a minimum dilution limit of 1.5 tends to overestimate the early mixing, the overall agreement is quite good. The use of no entrance mixing is rather unsatisfactory.

In conclusion, the empirical formulae developed from the Stolzenbach-Harleman model provide a good description of the entrance mixing process in the range of interest. For the very low mixing case

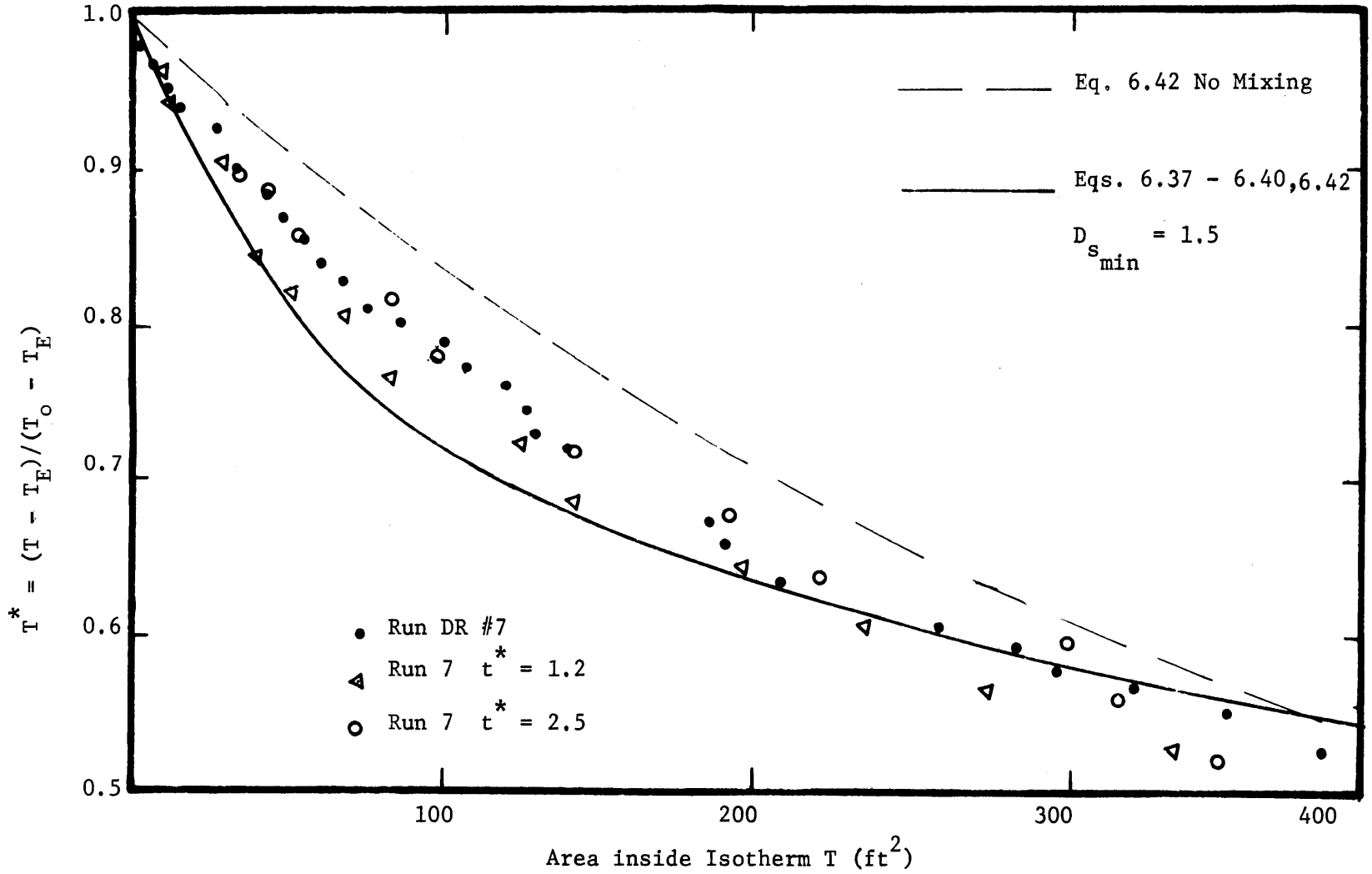

Figure 7-12 Surface Temperature Distribution for F_D=1, A_D=.065 (<<1), b_o = 1.25 ft, Q_o = 5 gpm

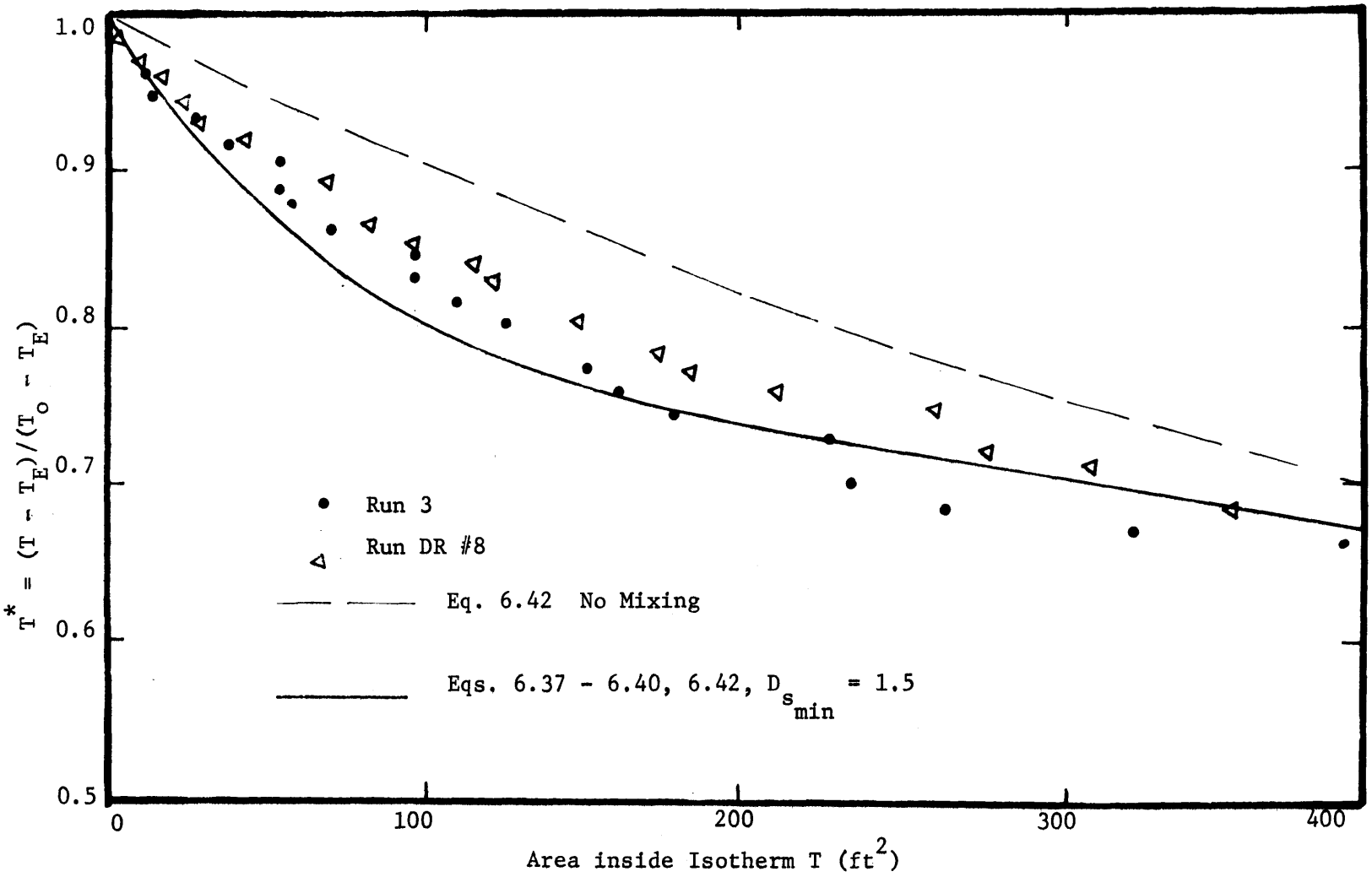

Figure 7-13 Surface Temperature Distribution near Outlet for F_D=1, A_D=.1(<<1), Q_o = 10 gpm

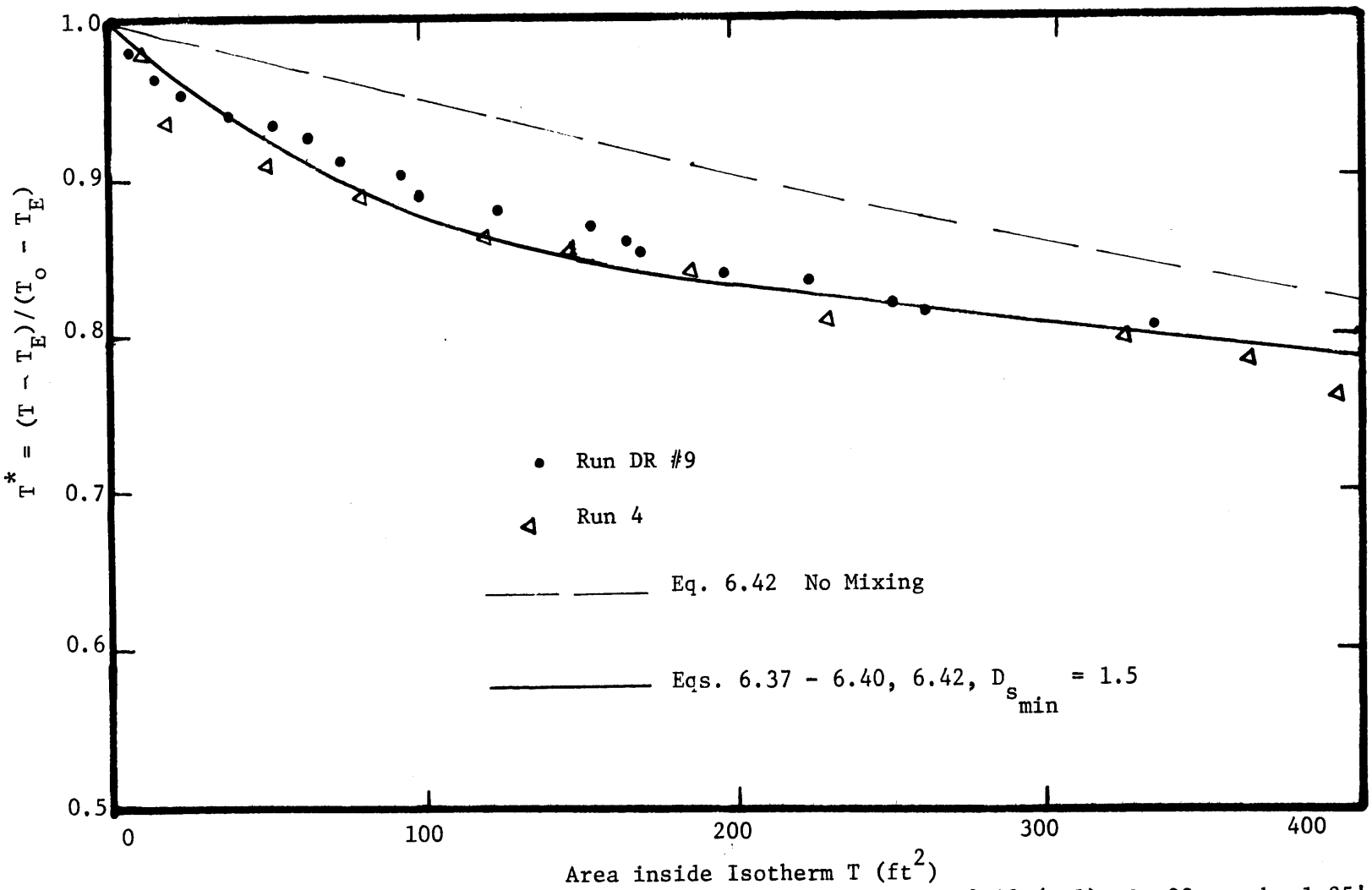

Figure 7-14 Surface Temperature Distribution near Outlet for F_D=1, A_D=0.18 ($\ll$1), Q_o=20gpm, b_o=1.25'

of $F_D = 1$ and $A_D \ll 1$, it is necessary to assume some minimum amount of mixing, and it appears that 50% entrainment ($D_s = 1.5$) leads to an adequate simulation of the measured surface temperature distribution for these conditions. It may be of interest to note that Stolzenbach and Harleman (1971) assume D_s of 1.5 in the formulation of their model. SEE ERRATA

7.5.2 Bottom Heat Loss Experiment

The heat flux through the bottom boundary can be significant in the laboratory case, and one experiment was designed solely to test the validity of the proposed treatment of this boundary condition. The temperature on the underside of the 0.6 ft. thick concrete floor was predicted by solving the diffusion equation

$$\frac{\partial T}{\partial t} = k_f \frac{\partial^2 T}{\partial z^2}$$

where k_f = thermal conductivity of concrete and T(0,t) is specified for all t. Details of the experiment have already been given. The emmissivity of the concrete floor, ϵ_f, is taken to be 0.97 (Buettner and Kern (1965)). Figure 7.15 shows that this simple approach gives quite satisfactory results. The predicted heat loss through the bottom is approximately 10 BTU/ft^2/hr for a water temperature of 97°F. Assuming molecular conduction in the bottom layer, this flux would require a gradient of 30°F/ft., which agrees well with the bottom gradients observed in the transient runs 4 and 5 where water temperatures were high (~96-98°F).

It is therefore concluded that the mathematical model treatment of the bottom heat loss is quite satisfactory.

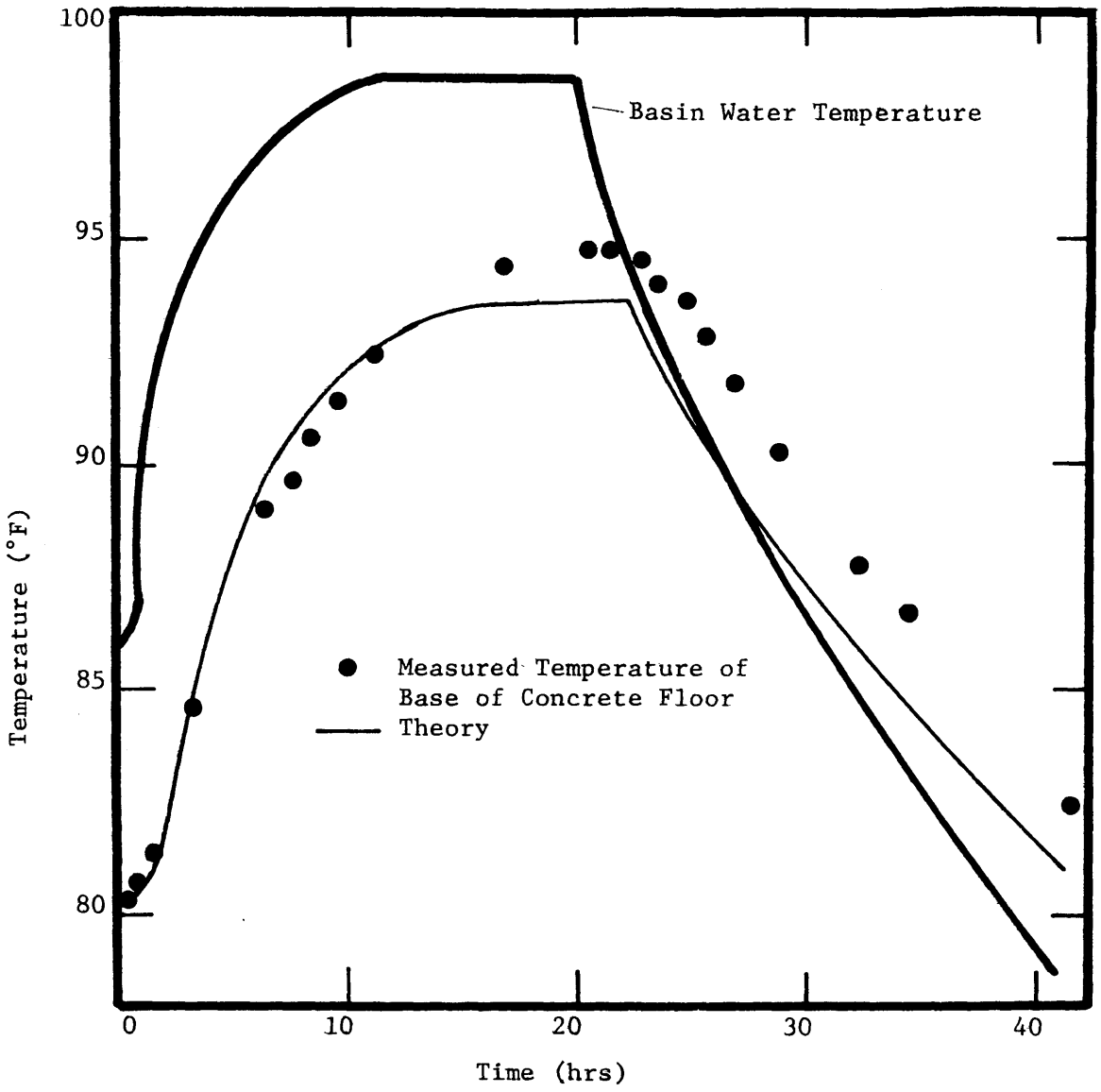

Figure 7-15 Predicted vs. Measured Concrete Floor Temperatures

7.5.3 Transient Cooling Pond Experiments

The results of the transient runs have already been described qualitatively in Chapter 4. The quantitative results will now be used to verify the mathematical model outlined in Chapter 6, and it will be shown that the proposed mathematical model adequately describes the transient behavior of the laboratory cooling pond. Note that the heat loading on the laboratory pond varies throughout the run since the discharge temperature is kept constant instead of the temperature rise between the intake and the outlet. This was done to simplify the problem of controlling the laboratory pond. The results for the five runs, Run 3-7, are now presented.

7.5.3.1 Run 3 - Low Entrance Mixing-Moderate Flowrate

This run demonstrates the behavior of an almost ideal cooling pond, with minimal entrance mixing ($IF_D = 1$, $A_D \simeq 0.1$). Outlet geometry, temperature and flowrate were kept constant during the run. Figure 7-16 demonstrates the transient heat loading, and shows the negligible response of the intake temperature to the imposed heat load until $t^* > 0.5$. The vertical motion of the warm interface near the intake is shown in Figure 7-17. Figure 7-18 illustrates the fact that the surface reaches steady state relatively quickly ($t^* = 0.5$-1) compared with the bottom layers ($t^* = 2$-3). The overall agreement between predicted and observed behavior is quite satisfactory. Figure 7-16 shows that the predicted intake temperature is somewhat high, but the transient behavior is very good. The predicted vertical profiles in Figure 7-17 are adequate, and the predicted surface temperature distribution in Figure 7-18 is excellent except at a very early time

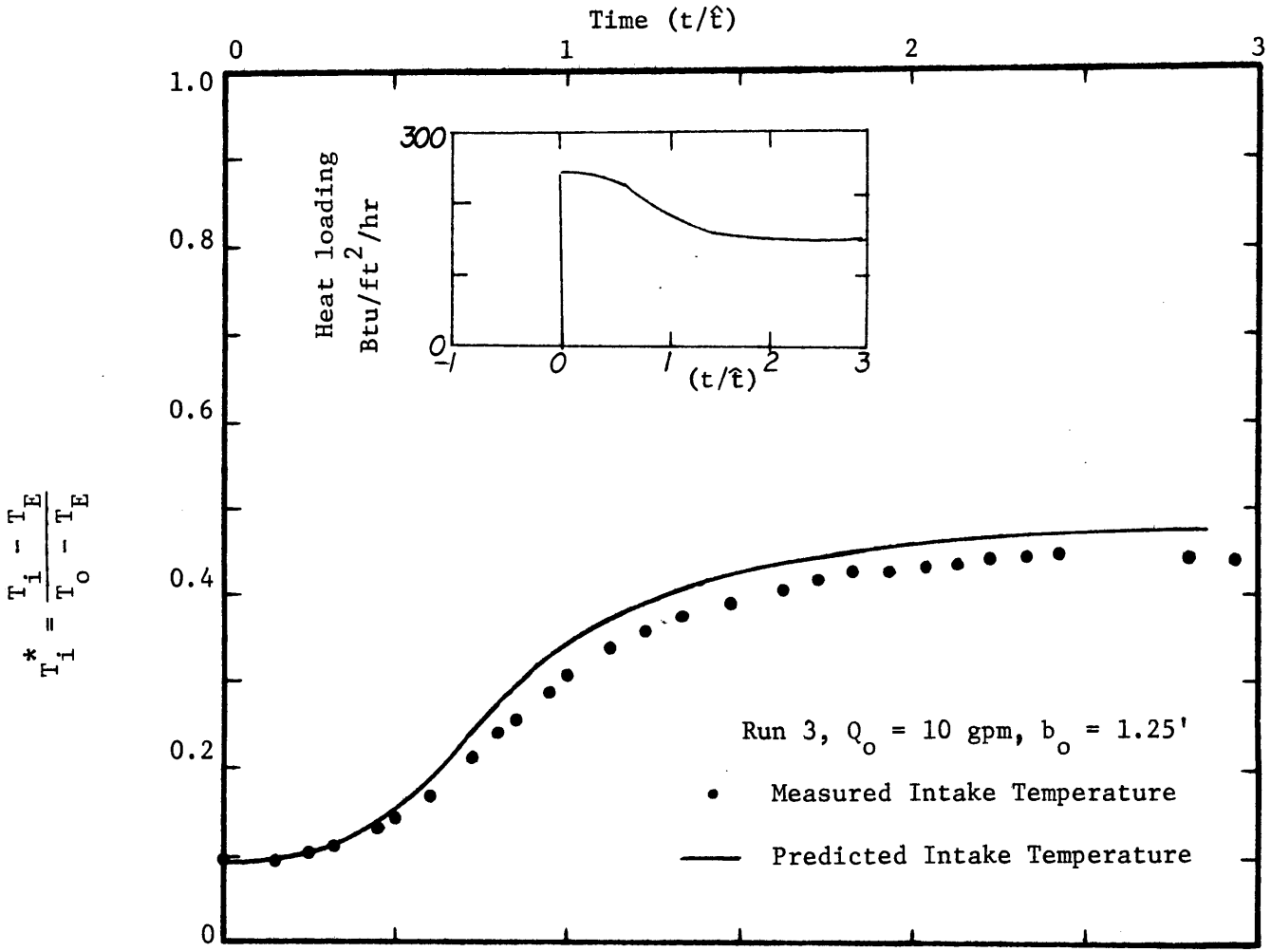

Figure 7-16 Transient Intake Temperature - Run 3

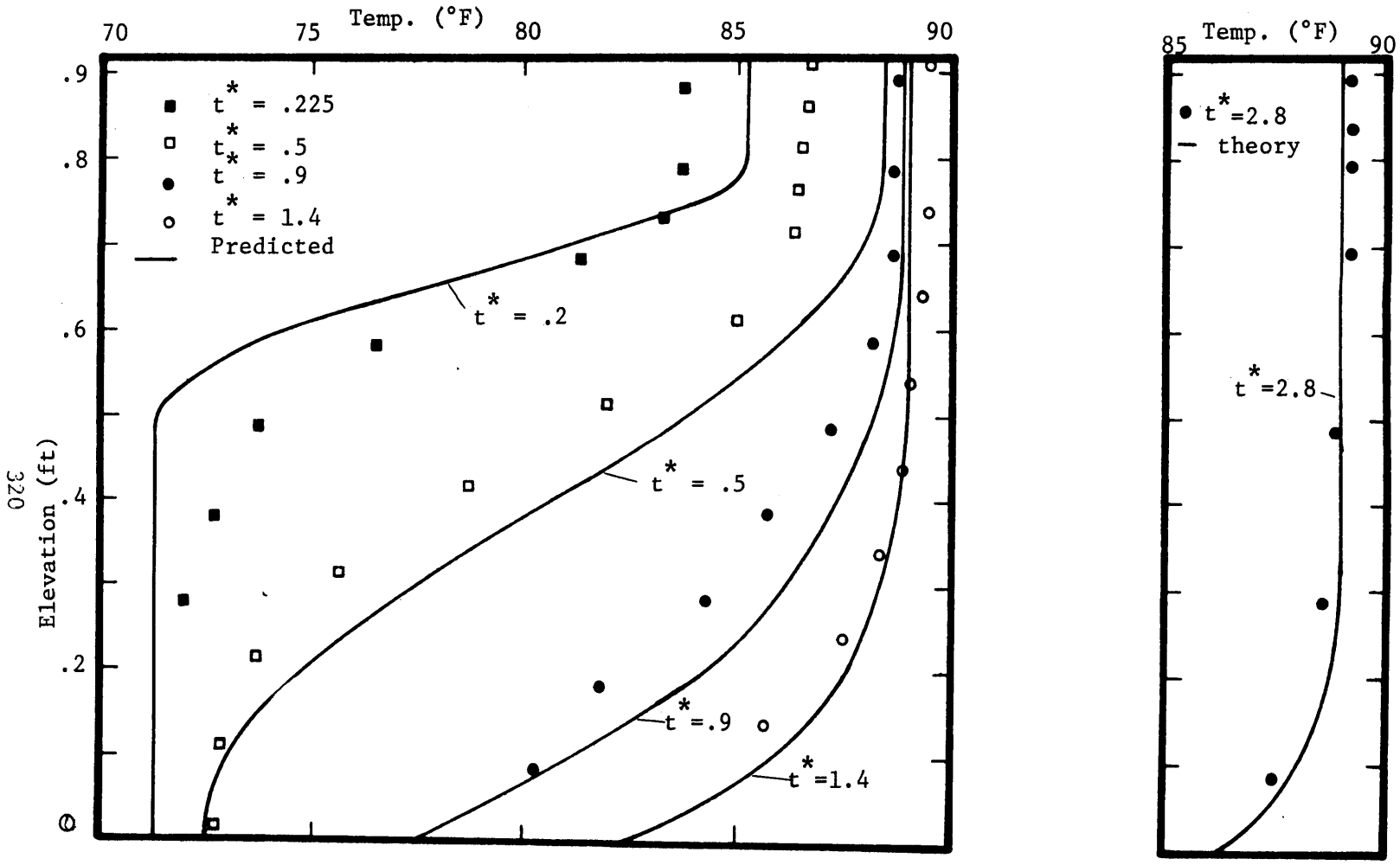

Figure 7-17 Predicted vs. Measured Temperature Profiles near the Intake - Run 3

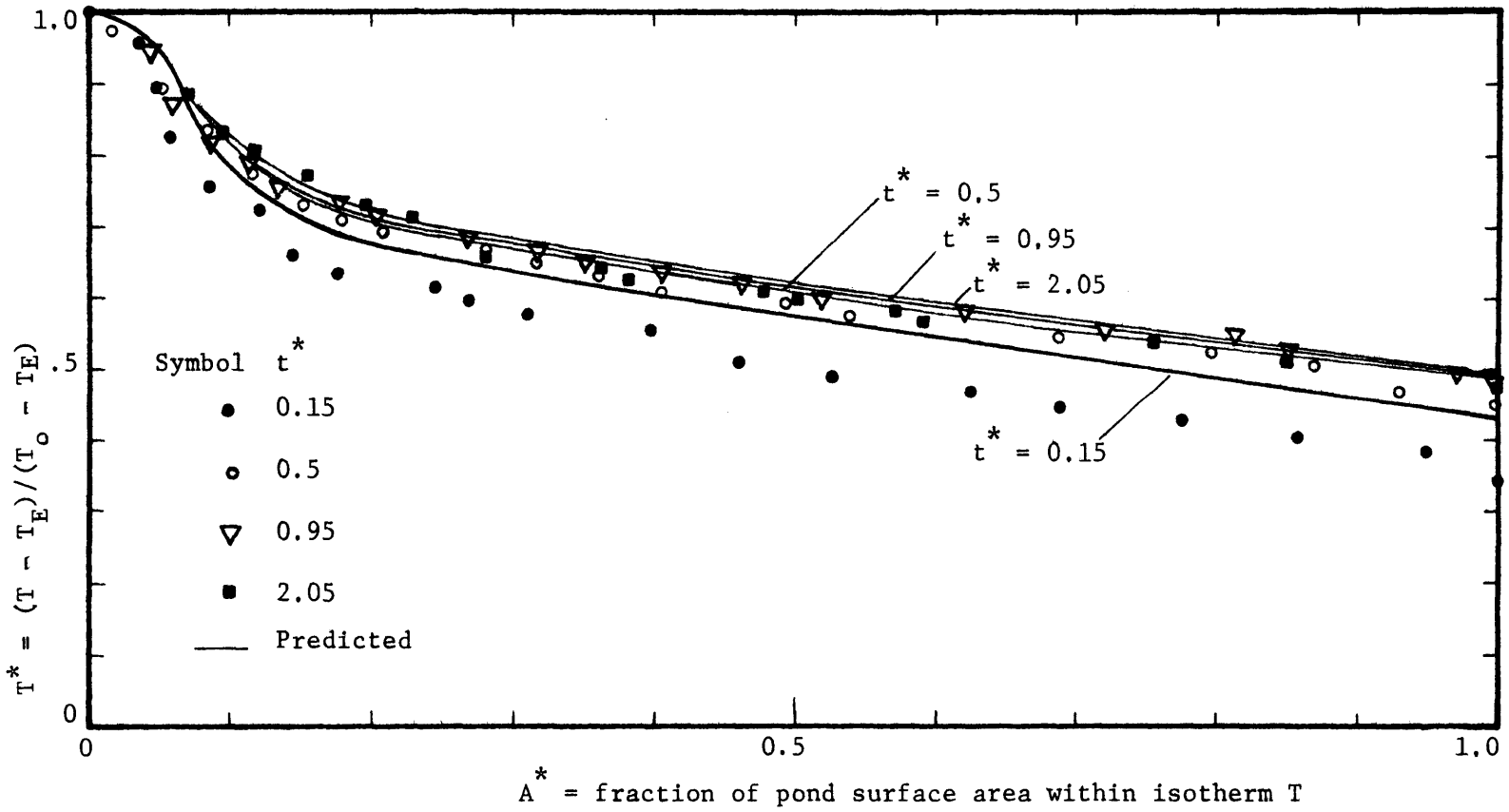

Figure 7-18 Predicted vs. Measured Surface Temperature Distribution - Run 3

$t^* < 0.5$. It appears that the establishment of a warm surface layer entails more mixing with the receiving water than is accounted for in the model, and this leads to predicted surface temperatures that are too high in the early stages. This effect is apparent in some other runs, but the lack of agreement is not considered too serious, since it lasts only for a short time, and occurs only for extreme loading changes.

7.5.3.2 Run 4 - Low Entrance Mixing-High Flowrate

This run is very similar to run 3, except that the flowrate has been doubled, leading to a doubling of the initial heat loading (see Figure 7-19). The agreement between predicted and observed behavior is relatively poor early in the runs (see Figures 7-19, 7-20), but excellent agreement is obtained as steady state is approached. Figure 7-21 shows an aspect of transient behavior that has not been discussed, namely that a sudden increase in flow rate leads to the formation of a strong vortex created by the surface discharge jet, which is "ineffective" in dissipating heat. After a relatively short time ($t^* < 0.5$) this vortex disappears. At this stage it appears that the model describes the steady state behavior very adequately, but the transient predictions are not as good. Run 5 with moderate entrance mixing will now be discussed, followed by runs 6 and 7 where the emphasis is on transient behavior.

7.5.3.3 Run 5 - Moderate Entrance Mixing-High Flowrate

Run 5 is similar to Run 4 except that the outlet width has been reduced from 1.25 ft. to 0.25 ft., resulting in a considerable increase in entrance mixing. Agreement between predicted and observed

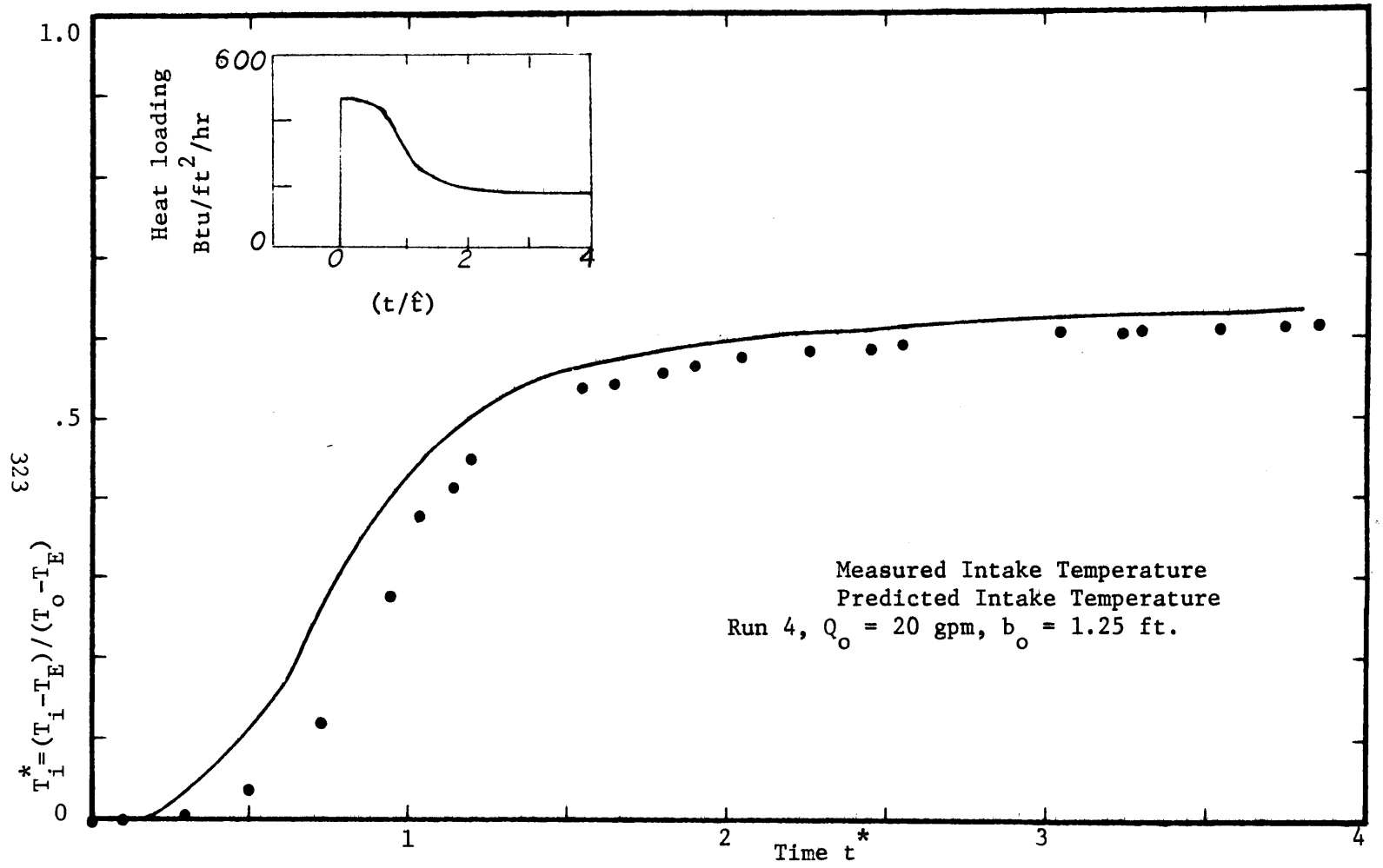

Figure 7-19 Predicted vs. Measured Intake Temperatures - Run 4

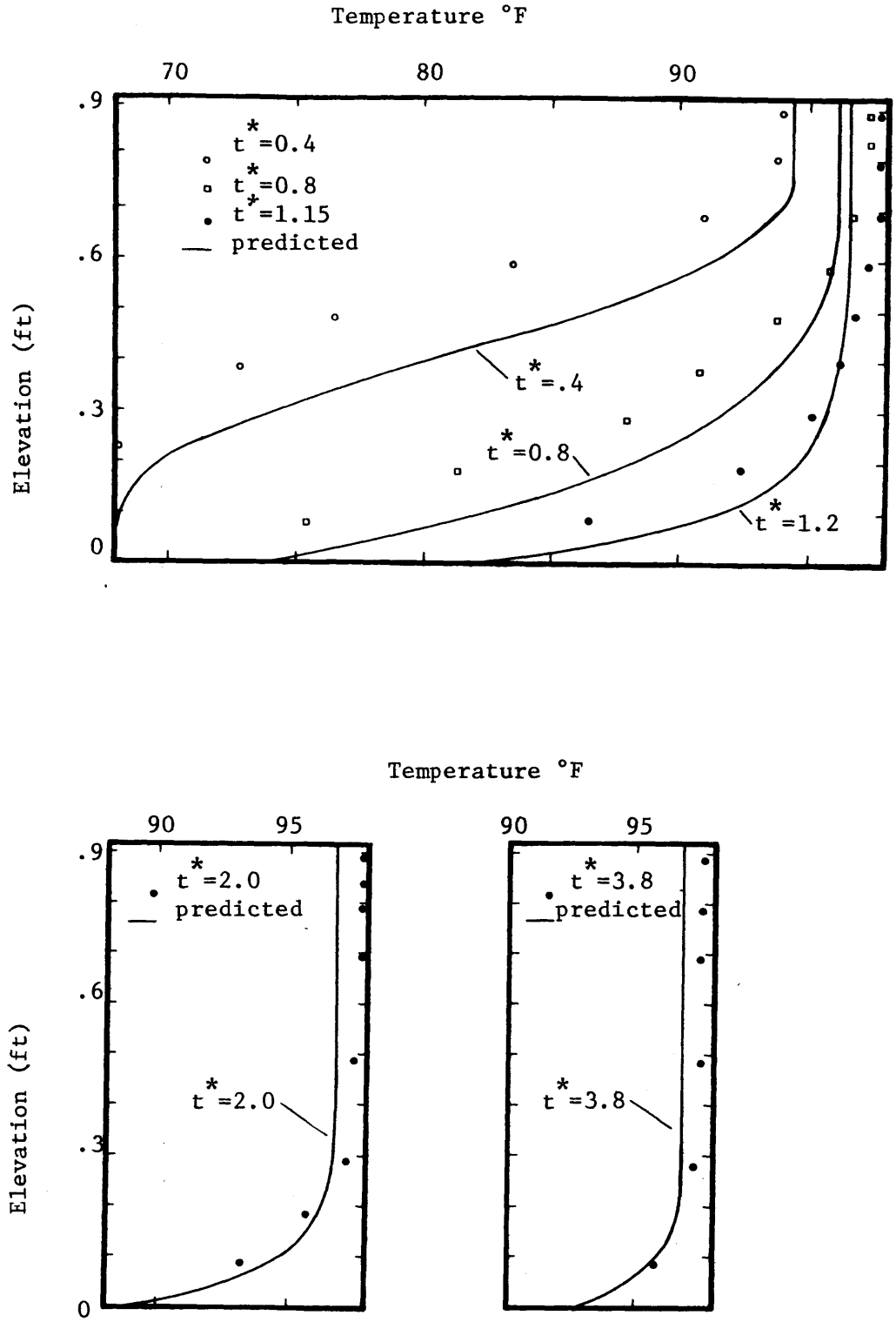

Figure 7-20 Predicted vs. Measured Temperature Profiles - Run 4

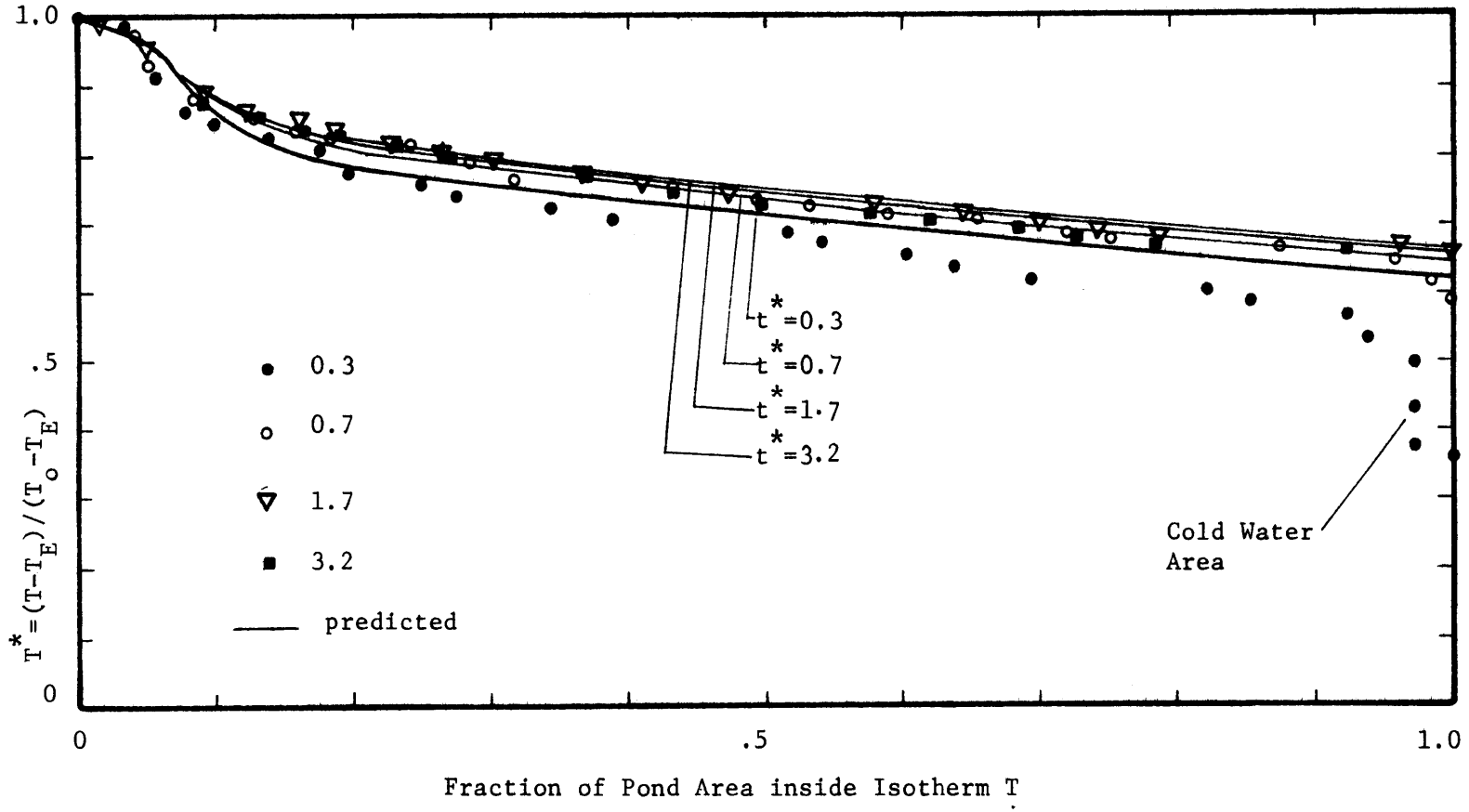

Figure 7-21 Predicted vs. Measured Surface Temperature Distribution - Run 4

behavior is excellent both at early and late times. Note the earlier response of the intake temperature, and the rapid decrease in temperature at the end of the discharge channel.See Figures 7-22 to 7-24.

7.5.3.4 Run 6 - Low-Moderate Entrance Mixing-Variable Flowrate

During this run the emphasis is on transient behavior. The flowrate was changed twice, from 5 gpm to 10 gpm at $t^* = 3.5$, and from 10 gpm to 5 gpm at $t^* = 4.3$. Outlet temperature and width were maintained constant. Figure 7-25 shows that the agreement between predicted and measured intake temperature is good to excellent at all times. Figures 7-26 and 7-27 show that the predicted surface temperature distribution is quite accurate. Figure 7-27 illustrates the fact that a reduction in loading leads to vertical mixing, but that this mixing is limited to the area of the pond where instability is present. Note that no horizontal gradients are present in about 30-40% of the pond surface area. The vertical profiles in Runs 6 and 7 are rather complex, and only those in Run 7 will be shown.

7.5.3.5 Run 7 - Low-High Entrance Mixing. Variable Flowrate

This run is an extreme example of transient behavior. Outlet temperature remains constant but changes occur both in flowrate and outlet width, resulting in four types of boundary conditions. The run starts with a low flowrate (5 gpm) and a wide outlet (1.25 ft.). $IF_D = 1$ and $A_D = .06$ and thus entrance mixing is very low. When steady state is almost reached ($t^* = 2.82$) the flowrate is quadrupled, and the outlet narrowed to 0.1 ft., resulting in very high mixing. When the new steady state is near ($t^* = 3.78$) the flowrate is halved, and later

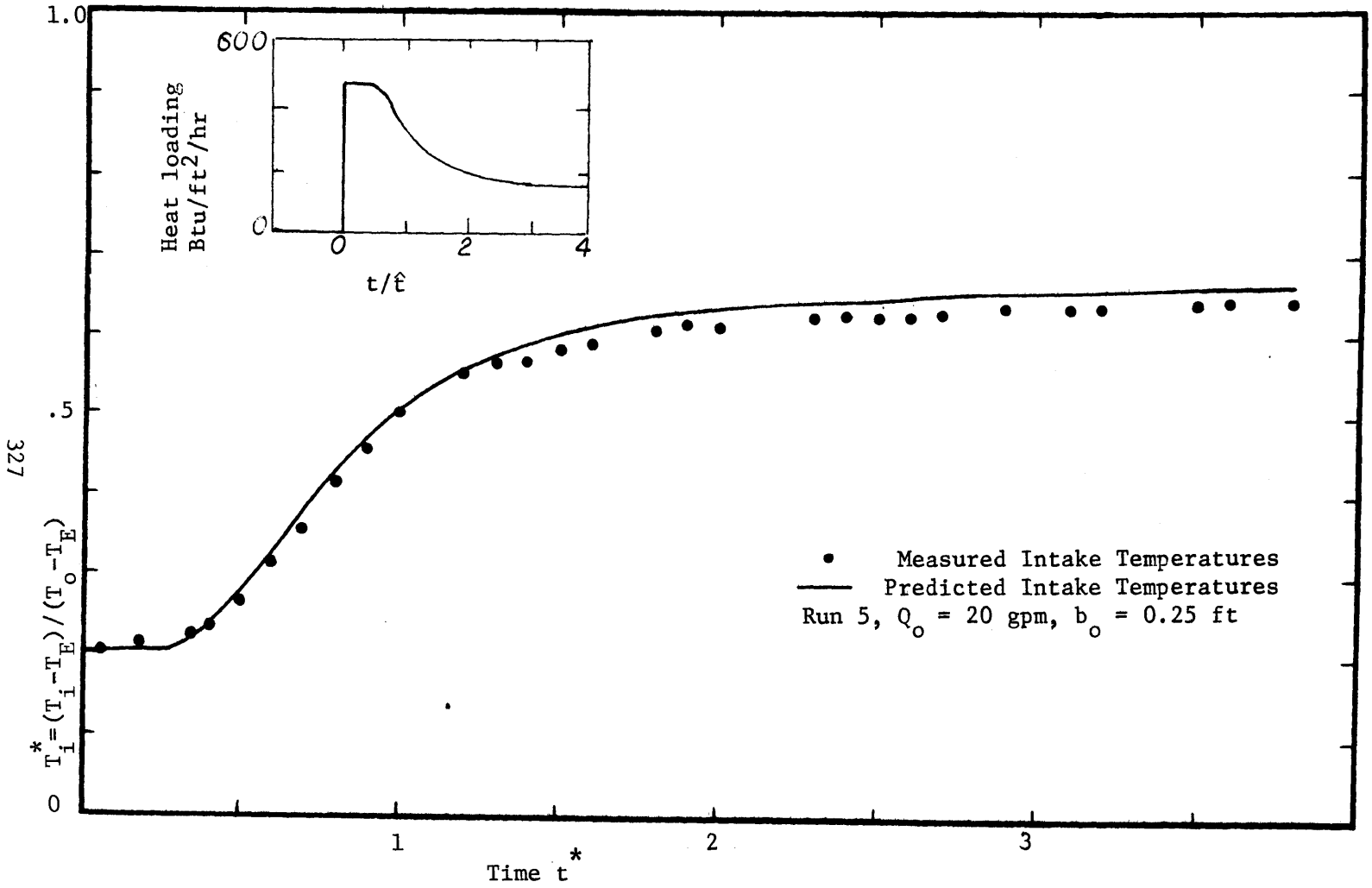

Figure 7-22 Predicted vs. Measured Intake Temperatures - Run 5

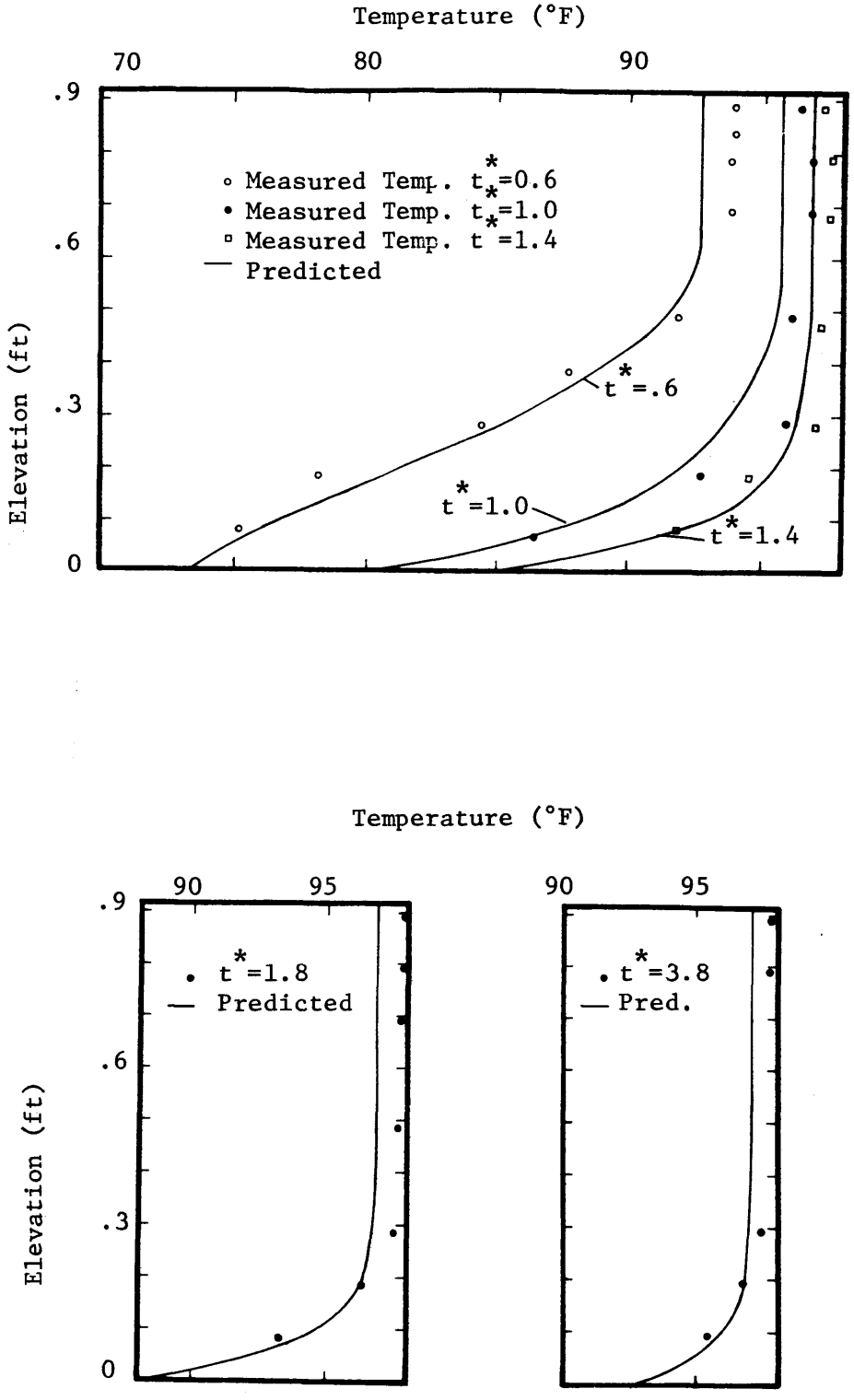

Figure 7-23 Predicted vs. Measured Temperature Profiles - Run 5

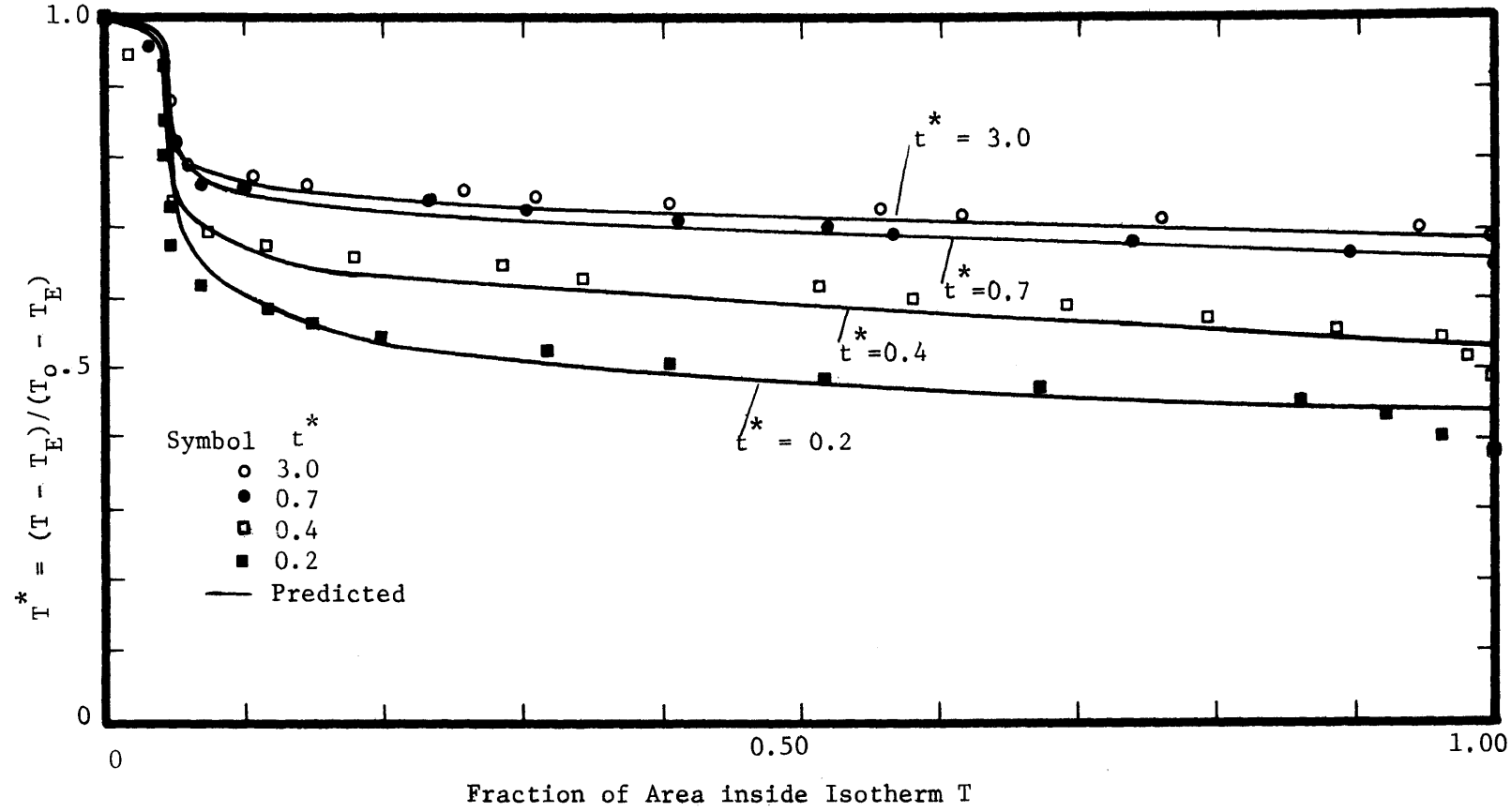

Figure 7-24 Predicted vs. Measured Surface Temperature Distribution - Run 5

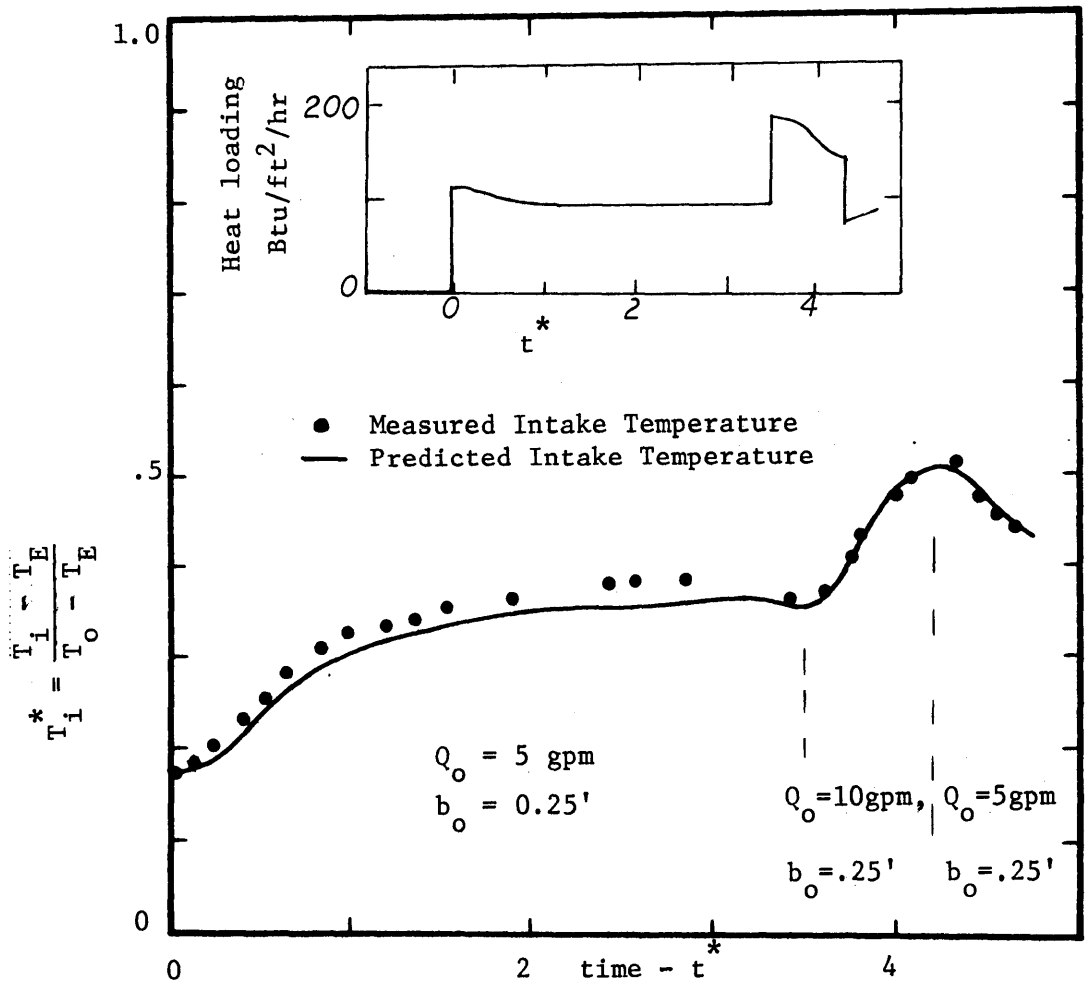

Figure 7-25 Predicted vs. Measured Intake Temperatures - Run 6

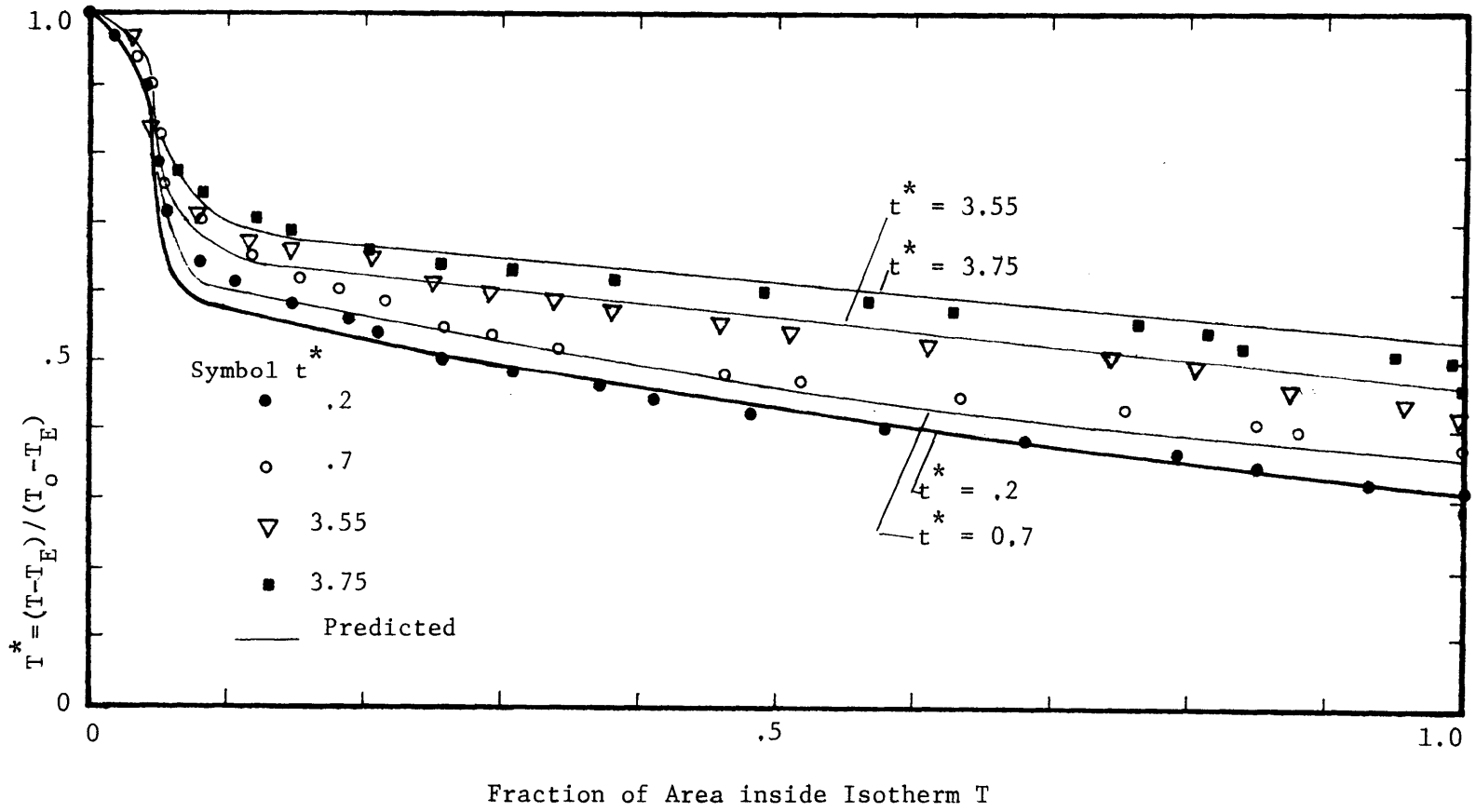

Figure 7-26 Predicted vs. Measured Surface Temperature Distribution - Run 6 - Load Increasing

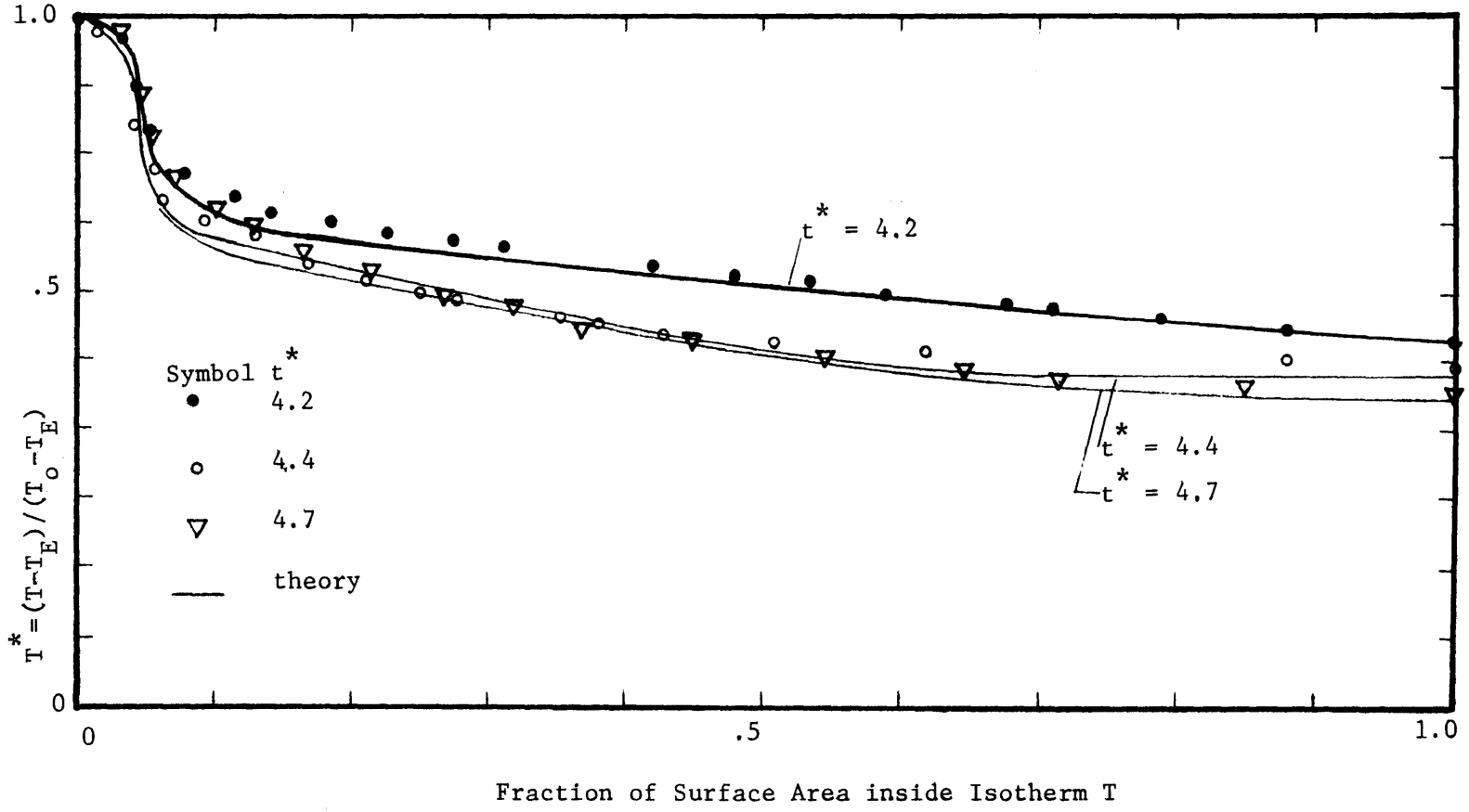

Figure 7-27 Predicted vs. Measured Surface Temperature Distribution - Run 6 - Load Decreasing

again ($t^* = 4.95$) the wide outlet is reinstated. All these changes in the boundary conditions are reflected in the intake temperature history in Figure 7-28. Initially the agreement between predicted and observed intake temperatures is excellent, but the predicted steady state intake temperature for the high flowrate, high mixing case is too high, and from here on the intake temperatures are too high, and agreement is only fair. Figure 7-29 shows the vertical profiles. Figures 7-29a and 7-29b show the transient behavior for the first two boundary conditions, reflecting an increase in loading. Agreement is quite good. Figure 7-29c shows the effect of a decrease in loading, showing that near the end of the run actual cooling is faster than predicted cooling, and agreement is becoming poor. Figure 7-30 shows that agreement between predicted and observed surface temperature distribution is excellent except at very early time where the mathematical model tends to be somewhat high. Overall, the agreement between observed and predicted behavior, for a complicated situation, is very satisfactory.

7.6 Summary of Laboratory Results

In general the transient behavior predicted by the proposed mathematical model agrees well with observed behavior with the exception of early times where agreement is fair. Discrepancies at small times must be expected since no attempt has been made to accurately simulate the horizontal motion of a warm interface through the surface layer. It should be stressed that the above agreement has been obtained with almost no attempt at curve fitting. The only place that an arbitrary parameter is related to measured data is the minimum limit placed on entrance mixing. Whenever possible separate experiments have been

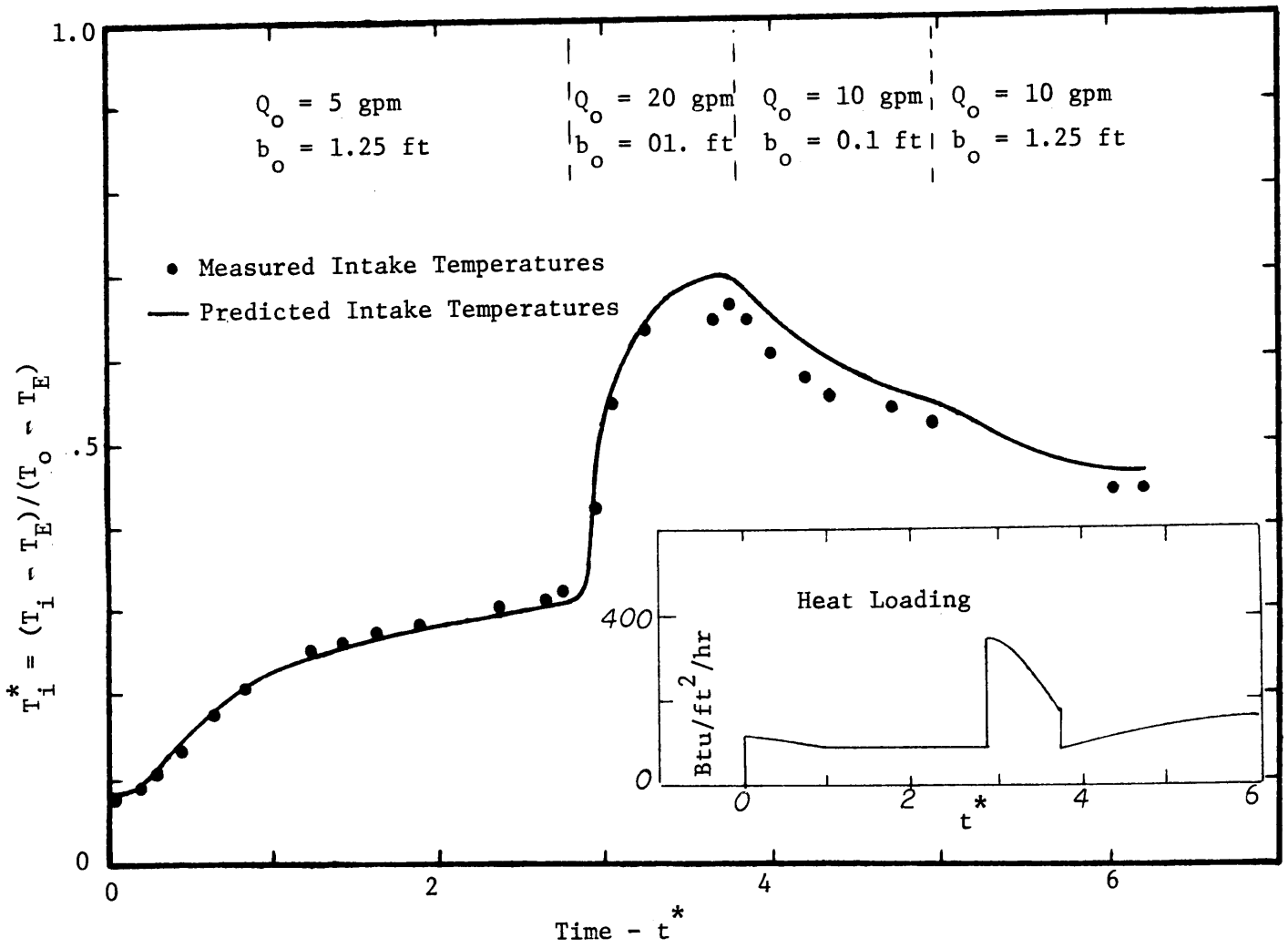

Figure 7-28 Predicted vs. Measured Intake Temperatures - Run 7

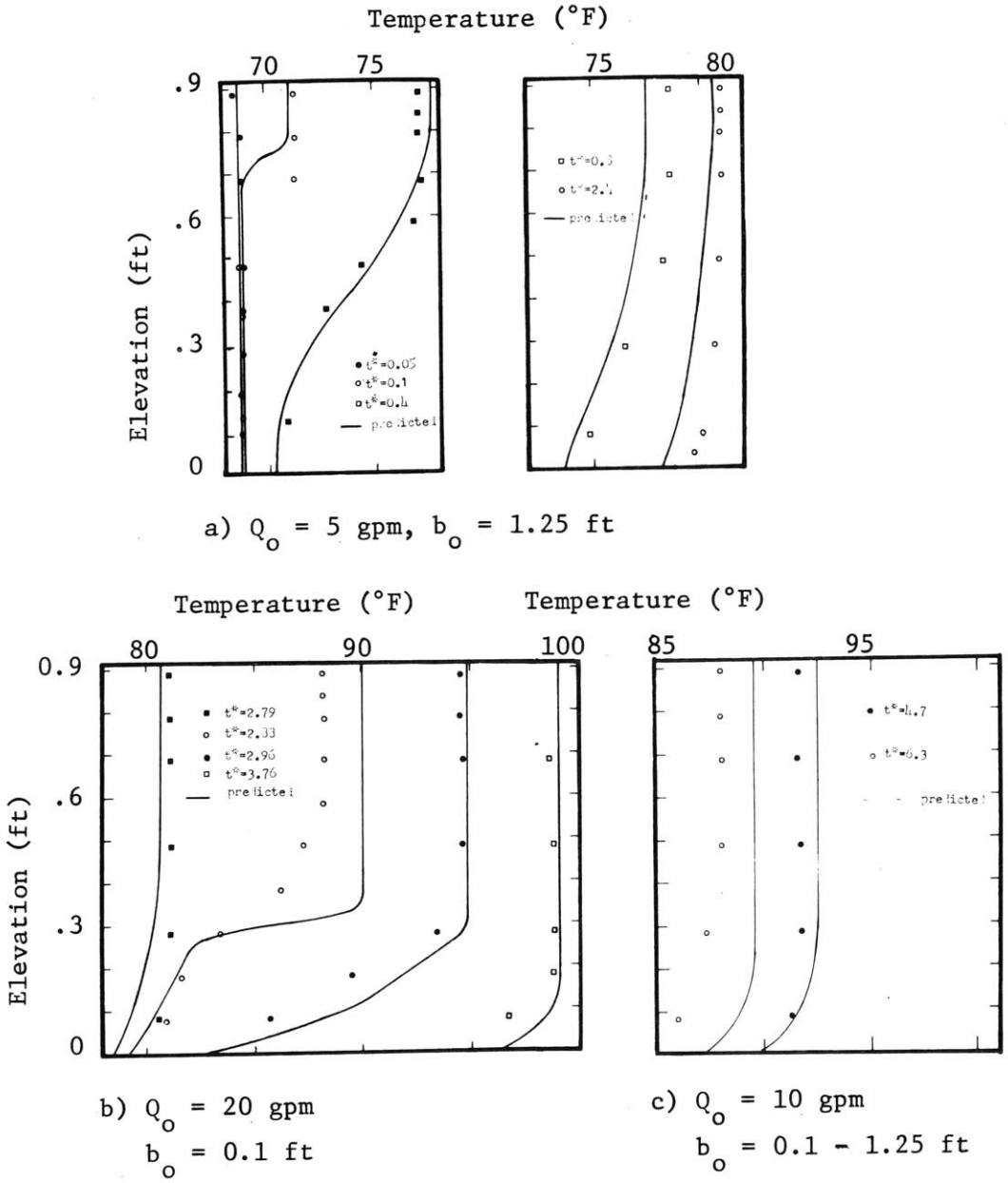

Figure 7-29 Predicted vs. Measured Temperature Profiles near Intake - Run 7

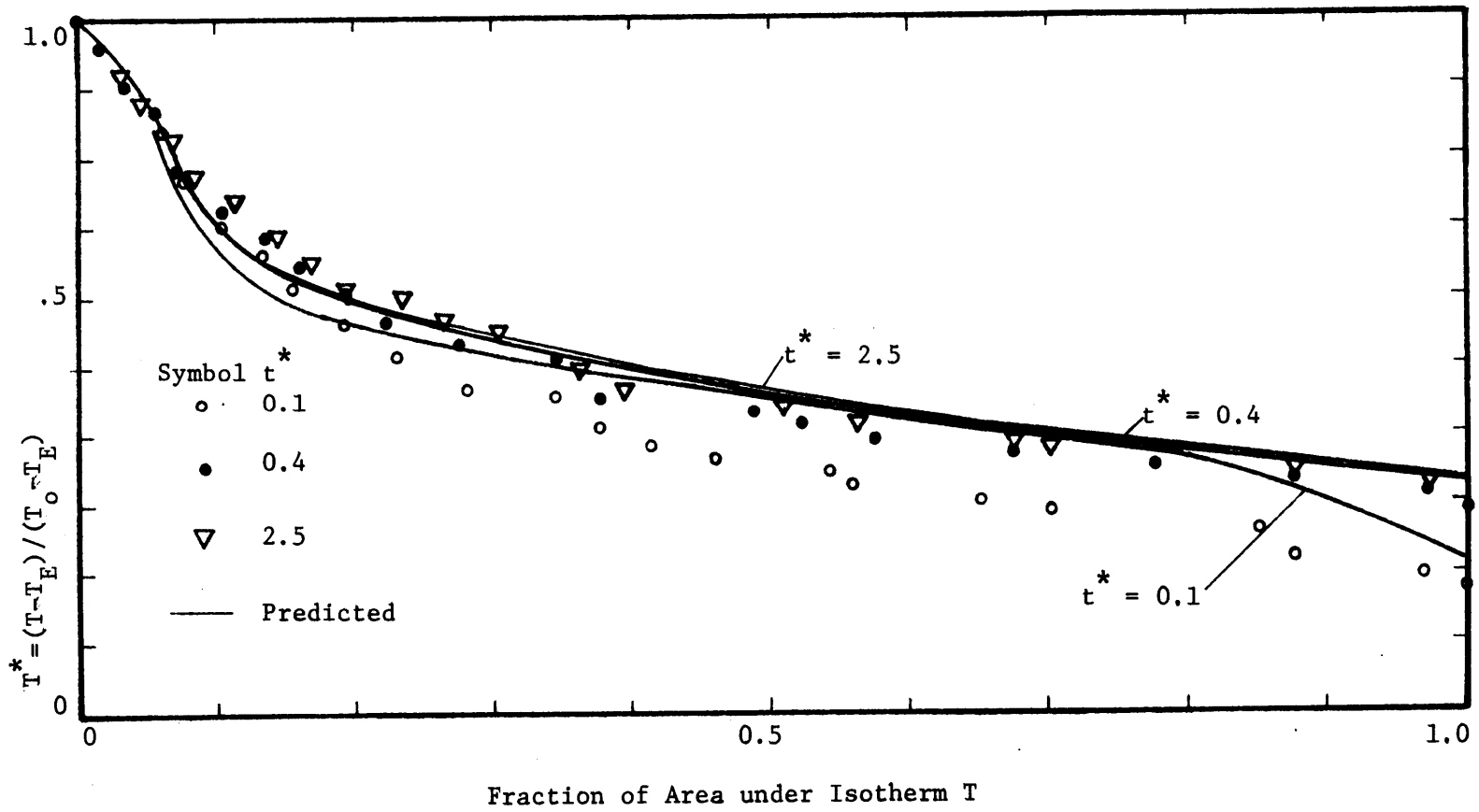

Figure 7-30a Predicted vs. Measured Surface Temperature Distribution
Run 7, Q_o = 5 gpm, b_o = 1.25 ft

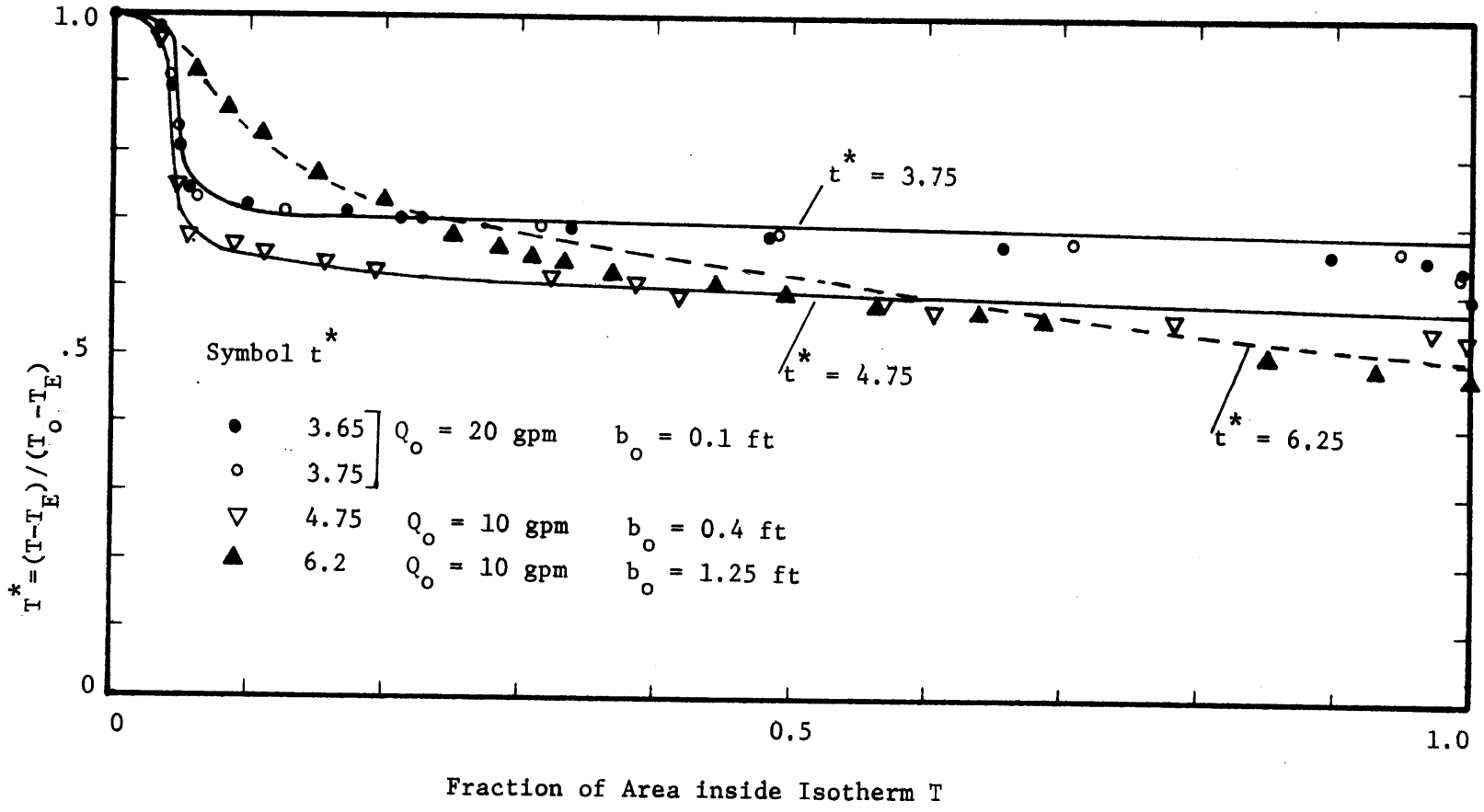

Figure 7-30b Predicted vs. Measured Surface Temperature Distribution
Run 7, Q_o = 20 - 10 gpm, b_o = 0.1 - 1.25 ft

carried out to define an unknown parameter such as minimum entrance mixing, or to test a theoretically based formulation of a boundary condition, such as surface or bottom heat loss. Based on the comparisons between calculated and observed laboratory cooling pond behavior, it is concluded that the proposed mathematical model is a predictive model for both transient and steady state conditions. In the next chapter the mathematical model will be tested against two sets of field data.

VIII. Application of the Mathematical Model to Field Cooling Ponds

8.1 Introduction

In chapter 7, the mathematical model was tested against a laboratory cooling pond, and was found to be quite satisfactory. In this chapter the model will be applied to two field cooling ponds, including a shallow artificial pond (Hazelwood) and a deep natural pond (Lake Norman). The emphasis will be on the prediction of the intake temperatures under transient meteorological and heat loading conditions, where possible other data such as surface temperature distributions, vertical temperature profiles, or surface outflow temperatures, will also be used to check the predictions of the mathematical model.

8.1.1 Input Data

As input, the mathematical model requires meteorological data to calculate the surface heat fluxes, hydrological and plant operating data to determine the heat input by stream flow and/or power plant, water quality data to determine the internal distribution of solar radiation, and geometrical data for the pond, including the outlet and intake, to determine the flow characteristics of the pond. Finally, the initial condition of the pond must be specified.

The meteorological data required are:

a) Air Temperature (dry bulb)

b) Air vapor pressure (wet bulb temperature, dew point temperature or relative humidity).

c) Solar Radiation

d) Wind-speed

e) Height at which wind speed is measured.

f) Cloud Cover or Atmospheric Radiation

The hydrological data required are:

a) Stream inflow and outflow rates

b) Stream inflow temperature

The plant data required are:

a) Plant power output

b) Heat rejection per unit power output

c) Condenser temperature rise,or condenser flow rate.

The water quality data required are:

a) The extinction coefficient of the water

b) The fraction of solar radiation absorbed near the water surface (usually 0.4-0.5).

The pond geometrical data required are:

a) The area-depth and length-depth relationship for the main pond

b) The length, surface area, average width and depth, and exit width and depth of the outlet channel

c) The elevation and opening height and width for the skimmer wall intake.

d) The elevation of the centerline of all outflows

e) The area depth relationship for the intake pond.

The initial condition data requirements are:

a) Initial surface elevation

b) Initial temperature distribution. (In many cases it is

reasonable to assume an isothermal initial condition. For an artificial cooling pond, the pond volume is small enough so that the initial condition is "forgotten" after a relatively short time. A deep natural type pond may be relatively homogeneous in early spring.)

8.1.2 Choice of Model Parameters

The use of the mathematical model in a field situation requires that decisions be made on the following subjects:

a) The applicability of the model,

b) length, area, and time increments,

c) minimum dilution limit for heated discharges, and entrance mixing ratio for stream inflows,

d) the appropriate intake withdrawal model,

e) schematization of the outlet channel.

For the model to be useful as a predictive tool, these decisions must be made without recourse to data, other than that which would be available on a proposed pond. The above decisions will be discussed, and guidelines will be given, but in some cases it may be necessary to test the sensitivity of the model to the choice of a particular parameter.

8.1.2.1 The Applicability of the Model

The model is judged applicable if the internal densimetric Froude number F_i is less than 0.2. F_i is defined in chapter 4 as

$$F_i = \frac{2q}{H\sqrt{g\,\frac{\Delta\rho}{\rho}\,H}} \qquad (8.1)$$

where for the purpose of judging the applicability of the model, the symbols are defined as

q = condenser flow/unit width (use the average pond width)

H = mean depth of pond

$\frac{\Delta\rho}{\rho}$ = characteristic density difference (use $\frac{\Delta\rho}{\rho} = 10^{-4}$ which is equivalent to 1-2°F).

8.1.2.2 Length, Area, Time Increments

For field use, a time increment of one day is the most suitable. A minimum of 15 depth increments and 20 area increments is considered advisable. The stability criteria, equations (6.63) to (6.65) can be checked using Δz, ΔA, and Δt chosen initially as above. A useful estimation of the vertical velocity V is given by

$$V = \frac{Q_T}{A_{av}} \tag{8.1a}$$

where Q_T = total through flow

A_{av} = horizontal area at mid-depth.

8.1.2.3 Entrance Mixing (Minimum Dilution Limit, Stream Inflows)

The behavior of a heated discharge with a low densimetric Froude No. ($F_D = 1$) and a low aspect ratio ($A_D << 1$) is not well known. In section 7.5.1 it was shown that a minimum dilution limit of 1.5 gave satisfactory results for the laboratory. For the field case, outlet conditions can rarely be specified accurately, and a more typical figure is 2.0. Since this is more conservative (i.e., predicts higher intake temperature) it is recommended that this value be used

initially, and the sensitivity of the model to the lower limit of 1.5 should be checked.

The entrance mixing for stream inflows has a feasible range of 25 to 50% (r_m = 0.25-.5) (see section 6.7.4.1). Initially the upper limit will be used, but the effect of the lower limit should be checked.

8.1.2.4 Withdrawal Model

The decision here is relatively straightforward. For an artificial pond with a skimmer wall intake, the Harleman and Elder (1965) two layer model (equation 6.55a) will be used. For a deep reservoir, Kao's model with constants obtained for TVA reservoirs (equation 6.54) will be used. The sensitivity of the model to the choice of withdrawal model should be checked.

8.1.2.5 Schematization of Outlet Channel

The outlet channel is schematized as a uniform rectangular channel. For a highly non-uniform channel such as at Hazelwood, the choice of the average width and depth of the channel may be rather arbitrary. If the behavior (e.g., intrusion length) is known, the channel dimensions may be adjusted to reproduce this behavior. For use in a predictive model, the average width will be chosen as the surface area of the channel divided by the length. The discharge Froude No. should be based on the actual exit conditions, which may differ from the average channel dimensions. The exit depth (h_o) is usually (118) taken as the maximum depth at the exit section, and the exit width ($2b_o$) is given by the exit area divided by the exit

depth (h_o).

8.1.3 Conclusions

The use of the mathematical model in a field situation requires that certain input data be available, and that some decisions be made on certain parameters within the model. The required input data is that which would be available before a pond is built. The choice of parameters within the model can be made without relying on field measurements, and hence the model is a predictive one. However, a sensitivity analysis on some parameters is advisable.

8.2 Hazelwood Cooling Pond

8.2.1 Description

The Hazelwood Power Station, installed capacity 1600 Mw, is situated on the extensive brown coal fields near Morwell, 90 miles east of Melbourne, Australia, (Latitude 38°S, Long. 147° E). The station is operated by the State Electricity Commission of Victoria, (SEC), and utilizes the local soft brown coal as fuel, rejecting approximately 5000-5200 Btu/Kw. hr to the condenser cooling water. Due to the absence of an extensive natural body of water in the vicinity, it was necessary to provide a closed circuit cooling system, and both capital cost and annual charges were in favor of a pond compared with towers. Other advantages gained were greater reliability and reduced make-up water requirements (Thompson (1971)). The lower water consumption with respect to cooling towers is probably due to the lack of a year round supply of make-up water, and hence the necessity of constructing a storage reservoir. The cooling pond is located

immediately south of the power station, and is formed by the construction of an embankment across the rather flat valley of Eel Hole Creek, and a second embankment across a long low saddle between this valley and an adjacent catchement to the south, (see figure 8-1, 8-2). The capacity of the pond at full level is 23,000 acre-feet, with a surface area of 1250 acres. The maximum depth is 45 ft. Due to the large proportion of the storage boundary in the form of embankments, the normally small annual changes in storage level (±0.5 ft.) result in insignificant changes in the surface area.

The cooling pond consists of a hot pond and outlet channel, total surface area approximately 100 acres, a main pond area 1080 acres, and an intake pond with a surface area of 50 acres, separated from the main pond by a skimmer wall. These features are shown in Figure 8-1, an aerial photograph of the power station and cooling pond. It can be seen that the local topography is relatively flat. The cooling pond was completed in 1963 and 200 Mw_e units were brought into service at approximately yearly intervals, the first in 1964 and the final unit in 1970. Data from two years of operation, 1968 and 1969, were used to check the model, and the installed capacity during these years increased from 800-1400 Mw_e. Figure 8-2 shows the hydrography of the pond. Surface level varied from R.L. 255.5 ft. to R.L. 256.5 ft. The skimmer wall opening was 250 ft. long, 8 ft. high with an invert level R.L. 223.0 ft.

8.2.2 Data

Meteorological and water temperature measuring instruments

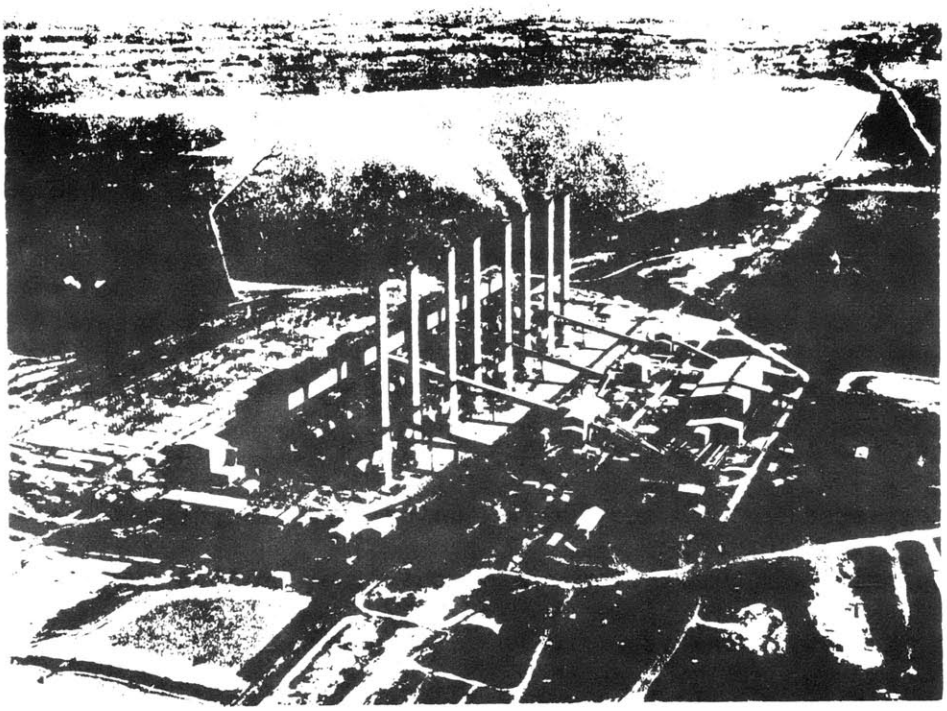

Figure 8-1 Aerial View Hazelwood Power Station and Cooling Pond

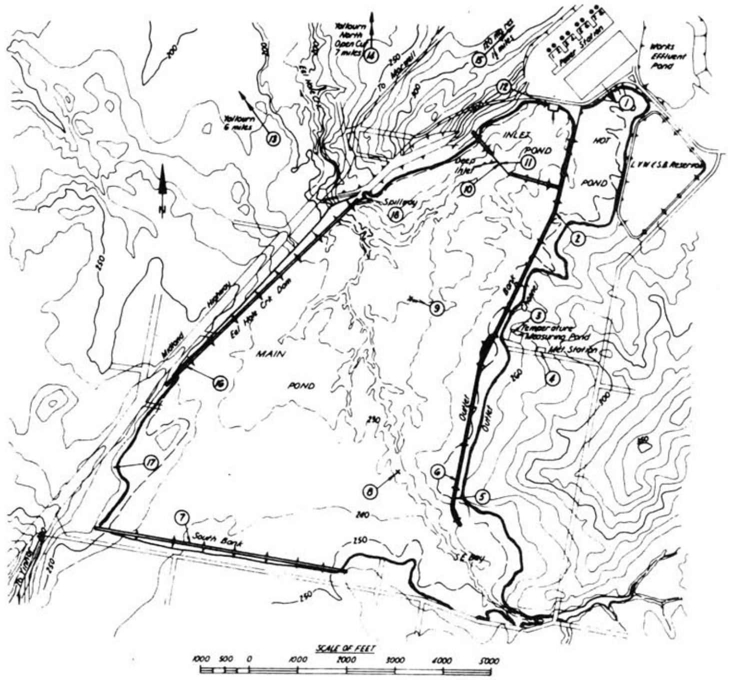

Figure 8-2 Cooling Pond Instrumentation & Topography (see also Table 8-1)

Station		Water Temperatures Recorders			Meteorological Instrumentation Recorders					Manual				LBS A 35 Water Level Recorder
Ref Fig 3	Identification	1'0 below surface	Approx at mid-depth	Approx at Bottom	Air Temp Dry Bulb Wet Bulb	Anemometer	Solarimeter	Nett Radiometer	Sunshine	Air Temp Max-Min	Anemometer	Evaporation Tank	Rain Gauge	
1	Power Station Outlet - Stage 1	-	9/63 A	-	-	-	-	-	-	-	-	-	-	-
1	" " " - 2	-	8/67 A	-	-	-	-	-	-	-	-	-	-	-
1	" " " - 3/4	-	12/68 A	-	-	-	-	-	-	-	-	-	-	-
2	End of Hot Pond	11/66 A	-	11/66 A	-	-	-	-	-	-	-	-	-	-
3	Temperature Measuring Pond	10/67 A	10/67 A	10/67 A	-	-	-	3/69 E	-	-	-	-	-	12/69
4	Hazelwood Met. Station	-	-	-	8/66 B	Pre '63 D	3/69 E	-	-	10/63	8/64	10/64	10/63	-
5	End of Outlet Channel	11/66 A	-	11/66 A	-	-	-	-	-	-	-	-	-	-
6	Outlet Bank	11/66 A	-	11/66 A	-		-	-	-	-	-	-	-	-
7	South Bank	9/63 A	-	-	-	-	-	-	-	-	-	-	-	-
8	Kent Recorder Buoy N° 2	5/69 G	-	5/69 G	-	-	-	-	-	-	-	-	-	-
9	" " N° 1	7/65 G	-	7/65 G	-	-	-	-	-	-	-	-	-	-
10	Deep Inlet - South Side	4/64 A	-	-	-		-	-	-	-	-	-	-	-
11	Deep Inlet - North Side	9/63 A	-	9/63 A			-	-	-	-	-	-	-	-
12	Inlet Structure - Stage 1	-	5/66 A	-	-	-	-	-	-	-	-	-	-	-
12	" " - Stage 2	-	5/66 A	-	-	-	-	-	-	-	-	-	-	-
12	" " - Mean	-	10/63 H	-	-	-	-	-	-	-	-	-	-	-
13	Yallourn Meteorological Station	-	-		Pre '63 B	-	-	-	Pre '63 F		Pre '63	Pre '63	Pre '63	-
14	Yallourn Nth Open Cut	9/66 A	-	9/66 A			-	-	-	-	-	-	9/66	-
15	120 mg Reservoir	Pre '63 A	-	-	Pre '63 C	-	-	-	-	Pre '63	Pre '63	-	Pre '63	-
16	Eel Hole Ck Bank (old loc)	-	-	-	-	-	-	-	-	-	5/63	-	5/63	-
17	" " " " (new loc)	-	-	-	-	-	-	-	-	-	8/68	-	8/68	-
18	Spillway	-	-	-	-	-	-	-	-	-	-	-	-	12/65

A = Cambridge - mercury & steel thermograph
B = Lambrecht - thermograph
C = Jules Richard - —"—
D = Rimco Sumner - recording anemometer
E = Middleton -
F = Campbell Stokes
G = Kent - mercury & steel thermograph
H = Siemens - —"—
7/66 = month/year for 1st record

Table 8-1 Details of Instrumentation - Cooling Pond

have been installed to check the performance of the pond. The instruments are described in Table 8-1, and their location shown in Figure 8-2. Thompson (1971) lists the accuracy for the temperature measurements as $\pm 0.5^{o}F$, for solar radiation as ± 0.5 Btu/ft^2/hr and wind velocity as ± 0.2 mph. Instruments were checked at regular intervals of 1-7 days and serviced monthly. Temperature checks were carried out monthly and records adjusted for any variation observed. Except for solar radiation, data was extracted from the recorder charts by hand. Three hourly temperature readings and average hourly wind speeds were recorded. The solar radiation data was recorded on paper tape, and was processed directly by computer. Cloud cover was observed twice daily at 0900 and 1500 hrs. Daily average wind velocities from the two anemometers were reduced to the 1 ft. level by the SEC, the observed wind velocities being corrected for elevation change and in one case for directional effects. Some doubt exists on the accuracy of wind correction (130), but in comparison with other cases, where only data from the nearest airfield is available, the wind speed data for Hazelwood must be regarded as excellent. All the above data, stored on magnetic tape, was made available by the SEC.

Further information on the surface temperature distribution within the pond was obtained using a small motor launch with a fast response thermometer which was capable of covering the pond surface on an intersecting grid in a period of 3 hours. This information was made available in the form of isotherm charts, as in Figure 4-18.

The above data is by far the best cooling pond data available

both with respect to quantity and quality, and provides an excellent opportunity to field test the mathematical model. Internal densimetric Froude Numbers, defined in section 4.4.3 as $F_i = \frac{2q}{H\sqrt{g\frac{\Delta\rho}{\rho}H}}$ are almost always < 0.1 (c.f. $F_c \simeq 0.2$), entrance mixing is low, and a deep skimmer wall is used (i.e., the pond is close to the defined ideal pond). Hence it is expected that the mathematical model will be applicable.

8.2.3 Inputs to the Mathematical Model

The computer program was usually run with a time step of one day and all data were reduced to daily averages.

Air temperatures (^oF), wet bulb temperatures (^oF), solar radiation ($Btu/ft^2/day$), wind speed (mph at 1 ft. elevation) and cloud cover (fraction) were read in directly. The air temperatures used were the mean of measurements taken at Hazelwood, and at Morwell, 3 miles away. Relative humidity was calculated from wet and dry bulb temperatures, using the simple relationship given in (129).

$$R_H = 2.8\left(\frac{T_a}{T_{wb}} - .655\right) \qquad (8.2)$$

For the year 1968 solar radiation was not measured directly, but the number of hours of sunshine was available for both 1968 and 1969. The SEC used a relationship developed by Hounam (1963) to fill in gaps in the 1969 solar radiation data. The formula

$$\frac{\phi_s}{\phi_{sc}} = 0.34 + 0.66\ (S_p) \qquad (8.3)$$

where S_p = fraction of possible sunshine. This formula, plus a tabulated function for the clear sky radiation, ϕ_{sc}, was developed for Australian conditions, and corresponded closely with measured values in 1969. The above formula was used to calculate solar radiation in 1968. Cloud cover for 1968 was also calculated, using known values of S_p, and a formula given by Wunderlich (1972).

$$C = (1-S_p)^{0.6} \tag{8.4}$$

Atmospheric radiation for both years was calculated using Swinbank's formula (equation 2.10).

Outlet temperatures and flow rates were determined from the power station output which was known on a daily basis. The input of correct heat loss was of prime importance, while the actual flow rate and condenser temperature rise are secondary. The heat input was determined from the power station output using a heat rejection value of 5175 Btu/Kw. hr (Thompson 1971). The SEC used a value of 5000 Btu/Kw. hr in computing heat loading, and the effect of this lower value was checked and found to be small. Condenser flow rates were not directly available, and although the units were rated at 1 cfs/Mw_c, this was deemed unreliable because of the practice of operating the circulating water pumps both prior and following the unit being on load. Measured values of condenser temperature rise were available on an average monthly basis, and these values were used, along with daily heat inputs, to determine the average daily flow rate. Other flows into the cooling pond were of the order of a few percent of the circulating water flow and were neglected. The surface level varied

between R.L. 255.5 and 256.5 and was assumed constant.

Geometric data was taken from a 1" = 1000 ft. contour map similar to that shown in Figure 8-2. The only problem was the schematization of the discharge channel. The average width of the channel (area/length) is approximately 400 ft., and this value was used initially. A width of 160 ft., the width of the narrower sections of the channel, gave a better prediction of intrusion length, and the effect of using this value was checked. If a cold wedge is present, the interface width is of the order of 40 ft., and this value was used in calculating interfacial entrainment.

The extinction coefficient, η, was not available, but it is known that the water is very turbid, with a Secchi disk depth of 1-3 ft. The effect of changing η within the range 0.5-1.7 ft.$^{-1}$ (see equation 6.60) was negligible. The interfacial friction factor was chosen to be 0.0086, the value obtained by Curtis on the basis of velocity measurements. The depth increment Δz was chosen as 2.0 ft. which satisfies the stability criteria (equations 6.64, 6.65) for most conditions. The two layer intake withdrawal model (equation 6.55a) is appropriate since the width of the skimmer wall opening (250 ft.) is much less than the pond width (4000 ft.) and the thickness of the withdrawal layer was determined using this model. A minimum dilution limit of 2.0 was used initially, and the effect of lowering this limit to 1.5 was checked. The minimum dilution limit has considerable significance in this case, since a cold wedge is usually present at the outlet (F_D=1) and the aspect ratio is low ($A_D \tilde{\sim} 1/40$).

8.2.4 Comparison of Theory with Field Measurements

Figure 8-3 compares the predicted and measured daily average intake temperatures for 1968. Note that when two intakes were used simultaneously, the intake temperatures could differ by up to $4^{o}F$, and it is felt that the accuracy of the average intake measurements is no greater than $\pm 1^{o}F$. Given the uncertainty in the input data it is felt that agreement of $\pm 2^{o}F$ between predicted and measured intake temperatures is all that can be expected. Figure 8-3 shows that the mathematical model almost always achieves this accuracy. Figure 8-4 shows that similar results were obtained for 1969. Measured intake temperatures were unavailable for three months during 1969, and during this period measured and predicted temperatures were compared at the skimmer wall opening. On the basis of 2 years of data it is concluded that the model predicts intake temperatures for an artificial pond with more than adequate accuracy.

A further check on the performance of the mathematical model was provided by the surface temperature distributions obtained by boat surveys. Typical daily fluctuations at 1 ft. depth are usually $3\text{-}4^{o}F$, but can reach $10^{o}F$. The boat survey took 3 hours, usually from 1000-1300 hrs, a time of rapid water temperature change, and it is felt that this limits the accuracy of the measured surface temperatures to $\pm 2^{o}F$. Figures 8-5, 8-6 show the predicted and measured surface temperature distributions for 5 cases including both summer and winter. The effect of reducing the minimum dilution limit from 2.0 to 1.5 is shown, and it is seen that the effect is relatively small.

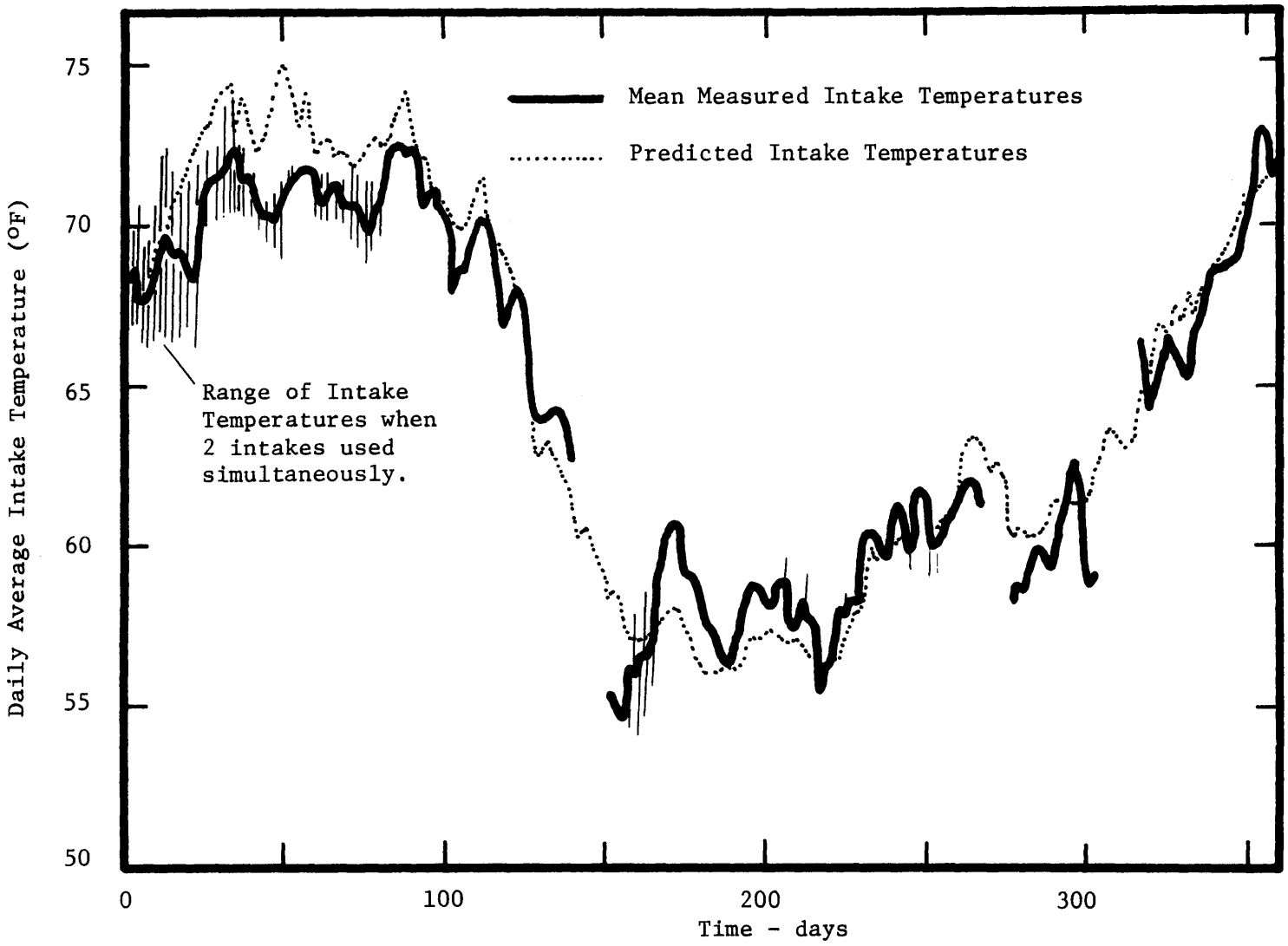

Figure 8-3 Predicted vs. Measured Intake Temperatures, Hazelwood 1968

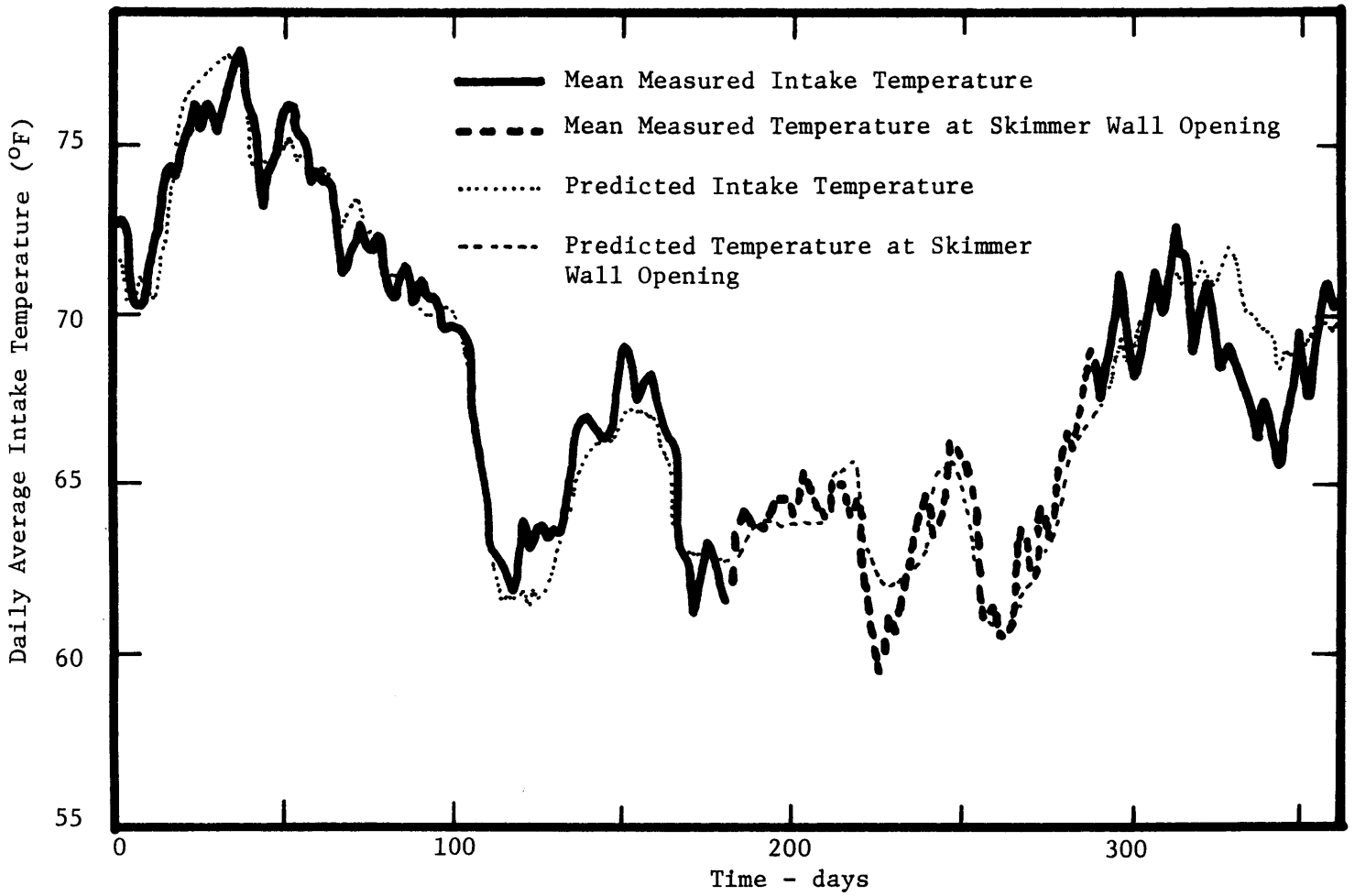

Figure 8-4 Predicted vs. Measured Intake Temperatures, Hazelwood 1969

The predicted discharge temperature $T_o(t)$ is determined within the model, and hence often varied from the measured discharge temperature by several degrees. To assist comparison, the curves in Figures 8-5 and 8-6 have been normalized against their respective (T_o-T_E). T_E was assumed the same for both measured and predicted curves.

The agreement between predicted and measured surface temperature distributions is fair. Generally the overall amount of entrance mixing is reasonable, but the predicted dilution takes place too quickly. The reason for this is apparent from Figure 8-2 where it is seen that after leaving the discharge channel, the heated water first enters a small bay with an area of about 50 acres, and then enters the main pond. This effect is clearly seen in Figures 8-5b and 8-6 where two mixing regions are apparently separated by a small plateau. Note that the second mixing region occurs about 50 acres (4 percent of area) from the end of the discharge channel. Although the shape of the predicted mixing region is not exact, nevertheless the temperature of 80-90 percent of the surface area is usually predicted within 2-3°F ($\Delta T^*=0.1$) of the measured surface temperature, i.e., the error in the predicted temperature for most of the surface is almost within the accuracy of measurement.

A final check on the performance of the mathematical model is obtained by examining the behavior of the skimmer wall both in the field and in the mathematical model. Figure 8-7 shows the daily average temperatures near the skimmer wall, at the surface and at the submerged opening. It is apparent that the actual skimmer wall does

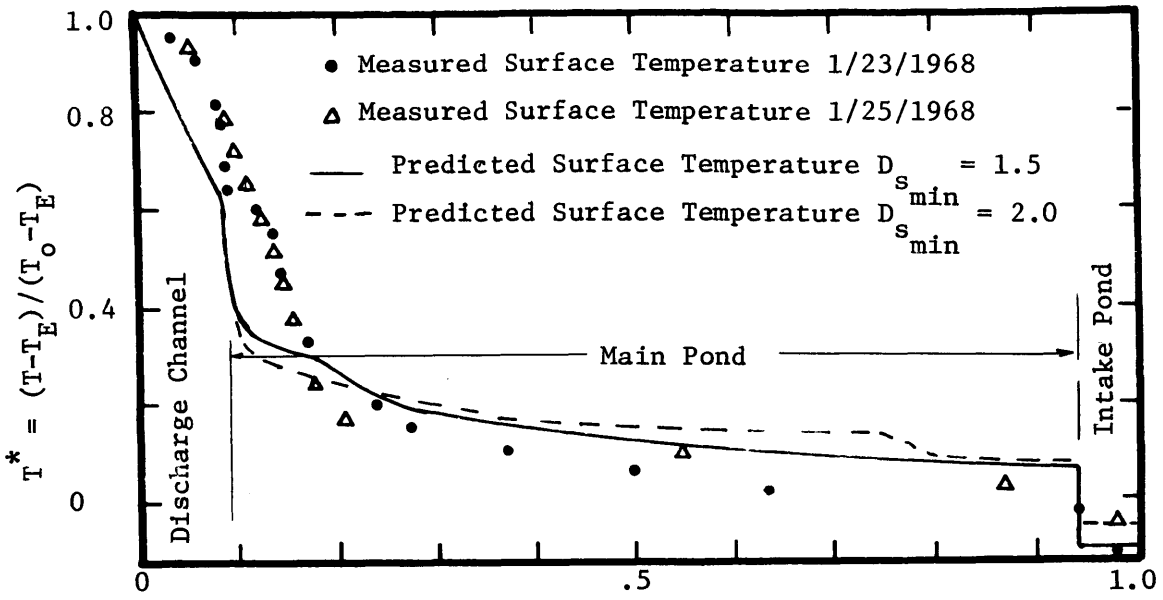

a) Surface Temperature Distribution - Summer

b) Surface Temperature Distribution - Autumn

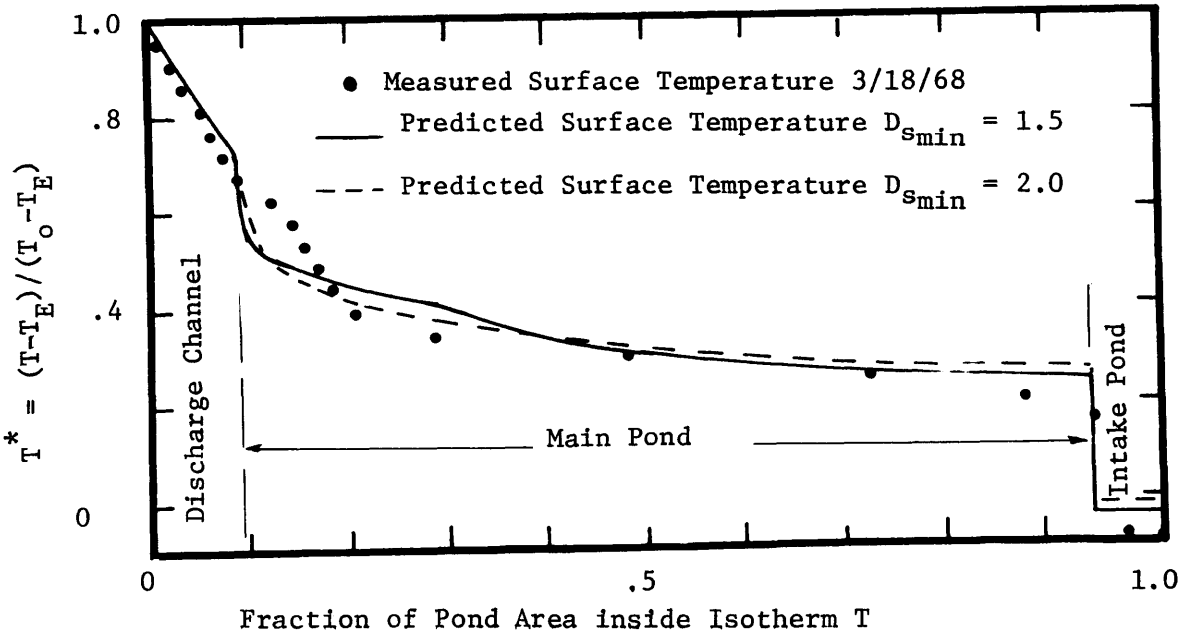

Figure 8-5 Predicted vs. Measured Surface Temperature Distribution - Hazelwood 1968

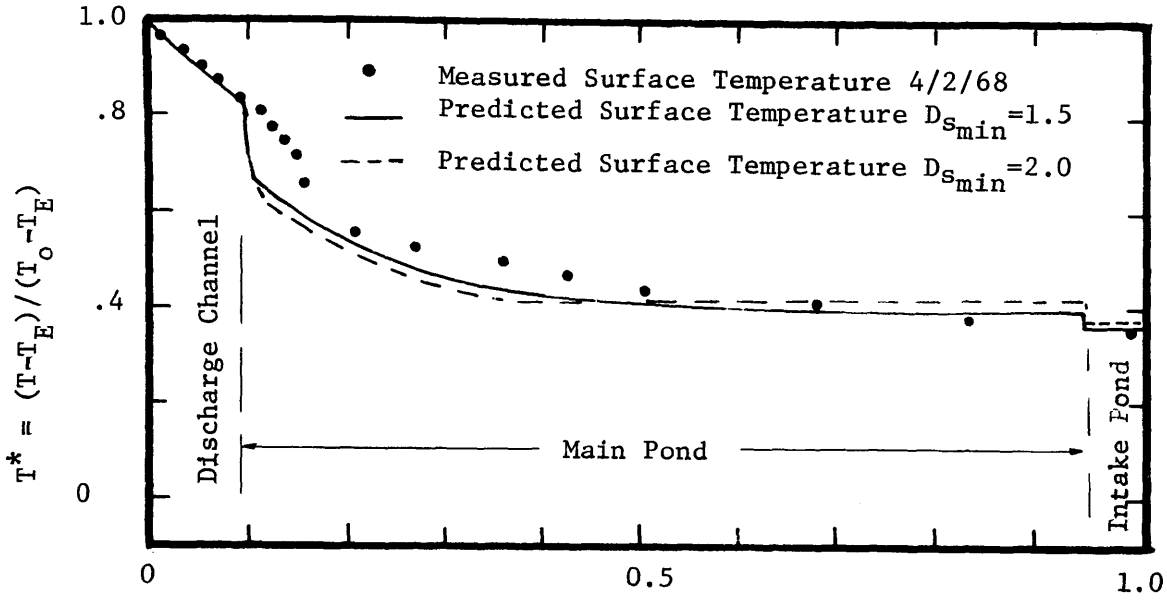

c) Surface Temperature Distribution - Autumn

d) Surface Temperature Distribution - Winter

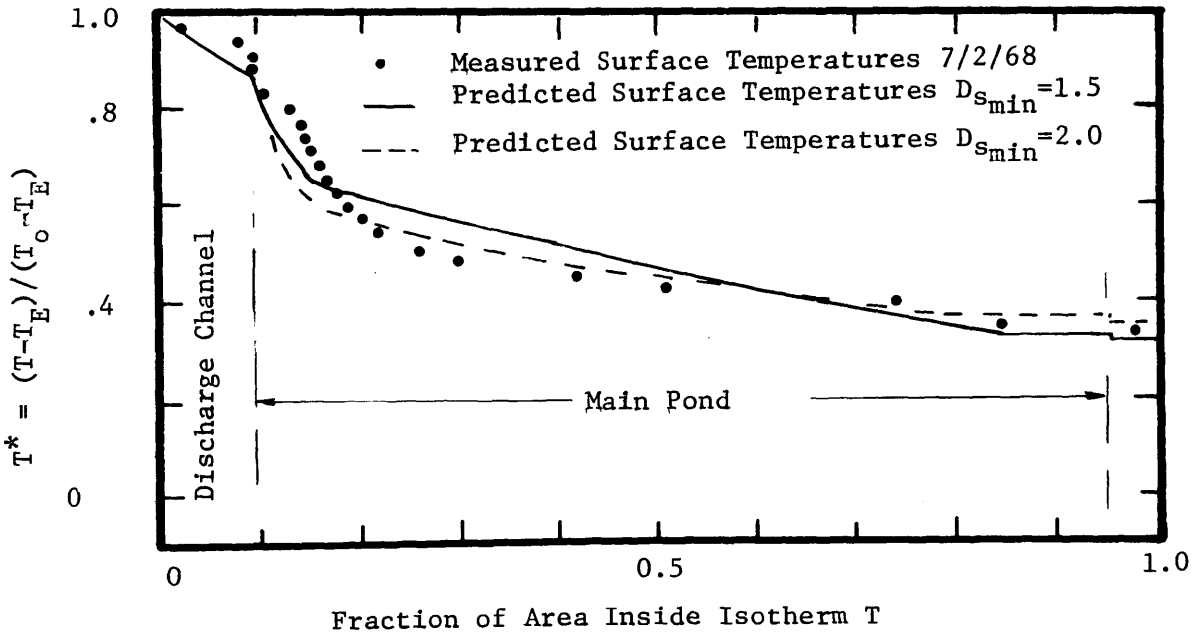

Figure 8-6 Predicted vs. Measured Surface Temperature Distribution - Hazelwood 1968

not work as well as the mathematical model assumes, but the great value of the skimmer wall in eliminating peak intake temperatures is illustrated. Figure 8-8 compares predicted and measured daily average temperatures at the skimmer wall both at the surface (1 ft. depth) and at the submerged opening (25 ft. depth). In general the agreement is excellent (i.e., within $\pm 2^{o}F$).

8.2.5 Sensitivity of Mathematical Model

A series of computer runs were done to test the sensitivity of the mathematical model to certain parameters such as the heat rejection rate and discharge channel schematization, for which a range of values are feasible. Other parameters checked were the type of selective withdrawal model used, and the minimum dilution limit for the surface discharge. Predicted intake temperatures are presented for the cases shown in Table 8-2. Run 6 and Run 8 are the basic predictive runs previously presented.

Table 8-2 Predicted Intake Temperatures for a Range of Parameters

Run	Year	Heat Rejection Btu/Kw hr	Discharge Channel Width (ft.)	Surface Discharge: Minimum Dilution Limit	Selective Withdrawal Model - Skimmer Wall Intake
1	1968	5000	160	1.5	Kao (1965
2	1968	5175	160	1.5	Kao (1965)
3	1968	5000	400	1.5	Kao (1965)
4	1968	5000	160	1.5	Two Layer Model
5	1968	5000	160	2.0	Kao (1965)
6	1968	5175	400	2.0	Two Layer Model
7	1969	5000	160	1.5	Kao (1965)
8	1969	5175	400	2.0	Two Layer Model

As expected, reducing the heat rejection rate and the minimum

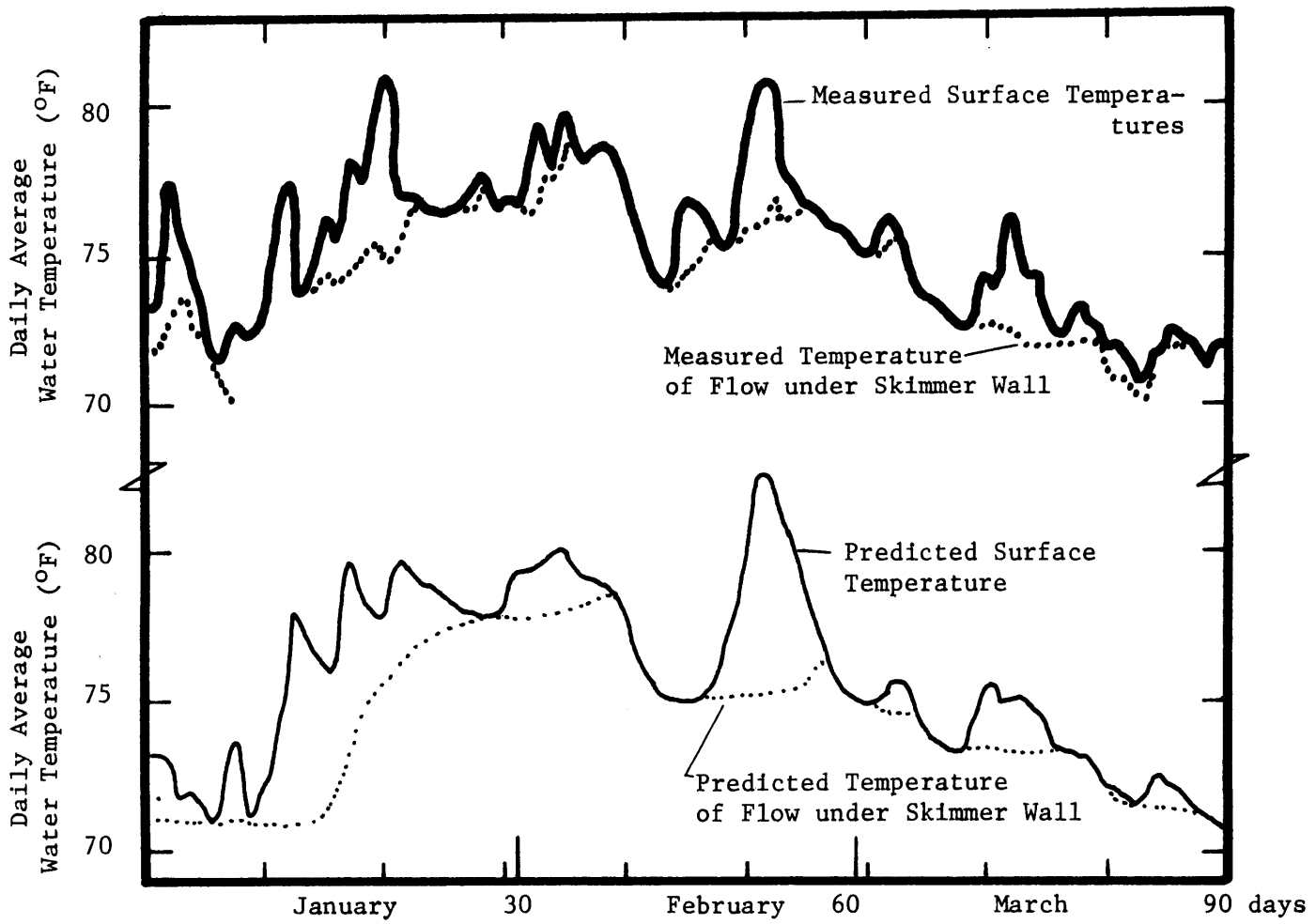

Figure 8-7 Behavior of Skimmer Wall - Measured and Predicted (Hazelwood - Summer 1969)

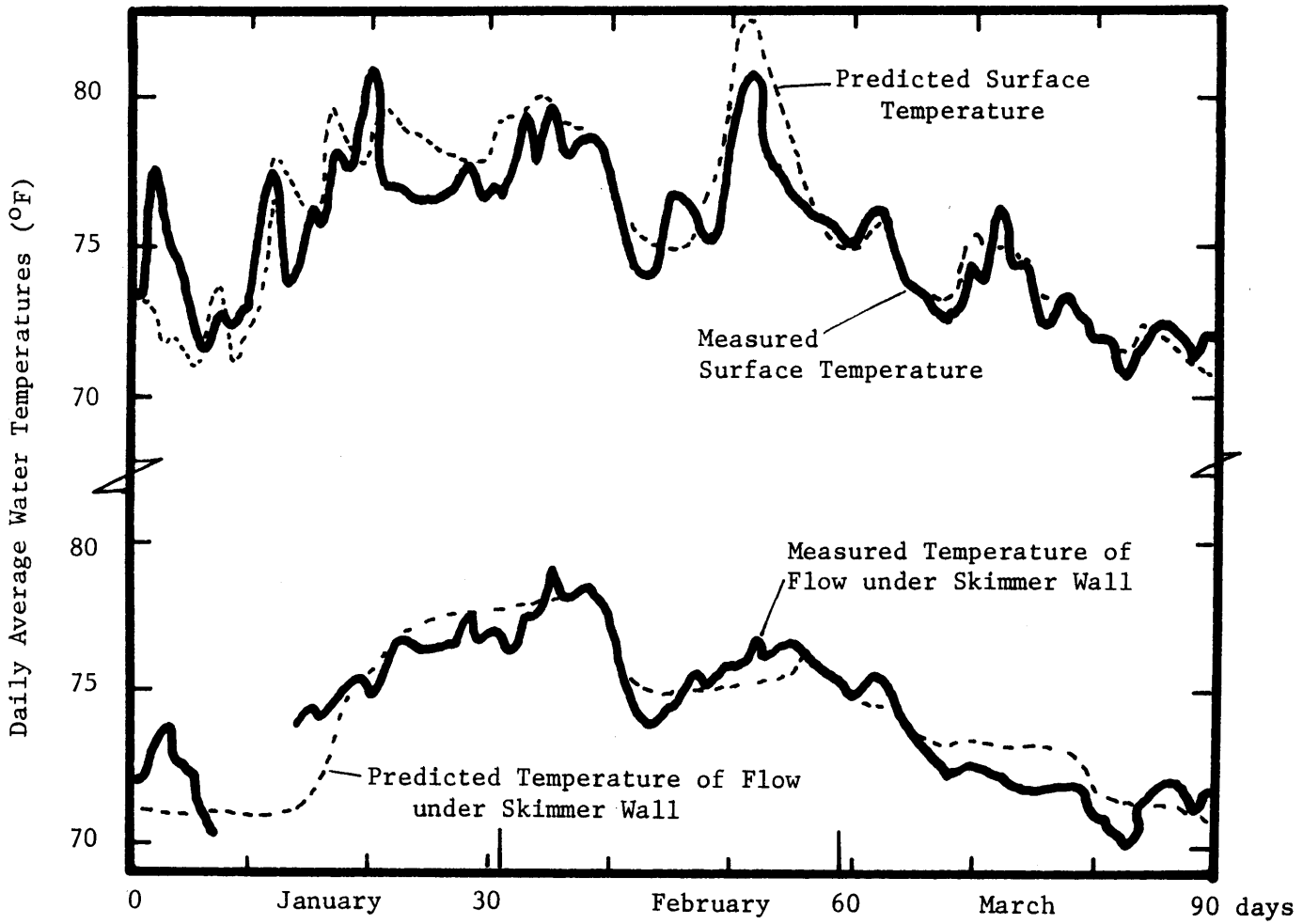

Figure 8-8 Predicted vs. Measured Temperatures at the Skimmer Wall - Surface and Opening at 25 ft. depth (Hazelwood, January-March 1969)

dilution limit led to a decrease in intake temperatures. Reduction in the width of the outlet channel also led to an intake temperature decrease. The reason for this is that entrainment within the channel itself is reduced, while the dilution at the end of the channel, which is usually specified by the minimum dilution limit, is unaffected. The use of the Kao withdrawal model, instead of the two layer model, caused a very slight decrease in intake temperature. Run 1 combines all these reduction effects, and Figure 8-9a compares the basic predictive run (Run 6) with the minimum intake temperature run (Run 1). It is seen that in the summer months, the critical design months, the range of feasible predicted intake temperatures is only about $1^{o}F$, with Run 1 giving slightly better results than Run 6. In winter the situation is reversed, with Run 6 giving better results, a feasible predictive range of about $2^{o}F$, and Run 1 being $3\text{-}4^{o}F$ low at some times. The larger difference between Run 1 and Run 6 in the winter months is due to the larger heat load and poorer heat loss conditions which exist in the winter. Figure 8-9a also shows that about half the difference between Run 1 and Run 6 is due to change in the minimum dilution limit (Run 5). Figure 8-9b shows the relatively small changes ($\sim \frac{1}{2}^{o}F$) which result from changing the heat rejection rate from 5175 to 5000 Btu/Kw hr, and changing the width of the outlet channel from 160-400 ft. The effect of changing the withdrawal layer model is insignificant and is not plotted. Figure 8-10 shows the range of predicted intake temperatures for 1969. Again it is seen that the feasible range in summer is small, $1\text{-}1.5^{o}F$, and agreement

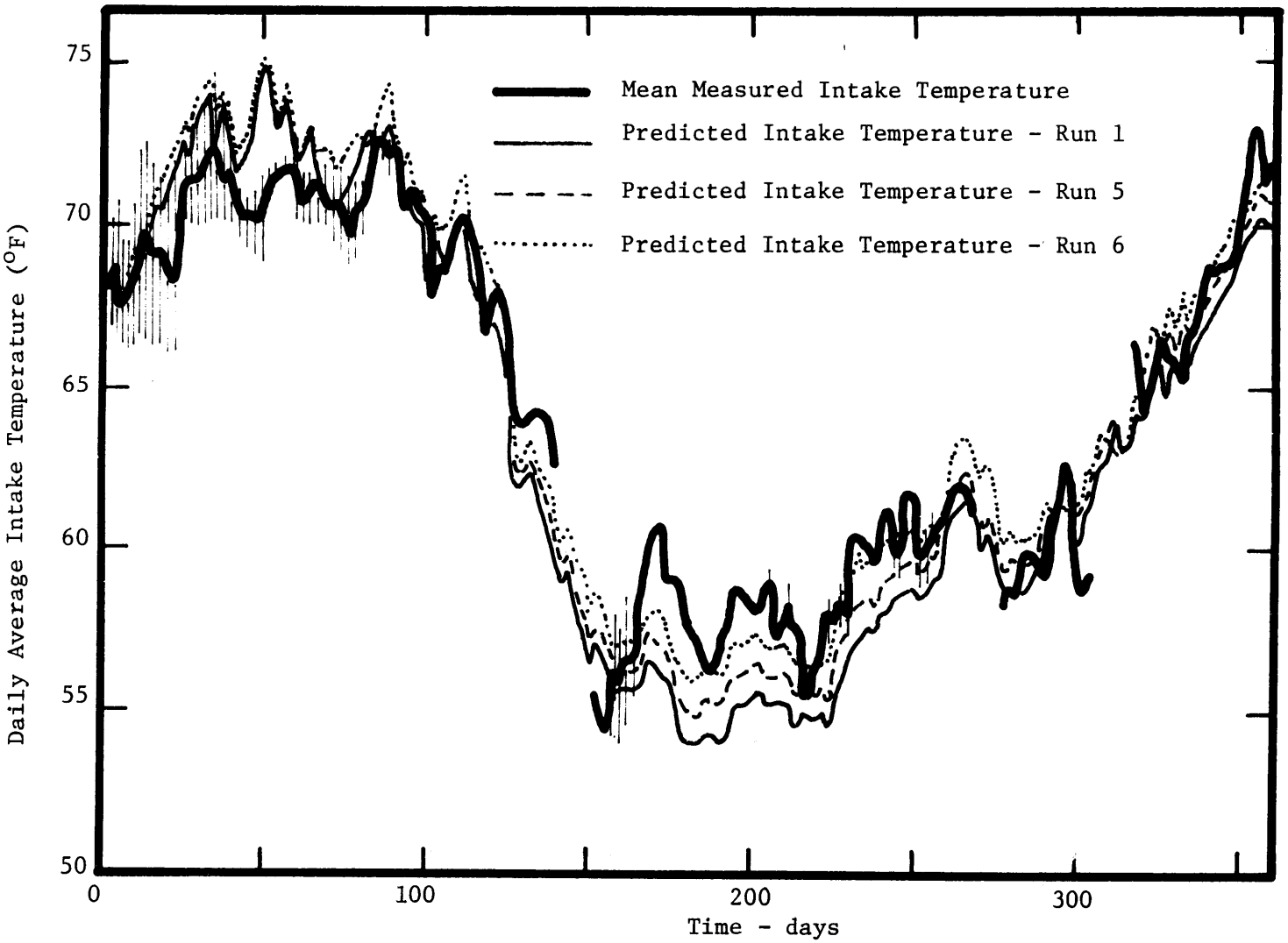

Figure 8-9a Predicted vs. Measured Intake Temperatures, Hazelwood, 1968

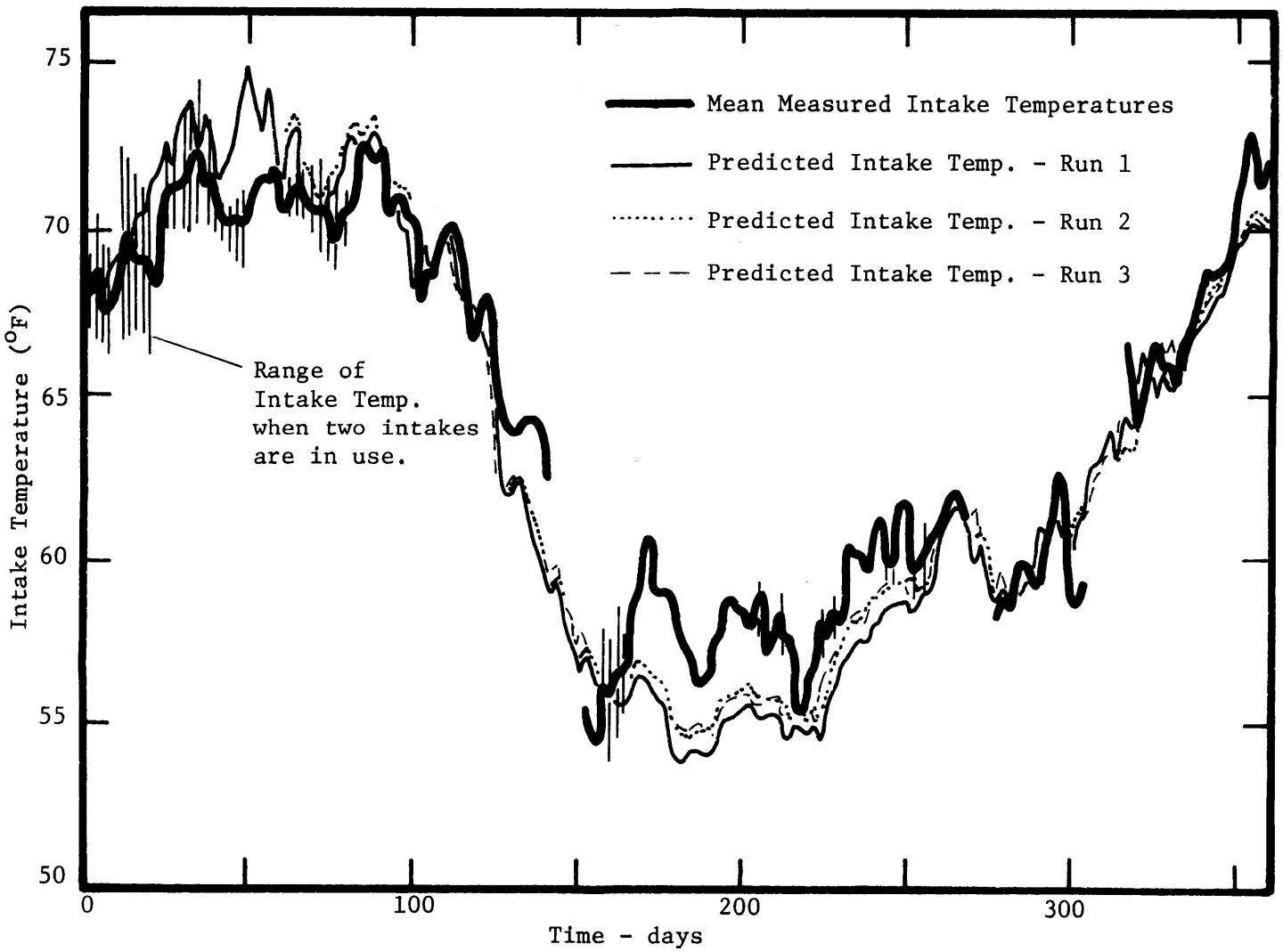

Figure 8-9b Predicted vs. Measured Intake Temperatures, Hazelwood, 1968

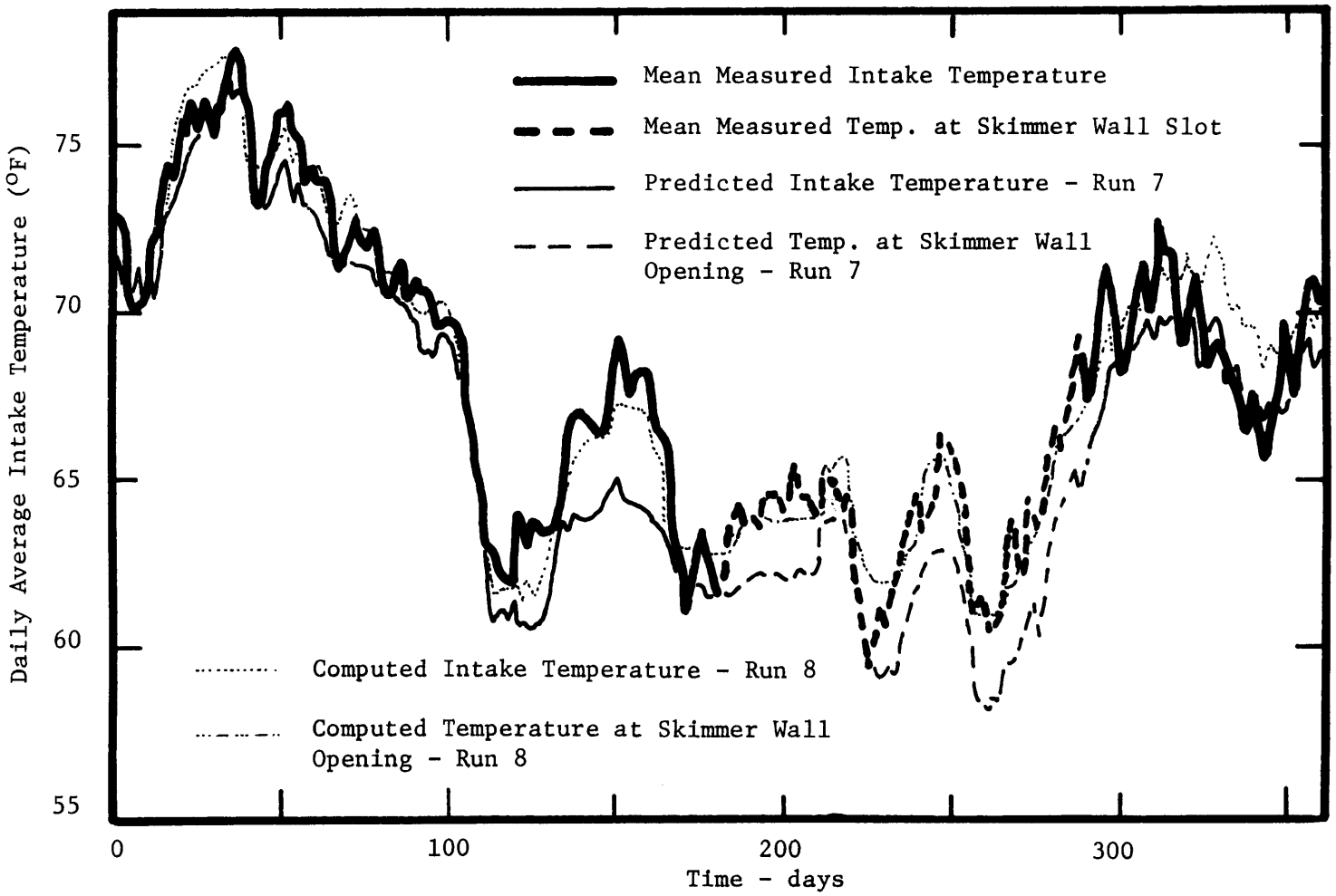

Figure 8-10 Predicted vs. Measured Intake Temperatures, Hazelwood 1969

between the measured intake temperature and both predicted temperatures is excellent. In the winter months, the feasible range is larger, up to 2.5°F, and the basic predictive run (Run 8) gives better results.

8.2.6 Summary

The mathematical model has been tested against two years of data (1968,1969) from the Hazelwood cooling pond. Certain inputs to the model, or parameters within the model, were not known with sufficient accuracy, and were varied over their feasible range. The combined effect of all the above changes was small (2-3°F). The accuracy of the field data, although of excellent quality is no better than ±1-2°F. The mathematical model predicted the mean daily intake temperatures for two years of data within 2°F for a high percentage of the time. The transient response of the model was excellent. Surface temperature distribution was only fair due to outlet topography which could not be reproduced in the mathematical model, but in the predicted temperature distribution was correct within 2-3°F for 80-90 percent of the surface area. Transient surface temperatures at the skimmer were checked over a 90 day period in the summer of 1969, and excellent results were obtained, usually within 2°F. Note that all inputs to the mathematical model are those which would be available before the pond was built. The execution time for the computer programs on an IBM 370/155 for a period of one year, was approximately one minute.

8.3 Lake Norman

8.3.1 Description

The mathematical model has been tested against data from a laboratory cooling pond, and a field cooling pond of the artificial type. An important use of the model is the prediction of the cooling performance of a natural lake or existing reservoir, or alternatively, the prediction of the effect of waste heat input on the thermal structure of an existing water body. The model has therefore been tested against three years of data from the Lake Norman power generating system, operated by the Duke Power Company in North Carolina.

Lake Norman (latitude 35.5°S, longitude 81°W) has a surface area of 32,500 acres, a maximum depth of 120 ft., and a mean depth of 34 ft. (see Figure 8-11). The impounding structure, Cowans Ford Dam was completed by Duke Power in 1963. The reservoir has a dual purpose, to provide hydroelectric power, and to serve as a cooling water source for thermal power stations. Existing stations are the Cowans Ford Hydroelectric Station and the Marshall Steam Station. The William B. McGuire Nuclear Station is now under construction. The principal inflow into the lake is the Catawba River, which first passes through the Lookout-Shoals Hydroelectric Station (19 Mw_e), 33.5 miles upstream of Cowans Ford Dam. The average detention time in Lake Norman at the mean river flow rate is about 200 days.

The Cowans Ford Hydroelectric Station was completed in 1967, and has a total capacity of 370 Mw_e. A unique feature of the station is the submerged dam in front of the intake, which allows only the

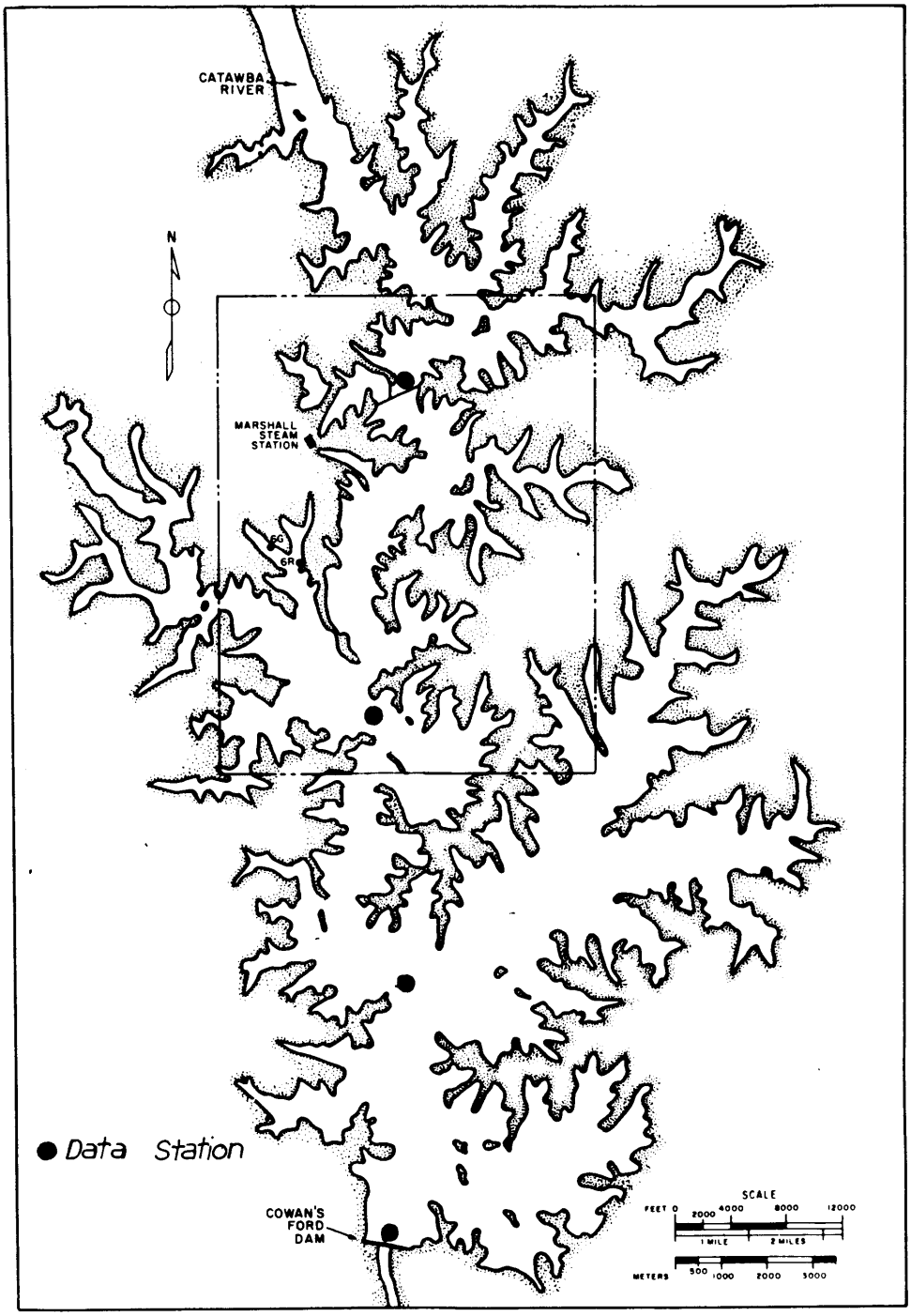

Figure 8-11 Lake Norman Showing Location of Cowan's Ford Dam, Marshall Steam Station and Data Stations.

warmer, well oxygenated surface waters to be released downstream, and therefore conserves the colder bottom waters for cooling purposes (see Figure 8-13).

The Marshall Steam Station is a fossil fuel station, and was completed in 1970. In 1966 the station's capacity was 770 Mw_e. In 1969 an extra unit was added, bringing the capacity to 1450 Mw_e, and in 1970 a final unit increased the capacity to 2136 Mw_e. A skimmer wall across the intake lagoon (Figure 8-12) enables the intake water to be selectively withdrawn from about the 60 ft. depth, and provides year round cool water to the condensers, with the result that Marshall rejects only 3930 Btu/Kw hr to the condenser water, and is rated as one of the most efficient (40%) thermal stations in the country. The surface area of the intake pond is approximately 205 acres, the mean depth is 28 ft., and at full load the detention time is 1.1 days. The heated water (2300 cfs. max.) is discharged into a narrow arm of the lake through a half mile long open channel as shown in Figure 8-12. For much of the year a cold wedge intrudes into the discharge channel, resulting in minimal mixing at the point of entry to the lake. However, during the summer the discharge is often at a lower temperature than the lake surface, and considerable entrance mixing is present.

Extensive meteorological, hydrological and plant operating data are available. Three years of data 1968, 1969 and 1971 were used to check the model. The plant capacity for these years was 772, 1454, and 2136 Mw_e respectively. Note that the maximum loading is

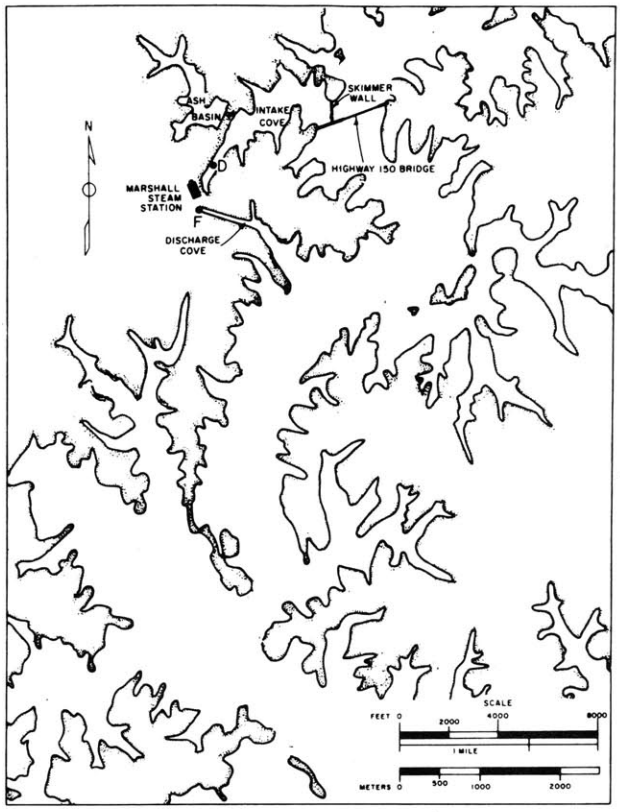

Figure 8-12 Marshall Steam Station Showing Location of Skimmer Wall and Discharge Channel

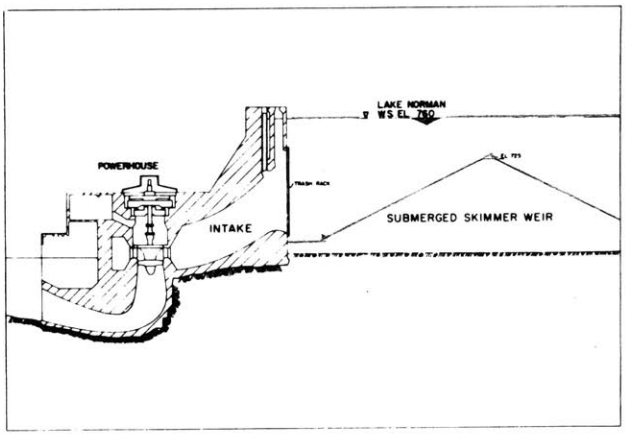

Figure 8-13 Submerged Skimmer Weir in Front of Cowan's Ford Dam

only 0.07 Mw_e/acre, compared with 1.1 Mw_e/acre at Hazelwood. Similarly the residence time for Lake Norman based on the maximum flow rate of the Marshall Steam Plant is $\sim$ 225 days (volume above intake level 1,000,000 acre ft.) compared with the residence time of Hazelwood of about 10 days. The important point is that the heat addition per unit surface area to the lake is small (about 10% of average summer solar radiation), and the principal effect of the Marshall Plant on the thermal structure is due to the withdrawal of cool water from a low level, which sets up a vertical advective flow and transports heat from near the surface into the body of the lake. The transient response of the system, rather than the surface heat loss, is the important parameter since water surface temperatures far from the outlet will be close to natural temperatures. The assumption of an effective area of unity is not important due to the light loading, but nevertheless would be reasonable, due to the large depth.

8.3.2 Data

The following daily average data was supplied by the Duke Power Company:

a) Dewpoint Temperature (^oF) or relative humidity (percent), dry bulb temperature (^oF), sky cover (tenths) or atmospheric radiation (K cal/m^2), and wind speed (mph at 8m. level) all measured at the Charlotte, North Carolina Weather Bureau (16 miles from the lake).

b) Solar radiation (cal/cm^2/day or Kcal/m^2/day) measured at Greensboro, North Carolina (80 miles from the lake)

c) Marshall Steam Station flow rates (cfs) and temperature

rise (for 1971) or discharge temperature (for 1968, 1969).

d) Lake Norman elevations (ft.)

e) Inflows (at Lookout Shoals) and outflows (at Cowans Ford Dam) ($10^6 ft^3$/day).

Water temperature profiles and secchi disk depths were taken approximately once a month at 8 stations within the lake. Data from four of these stations in the main body of the lake (see Figure 8-11) was averaged and either used in the mathematical model (secchi disk depths) or to check the model (temperature profiles).

The meteorological data suffers from the fact that it was not taken on site, but surface temperatures were correctly simulated in the mathematical model showing that this was not a serious defect.

Geometric data is shown in Table 8-3.

Table 8-3 Lake Norman Geometry

Water Surface Elev. ft.	Area Acres	Volume 10^3Acre-ft.	Length Miles	Important Elevations
760	32,510	1093	33.5	
750	25,950	801.9	29.7	
740	20,360	571.0	25.5	
730	15,660	391.6	23.7	
720	11,720	254.8	22.6	725.0 Top of sub-
710	8,242	155.5	21.8	merged weir in
700	5,427	87.5	20.8	front of Cowans
690	3,174	44.9	19.3	Ford Dam
680	1,786	20.4	15	
670	831	7.6	9.5	690.0 - 700.0
660	327	1.9	4.5	Marshall Steam
650	50	.05	0.2	Plant Intake

8.3.3 Inputs to Mathematical Model

The program was run with a nominal time increment of 1 day and a depth increment of 2.5 ft. All meteorological and flow data was read in directly in the units supplied by Duke Power, and conversion to the basic units of ft., days, btu's and ^{o}F was carried out internally. Swinbank's formula (equation 2.10) for atmospheric radiation was used, when direct measurements were not available.

All flows were supplied as daily averages, but Cowans Ford Hydroelectric Station was designed for 5% use, and hence daily average flow rates can be in error by an order of magnitude. Since Cowans Ford withdraws water over a submerged skimmer weir, equation (6.55a) was used to determine if drawdown of a warm surface layer or draw-up of a cold bottom layer occurred. Note that the displacement of the interface (Δh in Figure 8-14) is proportional to Q_{os}^2, where Q_{os} is the outflow rate, and hence correct specification of Q_{os} can be important. In contrast, the depth of the inflow layer is a function of inflow rate $(Q_{in})^{2/3}$, based on a fixed densimetric Froude No. (0.25), and hence correct specification of Q_{in} is not so crucial. For 1971, typical flow rates for Cowans Ford and Lookout Shoals were 12500 cfs (25% capacity) and 3800 cfs (100% capacity). These figures were not available for 1968 and 1969, and it was assumed that Cowans Ford operated for 2 hours/day for the five days a week that it usually operated. This is about 6% usage, compared with the 5% design figure. It was further assumed that the range of feasible flow rates was between 12,500 cfs (1 unit) and 50,000 cfs (all 4 units). The velocity

profile above the submerged weir was assumed uniform, while the profile in the region below the weir sill (R.L. 725.0 ft.) was assumed gaussian. See Figure 8-14.

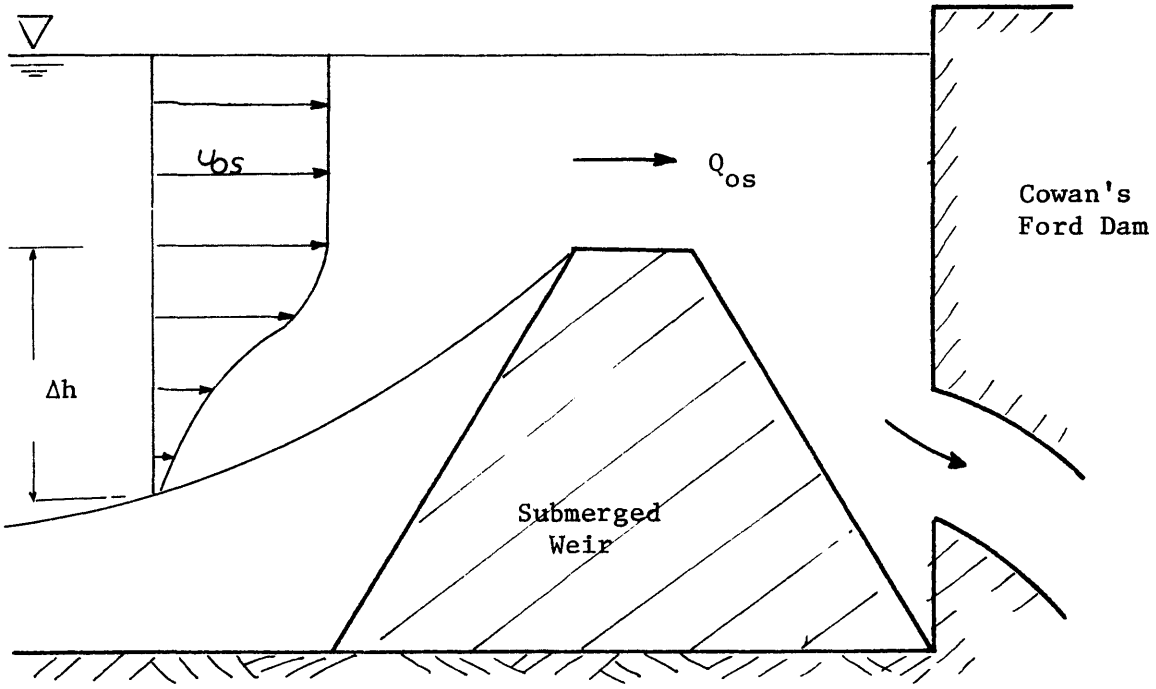

Figure 8-14 Assumed Velocity Profile for Outflow Through Cowan's Ford Dam

Lookout Shoals was assumed to operate at 100% capacity (3800 cfs), a reasonable assumption in view of its small capacity of 19 Mw_e. Note that the discussion above only refers to flow rates and correct mean daily flows were always used.

Extinction coefficients η were obtained from secchi disk depths (d_D) using the formula of Poole and Atkins (1929)

$$\eta = \frac{1.7}{d_D} \tag{8.4}$$

The average d_D from the four lake stations (see Figure 8-11) was first plotted against time, and average monthly values extracted and used in the model.

Other information such as the exit width and depth of the discharge channel (500 ft. and 40 ft.), and the effective length of the submerged weir (600 ft.) were obtained from topographical maps and engineering drawings supplied by the Duke Power Company. The entrance mixing of the stream inflow with the receiving water was assumed to be 50%, (r_m=0.5) a fairly typical figure as was discussed in section 6.7.4.1. The effect of this assumption was examined over the range r_m = 0.25 - 0.5 and found to be insignificant.

Model parameters which were important at Hazelwood, such as the minimum dilution limit, are not significant in this case because of the extremely light loading, and were kept constant in all runs.

The effect of the Marshall Steam Station submerged intake was simulated for all runs using the selective withdrawal formula based on Kao (1965).

Lake Norman behavior is complicated by the fact that during part of the summer (about 70 days in 1971), the Marshall discharge temperature is less than the surface temperature. It has been observed (61) that when this happens considerable mixing takes place, and this has been simulated in the model.

Early computer runs showed that the mathematical model

predicted an epilimnion that was too shallow and too warm in late spring. This was due to the fact that in April and early May high wind speeds could breakdown the weak stratification causing a deeper cooler epilimnion. This effect was included using the approach of Kato and Phillips (1969) by specifying an entrainment velocity, u_e, as

$$u_e = \frac{2.5 u_{*_w}^3}{g \frac{\Delta\rho}{\rho} H_e} \qquad (8.5)$$

where u_e = entrainment velocity at the bottom of the epilimnion

u_{*_w} = wind friction velocity and is determined using the approach of Van Dorn (1953).

H_e = depth of the epilimnion

$\frac{\Delta\rho}{\rho}$ = characteristic density difference, taken here to be the difference between the density of the upper layer and the mean density of the underlying layer of equal thickness (H_e).

The effect of including the wind mixing was primarily cosmetic, changing the near surface temperature profile in late spring, but having an insignificant effect on intake temperatures or later temperature profiles. This effect has been retained in the mathematical model.

8.3.4 Comparison of Theory with Field Measurements

The Lake Norman situation is rather complex compared with the Hazelwood case, primarily because of the river through-flow. The method of operation of the Cowans Ford Hydroelectric Station had a

measurable effect on the predicted intake temperature of the Marshall Steam plant as shown in Figure 8-15. At high flow rates the Cowans Ford plant withdraws water over the whole depth of the reservoir, which increases vertical advection and transports heat downward.

The results for the following computer runs are shown here:

Table 8-4 Computer Runs - Lake Norman Case

Run	Year	Cowans Ford Operation	Remarks
1	1971	12,500 cfs.	Supplied by Duke Power
2	1971	2 hrs/day Range 12,500-50,000 cfs.	Close to design use 5%
3	1969	2 hrs/day Range 12,500-50,000 cfs.	Close to design use 5%
4	1968	2 hrs/day Range 12,500-50,000 cfs.	Close to design use 5%

Computation starts on April 1, and the initial condition is the measured temperature profile on this date.

The performance of the mathematical model will be assumed primarily in terms of intake temperatures since the interest here is in the performance of the lake as a cooling pond. Further checks will be made using the outflow temperatures through Cowans Ford Dam and vertical temperature profiles within Lake Norman.

Figures 8-15 to 8-17 compare predicted and measured intake temperatures at Marshall Steam Station for 1971, 1969 and 1968, respectively. The significant influence of the outflow rate through the Cowans Ford Hydroelectric Station is clearly shown in Figure 8-15.

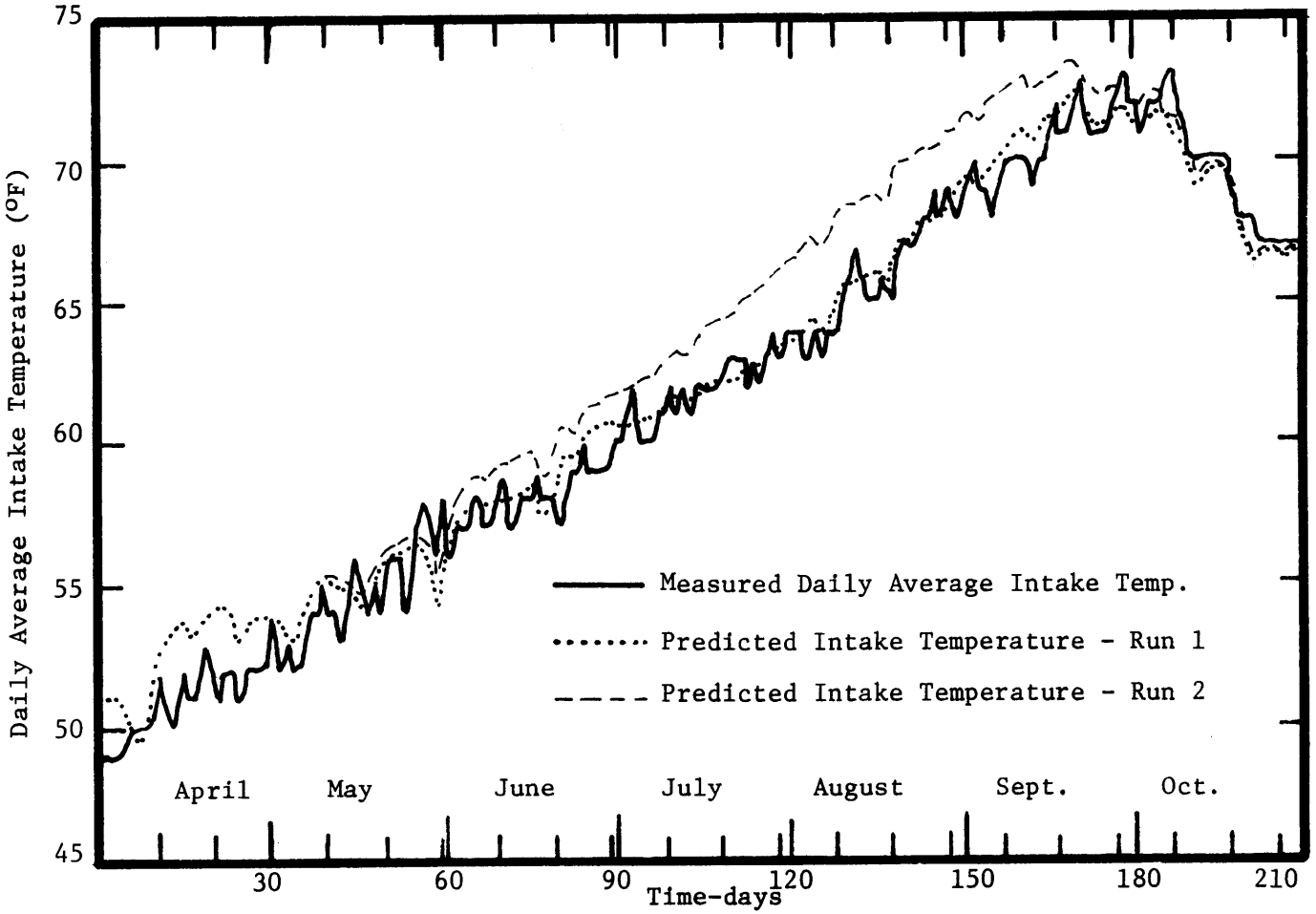

Figure 8-15 Predicted vs. Measured Intake Temperatures, Marshall Steam Plant, 1971

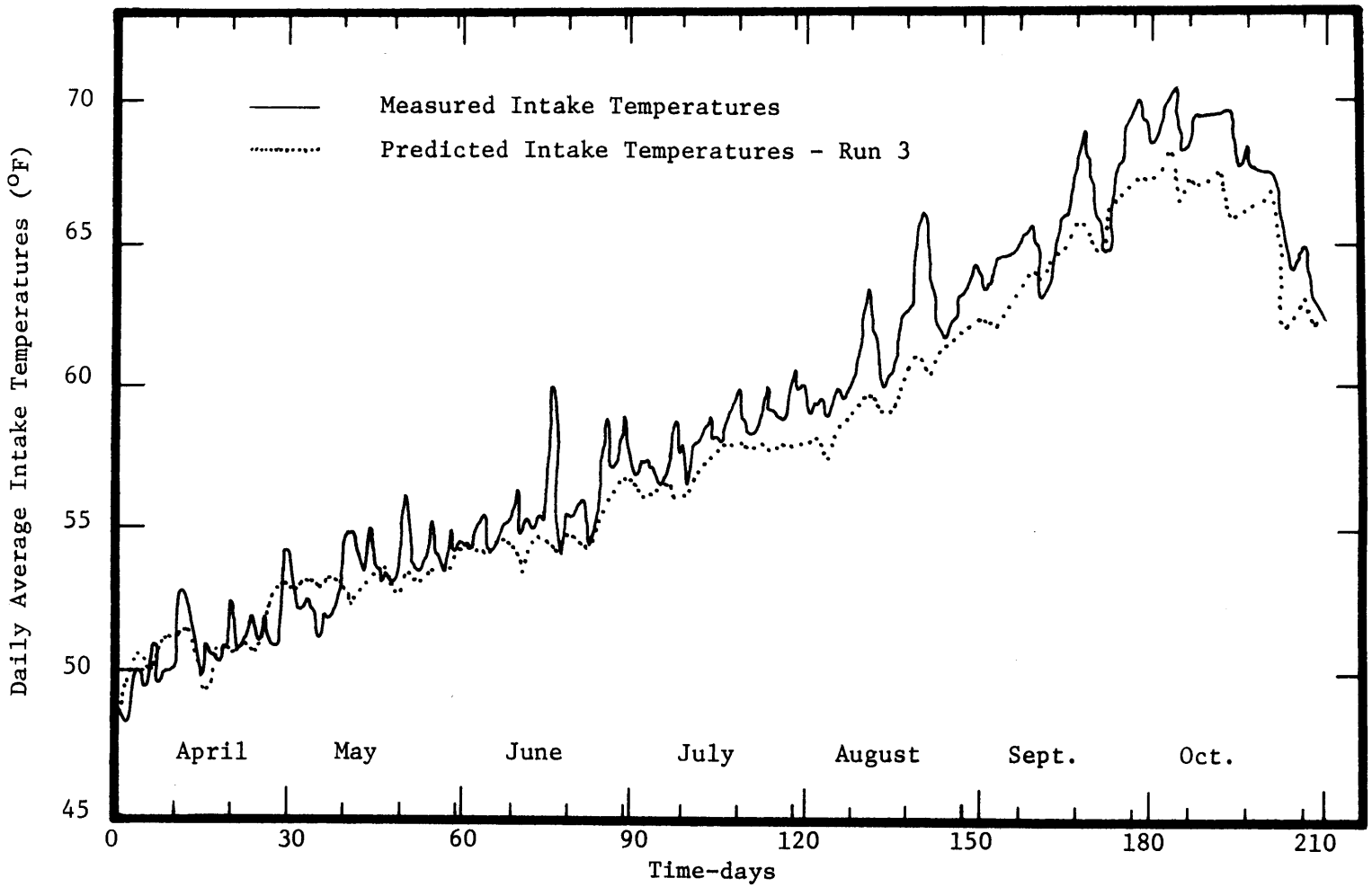

Figure 8-16 Predicted vs. Measured Intake Temperatures at Marshall Steam Station - April to October 1969

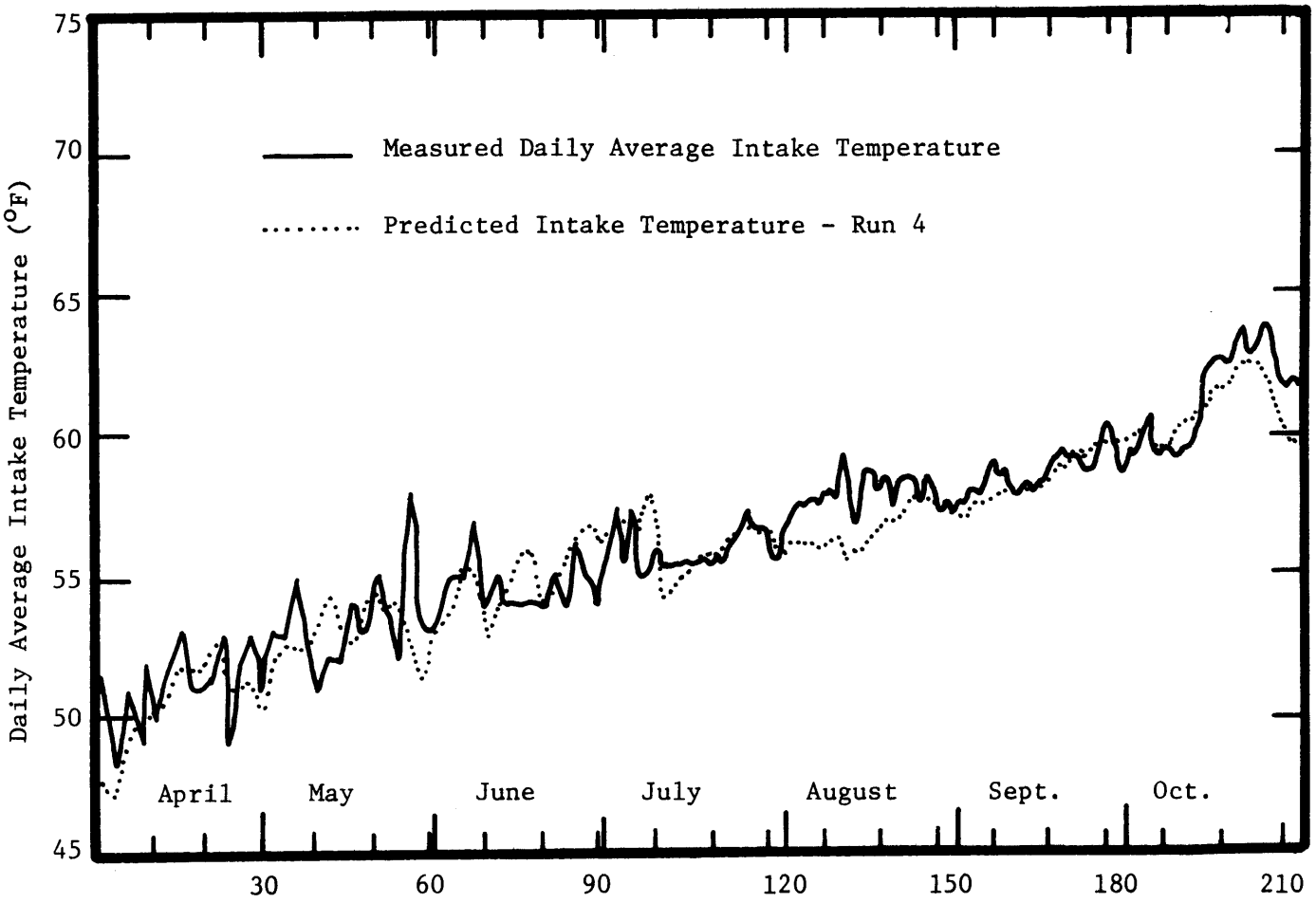

Figure 8-17 Predicted vs. Measured Intake Temperatures, Marshall Steam Plant, 1968.

Using the typical flow rate for 1971 supplied by Duke Power, excellent agreement is obtained, while if the flow rate is based on the design 5% usage, then predicted intake temperatures are too high by up to $3^{o}F$. For 1969 and 1968 limiting the usage to 2 hrs/day (the design usage) gives excellent agreement. The effect of the increasing capacity of Marshall from 772 Mw_e in 1968, to 1454 Mw_e in 1969 and 2136 Mw_e in 1970 is shown by the increase in intake temperatures, both predicted and measured, from 1968 to 1971.

Figures 8-18 and 8-19 compare the predicted and measured outflow temperatures at Cowans Ford Hydroelectric Station. Large short term fluctuations are apparent both in the measured and predicted temperatures for 1969. The fluctuation in the predicted temperatures is due to changes in the withdrawal layer thickness, δ. Since the latter depends on $(Q_{os})^2$, fluctuations in Q_{os} are immediately reflected in the outflow temperature. The minima in the predicted curves represent cases where Q_{os}, and hence δ, is large. Note that the minima agree better with the measured temperatures. Overall, the agreement with measured data is quite good, although the amount of data available is somewhat limited.

Figures 8-20 to 8-23 compare predicted and measured temperature profiles for the 3 years of interest. The measured temperature profile represents the average profile at the four stations shown in Figure 8-11. The range of temperatures at each depth is shown. Three of the four temperature measurement stations are a large distance from the Marshall Steam Plant, and it is felt that the range of measured

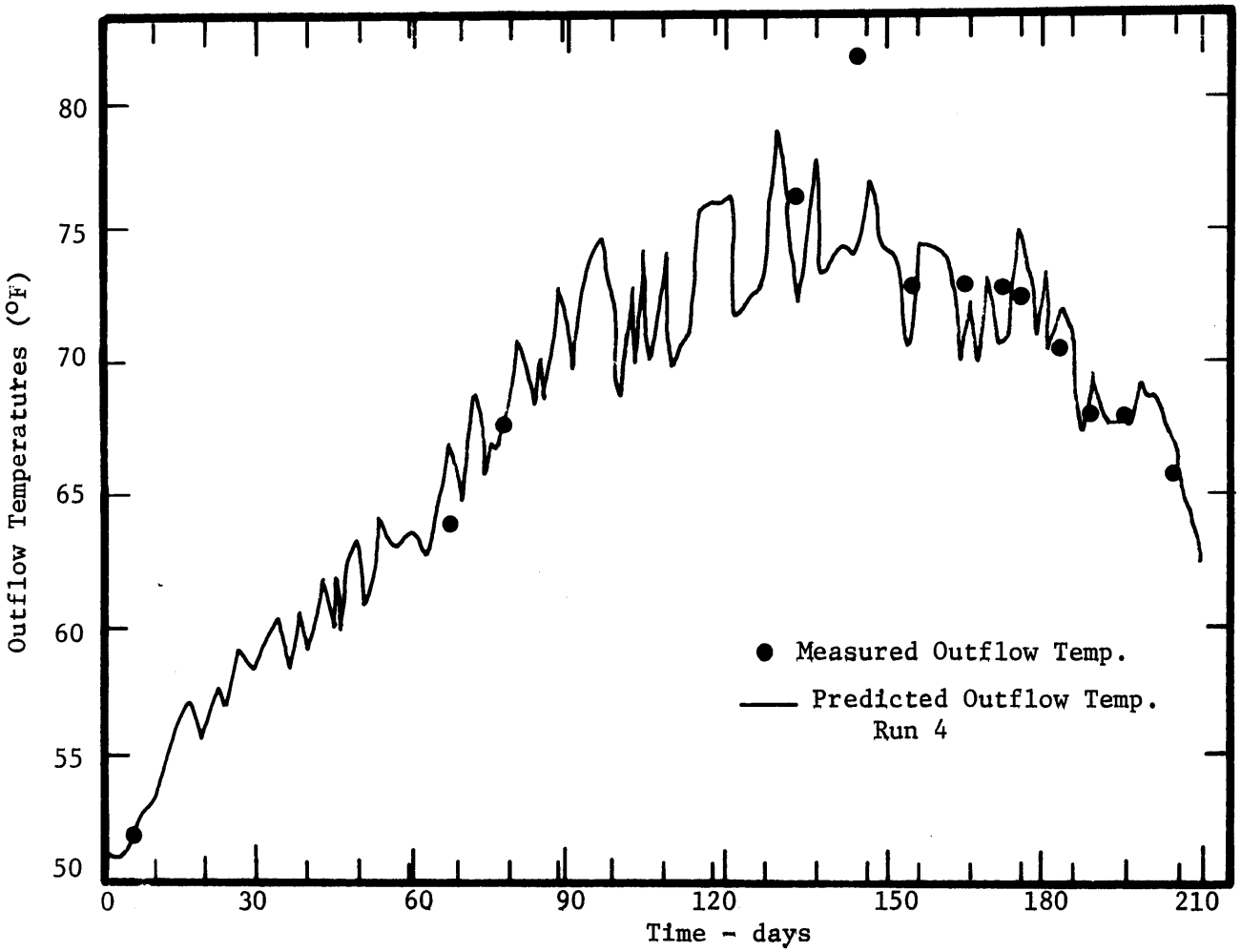

Figure 8-18 Predicted vs. Measured Outflow Temperatures at Cowan's Ford Hydroelectric Station, 1968

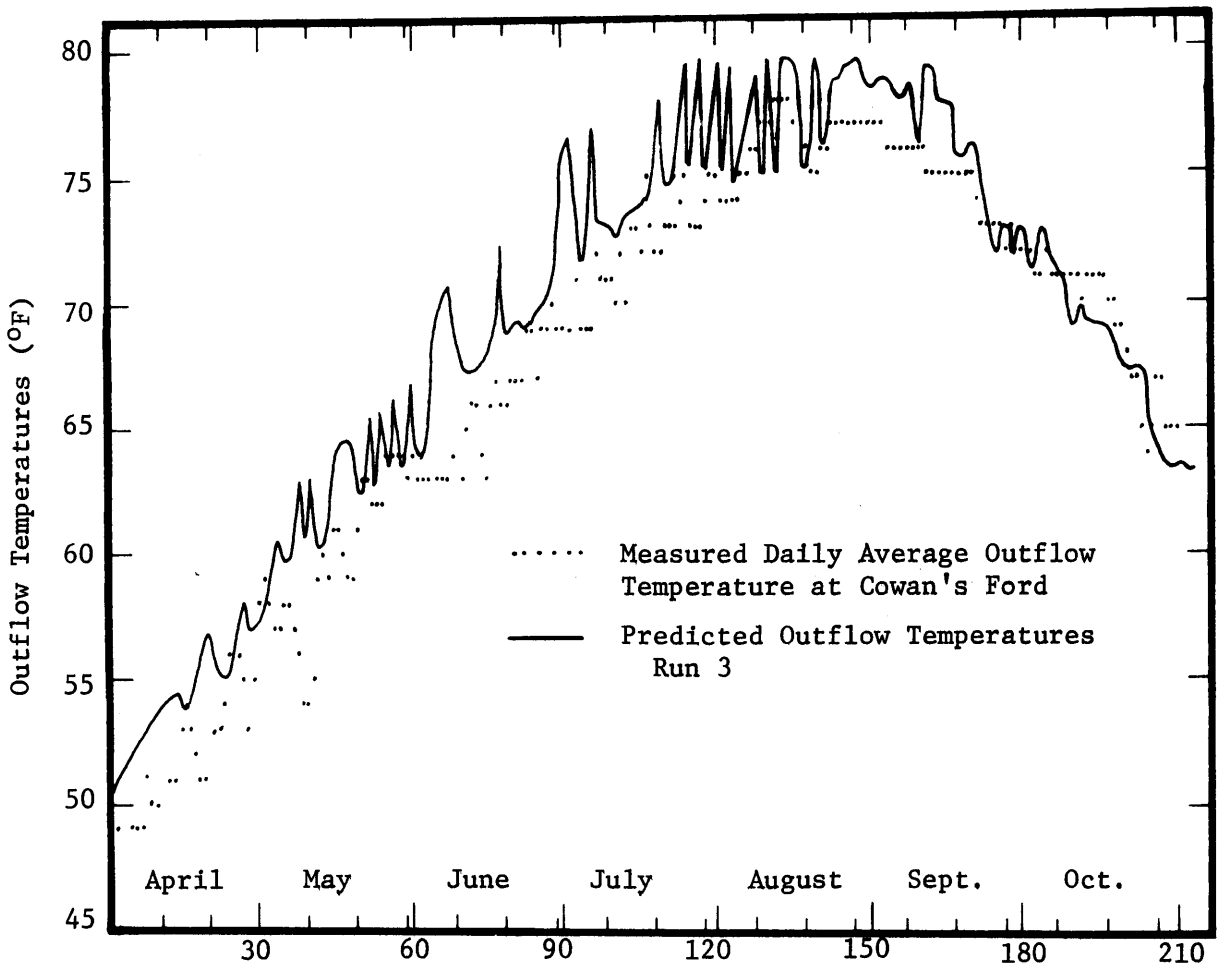

Figure 8-19 Predicted vs. Measured Outflow Temperatures at Cowan's Ford Hydroelectric Station, 1969

temperatures is probably due to different measurement times, and wind tilting of the isotherms, rather than the Marshall thermal plume.

Figures 8-20 and 8-21 show four profiles for 1971. Note that the predicted May profile in Figure 8-20 exhibits the shallow warm epilimnion which is not observed in the field, showing that wind effects in late spring are not simulated correctly. All the other profiles show a striking resemblance in that the predicted profile is in good agreement above the Marshall intake level, and shows poor agreement below this level. It was observed that the near bottom measured temperatures increased rather quickly during April, May and June, and then remained essentially constant. No satisfactory explanation is available. Predicted bottom temperatures can be increased by increasing the thickness of the stream inflow layer, or including the effect of turbulent diffusion. The former is reasonable because of the intermittent nature of the upstream hydroelectric plant, but the increase in thickness required to cause sufficient temperature rise was not considered realistic. Turbulent diffusion does improve the results, but a constant coefficient caused too little increase in the first few months, and far too high an increase in later months. Finally it was decided that it was better to keep the predictive form of the model, and accept the errors in the bottom temperatures, particularly since the agreement for the important variable, the intake temperature, is quite satisfactory.

8.3.5 Summary

The mathematical model has been tested against three years of

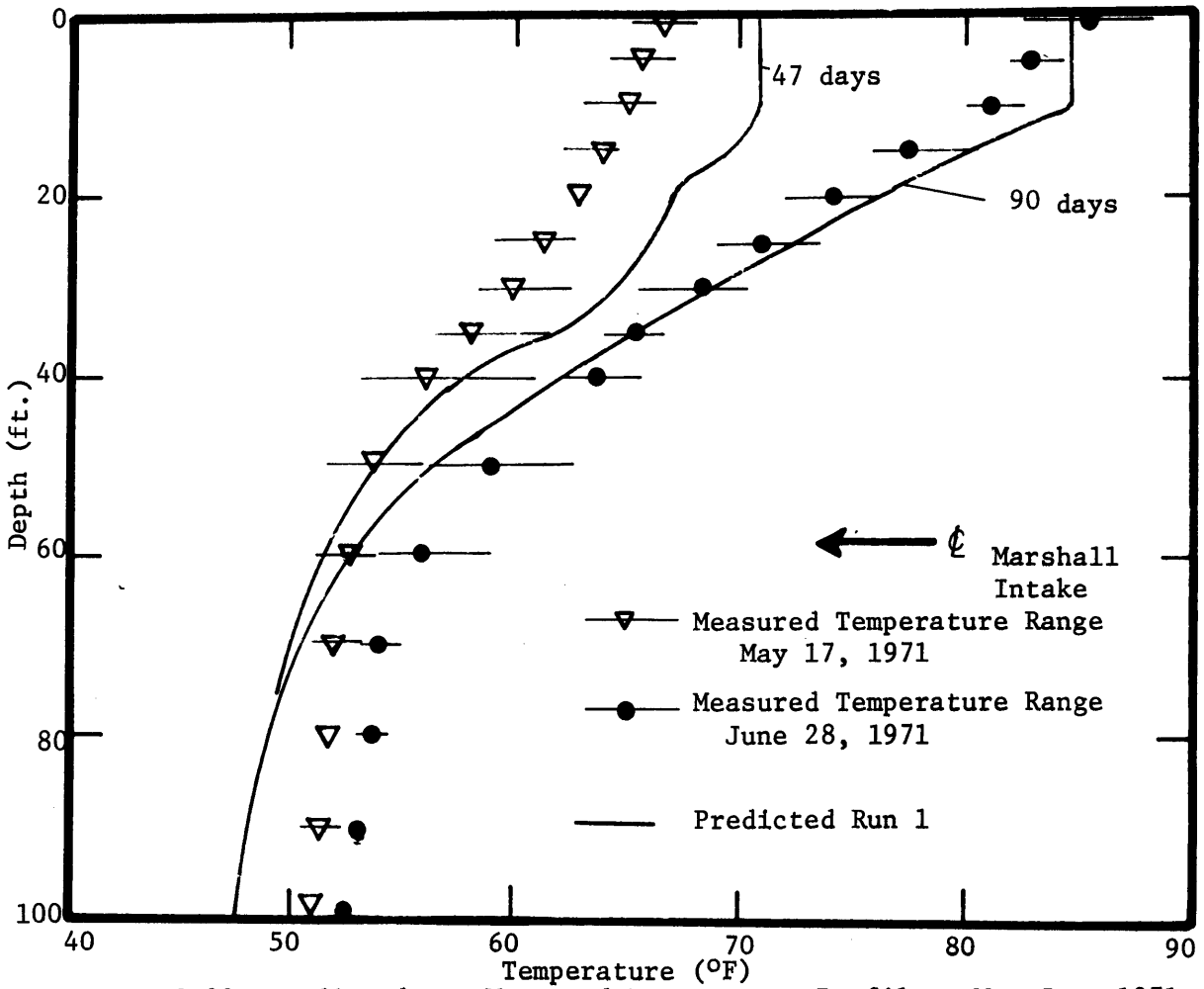

Figure 8-20 Predicted vs. Measured Temperature Profiles, May-June 1971

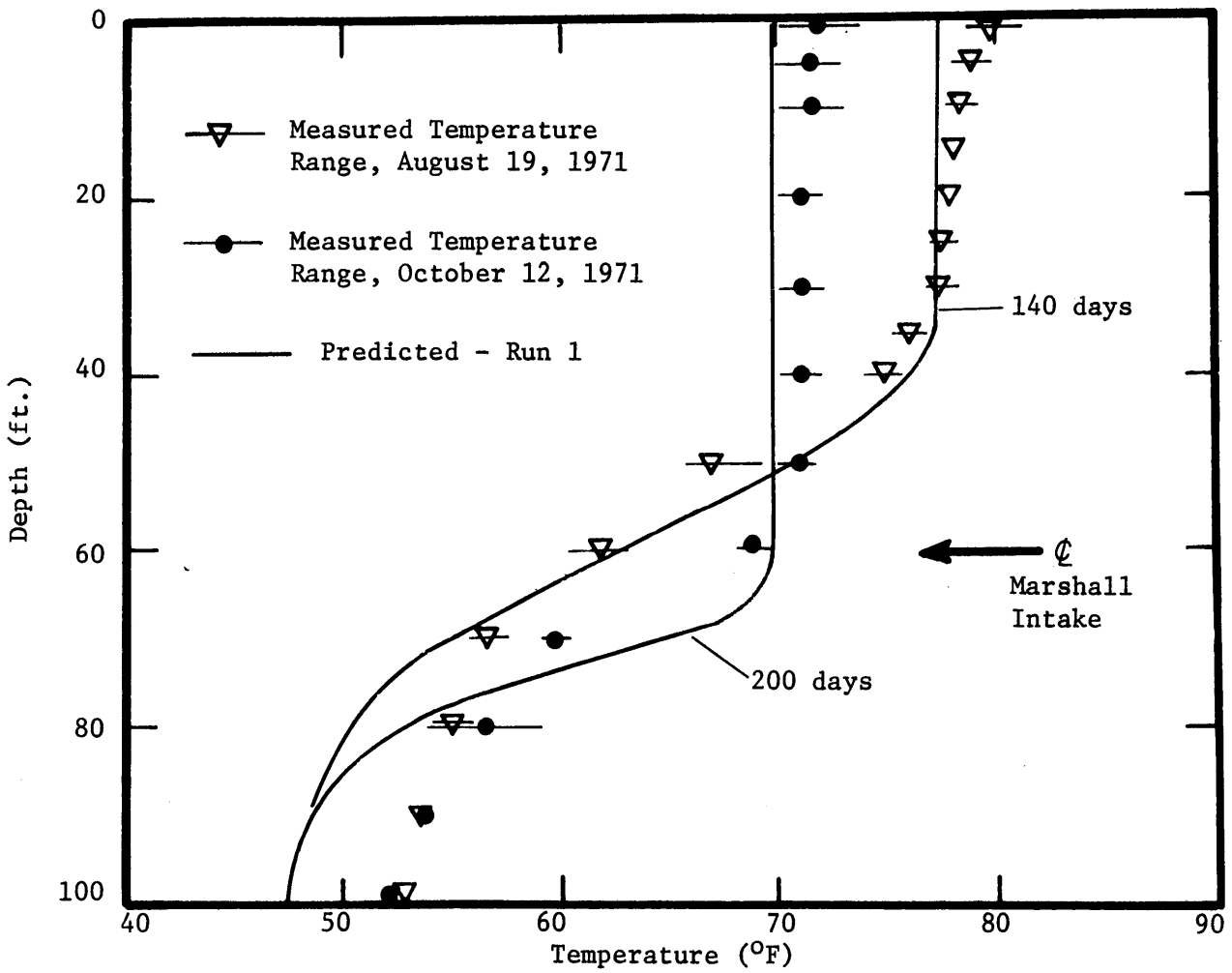

Figure 8-21 Predicted vs. Measured Temperature Profiles, August-October 1971

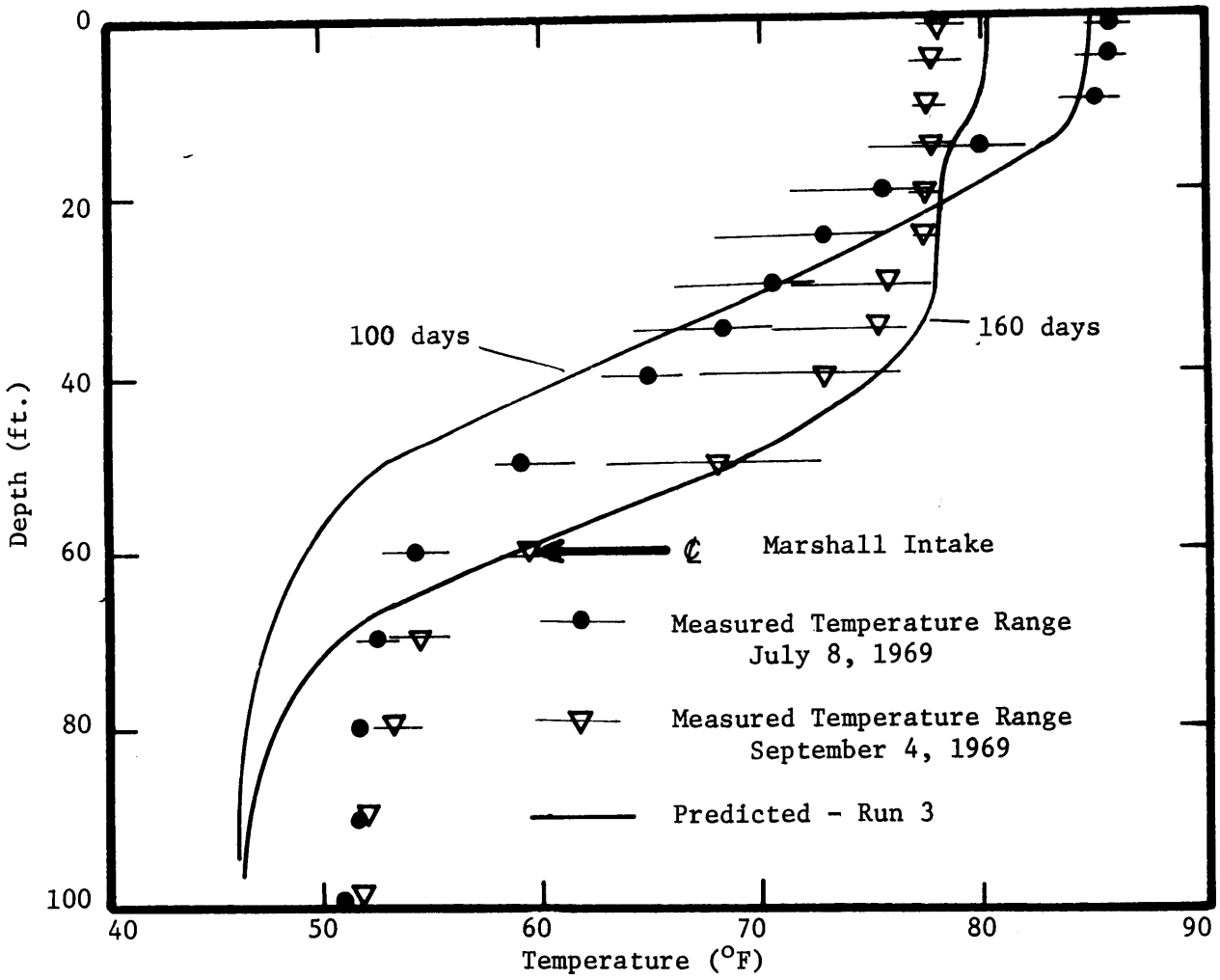

Figure 8-22 Predicted vs. Measured Temperature Profiles - 1969

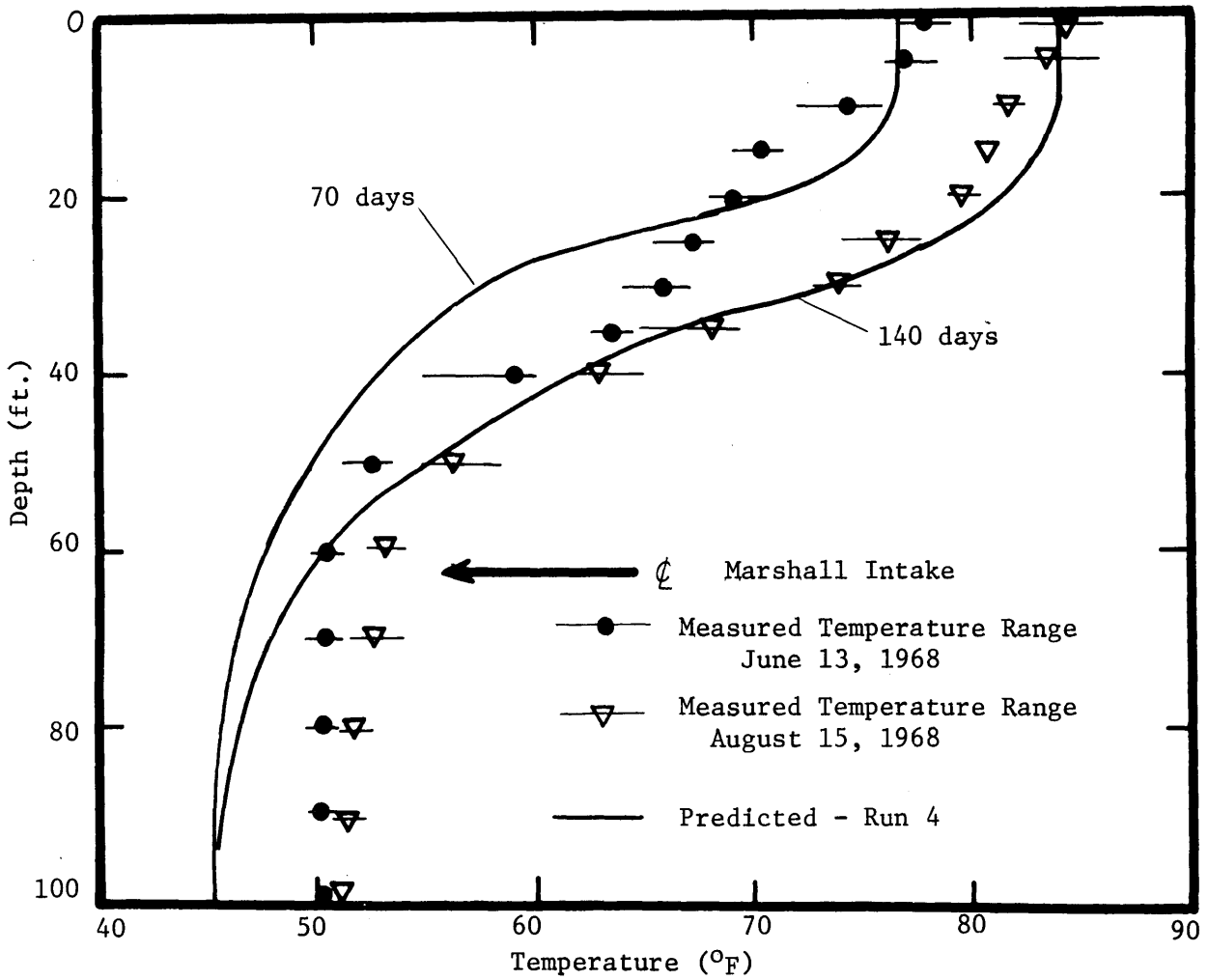

Figure 8-23 Predicted vs. Measured Temperature Profiles - Lake Norman 1968

data from Lake Norman, North Carolina, which serves both as a cooling pond for the Marshall Steam Plant (2136 Mw_e) and as a hydropower reservoir via the Cowans Ford Hydroelectric Station (370 Mw_e). It was found that the method of operation of the hydroplant had a significant influence on the predicted intake temperature for Marshall. In 1971 with Marshall at full capacity, the effect on the predicted intake temperature for Marshall of the method of operation of the hydroplant was $\sim 3^{o}F$. Using operating figures supplied by Duke Power for 1971, and design operation figures for 1968 and 1969, excellent agreement between measured and predicted intake temperatures for Marshall were obtained. Predicted outflow temperatures through the Cowans Ford turbines, and temperature profiles above the Marshall intake were satisfactory. Temperature profiles below the intake (about 5% of the lake volume) were poor. Methods for improving agreement here were discussed, but were rejected on the grounds that they detract from the predictive nature of the model.

The execution time for 214 days on an IBM 370/155 computer was approximately 30 seconds.

8.4 Conclusion

The mathematical model has been extensively field tested, using 2 years of data from a heavily loaded artificial pond (Hazelwood, Australia) and 3 years of data from a lightly loaded natural pond (Lake Norman, North Carolina). The results obtained were very satisfactory, with daily average intake temperatures usually predicted within $2^{o}F$. For the Hazelwood case, and for one year (1971) at Lake

Norman, the discharge temperature was calculated within the model, and only the condenser temperature rise was specified, i.e., only information, such as would be available on a proposed cooling pond, was used. Predicted surface temperature distribution, vertical profiles, near surface outflow temperatures and skimmer wall performance were all checked against field data with generally satisfactory results. In cases where input data or model parameters were not known with sufficient accuracy, the sensitivity of the model to the data or parameter was checked. The transient response of the model was good, except at early times when the effect of the simple treatment of the surface layer was apparent. The only obvious failure of the model was in predicting the heat transport to the region below the intake in Lake Norman, and from the point of view of the cooling capacity of the lake the volume of water in this region (5% of total volume) is not really significant.

IX. Summary and Conclusions

9.1 Objectives

If land is available cooling ponds offer many advantages as a means of closed cycle heat dissipation. These are simplicity, low maintenance and power requirements, aesthetic and possible recreational values, and high thermal inertia. A cooling pond is also subject to minimal environmental problems, since fogging tends to be localized, blowdown water can be stored for long periods, and make-up water requirements are intermittent and often lower than for other closed systems. In spite of the above advantages it is presently estimated that less than one-third of the closed cycle power stations, built in the next 30 years, will utilize cooling ponds. One reason for this is lack of land, but another reason is the lack of confidence in the ability to predict cooling pond performance under transient heat loads and meteorological conditions. The use of simple steady state models and various commonly used assumptions as to surface heat loss and circulation patterns can lead to differences of at least 100% in the required land area. This uncertainty leads to the use of conservative rules of thumb, such as 2 acres/MW_e, and often results in the rejection of the cooling pond alternative, which may be a mistake from economic, aesthetic and environmental considerations.

The guiding principle of this investigation is that a cooling pond can be designed on a rational basis to perform in a certain way. This cannot be done, however, until the desired pond behavior is first clearly defined, until the important mechanisms of heat transfer both

within the pond itself, and at the water surface, have been isolated and qualified, and until the transient response of the pond is known. The objectives of this study were therefore:

a) To determine the characteristics of an efficient cooling pond.

b) To examine the role, in such a pond, of factors such as entrance mixing, density currents, pond shape, internal diking and design and location of intake and outlet.

c) To examine the transient response of the pond to changes in the boundary conditions.

d) To critically examine the various surface heat loss formulae, and test them against the best available field data.

e) To develop a relatively simple, predictive, transient mathematical model for an efficient pond which will include the effects of all the significant parameters. The model should have the ability to simulate multiple inflows and outflows so that it is also applicable to a multi-purpose reservoir used as a cooling pond.

9.2 Surface Heat Loss

The various components of heat transfer at a water surface have been discussed, and where possible existing empirical formulae have been selected for use in this study. Existing formulae for predicting evaporative flux from an artificially heated water surface were found to be unsatisfactory. Field data indicates that a commonly used formula such as that of Brady (1969) may predict evaporative losses that are too

low by as much as 50% for a heavily loaded water surface. A new formula, Equation (2.35) has been proposed. The proposed formula, a modified form of that given by Shulyakovskiy (1969), explicitly accounts for mass transfer due to free convection, which can be very significant at low windspeeds. The formula is (in heat units)

$$\phi_e = [22.4(\Delta\Theta_v)^{1/3} + 14W_2][e_s - e_a] \qquad (2.35)$$

where ϕ_e = evaporative flux (Btu/ft^2/day)

$\Delta\Theta_v$ = virtual temperature difference (^{o}F) between the water surface and the air at 6.5 ft(2m.)

W_2 = wind speed in mph at 6.5 ft(2m.)

e_a = vapor pressure in mmHg at 6.5 ft(2m.)

e_s = saturation vapor pressure at the temperature of the water surface

The above formula has been shown to apply in the laboratory ($W_2 = 0$) and has been tested against a wide variety of field data with consistently good results. A heat exchange coefficient, K(Btu/ft^2/hr/^{o}F), has been defined which incorporates Equation (2.35) and charts are given relating K to meteorological parameters. This linear version of the surface heat loss formulae has been tested against additional field data.

9.3 Laboratory and Field Behavior

An efficient or ideal pond has been defined in terms of maximum surface heat transfer, and maximum response time. Maximum surface heat

transfer results from a surface that is as hot as possible and this requires a minimum of mixing at the entrance to the pond. Maximum response time to meteorological or operating fluctuations (thermal inertia) results from a large supply of cool water. This requires that the hot surface layer be as thin as possible and that the colder bottom water be selectively withdrawn. Thus the ideal pond is relatively deep, stratified, with minimal entrance mixing, and an effective skimmer wall type intake. This type of pond was examined in the laboratory. Boundary conditions such as pond geometry, discharge design and heat loading were varied in a systematic fashion. The emphasis was on determining the effect of entrance mixing and density currents on both the steady state and transient behavior of the pond. Where possible the laboratory results were supported by field observations. The conclusions from laboratory and field observations on ponds with the characteristics of an ideal pond are:

a) Horizontal temperature gradients are generally limited to a relatively thin surface layer (< 10'). The thickness of this layer is governed primarily by the discharge conditions. Under the surface layer, temperature gradients exist only in the vertical direction.

b) Entrance mixing has a significant effect on pond performance, the smaller the mixing, the more efficient the pond. This applies to all ponds regardless of depth.

c) Density currents are of paramount importance in the distribution of heated water into the backwater areas of the pond. As long as the internal densimetric Froude No. F_i of the flow in these areas is

less than 0.2, the effective area ratio of the pond will be close to unity. F_i is given by

$$F_i = \frac{2q}{H\sqrt{g\Delta\rho/\rho H}}$$

where q = flow/unit width

H = depth of backwater region

d) The shape of a stratified pond is important primarily from the point of view of entrance mixing effects and shortcircuiting, and both these effects can be minimized by good design. Thus it can be said that the performance of a well designed, stratified, cooling pond is independent of shape.

e) A deep, skimmer type intake can prevent shortcircuiting, except under unfavorable wind conditions. It also improves the transient response of the pond and enhances the effects of density currents.

f) The response of a pond can be approximately described by a time constant equal to the pond residence time.

g) Wind effects are important from the point of view of the heat transfer coefficient, inhibition of density currents by vertical mixing, reduction in active area and possible short circuiting.

9.4 Development of Predictive Analytical Models - Steady State and Transient

Existing analytical models are steady state, one-dimensional, and based on the extreme concepts of plug flow or complete mixing. These models are usually not predictive and require a fitting parameter such

as "effective area" to match observed results. The concept of "effective area" and some methods for its determination have been discussed. It was concluded that effective area usually does not have a physical basis, but merely represents a fitting parameter which accounts for the neglect of entrance mixing and inaccurate surface heat transfer. The need exists for analytical models that are both predictive and transient.

a) Some simple steady state analytical models have been proposed which consider the effect of entrance mixing, and these models include the plug flow and fully mixed ponds as special cases. The entrance mixing factor can be determined a priori from known pond parameters, and thus these proposed models, although highly idealized, and limited to the steady state case, are predictive. The most satisfactory model is described by the equation

$$\frac{T_i - T_E}{T_o - T_E} = \frac{e^{-r/D_s}}{D_s - (D_s - 1)e^{-r/D_s}} \tag{3.10}$$

where $r = \frac{KA_P}{\rho c Q_o}$

A_P = pond surface area

Q_o = condenser flow rate

K = heat transfer coefficient (see Figures 2-20 to 2-22)

$D_s = 1.4\sqrt{1+F_D^2}(A_D)^{1/4}$ (Equation 6.37)

F_D, A_D = densimetric Froude No. and aspect ratio of the discharge

T_E = equilibrium temperature

The entrance mixing models were tested against laboratory and field data, and performed better than the usual plug flow or fully mixed models.

b) The ideal cooling pond, defined as a deep stratified pond, with low entrance mixing, and a deep skimmer type intake, was shown to have temperature variations both in the horizontal and vertical plane. A realistic model of this type of pond must include horizontal variations in order to simulate heat loss correctly, and must include vertical variations in order to reproduce the transient response of the pond, i.e. a three dimensional model is required. Fortunately, the type of structure observed, and the significant role of density currents in an ideal type pond, make possible the use of two assumptions which greatly simplify the necessary mathematical model. The assumptions are:

(i) It is assumed that the cooling pond can be divided into two separate regions, a relatively thin vertically mixed surface layer, with temperature variations only in the horizontal plane, and a relatively deep sub-surface layer with temperature variations only in the vertical direction.

(ii) It is assumed that, due to the influence of density currents, the performance of the cooling pond is independent of the shape of the surface layer.

The effect of the above assumptions is to reduce the cooling pond to a series of regions where the temperature is a function of only one spatial parameter (area in the surface layer and depth in the sub-surface region). A relatively simple transient mathematical model was developed,

incorporating the above assumptions. Important aspects of the mathematical model are:

(i) The cooling pond was subdivided into five regions including an outlet channel, an entrance mixing region, a heat loss region, a sub-surface region and an intake pond.

(ii) A simplified form of the Stolzenbach-Harleman surface jet model (reference No. 116) was used to calculate the dilution in the entrance mixing region. The simplified model was tested in the laboratory over a wide range of outlet conditions, with generally good results.

(iii) The MIT deep reservoir model (57, 107) was used to simulate the sub-surface region.

(iv) The proposed evaporation (2.35) equation was used to calculate surface heat loss.

(v) The model predicts the transient surface temperature distribution $T(A_x,t)$, the transient vertical temperature distribution $T(z,t)$, and the transient intake temperature $T_i(t)$. The model can handle multiple inflows, each inflow being treated separately, and can predict individual outflow temperatures, $T_{os}(t)$, for multiple outflows.

(vi) The model can be used as a predictive tool, requiring as input only such information as is available before a pond is constructed.

9.5 Results for Transient Cases

The mathematical model was tested against the laboratory cooling pond, against 2 years of data on a moderately heavily loaded artificial cooling pond, (Hazelwood, Aust., 1250 acres, 800-1400 Mw_e), and against 3 years of data on a lightly loaded natural pond with multiple inflows and outflows, (Lake Norman, N.C., 32500 acres, 2136 MW_e (thermal), 370 MW_e (hydro)). The Hazelwood data is probably the best cooling pond data available. The most important parameter, transient intake temperature, showed good to excellent agreement in both the laboratory and field cases. Predicted surface temperature distribution was good for the laboratory case except for early times, but was only fair for the field case. Predicted transient vertical temperature profiles were fair to good both in the laboratory and the field, with the exception of the predicted profiles below the intake level in Lake Norman. Predicted outflow temperatures through the Cowans Ford Hydroelectric Station in Lake Norman were satisfactory, and reasonable agreement was obtained between the predicted and observed skimmer wall behaviour in Hazelwood.

On the basis of extensive laboratory tests, and 5 years of field data on two widely different cooling ponds, it is concluded that the mathematical model can predict daily average intake temperatures within $2^{o}F$ for a very large percentage of the time. The mathematical model is inexpensive to run, with an execution time of less than one minute on an IBM 370/155, for a model time of 1 year, using time increments of 1 day.

X. Cooling Pond Design Considerations and Future Research

10.1 Cooling Pond Design

The design of a cooling pond has been called an art rather than a science, because many of the factors that affect pond performance are so variable, and so peculiar to the individual situation (23). Decisions have to be made as to the pond area and depth, the type and location of the outlet and intake structures, the use of internal diking, the critical design period and the design method itself. These decisions will be briefly discussed.

a) Design Method - Physical and Analytical Models

Physical modeling of cooling pond behavior requires that similarity requirements for jet mixing, stratified flows, and surface heat loss all be satisfied along with the Froude and Reynolds criteria. It has been shown in Chapter V that each similarity requirement imposes its own distortion ratio, which ranges from no distortion for jet mixing, to 2-1/2 to 5 for surface heat loss, to 5-10 for stratified flow, to 5-15 for Reynolds effects. Obviously a problem exists as it is impossible to satisfy all these criteria simultaneously. It is strongly recommended that hydrothermal models not be used as the primary basis for cooling pond design. This does not rule out their use in examining local effects (e.g. using an undistorted model to examine the jet mixing at the outlet, or a distorted model to determine the effectiveness of a skimmer wall). Physical models may also be useful to compare qualitatively the effects of different internal dike arrangements, but it is felt that the use of hydrothermal models to predict intake temperatures may give very mislead-

ing results. Analytical models have their shortcomings, but they have the advantages of directly including the effects of surface heat loss, and can account for the different flow regimes in a cooling pond without the contradictions inherent in a physical model.

b) Choice of Pond Area and Depth

The design of a cooling pond usually reduces to the selection of the required area to dissipate the waste heat under critical operating and meteorological conditions, in order to meet constraints imposed by environmental factors (e.g. area under a specified isotherm), or by economic factors (e.g. turbine backpressure). The required area is affected by the depth which controls the pond's transient response and hence the length and severity of the critical design period, e.g. the "worst" day will be considerably more severe than the "worst" week. The depth may also affect the density current behavior, and hence even the steady state performance. The effective depth is in turn affected by the type of intake. A bottom, skimmer wall intake located in the deepest region in the pond will give best results, eliminating the effects of diurnal meteorological, and other short-term loading fluctuations.

An obvious economic trade-off exists between the area (initial cost) of a pond and the intake temperature (turbine back pressure, station efficiency) but a small, heavily loaded pond has advantages in addition to its lower initial cost.

(i) The heat transfer efficiency increases markedly at higher temperatures.

(ii) Less make-up water is required. The proportion of the waste heat dissipated by evaporation increases slightly

with increasing heat load (water temperature), but this is more than offset by the reduced natural evaporative losses due to the decrease in pond size.

(iii) Higher loading will promote stratification and ensure a fully active surface area.

c) Transient Behavior

Existing analytical design methods usually involve a steady state approach and assumed critical loading and meteorological conditions. As pointed out above, it is essential, if using this approach, to relate the length of the critical design period to the pond response time. However, it is felt that this approach is not really adequate, and the following approach is recommended:

(i) Choose several sets of feasible design parameters, such as area, depth and condenser water temperature rise, using the steady state approach and taking into account site considerations.

(ii) Examine the behavior of each feasible pond over a typical year using daily input data in the transient model, and generate a frequency distribution curve for the intake temperatures of each pond. Make-up water requirements for each pond should also be calculated.

(iii) Select the most promising designs and examine the pond behavior over a long period of time, such as the life of the plant (30 years). Using either

historical or synthetic meteorological data, and synthetic operating data, one could generate a statistically valid frequency distribution curve for the intake temperatures, which would be a far more realistic way of comparing a cooling pond with other cooling ponds or cooling towers. Costs for this approach need not be excessive (~$5 per simulated year).

d) Internal Diking

The traditional rationale for the use of internal diking is to increase the effective surface area of the pond by forcing pumping currents into well defined flow paths in order to eliminate stagnant or backwater areas. It has been shown, at least for moderately deep ponds (average depth > 15'), that this can be done far more simply by correctly designing the outlet and intake to achieve vertical stratification, thereby making use of density currents to distribute heat into backwater areas. Internal diking may be necessary to prevent short circuiting under unfavorable wind conditions, which could tilt the thermocline and force warm surface water through a skimmer wall opening. Usually, the length of diking necessary to prevent this type of short circuiting will be relatively short in comparison with the traditional diking pattern, designed to produce a long flow path for the pumping currents. If diking is necessary, it is important to avoid sudden contractions and expansions in the flow path, since these may promote internal mixing and destroy vertical stratification.

e) Design and Location of Outlet and Intake

The outlet should be designed so that the discharge densimetric Froude number based on the exit depth is approximately 0.5. This ensures a cold wedge in the outlet channel thus minimizing mixing at the exit, but at the same time restricts the length of the wedge. This ensures that the cold water does not penetrate to the plant end of the outlet channel where considerable mixing with the flow exiting from the condensers could occur. A short wedge length also restricts interfacial mixing in the outlet channel itself. The aspect ratio (depth/halfwidth) of the channel should be as low as possible (< 0.1).

The intake skimmer wall should be located in the deepest section of the pond. This minimizes the possibility of short circuiting, and insures that full use is made of the pond's cooling capacity (i.e. the thermal inertia of the pond is as large as possible). A problem exists here, as much of the benefit of a skimmer wall intake is lost if the intake pond behind the skimmer wall is too large, i.e. if the residence time of the intake pond is greater than a few hours. A possible solution is to use the selective withdrawal pipe described by Makarov (1972).

10.2 Future Work

The following aspects of cooling pond behavior need additional study:

a) Density Currents in Shallow Ponds: The role of density currents in shallow ponds needs to be examined in detail. It appears that density flows into stagnant areas are not inhibited when the internal densimetric Froude

No. F_i (see Section 4.4.3) is less than 0.2. However, it is not clear at what stage inhibition of the density flows significantly affects the pond heat loss efficiency.

b) Surface Intakes: The effect of a near surface intake on the role of density currents, and on the pond transient response, should be examined, since some ponds are not deep enough for an effective skimmer wall.

c) Low Froude No., Low Aspect Ratio Outlets: The behavior of low Froude No. ($F_D = 1$), low aspect ratio ($A_D << 1$) heated surface discharges should be examined in detail, including the effect of a stratified receiving water.

d) Buoyancy Effects on Forced Convective Heat Transfer Above a Horizontal Surface in the Turbulent Range: Some basic data on this problem is essential to the solution of mass transfer above a heavily loaded cooling pond. Both laboratory and field data are essential here.

e) Mathematical Model with Two-Dimensional Surface Layer: The mathematical model presented in this report specifies the area under a given surface isotherm, but does not give the temperature at a given point on the surface. In some cases this latter information may be of interest, and a mathematical model which solves the two-dimensional equations of conservation of momentum and heat in the surface layer would be of considerable value.

BIBLIOGRAPHY

1. Ackers, P., "Modelling of Heated Water Discharges", Ch. 6, Engineering Aspects of Thermal Pollution, Parker and Krenbel (Ed.), Vanderbilt University Press, 1969

2. AEC Report, "Heated Discharges - State of the Art", Report to AEC by Vanderbilt University, 1973

3. Anderson, E.R., "Energy Budget Studies", part of "Water Loss Investigations--Lake Hefner Studies", Technical Report, U.S.G.S. Prof. Paper 269, 1954

4. Angstrom, A., "The Study of Radiation of the Atmosphere", Smithsonian Institute, Misc. Coll. 65 (3) 1918

5. Asbury, J.G., "Effects of Thermal Discharges on the Mass/Energy Balance of Lake Michigan", Argonne National Laboratory, Report No. Es-1, July, 1970

6. Averkiev, A.G., Makarov, I.I. and Kind, K.Y., "Heat Transfer in a Cooling Pond", 14th Congress, I.A.H.R., Paris, September 1971

7. Bella, D.A. and Dobbins, W.E., "Difference Modelling of Stream Pollution", Proc. ASCE, SA5, October 1968

8. Berman, L.D., Evaporative Cooling of Circulating Water, Pergamon Press, 1961

9. Bird, R.B., Stewart, W.E. and Lightfoot, E.N., "Transport Phenomena", John Wiley & Sons, 1965

10. Bolz, R.E. and Tuve, G.E., "Handbook of Tables for Applied Engineering Science", Published by the Chemical Rubber Company, 1970

11. Bowen, I.S., "The Ratio of Heat Losses by Conduction and by Evaporation from Air Water Surface", Physical Review, Volume 27, 1926

12. Brady, D.K., Graves, W.L. and Geyer, J.C., "Surface Heat Exchange at Power Plant Cooling Lakes", Cooling Water Studies for Edison Electric Institute, Report No. 5, Johns Hopkins University, November 1969

13. Braslovskii, A.P. and Shergina, K.B., "Water Losses by Evaporation from Reservoirs in the Arid Zone of Kazakhstan. Izd", Nauka, Alma, Ata, 1965

14. Braslovskii, A.P. and Nurgaliev, S.N., Vyp. 4, 1966

15. Brooks, N.H. and Koh, R.C.Y., "Selective Withdrawal from Density Stratified Reservoirs", ASCE Specialty Conference on Current Research into the Effects of Reservoirs on Water Quality, Portland, Oregon, January 1968

16. Brown, F.S., "Waste Heat Disposal from Power Generating Stations", Proc. ASCE, PO3, June 1970

17. Brunt, D., "Notes on Radiation in the Atmosphere", Quart. Jour. Roy. Met. Soc., 58, 1932

18. Budyko, M., Beryland, T., Zubenok, L.-Izv., Akad, Nauk SSSR, Ser. Georgr., No. 3, 17-41, 1955

19. Buettner, K. and Kern, C., "Determination of Infrared Emissivities of Terrestrial Surfaces", Jour. Geophys. Res., Vol. 70, No. 6, March 15, 1965

20. Carter, H.H., "A Preliminary Report on the Characteristics of a Heated Jet Discharged Horizontally into a Transverse Current: Part I Constant Depth", Technical Report No. 61, Chesapeake Bay Institute, the Johns Hopkins University, November 1969

21. Christianson, A.G. and Tichenor, B.A., "Economic Aspects of Thermal Pollution Control in the Electric Power Industry", FWPCA Working Paper No. 67, September 1969

22. Committee on Power Plant Siting, National Academy of Engineering, "Engineering for Resolution of the Energy - Environment Dilemma", National Academy of Sciences Congress Catalog Card No. 79-186370 ISBN 0-309-01943-5, 1972

23. Cotter, T.J. and Lotz, R.W., "Cooling Pond Design in the Southwest", Journal of the Power Division, ASCE, 87, July 1961

24. Curtis, R.P., "Hazelwood Cooling Pond--A Method for Estimating the Effect of Thermal Density Currents on Performance", Engineering Study Report (Preliminary), State Electricity Commission of Victoria, 1966

25. Crawford, T.V., "Moisture Transfer in Free and Forced Convection", Quart. Jour. Roy. Met. Soc., Vol. 91, No. 387, 1965

26. Dake, J.M.K. and Harleman, D.R.F., "Thermal Stratification in Lakes, Analytical and Laboratory Studies", Water Resources Research, Vol. 5, No. 2, April 1969

27. Debler, W.R., "Stratified Flow in a Line Sink", Proc. ASCE, Engineering Science Division, EM3, July 1959

28. Dyer, A.J., "The Turbulent Transport of Heat and Water Vapour in an Unstable Atmosphere", Quart. Jour. Roy. Met. Soc., 93, 1967

29. Edinger, J.R. and Geyer, J.C., "Cooling Water Studies for Edison Electric Institute, Project No. RP-49--Heat Exchange in the Environment", The Johns Hopkins University, June 1, 1965

30. Edinger, J.E., "Shape Factors for Cooling Lakes", J. of Power Division, ASCE, Vol. 97, No. PO4, December 1971

31. Elder, R.A. and Wunderlich, W.O., "Evaluation of Fontana Reservoir Field Measurements", ASCE Specialty Conference on Current Research into the Effects of Reservoirs on Water Quality, Portland, Oregon, January 1968

32. Elder, R.A. and Wunderlich, W.O., "Inflow Density Currents in TVA Reservoirs", to be presented at International Symposium on Stratified Flows, Novosibirsk, 1972

33. Electrical World (1972), "23rd Annual Electrical Industry Forecast" by L.M. Olmsted, September 15, 1972, and "1972 Annual Statistical Report", March 15, 1972

34. Ellis, W.R., et. al., "The Use of a Radioactive Tracer (Iodine 131) in the Investigation of a Power Station Cooling Pond at Maitland, N.S.W.", Australian Atomic Energy Commission Report AAEC/E8, September 1958

35. Ellis, W.R., et. al., "A Power Station Cooling Pond Performance Test with Radioactive Tracer Iodine 131, Second Experiment at Maitland, N.S.W.", Australian Atomic Energy Commission Report AAEC/E51, April 1961

36. Ellison, T.H. and Turner, J.S., "Turbulent Entrainment in Stratified Flows", Jour. of Fluid Mech., Vol. 6, Part 3, October 1959

37. Federal Water Quality Administration, U.S. Dept. of Interior, "Feasibility of Alternative Means of Cooling for Thermal Power Plants Near Lake Michigan", August 1970

38. Fishenden, M. and Saunders, D.A., "An Introduction to Heat Transfer", Clarendon Press, 1950

39. Garrison, J.M. and Elder, R.A., "A Verified Rational Approach to the Prediction of Open Channel Water Temperatures", Proc. 11th Congress IAHR, Leningrad, 1965

40. Gates, D.M., "Radiant Energy, its Receipt and Disposal", Agricultural Meteorology, Met. Monogr., 28, Am. Met. Soc., Boston, 1965

41. Geiger, R., "The Climate Near the Ground", Harvard University Press, Cambridge, Massachusetts 1965

42. Georgiev, B. and Monev, E., "Measurements of Large Scale Circulation in a Cooling Reservoir by Means of Radioisotopes", IAHR Intern. Sym. on Stratified Flows, Novosibirsk, 1972

43. Goda, T., "Density Currents in an Impounding Reservoir", Eighth Congress, IAHR, 1959

44. Hamon, R.W., Weiss, L.L., Wilson, W.T., "Insolation as an Empirical Function of Daily Sunshine Duration", Monthly Weather Review, Vol. 82, No. 6, June 1954

45. Harbeck, G.E., et. al., "The Effect of the Addition of Heat from a Nuclear Power Plant on the Thermal Structure and Evaporation of Lake Colorado City, Texas", U.S. Geological Survey Professional Paper 272-B, 1959

46. Harleman, D.R.F., "Stratified Flow", Handbook of Fluid Dynamics, Section 26, McGraw-Hill Book Company, 1961

47. Harleman, D.R.F. and Elder, R.A., "Withdrawal from Two Layer Stratified Flows", Proc. ASCE, HY 4, Vol. 91, July 1965

48. Harleman, D.R.F., "Diffusion Processes in Stratified Flow", Chapter 12, Estuary and Coastline Hydrodynamics, A. T. Ippen, Ed., McGraw-Hill Book Company, New York, 1966

49. Harleman, D.R.F., Ch. 8: "Longitudinal Temperature Distributions in Rivers and Estuaries : One Dimensional Mathematical Models", Engineering Aspects of Heat Disposal from Power Generation, (D.R.F. Harleman, Ed.), R. M. Parsons Laboratory for Water Resources and Hydrodynamics, Department of Civil Engineering, MIT, Cambridge, Massachusetts, June 1971

50. Harleman, D.R.F. and Stolzenbach, K.D., "Fluid Mechanics of Heat Disposal from Power Generation", Annual Review of Fluid Mechanics, Vol. 4, 1972

51. Hauser, L.G., "Cooling Water Requirements for the Growing Thermal Generation Additions of the Electric Utility Industry", American Power Conference, April 1969

52. Hickok, G.H., "Evaporation from a Free Water Surface", ASCE Trans., Vol. III, Paper 2266, 1946

53. Hogan, W.T., Liepins, A.A., Reed, F.E., "An Engineering-Economic Study of Cooling Pond Performance", Littleton Research and Engineering Corp., Report G-179 to FWQA, May 1970

54. Hoopes, J.A., Zeller, R.W. and Rohlich, G.A., "Heat Dissipation and Induced Circulations from Condenser Cooling Water Discharges into Lake Monona, Report No. 35, Dept. of Civil Eng., University of Wisconsin, 1968

55. Hounam, C.E., "Estimates of Solar Radiation over Australia", Aust. Met. Mag. No. 43, December 1963

56. Howard, C.S., "Density Currents in Lake Mead", Proc. Minnesota International Hydraulics Convention, September 1953

57. Huber, W.C. and Harleman, D.R.F., "Laboratory and Analytical Studies of Thermal Stratification of Reservoirs", MIT, Hydrodynamics Laboratory Technical Report No. 112, October 1968

58. Hutchinson, G.E., A Treatise on Limnology, Vol. 1, Wiley & Sons, 1957

59. Idso, S.B. and Jackson, R.D., "Thermal Radiation from the Atmosphere", JGR, Vol. 74, No. 23, October 1969

60. Ippen, A.T. and Harleman, D.R.F., "Steady State Characteristics of Subsurface Flow", U.S. Dept. of Commerce, NBS Circular 521, "Gravity Waves", 1952

61. Jensen, L.D. and Geyer, J.C., "An Interim Report on Environmental Responses to Thermal Discharges from Marshall Steam Station, Lake Norman, North Carolina", Report to the Duke Power Company and Edison Electric Institute, August 1971

62. Jimeson, R.M. and Adkins, G.G., "Waste Heat Disposal in Power Plants", Chemical Engineering Progress, July 1971

63. Johnson, M.N. and Likens, G.E., "Steady State Thermal Gradient in the Sediments of a Meromictic Lake", Jour. Geophys. Res., Vol. 72, No. 12, June 1967

64. Jobson, H.E., "Effect of Using Averaged Data on the Computed Evaporation", Water Resources Research, Vol. 8, No. 2, April 1972

65. Kao, T.W., "The Phenomenon of Block in Stratified Flow", J.G.R., Vol. 70, No. 4, pp. 815-822, February 1965

66. Kato, H. and Phillips, D.M., "On the Penetration of a Turbulent Layer into a Stratified Fluid", J. Fluid Mech., Vol. 37, Part 4, 1969

67. Keulegan, G.H., Estuary and Coastline Hydrodynamics (A. T. Ippen, Ed.), Chapter 11, McGraw-Hill Book Company, 1966

68. Kirkwood, J.B., et. al., "Power Station Cooling Ponds", Research Note No. 45, The Electricity Commission of New South Wales, Australia, September 1964

69. Koh, R.C.Y., "Viscous Stratified Flow Towards a Line Sink", W. M. Keck Laboratory Report KH-R-6, California Institute of Technology, 1964

70. Koh, R.C.Y., "Two Dimensional Surface Warm Jets", Proc. ASCE, HY 6, June 1971

71. Kohler, M.A., "Lake and Pan Evaporation", USGS Prof. Paper 269, 1954

72. Lamb, N., "Report on the Behavior of Power Station Cooling Ponds", Power Development Branch, Projects Division, Electricity Commission of New South Wales, Australia, July 1958

73. Langhaar, J.W., "Cooling Pond May Answer Your Water Cooling Problems", Chemical Engineering, pp. 194-195, August 1953

74. Lean, G.H. and Whillock, A.Z., "The Behavior of a Warm Water Layer Flowing Over Still Water", IAHR, 11th Congress, Leningrad, 1965

75. Levenspiel, O. and Bischoff, K.B., "Patterns of Flow in Chemical Process Vessels", Advances in Chemical Engineering, Vol. 4, New York, 1963

76. Lima, D.O., "Pond Cooling by Surface Evaporation", Power, March 1936, pp. 142-144

77. Ljatkher, V.M., "Hydrothermal Modeling and Design Flows in Cooling Systems of Thermal and Nuclear Power Plants", IAHR Int. Symp. on Stratified Flows, Novosibirsk, 1972

78. Lofquist, K., "Flow and Stress Near the Interface Between Stratified Liquids", The Physics of Fluids, Vol. 3, No. 2, March-April 1960

79. Makarov, I.I. and Zisman, S.L., "On the Peculiarities of Water Supply to Thermal and Nuclear Power Plants from Stratified Streams and Reservoirs", IAHR Int. Symp. on Stratified Flows, Novosibirsk, 1972

80. Marciano and Harbeck, "Mass Transfer Studies", Water Loss Investigations: Lake Hefner, USGS Prof. Paper 269, 1954

81. Markofsky, M., "Evaporation in the Laboratory", M.S. Thesis in Dept. of Civil Engineering, MIT, Cambridge, 1968

82. McMillan, W., "Heat Dispersal--Lake Trawsfynydd Cooling Studies", Internal Symposium on Fresh Water Biology and Electrical Power, C.E.R.L., Leatherhead, U.K. April 1971

83. Messinger, H., "Dissipation of Heat from a Thermally Loaded Stream", Art 104, USGS Prof. Paper No. 475-C, 1963

84. Meyer, A.F., "Evaporation from Lakes and Reservoirs", Published by Minnesota Resources Comm., St. Paul, Minnesota, June 1942

85. Monin, A.S. and Obukhov, A.M., "Basic Regularity in Turbulent Mixing in the Surface Layer of the Atmosphere", U.S.S.R. Acad. Sci. Works on Geophys., Met. No. 24, 1954

86. Monin, A.S. and Yaglom, A.M., "Statistical Fluid Mechanics", MIT Press, 1971

87. Morgan, D.L., Pruitt, W.O. and Lourence, F.J., "Estimation of Atmospheric Radiation", Jour. App. Met., Vol. 10, June 1971

88. Mori, Y., Journal of Heat Transfer, Vol. 82, 1961

89. Mortimer, C.H., "Water Movements in Lakes During Summer Stratification", Phil. Trans. of Royal Society of London, Vol. 236, 1952

90. Morton, F.I., "Potential Evaporation and River Basin Evaporation", Proc. ASCE, HY6, November 1965

91. Motz, L.H. and Benedict, B.A., "Heated Surface Jet Discharged into a Flowing Ambient Stream", Report No. 4, Dept. of Environmental and Water Resources Engineering, Vanderbilt University, Nashville, Tennessee, August 1970

92. Munk, W.H. and Anderson, E.R., "Notes on the Theory of the Thermocline", Jour. Mar. Res., Vol. 7, 1948

93. Orlob, G.T. and Selna, L.G., "Progress Report on Development of a Mathematical Model for Prediction of Temperatures in Deep Reservoirs--Phase 3: Castle Lake Investigation", Water Resources Engineers, Inc., Lafayette, California, January 1967

94. Orlob, G.T., "Mathematical Models for Prediction of Thermal Energy Changes in Impoundments", a Final Report to FWOA by Water Resources Engineers, Inc., December 1969

95. Pasquill, F., "Eddy Diffusion of Water Vapor and Heat Near the Ground", Roy. Soc. of London, Proceedings, Ser. A, Vol. 198, No. 1052, July 1949

96. Policastro, A.J. and Tokar, J.V., "Heated-Effluent Dispersion in Large Lakes: State-of-the-Art of Analytical Modeling", Argonne National Laboratory, ANL/ES-11, January 1972

97. Poole, H.H. and Atkins, W.R.G., "Photoelectric Measurement of Submarine Illumination Throughout the Year", Jour. Mar. Biol. Assoc., Vol. 16, 1929

98. Priestley, C.B. and Swinbank, W.C., "The Vertical Transport of Heat by Turbulence in the Atmosphere", Proc. Roy. Soc., 189, 1947

99. Pritchard, D.W., "Design and Siting Criteria for Once-Through Cooling Systems", American Institute of Chemical Engineers, 68th Annual Meeting, Houston, Texas, March 1971

100. Pruitt, W.O. and Aston, M.J., "Atmospheric and Surface Affecting Evapotranspiration", Final Rept. Task 3A99-27-005-08, Dept. Ag. Eng., Dept. Irrig., University of California, Davis 1963

101. Rider, N.E., "Eddy Diffusion of Momentum, Water Vapor, and Heat Near the Ground", Phil. Trans. Roy. Soc., A246, No. 918, 1954

102. Rigter, B. P., "Density Induced Return Currents in Outlet Channels", Proc. ASCE, HY2, February 1970

103. Rimsha, V.A. and Donchencho, R.V., "The Investigation of Heat Loss from Free Water Surfaces in Wintertime", (in Russian) Trudy Leningrad Gosub. Gidrol. Inst. 64, 1957

104. Rohwer, E., "Evaporation from Free Water Surfaces", U.S. Dept. of Agriculture, Tech. Bulletin No. 271, 1931

105. Rouse, H. and Iamandi, C., "Jet Induced Circulation and Diffusion", Proc. ASCE, HY2, March 1969

106. Ryan, P.J., "Thermal Stratification and Overturn in Lakes and Reservoirs", M. Eng. Sc. Thesis, University of Melbourne, June 1968

107. Ryan, P.J. and Harleman, D.R.F., "Prediction of the Annual Cycle of Temperature Changes in a Stratified Lake or Reservoir: Mathematical Model and User's Manual", Ralph M. Parsons Laboratory for Water Resources and Hydrodynamics, Report No. 137, MIT, 1971

108. Ryan, P.J. and Stolzenbach, K.D., Chapter 1: "Environmental Heat Transfer", Engineering Aspects of Heat Disposal from Power Generation, (D.R.F. Harleman, Ed.), Ralph M. Parsons Laboratory for Water Resources and Hydrodynamics, Dept. of Civil Eng., MIT, Cambridge, Massachusetts, June 1972

109. Saunders, P.M., "The Temperature at the Ocean-Air Interface", Jour. Atmos. Sci., Vol. 24, May 1967

110. Schiff, J.B. and Schonfeld, J.C., "Theoretical Considerations on the Motion of Salt and Fresh Water", Proc. IAHR, Minnesota, 1953

111. Shulyakovskiy, L.G., "Formula for Computing Evaporation with Allowance for Temperature of Free Water Surface", Soviet Hydrology Selected Papers, Issue No. 6, 1969

112. Slotta, L.S. and Van Dyke, P., "Numerical Simulation of the Thermal Regime in Lake Norman", Hydronautics, Inc., Technical Report 7098-1, prepared for the Duke Power Company, October 1970

113. Smith, A.A., "The Effect of Gravity Waves on the Spread of an Effluent", Eleventh Congress IAHR, Leningrad, 1965

114. Sparrow, E.M. and Minkowycz, W.J., Int. Jour. Heat Mass Transfer, Vol. 5, 1962

115. Stolzenbach, K.D. and Harleman, D.R.F., "A Model Study of Thermal Stratification Produced by Condensed Water Discharge", MIT Hydrodynamics Laboratory Report No. 107, October 1967

116. Stolzenbach, K.D. and Harleman, D.R.F., "An Analytical and Experimental Investigation of Surface Discharges of Heated Water", Technical Report No. 135, Ralph M. Parsons Laboratory for Water Resources and Hydrodynamics, Dept. of Civil Eng., MIT, February 1971

117. Stolzenbach, K.D. and Harleman, D.R.F., Chapter 10: "Physical Modelling of Heated Discharges", Engineering Aspects of Heat Disposal from Power Generation, (D.R.F. Harleman, Ed.), Ralph M. Parsons Laboratory for Water Resources and Hydrodynamics, Dept. of Civil Eng., MIT, Cambridge, Mass., June 1972

118. Stolzenbach, K.D., Adams, E.E. and Harleman, D.R.F., "A Users Manual for Three Dimensional Heated Surface Discharge Computations", Technical Report No. 156, Ralph M. Parsons Laboratory for Water Resources and Hydrodynamics, MIT, Cambridge, Massachusetts, September 1972

119. Stone, H.L. and Brian, P.L., "Numerical Solution of Convective Transport Problems", Jour. A.I.Ch.E., Vol. 9, No. 5, 1963

120. Sundaram, T.R., Rehm, R.G., Rudinger, G. and Merrit, G.E., "A Study of Some Problems on the Physical Aspects of Thermal Pollution", Cornell Aeronautical Laboratory, Inc., Report VT-2616-0-2, November 1969

121. Sundaram, T.R. and Rehm, R.G., "Formation and Maintenance of Thermoclines in Temperate Lakes", AIAA Jour., Vol. 9, 1971

122. Sundaram, T.R. and Rehm, R.G., "The Effects of Thermal Discharges on the Stratification Cycle of Lakes", AIAA Jour., Vol. 10, 1972

123. Sutton, O.G., "Convection in the Atmosphere Near the Ground", Roy. Met. Soc., Quart. Jour., Vol. 74, No. 219, 1948

124. Sutton, O.G., "The Application to Micrometeorology of the Theory of Turbulent Flow over Rough Surfaces", Quart. Jour., Roy. Met. Soc., Vol. 75, No. 326, October 1949

125. Sverdrup, H.V., "On the Evaporation from the Oceans", Jour. Mar. Research, Vol. 1, No. 1, 1937-38.

126. Sverdrup, H.U., "Oceanography for Meterorologists", George Allen and Unwin Ltd., London, 1945

127. Sweers, H.E., "Vertical Diffusivity Coefficient in Thermocline", Limnology and Oceanography, Vol. 15, No. 2, March 1970

128. Swinbank, W.C., "Longwave Radiation from Clear Skies", Quart. J. of the Roy. Met. Soc. of London, Vol. 89, July 1963

129. Thackston, E.L. and Parker, F.P., "Effect of Geographical Location on Cooling Pond Requirements and Performance", Report for Project No. 16130-FDQ-03/71 to the EPA, March 1971

130. Thompson, D.M., "Hazelwood Cooling Pond - Data Collection and Analysis of Cooling Pond Performance", Fourth Australian Conference on Hydraulics and Fluid Mechanics, Monash University, Australia, December 1971

131. Throne, R.F., "How to Predict Lake Cooling Action", Power, pp. 86-89, September 1951

132. Tichenor, B.A. and Christianson, A.G., "Cooling Pond Temperature vs. Size and Water Loss", presented at ASCE National Water Resources Engineering Meeting, Phoeniz, Arizona, January 1971

133. Tilton, L.W. and Taylor, J.K., "Accurate Representation of the Refractivity and Density of Distilled Water as a Function of Temperature", J. of Research of the U.S. National Bureau of Standards, Vol. 18, February 1937

134. Tyler, J.E., "The Secchi Disk", Limn. and Oceanography Jour., Vol. 12, No. 1, 1968

135. United States Department of the Interior, "Techniques for Infrared Survey of Sea Temperature", Bureau Circular No. 202, November 1964

136. United States Department of the Interior, "Industrial Waste Guide on Thermal Pollution", FWPCA, Corvallis, Oregon, September 1968

137. U.S.G.S., "Water Loss Investigations: Lake Hefner Studies", USGS Prof. Paper 269, 1954

138. U.S.G.S., "Water Loss Investigations: Lake Mead Studies, USGS Prof. Paper 298, 1958

139. Van Dorn, W., "Wind Stress on an Artificial Pond", J. Marine Research, Vol. 12, No. 3, 1953

140. Webb, E., "On Estimating Evaporation with a Fluctuating Bowen Ratio", Jour. Geophys. Res., Vol. 65, No. 10, October 1960

141. Webb, E., "Evaporation from Lake Eucumbene", Div. of Met. Phys., Tech. Paper No. 10, CSIRO, Australia, 1960

142. Weeks, W.F., Keeler, C.M., Parrott, W. and Levine, D., "Wintertime Dissipation of Heat From a Thermally Polluted River", Water Resources Research, Vol. 7, No. 6, December 1971

143. Wunderlich, W.O. and Fan, L.N., "Turbulent Transfer in Stratified Reservoirs", presented at 19th Annual Specialty Conference of the ASCE Hydraulics Division, Iowa, August 1971

144. Wunderlich, W. and Elder, R.A., "Mechanics of Flow Through Man-Made Lakes", presented at Symposium on Man-Made Lakes, Their Problems and Environmental Effects", May 1971, Tennessee

145. Wunderlich, W.O., "Heat and Mass Transfer Between a Water Surface and the Atmosphere", Laboratory Report No. 14, T.V.A. Engineering Laboratory, Norris, Tennessee, 1972

146. Yen, Y. and Landvatter, G.R., "Evaporation of Water into a Sub-Zero Air Stream", Water Resources Research, Vol. 6, No. 2, April 1970

147. Yih, C.S., "On the Flow of Stratified Fluids", Proc. 3rd U.S. Congress on Applied Mechanics, June 1958

148. Zaykov, B.D., "Evaporation from the Water Surface of Ponds and Small Reservoirs in the USSR", Trans. State Hydrologic Institute (TRUDY GGI), 1949

149. Polk, E.M., Benedict, B.A., Parker, F.L., "Cooling Water Density Wedges in Streams", Proc. ASCE, HY10, October 1971.

DATA SOURCE REFERENCES

D1. Bachmann, R.W. and Goldman, C.R., "Hypolimnetic Heating in Castle Lake, California", Limnology and Oceanography, Vol. 10, No. 2, April 1965

D2. Goldman, C.R. and Carter, C.R., "An Investigation of Rapid Carbon-14 Bioassay of Factors Affecting the Cultural Eutrophication of Lake Tahoe, California-Nevada", Jour. Water Pollution Control Federation, July 1965

D3. Hazelwood Data Supplied by State Electricity Commission of Victoria (SEC), Monash House, 15 William St., Melbourne, Australia, Instrumentation Described in Thompson (1971)

D4. Lake Norman Data Supplied by Duke Power Company, 422 South Church St., Charlotte, North Carolina (see also Jensen and Geyer (1971))

D5. Tennessee Valley Authority, "Fontanna Reservoir 1966 Field Data, Part I, Temperature and Flow Data", Report No. 17-91, TVW, Division of Water Control Planning, Engineering Laboratory, Norris, Tennessee, March 1969

D6. Tennessee Valley Authority, "Notes on the Warming of Lake Water by Solar Radiation Absorption, based on Cherokee Reservoir Water Quality Study, 1967", Water Resources Research, Advance Report No. 3, Report No. 12-143

D7. TVA (1971) - A Series of Laboratory Reports Showing Velocity Profiles in TVA Reservoirs

LIST OF FIGURES

LIST OF TABLES

LIST OF SYMBOLS

A	-	surface area
A^*	-	non-dimensional surface area (A/A_p)
A_{av}	-	horizontal area at mid-depth
A_D	-	aspect ratio of outlet (h_o^*/b_o)
A_f	-	area of active zone (Ch. 3)
A_{IP}	-	surface area of intake pond
A_M	-	area of entrance mixing region
A_p	-	total surface area of pond
A_{p_m}	-	total surface area of completely mixed pond
A_{p_p}	-	total surface area of plug flow pond
A_s	-	area of stable region of surface
A_{th}	-	area of flow through zone (Ch. 3)
A_x	-	area swept out by heated discharge at distance x from origin
A_z	-	area in horizontal plane at elevation z
A_1	-	area of mixed flow zone (Figure 3-4)
a	-	evaporation constant-windspeed function at zero wind
a_1	-	constant in withdrawal layer formula (Eq. 6.53)
a_e	-	area of eddy zone (Ch. 3)
B	-	width of one-dimensional channel (e.g. discharge channel)
b	-	windspeed constant in Ch. 2
b_o	-	half width of discharge channel exit
b_s	-	width of surface layer

b_{si} - width of opening in skimmer wall

b_1 - width of mixed flow zone (Figure 3-4)

C - fraction of sky covered by clouds

C_1 - constant in Bowen's ratio

c - specific heat of water

c_f - specific heat of concrete

c_p - specific heat of air at constant pressure

D_f - thermal diffusivity of concrete

D_m - molecular diffusivity of heat in water

D_x - dilution after area A_x

d - depth of active layer (Ch. 3)

d_b - depth of water in experimental basin

d_D - Secchi disk depth

d_f - thickness of floor

d_M - depth at end of entrance mixing region

d_s - depth of surface layer

d_{si} - height of opening in skimmer wall

d_u - depth of upper layer (Eq. 5.9) in Ljatkher's model

E - mass flux due to evaporation (Ch. 2)

E - turbulent diffusivity

E_x, E_z - turbulent diffusivity in x,z direction

e - vapor pressure

e_a - vapor pressure in air

e_s - saturated vapor pressure at temperature of water surface

e_z - vapor pressure in air at height z

$F(W_z)$ - windspeed function for mass flux (Eq. 2.14)

$\mathbb{F}_c$ - critical densimetric Froude number density current flow into backwater areas

$$= \frac{u}{\sqrt{g \frac{\Delta\rho}{\rho} h_c}} \quad \text{(Eq. 4.1)}$$

$\mathbb{F}_D$ - densimetric Froude number of heated layer at outlet

$\mathbb{F}_i$ - internal densimetric Froude number at any point in the pond

$$= \frac{u}{\sqrt{g \frac{\Delta\rho}{\rho} H}}$$

$\mathbb{F}_L$ - local densimetric Froude number of flow in surface layer

$$\frac{u}{\sqrt{g \frac{\Delta\rho}{\rho} d_s}}$$

F_u - densimetric Froude number for two-layer flow (Eq. 6.29)

$\mathbb{F}^1$ - critical value of densimetric Froude number for withdrawal layer

$f(W_z)$ - windspeed function for heat flux

f - bottom friction coefficient

f_i - interfacial friction coefficient

Gr - Grashof No.

Gr.Pr. - Grashof Prandtl No.

g - acceleration due to gravity

H - depth of pond (mean or max. as shown)

H_c - heat transfer rate

H_e - depth of epilimnion

H_p - plant heat rejection rate

H_y - heat generation or dissipation per unit volume in body of fluid

h - average depth

h_c - critical depth at which density current is inhibited by actual water depth (Figure 4-14)

h_c - heat transfer coefficient (Ch. 2 only)

h_o - depth of discharge channel

h_o^* - depth of warm surface layer at exit of discharge channel (outlet)

h_r - hydraulic radius of moving layer in two-layer flow

h_1 - depth of upper layer in two-layer flow

h_2 - depth of lower layer in two-layer flow

K - heat transfer coefficient

K_h - eddy diffusivity of heat

K_m - eddy diffusivity of mass

K_o - diffusion coefficient for homogeneous case (Sundaram) (Eq. 5.5)

K_r - ratio of heat transfer coefficients in model and prototype

K_z - eddy diffusion coefficient (Sundaram) (Eq. 5.5)

k - cloudiness constant (Eq. 2.8)

k_e - coefficient of eddy utilization (Ch. 3)

k_f - thermal conductivity of concrete

k_{th} - coefficient of through-flow utilization (Ch. 3)

k_u - effective area ratio

L - length

L^* - length scale for lakes (Ch. 5 - Eq. 5.6)

L_x - horizontal length scale

L_{x_r} - horizontal length scale ratio

L_w - length of cold water wedge in discharge channel

L_z - vertical length scale

L_{z_r} - vertical length scale ratio

L_v - latent heat of vaporization of water

Nu - Nusselt No.

Pr - Prandtl No.

$P_1(t)$ - probability that the detention time of a particle in the upper layer is t

p - total air pressure (Ch. 2)

p - ratio of area of fully mixed pond to total pond surface area (Ch. 3, Eq.'s 3.14 to 3.16)

Q - flowrate

Q_d - volume flowrate of water entrained by condenser discharge

Q_{e_c} - entrained flowrate in channel

Q_{e_p} - entrained flowrate in pond itself

Q_b - blowdown flowrate

Q_e - evaporative flowrate

Q_{in} - stream inflow

$Q_{in}(z)$ - stream inflow below elevation z

Q_m - makeup water flowrate

Q_o - circulating water flowrate through condensers

Q_{os} - stream outflow through dam

Q_{os_k} - stream outflow through dam at outlet k

$Q_{os}(z)$ - stream outflow below elevation z

Q_r - ratio of flowrates in model and prototype

Q_s - total flowrate at stable region

Q_T - total through flow

Q_v - vertical flowrate

Q_x - flowrate at distance x from origin

Q_1 - flowrate at end of discharge channel

Q_2 - flowrate at end of entrance mixing region

Q_3 - flowrate at end of heat loss region

Q_4 - flowrate under skimmer wall = Q_o

Q_5 - flowrate through intake pond = Q_o

q - flow/unit width

q_b - heat flux out by advection (blowdown)

q_{c_i} - heat flux out by advection through intake

q_{c_o} - heat flux in by advection through outlet

q_{in} - stream inflow rate per unit height (Ch. 6)

q_L - heat flux out of surface

q_m - heat flux in by advection (makeup water)

$q_{os}(z,t)$ - outflow through dam per unit height

q_R - net heat influx by radiation

q_S - rate of change of heat stored in pond

q_1 - flow/unit width in upper layer

q_2 - flow/unit width in lower layer

R - gas constant for dry air (Eq. 2.25)

R - Bowen's Ratio (Eq. 2.45)

R_e - Reynolds number $=(4q/\nu)$

R_r - ratio of Reynolds numbers in model and prototype

R_H - relative humidity

R_i - Richardson No.

r - parameter which defines cooling potential of a simple pond $= (KA_p/\rho cQ_o)$

r_m - ratio of entrained water to stream inflow or condenser flow

S_x - bottom slope

S_o - bottom slope in discharge channel

S_p - fraction of possible sunshine

$T(x,y,z,t)$ - water temperature as a function of space, time

T^* - average temperature (Eq. 2.56)

$T^*(A^*,t^*)$ - non-dimensional surface temperature

T_{Am} - ambient temperature of receiving water

T_a - air temperature (°R, °F as defined)

T_{a_v} - virtual air temperature (Eq. 2.31b)

T_D - discharge temperature at exit from discharge channel

T_d - dewpoint temperature

T_E - equilibrium temperature

T_e - temperature of entrained flow

T_{e_c} - temperature of entrained flow in discharge channel

T_{e_p} - temperature of entrained flow in pond itself

$T_f(z)$ - initial temperature profile

T_m - temperature of the mixed discharge (Ch. 3)

T_m - average temperature of reservoir water entrained by stream inflow (Ch. 6)

T_i - intake temperature

T_i^* - non-dimensional intake temperature = $(T_i - T_E)/(T_o - T_E)$

T_{in} - stream inflow temperature

T'_{in} - mixed inflow temperature i.e. temperature of stream inflow after mixing with reservoir water

T_o - temperature of heated discharge from condensers

T_{os_k} - outflow temperature at dam outlet k (Ch. 6)

T_p - temperature of mixing water (Ch. 3)

T_{s0} - maximum water surface temperature

T_{s1} - minimum water surface temperature

T_s - bulk water surface temperature

T_s^* - average water surface temperature (Eq. 2.69 or 2.71)

T_s^* - non-dimensional surface temperature $\frac{T_s - T_E}{T_o - T_E}$

T_{s_v} - virtual temperature of a thin vapor layer in contact with the water surface

T_{wb} - wet bulb temperature

T_x - temperature at distance x from origin

T_l - temperature at cool end of surface layer (Ch. 1)

T_{l_d} - temperature at cool end of surface layer in daytime

T_{l_n} - temperature at cool end of surface layer at night

T_1 - temperature of heated discharge at exit from discharge channel (Ch. 6)

T_2 - temperature of heated discharge at end of entrance mixing region

T_3 - temperature of heated discharge at end of heat loss region

T_4 - temperature of flow under skimmer wall

T_5 - temperature of intake pond = T_i

t - time

$\hat{t}$ - residence time of pond ($\forall/Q_o$)

t^* - non-dimensional time ($t/\hat{t}$)

U - average velocity

u - velocity in x direction

u_D - discharge velocity at exit from discharge channel

u_e - entrained flowrate per unit horizontal area

$u_{in}(z)$ - stream inflow velocity at elevation z

u_o - average velocity of flow in discharge channel ($Q_o/2h_o b_o$)

u_o^* - exit velocity of heated layer from discharge channel ($Q_o/2h_o^* b_o$)

$u_{os}(z)$ - reservoir outflow velocity at elevation z

u_{*_w} - wind friction velocity (Eq. 5.6)

$\bar{V}$ - velocity vector

V - vertical velocity

V_c - relative velocity between two layers in discharge channel

$\forall$ - volume of pond

$\forall_u$ - volume of upper layer

$\forall_{Ip}$ - volume of intake pond

v - vertical velocity

W_z - windspeed (mph) at height z meters

W_2 - windspeed (mph) at height 2 meters

x - horizontal length scale

z - elevation above a datum (e.g. water surface in Ch. 2, bottom of cooling pond in Ch. 6)

z' - roughness height in vapor pressure profile (Eq. 2.47)

z_b - elevation of bottom

z_{in} - elevation of stream inflow

z_ℓ - elevation of bottom of mixed surface layer

z_o - roughness height in wind profile (Eq. 2.46)

z_{out} - elevation of stream outflow through dam

z_s - elevation of surface

α - molecular thermal diffusivity of air

α_v - volumetric expansion coefficient for water

β - gradient of vapor pressure - temperature curve (Ch. 2)

β^* - fraction of solar radiation absorbed near surface

β' - expansion coefficient for gas

β_o - parameter in Koh's withdrawal formula (Ch. 6,7)

β_s - gradient of vapor pressure - temperature curve at temperature T_s

Δ - increment

$\Delta z, \Delta A, \Delta t$ - length, area and time increments used in numerical model

ΔT - temperature rise through condenser

ΔT_c - temperature rise above ambient along the centerline of the heated discharge

ΔT_i - intake temperature elevation above natural surface temperature (Ch. 5)

ΔT_o - initial temperature difference between heated discharge and the receiving water

Δz - vertical length increment

$\Delta\theta$ - temperature difference between water surface or flat plate and the background air ($T_s - T_a$)

$\Delta\theta_v$ - virtual temperature difference between the water surface and air at two meters height (Eq. 2.306)

δ - thickness of withdrawal layer

ε - emmissivity of atmosphere (Ch. 2)

ε - normalized density gradient $\frac{1}{\rho}\frac{\partial\rho}{\partial z}$ (Ch. 6)

η - extinction coefficient of water

η' - ratio of depth of lower layer to total depth $[h_2/(h_1 + h_2)]$

θ - temperature of water in degrees C

ν - kinematic viscosity of gas

ρ - density of water

ρ_a - density of air

ρ_v - density of water vapor in air

σ - Stefan Boltzmann constant

σ_i - standard deviation of stream inflow (Ch. 6)

σ_i - constant (Eq. 5.5)

σ_o - standard deviation of outflow through dam, or through power station intake

τ, τ_o, τ_1 - time in Ljatkher's model (section 5.7)

τ_i - shear stress at interface between two layers of different density (Ch. 5, 6)

τ_o - bottom shear stress (Ch. 5,6)

τ_w - wind induced shear stress (Ch. 5,6)

ϕ - radiation (BTU/ft^2/day, cal/cm^2/day)

ϕ_a - incident atmospheric radiation (long wave)

ϕ_{a_c} - clear sky atmospheric radiation

ϕ_{ar} - reflected atmospheric radiation

ϕ_{an} - net incident atmospheric radiation = $\phi_a - \phi_{ar}$

ϕ_b - transmitted short wave radiation at depth z

ϕ_{br} - long wave radiation from the water surface

ϕ_c - conduction (sensible) heat flux

ϕ_e - evaporative heat flux

ϕ_n - net heat input

ϕ_R - net radiation from underside of concrete floor under laboratory cooling pond

ϕ_r - net radiation input from sun and atmosphere

ϕ_s - incident solar radiation (short wave)

ϕ_{sr} - reflected solar radiation

ϕ_{sn} - net incident solar radiation = $\phi_s - \phi_{sr}$

ϕ_{sc} - clear sky solar radiation

ERRATA for TR No. 161

p. 16, Figure 1 — L.H. Fig. Land Cost $ 500/acre
R.H. Fig. Land Cost $5000/acre

p. 23, line 2 — T_m should be r_m

p. 35, para.3, line 2 — ....., testing the formula against.....

p. 46, bottom of page — k = thermal conductivity of air

p. 48, Eqn. 2.26 should read

$$H_c = h_c \, \Delta\Theta = \rho_a \, c_p \, K_h \, \frac{\Delta\Theta}{\Delta Z} \qquad (2.26)$$

p. 60, line 10, ... Table 2-2 .....

p. 92, line 3, ...West Branch .....

p. 94, line 3, ...heat rejected.....

p.101, para. 2, ...Two cases will be treated separately, the case when .....

p.128, sec. 4.4, para. 1,

.....However, McMillan notes that field observations in Lake Trawsfynydd showed wind induced currents were an order of magnitude greater than density currents, and the latter were an order of magnitude greater than pumping currents. .....

p.131, sec. 4.4.2, line 3 .....indicates that heated water ....

p.138, Figure 4.12, ————————Temperature Profile
.....Velocity Profile

p.139, line 11, ...F_c has an upper limit of 0.5.

p.140, line 8, ...in support of $F_c \leq 0.5$. .....

p.171, line 6, ...Condenser water was withdrawn.....

p.177, line 5, ...Ljatkher's distribution function

p.208, Eqn. 6.14, last term is

$$\frac{1}{\rho c d_s} \left[\phi_n - \phi_{sn} (1-\beta^*) \, e^{-nd_s} \right]$$

p. 213, Figure 6-9, x axis represents F_u

p. 222, line 1, replace h_o by h_o^*

p. 254, line 3 .....profiles tend to be highly nonlinear.....

p. 259, line 6 $D_m = 0.133\ ft^2/day$

p. 262, bottom 2 lines .... Secchi disk ... .

p. 306, Eqn. 7.1

$$\rho = .999973 \left[1 - \frac{(\theta - 3.9863)^2}{508929.2} \cdot \frac{(\theta + 288.9414)}{(\theta + 68.12963)} \right]$$

p. 306, bottom line

$$\beta_o = \left(\frac{\varepsilon\, g}{D_m \nu} \right)^{\frac{1}{6}}$$

p. 316, line 5, ... assume $D_{s_{min}} = 1.5$ in the formulation of their model. .....

p. 376, para. 3, ...The performance of the mathematical model will be assessed primarily .....